Hashemite Kingdom of Jordan

Jordan Journal of Biological Sciences

An International Peer-Reviewed Scientific Journal

Financed by the Scientific Research and Innovation Support Fund

This title is indexed in Scopus

http://jjbs.hu.edu.jo/

المجلة الأردنية للعلوم الحياتية
Jordan Journal of Biological Sciences (JJBS)
http://jjbs.hu.edu.jo

Jordan Journal of Biological Sciences (JJBS) (ISSN: 1995–6673 (Print); 2307-7166 (Online)): An International Peer- Reviewed Open Access Research Journal financed by the Scientific Research and Innovation Support Fund, Ministry of Higher Education and Scientific Research, Jordan and published quarterly by the Deanship of Scientific Research , The Hashemite University, Jordan.

Submission Address

Professor Atoum, Manar F
The Hashemite Universit y
P.O. Box 330127, Zarqa, 13115, Jordan
Phone: +962-5-3903333 ext.4147
E-Mail: jjbs@hu.edu.jo

المجلة الاردنية للعلوم الحياتية
Jordan Journal of Biological Sciences (JJBS)
http://jjbs.hu.edu.jo

International Advisory Board (Arranged alphabetically)

Instructions to Authors

Scopes

Study areas include cell biology, genomics, microbiology, immunology, molecular biology, biochemistry, embryology, immunogenetics, cell and tissue culture, molecular ecology, genetic engineering and biological engineering, bioremediation and biodegradation, bioinformatics, biotechnology regulations, gene therapy, organismal biology, microbial and environmental biotechnology, marine sciences. The JJBS welcomes the submission of manuscript that meets the general criteria of significance and academic excellence. All articles published in JJBS are peer-reviewed. Papers will be published approximately one to two months after acceptance.

Type of Papers

The journal publishes high-quality original scientific papers, short communications, correspondence and case studies. Review articles are usually by invitation only. However, Review articles of current interest and high standard will be considered.

Submission of Manuscript

Manuscript, or the essence of their content, must be previously unpublished and should not be under simultaneous consideration by another journal. The authors should also declare if any similar work has been submitted to or published by another journal. They should also declare that it has not been submitted/ published elsewhere in the same form, in English or in any other language, without the written consent of the Publisher. The authors should also declare that the paper is the original work of the author(s) and not copied (in whole or in part) from any other work. All papers will be automatically checked for duplicate publication and plagiarism. If detected, appropriate action will be taken in accordance with International Ethical Guideline. By virtue of the submitted manuscript, the corresponding author acknowledges that all the co-authors have seen and approved the final version of the manuscript. The corresponding author should provide all co-authors with information regarding the manuscript, and obtain their approval before submitting any revisions. Electronic submission of manuscripts is strongly recommended, provided that the text, tables and figures are included in a single Microsoft Word file. Submit manuscript as e-mail attachment to the Editorial Office at: JJBS@hu.edu.jo. After submission, a manuscript number will be communicated to the corresponding author within 48 hours.

Peer-review Process

It is requested to submit, with the manuscript, the names, addresses and e-mail addresses of at least 4 potential reviewers. It is the sole right of the editor to decide whether or not the suggested reviewers to be used. The reviewers' comments will be sent to authors within 6-8 weeks after submission.
Manuscripts and figures for review will not be returned to authors whether the editorial decision is to accept, revise, or reject. All Case Reports and Short Communication must include at least one table and/ or one figure.

Preparation of Manuscript

The manuscript should be written in English with simple lay out. The text should be prepared in single column format. Bold face, italics, subscripts, superscripts etc. can be used. Pages should be numbered consecutively, beginning with the title page and continuing through the last page of typewritten material.

The text can be divided into numbered sections with brief headings. Starting from introduction with section 1. Subsections should be numbered (for example 2.1 (then 2.1.1, 2.1.2, 2.2, etc.), up to three levels. Manuscripts in general should be organized in the following manner:

Title Page

The title page should contain a brief title, correct first name, middle initial and family name of each author and name and address of the department(s) and institution(s) from where the research was carried out for each author. The title should be without any abbreviations and it should enlighten the contents of the paper. All affiliations should be provided with a lower-case superscript number just after the author's name and in front of the appropriate address.
The name of the corresponding author should be indicated along with telephone and fax numbers (with country and area code) along with full postal address and e-mail address.

Abstract

The abstract should be concise and informative. It should not exceed **350 words** in length for full manuscript and Review article and **150 words** in case of Case Report and/ or Short Communication. It should briefly describe the purpose of the work, techniques and methods used, major findings with important data and conclusions. No references should be cited in this part. Generally non-standard abbreviations should not be used, if necessary they should be clearly defined in the abstract, at first use.

Keywords

Immediately after the abstract, **about 4-8 keywords** should be given. Use of abbreviations should be avoided, only standard abbreviations, well known in the established area may be used, if appropriate. These keywords will be used for indexing.

Abbreviations

Non-standard abbreviations should be listed and full form of each abbreviation should be given in parentheses at first use in the text.

Introduction

Provide a factual background, clearly defined problem, proposed solution, a brief literature survey and the scope and justification of the work done.

Materials and Methods

Give adequate information to allow the experiment to be reproduced. Already published methods should be mentioned with references. Significant modifications of published methods and new methods should be described in detail. Capitalize trade names and include the manufacturer's name and address. Subheading should be used.

Results

Results should be clearly described in a concise manner. Results for different parameters should be described under subheadings or in separate paragraph. Results should be explained, but largely without referring to the literature. Table or figure numbers should be mentioned in parentheses for better understanding.

Discussion

The discussion should not repeat the results, but provide detailed interpretation of data. This should interpret the significance of the findings of the work. Citations should be given in support of the findings. The results and discussion part can also be described as separate, if appropriate. The Results and Discussion sections can include subheadings, and when appropriate, both sections can be combined

Conclusions

This should briefly state the major findings of the study.

Acknowledgment

A brief acknowledgment section may be given after the conclusion section just before the references. The acknowledgment of people who provided assistance in manuscript preparation, funding for research, etc. should be listed in this section.

Tables and Figures

Tables and figures should be presented as per their appearance in the text. It is suggested that the discussion about the tables and figures should appear in the text before the appearance of the respective tables and figures. No tables or figures should be given without discussion or reference inside the text.

Tables should be explanatory enough to be understandable without any text reference. Double spacing should be maintained throughout the table, including table headings and footnotes. Table headings should be placed above the table. Footnotes should be placed below the table with superscript lowercase letters. Each table should be on a separate page, numbered consecutively in Arabic numerals.

Each figure should have a caption. The caption should be concise and typed separately, not on the figure area. Figures should be self-explanatory. Information presented in the figure should not be repeated in the table. All symbols and abbreviations used in the illustrations should be defined clearly. Figure legends should be given below the figures.

References

References should be listed alphabetically at the end of the manuscript. Every reference referred in the text must be also present in the reference list and vice versa. In the text, a reference identified by means of an author's name should be followed by the year of publication in parentheses (e.g.(Brown,2009)). For two authors, both authors' names followed by the year of publication (e.g.(Nelson and Brown, 2007)). When there are more than two authors, only the first author's name followed by "*et al*." and the year of publication (e.g. (Abu-Elteen *et al*., 2010)). When two or more works of an author has been published during the same year, the reference should be identified by the letters "a", "b", "c", etc., placed after the year of publication. This should be followed both in the text and reference list. e.g., Hilly, (2002a, 2002b); Hilly, and Nelson, (2004). Articles in preparation or submitted for publication, unpublished observations, personal communications, etc. should not be included in the reference list but should only be mentioned in the article text (e.g., Shtyawy,A., University of Jordan, personal communication). Journal titles should be abbreviated according to the system adopted in Biological Abstract and Index Medicus, if not included in Biological Abstract or Index Medicus journal title should be given in full. The author is responsible for the sccuracy and completeness of the references and for their correct textual citation. Failure to do so may result in the paper being withdraw from the evaluation process. Example of correct reference form is given as follows:-

Reference to a journal publication:

Bloch BK. 2002. Econazole nitrate in the treatment of *Candida vaginitis*. *S Afr Med J.* , **58**:314-323.

Ogunseitan OA and Ndoye IL. 2006. Protein method for investigating mercuric reductase gene expression in aquatic environments. *Appl Environ Microbiol.*, **64**: 695-702.

Hilly MO, Adams MN and Nelson SC. 2009. Potential fly-ash utilization in agriculture. *Progress in Natural Sci.*, **19**: 1173-1186.

Reference to a book:

Brown WY and White SR.1985. **The Elements of Style**, third ed. MacMillan, New York.

Reference to a chapter in an edited book:

Mettam GR and Adams LB. 2010. How to prepare an electronic version of your article. In: Jones BS and Smith RZ (Eds.), **Introduction to the Electronic Age**. Kluwer Academic Publishers, Netherlands, pp. 281–304.

Conferences and Meetings:

Embabi NS. 1990. Environmental aspects of distribution of mangrove in the United Arab Emirates. Proceedings of the First ASWAS Conference. University of the United Arab Emirates. Al-Ain, United Arab Emirates.

Theses and Dissertations:

El-Labadi SN. 2002. Intestinal digenetic trematodes of some marine fishes from the Gulf of Aqaba. MSc dissertation, The Hashemite University, Zarqa, Jordan.

Nomenclature and Units

Internationally accepted rules and the international system of units (SI) should be used. If other units are mentioned, please give their equivalent in SI.

For biological nomenclature, the conventions of the *International Code of Botanical Nomenclature, the International Code of Nomenclature of Bacteria,* and the *International Code of Zoological Nomenclature* should be followed.

Scientific names of all biological creatures (crops, plants, insects, birds, mammals, etc.) should be mentioned in parentheses at first use of their English term.

Chemical nomenclature, as laid down in the *International Union of Pure and Applied Chemistry* and the official recommendations of the *IUPAC-IUB Combined Commission on Biochemical Nomenclature* should be followed. All biocides and other organic compounds must be identified by their Geneva names when first used in the text. Active ingredients of all formulations should be likewise identified.

Math formulae

All equations referred to in the text should be numbered serially at the right-hand side in parentheses. Meaning of all symbols should be given immediately after the equation at first use. Instead of root signs fractional powers should be used. Subscripts and superscripts should be presented clearly. Variables should be presented in italics. Greek letters and non-Roman symbols should be described in the margin at their first use.

To avoid any misunderstanding zero (0) and the letter O, and one (1) and the letter l should be clearly differentiated. For simple fractions use of the solidus (/) instead of a horizontal line is recommended. Levels of statistical significance such as: $^{*}P < 0.05$, $^{**}P < 0.01$ and $^{***}P < 0.001$ do not require any further explanation.

Copyright

Submission of a manuscript clearly indicates that: the study has not been published before or is not under consideration for publication elsewhere (except as an abstract or as part of a published lecture or academic thesis); its publication is permitted by all authors and after accepted for publication it will not be submitted for publication anywhere else, in English or in any other language, without the written approval of the copyright-holder. The journal may consider manuscripts that are translations of articles originally published in another language. In this case, the consent of the journal in which the article was originally published must be obtained and the fact that the article has already been published must be made clear on submission and stated in the abstract. It is compulsory for the authors to ensure that no material submitted as part of a manuscript infringes existing copyrights, or the rights of a third party.

Ethical Consent

All manuscripts reporting the results of experimental investigation involving human subjects should include a statement confirming that each subject or subject's guardian obtains an informed consent, after the approval of the experimental protocol by a local human ethics committee or IRB. When reporting experiments on animals, authors should indicate whether the institutional and national guide for the care and use of laboratory animals was followed.

Plagiarism

The JJBS hold no responsibility for plagiarism. If a published paper is found later to be extensively plagiarized and is found to be a duplicate or redundant publication, a note of retraction will be published, and copies of the correspondence will be sent to the authors' head of institute.

Galley Proofs

The Editorial Office will send proofs of the manuscript to the corresponding author as an e-mail attachment for final proof reading and it will be the responsibility of the corresponding author to return the galley proof materials appropriately corrected within the stipulated time. Authors will be asked to check any typographical or minor clerical errors in the manuscript at this stage. No other major alteration in the manuscript is allowed. After publication authors can freely access the full text of the article as well as can download and print the PDF file.

Publication Charges

There are no page charges for publication in Jordan Journal of Biological Sciences, except for color illustrations,

Reprints

Ten (10) reprints are provided to corresponding author free of charge within two weeks after the printed journal date. For orders of more reprints, a reprint order form and prices will be sent with article proofs, which should be returned directly to the Editor for processing.

Disclaimer

Articles, communication, or editorials published by JJBS represent the sole opinions of the authors. The publisher shoulders no responsibility or liability what so ever for the use or misuse of the information published by JJBS.

Indexing

JJBS is indexed and abstracted by:

DOAJ (Directory of Open Access Journals)	CABI
Google Scholar	EBSCO
Journal Seek	CAS (Chemical Abstract Service)
HINARI	ETH- Citations
Index Copernicus	Open J-Gat
NDL Japanese Periodicals Index	SCImago
SCIRUS	Clarivate Analytics (Zoological Abstract)
OAJSE	Scopus
ISC (Islamic World Science Citation Center)	AGORA (United Nation's FAO database)
Directory of Research Journal Indexing (DRJI)	SHERPA/RoMEO (UK)
Ulrich's	

المجلة الأردنية للعلوم الحياتية
Jordan Journal of Biological Sciences (JJBS)
ISSN 1995- 6673 (Print), 2307- 7166 (Online)
http://jjbs.hu.edu.jo

The Hashemite University

Deanship of Scientific Research

TRANSFER OF COPYRIGHT AGREEMENT

Journal publishers and authors share a common interest in the protection of copyright: authors principally because they want their creative works to be protected from plagiarism and other unlawful uses, publishers because they need to protect their work and investment in the production, marketing and distribution of the published version of the article. In order to do so effectively, publishers request a formal written transfer of copyright from the author(s) for each article published. Publishers and authors are also concerned that the integrity of the official record of publication of an article (once refereed and published) be maintained, and in order to protect that reference value and validation process, we ask that authors recognize that distribution (including through the Internet/WWW or other on-line means) of the authoritative version of the article as published is best administered by the Publisher.

To avoid any delay in the publication of your article, please read the terms of this agreement, sign in the space provided and return the complete form to us at the address below as quickly as possible.

Article entitled:----------

Corresponding author: ----------

To be published in the journal: Jordan Journal of Biological Sciences (JJBS)

I hereby assign to the Hashemite University the copyright in the manuscript identified above and any supplemental tables, illustrations or other information submitted therewith (the "article") in all forms and media (whether now known or hereafter developed), throughout the world, in all languages, for the full term of copyright and all extensions and renewals thereof, effective when and if the article is accepted for publication. This transfer includes the right to adapt the presentation of the article for use in conjunction with computer systems and programs, including reproduction or publication in machine-readable form and incorporation in electronic retrieval systems.
Authors retain or are hereby granted (without the need to obtain further permission) rights to use the article for traditional scholarship communications, for teaching, and for distribution within their institution.

☐ **I am the sole author of the manuscript**

☐ **I am signing on behalf of all co-authors of the manuscript**

☐ **The article is a 'work made for hire' and I am signing as an authorized representative of the employing company/institution**

Please mark one or more of the above boxes (as appropriate) and then sign and date the document in black ink.

Signed:_____ **Name printed:** _____
Title and Company (if employer representative) : _____
Date: _____

Data Protection: By submitting this form you are consenting that the personal information provided herein may be used by the Hashemite University and its affiliated institutions worldwide to contact you concerning the publishing of your article.

Please return the completed and signed original of this form by mail or fax, or a scanned copy of the signed original by e-mail, retaining a copy for your files, to:

Hashemite University
Jordan Journal of Biological Sciences
Zarqa 13115 Jordan
Fax: +962 5 3903338
Email: jjbs@hu.edu.jo

EDITORIAL PREFACE

Jordan Journal of Biological Sciences (JJBS) is a refereed, quarterly international journal financed by the Scientific Research and Innovation Support Fund, Ministry of Higher Education and Scientific Research in cooperation with the Hashemite University, Jordan. JJBS celebrated its 12th commencement this past January, 2020. JJBS was founded in 2008 to create a peer-reviewed journal that publishes high-quality research articles, reviews and short communications on novel and innovative aspects of a wide variety of biological sciences such as cell biology, developmental biology, structural biology, microbiology, entomology, molecular biology, biochemistry, medical biotechnology, biodiversity, ecology, marine biology, plant and animal biology, plant and animal physiology, genomics and bioinformatics.

We have watched the growth and success of JJBS over the years. JJBS has published 14 volumes, 60 issues and 800 articles. JJBS has been indexed by SCOPUS, CABI's Full-Text Repository, EBSCO, Clarivate Analytics- Zoological Record and recently has been included in the UGC India approved journals. JJBS Cite Score has improved from 0.7 in 2019 to 1.4 in 2021 (Last updated on 6 March, 2022) and with Scimago Institution Ranking (SJR) 0.22 (Q3) in 2021.

A group of highly valuable scholars have agreed to serve on the editorial board and this places JJBS in a position of most authoritative on biological sciences. I am honored to have six eminent associate editors from various countries. I am also delighted with our group of international advisory board members coming from 15 countries worldwide for their continuous support of JJBS. With our editorial board's cumulative experience in various fields of biological sciences, this journal brings a substantial representation of biological sciences in different disciplines. Without the service and dedication of our editorial; associate editorial and international advisory board members, JJBS would have never existed.

In the coming year, we hope that JJBS will be indexed in Clarivate Analytics and MEDLINE (the U.S. National Library of Medicine database) and others. As you read throughout this volume of JJBS, I would like to remind you that the success of our journal depends on the number of quality articles submitted for review. Accordingly, I would like to request your participation and colleagues by submitting quality manuscripts for review. One of the great benefits we can provide to our prospective authors, regardless of acceptance of their manuscripts or not, is the feedback of our review process. JJBS provides authors with high quality, helpful reviews to improve their manuscripts.

Finally, JJBS would not have succeeded without the collaboration of authors and referees. Their work is greatly appreciated. Furthermore, my thanks are also extended to The Hashemite University and the Scientific Research and Innovation Support Fund, Ministry of Higher Education and Scientific Research for their continuous financial and administrative support to JJBS.

Professor Atoum, Manar F.
March, 2021

JJBS

Volume 16, Number 1, March 2023
ISSN 1995-6673

Jordan Journal of Biological Sciences

CONTENTS

Original Articles

JJBS

Volume 16, Number 1,March 2023
ISSN 1995-6673
Pages 1 – 6
https://doi.org/10.54319/jjbs/160101

Jordan Journal of Biological Sciences

Effect of Silver Nanoparticles on Growth and Physiological Responses of Spinach (*Spinacia oleracea* L.) under Salt Stress

Emad Y. Bsoul*, Sabreen A. Othman, Abdul Latief A. Al-Ghzawi and Muhannad I. Massadeh

Department of Biology and Biotechnology, The Hashemite University, Zarqa, Jordan

Received: June 26, 2022; Revised: September 19, 2022; Accepted: September 26, 2022

Abstract

Saline soil or water can highly affect plant physiological and biochemical responses including general disruption in the nutritional status of plants, osmotic stress, and ion-specific toxicity The rapid development and potential release of engineered nanoparticles (ENPs) have raised considerable concerns due to the unique properties of nanomaterials. Spinach is considered a model plant in hydroponic system production and is of research interest all over the world. In this study, we aim to study the physiological responses of spinach under different concentrations of both silver nanoparticles and salt stress. Spinach seedlings were exposed to 16 treatments asthreesalinity concentrations (4.0, 6.0, and 10.0 $dS.m^{-1}$),three silver nanoparticles concentrations (20, 40, 60 ppm), nine treatments as combination of salinity and silver nanoparticles and control.Relative water content (RWC), stomatal conductance (g_s), chlorophyll content index (CCI),), dry weights (DW), leaf area (LA), and specific leaf area (SLA) of 41 days old spinach seedlings were examined and recorded for 6 weeks. The application of Silver nanoparticles had affected plant growth and altered many plant physiological responses. We concluded that silver nanoparticles might have positive effects on the physiological parameters but only under non-saline stress. However, it negatively impacts plants when it was added under saline conditions.

Keywords: spinach, silver nanoparticles, hydroponic, salt stress, water relations, gas exchange, relative growth rate, net assimilation rate.

1. Introduction

Salt stress (salinity) is the most abiotic stress that extremely influences plant growth and production. Saline soil or water can highly affect plant physiological and biochemical responses, including general disruption in the nutritional status of plants, osmotic stress, and ion-specific toxicity as a result of the accumulation of sodium (Na) and chloride (Cl) ions (Nazar et al. 2011). One of the essential goals for plant researchers is to investigate the physiological responses that help to develop salt tolerance in plants. In addition, soil salinity also affected the quality of many crops, which had a negative impact on the agriculture economy.

Soil salinity in many countries is mainly a consequence of arid climatic conditions. Most crops are sensitive to salt stress that cause subsequent yield loss. To cope with salinity, plants implement many physiological and anatomical traits as adaptation strategies that reduce the effect of salt stress (Bsoul et al., 2017)

Green leafy vegetables are an important part of healthy diets. Spinach (*Spinacia oleracea* L) is an annual edible flowering plant belongs tothe Amaranthaceae. Spinach leaves are a superfood that is loaded with many nutrients in a low-calorie package (Giri et al., 2016). It was found that spinach could tolerate irrigation with salinity around 5.7 dS/m (Uçgun et al,.2020).

Hydroponics is a method of growing plants in water based nutrient rich solution. Growing with hydroponics comes with many advantages, the biggest of which is the significantly increased rate of plant growth. With the proper setup, plants will mature up to 25% faster and produce up to 30% more than the same plants grown in soil (Ritter et al. 2001). Spinach grows quickly in a hydroponic system.

Engineered nanomaterials have received a particular attention for their positive impact on improving many sections of economy, including agriculture(Nowack and Bucheli 2007).The European Union has defined a nanomaterial as a natural, incidental or manufactured material containing particles, in an unbound state or as aggregate or as agglomerate. One more external dimension is the size range 1 – 100 nm" (Rauscher et al., 2015). Nanoparticles (NPs) are used to improve agriculture production and crop protection. However, using them is relatively new and needs further exploration in field of agriculture(Lijuan et al., 2020).Nanoparticles interact with plants causing many morphological and physiological changes, depending on the properties of NPs. Research findings suggested both positive and negative effects on plant growth and development, and the impact of engineered nanoparticles (ENPs) on plants depends on the composition, concentration, size, and physical and chemical properties of ENPs as well as plant species (Xingmao et al. 2010).

* Corresponding author. e-mail: ebsoul@hu.edu.jo.

Silver nanoparticles (AgNPs) are increasingly used in various fields, including medical, food, health care, consumer, and industrial purposes, due to their unique physical and chemical properties (Zhang et al. 2016).Both positive and negative effects of Ag NPs on plant growth have been reported (Abdel Kareem et al. 2017). However, scarce studies have reported the role of NPs on plants under salinity (Almutairi, 2016). Our objective in this study is to investigate the physiological responses of spinach under different concentrations of both silver nanoparticles and salt stress.

2. Materials and Methods

2.1. Study location

This study was conducted in a greenhouse at The Hashemite University, Zarqa, Jordan. 32°05' N Latitude and 36°06 E Longitudes. Greenhouse day temperature, humidity and the light intensity were (24.6 ± 0.039 °C), (51%± 1.48), respectively. Mean midday photosynthetic photon flux density (PPFD) was (365± 0.71 µmol· s^{1}·m^{-2})measured by a quantum sensor (LI-250A; LICOR.)

2.2. Plant material and experimental design

Seeds of baby spinach from the local market were used for this experiment. Seeds were germinated in the greenhouse in trays containing peatmoss (KEKKILA, European Union). After the appearance of the primitive stem, spinach seedlings were then grown in a hydroponic system to prevent any interaction that can impede nanoparticles from the plants. Aftertwo weeks, uniform plants were selected and randomly assigned toexperimental treatments. Each plant was moved to 200 ml flask covered with Aluminum foil (Figure 1) and filled with sterile perlite and Hoagland's solution. Spinach seedlings were left in the flask under greenhouse conditions for four days as adaptation period (Alkhatib et al., 2019).

Uniform spinach plants were assigned randomly to one of 16 treatments ((control), (S1) 4.0dS.m^{-1}, (S2) 6.0 dS.m^{-1}, (S3)10.0dS.m^{-1}, (N1) 20 ppm AgNPs,(N2) 40 ppm AgNPs,(N3) 60 ppm AgNPs,(S1N1)4.0dS.m^{-1} + 20 ppm AgNPs, (S1N2)4.0dS.m^{-1} + 40 ppm AgNPs,(S1N3)4.0dS.m^{-1} + 60 ppm AgNPs,(S2N1)6.0dS.m^{-1} + 20 ppm AgNPs, (S2N2)6.0dS.m^{-1} + 40 ppm AgNPs,(S2N3)6.0dS.m^{-1} + 60 ppm AgNPs(S3N1)10.0dS.m^{-1} + 20 ppm AgNPs, (S3N2)10.0dS.m^{-1} + 40 ppm AgNPs,(S3N3)10.0dS.m^{-1} + 60 ppm AgNPs) for 65 days. The experimental design was Randomize Completely Block Design (RCBD). There were five experimental replications, each containing a total of 16 plants and the total number was 80 seedlings. Plants were grown in a 200 ml flask filled with perlite and the designated solution treatment

All the spinach seedlings from all the treatments had equal and appropriate amount of Hoagland's solution during the experiment period with pH = 5.9. In addition, a fungicide (Vapco Top 70 %,Thiophanate- methyl) was added to the treatment solutions(2 g L^{-1}) to prevent the growth of fungal species.

2.3. Initial seedling traits

After30 days of acclimatization, uniform plants were randomly selected as experimental units. Extra 16 seedlings were harvested to determine the initial dry weights on the same day when the treatments were applied. The harvested plants were separated into shoots and roots. Oven dry weights of shoot and root were determined at 65º C for 3 days.

2.4. Salinity and silver nanoparticles treatments

A 3:1 proportion of calcium chloride and sodium chloride was diluted in water to make a stock solution. Treatment solutions were made by adding stock solution to distilled water until the desired salinity levels were achieved. All readings were recorded using an EC meter (Milwaukee SPEM500).Silver nanoparticles (AgNPs) water dispersion was used in this study has the APS: 2 nm.

2.5. Physiological traits

Two youngest fully-expanded mature healthy leaves were selected to measure the chlorophyll Content Index by using chlorophyll content meter (Optic- Sciences, CMM 200) every two weeks. Stomatal conductance (g_s) was measured biweekly using AP4 Porometer(Delta-A Devices-Cambridge-U. K).

2.6. Final harvest

At the end of the experiment after 41 days, all plant parts were harvested and separated into leaves, shoots and roots.Leaf area was recorded using the leaf area meter (LI-3050C; LI-COR, Lincoln, Nebr.).All plant parts were oven dried at 68°C for three days.Plant stem diameter was measured at the harvest day by using digital Vernier caliper (US 7533474B2, United States).Relative growth rates were calculated using the equation of Gutschick and Kay (1995): RGR = (ln W2 - ln W1)/ (T2 - T1), where W2 was the final dry weight at day 41 (T2), and W1 was the initial DW determined from initial data harvest on day one (T1). Net assimilation rates (NAR) were calculated as: NAR = M2 - M1/T2 - T1 X log L2 - log L1/L2 - L1, where M2 was the final dry weight at day 41 (T2), and M1 was the initial DW determined from the initial recorded on day one of the experiment (T1). Leaf area ratio ($cm^2.g^{-1}$) was calculated as SLA= leaf area/leaf dry weight. Specific stem length ($cm.g^{-1}$) was calculated as SSL= stem height/ stem dry weight.

Leaf discs from five of the youngest fully expanded mature leaves from the median portion of the stem of two randomly selected plants from each treatment were selected. RWC was calculated using the equation: RWC (%) = (FW-DW/SW-DW) * (100) where: FW is the fresh weight and DW represents fresh weight sample oven dried at 68 °C and SW represents saturated weight of sample, which was immersed overnight in distilled water (Bsoul et al., 2007).

2.7. Statistical analysis

Statistical analysis was performed using SAS 9.1 software for Windows (2003). Significant differences between values of all parameters were determined at $P \leq 0.05$ using Proc Glm, PDIFF, ANOVA and Least Significant Difference (LSD).

3. Results

Salinity and silver nanoparticles had affected plant growth parameters. There were no significant differences among treatments in root DW ($P \leq 0.28$), shoot DW ($P \leq$

0.25), total plant DW ($P \leq 0.49$). However, there were significant differences among treatments in root/shoot ratio ($P \leq 0.04$) and stem diameter ($P < 0.0001$) (Table 1).

Plants treated with (S3) had the highest root/shoot DW ratio (6.7) while plants treated with moderate salinity (S2) concentration (6.0 $dS.m^{-1}$), 40 ppm of Ag nanoparticles, (S1N1), (S1N2) and plants with (S1N3) treatments had the lowest value (1.9), (1.2), (1.8), (1.8) and (1.9), respectively. Moreover, plants irrigated with 20 ppm of Ag nanoparticles had the highest stem diameter (0.29 mm), while plants with high salinity concentration (10 $dS.m^{-1}$), (S3N1), (S3N2) and (S3N3) treatments had the lowest and similar stem diameter (Table 2).

Spinach seedlings had no significant differences among treatments in their specific leaf area (SLA) ($P \leq 0.58$) and leaf area ratio (LAR) ($P \leq 0.17$). However, there were significant differences among treatments in leaf area (LA) ($P < 0.0006$), specific leaf weight (SLW) ($P \leq 0.04$) and leaf weight ratio (LWR) ($P \leq 0.03$). The highest leaf area value (5.1 cm^2) was recorded for control, but plants treated with high salinity concentration had among the lowest LA (3.1 cm^2) (Table 2).

Table 1: Effects of salinity and silver nanoparticles treatment onRoot DW, Shoot DW, Plant DW, root to shoot ratio and stem diameter (SD) subjected to irrigation treatments and harvested on day 41 of the experiment.

Treatment	Root DW (g)	Shoot DW (g)	Plant DW (g)	Root/Shoot	SD (mm)
Control	0.061[a*]	0.024 [a]	0.086 [a]	2.5 [cd]	0.33 [a]
S1 (4.0 dS/m)	0.053[a]	0.023 [a]	0.076 [a]	2.3 [cd]	0.08 [dc]
S2 (6.0dS/m)	0.042[a]	0.022 [a]	0.064 [a]	1.9 [d]	0.12 [c]
S3 (10.0dS/m)	0.134 [a]	0.020 [a]	0.155 [a]	6.7 [a]	0.01 [f]
N1(20 ppm)	0.062 [a]	0.022 [a]	0.084 [a]	2.8 [cd]	0.29 [ab]
N2(40 ppm)	0.037 [a]	0.030 [a]	0.067 [a]	1.2 [d]	0.28 [b]
N3(60 ppm)	0.061 [a]	0.022 [a]	0.083 [a]	2.7 [cd]	0.28 [b]
S1N1	0.068 [a]	0.038 [a]	0.105 [a]	1.8 [d]	0.07 [cde]
S1N2	0.066 [a]	0.036 [a]	0.101 [a]	1.8 [d]	0.07 [cde]
S1N3	0.045 [a]	0.024 [a]	0.068 [a]	1.9 [d]	0.07 [cde]
S2N1	0.080 [a]	0.013 [a]	0.093 [a]	6.2 [abc]	0.04 [ef]
S2N2	0.130 [a]	0.021 [a]	0.151 [a]	6.2 [abc]	0.05 [def]
S2N3	0.074 [a]	0.026 [a]	0.099 [a]	2.8 [cd]	0.04 [def]
S3N1	0.091 [a]	0.023 [a]	0.113 [a]	4.0 [abcd]	0.02 [f]
S3N2	0.074 [a]	0.017 [a]	0.091 [a]	4.4 [abcd]	0.01 [f]
S3N3	0.073 [a]	0.021 [a]	0.094 [a]	3.5 [bcd]	0.01[f]
Mean	0.072	0.024	0.096	03.3	0.11
P-value	0.28	0.25	0.49	0.04	<0.0001

* Means within the columns followed by the same letter are not significantly different.

Table 2: Effects of salinity and silver nanoparticles treatment onLeaf Area (LA), Specific Leaf Area (SLA), Specific Leaf Weight (SLW), Leaf Weight Ratio (LWR) and Leaf Area Ratio (LAR) of spinach seedlings subjected to irrigation treatments and harvested on day 41 of the experiment

Treatments	LA (cm^2)	SLA ($cm^2.mg^{-1}$)	SLW ($mg.cm^{-2}$)	LWR ($g.g^{-1}$)	LAR($cm^2.mg^{-1}$)
Control	5.1[* a]	1.49[a]	0.44 [abcd]	0.049 [abc]	0.86 [a]
S1 (4.0 dS/m)	4.8 [ab]	0.78 [a]	0.32 [abcde]	0.038 [abcde]	0.61 [a]
S2 (6.0 dS/m)	3.9 [defg]	0.36 [a]	0.11 [de]	0.018 [bcde]	0.32 [a]
S3 (10.0 dS/m)	3.1 [g]	1.11 [a]	0.04 [e]	0.004 [e]	0.21 [a]
N1 (20 ppm)	4.4 [abcdef]	1.39 [a]	0.58 [abc]	0.042 [abcd]	0.73 [a]
N2 (40 ppm)	4.7 [abcd]	0.96 [a]	0.39 [abcde]	0.037 [abcde]	0.55 [a]
N3 (60 ppm)	4.4 [abcdef]	2.30 [a]	0.40 [abcde]	0.024 [bcde]	0.75 [a]
S1N1	4.8 [abc]	1.61 [a]	0.66 [a]	0.051 [ab]	0.81 [a]
S1N2	4.6 [abcde]	1.38 [a]	0.49 [abcd]	0.031 [abcde]	0.52 [a]
S1N3	4.6 [abcde]	1.78 [a]	0.60 [ab]	0.065 [a]	1.15 [a]
S2N1	4.0 [cdef]	0.78 [a]	0.20 [cde]	0.010 [de]	0.19 [a]
S2N2	3.7 [fg]	1.08 [a]	0.42 [abcd]	0.011 [de]	0.18 [a]
S2N3	3.7 [fg]	0.85 [a]	0.19 [cde]	0.016 [bcde]	0.34 [a]
S3N1	4.2 [bcdef]	0.72 [a]	0.22 [bcde]	0.012 [cde]	0.21 [a]
S3N2	4.2 [bcdef]	1.22 [a]	0.14 [de]	0.011 [de]	0.38 [a]
S3N3	3.8 [efg]	0.17 [a]	0.23 [bcde]	0.009 [de]	0.08 [a]
Mean	4.3	1.13	0.34	0.027	0.49
P-value	0.0006	0.58	0.04	0.03	0.17

* Means within the columns followed by the same letter are not significantly different.

At the end of the experiment relative growthrateRGR results indicated that there were no significant differences among treatments (P= 0.6373) (Fig. 1).

significant differences among treatments (P= 0.6373) (Fig. 3).

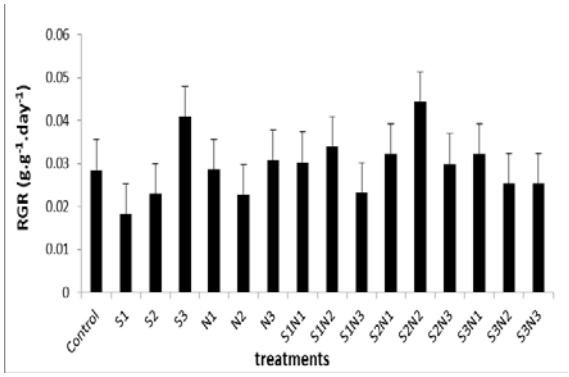

Figure 1: Relative Growth Rate($g.g^{-1}.day^{-1}$): RGR values for all treatments at the end of the experiment (41 days after planting) under the effect of salt stress and nanoparticles irrigation.

Net assimilation rate had significant differences among treatments under salt stress and nanoparticles irrigation (P<0.0469). Plants treated with high salinity (S3=10 $dS.m^{-1}$), (S2N2) had the highest NAR value (1.104, $0.8566mg.cm^{-2}.day^{-1}$) respectively, while other treatments had similar values(Fig. 2).

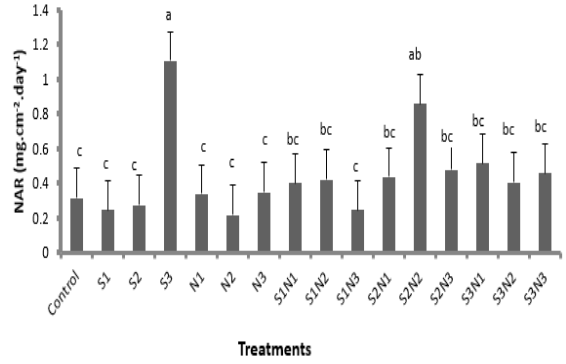

Figure 2: Net Assimilation Rate($mg.cm^{-2}.day^{-1}$): NAR values for all treatments at the end of the experiment (41 days after planting) under the effect of salt stress and nanoparticles irrigation. Data are means ± SE of 5 replicates. Means within the columns marked with the same letter were not significantly different at the $P \leq 0.05$.

Relative water contents RWC results showed significant differences among treatments (P = 0.006). (S1N3) had the highest RWC value (40%). However, the lowest RWC value was (3%) and (4%) for the plants treated with (S3) and (S3N1), respectively (Fig. 3).

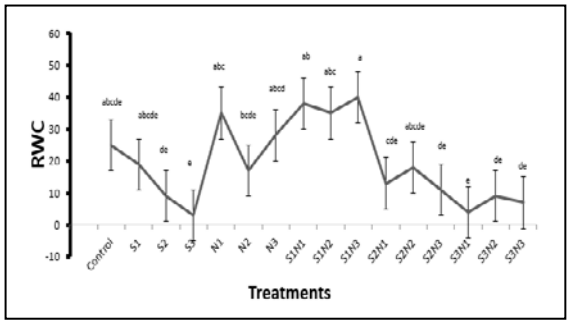

Figure 3: Relative Water Content RWC %:Treatments of nanoparticles irrigation compared with control after 41 days.Data are means ± SE of 5 replicates. Means within the columns marked with the same letter were not significantly different at the $P \leq 0.05$.

Stomatal conductance (g_s) had significant differences among treatments (P=0.0169) in the 6thweek, plants irrigated with 40 ppm of silver nanoparticles (N2) and(S1N1)had the highest stomatal conductance ($0.14cm.s^{-1}$), while S2 and S3 had the lowest stomatal conductance (0.03 and $0.02cm.s^{-1}$), respectively. However, in the 2nd and 4thweek, plants had no significant differences in g_s (P = 0.4391)**,** (P = 0.3762) (Table 3).

Table3 . Biweekly stomatal conductance (g_s) under salt stress and NPs irrigation

Treatment	(g_s) ($mmol.m^{-2}.s^{-1}$) 2nd week	(g_s) ($mmol.m^{-2}.s^{-1}$) 4th week	(g_s) ($mmol.m^{-2}.s^{-1}$) 6th week
Control	0.13 ^{a*}	0.11 ^{a}	0.14 ^{ab}
S1 (4.0 dS/m)	0.2 ^{a}	0.09 ^{a}	0.08 ^{abcd}
S2 (6.0 dS/m)	0.09 ^{a}	0.06 ^{a}	0.03 ^{d}
S3 (10.0 dS/m)	0.03 ^{a}	0.02 ^{a}	0.02 ^{d}
N1 (20 ppm)	0.15 ^{a}	0.11 ^{a}	0.08 ^{abcd}
N2 (40 ppm)	0.17 ^{a}	0.15 ^{a}	0.14 ^{a}
N3 (60 ppm)	0.12 ^{a}	0.1 ^{a}	0.11 ^{abc}
S1N1	0.19 ^{a}	0.12 ^{a}	0.14 ^{a}
S1N2	0.13 ^{a}	0.1 ^{a}	0.07 ^{abcd}
S1N3	0.13 ^{a}	0.09 ^{a}	0.07 ^{bcd}
S2N1	0.14 ^{a}	0.09 ^{a}	0.09 ^{abcd}
S2N2	0.15 ^{a}	0.05 ^{a}	0.06 ^{cde}
S2N3	0.18 ^{a}	0.1 ^{a}	0.07 ^{abcd}
S3N1	0.13 ^{a}	0.09 ^{a}	0.09 ^{abcd}
S3N2	0.15 ^{a}	0.04 ^{a}	0.04 ^{cd}
S3N3	0.09 ^{a}	0.04 ^{a}	0.04 ^{cd}
Means	0.14	0.09	0.08
P-value	0.44	0.38	0.02

*Means within the columns followed by the same letter are not significantly different.

4. Discussion

The current study showed that salinity treatments had no effect on whole plant dry weights, shoot dry weight and root dry weight but significantly affected other growth root to shoot ratio and stem diameter. Guenther et al. (1987) reported that salinity stress is a serious abiotic stress that influences the growth of spinach seedlings and they reported that the reasons were the excessive uptake of (Na^+) and (Cl^{-1}) ions, the accumulation of Na+ in the leaves and nutritional imbalance. Salinity significantly increased root/shoot ratio in spinach seedlings because plants usually invest more in roots than in shoots under salt or drought stress. The application of silver nanoparticles in the current study had no effect on root to shoot ratio that had values similar to the control. These finding were consistent with Mazumdar (2014) who reported that root fresh weight and shoot fresh weight were not affected at low concentration below of 50 µg/mL of silver nanoparticle. This implied that the effect on the root/shoot ratio was due to salinity only.

Salinity treatments reduced spinach stem diameter because plants reduce their hydrolytic conductivity when they are subjected to water stress. Similar results were reported in *Spondias tuberosa* plants (Da silva et al., 2008).

Salinity treatments significantly reducing leaf area of spinach might be attributed to the fact that plants usually reduce their leave's surface area under water deficit or unavailable water in order to reduce transpiration and prevent dehydration. In addition, salinity reduces the total plant growth in general. Beinsan et al. (2003) reported that the negative impact of salt stress on leaf area is due of the reduction in both photosynthesis rate and chlorophyll content in *Phaseolus vulgaris L* plants. The Application of silver nanoparticles had almost similar effect on spinach leaf area that was only under salt stress, and silver nanoparticles had no advantage in improving the plant response to salinity. On the other hand, the application of silver nanoparticles might have a negative impact on the plant under salinity. Almutairi(2016) reported that AgNPs play an important role in moderating the inhibition of plant growth in saline environments by inducing salt tolerance in plants. It was found that exposure to AgNPs is capable of increasing the germination percentage, the germination rate, the root length and the seedling fresh and dry weights of tomato plants under NaCl stress, if applied AgNP on seeds through seed germination. Based on that, we might conclude that it is important to consider the plant growth stage when we apply nanoparticles under saline conditions.

RGR represents the extent to which a plant invests its photosynthesis in current growth and enhances its capacity for future photosynthesis (Fitter and Hay, 2002). Current work indicated that spinach RGR were not significantly affected when treated with the different salt levels. Water availability is a factor that usually reduces NAR and growth. El-Hendawy et al. (2005) reported that the salinity stress reduced NAR values in wheat. The authors attributed the reasons behind that to the reduction in plant relative water content in some cases. Current research indicated a decrease in NAR values when Ag nanoparticles were applied and that might be because silver nanoparticles were able to decrease plant's chlorophyll content.

Relative water content RWC is an important salinity stress indicator and its response varies depending on salinity severity(Galmés et al., 2007).In this study, salinity treatments decreased RWC values. That might be because the plant roots were unable to absorb enough water from the surrounding medium. Yang et al. (2011) reported that RWCin *Medicago ruthenica*plants was decreased under salt stress, as the plants were unable to compensate for water lost by transpiration. Application of silvernanoparticles at concentration of 20 ppm of Ag nanoparticles (N1) had the highest RWC, contra the results of Çekiç et al. (2017) who reported that AgNPs did not significantly affect the water status of *S. lycopersicum*. Applying both salt and Ag nanoparticles together had a negative effect on spinach RWC because saline water might reduce the free Ag nanoparticles amount. As a result, the effect of salinity and Ag nanoparticles treatments was similar to the effect of salinity treatment alone.

Stomatal conductance had no significant differences among treatments in the 2^{nd} and 4^{th}week. However, Stomatal conductance had significant differences among treatments in the 6^{th} week and reduced under salinity. Reduction of stomatal conductance and transpiration rate are considered as adaptations to protect plants from dehydration (Romero et al., 2001). Application of silvernanoparticles had a positive effect on the 6^{th}week and the reason behind that might be the increase in the available amount of water for spinach plants under hydroponic system.

Chlorophyll is one of the major chloroplast components necessary for photosynthesis, and the chlorophyll content index has a positive relationship with the photosynthetic rate. The decrease in chlorophyll content under salinity stress has been considered as chlorophyll degradation. Decreased chlorophyll level during salinity stress has been reported and considered the main cause of inactivation of photosynthesis and loss of chlorophyll and found to be dependent on the duration and severity of salinity. Omoto et al. (2010) reported that the negative effect of salinity on plant's chlorophyll content index was due to chlorophyll deficiency. Chlorophyll deficiency is attributed to the inhibition of chlorophyll synthesis. In our study, the application of silver nanoparticles had a negative effect on spinach chlorophyll content index. Xingmao et al. (2010) reported that silver nanoparticles concentration below 20 ppm can be taken up by plants and transport from intracellular spaces to inside plant cells through plasmodesmata of root cells. These nanoparticles then pass through shoots and accumulate in the leaves which cause an adverse effect on total chlorophyll content index of tested plants. In addition, the Ag NP treatments may cause toxicity to the plants. In greenhouse experiments, Song et al. (2013) reported that mature tomato plants showed evidence of phytotoxicity due to AgNPs by exhibiting low chlorophyll contents and less fruit production. Application of both salt and AgNPs had a negative effect on spinach chlorophyll content, and this might have been attributed to increase in chlorophyllase enzyme activity. Abdel Kareem et al. (2017) reported that total chlorophyll contents decreasing under salt might be due to AgNPs toxicity in plants.

5. Conclusion

Application of silver nanoparticles up to 20 ppm concentration might be considered as a successful method for spinach seedlings under non-saline irrigation conditions and might be successfully used to enhance physiological responses of spinach seedlings. For plants under salinity stress, silver nanoparticles were not able to alleviate the salinity stress with a complement amount of specific nanoparticles concentration. In addition, the application of Ag nanoparticles had a negative effect on stomatal conductance and chlorophyll content when mixed with saline water. Ag nanoparticles did not improve the physiological parameters under salinity stress. Nanoparticles application method and the stage of application might have a great importance when it is used for spinach plants.

Acknowledgements

We deeply thank The Hashemite University for allowing us to use their facilities and equipment. In addition, we are thankful for the greenhouse technicians Yahya Al-Sayfi and Ayoub for their help during the experiment.

References

Alkhatib, R, Alkhatib B, Abdo N, Laith AE and Creamer R. 2019. Physio-biochemical and ultrastructural impact of (Fe_3 O_4) nanoparticles on tobacco. *BMC Plant Biol* **19**:253.

Abdel Kareem SH. Mohamed FQ, Abdel-Hadi AM, Rabia AR, Shafaqat A and Muhammad R. 2017. Interactive effect of salinity and silver nanoparticles on photosynthetic and biochemical parameters of wheat, *Archives of Agronomy and Soil Science*, **63(12):**1736-1747.

Almutairi ZM. 2016. Influence of silver nano-particles on the salt resistance of tomato (*Solanum lycopersicum*) during germination. *Int. J. Agric. Biol.*, **18**: 449–457.

Beinsan, C, Camen D, Sumalan R, and Babau M. 2003. *'Study concerning salt stress effect on leaf area dynamics and chlorophyll content in four bean local landraces from Banat area', Faculty of Horticulture*, 119: 416-19.

Bsoul E., Hilaire RSt., and VanLeeuwen D. 2007. Bigtooth maples from selected provenances effectively endure deficit irrigation. *Hortscience*: **42:**1167-1173.

Bsoul, EY, Shahrestani SA and Shdiefat SM. 2017. Growth, nutrient acquisition, and physiological responses of three olive cultivars to induced salt stress. *Journal of Plant Nutrition* **40(14):** 1955-1968.

Çekiç, FÖ, Ekinci S, İNAL MS, and ÖZAKÇA D. 2017. Silver nanoparticles induced genotoxicity and oxidative stress in tomato plants. *Turkish Journal of Biology*, **41:** 700-707.

Da Silva EC, Nogueira RJMC, de Araújo FP, de Melo NF and de Azevedo Neto AD. 2008. Physiological responses to salt stress in young umbu plants. *Environmental and Experimental Botany* **63(1-3):** 147-157.

El-Hendawy, Salah E, Yuncai Hu, and Urs Schmidhalter. 2005. Growth, ion content, gas exchange, and water relations of wheat genotypes differing in salt tolerances. *Australian Journal of Agricultural Research*. **56:** 123-34.

Fitter A. and Hay R. 2002. **Environmental Physiology of Plants**, Academic Press, San Diego,

Galmés J, Medrano H, and Flexas J. 2007. Photosynthetic limitations in response to water stress and recovery in Mediterranean plants with different growth forms. *New phytologist*, **175:** 81-93.

Giri A, Armstrong B, Rajashekar CB .2016. Elevated carbon dioxide level suppresses nutritional quality of lettuce and spinach. *Am J Plant Sci* **7**:246–258.

Guenther, J.E., Melis, A. 1987. Targets of Salinity Stress in Spinach. In*: Biggins, J. (eds) Progress in Photosynthesis Research. Springer, Dordrecht.*

Gutschick VP and KayLE.. 1995. Nutrient-limited growth rates: quantitative benefits of stress responses and some aspects of regulation. *J. Exp. Bot.***46:** 995-1009.

Lijuan Z, Li Lu, Wang A, Zhang H, Huang M, Wu H, Xing B, Wang Z, and Ji R. 2020.Nano-Biotechnology in Agriculture: Use of Nanomaterials to Promote Plant Growth and Stress Tolerance. *Journal of Agricultural and Food Chemistry* **2020** ***68*** **(7):** 1935-1947.

Mazumdar H. 2014. The impact of silver nanoparticles on plant biomass and chlorophyll content. *Int. J. Eng. Sci*, **4:** 12-20.

Nazar, R, Noushina I, Asim M, Shabina S and Nafees A K. 2011. Understanding the significance of sulfur in improving salinity tolerance in plants. *Environmental and Experimental Botany*, **70:** 80-87.

Nowack B, and Bucheli TD. 2007. Occurrence, behavior and effects of nanoparticles in the environment. *Environmental pollution,***150:** 5-22.

Omoto E, Taniguchi M and Miyake H. 2010. Effects of salinity stress on the structure of bundle sheath and mesophyll chloroplasts in NAD-malic enzyme and PCK type C4 plants. *Plant Production Science***13(2):** 169-176.

Rauscher, H., Roebben, G., Sanfeliu, A., Emons, H., Gibson, N., Koeber, R., Linsinger, T.,Rasmussen, K., Sintes, J., Sokull-Klüttgen, B., & Stamm, H. (2015). *Towards a review of the EC recommendation for a definition of the term nanomaterial*. Report by the Joint Research Centre of the European Commission, European Union. Ispra, Italy.

Ritter E, Angulo B, Riga P, Herran C, Relloso J, San Jose M. 2001. Comparison of hydroponic and aeroponic cultivationsystems for the production of potato minitubers. *Potato Research.* **44(2):**127-135.

Romero-Aranda R, Soria T. and. Cuartero J. 2001. Tomato plant-water uptake and plant-water relationships under saline growth conditions. *Plant science***160 (2):** 265-272.

Song U, Jun H, Waldman B, Roh J, Kim Y, Yi J and Lee EJ. 2013. Functional analyses of nanoparticle toxicity: a comparative study of the effects of TiO_2 and Ag on tomatoes (*Lycopersicon esculentum*). *Ecotoxicol Environ Saf*. **93**:60-7.

Uçgun, K., Ferreira, JFS, Liu, X, da Silva Filho, JB, Suarez DL, Lacerda CFd and Sandhu D. **2020**. Germination and Growth of Spinach under Potassium Deficiency and Irrigation with High-Salinity Water. *Plants* , ***9:*** 1739.

Xingmao M, Geiser-Lee J, Deng Y, Kolmakov A, 2010. Interactions between engineered nanoparticles (ENPs) and plants: phytotoxicity, uptake and accumulation', *Science of the total environment*, **408:** 3053-61.

Yang J, Zheng W, Tian Y, Wu Y, and Zhou D. 2011. Effects of various mixed salt-alkaline stresses on growth, photosynthesis, and photosynthetic pigment concentrations of Medicago ruthenica seedlings. *Photosynthetica***49(2):** 275-284.

Zhang XF, Liu ZG, Shen W, Gurunathan S. 2016. Silver Nanoparticles: Synthesis, Characterization, Properties, Applications, and Therapeutic Approaches. *International Journal of Molecular Sciences*. **17(9):**1534.

JJBS

Volume 16, Number 1,March 2023
ISSN 1995-6673
Pages 7 – 12
https://doi.org/10.54319/jjbs/160102

Jordan Journal of Biological Sciences

An In-Silico Study on Allicin Compound in Garlic (Allium Sativum) as A Potential Inhibitor of Human Epidermal Growth Factor Receptor (Her)-2 Positive Breast Cancer

Ardyarini Dyah Savitri[1], Hanik Badriyah Hidayati[2,*], Lysa Veterini[3], Meidyta Sinantryana Widyaswari[4], Akbar Reza Muhammad[5], Ainiyah Fairus[5], Mohammad Qoimam Bilqisthi Zulfikar[5], Mega Astri[5], Nosa Abdellah Ramasima[5], Dini Putri Anggraeni[5], Reghina Salsabila Ayuantia Nainatika[5], Juliana[6]

[1]Lecturer, Department of Internal Medicine, Faculty of Medicine - Unversitas Nahdlatul Ulama, Surabaya; [2]Lecturer, Department of Neurology, Faculty of Medicine - Unversitas Airlangga, Surabaya; [3]Lecturer, Department of Pathology and Anatomy, Faculty of Medicine - Unversitas Nahdlatul Ulama, Surabaya ;[4]Lecturer, Department Dermatology and Venereology, Faculty of Medicine - Unversitas Nahdlatul Ulama, Surabaya; [5]Medical Student, Faculty of Medicine - Unversitas Nahdlatul Ulama, Surabaya; [6]Medical Student, Faculty of Medicine - Unversitas Airlangga, Surabaya

Abstract

Allicin is the major sulfur-containing compounds in a single garlic (Allium Sativum) that play an important protective part in the oxidative processes. Because of its less toxicity and its potency in preventing and attenuating outcomes of several cancer types, it makes Allicin as a potential natural therapy for breast cancer. Moreover, because of the similar structure of N-Acetylcysteine (NAC) and Allicin, it predicts that Allicin may give the same therapeutic effects with NAC, which NAC is able to show the anti-tumor effect on Human Epidermal Growth Factor Receptor (HER-2) protein of breast cancer. Breast cancer as the most common cancer in women and the second-highest prevalence of cancer in the world, might provide benefits using Allicin in order to prevent cancer progression with a better safety profile. However, little study has been carried out on the functional role of Allicin in HER-2 positive breast cancer. In this study, we calculated and compared the binding energy, pharmacokinetic properties, and toxicity of Allicin and NAC with HER-2 receptor using in-silico study in order to evaluate the potency as HER-2 positive breast cancer alternative therapy. By using Molegro Virtual Docker, the affinity between Allicin and NAC to HER-2 receptor showed an equal result, -62,1239 kcal/mol for Allicin, and -65,8084 kcal/mol for NAC. Meanwhile, study on their pharmacokinetic properties and toxicity using pkCSM online tool showed that Allicin has a safer profile than NAC. Thus, it can be concluded that the Allicin compound has a relatively same anti-tumor potency in HER-2 positive breast cancer compared to NAC. Moreover, Allicin also has a fairly good pharmacokinetic profile and more tolerable toxicity properties, rather than NAC.

Keywords : Allicin, in silico, HER-2 positive breast cancer

1. Introduction

Breast cancer is the most common cancer in women. It is the second-highest prevalence of cancer in the world, which was found in 2.1 million people (11.6%) with 626,679 deaths (6.6%), based on the International Agency for Research on Cancer data in GLOBOCAN (Global Cancer Statistics) in 2018 (Bray *et al.,* 2018). About 1 of 5 women with breast cancer have the Human Epidermal Growth Factor Receptor (HER)-2 protein on the surface of their cancer cells. It is known that HER-2-positive breast cancer has more aggressive tumor phenotypes. Unfortunately potential therapeutics including trastuzumab, lately developed therapeutic resistance which lead to therapeutic failure.

Allicin as the main active compound of single garlic contains quite high sulfur. Some studies revealed that Allicin exhibits not only as an antioxidant but also as antibacterial and anticarcinogenic (Nikolic *et al.,* 2004). Several sulfur-containing antioxidants are known to provide benefits in inhibiting cancer progression, one of which is N-Acetylcysteine (NAC). It is said that NAC has an anti-tumor effect on Human Epidermal Growth Factor Receptor (HER-2) protein of breast cancer (Wang and Xu, 2019; Wimana *et al.,* 2017). Based on this fact, we predict that Allicin has the same potential effect in inhibiting HER-2 positive breast cancer as NAC. Unfortunately, there is still no study about this recently.

This study aimed to compare the potential of Allicin and NAC in inhibiting HER-2 positive breast cancer. In addition to their potency, NAC and Allicin compounds will be tested for their pharmacokinetic properties consisting of absorption, distribution, metabolism, and excretion (ADME) along with the toxicity properties using the pkCSM online tool.

This study began with downloading HER-2 receptor from Protein Data Bank with ID code: 3PP0 and native

* Corresponding author. e-mail: hanikhidayati@fk.unair.ac.id.

ligand 03Q. Prediction using Molegro Virtual Docker was carried out by re-docking between the HER-2 receptor and the native ligand. The docking method is valid if Root Mean Square Deviation (RMSD) is equal to or less than 2 Å. Allicin and NAC were docked alternately to target protein using Molegro Virtual Docker. The results achieved were in the form of Rerank score, which explains the energy required for binding of the compound (ligand) to the receptor. A comparison of scores between Allicin and NAC was carried out, in which a higher Rerank score indicated that the required binding energy between ligand and receptor was greater, which means that the interaction was less stable than the lower score (Kufareva and Abagyan, 2012).

Before the docking process is commenced, it is necessary to check the properties of the ligands using the pkCSM online tool. In addition, Allicin and NAC compounds will also be tested for their pharmacokinetic properties consisting of absorption, distribution, metabolism, and excretion (ADME) along with compounds' toxicity properties using the pkCSM online tool (Pires *et al*., 2015).

2. Materials and Methods

2.1. Tools

This study uses a set of computers with Windows 10 specifications, 64 bit. The programs used in this study are ChemDraw Professional 16.0, Chem 3D 16.0, and Molegro Virtual Docker 5.

2.2. Ligand and Receptor Preparation

Allicin was used as the ligand tested in this study, and its potency will be compared with N-Acetylcysteine (NAC). The structures of Allicin and NAC were downloaded from https://pubchem.ncbi.nlm.nih.gov/. The 2-dimensional structure of both ligands was redrawn using ChemDraw Professional 16.0 and converted to a 3-dimensional structure using Chem3D 16.0. The structure obtained in Chem3D determined the most stable conformation and the minimum energy. Data is stored in the form mol2 {SYBYL2(*.mol2)}.

The receptor used in this study is HER-2 and its 3-dimensional structure obtained from https://www.rcsb.org/structure/3PP0 with ID code: 3PP0. The downloaded results show that HER-2 binds to the native ligand 03Q. Data is saved in PDB format. By using Molegro Virtual Docker 5, cavity detection is carried out on the receptor. The cavity in which there is an active native ligand 03Q is used as a docking location between the receptor and the ligand.

2.3. Molecular Docking and Compound Potential Prediction

The first step that needs to be done in predicting the potential of a compound is to validate the molecular docking method by re-docking between the receptor and the native ligand. It is indicated by the Root Mean Square Deviation (RMSD) value. If the RMSD is equal to or less than 2 Å, then it can be continued with the docking process between the receptor and both ligands (Purnomo, 2013; Nauli, 2014). Prediction of Allicin and NAC potential activity on HER-2 protein is in the form of Rerank score. A lower score indicates that the energy required for ligand and receptor interaction is smaller, so that the bond is more stable, and vice versa.

The amino acid residues was formed and observed in the interaction between the receptor and the ligand. These bond interactions can be in the form of hydrogen bonds, steric interactions, and electrostatics.

2.4. Prediction of Pharmacokinetic and Physicochemical Properties and Compounds' Toxicity

The physicochemical properties of Allicin and NAC were predicted using the pkCSM online tool. These properties include molecular weight (BM), Log P, number of rotating atomic bonds (Torsion), number of hydrogen bond acceptors (HBA), number of hydrogen bond donors (HBD), and Polar Surface Activity (PSA). Compliance to Lipinski's rule consisting of a molecular weight of fewer than 500 Daltons, hydrogen bond donors less than 5, log P value of less than 5, and hydrogen bond acceptor number of less than 10 is required for docking preparation (Lipinski *et al*., 2001).

Prediction of pharmacokinetic parameters and toxicity properties were performed using the pkCSM online tool. Using ChemDraw Professional 16.0 program, the 2-dimensional structure of the Allicin Compound and NAC was drawn. Then it converted into a 3-dimensional structure using Chem3D 16.0 program. The 3-dimensional image was then saved in the form of *.sdf file. The structure obtained was translated into a SMILES structure with the help of the Online SMILES Translator (https://cactus.nci.nih.gov/translate). After that, the compounds were processed with the pkCSM online tool (http://biosig.unimelb.edu.au/pkcsm/prediction) for predicting the pharmacokinetic properties and toxicity tests by inputting the compound's SMILES structure into the program (Pires *et al*., 2015).

3. Results

3.1. Ligand and Receptor Preparation

The 2-dimensional structures of the ligands are shown in Figure 1. The image was converted into 3-dimensional structure using Chem3D 16.0. The results obtained conform to the most stable form with the least energy for optimization of the compound structure. The data obtained is kept in the form mol2 {SYBYL2(*.mol2)}. The results of optimization of both compounds can be seen in Figure 2.

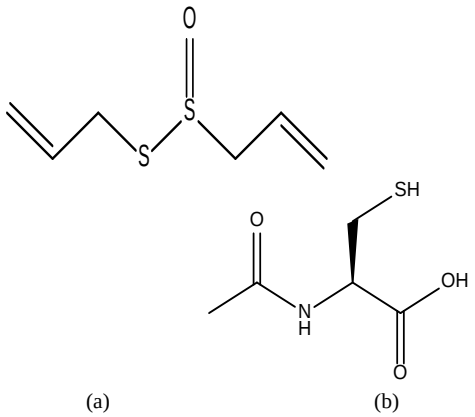

(a) (b)

Figure 1. 2D Structure (a) Allicin; (b) *N-Acetylcysteine* (NAC)

(a) (b)

Figure 2. 3D Structure with Optimization (a) Allicin (b) *N-Acetylcysteine*

The HER-2 protein was downloaded through the Protein Data Bank with ID code: 3PP0, which has 03Q as the native ligand. After downloading the receptor, the cavity was detected using Molegro Virtual Docker. The compound-complex in the cavity is shown in Figure 3.

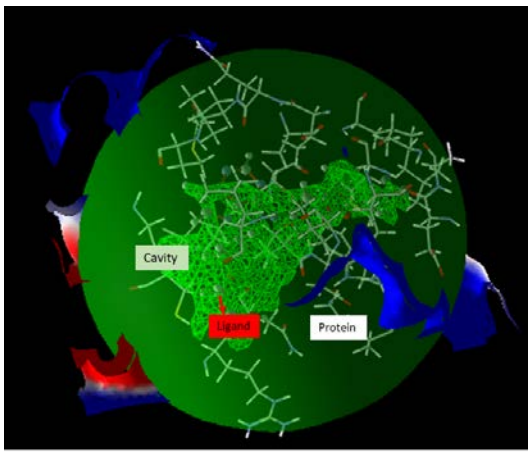

Figure 3. HER-2 complex (3PP0) with native ligand 03Q in the cavity

Before docking process, it is necessary to undergo re-docking process between the receptor and the native ligand in order to know the validation docking method. The re-docking process showed 1,695Å for RMSD result (Lipinski *et al*., 2001). On the other hand, the re-docking process between native ligand 03Q and HER-2 receptor showed quite low energy, with rerank score of -165,051 Kcal/mol. The interaction of the HER-2 receptor with the native ligand 03Q is shown in Figure 4. Figure 6 and Table 1 showed the amino acid residues formed during the interaction, and those are:

1. Hydrogen bond: Asp863, Thr862, Met801, Ser728
2. Steric bond: Asp863, Met774, Met801, Ala751

Since molecular docking has shown valid results, docking was then carried out between the receptor with the test and comparison ligands. The interaction between HER-2 receptor and the Allicin and NAC ligands is shown in Figures 5(a) and 5(b).

1. Interaction between HER-2 receptor and Allicin

The prediction of the required binding energy in the interaction between the HER-2 receptor and the Allicin is shown in Table 2. It is predicted that the affinity between Allicin and HER-2 receptor is -62.1239 Kcal/mol. The amino acid residues formed during the interaction process between Allicin and the receptor are shown in Figure 6 and Table 1, and the residues are Thr798 and Ser783 for hydrogen bond and Leu785 for steric bond.

2. Interaction between HER-2 receptor and NAC

The prediction of the required binding energy in the interaction between the HER-2 receptor and the NAC is shown in Table 2. It is predicted that the affinity between NAC and HER-2 receptor is -65.8084 Kcal/mol. The amino acid residues formed during the interaction process between NAC and the receptor are shown in Figure 6 and Table 1, and the residues are hydrogen bonds only and those are Asp863, Thr862, Thr798, and Ser783.

Table 1. Amino Acid Residues formed in the interaction between the HER-2. Receptor and the Ligand

Ligand	Hydrogen Bond	Steric Bond	Electrostatic Bond
03Q	Asp863, Thr862, Met801, Ser728	Asp863, Met774, Met801, Ala751	-
Allicin	Thr798, Ser783	Leu785	-
NAC	Asp863, Thr862, Thr798, Ser783	-	-

Table 2. Prediction of bond energy between receptor and ligand lig

Ligand	***Rerank score***
03Q	-165,051
Allicin	-62,1239
NAC	-65,8084

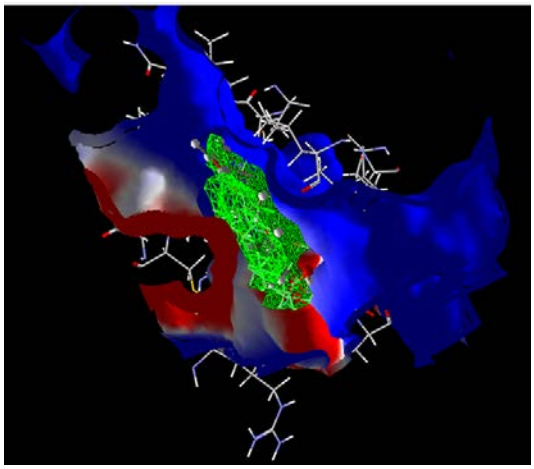

Figure 4. HER-2 Receptor Interaction with native ligand 03Q

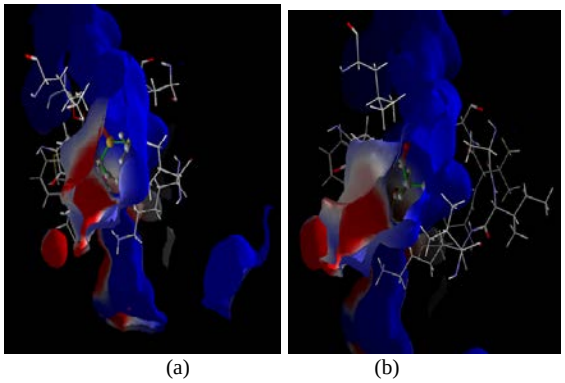

(a) (b)

Figure 5. HER-2 Receptor Interaction with ligand (a) Allicin (b) NAC

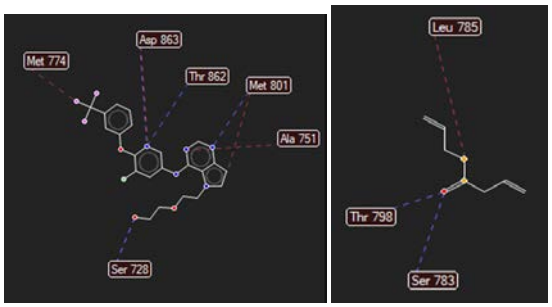

(a) (b)

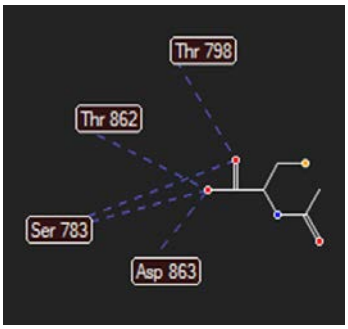

(c)

Figure 6. Receptor Interaction with Ligand and Amino Acid Residue formed (a) 03Q (b) Allicin (c) NAC

3.2. Prediction of Pharmacokinetic, Physicochemical, and Toxicity of Compounds

1. Allicin

Compliance with Lipinski's rule for Allicin was shown in Table 3. The analysis shows that Allicin has low molecular weight, hydrogen bond donors less than 5, log P value of less than 5, and hydrogen bond acceptor number of less than 10.

Prediction of pharmacokinetic properties and toxicity of Allicin is shown in Table 4. The intestinal absorption of Allicin is 96,299% and the skin permeability is -1,877 log Kp. The volume distribution of Allicin is -0,045 log L/kg, and its blood-brain barrier penetration properties are 0,506 logBB. Allicin is also neither a substrate nor inhibitor of CYP3A4.

The ability of Allicin to be excreted from the body, either through the liver or kidneys, was shown by the total the clearance of Allicin, which is 0,714 log ml/min/ kg. According to the results, Allicin is not renal Organic Cation Transporter (OCT)-2.

Table 3. Prediction test results of physicochemical properties of Allicin and NAC. compounds

	Allicin	**NAC**
BM	162,279	163,198
Log P	1,7553	-0,4945
Torsion	5	3
HBA	2	3
HBD	0	3
PSA (A^2)	62,082	64,021

BM = Molecular Weight; Log P = Octanol logarithm / water partition coefficient; HBD = hydrogen bond donor; PSA = Polar Surface Area; HBA = hydrogen bond acceptor

Another safety profile that must be considered is the mutagenic ability of the drug candidate. This can be seen from the AMES toxicity test (Mortelmans and Zeiger, 2000). Table 4 shows that Allicin is not mutagenic.

The safety of drug administration in experimental animals is known from the LD50. LD50 is the dose given to animals that produce 50% of animal death in the population within a certain time (Chan *et al*., 1989). Table 4 shows that the LD50 of Allicin is 2.366 mol/kg

Table 4. Pharmacokinetic prediction test results (ADME) of Allicin and NAC

ADME & Toxicity	**Allicin**	**NAC**
Intestinal Absorption (human) (%)	96,229	77,922
VDss (human) (log L/kg)	-0,045	-1,355
Skin Permeability (log Kp)	-1,877	-2,735
Blood Brain Barrier Permeabelity (log BB)	0,506	-0,355
CYP3A4 subtrate (Yes/ No)	No	No
CYP3A4 inhibitor (Yes/ No)	No	No
Renal OCT2 substrate (Yes/ No)	No	No
Total Clearance (log ml/ min/ kg)	0,714	0,309
AMES Toxicity (Yes/ No)	No	Yes
LD50 (mol/ kg)	2,366	1,626

VDSS = Volume Distribution *Steady State*; CYP3A4 = Cytochrome P3A4; Renal OCT2 = Renal *Organic Cation Transporter* 2

2. N-Acetyl Cysteine (NAC)

As with Allicin, NAC shows good compliance with Lipinski's rule. As shown in Table 3, NAC has low molecular weight, hydrogen bond donors less than 5, log P value of less than 5, and hydrogen bond acceptor number of less than 10.

Prediction of pharmacokinetic properties and toxicity of NAC is shown in Table 4. Intestinal absorbtion of NAC is 77,992%, and the skin permeability is -2,735 log Kp. Volume distribution of NAC is -1,355 log L/kg and the blood-brain barrier penetration properties is -0,355 logBB. NAC is also neither a substrate nor inhibitor of CYP3A4.

The total clearance of NAC is 0,309 log ml/min/ kg. According to the results, NAC is not renal Organic Cation Transporter (OCT)-2.

The mutagenic ability of NAC from AMES toxicity test shows positive results, which means NAC is a mutagenic drug (Mortelmans and Zeiger, 2000).

The safety of drug administration in experimental animals for NAC is 1,626 mol/kg as shown in Table 4.

4. Discussion

HER-2 positive type breast cancer is a quite aggressive breast cancer type. Strong positive HER-2 expression also indicates a high risk of breast cancer relapse. HER-2 itself is a transmembrane protein encoded by the gene c-ERBB-(Her-/neu) located on chromosome 17 and it is an ideal target for targeted therapy in breast cancer (Ferrero *et al.*, 2000).

Because of the same sulfur-containing structure, in this research, we used Allicin as the test ligand, and NAC as the comparison ligand to be docked to the HER-2 receptor. Both chemical structures are shown in Figures 1 and 2.

The predictive physicochemical properties test in Table 3 shows that both ligands meet Lipinski's rules. It means that both of them have met the criteria of drug-likeness and both ligands have high permeability properties and are easily absorbed by the body (Purnomo, 2013).

The result of re-docking process between native ligand 03Q and HER-2 receptor showed the lowest energy, with rerank score of -165,051 Kcal/mol. On the other hand, Allicin showed the highest energy (-62.1239 Kcal/mol). It is shown in Table 2. The result obtained by Allicin is less stable than other ligands. However, the energy required for the bond between Allicin and NAC on HER-2 is not significantly different.

In the ligand and receptor interaction, amino acid residues are formed, both in hydrogen bonds, steric and electrostatic interactions. This is as shown in Figure 6 and Table 1, which there are similarities in the amino acid residues formed in the hydrogen bonds of native ligand and NAC, namely Asp863 and Thr862. However, there was no similarity of amino acid residues formed between Allicin and the other two ligands. This indicates that NAC has more similar activity with the native ligand on the HER-2 receptor, compared to Allicin (Cosconati *et al.*, 2010).

The pharmacokinetic properties and toxicity of the two ligands are shown in Table 4. From these results, it can be concluded that Allicin has better intestinal absorption (96.2%) compared to NAC (77.9%). However, both compounds are generally well absorbed. A compound is said to have good intestinal absorption if its absorption ability reaches > 80%, and bad if its ability is < 30% (Chander *et al.*, 2017).

For absorption through the skin, Table 4 above shows that Allicin has lower skin permeability than NAC, where the log Kp value of Allicin is -1.877 and NAC is -2.735. This is following what was stated by Pires et al (2015), that the drug has low skin absorption if the log Kp value is > -2.5 (Pires *et al.*, 2015).

Drug distribution throughout the body is needed to increase the drug's effectiveness. This is expressed from VDss value, where a higher value of VDss means there is more drug distributed into the network. A compound is said to have a low VDss if the value is <-0.15 and high if it > 0.45 (Tedjamartono *et al.*, 2020). The results in Table 4 above show that Allicin has a better volume of distribution than NAC, where the Allicin VDss reaches -0.045, while NAC is -1,355.

Breast cancer with HER-2 overexpression is a very aggressive cancer type with a higher risk for brain metastases (Zhou, 2008). Therefore, the most ideal HER-2 positive breast cancer drug is one that can penetrate the blood-brain barrier. According to Pires et al. (2015), a drug is said to have good penetration inside the brain if the log BB value reaches > 0.3. On the contrary, it would have poor brain penetration if the BB log value reaches < -1 (Pires *et al.*, 2015). From Table 4 above, it can be concluded that both compounds have good blood-brain barrier penetration properties, but Allicin has a higher ability to penetrate the blood-brain barrier than NAC.

Drug metabolism process needs Cytochrome P450 (CYP450) super enzymes. CYP450 enzymes are essential for the metabolism of many medicines and endogenous compounds. There are seventeen CYP families recognized in humans, including CYP3A4 as the most abundant and important subfamily of the CYP isoforms in the liver. It contributes to bile acid detoxification, the termination of action of steroid hormones, and elimination of phytochemicals in food and the majority of medicines (Šrejber *et al.*, 2018). Drugs that can inhibit this enzyme are called CYP3A4 inhibitors. On the contrary, drugs that can induce cytochrome P450 are referred to as CYP3A4 substrates. Drugs that inhibit CYP3A4 will result in decreased drug metabolism and increased drug levels in the blood. However, drugs that can induce this enzyme will result in increased drug metabolism and consequently decrease the drug levels in the blood (Aslam *et al.*, 2003). Table 4 shows that both Allicin and NAC are neither inducers nor inhibitors CYP3A4, so they are safe when they were given together with other drugs that affect this enzyme activity.

Total clearance indicates the ability of the drug to be excreted from the body, either through the liver or kidneys (Belzer *et al.*, 2013). Table 4 shows that the clearance of Allicin is slower than that of NAC, so Allicin stays in the body longer than NAC.

Organic Cation Transporter (OCT)-2 is a transporter in the kidney that functions to increase drug uptake from the blood, then passes through the basal membrane of kidney, reaches the proximal tubular cells, and waste from the body. OCT-2 substrate has the capability to cause side effects when given along with OCT2 inhibitor (Zhou,2008). According to predictive pharmacokinetic properties, it was found that both Allicin and NAC are not

renal OCT2 substrates, so they are safe when given together with OCT2 inhibitors.

Another safety profile that must be considered is the mutagenic ability of the drug. This can be seen from the AMES toxicity test (Mortelmans and Zeiger, 2000). Table 4 shows that Allicin is not mutagenic, while NAC is mutagenic.

The safety of drug administration in experimental animals is known from the LD50. LD50 is the dose given to animals that produce 50% of animal death in the population within a certain time (Chan *et al.*, 1989). Table 4 shows that the LD50 of Allicin is 2.366 mol/kg and NAC is 1.626 mol/kg. Thus, Allicin has a higher safe dose limit than NAC.

5. Conclusion

In-silico study showed that the Allicin compound of single garlic (Allium Sativum) relatively has the same ability to NAC as an anti-tumor in HER-2 positive breast cancer. Moreover, Allicin also has a fairly good pharmacokinetic profile, such as intestinal absorption, volume distribution, the ability to penetrate blood brain barrier, and the safety of combining drugs, especially drugs that affect CYP3A4 activity or when it is given together with OCT2 inhibitor drugs. Moreover, Allicin stays longer in the human body, with no mutagenic effect and lesser animal death in experimental studies. Nevertheless, in vitro and in vivo studies should be conducted to ensure the results of this study.

Funding Acknowledgements

The author(s) received no financial support for the research, authorship, and/or publication of this article.

References

Aslam M, Tan CK, and Prayitno A. 2003. **Farmasi Klinis (Clinical Pharmacy) Menuju Pengobatan Rasional Dan Penghargaan Pilihan Pasien**. Elex Media Komputindo, Jakarta.

Belzer M, Morales M, Jagadish B, Mash E, and Wright S. 2013. Substrate-Dependent Ligand Inhibition of the Human Organic Cation Transporter OCT2. *J Pharmacol Exp Ther*., **346(2)**: 300-310.

Bray F, Ferlay J, Soerjomataram I, Siegel RL, Torre LA and Jemal A. 2018. Global Cancer Statistics 2018: GLOBOCAN estimates of Incidence and Mortality Worldwide for 36 Cancers in 185 Countries. *CA Cancer J Clin*., **68(6)**: 394- 424.

Chan PK and Hayes AW. 1989. **Principles and Methods of Acute Toxicity and Eye Irritancy**. In: Hayes AW (Eds), Principles and Methods of Toxicology. Raven Press, New York.

Chander S, Tang CR, Al-Maqtari HM, Jamalis J, Penta A, Hadda TB, Sirat HM, Zheng YT, and Sankaranarayanan M. 2017. Synthesis and study of anti-HIV- 1 RT activity of 5-benzoyl-4-methyl-1,3,4,5-tetrahydro-2h-1,5-benzodiazepin-2-one derivatives. *Bioorg Chem*., **72**: 74-79.

Cosconati S, Forli S, Perryman A, Harris R, Goodsell D, and Olson A. 2010. Virtual screening with AutoDock: theory and practice. *Expert Opin Drug Discov*., **5(6)**: 597-607.

Ferrero-Pous M, Hacene K, Bouchet C, Le Doussal V, Tubiana-Hulin M, and Spyratos F. 2000. Relationship between c-erbB2/HER2 and other tumor Characteristics in Breast Cancer Prognosis. *Clin Cancer Res.*, **6(12)**: 4745–4754.

Kufareva I and Abagyan R. 2012. Methods of protein structure comparison. *Methods Mol Biol*., **857**: 231–257.

Lipinski CA, Lombardo F, Dominy BW, and Feeney PJ. 2001. Experimental and computational approaches to estimate solubility and permeability in drug discovery and development settings. *Adv Drug Deliv Rev*., **46(1-3)**: 3-26.

Mortelmans K and Zeiger E. 2000. The Ames Salmonella/microsome mutagenicity assay. *Mutat Res-Fund Mol M.*, **455(1-2)**: 29-60.

Nauli T. 2014. Penentuan sisi aktif Selulase Aspegillus Niger dengan Docking Ligand. *J Kim Terap Indones*, **16(2)**: 94-100.

Nikolic V, Stankovic M, Nikolic Lj and Cvetkovic D. 2004. Mechanism and kinetics of synthesis of allicin. *Pharmazie.*, **59(1)**: 10–14.

Pires D, Blundell T, and Ascher D. 2015. pkCSM: Predicting Small-Molecule Pharmacokinetic and Toxicity Properties Using Graph-Based Signatures. *J Med Chem.*, **58(9)**: 4066-4072.

Purnomo H. 2013. **Kimia Komputasi Uji In Silico Senyawa Anti Kanker**. Pustaka Pelajar, Yogyakarta.

Šrejber M, Navrátilová V, Paloncýová M, Bazgier V, Berka K, Anzenbacher P, and Otyepka M. 2018. Membrane-attached mammalian cytochromes P450: an overview of the membrane's efects on structure, drug binding, and interactions with redox partners. *J Inorg Biochem*., **183**:117–136.

Tedjamartono TD, Sudarsa IW, Winata A and Wetan NGAAMY. 2020. Overekspresi Her-2 Sebagai Faktor Risiko Terjadinya Metastasis Otak Pada Pasien Kanker Payudara. *E-J Medika Udayana*., **9(9)**: 58-64.

Wang J, and Xu B. 2019. Targeted therapeutic options and future perspectives for HER2-positive breast cancer. *Sig Transduct Target Ther*., **4**:34.

Wimana Z, Gebhart G, Guiot T, Vanderlinden B, Larsimont D, and Doumont G, Van Simaeys G, Goldman S, Flamen P and Ghanem G. 2017. N-Acetylcysteine breaks resistance to trastuzumab caused by MUC4 overexpression in human HER2 positive BC-bearing nude mice monitored by 89Zr-Trastuzumab and 18F-FDG PET imaging. *Oncotarget*., **8(34)**: 56185-56198.

Zhou S. 2008. Potential Strategies for Minimizing Mechanism-Based Inhibition of Cytochrome P450 3A4. *Curr Pharm Des.*, **14(10)**: 990-1000.

JJBS

Volume 16, Number 1,March 2023
ISSN 1995-6673
Pages 13 – 20
https://doi.org/10.54319/jjbs/160103

Jordan Journal of Biological Sciences

Oxidative and Histological Effects of Herbicide Glufosinate-Ammonium and Cyanobacteria Extracted Anatoxin-a on Land Snails *Monacha cartusiana*

Radwa M. Said[1], Asmaa H. Al-Badwy[2,*], Aya A. Mohamed[1]

[1]*Zoology Department, Faculty of Science, Zagazig University, Zagazig 44519, Egypt;*[2]*Plant Biotechnology Laboratory (PBL), Botany and Microbiology Department, Faculty of Science, Zagazig University, El-Gamaa Street 1, 44519 Zagazig- Sharkia- Egypt.*

Received: March 22, 2022; Revised: May 26, 2022; Accepted: June 6, 2022

Abstract

Pesticides are widely used in a variety of applications, resulting in significant discharge into the terrestrial environment. Hence, the present study was performed to evaluate the effect of two pesticides (Glufosinate-ammonium and Anatoxin- a) on biochemical parameters, oxidative stress, nuclear factor kappa B (NF-KB) activity, and histopathology of the digestive gland of the land snail *Monacha cartusiana*, which is often employed as a bioindicator of terrestrial pollution. There are no further studies on the effect of *Anabaena flos-aquae* extract on land snails. The results showed that LC_{50} of Glufosinate-ammonium and Anatoxin-a after exposure to land snail *Monacha cartusiana* for 96 hrs were 66.6 and 5.3 mg L^{-1}, respectively. LC_{50} values reveal the potential activity of Anatoxin-a than Glufosinate-ammonium against the tested snails. Within four days of exposure to glufosinate-ammonium, there were no deaths among treated snails. After the second day of exposure to Anatoxin-a, mortality percentages appeared and gradually rose with increasing concentrations and exposure time. After 28 days of exposure to LC_{25} of tested pesticides, AST, ALT, ALP, MDA, CAT, GPX, and GST levels increased while TAC levels were decreased. NF-KB immunopositivity was much more severe in the cells of tested snails treated with Anatoxin-a than Glufosinate-ammonium. Histopathological examination of the digestive gland showed that sublethal concentration of Glufosinate-ammonium produced excessive secretion and vacuolation. Anatoxin-a induced severe cellular damage in digestive tubules. In conclusion, two pesticides caused alterations in oxidative stress, NF-KB activity, and histological nature of *M. Cartusiana* that confirmed the toxicity of both pesticides for the living species in the terrestrial environment.

Keywords: *Monacha cartusiana*; Glufosinate-ammonium; Anatoxin-a; Oxidative stress; NF-KB activity; Histopathological changes.

1. Introduction

Environmental contamination is a recurring issue as well as an undesirable byproduct of human activity (Desouky *et al.,* 2013). An increasing human population necessitates increased agricultural productivity, which may need the usage of industrially generated chemicals, such as pesticides. These compounds are beneficial in certain ways, but they frequently have negative effects on the environment and, as a result, endanger human health (Stara *et al.,* 2018). Pesticides are undeniably a source of public concern due to their propensity for movement from one environmental compartment to another, as well as their effects on non-target biota. In Egypt, the widespread usage of pesticides in agricultural areas is commonplace. The application of these contaminants may cause hazards to non-target organisms (Klassen, 1986).

Herbicides, which are used to control weeds, comprise a diverse group of chemical products. One of the most often utilized herbicides in natural areas is Glufosinate-ammonium. Due to its high crop safety, ability to inhibit the synthesis of amino acids required for protein formation in vulnerable plants, and potential to be rapidly degraded in the soil, Glufosinate-ammonium is a highly effective herbicide used to control weeds **(**Hack *et al*., 1994; David *et al*., 2010).

The most studied classes of cyanotoxins are microcystins, nodularin, saxitoxins, cylindrospermopsin, and anatoxins. The literature on their environmental prevalence, biosynthesis, characteristics, and health importance evaluated was published after 2000 (Svircev *et al*., 2019). Cyanobacterial neurotoxins are divided into three classes (anatoxin-a, homoanatoxin, and saxitoxins) based on their structure: alkaloids. Neurotoxicity mechanism includes: anti acetylcholinesterase activity, anti-phosphatase activity, postsynaptic cholinergic agonist action (Metcalf and Codd, 2004), and protein kinase C activators are some of the mechanisms of neurotoxicity (Fujiki *et al*., 1990). Moreover, Cyanotoxins like organophosphorus insecticides cause toxicity by irreversibly inhibiting acetylcholinesterases (Metcalf and Bruno, 2017). Anatoxin-a is derived from cyanobacteria *Anabaena flos-aquae* and may play an important role in insect control (Saber *et al*., 2018). In addition to toxigenic cyanobacteria or particular cyanotoxins, there are some indications of relevant exposure to environmental health problems in animal poisoning occurrence (Krienitz *et al*., 2005). Anatoxin-a showed promising larvicidal

* Corresponding author. e-mail: bio_asmaa88@yahoo.com.

activity against some insects such as mosquitoes (Costa *et al*., 2019).

Terrestrial snails are helpful models for assessing the risk of metals and pesticides in soil (Scheifler *et al*., 2003; Laguerre *et al*., 2009). They may be exposed to three sources of pollution: soil, plants, and air. Land snails are a suitable model organism for ecotoxicological investigations of pollutant-induced alterations and are frequently utilized as a bioindicator of soil contamination because they can accumulate and respond to both organic and inorganic substances of various origins at the organism and cellular levels (Regoli *et al*., 2005). *Monacha cartusiana* (Phylum: Mollusca, Class: Gastropoda, Muller 1774) is a land snail found throughout a wide geographical range in the Mediterranean and Southeastern Europe (Pieńkowska *et al*., 2019). In Egypt, *M. cartusiana* snails infest various economic crops with a high occurrence and population density (Lokma, 2013).

Glufosinate-ammonium and Anatoxin-a in animal tissues have been studied in only a few research studies. Therefore, the goal of the current study was to scrutinize the impacts of Glufosinate-ammonium and Anatoxin-a on the biochemical parameters, oxidative stress, NF-KB activity, and histopathology of the digestive gland of the land snail *M. cartusiana* and to censoriously assess its utility as a bioindicator for Glufosinate-ammonium and Anatoxin-a toxicity in the terrestrial environment.

2. Materials and Methods

2.1. Chemicals

Glufosinate ammonium was obtained from Sigma-Aldrich (Germany). Different concentrations of Glufosinate ammonium ($C_5H_{15}N_2O_4P$) were freshly-prepared daily. It is a liquid form with the commercial name ‘‘Basta’’. Percentage of Glufosinate ammonium equals 40% w/v, and inert ingredients equal 60 %w/v. One liter of Glufosinate ammonium equals 400 g of active ingredient (400 g/l). The stock solution was prepared by adding 2.5 ml (=1 gram) of Glufosinate ammonium and was completed to1L by adding distilled water to give following concentrations (30, 60, 90 and 120 $mg.L^{-1}$)

2.2. Preparation of Cyanobacterial extract

The alga *Anabaena flos-aquae* was obtained from Prof. Dr. Yassin El-ayouty at Zagazig University's Phycology Lab. *Anabaena flos-aquae* was grown on BG-11 medium (Stanier *et al.,* 1971). The algal culture was maintained at 25°C ± 2°C, under white fluorescent illumination of 120 $\mu Em^{-2}s^{-1}$ provided by fluorescent tubes. The culture was aerated with air current and subjected to photoperiod of light: dark (16:8hrs). A pH meter was used to adjust the pH of the medium to 7.4 using 0.1N HCl and NaOH. At the mid-logarithmic phase, algal cells were harvested by centrifugation at 10,000 rpm (4°C) for 15 minutes using Multi-tube under cooling centrifuge (Vision SCIENTIFIC CO., LTD., South Korea), washed three times with sterile distilled water, and air-dried. Anatoxin-a was extracted from *Anabaena flos-aquae* using the modified method (Harada *et al.,* 1993).

Approximately 10 grams of dried algal cells were extensively grounded in 5 ml methanol and 50 mM acetic acid, agitated for 24 hours at 150 rpm in dark, and the supernatant was collected by centrifuging at 8000 rpm. The extraction was carried out three times. The solution's pH was raised to 7.7 by adding 7% ammonium hydroxide. The extract was dried on a vacuum evaporator and recorded as the yield of crude extract. The sample was dissolved in water to finally achieve stock concentration of 2 $g.L^{-1}$ and stored in darkness at 4°C. Extraction with 50 mM acetic acid–methanol was determined to be the most successful since it yielded better recovery and allowed less pigment to be extracted from cell pellets (Harada *et al.,* 1989). The sample was determined using a T80, UV/VIS Spectrophotometer within the wavelength range of 200-400 nm. The extract had a single absorption peak at 225 nm (Figure 1) which may give indication for the presence of *Anabaena* toxin. A single absorption peak of anatoxin-a at 225 nm was confirmed by AL-Sultan and Aubaed (2017) and Gugger *et al.* (2005).

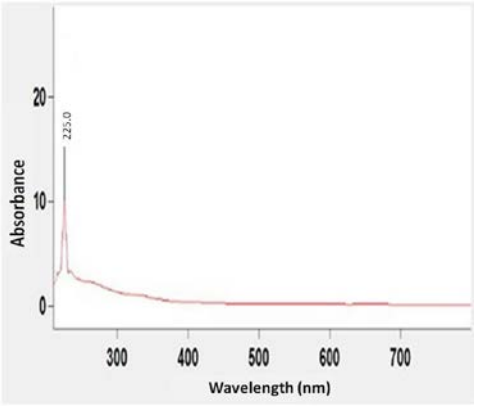

Figure 1. Ultraviolet spectrum of *Anabaena* extract

2.3. Collection and acclimatization of snails

Adult *M. cartusiana* snails (Muller, 1774) (8 ± 0.4 mm lengths, 10.3 ± 0.6 mm width, and 1.6 ± 0.1 g weights) were gathered by hand from fields cultured with Egyptian clover at Alashraf village, Zagazig District, Sharkia Governorate, Egypt, during September 2020. The gathered snails were taken to the laboratory and maintained in glass boxes (40 x 30 x 30 cm) filled with moist soil of about 10 cm height and covered with a nylon-mesh covering. They nourished on fresh lettuce leaves every day for a week. The tested snails were housed at 22°C± 3°C and a humidity of 80-90%**.**

2.4. Toxicity test and Experimental design

The tested snails were categorized into three groups. The first group is the control group (n=10), whereas the second group was divided into two subgroups (each subgroup is pooled of 40 snails, 10 snails for each concentration of two pesticides) the first subgroup treated with four concentrations of Anatoxin-a (2, 4, 6, 8 mg/l) and the 2nd subgroup exposed to Glufosinate-ammonium concentrations (30, 60, 90, 120 mg/l) for five days for the toxicity test. The toxicity test occurred using the poisonous bait technique. Each concentration was combined with 5 grams of sugarcane syrup. The mixture was then completed with wheat bran to 100 grams and humidified with little quantities of water. The LC_{50} was calculated using three replicates per concentration. Tested snails were investigated by a stainless steel needle (WHO, 1965), and mortality percentages were counted after 24, 48, 72 and 96 days treatments. The third group was fed baits comprising LC_{25} of the used pesticides for 28 days for biochemical,

oxidative stress, immune-histochemical and histological investigations. The ethical guidelines for animal experiments stated in the Declaration of Helsinki were followed, approval number 55.

2.5. Biochemical and oxidative stress biomarkers

Snail shell was detached, and the foot muscle was isolated under ice (4^0C). 0.5gm of the digestive gland of unexposed and LC_{25}-exposed snails for 28 days were dissected out and homogenized in 10mL of ice-cold 0.05M Phosphate buffer saline. The homogenates were centrifuged at 8000 rpm at 5 °C, and the supernatants were kept at - 80 °C. Alanine aminotransferase (ALT) and Aspartate aminotransferase (AST) were analyzed according to Breuer (1996). Assay of alkaline phosphatase (ALP) was carried out according to Moss (1982). Malondialdehyde (MDA), total antioxidant capacity (TAC), Catalase (CAT), Glutathione peroxidase (GPX), and glutathione s-transferase (GST) were analyzed according to the corresponding assay kit protocol (Sat 450, AMS, Italy).

2.6. Immunohistochemical studies

Paraffin sections (5 µ) were mounted on positively charged glass slides (Biogenex, USA). The slides were placed in an open plastic container with enough antigen retrieval solution to completely cover them (Citrate buffer solution, pH 6). Slides were put in a microwave oven (Samsung 800 Watts) at power 10 for 5 minutes. The slides were then washed several times in deionized water before being immersed in PBS for 5 minutes. Endogenous peroxidase blocking reagent comprising hydrogen peroxide and sodium azide was used to incubate tissue sections (DAKO peroxidase blocking reagent, Cat. No. S 2001). Except for the tissue portion, the excess buffer was blotted off and the slides were dried. The sections were then treated with one to two drops of a supersensitive primary monoclonal antibody [against Nuclear Factor Kappa B (NF-B)]. For 60 minutes, slides were incubated horizontally in a humid chamber at room temperature. The slides were washed for 5 minutes after the excess reagent was thrown away. In two successive phosphates buffer saline jars (PBS). 1-2 drops of the ready-to-use DAKO EnVision + system were applied for 20 minutes at room temperature after blotting excess buffer. The sections were rinsed with PBS as before and blotted. DAB (diaminobenzidine) was used as a chromogen and counterstained with Mayer's hematoxylin. NFkB immunoreactivity was evaluated under light microscopy in terms of severity (Eissa and Shoman, 1998).

2.7. Histological examinations

Both control and treated digestive glands of the snail were dissected out and fixed in Formalin. Specimens were dehydrated in ascending series of ethanol concentrations, and then cleaned in Xylene for 20 minutes before being embedded in paraffin wax. Sections (4–5 m thick) were cut, mounted, and stained with Eosin and Hematoxylin.

2.8. Statistical analysis

All results were executed using SPSS version 20 (SPSS, Richmond, VA, USA). One-way ANOVA followed by Duncan's multiple range tests as a post-hoc test was used to compare the significant differences among treatments at $P < 0.05$. Probit analysis was used to determine LC_{50} by the graphic way of the curve dose-effect according to Finney (1971).

3. Results

3.1. Toxicity test

Table 1 showed that glufosinate-ammonium exposure resulted in no deaths among exposed snails within four days. After the second day of Anatoxin-a exposure, mortality percentages occurred. With increasing concentrations of tested pesticides and exposure periods, mortality percentages increased. The LC_{50} values of Anatoxin-a and Glufosinate-ammonium were 5.3 and 66.6 mg/l, respectively, whereas LC_{25} were 1.33 and 16.65 mg/l, respectively. Anatoxin-a had a toxicity index of 100%, whereas Glufosinate-ammonium had a toxicity index of 7.9% (Table 2).

Table 1. Effect of different concentrations of Glufosinate-ammonium and Anatoxin- a on mortality percentages of *M. cartusiana* at different exposure periods.

Tested pesticides	Time / Conc.	Percentage mortality (%)			
		24 hr.	48 hr.	72 hr.	96 hr.
Glufosinate-ammonium ($mg.L^{-1}$)	30	0±0.00	0±0.00	0±0.00	0±0.00
	60	20±5.8	20±5.8	26.7±3.3	40±0.00
	90	56.7±3.3	70±0.00	70±0.00	76.7±3.3
	120	66.7±3.3	86.7±3.3	100±0.00	100±0.00
Anatoxin- a ($mg.L^{-1}$)	4	0±0.00	23.3±3.3	30±0.00	36.7±3.3
	6	40±0.00	46.7±6.7	46.7±6.7	50±0.00
	8	50±0.00	63.3±3.3	66.7±3.3	70±0.00
	10	83.3±3.3	100±0.00	100±0.00	100±0.00

- Data are represented as means of samples ±SE. Concentration (Conc.)

Table 2. Lethal toxicity values, sublethal concentrations, and toxicity index of Glufosinate ammonium and Anatoxin-a against *M. cartusiana* under laboratory conditions.

Tested pesticide	LC_{50} ($mg.L^{-1}$)	LC_{25} ($mg.L^{-1}$)	Toxicity index (%)	Slope
Glufosinate-ammonium	66.6	16.65	7.9	7.81±0.73
Anatoxin-a	5.3	1.33	100	4.54±0.49

3.2. Biochemical biomarker in clover snail M. cartusiana exposed to LC_{25} of two tested pesticides.

Table 3 shows that after 28 days of exposure, ALT, AST, and ALP levels in clover snails treated with Glufosinate-ammonium were significantly increased ($P < 0.05$) by 20.7%, 19.7%, and 144.5% while the exposure of clover snails to Anatoxin-a caused a significant increase by 56.9%, 91.2%, and 192.6% as compared with the control groups.

Table 3. Physiological parameters of *M. cartusiana* treated with LC_{25} of Glufosinate-ammonium and Anatoxin-a for 28 days.

Pesticides	ALT (U/l)	AST (U/l)	ALP (U/L)
Control	23.2 ± 0.6^{a}	28.4 ± 0.50^{a}	136.0 ± 6.0^{a}
Glufosinate-ammonium	28.0 ± 0.9^{b}	34.0 ± 0.95^{b}	332.5 ± 2.5^{b}
Anatoxin-a	36.4 ± 0.55^{c}	54.3 ± 1.25^{c}	398 ± 20^{c}
F-value	91.44	200.18	126.11
P-value	0.002	0.001	0.001

Each value is mean of 3 samples ± SE -Means with different alphabetical superscripts at each column among tested pesticides are significantly different at $P < 0.05$ (one way ANOVA and subsequent post hoc multiple comparisons with Duncan's Multiple Range Test).

3.3. Oxidative stress and antioxidant biomarkers in clover snail M. cartusiana exposed to LC25 of two tested pesticides.

Table 4 shows that after 28 days of exposure, MDA, CAT, GPx and GST levels in clover snails treated with Glufosinate-ammonium were significantly increased ($P<0.05$) by 32.3%, 77.1% ,14.5% and 49.4% while the exposure of clover snails to Anatoxin-a caused a significant increase by 310.1%, 95.8%, 78.9% and 182.4% compared by the control groups. TAC levels in clover snails treated with Glufosinate-ammonium were significantly decreased ($P<0.05$) by -23.5 % while the exposure of clover snails to Anatoxin-a caused a significant decrease by -80.9% compared by the control groups**.**

Table 4. Oxidative stress and antioxidant biomarkers of *M. cartusiana* treated with LC_{25} of tested pesticides for 28 days.

Pesticides	MDA (nmol)	TAC (µmol/l)	CAT (U/g)	GPX (U/g)	GST(U/g)
Control	14.4 ± 1.2^{a}	2.30 ± 0.34^{a}	0.48 ± 0.02^{a}	0.76 ± 0.04^{b}	1.76 ± 0.35^{a}
Glufosinate-ammonium	19.1 ± 2.1^{a}	1.76 ± 0.22^{b}	0.85 ± 0.11^{b}	0.87 ± 0.03^{b}	2.63 ± 0.67^{a}
Anatoxin-a	59.05 ± 9.55^{b}	0.44 ± 0.11^{b}	0.94 ± 0.05^{b}	1.36 ± 0.16^{b}	4.97 ± 0.93^{b}
F-value	18.61	16.63	27.42	10.86	14.16
P-value	0.02	0.02	0.01	0.04	0.03

Each value is mean of 3 samples ± SE -Means with different alphabetical superscripts at each column among tested pesticides are significantly different at $P < 0.05$ (one way ANOVA and subsequent post hoc multiple comparisons with Duncan's Multiple Range Test).

3.4. NF-kB immunoreactivity

NF-kB immunopositivity was observed in the digestive gland cells of clover snail *M. cartusiana*. NF-kB positivity was detected in the perinuclear areas of cells of digestive tubules (Plate 1 B, C, and D) of exposed snails compared to the control groups (plate 1 A). Immunopositivity was much more severe in snails treated with Anatoxin-a than Glufosinate-ammonium.

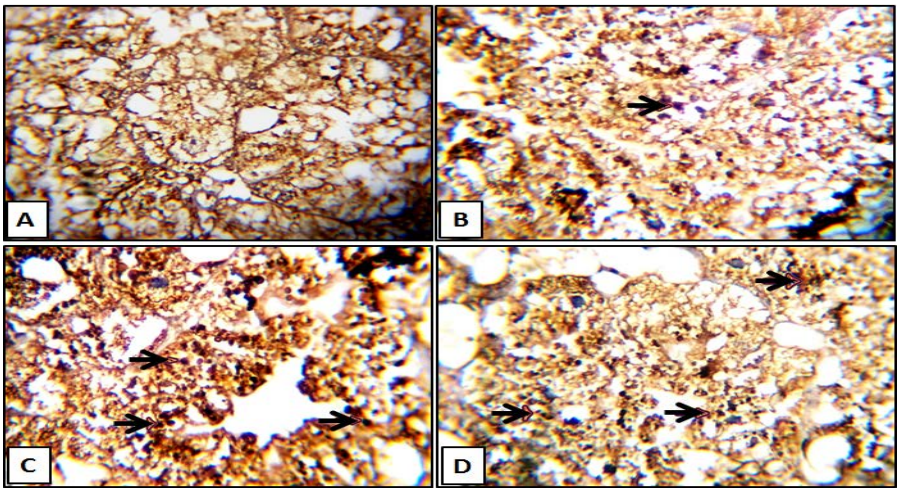

Plate 1. Nuclear factor kappa B staining of snail digestive gland. (A) NF-kB staining of digestive gland of control snails. (B) NF-kB staining of digestive gland of snail exposed to LC_{25} Glufosinate-ammonium after 28 days of exposure (arrows refer to NF-kB immunopositivity). (C and D) NF-kB staining of digestive gland of snail exposed to LC_{25} Anatoxin-a after 28 days of exposure (arrows refer to NF-kB immunopositivity).Magnifiction power (400X).

3.5. Histological changes of the digestive gland of M. cartusiana

The digestive glands comprise branched blindly ending follicles circumscribed by connective tissue (Plate 2A). Each follicle of the digestive gland is encircled by a thin layer of circular muscle fiber. The cells constituting the wall of each tubule are predisposed around an irregular lumen. Investigation of such cells demonstrated the presence of three types of cells digestive, excretory, and calcium cells (plate 2B). The digestive cells are the most plentiful cell type and fill most of the volume of each tubule. The excretory cells are less abundant and more significant than digestive cells, and cytoplasm of these cells is occupied by large vacuole having one or more yellow-brownish secretory granules. The calcium cells are the least abundant compared to the digestive and excretory cells, and their nuclei are situated at the basal half of the cell and are spherical ovoid in shape (plate 2A). After exposure to Glufosinate-ammonium, mild histological abnormalities such as mild tubular disruptions, excessive luminal secretion, and vacuolation (plate 2C), excretory cells showed an increase in the number and size of brownish-yellow granules (plate 2 D).

Anatoxin-a caused an increase in the number of vacuoles in the tubular epithelial cells of the digestive gland of snails and resulted in a widening of the lumen. The digestive and secretory cells are swollen and vacuolated with a thin cytoplasmic layer surrounding the large vacuole (plate 2E). Excessive tubular disruption is observed, including epithelial cell lysis, extensive vacuolation, and lumen reduction (plate 2F).Discussion

Investigating the impacts of pesticides discharged into the terrestrial environment on the terrestrial ecosystem becomes a topic of interest. Several studies were conducted to investigate the release of these pesticides into the terrestrial environment in response to these concerns. The current study focuses on the impact of two pesticides (Glufosinate-ammonium and Anatoxin-a) on the land snail *M. cartusiana*, which is frequently used as a bioindicator of terrestrial pollution.

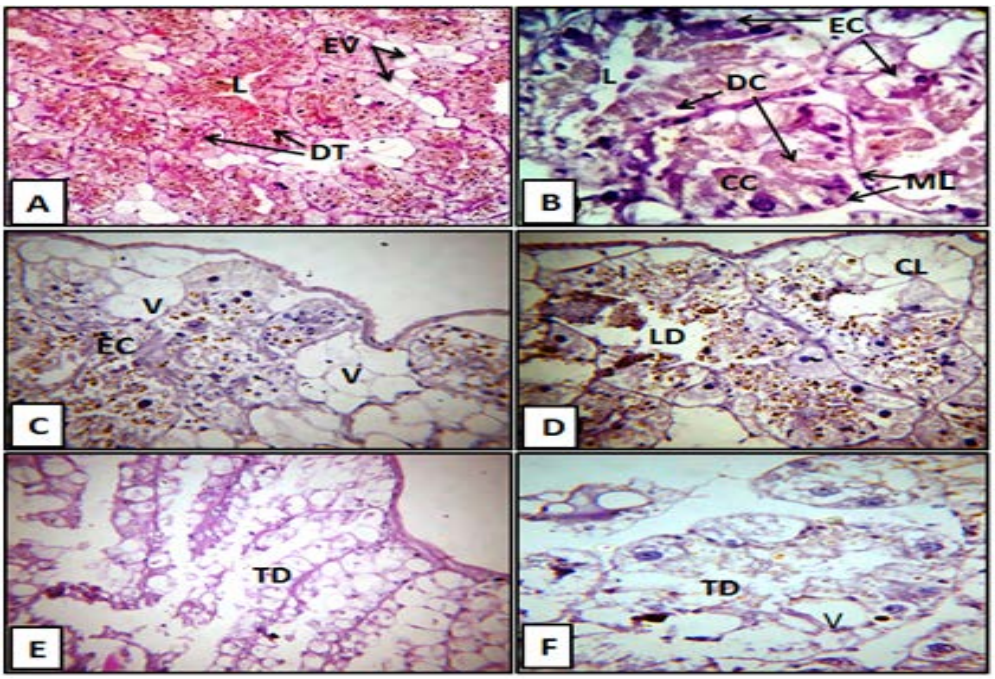

Plate 2. Light micrograph of the digestive gland of *M. cartusiana* snails. (A): The digestive gland of control group displaying the usual cellular structure (X100). (B): The digestive gland of control group displaying different types of cells forming the digestive tubules (X 400). (C&D): T.S. of digestive tubules after exposure to $LC_{25}$of Glufosinate-ammonium for 28 days showing mild tubular disruptions such as excessive secretion and Vacuolation (X100 & 200). (E&F): T.S. of digestive tubules after exposure to $LC_{25}$of Anatoxin-a for 28 days showing tubular degeneration(X100 & 400). **CC:** Calcium cell; **CL:** Cell lysis; **DC:** Digestive cell; DT**:** Digestive tubules; **EC:** Excretory cell; **EV:** Excretory vacuoles; **L:** Lumen; **LD:** Lumen dilatation; **ML:** Muscle layer; **TD:** Tubular disruption; **V:** Vacuolation.

3.6. Toxicity test

According to the results, Anatoxin-a was more toxic to *M. cartusiana* than Glufosinate-ammonium. These findings are compatible with those of Druart *et al.* (2011), who reported that Glufosinate-ammonium has a diminished toxic effect on land snail *Helix aspersa*. Silva dos Santos *et al.* (2019) recorded that Anatoxin-a has a neurotoxic effect on *Nauphoeta cinerea* cockroaches. The differences in toxicity between two pesticides may be accredited to the differences in susceptibility and tolerance associated with its accumulation, biotransformation, and excretion (Reddy *et al.*, 2012). Furthermore, the susceptibility of adult snails to pesticides varies depending on the mode of action, biological agent against the target organism, and the chemical component produced by the microorganisms. Two mechanisms mediate the toxic action of Anatoxin-a; first, it stimulates muscle contraction by acting as an ACh agonist, but it is continuous, unlike Ach; second, by inhibiting acetylcholinesterase, it increases the neurotransmitter within the synaptic cleft. The result of these two mechanisms is paralysis which could lead to the death of snails (Osterbauer and Dobbs, 2009). On the contrary, Glufosinate-ammonium does not inhibit neurotransmitter receptors or affect the catecholamine neurotransmitter tissue concentrations. This reason may be due to the weak toxic effect of Glufosinate-ammonium.

3.7. Biochemical biomarker in clover snail M. cartusiana exposed to LC_{25} of two tested pesticides.

Biochemical investigations have been used for evaluating the health status, impacts of stressors, and the adaptive capability of organisms to the external environment (El-Sayed *et al.*, 2019). Amino-transferase enzymes (ALT&AST) catalyze the inter-conversion of α-ketoacids and amino acids, and their echelons indicate heart dysfunction and liver impairment (Ghouri *et al.*, 2010). The current study found that ALT and AST increased in the digestive gland of treated snail with two pesticides. This increase may result from toxin exposure or destruction of the hepatic cell (Farkas *et al.*, 2004). These findings are in agreement with Abdel-Halim *et al.* (2020) and Gaber *et al.* (2021) who stated that ZnONPs and Methomyl (Copter 90%) caused an increase in the activity of AST and ALT in treated *M. cartusiana*, respectively. Also, Abd El-Atti *et al.* (2020) stated that Biozed (fungal) and Biogard (Bacterial) biocide caused an increase in the levels of ALT and AST in *M. cartusiana*. ALP is an enzyme responsible for removing phosphate groups from several kinds of molecules such as proteins and nucleotides by hydrolysis and is used to detect liver damage (Thomas, 2006). The present study revealed that Anatoxin-a and Glufosinate-ammonium significantly increased ALP levels in the digestive gland of treated *M. cartusiana*. Such increments are in harmony with the results of Sharaf *et al.* (2015) who stated that Diazinon, Lambda-cyhalothrin, and Methomyl exposure increased ALP levels in *M. cartusiana*. This increase may be due to destruction of the hepatic cell.

3.8. Oxidative stress and antioxidant biomarkers in clover snail M. cartusiana exposed to LC_{25} of two tested pesticides.

The reactive oxygen species (ROS) has a substantial role in the biological system's physiological control of cell function. Enzymatic and non-enzymatic antioxidant mechanisms are adequate in biological systems to cope with the continuous generation of ROS. When the generation of ROS exceeds their neutralization by antioxidant mechanisms within an organism, oxidative stress (OS) occurs (Regoli and Giuliani, 2014). Malondialdehyde (MDA) used as a biomarker of oxidative stress is one of the final products of polyunsaturated fatty acids peroxidation in the cells (Davey *et al.*, 2005). The current study displayed that MDA levels increased significantly in clover snail *M. cartusiana* after treatment with two pesticides. Likewise, Sharaf *et al.*, (2015) illustrated that MDA levels increased in the clover snail, *M. cartusiana*, after exposure to Diazinon, Lambda-cyhalothrin, and Methomyl. The increment may induce this elevation in free radicals, which causes the overproduction of MDA. Total antioxidant capacity (TAC) measures an organism's antioxidant state by assessing the antioxidant response against the free radicals accumulated in a tissue sample (Richetti *et al.*, 2011). In addition, the current study revealed that the TAC level was decreased in pesticides exposed to the snail. In agreement with the current study, Morad *et al*., 2022 found that TAC levels decreased in *Biomphlaria alexandrina* snails, after exposure to myco-synthesized nano-selenium. This reduction can be attributed to its defensive role against damages induced by free radicals. Catalase (CAT) and Glutathione peroxidase (GPx) are antioxidant enzymes and are considered the first line of defense against ROS (Van der Oost *et al*., 2003). In the current study, CAT and GPX activity was increased in the digestive gland of *M. cartusiana* upon exposure to two pesticides. Such increment in CAT and GPX activities may be an adaptive mechanism to prevent the accumulation of toxic reactive oxygen (Regoli *et al.*, 2006). In the same regard, Sharaf *et al.* (2015) found that CAT activity increased in the digestive gland of the clover snail, *M. cartusiana*, after treatment with Diazinon, Lambda-cyhalothrin, and Methomyl. Glutathione-s-transferase (GST) plays a vital role in defending cells and tissues from oxidative stress (Havelková *et al.*, 2008). GST activity was found to be significantly increased in the digestive gland of clover snail *M. cartusiana* following exposure to the tested pesticides. This increase may be attributed to its defensive role against damages induced by oxyradical. On the contrary, Abdel-Halim *et al.* (2020) reported that ZnONPs caused a decrease in the activity of GPX and GST in treated *M. cartusiana*.

3.9. NF-kB immunoreactivity

Nuclear factor Kappa B (NF-KB) is present in an inactive form in the cytosol linked to inhibitory regulatory proteins called IKB. There are different inducers to NF-KB activity, comprising oxidative stress resulted from reactive oxygen species and hypoxia, leading to NF-KB immunopositivity in tissues (Topal *et al.*, 2015). Another inducer is the lipid peroxidation intermediates (Campo *et al.*, 2008). Furthermore, the treatment of cells with Anatoxin-a and Glufosinate-ammonium increases the activity of NF-KB in the digestive gland of clover snail *M. cartusiana*. Immunopositivity was much more severe in snails treated with Anatoxin-a than Glufosinate-ammonium. The increment in the activity of NF-KB may be due to this elevation in reactive oxygen species.

3.10. Histological changes of the digestive gland of M. cartusiana

Histological investigations are significant biomarkers in toxicological studies. They are utilized as indicators of environmental stress since they deliver a particular biological end-point of historical exposure and divulge the direct effect of the toxicant in the organs (Ramesh *et al.*, 2018). In the current study, many histopathological alterations were estimated in the digestive gland, which is the vital organ that performs the detoxification mechanism (Henry *et al.*, 1991). The digestive gland of untreated snail is composed of three types of cells (digestive, excretory, and calcium cells). This finding agrees with Ismail *et al.* (2013), who detected the presence of three types of cells in the wall of tubules of the digestive gland. Based on the Histological examination of the digestive gland, the sub-lethal concentrations of Glufosinate-ammonium caused mild tubular disruptions such as excessive luminal secretion and vacuolation. Sub-lethal concentrations of Anatoxin-a resulted in severe tubular disruption, including cellular destruction. Similar changes were detected in the digestive gland of clover snail, *M. cartusiana* treated with Biozed (fungal), and Biogard (Bacterial) biocide (Abd El-Atti *et al.*, 2020).

In conclusion, this study has revealed that two pesticides (Glufosinate-ammonium and Anatoxin-a) have toxic effects against *M. cartusiana*. However, Anatoxin-a

was more toxic to treated snails than Glufosinate-ammonium. Anatoxin-a and Glufosinate-ammonium caused alterations in biochemical, oxidative stress biomarkers, NF-KB activity, and severe histopathological changes of *M. Cartusiana*. Therefore, these pesticides must be used prudently, and their release into the terrestrial environment should be closely monitored and regulated. Furthermore, the current study demonstrated the efficacy of land snails, *M. cartusiana*, as a bioindicator for Anatoxin-a and Glufosinate-ammonium toxicity. Furthermore, it suggested that long-term treatment could reveal the dangers of pesticide addiction on macroinvertebrates and human life.

Acknowledgements

The authors are grateful to Zoology and botany Department, Faculty of Science, Zagazig University, Zagazig, Egypt, for providing the appropriate laboratory to conduct the experiment. We would like to express our deep thanks and gratitude to Prof. Dr. Yassin El-ayouty (Botany and Microbiology Department, Faculty of Science, Zagazig University, Egypt) for providing the *Anabaena flos-aquae* strain. We would like to thank Marwa Abolfotouh for her helpful comments on the manuscript.

Author contribution

R.M. Said conceived and designed the experiment. A H. Al-Badwy conceived and designed the experiment. A. A. Mohamed conceived and performed the experiment. All authors contributed to writing, reading, and approving the final manuscript.

Funding statement

This research did not receive any specific grant from funding agencies in the public, commercial, or not-for-profit sectors.

Data availability

Data included in the article.

Declarations

Conflict of interest

The authors declare no competing interests.

Additional information

No additional information is available for this paper.

References

Abd El-Atti MS, Khalil AM, Elsheakh AA and Wesam SE. 2020. Biological control of *Monacha cartusiana* glassy clover land snails by microbial biopesticides Biozed and Biogard, using bait. *Tech Biocat Agricul Biotech.*, **25:**1-6.

Abdel-Halim KY, Osman SR and Abdou GY. 2020. In vivo evaluation of oxidative stress and biochemical alteration as biomarkers in glass clover snail, *Monacha cartusiana* exposed to zinc oxide nanoparticles. *Environ Pollut.*, **257:** 113120.

AL-Sultan EYA and Aubaed MAA. 2017. Extraction and Purification of Neurotoxin (Anatoxin-a) From Blue-green Alga *Pesudoanabaena limnetica* and Indicating Its Histopathological Effects on The Brain of Male Laboratory Mice (*Mus Musculus* L.). *J Biol Agricul Health.*, **7(18):** 77-87.

Breuer j. 1996. Report on the symposium “drug effect in clinical chemistry methods. *Eur J Clin Chem Clin Biochem.*, **34:** 385-386.

Campo GM, Avenoso A, Campo S, D'Ascola A, Traina P, Samà D and Calatroni A. 2008. NF-kB and caspases are involved in the hyaluronan and chondroitin-4-sulphate-exerted antioxidant effect in fibroblast cultures exposed to oxidative stress. *J Appl Toxicol.*, **28(4):** 509-517.

Costa JAV, Freitas BCB, Cruz CG, Silveira J and Morais MG. 2019. Potential of microalgae as biopesticides to contribute to sustainable agriculture and environmental development. *J Environ Sci Health-B.*, **54(5):** 366-375.

Davey MW, Stals E, Panis B, Keulemans J and Swennen RL. 2005. High-through put determination of malondialdehyde in plant tissues. *Anal Biochem.*, **347(2):** 201- 207.

David DW, David D, Tompkins DM and Townsend CR. 2010. Synergistic effects of glyphosate formulation and parasite infection on fish malformations and survival. *J Appl Ecol.*, **47(2):** 498–504.

Desouky MMA, Abdel-Gawad H, and Hegazi B. 2013. Distribution, fate and histopathological effects of Ethion insecticide on selected organ of the crayfish, *Procambarus clarkia*. *F Chem Toxicol.*, **52:** 42-52.

Druart C, Millet M, Scheifler R, Delhomme O and Vaufleury de Annette. 2011. Glyphosate and glufosinate-based herbicides: fate in soil, transfer to, and effects on land snails. *J Soil Sediment.*, **11(8):** 1373–1384.

Eissa S and Shoman S. 1998. **Markers of invasion and metastasis and markers of tumor proliferation and apoptosis in Tumors markers**. Chapman and Hall, Lippincott- Raven Publisher Inc., London, UK, pp. 131-153.

El-Sayed AS, Shindia AA, AbouZeid AA, Yassin AM, Sitohy M and Sitohy B. 2019. *Aspergillus nidulans* thermostable arginine deiminase - Dextran conjugates with enhanced molecular stability, proteolytic resistance, pharmacokinetic properties and anticancer activity. *Enzyme Microb Technol.*, **131:**109432.

Farkas JP, Farkas P and Hyde D. 2004. Liver and gastroenterology tests. In: Lee M (ed) **Basic Skills in Interpreting Laboratory Data**, third ed. American Society of Health System Pharmacists Inc, USA. Pp. 330 -336.

Finney DJ. 1971. **Probit analysis**, third ed. Combrige University Press, London.

Fujiki H, Suganuma M, Suguri H, Yoshizawa S, Takagi K, Nakayasu M, Ojika M, Yamada K, Yasumoto T, Moore RE and Sugimura T. 1990. New tumor promoters from marine natural products. In: Hall S, Strichartz G (Eds.), **Marine toxins, origin, structure and molecular pharmacology**. American Chemical Society, Washington DC, pp. 232–240.

Gaber OA, Asran A, Elfayoumi HMK, El-shahawy G, Khider FK, Abdel-Tawab H and Mahmoud KA. 2021. Influence of Methomyl (Copter 90%) on certain biochemical activities and histological structures of land snails *Monacha cartusiana*. *Saudi J Biol Sc.*, **29(4):** 2455-2462.

Ghouri N, Preiss D and Sattar N. 2010. Liver enzymes, nonalcoholic fatty liver disease, and incident cardiovascular disease: a narrative review and clinical perspective of prospective data. *Hepatology*., **52(3):** 1156-1161.

Gugger M, Lenoir S, Berger C, Ledreux A, Druart JC, Humbert JF, Guette C and Bernard C. 2005. First report in a river in France of a benthic cyanobacterium *Phormidium favosum* producing anatoxin-a associated with dog neurotoxicosis. *J Toxicon.*, **45(7):** 919-928.

Hack R, Ebert E, Ehling G and Leist KH. 1994. Glufosinate ammonium-some aspects of its mode of action in mammals. *Food Chem Toxicol*., **32(5):** 461-470.

Harada K, Kimura Y, Ogawa K, Suzuki M, Dahlem AM, Beasley VR and Carmichael WW. 1989. A new procedure for the analysis and purification of naturally-occurring anatoxin-a from the blue–green alga *Anabaena-flos-Aquae*. *J Toxicon*., **27(12):** 1289–1296.

Harada KI, Nagai H, Kimura Y, Suzuki M, Park HD, Watanabe MF, Luukkainen R, Sivonen K and Carmichael WW. 1993. Liquid chromatography/mass spectrometric detection of anatoxin-a, a neurotoxin from cyanobacteria. *Tetrahedron*., **49(41):** 9251-9260.

Havelková M, Randák T, Blahová J, Slatinská I and Svobodová Z. 2008. Biochemical markers for the assessment of aquatic environment contamination. *Interdisc Toxicol*., **1(2):** 169–181.

Henry M, Boucaud-Camou E and Lefort Y. 1991. Functional microanatomy of the digestive gland of the scallop *Pecten maximus* (L.) *Aquat Living Resour*., **4(3):** 191-202.

Ismail SH, Rashed A, Abou –senna FM and Abed M. 2013. Physiological and histochemical studies on the land snail, *Monacha cartusiana* in Sharkia Governorate. *Egypt J Agric Res.*, **91(1):** 207–216.

Klassen CD. 1986. **Cassarett's & Doulls Toxicology: The Basic Science of Poisons**, third ed. MacMillan Publ. Co., New York, pp. 1628–1650.

Krienitz L, Ballot A, Caspar P, Codd GA, Kotut K, Metcalf JS, Morrison LF, Pflugmacher S and Wiegand C. 2005. Contribution of toxic cyanobacteria to massive deaths of Lesser Flamingos at saline-alkaline lakes. *Proc Int Assoc Theor Appl Limnol*., **29:** 783–786.

Laguerre C, Sanchez-Hernandez JC, Köhler HR, Triebskorn R, Capowiez Y, Rault M and Mazzia C. 2009. B-type esterases in the snail *Xeropicta derbentina*: an enzymological analysis to evaluate their use as biomarkers of pesticide exposure. *Environ Pollut*., **157(1):** 199–207.

Lokma MH. 2013. Studies on Some Terrestrial Mollusca Injurious to
Vegetables and Field Crops in East Delta Locality (Sharkia and Ismailia). Ph.D. Plant Protection Department, Faculty of Agriculture, Moshtohor, Benha University, pp. 174.

Metcalf JS and Bruno M. 2017. **Anatoxin-a(S)**. In Handbook of Cyanobacterial Monitoring and Cyanotoxin Analysis, Wiley, Chichester, UK, pp. 155–159.

Metcalf JS and Codd GA. 2004. **Cyanobacterial toxins (cyanotoxins) in water**. Foundation for Water Res Allen House, The Listons, Liston Road, Marlow, Bucks SL 71 FD, UK.

Morad MY, El-Sayed H, Elhenawy AA, Korany SM, Aloufi AS, Ibrahim AM. 2022. Myco-Synthesized Molluscicidal and Larvicidal Selenium Nanoparticles: A New Strategy to Control *Biomphalaria alexandrina* Snails and Larvae of *Schistosoma mansoni* with an In Silico Study on Induced Oxidative Stress. *J Fungi*., **8(3)**:262.

Moss DW. 1982. Alkaline phosphatase isoenzymes. *Clin Chem*., **28(10):** 2007- 2016.

Osterbauer PJ and Dobbs MR. 2009. Neurological weapons. *Clin Neurotoxicol*., 675- 691.

Pieńkowska JR, Manganelli G, Giusti F, Barbato D, Hallgass A and Lesicki A. 2019. Exploration of phylogeography of *Monacha cantiana* s. l. continues: the populations of the Apuanalps (NW Tuscany, Italy) (Eupulmonata, Stylommatophora, Hygromiidae). *ZooKeys*, **814:** 115-149.

Ramesh M, Selvaraj A, Rama KP and Chellappan S. 2018. Evaluation of acute and sublethal effects of chloroquine ($C_{18}H_{26}CIN_3$) on certain enzymological and histopathological biomarker responses of a freshwater fish *Cyprinus carpio*. *Toxico Rep.*, **5:** 18-27.

Reddy NM, Reddy RR and Rajender K. 2012. Sub-acute toxicity effects of chlorpyrifos on acetylcholinesterase activity and recovery in the freshwater field crab *Barytelphusa guerini*. *Int J Environ Sci*., **3(1):** 98-107.

Regoli F and Giuliani ME. 2014. Oxidative pathways of chemical toxicity and oxidative stress biomarkers in marine organisms. *Mar Environ Res*., **93**: 106-117.

Regoli F, Gorbi S, Fattorini D, Tedesco S, Notti A, Machella N, Bocchetti R, Benedetti M and Piva F. 2006. Use of the land snail *Helix aspersa* as sentinel organism for monitoring ecotoxicologic effects of urban pollution: an integrated approach. *Environ Health Perspect*., **114(1):** 63-69.

Regoli F, Gorbi S, Machella N, Tedesco S, Beneditti M and Bochetti R. 2005. Pro oxidant effects of extremely low frequency electromagnetic fields (ELF-EM) in the land snail *Helix aspersa. Free Radic Biol Med*., **39:** 1620-1628.

Richetti SK, Rosemberg DB, VenturaLima J, Monserrat JM, Bogo MR and Bonan CD. 2011. Acetylcholinesterase activity and antioxidant capacity of zebrafish brain is altered by heavy metal exposure. *Neurotoxicol*., **32(1):** 116-122.

Saber AA, Hamed SM, Abdel-Rahim EFM and Cantonati M. 2018. Insecticidal prospects of algal and cyanobacterial extracts against the cotton leaf worm *Spodoptera littoralis*. *VIE MILIEU*., **68:** 199-212.

Scheifler R, Brahim MB, Gomot-de Vaufleury A, Carnus JM and Badot PM. 2003. A field method using microcosms to evaluate transfer of Cd, Cu, Ni, Pb and Zn from sewage sludge amended forest soils to *Helix aspersa* snails. *Environ Pollut*., **122(3):** 343–350.

Sharaf HM, Abd El-Atti MS and Salama MA. 2015. Toxic effects of some pesticides on the enzymatic activities and spermatogenesis of the land snail *Monacha cantiana. J Biosci Appl Res*., **1(3):** 139-146.

Silva dos Santos D, Rosa ME, Zanatta AP, Oliveira RS, Moreira de Almeida C G, Leal AP, Sanz M, Fernandes KA, Queiroz de Souza V, Reis de Assis D, Pinto E and André Dal Belo C. 2019. Neurotoxic effects of sublethal concentrations of cyanobacterial extract containing anatoxin-a(s) on Nauphoeta cinerea cockroaches. *Ecotoxicol Environ Saf*., **171:** 138-145.

Stanier R, Kunisawa R, Mandel M and Cohen-Bazire G. 1971. Purification and properties of unicellular blue-green algae (order Chroococcales). *Bacteriol Rev*., **35(2):** 171-205.

Stara A, Kouba A and Velisek J. 2018. Biochemical and histological effects of sub-chronic exposure to atrazine in crayfish *Cherax destructor*. *Chem Biol Interact*., **291:** 95-102.

Svircev Z, Lali´c D, Savi´c GB, Tokodi N, Backovic DD, Chen L, Meriluoto J and Codd GA. 2019. Global geographical and historical overview of cyanotoxins distribution and cyanobacterial poisonings. *Arch Toxicol*., **93:** 2429–2481.

Thomas A. 2006. Hematologic effects of Systemic Disease and Nonhematopoietic Tumors. In: Arceci RJ, Hanna IM and Smith OP (Eds.), **Pediatric hematology**, third ed, Blackwell Publishing Ltd. pp. 763.

Topal A, Atamanalp M, Oruç E, Halıcı MB, Şişecioğlu M, Erol HS, Gergit A and Yılmaz A. 2015. Neurotoxic effects of nickel chloride in the rainbow trout brain: assessment of c-Fos activity, antioxidant responses, acetylcholinesterase activity, and histopathological changes. *Fish Physiol Biochem*., **41:** 625-634.

Van der Oost R, Beyer J and Vermeulen NPE. 2003. Fish bioaccumulation and biomarkers in environmental risk assessment: a review. *Environ Toxicol Pharm*., **13(2):** 57-149.

WHO .1965. Molluscicdal screening and evaluation. *Bull World Health Organ*., **33(4):** 567–581.

JJBS

Volume 16, Number 1,March 2023
ISSN 1995-6673
Pages 21 – 26
https://doi.org/10.54319/jjbs/160104

Jordan Journal of Biological Sciences

Concomitant Administration of L-carnitine and Performing High-Intensity Interval Training Effects on the Genes Involved in Mitochondrial Fusion and Apoptosis in Rat Liver

Beydolah Shahouzehi[1], Yaser Masoumi-Ardakani[2], Hossein Fallah[3], Soheil Aminizadeh[4,*]

[1]*Cardiovascular Research Center, Institute of Basic and Clinical Physiology Sciences, Kerman University of Medical Sciences, Kerman, Iran;* [2]*Physiology Research Center, Institute of Neuropharmacology, Kerman University of Medical Sciences, Kerman, Iran;* [3]*Department of Clinical Biochemistry, Faculty of Medicine, Kerman University of Medical Sciences, Kerman, Iran;* [4]*Department of Physiology and Pharmacology, Afzalipour School of Medicine, and Physiology Research Center, Institute of Neuropharmacology, Kerman University of Medical Sciences, Kerman, Iran*

Received: February 22, 2022; Revised: May 14, 2022; Accepted: June 22, 2022

Abstract

Mitochondria as dynamic organelles go through coordinated processes, including fusion and apoptosis. This study was designed to assess the effects of L-carnitine supplement and high-intensity training on the mitochondria fusion and apoptosis in liver tissue. Thirty-two Wistar rats were assigned into four groups, and eight rats were entered into each group, including the untreated control group (CTL), L-Carnitine group (LCAR; 200 mg/kg/day, i.p), High-intensity interval training group (HIIT), HIIT+L-Carnitine group (LCAR-HIIT; received 200 mg/kg/day L-Carnitine and performed HIIT). Real-Time PCR was used to quantify the expression of liver genes. LCAR-HIIT significantly decreased Parkin ($p<0.0001$), MFN-1 ($p=0.014$), Caspase-3 ($p=0.039$), Bax ($p<0.0001$) expression in the liver compared with the CTL. However, HIIT with LCAR significantly increased the expression of Bcl-2 compared with the CTL ($p=0.049$), while LCAR significantly reduced Bax expression compared to the CTL ($p=0.006$). LCAR-HIIT induced positive physiological changes in the liver through negative regulation of Bax and caspase-3. In addition, LCAR-HIIT may provide a new approach for ameliorating mitochondria fusion in the liver tissue.

Keywords: L-Carnitine, HIIT, Parkin, mitochondria fusion, Apoptosis

1. Introduction

Mitochondrial in eukaryotic cells acts as the ATP production site and also coordinates multiple metabolic reactions by the Krebs cycle and fatty acids metabolism. Mitochondria, as an essential organelle in the cells, regulate cell proliferation and survival, inflammatory pathways, and anti-inflammatory responses (Suliman, 2014).

Fission and fusion processes are related to the division or fusion of mitochondria. Still, the process of biogenesis of mitochondrial promotes mitochondrial mass and a regulatory network including Peroxisome proliferator-activated receptor-γ coactivator-1α (PGC-1α), NRFs (Nuclear Respiratory Factors), mitochondria transcription factor A, MFN1, and MFN2 coordinate their dynamic (Litvinova et al., 2015, Palikaras et al., 2015, Norat et al., 2020). Mitochondrial biogenesis is thought to occur in response to increased workload, such as that present in training skeletal muscle or changes in the availability of substrates that occur during starvation (Suliman, 2014). Impaired quality control of mitochondria leads to the mitochondrial disturbance that contributes to some complications such as cardiovascular disease, diabetes mellitus, and aging. Parkin is an essential mediator of these processes (LaRocca et al., 2014).

Every cell in the body has a hidden program to destroy itself through apoptosis. Under normal circumstances, this program is kept off by inhibitory agents. One of the mechanisms of inhibition of apoptosis is the maintenance of molecules involved in apoptosis in organelles such as lysosomes and mitochondria (Vieira, 2003). Mitochondria are one of the main targets in apoptosis. Dynamic changes of proteins such as MFN2 and Drp1, and the apoptotic regulators Bax and Bcl-2 contributed to the mitochondrial fragmentation during apoptosis. Inhibition of the mitochondrial fission process is associated with activation of downstream caspases, thus delaying apoptosis, and overexpression of MFN1 and MFN2 also suppress the apoptotic process. The apoptotic proteins -caspase-3andBax- play a pivotal role in the prognosis of apoptosis in mitochondrial membrane permeability(Steiner et al., 2011, LaRocca et al., 2014, Palikaras et al., 2015, Dagda, 2018).Elevated levels of inflammatory cytokines, some growth factors, etc., reduced the expression of MFN2, while processes that increase energy consumption (such as exercise) increased its expression (Schrepfer and Scorrano,

* Corresponding author. e-mail: soheilaminizadeh@gmail.com.

2016). Several other intracellular pathways, such as cell cycle progression, mitochondrial bioenergetics maintenance, apoptosis, and autophagy, have been shown modulated MFN2 (Filadi et al., 2018).

Carnitine (beta-hydroxy-gamma trimethyl ammonium butyrate) is known as a vitamin-like and amino-acid-like substance. It was documented that the L-isoform of carnitine is physiologically active. Its prominent role in the body is to promote the β-oxidation of lipids by transferring them to the mitochondrial matrix. Therefore, if carnitine is not present, most dietary lipids cannot be available for oxidation (Eskandari et al., 2004, Cha, 2008).

High-Intensity Interval Training (HIIT) is intense training period with short rest intervals that reduces the total training time and has aerobic-like effects (Nutrients Editorial, 2018).Steiner et al. showed that exercise increased mitochondrial biogenesis through PGC-1a and other mediators (Steiner et al., 2011). Carnevali et al. showed that HIIT increases mitochondrial fat transfer capacity (by increasing the activity of the enzyme carnitine palmitoyl transferase), which facilitates the beta-oxidation process (Carnevali, Eder et al., 2012). Also, HIIT improved the muscle oxidation direction of animals with hypertension (Holloway et al., 2015). Overall, HIIT increases energy efficiency and physical function (Kwak, 2013, Holloway et al., 2015, Fallahi et al., 2016). Kwak has described that exercise has a protective effect against apoptosis (Kwak, 2013).L-carnitine supplementation with regular aerobic exercise improved liver tissue apoptosis in type 2 diabetic subjects (Gholami et al., 2019).

Given the vital liver roles in the body's metabolic processes and the high content of mitochondria in the hepatocytes and the critical role of the liver in regulating metabolic processes and pathways related to exercise physiology, we evaluated the effect of L-carnitine supplementation and performing high-intensity exercise on the genes variations elaborated in mitochondrial dynamic and apoptosis in rat liver tissue to investigate how L-carnitine and intense intermittent exercise interact with each other.

2. Materials and Methods:

2.1. Materials

L-carnitine hydrochloride (Sigma, C0283-25G), EZ-10 Spin Column Animal Total RNA Miniprep extraction kit (BS82312, BIO BASIC), cDNA synthesis kit (Pars TousInc., A101161), RealtimeQPlus Master GreenMix (Ampliqon, 5000830high ROX™), primers were purchased from Metabion International Company.

2.2. Methods

Thirty-two Wistar rats (male, 8-9 weeks of age) were purchased from Physiology Research Center. Rats were kept in the standard condition with a temperature of 23 ± 2 °C and a light-dark cycle of 12/12 h. Rats had free access to food & water. The animals were monitored for one week to familiarize themselves with the new environment and separated into 4 groups (n = 8), including Untreated control group (CTL; with no intervention), the L-Carnitine group (LCAR; 200 mg/kg/day, i.p), High-Intensity Interval Training group (HIIT), HIIT+L-Carnitine group (LCAR-HIIT; received 200 mg/kg/day L-Carnitine and performed HIIT), randomly. The groups that needed to do the exercise were given a 2-week treadmill adaptation, and then the study was begun. The study lasted for four weeks. The current study was approved (Code number: IR.KMU.REC.1399.378) by the Ethics committee of Karman Medical University.

2.2.1. L-carnitine Administration:

L-carnitine is dissolved in the sterile normal saline and administrated by daily i.p injection (200 mg/kg) (Masoumi-Ardakani et al., 2020, Karabulut et al., 2021).

2.2.2. Training Protocol:

Familiarity of rats lasted for two weeks (15 meters/minute for 15 min). Exercise intensity was calculated by lactometer (Lactate Scout Company/Code: 37, Germany), which quantified the blood lactate levels directly after exercise, and levels > 6 mmol/L were considered high intensity (Verboven et al., 2019) (Table 1). For calculation of the intensity, the speed test starts with a warm-up of 10 meters per minute and then increases the speed (0.3 meter/minute) till exhaustion (Hu et al., 2021). Each session consisted ten 2 minutes work bouts/day at about 22 m/min, 29° slope separated by 2-minutes rest periods (5 days/week, 4-week) (Batacan et al., 2016). Finally, forty-eight hours after the final training session, the animals were anesthetized and sacrificed. The liver tissue of each rat was dissected, and rinsed with cold saline and frozen until future examinations.

Table 1. The blood levels of lactate measured directly after exercise

group	Lactate (mmol/L)
HIIT (n=8)	6.3
LCAR-HIIT (n=8)	6.1

2.2.3. Real Time-PCR carried out to measure genes expression

The Real-Time PCR method was carried out to determine the relative expression of target genes in this study. For this purpose, total liver RNA was extracted. The process of RNA extraction typically involves the destruction of cells in a chemical environment that simultaneously inactivates ribonucleases and then uses columns that can capture RNA molecules and pass other molecules through. In the final step, the RNAs were washed from the column using an elution buffer and collected in sterile tubes. Then the purity and concentration of the extracted RNA were set out by the Nano-drop device. The cDNA was synthesized from total RNAs, and to inhibit the RNase enzyme, RNasin (RNase inhibitor) was added to the reaction mixture. The obtained cDNA was then used for the next step. Real-time PCR was carried out with polymerase enzyme and specific primers (Table 2) for the target genes. The 18s rRNA gene was used as the housekeeping gene. After Real-time PCR, Ct values were obtained for samples and reference genes. The formula $2^{-\Delta\Delta CT}$was used to calculate relative expression of genes (Mohammadi et al., 2018).

Table 2. The sequences of primers to perform Real-time PCR

Gene	Forward	Reverse
Bax	ATCCAAGACCAGGGTGGCTG	CACAGTCCAAGGCAGTGGGA
Bcl-2	TATATGGCCCCAGCATGCGA	GGGCAGGTTTGTCGACCTCA
Caspase-3	GTGGAACTGACGATGATATGGC	CGCAAAGTGACTGGATGAACC
MFN1	ACCAATCCCGCTGGGGAGGA	TGGGGAGGTGCTGTCTCGGA
MFN2	TTCCACACCACTCCTCCGAC	AGCGTCCTCTCCCTCTGACA
NRF-1	TAGCCCATCTCGTACCATCAC	TTTGTTCCACCTCTCCATCAG
Parkin	CTGGCAGTCATTCTGGAC	CTCTCCACTCATCCGGTTT
18S	GCAATTATTCCCCATGAACG	GGCCTCACTAAACCATCCAA

2.3. Statistical Analysis:

To analyze the data, we used SPSS version 22. We carried out the one-way analysis of variance (One-Way ANOVA) test, and to the pairwise comparison between groups, we performed Tukey's test. The data was expressed as Mean±SEM and the p value <0.05 was significant.

3. Results

The combination of LCAR+HIIT significantly reduced Parkin, MFN1, and caspase-3 expressions compared with the CTL (Figs 1, 3, and 5). The combination of LCAR+HIIT significantly reduced Parkin expression compared to the LCAR (p = 0.023) as well as HIIT (p = 0.012) groups (Fig 1). LCAR and combination of LCAR+HIIT significantly reduced Bax expression (Fig 6). The Bcl-2 expression in 3 intervention groups increased compared to the control, but only the combination of LCAR-HIIT caused a significant elevation (Fig 7). The expression of NRF-1 and MFN2 genes was not significant between the studied groups (Figs 2 and 4)

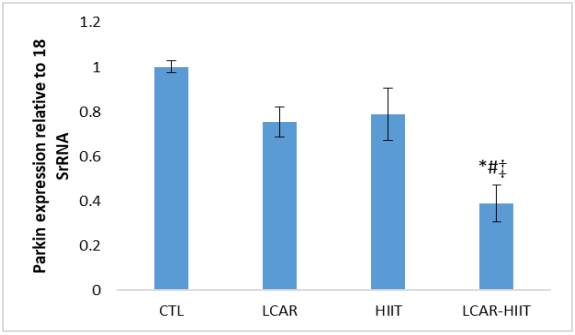

Figure 1. Parkin gene relative expression (Mean±SEM) in 4 studied groups, including control (CTL), received L-carnitine (LCAR), high-intensity interval training (HIIT), and LCAR+HIIT. P< 0.05 was considered as significant difference. * Statistically significant compared to control, # statistically significant compared to LCAR, ‡ statistically significant compared to HIIT.Significant signs are the same in the rest of the figures.

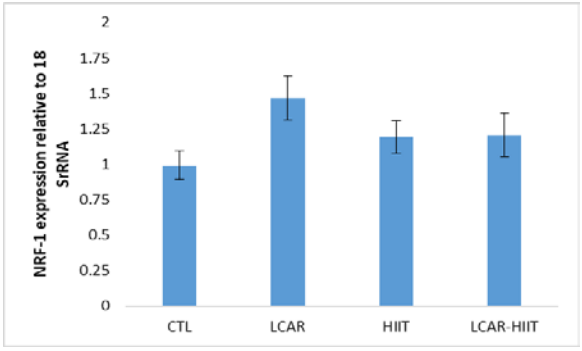

Figure 2. NRF-1 gene relative expression (Mean±SEM) in 4 studied groups, including control (CTL), received L-carnitine (LCAR), high-intensity interval training (HIIT), and LCAR+HIIT. P< 0.05 was considered as significant difference.

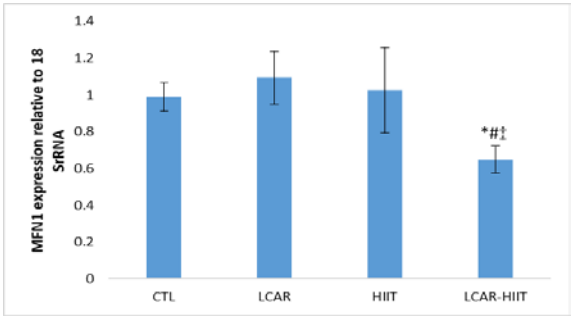

Figure 3. MFN1 gene relative expression (Mean±SEM) in 4 studied groups, including control (CTL), received L-carnitine (LCAR), high-intensity interval training (HIIT), and LCAR+HIIT. P< 0.05 was considered as significant difference.

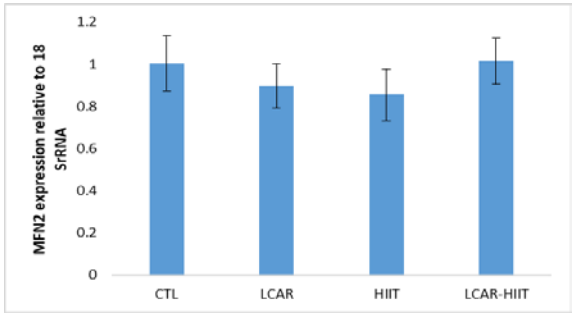

Figure 4. MFN2 gene relative expression (Mean±SEM) in 4 studied groups, including control (CTL), received L-carnitine (LCAR), high-intensity interval training (HIIT), and LCAR+HIIT. P< 0.05 was considered as significant difference.

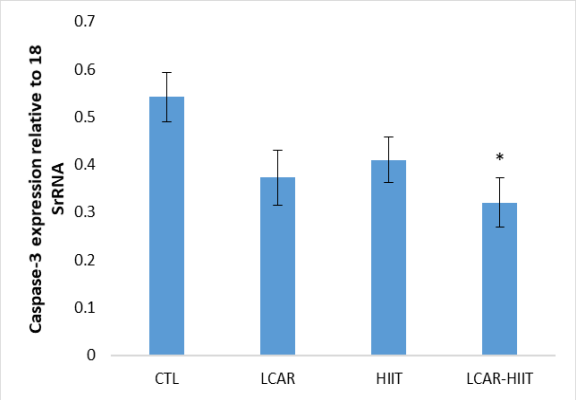

Figure 5. Caspase-3 gene relative expression (Mean±SEM) in 4 studied groups, including control (CTL), received L-carnitine (LCAR), high-intensity interval training (HIIT), and LCAR+HIIT. P< 0.05 was considered as significant difference.

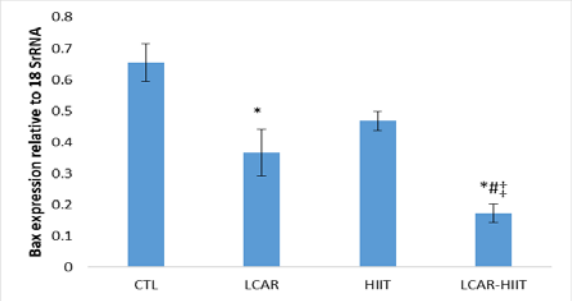

Figure 6. Bax gene relative expression (Mean±SEM) in 4 studied groups, including control (CTL), received L-carnitine (LCAR), high-intensity interval training (HIIT), and LCAR+HIIT. P< 0.05 was considered as significant difference.

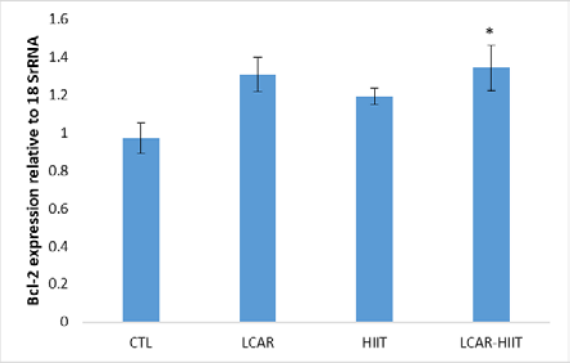

Figure 7. Bcl-2 gene relative expression (Mean±SEM) in 4 studied groups, including control (CTL), received L-carnitine (LCAR), high-intensity interval training (HIIT), and LCAR+HIIT. P< 0.05 was considered as significant difference.

4. Discussion

These current findings demonstrate the first evidence that L-CAR and HIIT contribute to the mRNA level of Parkin, MFN-1, Caspase-3, and Bax in liver tissue. Also, our current study provides evidence that HIIT and LCAR ameliorated Bcl-2 in liver tissue, possibly by suppressing the Parkin expression in the liver. Specifically, our results demonstrate that 1) HIIT and L-CAR decreased the mRNA expression level of apoptotic signaling, including Caspase-3, and Bax in the rat liver tissue, 2) L-CAR with HIIT elevated liverBcl-2expression, 3) L-carnitine and HIIT reduced the mRNA expression of MFN-1.

Based on the present study, four weeks of HIIT and L-CAR supplementation led to a remarkable reduction of Bax and the ratio of Bcl-2/Bax and also an increase in Bcl-2 levels of liver tissue. This indicates the protective effect of HIIT and LCAR supplementation through optimal regulatory pathways of apoptotic indices. Keleshian et al. reported that with increasing age, mRNA expression of pro-apoptotic Bax index and inflammatory and oxidative indexes in the frontal cortex of the brain increases, and Bcl-2 levels decrease (Keleshian et al., 2013). When there is no death receptor stimulus, the anti-apoptotic protein Bcl-2 is heterodimerized intracellularly with Bax. In case Bcl-2 overexpression, these molecules form homodimers and simultaneously inhibit apoptosis. Conversely, Bax overexpression leads to its homodimerization, resulting in increased sensitivity to apoptotic stimuli (Naim and Kaufmann, 2020). Therefore, disruption of the apoptotic balance and its shift to increased Bcl-2 following HIIT and L-CAR supplementation may be associated with the effects of support for liver tissue. In this regard, Um et al. showed that after 16 weeks of training, Bax levels in mice brains decreased, and Bcl-2 levels increased significantly (Um et al., 2008). Shirpour et al. observed that curcumin supplementation and HIIT showed an apoptosis inhibitory effect in hepatocytes (shirpour et al., 2017). Also, HumayunFard et al. reported that performing HIIT with selenium administration showed interactive properties on apoptosis proteins in rats (Humayun Fard et al., 2019). Although there are limited numbers of studies that evaluated the effect of HIIT and LCAR on the liver of rats and comparing the studies discussed with the results of our research, it appears that regular exercise has protective effects. Exercise training through phosphorylation of protein kinase B may reduce Bax and cytochrome C levels and therefore suppress apoptosis in the liver. Based on previous observations, HIIT was associated with a more significant impact on the development of liver function than continuous training (Rezaei et al., 2017). Jabbari et al. reported that L-carnitine supplementation and exercise training showed remarkable beneficial properties against apoptosis in diabetic rats (Jabbari et al., 2019). In sum, the results are not conclusive. Human elevated MFN1 during aging is reversed by running (Bori et al., 2012) or by six-week treadmill running in rats (Koltai et al. 2012); however, there were other human studies that demonstrated unaltered MFN1 in response to physical activity (Joseph et al., 2012, Gioscia-Ryan et al., 2016). Although they have shown that MFN1 expression up-regulated after cycling (12 weeks)(Konopka et al., 2014), after the same aerobic protocol, with the same duration and higher intensity, there was no increased MFN1 expression (Moreira et al., 2017).

Parkin, a cytosolic E3-ubiquitin ligase, functions in mitophagy. Specifically, the pol yubiquitination of Parkin substrates, such as MFN1/2, leads to their degradation by the proteasome. Induced mitochondrial fission and mitophagy after MFN1/2 destruction make a strong connection between mitochondrial dynamics to mitophagy. Mitophagy occurs in basal conditions constantly. Some specific physiological conditions can induce this process (Yoo and Jung, 2018).We demonstrated that Parkin is necessary for exercise-induced mitophagy. Interestingly, mitophagy induced after exercise was attenuated by training probably because of the promotion of basal

mitochondrial content and quality. It seems that Parkin is necessary for the preservation of basal mitochondrial function and increased good functioning mitochondria pool due to training adaptations (Chen et al., 2018). But HIIT and low-intensity interval training (LIIT), despite increasing PGC-1α and reducing DRP1, failed to improve mitochondrial fusion and fission (Ebadi and Damirchi, 2018).

One important issue that may be of interest in this study is the potential stress associated with performing high-intensity training and daily L-carnitine intraperitoneal injections. Previous studies have shown that exercise improves redox status by reducing pro-oxidant factors and increasing antioxidant intermediates. Poblete Aro et al. (2015) reported that HIIT (12 weeks) significantly reduced oxidative stress in diabetic patients (Poblete Aro et al., 2015). In a systematic review by Lu et al. (2021), they concluded that high-intensity exercise increased antioxidant capacity (Lu et al., 2021).

On the other hand, concerning L-carnitine administration, it was reported that L-carnitine intraperitoneal injections improved the redox state in diabetic rats (Masoumi-Ardakani et al., 2020). Hussein et al. (2013) reported that in high-fructose diet rats, L-carnitine increased liver catalase and superoxide dismutase (SOD) and reduced serum malondialdehyde level (Hussein et al., 2014). Also, L-carnitine administration reduced lipid peroxidation and increased serum SOD, catalase, and α-tocopherol in rats (Rajasekar, 2007). Lee et al. (Randomized clinical trial) linked reduced ROS levels to L-carnitine as its protective properties (Lee et al., 2014). It was also reported that L-carnitine i.p. administration promoted antioxidant defense status (Irat et al., 2003).

Finally, oxidative stress induces apoptosis and if HIIT and L-carnitine injection caused stress induction; therefore; we expect that apoptosis must increase in this group (LCAR-HIIT). On the contrary, we found that the expression of Caspase-3 and Bax reduced in LCAR-HIIT group, which indicates that there is probably no significant stress effect due to performing HIIT or L-carnitine injections.

In our study, in LCAR-HIIT group, both Parkin and MFN1 decreased in the same direction, so both mitophagy and mitochondrial fusion appear to be in equilibrium. By down regulation of Parkin we expected an increase in MFN1 levels, but the combination of exercise and carnitine administration reduced its expression, a balance has been struck between these processes. There are some limitations in this study; oxidative stress and antioxidants were not determined, and we did not examine the oxidative stress made by several injections and performing exercise.

5. Conclusion

In conclusion, the current study demonstrates that L-carnitine supplementation and performing HIIT improved positive physiological changes in the liver through negative regulation of Bax, caspase-3. In addition, LCAR-HIIT may provide a new approach for facilitating mitochondria fusion in the liver.

References

Batacan RB, Duncan MJ, Dalbo VJ, Connolly KJ and Fenning AS. 2016. Light-intensity and high-intensity interval training improve cardiometabolic health in rats. *Appl Physiol Nutr Metab.*, **41**(9): 945-952.

Bori Z, Zhao Z, Koltai E, Fatouros IG, Jamurtas AZ, Douroudos G, Terzis A and et al. 2012. The effects of aging, physical training, and a single bout of exercise on mitochondrial protein expression in human skeletal muscle. *Exp Gerontol.*, **47**(6): 417-424.

Carnevali LC, Eder R, Lira FS, Lima WP, Goncalves DC, and et al. 2012. Effects of high-intensity intermittent training on carnitine palmitoyl transferase activity in the gastrocnemius muscle of rats. *Braz J Med Biol Res*., **45**(8): 777-783.

Cha YS. 2008. Effects of L-carnitine on obesity, diabetes, and as an ergogenic aid. *Asia Pac J Clin Nutr*.,17 Suppl 1: 306-308.

Chen CCW, Erlich AT and Hood DA. 2018. Role of Parkin and endurance training on mitochondrial turnover in skeletal muscle. *Skelet Muscle*., **8**(1): 10.

Dagda RK. 2018. Role of Mitochondrial Dysfunction in Degenerative Brain Diseases, an Overview. *Brain Sci.*, **8**(10).

Ebadi B and Damirchi A. 2018. Effect of exercise training intensity on mitochondrial dynamics and mitophagy in post myocardial infarction rats. *Inter J of Applied Exercise Physiology*., 4 (6).

Eskandari HG, Cimen MY, Tamer L, Kanik A and Atik A. 2004. Short term effects of L-carnitine on serum lipids in STZ-induced diabetic rats. *Diabetes Res Clin Pract*., **66**(2): 129-132.

Fallahi AA, Shekarfroush S, Rahimi M, Jalali A and Khoshbaten A. 2016. Alteration in cardiac uncoupling proteins and eNOS gene expression following high-intensity interval training in favor of increasing mechanical efficiency. *Iran J Basic Med Sci*., **19**(3): 258-264.

Filadi R, Pendin D and Pizzo P. 2018. Mitofusin 2: from functions to disease. *Cell Death Dis*., **9**(3): 330.

Gioscia-Ryan RA, Battson ML, Cuevas LM, Zigler MC, Sindler AL and Seals DL. 2016. Voluntary aerobic exercise increases arterial resilience and mitochondrial health with aging in mice. *Aging (Albany NY)*., **8**(11): 2897-2914.

Holloway TM, Bloemberg D, Da Silva ML, Quadrilatero J and Spriet LL. 2015. High-intensity interval and endurance training are associated with divergent skeletal muscle adaptations in a rodent model of hypertension. *Am J Physiol Regul Integr Comp Physiol.*, **308**(11): R927-934.

Holloway TM, Bloemberg D, Da Silva JA, Simpson J, Quadrilatero J, and Spriet LL. 2015. High intensity interval and endurance training have opposing effects on markers of heart failure and cardiac remodeling in hypertensive rats. *PLoS One*., **10**(3): e0121138.

Hu J, Cai M, Shang Q, Li Z, Feng Y and et al. 2021. Elevated Lactate by High-Intensity Interval Training Regulates the Hippocampal BDNF Expression and the Mitochondrial Quality Control System. *Front Physiol*.,**12**: 629914.

Humayun Fard H, Hosseini SA, Azarbayjani MA and Nikbakht M. 2019. The Effect of Interval Training with Selenium Consumption on Gene Expression of Caspase- 3 and Cyclin-D in Liver Tissue of Cadmium-Exposed Rats. *Jundishapur J Health Sci.*, **11**(2): e88598.

Hussein SA, Abd El-Hamid OM and Hemdan HS. 2014. Protective Effect of L-carnitine on Metabolic Disorders, Oxidative Stress, Antioxidant Status and Inflammation in a Rat Model. *Inter J of Biological Chemistry*., **8**(1): 21-36.

Irat AM, Aktan F and Ozansoy G. 2003. Effects of L-carnitine treatment on oxidant/antioxidant state and vascular reactivity of streptozotocin-diabetic rat aorta. *J Pharm Pharmacol.*, **55**(10): 1389-1395.

Jabbari EM, Gholami H, Nikbakht N, Shakeri S and Ghazaliyan F. 2019. Effect of aerobic training and L-carnitine supplementation on some apoptotic factors in diabetic rat liver. *Razi Journal of Medical Sciences.*, **26**(7): 131-140.

Joseph AM, Adhihetty PJ, Buford TW, Wohlgemuth SE, Lees HA, Nguyen LM, Aranda JM, and et al. 2012. The impact of aging on mitochondrial function and biogenesis pathways in skeletal muscle of sedentary high- and low-functioning elderly individuals. *Aging Cell*,. **11**(5): 801-809.

Karabulut D, Akin AT, Unsal M, Lekesizcan A, Ozyazgan TM, Keti DB, and et al. 2021. L-Carnitine ameliorates the liver by regulating alpha-SMA, iNOS, HSP90, HIF-1alpha, and RIP1 expressions of CCL4-toxic rats. *Iran J Basic Med Sci*., **24**(2): 184-190.

Keleshian VL, Modi HL, Rapoport SI and Rao JS. 2013. Retracted: aging is associated with altered inflammatory, arachidonic acid cascade, and synaptic markers, influenced by epigenetic modifications, in the human frontal cortex. *Journal of neurochemistry*,. **125**(1): 63-73.

Koltai E, Hart N, Taylor AW, Goto S, Ngo JK and et al. 2012. Age-associated declines in mitochondrial biogenesis and protein quality control factors are minimized by exercise training. *Am J Physiol Regul Integr Comp Physiol*., **303**(2): R127-134.

Konopka AR, Suer MK, Wolff CA and Harber MP. 2014. Markers of human skeletal muscle mitochondrial biogenesis and quality control: effects of age and aerobic exercise training. *J Gerontol A Biol Sci Med Sci*., **69**(4): 371-378.

Kwak HB. 2013. Effects of aging and exercise training on apoptosis in the heart. *J Exerc Rehabil*,. **9**(2): 212-219.

LaRocca TJ, Hearon CM, Henson GD and Seals DR. 2014. Mitochondrial quality control and age-associated arterial stiffening. *Exp Gerontol*,. **58**: 78-82.

Lee BJ, Lin JS, Lin YC and Lin PT. 2014. Effects of L-carnitine supplementation on oxidative stress and antioxidant enzymes activities in patients with coronary artery disease: a randomized, placebo-controlled trial. *Nutr J*., **13**: 79.

Litvinova L, Atochin DN, Fattakhov N, Vasilenko M, Zatolokin P and Kirienkova E. 2015. Nitric oxide and mitochondria in metabolic syndrome. *Front Physiol*., **6**: 20.

Lu Y, Wiltshire HD, Baker JS and Wang Q. 2021. Effects of High Intensity Exercise on Oxidative Stress and Antioxidant Status in Untrained Humans: A Systematic Review. *Biology (Basel)*., **10**(12).

Masoumi-Ardakani Y, Aminizadeh S, Fallah H and Shahouzehi B. 2020. l-carnitine different doses affect serum and pancreas tissue Antioxidative defense and histopathology in STZ-induced diabetic rats. *Biologia*., **75**(9): 1415-1423.

Mohammadi A, Fallah H, Shahouzehi B and Najafipour H. 2018. Effect of LXR agonist T0901317 and miR-33inhibitor on SIRT1-AMPK and circulating HDL-C levels. *Bulgarian Chemical Communications*., **50**(1): 111-118.

Moreira OC, Estebanez B, Martinez-Florez S, Depaz JD, Cuevas MJ and Gonzalez-Gallego J. 2017. Mitochondrial Function and Mitophagy in the Elderly: Effects of Exercise. *Oxid Med Cell Longev*., **2017**: 2012798.

Naim S and Kaufmann T. 2020. The multifaceted roles of the bcl-2 family member bok. *Frontiers in cell and developmental biology*., 4 **(8)**.

Norat P, Soldozy S, Sokolowski JD, Gorick CM, Kumar JS, Chae Yand et al. 2020. Mitochondrial dysfunction in neurological disorders: Exploring mitochondrial transplantation. *NPJ Regen Med.*, **5**(1): 22.

Nutrients Editorial Office. 2018. Erratum: l-Carnitine Supplementation in Recovery after Exercise; Nutrients 2018, 10, 349. *Nutrients.*, **10**(5).

Palikaras K, Lionaki E and Tavernarakis N. 2015. Balancing mitochondrial biogenesis and mitophagy to maintain energy metabolism homeostasis.*Cell Death Differ*.,**22**(9): 1399-1401.

Poblete Aro CE, Russell Guzman JA, Soto Munoz AE and Villegas Gonzalez BE. 2015. Effects of high intensity interval training versus moderate intensity continuous training on the reduction of oxidative stress in type 2 diabetic adult patients: CAT. *Medwave*., **15**(7): e6212.

Rajasekar P and Anuradha CV. 2007. Effect of L-carnitine on skeletal muscle lipids and oxidative stress in rats fed high-fructose diet. *Experimental Diabe Research.*, **2007 (5)**.

Rezaei R, Nourshahi M, Khodagholi F, Haghparast A, Nasoohi S, Bigdeli M and Ashabi G. 2017. Differential impact of treadmill training on stroke-induced neurological disorders. *Brain injury*., **31**(13-14): 1910-1917.

Schrepfer E, and Scorrano L. 2016. Mitofusins, from Mitochondria to Metabolism. *Mol Cell*., **61**(5): 683-694.

Shirpour S, Azarbayjani MA, Peeri M and Farzanegi P. 2017. Effect of High Intensity Interval Training with Curcumin on Gene Expression of Bax, Bcl- 2, and Caspase- 3 in Aged Female Rat Hepatocytes. *Report of Health Care*., **3**(3): 8-14.

Steiner JL, Murphy EA, McClellan JL, Carmichael MD and Davis JM. 2011. Exercise training increases mitochondrial biogenesis in the brain. *J Appl Physiol (1985).*, **111**(4): 1066-1071.

Suliman HB and Piantadosi CA. 2014. Mitochondrial biogenesis: regulation by endogenous gases during inflammation and organ stress. *Curr Pharm Des.*, **20**(35): 5653-5662.

Um HS, Kang EB, Leem YH, Cho YH, Yang CH, Chae KR and et al. 2008. Exercise training acts as a therapeutic strategy for reduction of the pathogenic phenotypes for Alzheimer's disease in an NSE/APPsw-transgenic model. *International journal of molecular medicine.*, **22**(4): 529-539.

Verboven M, Cuypers A, Deluyker D, Lambrichts I, Eijnde BO, Hansen D and Bito V. 2019. High intensity training improves cardiac function in healthy rats. *Sci Rep*., **9**(1): 5612.

Vieira H and Kroemer G. 2003. Mitochondria as targets of apoptosis regulation by nitric oxide. *IUBMB Life*., **55**(10-11): 613-616.

Yoo SM and Jung YK. 2018. A Molecular Approach to Mitophagy and Mitochondrial Dynamics. *Mol Cells.*, **41**(1): 18-26.

Jabbari E, Gholami M, NikBakht H, Shakeri N, Ghazaliyan F. 2019. Effects of aerobic training and L-carnitine on the apoptosis in liver of male diabetic rats. *Razi Journal of Medical Sciences.*, **26**(7) .

JJBS

Volume 16, Number 1,March 2023
ISSN 1995-6673
Pages 27 – 34
https://doi.org/10.54319/jjbs/160105

Jordan Journal of Biological Sciences

Species Diversity of Freshwater Microalgae in Dramaga, Bogor Based on Morpho-ecological Identification between Low and High Light Intensity Environment

Miftahul Huda Fendiyanto[1,2], Mentari Putri Pratami[1,*], Rizky Dwi Satrio[1,2] , Isna Arofatun Nikmah[1], Nastiti Intan Permata Sari[1], Mo Awwanah[1], Nadya Farah[1], Nurhadiyanta[1]

[1]Study Program of Biology, Faculty of Military Mathematics and Natural Sciences, Indonesia Defense University. Kampus Universitas Pertahanan Sentul Bogor, Kawasan IPSC, 16810, West Java, Indonesia; [2]Laboratory Plant Physiology and Molecular Biology, Department of Biology, Faculty of Mathematics and Natural Sciences, IPB University. Kampus IPB Darmaga Bogor 16680, West Java, Indonesia

Received: April 1, 2022; Revised: June 9, 2022; Accepted: June 24, 2022

Abstract.

Microalgae are prokaryotic or eukaryotic organisms that have photosynthetic anabolic activity. This anabolic photosynthesis is related to the abiotic factor of light. Therefore, this study aimed to identify the morphological diversity level of microalgae based on their environment, especially light intensity. We collected samples based on two types of environment, namely high light community (HL-1D and HL-2D) and low light community (LL-1D and LL-2D). The Data were analyzed using Species Richness Indices (Menhinick and Margalef indices), Species Diversity (Shannon-Wiener and Simpson Indices), and Eveness Index. Based on the results of morphological identification, we found the presence of algae from the divisions Cyanophyta, Chlorophyta, and Euglenophyta in both communities. The most dominant species found in the HL environment were Cyanophyta (*Chroococcus* sp., *Microcystis* sp., *Nostoc* sp., *Oscilatoria* sp.), Chlorophyta (*Actinastrum* sp., *Ankistrodesmus* sp., *Centritractus belanophorus*, *Coelastrum* sp., *Closterium* sp., *Gleocapsa* sp., *Mougeutia* sp., *Pediastrum* sp., *Scenedesmus* sp., *Selenastrum* sp., *Sphaeroplea* sp., *Tetraspora cylindrica*, *Ulothrix* sp., and *Volvox* sp.), Euglenophyta (*Cryptoglena* sp. and *Lepocinclis* sp.). Species found in the LL environment were Cyanophyta (*Bulbochaeta* sp.) and Chlorophyta (*Pleurotaenium* sp., *Uronema elongasi*, and *Zygnema* sp.). Microalgae communities in high light communities have higher diversity than low light communities. This study can be used as a reference for the diversity of microalgae in two different types of environments, especially in the tropics and in freshwater microalgae communities. This diversity data could be a reference for researchers and provide preliminary information of microalgae potency as alternative biofuels in the future.

Keywords: Abiotic Factor, Freshwater Microalgae, Light Intensity, Photosynthesis

1. Introduction

Fossil fuels or mineral fuels are natural resources that contain hydrocarbons such as coal, oil, and natural gas. Along with the increase in the world's population, the availability of fossil-based fuels has been dwindling. This condition will have an impact on various sectors such as transportation, industry, agriculture, and others. With the limited amount of fossil fuels available, humans will switch to using petroleum. If used continuously, there will be an increase in CO_2 emission levels in the atmosphere, which will affect global warming and climate change (Chisti, 2007; Handoko *et al.*, 2008; Paynter and Frölicher, 2015; Williams *et al*., 2017). To overcome this problem, we need a substitute fuel that is renewable and environmentally friendly such as biodiesel (Mahyudin and Kusnandar, 2006; Williams *et al.*, 2017). Biodiesel is an alternative fuel derived from plants or animals through a transesterification process with alcohol (Chisti, 2007; Litinas *et al*., 2020). Indonesia is an archipelagic country with abundant aquatic biological resources, both in type and quantity. One aspect of the richness of biological resources is the abundance of plants that have the potential as a source of biodiesel, one of which is microalgae. Microalgae can produce 150-200 times more lipids than lipid-producing plants, i.e., *Elaeis* sp. and *Jatropha* sp.(Chisti, 2007).

Microalgae are a group of microscopic low-level plants that live in both fresh and marine waters. Microalgae are unicellular organisms that live in colonies or live as solitary and are generally photosynthetic because they live by utilizing light energy. Microalgae are rich in nutrients that can be developed as a source of raw materials for the pharmaceutical, cosmetic, and biofuel industries (Ghufran and Kordi, 2010). In addition, the biomass of many microalgae has a high lipid content of approximately 60% of the dry weight. Such microalgae are also tolerant of changes in extreme environmental conditions such as soil,

* Corresponding author. e-mail: mentariry@gmail.com.

lakes, wastewater, snow, high temperatures of as hot springs, and high salt content of the sea (Agustini, 2006).

Several types of microalgae are being developed in several countries as producers of bio-oil which can be further utilized in biodiesel (Moshood *et al.*, 2020). In addition, the potential of microalgae which is currently receiving special attention is as a producer of biohydrogen that can be used as renewable energy (Richmond and Emeritus, 2013; Moshood *et al*., 2020). The advantages of microalgae for biodiesel raw materials include not only requiring a large area of land, but also fast harvesting time; the biomass has a high lipid content and a fast cell growth rate with cell doubling occurring every 3.5 hours and not causing competition between energy and food needs (Chisti, 2007; Moshood *et al*., 2020).

The growth and production of microalgae are strongly influenced by environmental conditions. The environmental factors that affect the growth and productivity of microalgae lipids include light intensity, temperature, osmotic pressure, pH, and nutrient concentration in the media (Becker, 1994). Nybakken (1982) suggested that the main inorganic nutrients needed by phytoplankton to grow and reproduce are N in the form of NO^{3-} and P in the form of PO_4^{3-}. One of the known cell disruption methods is the osmotic shock method. It performs a sudden decrease in osmotic pressure on a microorganism so that it will cause cell damage. This method can be used to remove cellular components such as oil.

According to Teresa *et al.*, (2010), *Botryococcus braunii* can contain quite a lot of lipids up to 20-75% dry weight of biomass. Long-chain hydrocarbons in the form of oil or unbranched triterpenes of this species are known as botryococcene is very potential as an energy source or biodiesel (Metzger and Largeau, 2005; Rao *et al.*, 2007).

Several groups of microalgae can be used as biodiesel raw materials, namely diatoms (Bacillariophyceae), green microalgae (Chlorophyta), and blue-green microalgae (Cyanophyta) (Griffiths and Harrison, 2009). Microalgae contain several important components including carbohydrates, fatty acids, and proteins so that microalgae can be used as raw materials to produce their derivative products. The content and productivity of microalgae lipids are influenced by nitrogen concentration and light intensity (Gunawan, 2010). Microalgae have been investigated as an alternative as substitute for land plant commodities as a source of oil production because of their ability to grow in a short time with abundant biomass (Prartono *et al.*, 2013). To utilize microalgae as raw material for biodiesel, it is necessary to characterize and identify species first (Moshood *et al.*, 2020). Species identification is a step that can be taken to determine the types and relationships of a group at the taxonomic level and is important to be the basis for applied research from Microalgae (Prartono *et al.*, 2013). Therefore, the purpose of this study is to identify morphologically the diversity level of microalgae based on their environment, especially light intensity to provide a primary data to get a species which used a fossil fuels as renewable energy sources for the next research.

2. Materials And Methods

2.1. Sample collection

Freshwater samples were collected from two sites in Dramaga, Bogor Regency based on high (open, 6.500-10.000 lux) and low light intensity (shaded, 1.000-2.000 lux) environments. We used four sites with 20 replicates, so in total we evaluated 80 samples.. The sites in this study included high light community 1 (HL-1D), high light community 2 (HL-2D), low light community 1 (LL-1D), and low light community 2 (LL-2D). We collected fresh water at these four locations particularly 5 plots with 5 m in distance, respectively and then observed it directly using a compound microscope (Olympus, Japan). Sampling was carried out by filtering 5-10 liters of water with a vacuum pump in which a 0.45-micrometer millipore was installed. Water was taken at a depth of 50 cm to 1 m depending on the intensity of sunlight in the research location so that the filtered microalgae were microalgae that live above the water surface and float in the water. Then, the millipore was taken and put into a falcon bottle that had been filled with Industry Daigo Microalgae (IMK) media (Gunawan, 2010). For the microalgae samples to be identified, 4% formalin was added to keep the chlorophyll from being damaged (Gunawan, 2010).

2.2. Morphological identification

Microalgae from freshwater collections were identified based on cell surface structure, cell shape (globose, filamentous), living type (solitary or colony), species or genus characteristics, and cell motility. These three algae are very abundant in freshwater, according to a report by Gunawan (2010). Identification of microalgae morphology was carried out by observing using a light microscope (Olympus CX41, Japan), and identification was carried out by referring to the identification book entitled "The Freshwater Algae" (Prescot, 1978) and the book “Key to Freshwater Algae: A Web-Based Tool to Enhance Understanding of Microscopic Biodiversity” (Shayler and Siver, 2006).

2.3. Diversity parameter analysis

We tested the species richness (SR) parameter using the R program with the syntax “apply(data[,-1]>0,1, sum)” (Lander, 2014). Species richness was measured based on the number of species at each site specifically in the four communities HL-1D, HL-2D, LL-1D, and LL-2D. In addition to species richness, we also measure richness based on two kinds of indices, namely Menhinick's index (May) and Margalef's index (Mai) with the following formula (Peng *et al.*, 2018) where n was the number of species and N was the total number of individuals.

$$MeI = \frac{n}{\sqrt{N}}$$

$$MaI = \frac{n-1}{lnN}$$

For species abundance, we used the syntax "apply(data[,-1],1,sum)" in the R program. We also tested Rarefaction (Ra) with the formula below, where n was the sub-sample, N was the total number of individuals in the new rarefied taxa, and Ni was the total number of individuals in each of the original taxa (Peng *et al.*, 2018).

$$Ra = \sum 1 - \left[\frac{\left(\frac{N - Ni}{n} \right)}{\left(\frac{N}{n} \right)} \right]$$

For species diversity, we used the Shannon-Wiener Index (H') and Simpson's Index (λ) formulas (Peng *et al.*, 2018) with the syntax "diversity(data[-1], index="Shannon")" and "diversity(data[-1], index= "Simpson")" in the vegan package in the R program where ni is the number of individuals of the amount of each of the i species and N is the total number of individuals for the site. The criteria of species diversity was H' < 1 considered low; 1< H' < 3 is in the middle, and H' > 3 is high.

$$H' = -\sum \left(\frac{ni}{N} \times \ln \frac{ni}{N} \right)$$

$$\lambda = \sum \frac{ni(ni-1)}{N(N-1)}$$

For the evenness parameter, we used Pilou evenness (J) and Hill's ratios (Ea:b) as below (Peng *et al.*, 2018), where H' is the actual diversity value (the Shannon-Wiener Index) and Hmax is the maximum possible diversity value. In addition, Na is the diversity numbers of order a (community 1) and Nb is the diversity numbers of order b (community 2).

$$J = \frac{H'}{H \max}$$

$$Ea : b = \frac{Na}{Nb}$$

2.4. Statistical test and data analysis

Morphological characteristic data were analyzed descriptively to obtain a complete description of each species. For data analysis, we tested the data statistically (descriptive statistics, analysis of variance, and T-test) by using the program R version 3.5.1 (Lander, 2014).

3. Results and Discussion

3.1. Biodiversity of freshwater microalgae in Dramaga, Bogor in four sites community

Freshwater microalgae in Dramaga showed a relatively abundant level of diversity, especially in high light communities (HL-1D and HL-2D) compared to low light communities (LL-1D and LL-2D). In the high light community (HL), we found many species, i.e. *Actinastrum* sp., *Ankistrodesmus* sp., *Chroococcus* sp., *Coelastrum* sp., *Gleocapsa* sp., *Microcystis* sp., *Oscilatoria* sp., *Pediastrum* sp., *Scenedesmus* sp., *Selenastrum* sp., *Ulothrix* sp., and *Volvox* sp. (Figure 1). In the low light community (LL), we found species *Bulbochaeta* sp., *Closterium* sp., *Closterium* sp2, *Pleurotaenium* sp., *Uronema* sp., and *Zygnema* sp. (Figure 1).

Chroococcus sp. has general characteristics, namely prokaryotic organisms, coccus cell shape, is unicellular, has chlorophyll pigment, and forms a mucous membrane. We found the species *Chroococcus* sp. in abundance in the HL community. *Chroococcus* sp. is classified as division Cyanophyta, Class Cyanophyceae, Order Chroococcales, and Genus *Chroococcus*. In the new classification system, *Chroococcus* sp. is classified closer to bacteria than other eukaryotic algae organisms based on microalgae phylogeny studies (Shayler and Siver, 2006).

Volvox sp. tends to form colonies where it is divided into two types, i.e. main colonies and auto-colonies. Another characteristic that we found in the species *Volvox* sp. In this study, the colonies were spherical, the cells were round in shape, and each cell was covered with mucilage (Figure 1). *Volvox* sp. has a classification system, namely Kingdom Protista, Division Chlorophyta, Class Chlorophyceae, Order Volvocales, Family Volvocaceae, Genus *Volvox*. Different from *Chroococcus* sp., *Volvox* sp. tend to be advanced because they have a nuclear membrane and are classified as eukaryotic organisms. Different from *Volvox* sp., *Coelastrum* sp. Morphologically, no mucilage was found even though they were both Division Chlorophyta.

Other microalgae belonging to the Division Chlorophyta include *Gleocapsa* sp., *Sphaeroplea* sp., *Scenedesmus* sp., and *Actinastrum* sp. *Gleocapsa* sp. is a eukaryotic organism belonging to the division Chlorophyta and Class Chlorophyceae. We identified this species based on the presence of a gelatinous cell envelope. *Sphaerolea* sp. has a characteristic where cells tend to be filamentous and chloroplasts are spiral. *Scenedesmus* sp. in this study has a morphological structure where the spine is relatively long, cells are oval, chloroplasts are found in almost all parts of the cell, and visually it is found the presence of pyrenoid as a place to store food reserves. In this study, *Scenedesmus* sp. also has the number of cells in the colony as many as four, the form of chloroplast laminate, and the colony is coenobitic. *Actinastrum* sp. Morphologically has a cell shape that resembles a star.

Oscilatoria sp. belongs to the Kingdom Monera group, especially the Cyanophyta Division where the cell structure is in the form of filaments.

Based on the identification results, we found that *Pediastrum* sp., has a polygonal cell shape where the colonies are without a conspicuous gelatin sheath, and the cells tend to be green indicated by the presence of high chlorophyll (Figure 1). *Pediastrum* sp. is classified into Kingdom Protista, Division Chlorophyta, Class Chlorophyceae, Order Chlorooccales, Family Hydrodictyaceae, and Genus *Pediastrum*.

Ulothrix sp. has a characteristic filamentous (thread) and cylindrical cell shape (Figure 1). In this study, we found the presence of chlorophyll in the filaments of *Ulothrix* sp. *Ulothrix* sp. classified into Kingdom Protista, Division Chlorophyta, Class Chlorophyceae, Order Ulotrichales, Family Ulotrichaceae, and Genus *Ulothrix*.

Microcystis sp. has a characteristic that is unicellular and round cells (Figure 1). Based on the results of our identification, the chlorophyll in *Microcystis* sp. is located in almost all parts of the cell. *Microcystis* sp. has a classification system, namely Kingdom Monera, Division Cyanophyta, Class Cyanophyceae, Order Nostocales, Family Nostocaceae, and Genus *Microcystis*.

Uronema sp. In this study, it can be categorized as an elongated *Uronema* where the cells are filamentous and there is a partition between the filaments in the microalgae. The elongated *Uronema* in this study is classified as Division Chlorophyta with the cell nucleus surrounded by a nuclear membrane or eukaryotic. *Zygnema* sp. relatively

have the same cell shape as *Uronema* sp. mainly in the form of filaments, but both are distinguished by the location of the bulkhead, and morphologically in the structure of the ends of the filaments.

Based on the identification results, we found the presence of *Bulbochaeta* sp. on the LL site. *Bulbochaeta* sp. grouped into Kingdom Monera, Division Cyanophyta, Class Cyanophyceae, Order Oedogenales, Family Oedogoniaceae, and Genus *Bulbochaeta*. We identified the species *Bulbochaeta* sp. based on the characteristics in the form of branched filaments and chloroplasts are morphologically shaped like a net.

Pleurotaenium sp. and *Closterium* sp. both have cell forms in the form of filaments and belong to the Division Chlorophyta, Kingdom Protista, including eukaryotic organisms. Both differ in cell shape and chloroplasts, where *Pleurotaenium* sp. is wider in shape with rectangular chloroplasts while the cell and chloroplast forms of *Closterium* sp. are slender in shape with relatively tapered ends.

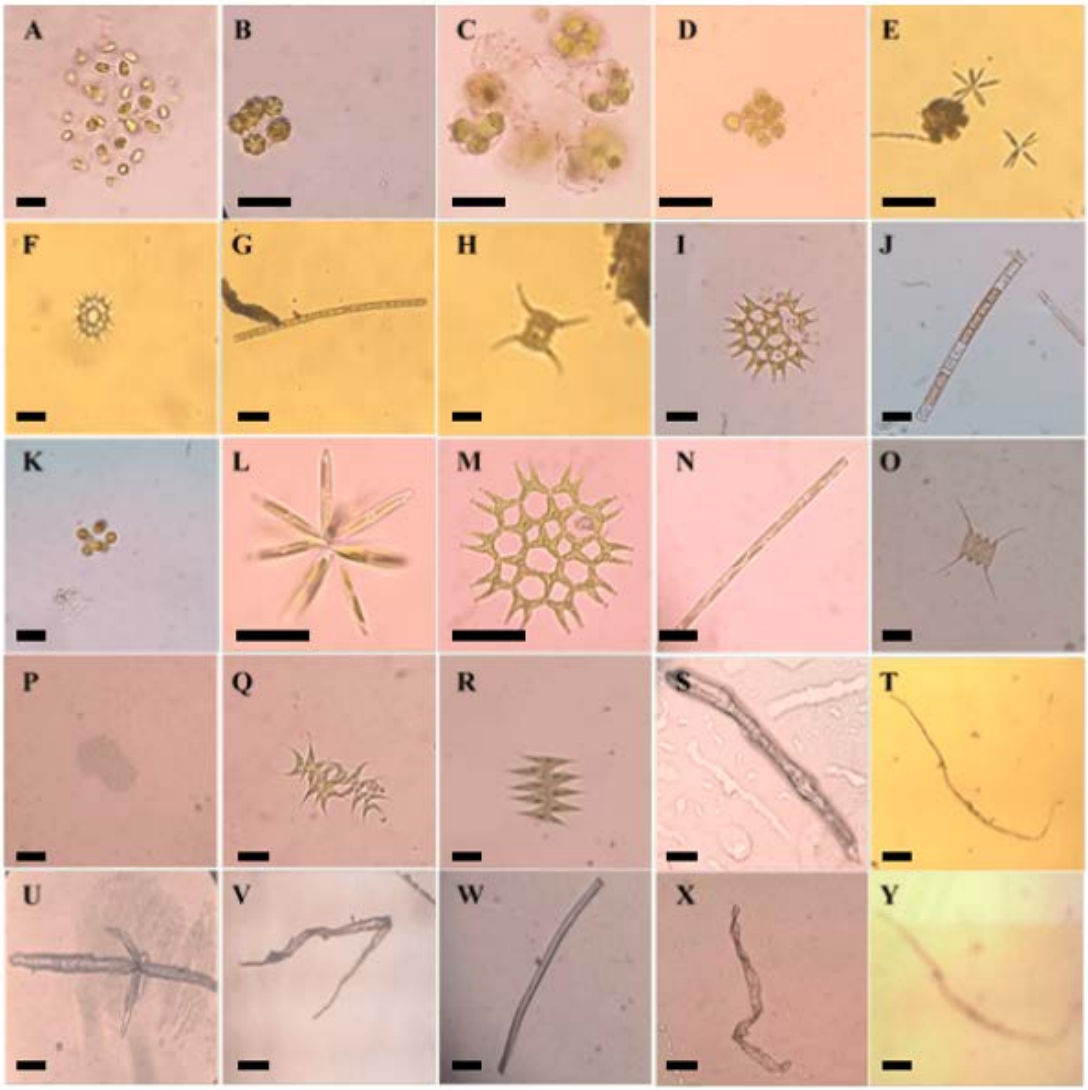

Figure 1. Freshwater-Microalgae Diversity in Dramaga, Bogor particularly in each site. HL-1D: high light community 1: A-H (A: *Chroococcus*, B: *Volvox* sp., C: *Coelastrum*, D: *Gleocapsa*, E: *Actinastrum*, F: *Pediastrum*, G: *Oscilatoria*, H: *Scenedesmus*), HL-2D: high light community 2: I-R (I: *Pediastrum*, J: *Ulothrix* sp1, K: *Microcystis*, L: *Actinastrum*, M: *Pediastrum*, N: *Ulothrix* sp2, O: *Scenedesmus*, P: *Mycrocystis*, Q: *Selenastrum*, R: *Ankistrodesmus*) LL-1D: low light community 1: S-T (S:*Uronema*, T: *Closterium*), LL-2D: low light community 2: U-Y (U: *Bulbochaeta*, V: *Pleurotaenium*, W: *Closterium* sp1., X: *Zygnema*, Y: *Closterium* sp2.). Bar = 10 μm.

Table 1. Species diversity of microalgae in four sites community in Dramaga, Bogor

No.	Sites	Species	Division
1	HL-1D	*Volvox* sp.	Chlorophyta
2		*Chroococcus* sp.	Cyanophyta
3		*Coelastrum* sp.	Chlorophyta
4		*Tetraspora cylindrica*	Chlorophyta
5		*Mougeutia* sp.	Chlorophyta
6		*Lepocinclis* sp.	Euglenophyta
7		*Gleocapsa* sp.	Chlorophyta
8		*Sphaeroplea* sp.	Chlorophyta
9		*Scenedesmus* sp.	Chlorophyta
10		*Cryptoglena* sp.	Euglenophyta
11		*Actinastrum* sp.	Chlorophyta
12		*Pediastrum* sp.	Chlorophyta
13		*Oscilatoria* sp.	Cyanophyta
14		*Nostoc* sp.	Cyanophyta
15	HL-2D	*Volvox* sp.	Chlorophyta
16		*Ulothrix* sp.	Chlorophyta
17		*Pediastrum* sp.	Chlorophyta
18		*Microcystis* sp.	Cyanophyta
19		*Actinastrum* sp.	Chlorophyta
20		*Closterium* sp.	Chlorophyta
21		*Scenedesmus* sp.	Chlorophyta
22		*Gleocapsa* sp.	Chlorophyta
23		*Selenastrum* sp.	Chlorophyta
24		*Centritractus belanophorus*	Chlorophyta
25		*Coelastrum* sp.	Chlorophyta
26		*Ankistrodesmus* sp.	Chlorophyta
27	LL-1D	*Closterium* sp.	Chlorophyta
28		*Uronema elongasi*	Chlorophyta
29	LL-2D	*Bulbochaeta* sp.	Cyanophyta
30		*Zygnema* sp.	Chlorophyta
31		*Closterium* sp.	Chlorophyta
32		*Pleurotaenium* sp.	Chlorophyta

Note: HL-1D: high light community 1, HL-2D: high light community 2, LL-1D: low light community 1, LL-2D: low light community 2

In general, we found differences in species composition or division among the two sites in this research. Specifically, to site HL, we can find all Division Chlorophyta, Cyanophyta, and Euglenophyta. In low light community (LL), we did not find Euglenophyta in our freshwater sample. This is probably related to the behavior of the motile and the presence of eye-spot in Euglenophyta, which tends to like high light intensity. At the species level, we found few species of microalgae at the LL sites but the species at these sites tended to be unique and were not found at the HL sites, i.e., *Uronema elongation*, *Bulbochaeta* sp., *Pleurotaenium* sp., and *Zygnema* sp. Interestingly, at the HL sites, we found *Lepocinclis* sp. and *Cryptoglena* sp. where both are classified as Division Euglenophyta and are motile and have chloroplasts. Species that can be found at both HL and LL sites are *Closterium* sp. Meanwhile, species that could only be found at HL sites were *Volvox* sp., *Chroococcus* sp., *Coelastrum* sp., *Tetraspora cylindrica*, *Mougeutia* sp., *Lepocinclis* sp., *Gleocapsa* sp., *Sphaeroplea* sp., *Scenedesmus* sp., *Cryptoglena* sp., *Actinastrum* sp., *Pediastrum* sp., *Oscilatoria* sp., *Nostoc* sp., *Ulothrix* sp., *Pediastrum* sp., *Microcystis* sp., *Closterium* sp., *Selenastrum* sp., *Centritractus belanophorus*, and *Ankistrodesmus* sp.

3.2. Species richness, abundance, diversity, and evenness indices of freshwater microalgae among high and low light intensity environment

The highest species richness of freshwater microalgae was obtained at the HL-1D site and the lowest was at the LL-1D site. In general, species richness in high light intensity communities (HL-1D and HL-2D) was higher than in low light intensity communities (LL-1D and LL-2D). Richness can also be tested with Menhinick's index (MeI) and Margalef's index (MaI). The values of the MeI and MaI indices are relatively similar to the SR values where the order of communities that have the highest to lowest species richness are HL-1D, HL-2D, LL-2D, and LL-1D (Table 2). Species abundance in this study shows something different from species richness where the highest value is indicated by the HL-2D site, while the LL-1D and LL-2D sites are relatively similar.

On the other hand, the Rarefaction value also shows that the highest Ra value is in the LL-2D community. This means that the species at the site are unique, and the majority can only be found in that community.

In addition to the value of species richness, abundance, and rarefaction, Diversity of Microalgae can also be tested with two types of indices, namely the Shannon-Wiener Index (H') and Simpson's Index (λ). Based on the test of the two types of indices, it shows that the microalgae community as a whole has relatively varied diversity, from low to relatively high. Based on the values of the Shannon-Wiener Index and Simpson's Index, the HL-1D and HL-2D sites have relatively high biodiversity, the LL-2D sites are classified as having moderate biodiversity, and the LL-1D sites are grouped as communities with relatively low biodiversity. In general, the biodiversity of freshwater microalgae in a high light environment is higher than that in a low light environment (Table 2).

Evenness values usually show the inverse value of the diversity index value (both in the Shannon-Wiener Index or Simpson's Index). In this study, we used two kinds of evenness index, namely Pilou evenness (J) and Hill's ratios (Ea:b). Although the two indices have different statistical calculations, they both show the same trend where the LL-1D site has a high Pilou evenness and Hill's ratios value, while the HL-1D site shows a low value (Table 1).

Table 2. Species richness, abundance, diversity, and evenness indices of four community of microalgae

Sites	SR	MeI	MaI	SA	Ra	H'	λ	J	$E_{a:b}$
HL-1D	13±0.03	3.15±0.01	4.24±0.02	17±0.21	3.79±0.01	2.48±0.01	0.91±0.01	0.35±0.00	0.19±0.01
HL-2D	11±0.11	2.40±0.00	3.28±0.01	21±0.32	3.64±0.00	2.31±0.02	0.89±0.01	0.37±0.00	0.22±0.00
LL-1D	2±0.02	1.15±0.01	0.91±0.00	3±0.52	2.00±0.00	0.64±0.01	0.44±0.00	0.64±0.01	0.78±0.02
LL-2D	4±0.01	2.00±0.00	2.16±0.01	4±0.31	4.00±0.01	1.39±0.01	0.75±0.01	0.54±0.01	0.53±0.01

Note: SR: Species richness; MeI: Menhinick's index; MaI: Margalef's index; SA Species abundance Ra Rarefaction; H': Shannon-Wiener Index; λ: Simpson's Index; J: Pilou evenness; $E_{a:b}$: Hill's ratios

3.3. Shannon-Wiener index in each dominant species of microalgae

The Shannon-Wiener Index is a biodiversity parameter that is commonly used in several communities of organisms, both organisms in the blood and in the waters. Specifically, on the calculation of the Shannon-Wiener Index in aquatic environments, we tested the level of H' value in several species of microalgae. Species that have a high level of diversity in freshwater microalgae in this study is *Closterium* sp., *Gleocapsa* sp., *Actinastrum* sp., *Volvox* sp., *Coelastrum* sp., *Scenedesmus* sp., and *Pediastrum* sp. (Table 3).

Table 3. Top seven species diversity of microalgae

Code	Species	H’
Sp17	*Closterium* sp.	1.055±0.02
Sp7	*Gleocapsa* sp.	0.693±0.01
Sp11	*Actinastrum* sp.	0.693±0.01
Sp1	*Volvox* sp.	0.637±0.01
Sp3	*Coelastrum* sp.	0.562±0.01
Sp9	*Scenedesmus* sp.	0.562±0.03
Sp12	*Pediastrum* sp.	0.562±0.01

4. Discussion

Microalgae are microorganisms that have a relatively wide distribution in both freshwater and seawater. Microalgae are divided into two types based on the Whittaker classification system, especially from the presence or absence of a nuclear membrane. The two types are prokaryotic microalgae and eukaryotic microalgae (Branco-Vieira *et al.*, 2020). Prokaryotic microalgae are classified into two divisions, i.e. Prochlorophyta and Cyanophyta. Eukaryotic microalgae are divided into nine divisions, i.e. Glaucophyte, Rhodophyta, heterokont, Haptophyta, Cryptophyta, Dinoflagellate, Euglenophyta, Chlorarachniophyta, and Chlorophyta (Barsanti and Gualtieri 2006). In this study, we found Division Cyanophyta, Chlorophyta, and Euglenophyta (Figure 1, Table 1).

Microalgae have a lot of potential in their utilization such as biofuels, bioenergy, cosmetics, pharmaceuticals, and health (Ghufran and Kordi, 2010; Chia *et al.*, 2018). Especially for the use of microalgae as biofuels and bioenergy, the important macromolecules produced in microalgae are lipids. High lipid content can determine a high level of biofuel potential in microalgae. The use of markers (morphological, anatomical, metabolite, and molecular markers) can be considered to exploit triacylglyceride-producing metabolic pathways in microalgae such as in higher plants.

Microalgae are photosynthetic microorganisms that have the potential to be used for fine chemicals products (Ghufran and Kordi, 2010; Barbera *et al*., 2018), food additives for humans and animals, immobilization systems for the formation of extracellular compounds, heavy metal biosorption, and CO_2 fixation. With an oil content of 77%, microalgae also have the potential to be used as biodiesel, which is an alternative energy source; and based on calculations, microalgae can produce 200 times more oil than other vegetable sources (Litinas *et al.*, 2020). The advantage of microalgal biodiesel is that it is a renewable source (Moshood *et al.*, 2020). In addition, with its location at the equator, Indonesia has a very sufficient source of sunlight as an energy source for photosynthetic microalgae (Gunawan, 2010).

Microalgae are the only source of biodiesel that has the potential to completely replace fossil fuels (Brennan and Owende, 2010; Hajar *et al*., 2017; Pratami *et al*., 2022). Unlike other plants, microalgae grow very rapidly and contain lots of oil/lipids. Microalgae undergo exponential growth in about 3.5 hours. The lipid content of microalgae can exceed 80% of their dry weight. Each microalga has a different amount of lipid content (Gunawan, 2010; Pratami *et al*., 2022). In other organisms, for example in snake fruit, lipid metabolites are relatively diverse (Fendiyanto *et al*., 2020; Fendiyanto et al., 2021).

Microalgae collection in the laboratory can use one or more types of microalgae which are given special nutrients into a culture such as NO^{3-} or PO_4^{3-} and carried out with lamp irradiation (Bold and Wynne, 1985; Moshood *et al*., 2020). The microalgae growing media used must contain inorganic elements in the form of N, P, Fe, and Si (Chisti, 2007). Microalgae culture requires inorganic nutrients in the form of macronutrients including C, H, O, N, P, K, S, Mg, Si, and Ca, while microelements include Fe, Zn, Cu, Na, Mo, Co, B, Mn, Cl and Ni (Agustini, 2006; Hamim, 2007). The main macronutrients in the form of N in the form of NO3⁻ and P in the form of PO43- are needed for microalgae growth, so that these two elements are limiting factors in microalgae growth. Research conducted by Griffiths and Harrison, (2009) reported that the reduction of nitrogen concentration in microalgae media Greens can increase the lipid content from 41% to two times. Elemental P is needed by microalgae in regulating growth and metabolic processes, which is used to compose cell membranes (phospholipids), as a basic material for ATP and nucleic acid synthesis (Theodorou *et al*., 1991; Barbera et al. 2018). Elemental P in the nutrient solution is usually in the form of PO_4^{3-} which will be absorbed by microalgae under conditions that receive a lot of light and in a pH between 6-7 (Lewin 1962). Macronutrients such as

P are important in the formation of proteins. Restriction of P in green microalgae *Selenastrum minutum* reduces its protein content (Theodorou *et al*., 1991). Gunawan (2010) also reported that microalgae produced high lipid content at 0.2 M concentration of N and 0.6 mM of P concentration in BG 11 medium. K element functions in carbohydrate metabolism, Fe and Na elements play a role in the formation of chlorophyll. The elements Si and Ca are materials in the formation of cell walls.

Micronutrients are given in small amounts and must remain with the function of a catalyst during the biosynthetic process to support the growth of organisms. In microalgae growing media, EDTA or citrate is usually added to stabilize the micronutrient function and also functions as a chelator (Widianingsih *et al*., 2008). In addition, the addition of phosphate salts as a buffer solution or buffer solution will cause the pH of the growing medium to become stable (Sidabutar, 1999). Microalgae culture is usually in the pH range between 7 to 9 and the optimum pH is between 8.2-8.7 which will increase the growth rate of microalgae (Abdulazis, 2010). There are many variations of the growing media used on a laboratory scale or cultivation scale with different mineral compositions according to the needs and types of microalgae used. Microalgae culture under exponential phase conditions is usually carried out within 4 to 7 days of inoculation, during which time microalgae should be given medium conditions with optimal nutrient concentrations for microalgae growth (Sutomo *et al*., 2007). Based on research conducted by Gunawan, (2010), it is known that BG 11 medium is the best culture medium for microalgae. According to Gunawan, (2010), BG 11 is usually used to isolate Cyanophyta and freshwater microalgae. BG 11 medium contains NO^{3-} as a source of N, while HPO_4^{2-} and H_2PO^{4-} as a source of P and as buffering agents (Reine and Trono, 2002).

Molecular identification using DNA is not influenced by morphological characteristics, is easier, and accurate (Pandin, 2010; Fendiyanto *et al*., 2019a; Fendiyanto *et al*., 2019b; Satrio *et al*., 2019; Miftahudin *et al*., 2021; Satrio *et al*., 2022; Pratami *et al*., 2022), i.e. gene expression analysis and metabolomic approaches are used in broad studies especially in many crops (Bendjedid *et al*., 2022; Deabes *et al*., 2022; Kamillah *et al*., 2022). One of the molecular markers that can be used in the identification process of microalgae is the 18S rRNA gene. Wang *et al*., (2014) in their study used the 18S rRNA marker which is a ribosomal recommendation genome used to detect eukaryotic microscopic organisms in ecosystems. In this study, we tried to find ecological markers (especially abiotic factors) to predict the level of microalgae diversity.

5. Conclusion

In general, we found differences in species composition or division among the two sites in this research. Specifically, to site HL, we can find all Division Chlorophyta, Cyanophyta, and Euglenophyta. In low light community (LL), we did not find Euglenophyta in our freshwater sample. The most dominant species found in the HL environment were *Volvox* sp., *Chroococcus* sp., *Coelastrum* sp., *Tetraspora cylindrica*, *Mougeutia* sp., *Lepocinclis* sp., *Gleocapsa* sp., *Sphaeroplea* sp., *Scenedesmus* sp., *Cryptoglena* sp., *Actinastrum* sp., *Pediastrum* sp., *Oscilatoria* sp., *Nostoc* sp., *Ulothrix* sp., *Pediastrum* sp., *Microcystis* sp., *Closterium* sp., *Selenastrum* sp., *Centritractus belanophorus*, and *Ankistrodesmus* sp. Species found in the LL environment were *Uronema elongasi*, *Bulbochaeta* sp., *Pleurotaenium* sp., and *Zygnema* sp. Microalgae communities in high light communities have higher diversity than low light communities. This study can be used as a reference for the diversity of microalgae in two different types of environments, especially in the tropics and in freshwater microalgae communities. This diversity data could be a reference for researchers and provide preliminary information of microalgae potency as alternative biofuels in the future.

Acknowledgements

This research was funded by Ministry of Defense, the Republic of Indonesia through Dr. Mentari Putri Pratami, S.Si., M.Si fiscal year 2021 through LP2M, particularly the Republic of Indonesia Defense University (RIDU) Funding. We thank Laboratory of Plant Physiology and Genetics, Department of Biology, IPB University for supporting facilities to algal culture.

References

Abdulazis SNB. 2010. A Cultivation of *Chlorella vulgaris* under Heterotrophic Condition for Growth and Lipid Production in Various Waste. Universiti Teknologi Malaysia Press, Kuala Lumpur.

Agustini R. 2006. Utilization of thermophilic proteases that live in the hot springs of Batu Cangar Malang. *Indones J Chem.*, **6(2)**: 205-211.

Barbera E, Bertucco A and Kumar S. 2018. Nutrients recovery and recycling in algae pro- cessing for biofuels production. *Renew Sustain Energy Rev.*, **90**: 28-42.

Barsanti L and Gualtieri P. 2006. Microalgae. CRC Press-Taylor & Francis, Paris.

Becker. 1994. Microalge Biotechnology and Microbiology. Cambridge University Press, New York.

Bendjedid S, Bazine I, Tadjine A, Djelloul R, Boukhari A and Bensouici C. 2022. Analysis of phytochemical constituents by using LC-MS, antifungal and allelopathic activities of leaves extracts of aloe vera. *Jordan J Biol Sci.*, **15(1):** 21-28.

Bold HC and Wynne MJ. 1985. Introduction to the Algae Structure and Reproduction Second edition. Prentice-Hall Inc, New Jersey.

Branco-Vieira M, Costa D, Mata TM, Martins AA, Freitas MAV and Caetano NS. 2020. A life cycle inventory of microalgae-based biofuels production in an industrial plant concept. *Energy Rep.*, **6**:397-402.

Brennan L and Owende P. 2010. Biofuels from microalgae- a review of technologies for production, processing, and extractions of biofuels and co-products. *Renew Sustain Energy Rev.*, **14**: 557–577.

Chia SR, Chew KW, Show PL, Yap YJ, Ong HC, Ling TC and Chang J. 2018. Analysis of economic and environmental aspects of microalgae biorefinery for biofuels production: a review. *Biotechnol J*., **13(6):** 1700618.

Chisti Y. 2007. Biodiesel from microalgae. *J Biotech Advances.*, **25**: 294–306.

Deabes MM, Khalil WKB, SKh AEA, Ibrahim SD and Naguib KM. 2022. The Inhibitory Effect of Different Ephedra Plant Extracts on the Aspergillus flavus Growth and Aflatoxin B1 Gene Expression. *Jordan J Biol Sci.*, **15(1):** 59-66.

Fendiyanto MH, Satrio RD, Suharsono, Tjahjoleksono A and Miftahudin. 2019a. Correlation among Snpb11 markers, root growth, and physiological characters of upland rice under aluminum stress. *Biodiversitas.*, **20(5):** 1243-1254.

Fendiyanto MH, Satrio RD, Suharsono, Tjahjoleksono A, Hanarida I and Miftahudin. 2019b. QTL for aluminum tolerance on rice chromosome 3 based on root length characters. *SABRAO J Breed Genet.*, **51(4):** 451-469.

Fendiyanto MH, Satrio RD and Darmadi D. 2020. Metabolic profiling and pathway analysis in red arillus of Salacca sumatrana demonstrate significant pyruvate, sulfur, and fatty acid metabolisms. *Biodiversitas.*, **21(9):** 4361-4368.

Fendiyanto MH, Satrio RD, Widana IDKK, Pratami MP, Nikmah IA and Darmadi D. 2021. Differential hierarchical metabolites expression of red/white Salacca sumatrana arillus and its molecular docking studies. *Biodiversitas.*, 22(2): 1014-1024.

Griffiths MJ and Harrison STL. 2009. Lipid productivity as a key characteristic for choosing algal species for biodesel production. *J Appl Phycol.*, **21**:493- 507.

Ghufran A and Kordi L. 2010. Aquatic Bioata Cultivation for Food, Cosmetics, and Medicine. Andi, Yogyakarta.

Gunawan. 2010. Diversity and characterization of microalgae from hot springs in West Java which are potential sources of biodiesel. Thesis, IPB University, Bogor.

Hajar HAA, Riefler RG and Stuart BJ. 2017. Cultivation of the microalga Neochloris oleoabundans for biofuels production and other industrial applications. *Appl Biochem Microbiol.*, **53(6):** 640-653.

Hamim. 2007. Fisiologi Tumbuhan. Universitas Terbuka Press, Jakarta.

Handoko, Sugiarto Y and Syaukat Y. 2008. The Linkage of Climate Change and Strategic Food Production: An Independent Policy Review in the Sector of Trade and Development. SEAMEO Biotrop, Bogor.

Kamillah WO, Kusumaningrum HP, Ferniah RS, Herida AP and Nasansia GL. 2022. Physiological response and detection of *Inh2* gene in dieng red potato (*Solanum tuberosum* L.) Affected by Frost. *Jordan J Biol Sci.*, **15(1):** 101-106.

Lander JP. 2014. R for Everyone: Advanced Analytics and Graphics. Addison-Wesley, Boston.

Litinas A, Geivanidis S, Faliakis A, Courouclis Y, Samaras Z, Keder A, Krasnoholovets V, Gandzha I, Zabulonov Y, Puhach O and Dmytriyuk M. 2020. Biodiesel production from high FFA feedstocks with a novel chemical multifunctional process intensifier. *Biofuel Res J.*, **26**: 1170-1177.

Mahyudin AR and Koesnandar. 2006. Biohydrogen production: prospects and limitations to practical application. *Akta Kimia Indonesia.*, **1**:73-78.

Metzger P and Largeau C. 2005. *Botryococcus braunii*: a rich source for hydrocarbons and related ether lipids. *Appl Microbiol Biotech.*, **66(5):** 486–496.

Miftahudin M, Roslim DI, Fendiyanto MH, Satrio RD, Zulkifli A, Umaiyah EI, Chikmawati T, Sulistyaningsih YC, Suharsono S, Hartana A, Nguyen HT and Gustafson JP. 2021. *OsGERLP*: A novel aluminum tolerance rice gene isolated from a local cultivar in Indonesia. *Plant Physiol Biochem.*, **162**: 86-99.

Moshood TD, Nawanir G and Mahmud F. 2020. Microalgae biofuels production: A systematic review on socioeconomic prospects of microalgae biofuels and policy implications. *Environmental Challenges.*, **5**: 1-18.

Nybakken JW. 1982. Marine Biology, An Ecologycal Approach. Harper and Row Publisher, New York.

Pandin DS. 2010. Penanda DNA untuk pemulian tanaman kelapa (*Cocos nucifera* L). *Jurnal Perspektif.*, **9(1):** 21-35.

Paynter D and Frölicher TL. 2015. Sensitivity of radiative forcing, ocean heat uptake, and climate feedback to changes in anthropogenic greenhouse gases and aerosols. *J Geophys Res Atmos.*, **120**: 9837-9854.

Peng Y, Fan M, Song J, Cui T, and Li R. 2018. Assessment of plant species diversity based on hyperspectral indices at a fine scale. *Sci Rep*., **8**: 4776.

Pratami MP, Fendiyanto MH, Satrio RD, Nikmah IA, Awwanah M, Farah N, Sari NIP, Nurhadiyanta N. 2022. In-silico Genome Editing Identification and Functional Protein Change of Chlamydomonas reinhardtii Acetyl-CoA Carboxylase (CrACCase). *Jordan J Biol Sci.*, **15(5):** 431-440.

Prartono T, Kawaroe M and Katili V. 2013. Fatty acid composition of three diatom species *Skeletonema costatum*, *Thalassiosira* sp. and *Chaetoceros gracilis*. *Int J Environ Bioenergy.*, **6(1):** 28-43.

Prescott GW. 1978. How to Know the Freshwater Algae, Third edition. Wm C Brown Company Publishers, New York.

Rao AR, Dayananda C, Sarada R, Shamala TR and Ravishankar GA. 2007. Effect of salinity on growth of green alga *Botryococcus braunii* and its constituents. *Biores Technol*., **1(98):** 560–564.

Reine WFP and Trono JGC. 2002. Cryptograms: Algae. Prosea Foundation, Bogor.

Richmond A and Emeritus C. 2013. Handbook of Microalgal Culture Applied Phycology and Biotechnology. Wiley-Blackwell, New York.

Satrio RD, Fendiyanto MH, Suharsono, Supena EDJ and Miftahudin. 2019. Identification of drought-responsive regulatory genes by hierarchical selection of expressed sequence tags and their expression under drought stress in rice. *Intl J Agric Biol.*, **22(6):** 1524-1532.

Satrio RD, Fendiyanto MH, Suharsono, Supena EDJ and Miftahudin. 2021. Genome-wide SNP discovery, linkage mapping, and analysis of QTL for morpho-physiological traits in rice during vegetative stage under drought stress. *Physiol Mol Biol Plants*., **27(11):** 2635-2650.

Shayler HA and Siver PA. 2006. Key to freshwater algae: a web-based tool to enhance understanding of microscopic biodiversity. *J Sci Educ Technol*., **15**: 298–303.

Sidabutar EA. 1999. The Effect of the Type of Microalgae Growth Medium *Chlorella* sp. to the Growth-Promoting Compounds Produced. IPB University Pr, Bogor.

Sutomo A, Ani G and Sutomo G. 2007. Kultur tiga jenis mikroalga (*Tetraselmis* sp., *Chlorella* sp.dan *Chaetoceros gracilis*) dan pengaruh kepadatan awal terhadap pertumbuhan *C. Gracilis* di laboratorium. *Oseano Limnol*., **37**: 43-58.

Teresa M, Anto´nio A, Martins and Nidia SC. 2010. Microalgae for biodiesel production and other application. *Biotech.*, **14**:217–232.

Theodorou ME, Elrifi IR, Turpin DH and Plaxton WC. 1991. Effects of phosphorus limitation on respiratory metabolism in the green alga *Selenastrum minutum*. *Plant Physiol.*, 95: 1089-1095.

Wang Y, Tian RM, Gao ZM, Bougoffa S and Qian PY. 2014. Optimal eukaryotic 18S and universal 16S/18S ribosomal RNA primers and their application in a study of symbiosis. *PloS One*., **9(3):**e90053.

Widianingsih, Ridho A, Hartati R and Harmoko. 2008. Kandungan nutrisi Spirulina platensis yang dikultur pada media yang berbeda. Ilmu Kelautan., **3:** 167-170.

Williams RG, Roussenov V, Goodwin P, Resplandy L and Bopp L. 2017. Sensitivity of global warming to carbon emissions: effects of heat and carbon uptake in a suite of earth system models. *J Climate.*, **12:**9343–9363.

JJBS

Volume 16, Number 1,March 2023
ISSN 1995-6673
Pages 35 – 40
https://doi.org/10.54319/jjbs/160106

Jordan Journal of Biological Sciences

Calcium Nitrate Toxicity on Rat Liver and Kidney Functions: A Biochemical and Histopathological Evaluation

Araar Samia[1,2,*], Khaldi Fadila[1,2], Sayah Sarra[1,2], Chaib Sakina[3] and Gheid Abdelhak[1]

[1]*Laboratory of Sciences and Technology of Water and Environment. Mohamed-CherifMessaadia University, BP 1553, Souk Ahras 41000, Algeria;*[2]*Department of Biology, Faculty of Natural and Life Sciences, Mohamed-CherifMessaadia University, BP 1553, Souk Ahras 41000, Algeria;*[3]*Laboratory of Environmental Biosurveillance (LBSE), Department of Biology,Faculty of Sciences, Badji MokhtarUniversity, BP 12 Sidi Amar, 23000 Annaba, Algeria*

Received: March 8, 2022; Revised: June 17, 2022; Accepted: June 30, 2022

Abstract

Calcium NitrateTetrahydrate is a wide-used nitrogen fertilizer in Algerian agriculture. The present study was aimed to examine the toxic effects of calcium nitrate on kidney and liver functional biochemical markers. Twenty-eight male albino *wistar* male rats were divided into three treated groups receiving orally 200, 400 and 800mg/kg of calcium nitrate, and one untreated control group. Results showed a dose- dependent increase in kidney and liver relative weights, serum levels of glucose, cholesterol, triglyceride, blood urea, creatinine, and uric acid, and enzymatic activity of transaminases and alkaline phosphatase. However, serum protein and albumin levels were significantly decreased in a dose dependent manner as compared with those of control group. In addition, hepatic and renal histological changes were evidenced by hepatocyte degeneration, necrosis, dilation and sinusoid congestion, atrophy of glomeruli, vascular congestion, and infiltration of inflammatory cells. It is noteworthy that these adverse stress effects were higher in 400 and 800 mg/kg calcium nitrate treated rats than those treated with 200mg/kg and control group. In conclusion, the study proved the effective ability of subacute exposure of calcium nitrate to induce liver and kidney stress dysfunctions.

Keywords: Calcium Nitrate; Histology; Liver and kidney stress dysfunctions; Rats

1. Introduction

Synthetic fertilizers are widely used in agriculture as a quick and less expensive source of delivering plant nutrients leading to increase productivity (Ahmad et *al*., 2017) and agricultural yield, but soil, air and water contamination effects on human and environmental health limit its use (Panico et *al*., 2020; Elahi et *al.*, 2019; Li et *al.*, 2019). Calcium is an essential macronutrient for a variety of biological functions (Meriño-Gergichevich et *al*., 2010), including regulation of plant growth and development (Hepler, 2004). Hence, calcium fertilizers such as calcium nitrate and calcium chloride, the most common calcium fertilizer forms, can be used to increase the calcium content of fruits (Lanauskas et *al.*, 2012). Calcium can be delivered quickly from calcium nitrate to crops in fertigation systems, as well as to those of rapid growth and those undergoing specific periods of high calcium demand(Martínez et *al.*, 2013).Further, nitrates, the end product of nitrogen fertilization, can be washed into water streams when it is not absorbed by plant roots, and, noteworthy, the green leafy foods like lettuce have the highest nitrate levels, the 60% of total nitrousoxide emissions could be linked to agricultural soil management practices (Vitale et al., 2017; Liu et *al*., 2014).Additionally, consumption of nitrates or nitrite in drinking water and food may result in the onset of health condition disorders, such as methemoglobinemia and cancers of the stomach, liver, colon, and lungs in humans, and particularly thyroid and kidney cancers, and non-Hodgkin's lymphoma (Espejo-Herrera et *al.*, 2015).Moreover, the nitrate reduction process starts with mouth bacterial flora producing nitrate reductase enzymes, and hence about 25% of ingested nitrate can be converted to NO_2 in the mouth. The acidic pH of the stomach promotes the formation of nitrous acid, which can be metabolized into various nitrogen oxides, including nitrogen dioxide (NO_2^{-2}) and dinitrogen trioxide (N_2O_3) depending on the redox environment and gastric content. In addition, enterosalivary circulation of nitrate has been described after its absorption in the intestine, where it is converted into nitrite in the mouth and, then the cycle is restarted (Pereira et *al*., 2013). Of note, the metabolism of nitric oxide and nitrosamine in the body results in the formation of nitrate which is reported as the highly carcinogenic agent leading to carcinoma of the stomach, liver, and esophagus (Kim et *al.*, 2002).Several studies have reported the effects of nitrate induced-alterations liver and kidney biochemical markers in experimental animals(Azzez et *al*., 2011).Therefore, the present work aims to study the biochemical and histological stress effects of calcium nitrate on hepatic and renal functions in rats.

* Corresponding author. e-mail: araar.samia01@gmail.com.

2. Materials and Methods

2.1. Chemical materials

Calcium nitrate tetra-hydrate ($Ca(NO_3)_2$-$4H_2O$) as Calnisol® (Case number: 10124-37-5) was purchased from a fertilizer company named Profert, Bejaia, Algeria.

2.2. Biological materials

Twenty-eight male albino wistar rats weighing 240 ± 20 g and obtained from the Pasteur Institute, Algiers of Algeria were housed on sawdust in plastic cages in an animal house of our Institution maintained with a temperature of 25±2° C, humidity 50±10%, and natural photoperiod. Animals were fed ad-libtium with sticks consisting of corn, barley, milk and vitamin supplements, and tap drinking water.

2.3. Experimental procedures

Rats were acclimated 21days before experiments, and then were divided randomly into three (seven rats/group) treated groups that received 200, 400, and 800mg/kg doses of calcium nitrate respectively, and one untreated control group of seven rats per group. Calcium nitrates were dissolved in mineral water and were given orally to rats for 30 days. Thereafter, animals were sacrificed by cervical decapitation, and blood samples were collected into heparinized tubes for the biochemical analyses. Liver and kidney organs were removed for histo-pathological evaluation.

2.4. Biochemical analyses

The blood samples were centrifuged for 15 minutes at 3000 rpm, and the resulting plasma was stored at -20°C to be used for the spectrophotometric evaluation of biochemical parameters (glucose, cholesterol, triglycerides, transaminases (ASAT and ALAT), alkaline phosphatase (ALP), total proteins, albumin, creatinine, urea and uric acid) using commercially available diagnostic kits (Diagnopharm, Bouira, Algeria;Réf, B07050012, B11010011, B16010011, B18005022, B17005022, B20005022,, B08030013, B24050012, B05020022, B10020024 and B01010011 respectively) using a fully automated chemistry analyzer.

2.5. Histological examination

The liver and kidney from the experimental rats were removed, rinsed with physiological water and fixed in Bouin's solution for 24 hours, and embedded in paraffin wax. The tissue sections were then cut into slices of 5 µm thickness by a rotary microtome, and stained with hematoxylin and eosin (Hould, 1984). The preparations were dried and observed with an optical microscope (OPTIKA brand).

2.6. Statistical analysis

Data were expressed as mean ± SD values. The comparison between control and treatments was tested by Student's t-test using IBM SPSS Statistics 23.0 software. Differences were considered statistically significant at $p<0.05$.

3. Results

3.1. Physiological observations

The liver relative weights (bwt) per 100g of the animal body were significantly higher in 400 and 800 mg/kg calcium nitrate treated rats than those of 200mg/kg and controls since kidney relative weights showed no significant changes (Tab.1).

Table 1. Changes in hepatic and renal relative weights in control rats and treated rats (data are given as mean ± SD, 7rats/group).

Parameters	Treatments			
	Control	200mg /kg	400mg/ kg	800mg/kg
Relative liver weight (g/100 g b.w) Relative kidney weight (g/100 g b.w)	2.70±0.14 0.23±0.01	2.74±0.14 0.24±0.02	3.01±0.24* 0.24±0.02	3.06±0.17*** 0.24±0.02

*p <0.05; ***p < 0.001: Significant difference compared to the control group.

3.2. Biochemical results

The serum levels of glucose, cholesterol and triglycerides were significantly increased in treated groups compared with control group (Table 2). As indicated in Tables 3, calcium nitrate treatments caused a significant elevation in the enzymatic activity of transaminases (ASAT, ALAT) and alkaline phosphatase (ALP) enzymatic activities, along with a marked decrease in protein and albumin levels. In addition, the levels of serum blood urea, creatinine, and uric acid levels were higher in calcium nitrate treated rats compared to controls (Table.4).

Table 2. Lipid profiles in control and treated rats (Data are given as mean ± SD, 7 rats/group).

Parameters	Treatments			
	Control	200mg/kg	400mg/kg	800mg/kg
Glucose (g/l)	1.12±0.07	1.15±0.09	1.21±0.05**	1.25±0.05***
Cholesterol (g/l)	0.96±0.08	0.96±0.07	1.05±0.05*	1.11±0.05***
Triglycerides (g/l)	0.68±0.17	0.67±0.07	0.80±0.03*	0.86±0.04**

*p < 0.05; **p < 0.01; ***p < 0.001: Significant difference compared to the control group.

Table 3. Hepatic biochemical profiles in control and treated rats (data are given as mean ± SD, 7 rats/group).

Parameters	Treatments			
	Control	200mg/kg	400mg/kg	800mg/kg
ASAT (U/L)	114.61±16.29	111.73±10.30	123.37±5.35	134.67±5.29**
ALAT (U/L)	67.60±9.03	63.40±9.50	73.41±4.45	78.73±5.69**
ALP (U/L)	117.16±5.46	118.31±10.02	129.67±5.41	137.14±7.40**
Total protein (g/l)	71.17±5.18	64.37±8.17	60.87±4.09***	59.56±3.12***
Albumin (g/l)	36.00±1.85	35.04±1.14	33.98±1.70*	33.51±1.27**

*p < 0.05; **p < 0.01; ***p < 0.001: Significant difference compared to the control group.

Table 4. Renal biochemical profiles in control and treated rats (Data are given as mean ± SD, 7 rats/group).

Parameters	Treatments			
	Control	200mg/kg	400mg/kg	800mg/kg
Urea (mg/dL)	40±0.2	40±0.3	42±0.2	43±0.2**
Creatinine (mg/dL)	1.17±0.10	1.19±0.09	1.21±0.08	1.30±0.05**
Uric acid (mg/dL)	4.75±0.54	4.59±0.48	4.94±0.44	5.31±0.44*

*p < 0.05; **p < 0.01: Significant difference compared with the control group.

3.3. Histopathological observations

As shown in Figs 1 & 2, liver and kidney sections from rats treated with 200, 400, and 800 mg/kg doses of (Ca $(NO_3)_2 4H_2O$) for 30 days revealed marked histological alterations when compared with those of control rats, showing regular histological architecture with hexagonal lobules, and visible capillary sinusoids (Fig1A, B). No histological damage was found in the liver of the 200mg/kg (Ca $(NO_3)_2 4H_2O$) treated group compared with the control group, while the higher doses (400 and 800mg/kg) showed considerable vascular dilation and congestion, degeneration of hepatocytes, hemorrhage, and lipid vacuolation, and thus moderate inflammations compared to the control group (Fig 1, C – F). Moreover, Microscopic observations of renal tissues from (Ca $(NO_3)_2 4H_2O$) treated rats showed severe histopathological changes evidenced by glomerular atrophy associated with dilation of Bowman's space, intra-glomerular hemorrhage, and vascular congestion (Fig 2, B- D) when compared with kidney from control rats showing normal renal parenchyma with well-defined renal glomeruli and tubules (Fig 2A).

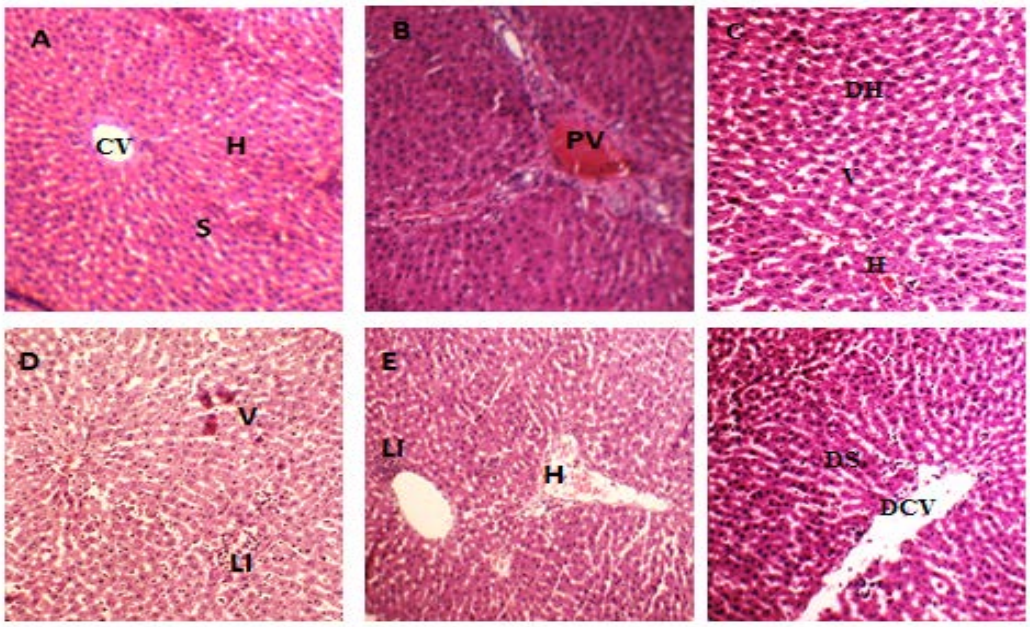

Figure 1. Photomicrograph of liver histology stained with H&E from control rats and rats treated with calcium nitrate for 30 days. The control group's liver sections revealed normal preserved histoarchitecture (A-B). The damage caused by calcium nitrate in liver sections (C–H) increases in a concentration-dependent manner.

CV, centralvein; S, sinusoids; H, hepatocyte;DH, degenerated hepatocyte; V,vacuoles; H, hemorrhage; LI, leucocyte infiltrations; DCV,dilated central vein; DS, dilatedsinusoid;

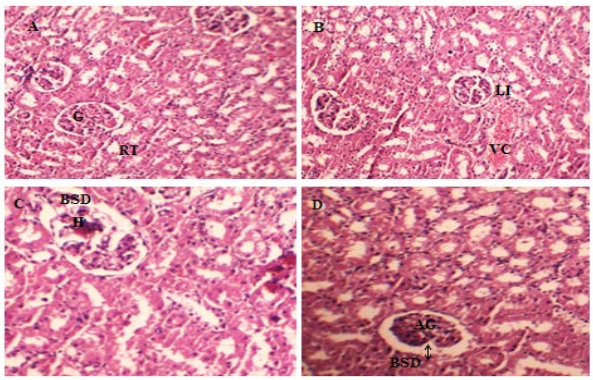

Figure 2. Photomicrographs of H&E-stained kidney histological sections from control and treated rats. The control group's kidney sections revealed normal preserved histoarchitecture (A). The damage caused by calcium nitrate in kidney sections (B–D) increases in a concentration-dependent manner.

AG, atrophy of glomerulus; BSD, Bowman's space dilatation; VC,vascular congestion; LI, lymphocyte infiltration; H, haemorrhage

4. Discussion

The intensified use of synthetic fertilizers, including nitrate fertilizers leads to multiple human health problems (WHO, 2006). The chemical components of the fertilizers can affect the digestion and absorption processes and the metabolic use of ingested food(Weil and McCollister, 1963; OCDE, 2000).Nitrates from fertilizers applied on soil surface or animal excrements contaminated drinking water reserves can seep into groundwater, and cause consequently human and animal health problems (Lockhart, 2013).Thus, the present study was conducted to evaluate the potential toxicity of (Ca $(NO_3)_2 4H_2O$), a nitrogen fertilizer, in rats. The organ weights are a valuable tool in assessing the in vivo toxicity of a xenobiotic (Bailey et *al.*, 2004; Sellers et *al.*,2007). In this regard, our results revealed significant increase in the liver relative weights. This result is in agreement with the study of Lee et al. (2020) reporting an increase in the hepato-somatic ratio in rats that received 1000mg/kg/day of ammonium nitrate, in addition to the result of Bouaziz-Ketata et *al.*, (2014) showing an increase in relative liver weight in rats treated with $NaNO_3$ for 7 weeks. This hepatomegaly can be explained by the over-espression of oxidative stress and over-excitation of the liver detoxification process in response to the harmful effect of xenobiotics (Guerriero et *al.*, 2014; Abdel-Gawad et *al.*, 2020).Furthermore, blood glucose level was significantly increased in treated rats compared with controls, and this concords with those previously reported (Azzez et *al*., 2011; Delgadoa et *al.*,2018).The hyperglycemia due to calcium nitrate treatment is likely explained by the activation of the glycogenolysis process, resulting in the release of glucose by glycogen phosphorylase under the action of amylase(Hijmans et *al.*, 2014).Several European research studies have attempted to discover a close association between nitrate concentration in drinking water and insulin-dependent diabetes by increasing blood glucose while decreasing hepatic glycogen (IDD), but the comparison revealed sparse and contradictory data(Moltchanova et *al.*,2004).On the other hand, results showed a very highly significant increase in the levels of cholesterol and triglycerides. This hyperlipidemia can be explained by hypothyroidism(Jublanc and Bruckert, 2004; Pearce, 2004).Previous *in vivo* experimental studies have proven that inorganic nitrate is a short-term goitrogenic agent causing hypertrophy of the epithelial cells of the thyroid gland(Boukerche et *al*., 2007; Gatseva and Argirova, 2008; Messaadia et *al*, 2013).On top of that, (Ca $(NO_3)_2 4H_2O$) treated rats for 30 days resulted in an elevation of enzymatic activity of transaminases (AST, ALT) and alkaline phosphatase (ALP) and bilirubin level, and a lowering of total protein and albumin levels. This result is in line with that previously reported (Messaadia et *al*., 2013; Fouad et *al.*, 2017; Kattiaa et *al.*, 2017). In addition, increased levels of ALT and AST in the blood indicate their increased release in blood following hepatocyte necrosis leading to liver impaired function (Krim et *al.*,2013). As previously reported, the concentration of transaminases (AST, ALT) may become high in ammonium nitrate (Messaadia et *al*., 2013) or sodium nitrate treated rats (Delgadoa et *al*.,2018). In this study, calcium nitrates induced a marked decrease in blood total protein levels. A similar result was reported in adult rats treated with sodium nitrate in drinking water at concentrations of 550 mg/L for four months (Azza *et al*., 2011). The decline in blood total protein levels is mainly due to the effects of nitrate on the liver, either through necrotic alterations or other mechanisms (Anthony et *al*., 1994). Additionally, waste products from protein metabolism that are eliminated by the kidneys, such as blood creatinine, urea, and uric acid concentrations, are usually regarded as indicators of kidney function (Tootian et *al*., 2012). Accordingly, our results showed a significant increase in blood urea, creatinine, and uric acid levels in response to ($Ca(NO_3)_2 4H_2O$)toxicity, similar to those previously reported (Messaadia *et al.*, 2013).The increased blood urea, uric acid, and creatinine levels suggested impaired renal function as evidenced by changes in reabsorption threshold, renal blood flow, and glomerular filtration. The results of the present work indicated that (Ca $(NO_3)_2 4H_2O$) induces histopathological alterations in the liver characterized by venous congestion, mononuclear cell infiltration, cytoplasmic vacuolation of hepatocytes, and fatty degeneration. These histological alterations were similarly reported in some previous studies (Bouaziz-Ketata et *al*., 2014; Kattaia et *al*., 2017; Delgadoa et *al*., 2018; Ikele et *al*., 2021), and in return, calcium nitrate treatment resulted in the dilation of the renal tubules, atrophy of the glomeruli, and leukocyte infiltration. In this regard, Anwar and Mohamed (2015) reported glomerular atrophy and renal blood vessel congestion in the kidneys of rats treated with 500 mg/L $NaNO_3$ for 4 and 6 weeks.

5. Conclusion

(Ca $(NO_3)_2 4H_2O$) caused marked dose-dependent changes in liver and kidney biochemical stress profiles and consequently led to renal insufficiency without hepatotoxicity. Conclusively, the excessive use of higher doses of calcium nitrate may place mammalian and human health at risk.

Acknowledgments

The results were obtained within the project ATRP/ code N°: D01N01UN410120180001"Origin and diversification of pollution (water, air and soil) by heavy metals of some biotopes by the use of bio-indicator models" funded by Directorate General for Scientific Research and Technological Development (DGRSDT)

Conflict of Interests

None.

References

Abdel-GawadFKh, Khalil WKB, Bassem SM, Kumar V, Parisi C, Inglese S,Temraz TA,Nassar HF, Guerriero G. 2020.The duckweed, *Lemna minor* modulates heavy metal-induced oxidative stress in the Nile tilapia *Oreochromisniloticus. Water*,**12**(11): 2983. https://doi.org/10.3390/w12112983.

Ahmed M, Rauf M, Mukhtar Z and Saeed NA. 2017. Excessive use of nitrogenous fertilizers: an unawareness causing serious threats to environment and human health. *Environ Sci Poll Res*, **24**(35): 26983-26987.https://doi.org/10.1007/s11356-017-0589-7.

Anthony ML, Gartland KP, Beddell CR, Lindon JC and Nicholson JK. 1994. Studies of the biochemical toxicology of uranyl nitrate in the rat. *Arch Toxicol*, **68**(1): 43-53.

Anwar M.M and Mohamed NE. 2015. Amelioration of liver and kidney functions disorders induced by sodium nitrate in rats using wheat germ oil. *J Radiat Res Appl Sci*, **8** (1) : 77–83. https://doi.org/10.1016/j.jrras.2014.11.004

Azza M, El-Wakf MES, Elhabiby MW, El-kholy EGE and El-Ghany EA. 2011. Use of tumeric and curcumin to alleviate adverse reproductive outcomes of water: Nitrate pollution in male rats. *Nat Sci*, **9**: 229-239.

Azzez OH, Mahmood MB and Hassan. 2011. Effect of nitrate poisoning on some biochemical parameters in rats. *Iraqui J Vet Sci*,**25** (2): 47–50.

Bailey SA, Zidell RH and Perry RW. 2004. Relationships between organ weight and body/brain weight in the rat: what is the best analytical endpoint?.*Toxicol Pathol*, **32**(4) :448-466.https://doi.org/10.1080/01926230490465874

Bouaziz-Ketata H, Salah GB, Salah HB, Marrekchi R, Jamoussi K, Boudawara T, Fakhfekh F and Zeghal N .2014. Nitrate-induced biochemical and histopathological changes in the liver of rats: ameliorative effect of Hyparrheniahirta. *Biomed Environ Sci* ,**9**: 695–706. https://doi.org/10.3967/bes2014.105.

Boukerche S, Aouacheri W and Saka S. 2007. The toxic effects of nitrates : biological study in, humans and animals. *Ann Biol Clin*,**65**(4): 385-391.https://doi.org/10.1684/abc.2007.0136.

Delgado MG, Zamora AG, Gonsebatt ME, Mata EM, Vargas GG, Rincón E C and Morales R P. 2018. Subacute intoxication with sodium nitrate induces hematological and biochemical alterations and liver injury in male Wistar rats. *Ecotoxicol Environ Saf*, **166**: 48-55. https://doi.org/10.1016/j.ecoenv.2018.09.060

ElahiE,Weijun C, Zhang HandNazeer M .2019. Agricultural intensification and damages to human health in relation to agrochemicals: application of artificial intelligence. *Land Use Policy*,**83:** 461–474. https://doi.org/10.1016/j.landusepol.2019.02.023.

Espejo-Herrera N, Cantor K, Malats N, Silverman D, Tardon A and García-Closas, 2015. Nitrate in drinking water and bladder cancer risk in Spain. *Environ Res*, **137**: 299–307. https://doi.org/10.1016/j.envres.2014.10.034

Fouad SS, Mohi-Eldin M, HaridyM and Khalil A. 2017. Ameliorative effects of ascorbic acid (Vit. C) against sodium nitrite toxicity in albino rats: hematological, biochemical and histopathological studies. *Am-Euras. J. Toxicol. Sci*, **9** (1): 01 06.https://doi.org/10.5829/idosi.aejts.2017.01.06.

Hepler PK. 2005. Calcium: a central regulator of plant growth and development. *Plant Cell*, **17**(8): 2142-2155.https://doi.org/10.1105/tpc.105.032508.

Hijmans BS, Grefhorst A, Oosterveer MH and Groen AK. 2014. Zonation of glucose and fatty acid metabolism in the liver: mechanism and metabolic consequences. *Biochem*, **96:** 121–129. https://doi.org/10.1016/j.biochi.2013.06.007.

Hould R. 1984. **Techniques d'histopathologie et de cytopathologie.** Ed Maloine**19**(21):225–227

Ikele, C. B., Okwuonu, E., andIjem, A. N. 2021. Further studies on evaluation of the toxicity potential of Terminalia catappa Lin. Combretaceae leaf extract: effects on the histology, liver enzymes, and haematology profile of albino rats. *JJBS*, **14**(5), 890-897.https://doi.org/10.54319/jjbs/140502.

Guerriero G, Trocchia S, Abdel Gawad FKh, Ciarcia G. 2014. Roles of reactive oxygen species in the spermatogenesis regulation. *Front. Endocrinol.*, 5:56. https://doi.org/10.3389/fendo.2014.00056

Jublanc C and Bruckert E. 2004. Hypothyroidism and cardiovascular disease : role of new risk factors and coagulation parameters. *Semin Vasc Med* ,**4**(2) : 145-151 . https://doi.org/10.1055/s-2004-835372.

Kattaia A, El-Baseta S, Mohameda E, Abdul-Maksoub R and Elfakharanyc Y. 2017. Molecular mechanisms underlying histological and biochemical changes induced by nitrate in rat liver and the efficacy of S-Allylcysteine. *Ultrastruct. Pathol*, 41(1): 10–22. https://doi.org/10.1080/01913123.2016.1252821.

Kim HJ, Chang WK, Kim MK, Lee SS and Choi BY. 2002. Dietary factors and gastric cancer in Korea: Case-control study. *Int Jr Cancer*, **97**: 531-535.https://doi.org/10.1002/ijc.10111.

Krim M, Messaadia A, Maidi I, Aouacheri O and Saka S. 2013. Protective effect of ginger against toxicity induced by chromate in rats. *Ann Biol Clin*, **71**(2): 165-173.

Lanauskas J, Kviklienė N, Uselis N, Kviklys D, Buskienė L, Mažeika R and Staugaiti G. 2012. The effect of calcium foliar fertilizers on cv. *Ligol Appless Plant Soil Environ*, **58:** (10): 465–470.

Lee MJ, Chung YH, Choi HY and Cha HG. 2020. Evaluation of subchronic repeated administration toxicity of ammonium nitrate in rats. *Toxicol Res*, **36**(2): 115-122. https://doi.org/10.1007/s43188-019-00022-4.

Li M, Wiedmann T andHadjikakou M. 2019. Towards meaningful consumption-based planetary boundary indicators: the phosphorus exceedance footprint. *Glob Environ Change*,**54 :** 227–238. https://doi.org/10.1016/j.gloenvcha.2018.12.005.

Liu CW, Sung Y, Chen BC and Lai HY. 2014. Effects of nitrogen fertilizers on the growth and nitrate content of lettuce (Lactucasativa L.) *Intl J Environ Res Public Health*, 11: 4427–4440.https://doi.org/10.3390/ijerph110404427

Lockhart KM, King AM and Harter T. 2013. Identifying sources of groundwater nitrate contamination in a large alluvial groundwater basin with highly diversified intensive agricultural production. *J Contam. Hydrol*, **151:** 140-154.https://doi.org/10.1016/j.jconhyd.2013.05.008

Martínez LM, Velasco VAV, Luna JR, Valle JRE, Ángeles GVC and Lugo MLM. 2013. Effect of calcium nitrate and substrates on tomato yield. *Rev Mex Cienc Agríc*, **4:**1175–1184.

Meriño-Gergichevich C,Alberdi M, Ivanov AG and Reyes-Díaz M. 2010. Al3+–Ca2+ interaction in plants growing in acid soils: Al phytotoxicity response to calcareous amendments. *J Soil Sci Plant Nutr*, **10**:217–243.

Messaadia A, Saka S, Krim M, Maidi I, Aouacheri O and Djafer R. 2013). Ginger supplemented diet ameliorates ammonium nitrate-induced oxidative stress in rats. *Afr J Biotechnol*, **12** (49): 5909–5916. https://doi.org/10.5897/AJB2013.13118.

Moltchanova E, Rytkonen M, Kousa A, Taskinen O, Tuomilehto J and Karvonen M. 2004. Zinc and nitrate in the ground water and the incidence of type 1 diabetes in Finland. *Diabetes Med*, **21**: 256-261.https://doi.org/10.1111/j.1464-5491.2004.01125.x

Organization for Economic Cooperation and Development (OECD). 2000. Guidance Notes for the Analysis and Evaluation of Repeat Dose Toxicity Studies. Environment, Health and Safety Publications Series on Testing and Assessment, Environment Directorate, OECD, Paris, pp. 27–72.

Panico S C, Esposito F, Memoli V, Vitale L, Polimeno F, Magliulo V, Maisto G, De Marco A. 2020. Variations of agricultural soilqualityduring the growth stages of sorghum and sunflower. *Applied Soil Ecology*,**152** : 103569. https://doi.org/10.1016/j.apsoil.2020.103569.

Pearce EN. 2004. Hypothyroidism and dyslipidemia: modern concepts and approaches. *Curr Cardiol Rep*,**6**(6): 451-456.

Pereira C, Ferreira N, Rocha B, Barbosa R andLaranjinha J. 2013. The redox interplay between nitrite and nitric oxide: from the gut to the brain. *Redox Biol*, **1:** 276–284. https://doi.org/10.1016/j.redox.2013.04.004

Sellers R S, Mortan D, Michael B, Roome N, Johnson JK, Yano BL, Perry R and Schafer K. 2007. Society of Toxicologic Pathology position paper: organ weight recommendations for toxicology studies. *Toxicolpathol*, **35**(5) :751-755.https://doi.org/10.1080/01926230701595300

Tootian Z, Monfared AL, Fazelipour S, Shybani MT, Rouhollah F, Sasani F and Molaemi E. 2012. Biochemical and structural changes of the kidney in mice exposed to phenol. *Turkish J Med Sci*, **42**(4): 695-703.

Vitale L, Polimeno F, Ottaiano L, Maglione G, Tedeschi A, Mori M, De Marco A, Di Tommasi P, Magliulo V. 2017. Fertilizer type influences tomatoyield and soil N2O emissions. *Plant Soil Environ*, **63** : 105–110. https://doi.org/10.17221/678/2016-PSE.

Weil SC and McCollister DD .1963. Relationship between short and long-term feeding studies in designing an effective toxicity test. *J Agric Food Chem*, **11**: 486 – 491.

WHO .2006. World Health Organization, Nitrate and potential endogenous formation of N-nitrosocombounds Food Additives Series: no 50 Who. Geneva, P1-9 24. Kostogrys, R. B., Pisulewski,

JJBS

Volume 16, Number 1,March 2023
ISSN 1995-6673
Pages 41 – 53
https://doi.org/10.54319/jjbs/160107

Jordan Journal of Biological Sciences

Astragalus sarcocolla Gum-mediated a Novel Green-synthesis of Biologically Active Silver-Nanoparticles with Effective Anticancer and Antimicrobial activities

Abeer A. Abd El Aty[1,*], Shifaa O. Alshammari[1], Reem M. Alharbi[1], Ahmed AF. Soliman[2]

[1]*Department of Biology, College of Science, University of Hafr Al Batin, P.O. Box 1803, Hafr Al Batin, Saudi Arabia;* [2] *Drug Bioassay-Cell Culture Laboratory, Pharmacognosy Department, National Research Center, Dokki, Giza, 12622, Egypt.*

Received: May 4, 2022; Revised: June 28, 2022; Accepted: July 6, 2022

Abstract

Cancer diseases and microbial infections are the subject of several ongoing recent researches. In this paper, aqueous extract of red and yellow *Astragalus sarcocolla* gum was used as safe and green agent, for the synthesis of novel biologically active silver-nanoparticles. Six silver nanoparticles (AgNPs) with different characters were obtained using *sarcocolla* gum at (5, 10 and 20 mg/ml (w/v)) concentrations. All biosynthesized AgNPs were characterized using UV–visible spectroscopy, Transmission Electron Microscopy (TEM), and Dynamic light scattering (DLS). Cytotoxic effect of *sarcocolla* gum-AgNPs against five human cancer cells and one normal cells was determined using the MTT (3-(4, 5-dimethylthiazol-2-yl)-2, 5-diphenyltetrazolium bromide) assay. The semi rounded particles formed from 5mg/ml red gum (AgNPs-RG1) and having 9.23±3.66 nm size range were the most active and possessed high cytotoxic effect against, A549 lung, pc3 prostate, Mcf-7 breast and paca2 pancreatic cancers, with IC_{50} values (88.4,75.6, 72.2& 55.0 ug/ml, respectively), but showed low cytotoxic effect (20 % at 100ug/ml) against human normal cells (BJ-1). On the other hand, the spherical to cubic shaped nanoparticles obtained from 5mg/ml yellow gum (AgNPs-YG1) with 10.92 ± 5.48 nm size range, showed good cytotoxic effect against three cancer cells (PC3 prostate, MCF-7 breast and paca2 pancreatic) with IC_{50} values (75.0, 82.8 and 81,6ug/ml respectively), and normal cells(BJ-1) with IC_{50} value (81.8ug/ml). Antibacterial and antifungal activities of the synthesized red and yellow gum-mediated AgNPs with different sizes and shapes were also investigated. Particles biosynthesized from 5 and 10 mg/ml red gum (AgNPs-RG1, RG2) and 5mg/ml yellow gum (AgNPs-YG1) exhibited broad spectrum antimicrobial effects against all tested pathogenic gram-positive, gram-negative bacterial strains, unicellular yeast and filamentous fungi. Based on these results, it can be concluded that the synthesized silver nanoparticles from low concentrations of *sarcocolla* gum have significant biomedical applications.

Keywords: Green-synthesis, *Astragalus sarcocolla* gum, Biosynthesis, AgNPs, Anticancer, Antimicrobial.

1. Introduction

Different microbial infection diseases and severe cancers are the most widely spread and diagnosed diseases worldwide (Mackey *et al*., 2014). Repeated use of current conventional treatments of synthetic antibiotics against microbial infection diseases, causes the antibiotic resistance, and inadequate treatments of these drugs (Bisht *et al*., 2010). On the other hand, using synthetic radiation therapy, surgery, generic drugs, chemotherapy, and hormone therapy did not show an effective result in cancer disease treatments (Qi *et. al.*, 2015; Akram *et al*., 2017). Therefore, more effort has been made to search for new low-cost materials with high efficiency for treating these diseases. The production of metal nano-particles made with natural biomolecules was considered as novel and effective alternative antimicrobial and anticancer modalities (Vasan *et al*., 2019).

Silver nanoparticles (AgNPs) are considered one of the most potential researched metal nanoparticles with high biological activities due to their unique physical properties, particularly their small size, large surface area, stability, and tunable size (Raghavendra *et al*., 2016; Pandey *et al*., 2016, Alharbi *et al.*, 2023). The biological applications of AgNPs have been greatly demonstrated in the fields of biotechnology, pharmaceuticals and medicine (Raghavendra *et al*., 2016; Lee and Jun, 2019). In addition, several researches indicated that involving the integration of nano-particles with biological molecules led to the development of antimicrobial agents, therapies in cancer, therapeutic medicines, drug delivery systems, labeling agents, etc. (Roy *et al*., 2015a, Song and Kim 2009, Kokila *et al.*, 2015, Daniel and Astruc 2004).

AgNPs are generally synthesized using various synthetic methods such as photochemical, chemical, electrochemical and γ-irradiation (Li *et al*., 2007; Raju *et al*., 2014). Most of these synthetic methods are hazardous due to application of toxic chemical agents which pose

* Corresponding author. e-mail: abeerab@uhb.edu.sa, aabass44@yahoo.com.

environmental problems and biological hazards (Mehndiratta *et al*., 2013). In recent times, much effort is being focused, by researchers, to prepare AgNPs using "green chemistry approaches", in which silver salts are biologically reduced to AgNPs using nontoxic and natural low cost polymers such as bacterial biomass (Abd El Aty and Zohair, 2020), Fungi (Abd El Aty *et al.*, 2020), algae (Alharbi *et al*., 2020), Yeasts (Ammar *et al.*, 2021), plant extracts (Parveen *et al*., 2016) and extracts of different natural gums, i.e., *kondagogu*-gum (Rastogi et al., 2014), *salmalia malabarica* gum (Murali krishna *et al.*, 2015) guar gum (Pandey and Mishra 2014, Pandey and Mishra, 2016), ghatti gum (Kora *et al.*, 2012). These biopolymers are used as both stabilizing and reducing agents (Demchenko *et al.*, 2020; Wang *et al.*, 2021). *Astragalus sarcocolla* a historical shrub, belongs to the Fabaceae family able to form the gum as a secondary metabolite. *Sarcocolla* gum is one of the most famous gum resins in Kingdom of Saudi Arabia used in folk medicine for treating wounds, flatulence and used as antiviral agent to prevent various winter diseases in children (Ababutain, 2017).

Based on the research articles published on the medicinal applications of the genus "*Astragalus*", we have noticed that *sarcocolla* gum resin has not been studied as a reducing and capping agent for biological synthesis of AgNPs. Therefore, the objective of this study is to explore the potential green synthesis of AgNPs with *Astragalus sarcocolla* gum aqueous extract as a reducing, capping, and stabilizing agent and ascertain characterization of gum-AgNPs. Also, the biological activity of silver-nanoparticles as antibacterial and anticancer agents was evaluated on Gram-positive and Gram-negative bacteria, yeast, fungi and five carcinoma cell lines for their potential biomedical applications.

2. Materials and Methods

2.1. Preparation of Astragalus sarcocolla gum aqueous extract

Sarcocolla red and yellow gum of the *Astragalus sarcocolla* tree was obtained from local herbarium market in Hafr Al Batin City, Saudi Arabia. Red (**RG**) and yellow (**YG**) gum was ground separately using ceramic mortar into a fine powder in a 100 ml Erlenmeyer flask. 1 g of fine powder along with 20 ml of distilled water was stirred for 60 min on magnetic starrier (60rpm and 30°C). Further, the aqueous extracts were centrifuged at 5000 cycle/min for 10 min., and the stock extracts of (50 mg/ml) concentration were stored at 4 °C for future studies.

2.2. Protein content

According to Lowry *et al.* (1951), the protein concentration in stock extracts of red and yellow gum was assayed.

2.3. Green-synthesis of silver nanoparticles

Three different concentrations of (5, 10, 20 mg/ml) were prepared from red and yellow stock aqueous extracts and evaluated for biosynthesis of nano-silver. 10 ml of each prepared concentration was mixed with 5 ml of 4mM $AgNO_3$ separately at 10 pH and incubated in a dark rotating shaker of 150 rpm and 28-30 °C for 24 hours (Abd El Aty *et al.*, 2020).

2.4. Characterization techniques

2.4.1. UV–visible spectroscopy

The formation of silver nanoparticles was initially detected by visual observation of color change from pale red and pale yellow to reddish-brown color. The bio-reduction of silver ions was monitored by UV–Visible spectrophotometer. The absorption spectrum of the aqueous filtrate was scanned in the range of 200–800 nm. The sharp peak given by UV visible spectrum indicated the formation of AgNPs at the absorption range 400–450 nm.

2.4.2. Transmission Electron Microscopy (TEM)

TEM analysis was performed to determine the morphology, size and shape of the silver nanoparticles. TEM measurements were done by (TEM; JEOL, JEM-2100, Japan) according to Ammar *et al*. (2021).

2.4.3. 2.4.3. Dynamic light scattering (DLS)

Zeta potential and distribution of particle size were measured using Dynamic Light Scattering (Particle Sizing Systems, Inc. Santa Barbara, California, USA) in the range of 0.1–1000 μm. Dynamic light scattering system (DLS) was used for the analysis of average size and distribution of particles in solution which gives the hydrodynamic diameter of particles.

2.5. Cytotoxicity assay

2.5.1. Cell culture

Cytotoxic assays were performed using five human cancer cell lines namely (A549 lung cancer, HCT116 colon cancer, MCF-7 breast cancer, PC3 prostate cancer, and paca2 pancreatic cancer) and one humane normal cell line (BJ-1), all cells purchased from the karolinska center, Department of oncology and pathology, Karolinska institute and hospital, Stockholm. Cancer cells were maintained in DMEM medium and DMEM F12 in case of normal cells. All media were supplemented with 10% fetal bovine serum and 100 μg ml^{-1} streptomycin, and 100 IU ml^{-1} penicillin. And then the cells were incubated at 37C^{o} in 5 %CO_2 and 95% humidity. Cells were sub-cultured using trypsin 0.15 % (Abd El Aty *et al.*, 2020; Alharbi *et al.*, 2020).

2.5.2. MTT Assay for testing cell viability

Cancer cells were seeded at a density of 1×10^4 and 1×10^5 (in case of normal cells) per well into 96-well plates in appropriate culture medium and pre-incubated for 24 h at 37°C humidified atmosphere containing 5% CO2. After that, the cells were treated for 48 h with different concentrations of sample (12.5, 25, 50 and 100 μg ml^{-1}) in the respective cell culture medium. Doxorubicin was used as positive control and 0.5 % DMSO was used as negative control. Cell viability was determined using the MTT (3-(4, 5-dimethylthiazol-2-yl)-2, 5-diphenyltetrazolium bromide) assay as described by Mosmann (1983). The equation used for calculation of percentage cytotoxicity was:

Percentage of cytotoxicity %= (1- (av(x) / (av(NC))) * 100

Where Av: average, X: absorbance of sample well measured at 595 nm with reference 690 nm, NC: absorbance of negative control measured at 595 nm with reference 690.

The IC_{50} values were determined using probit analysis and utilizing the SPSS computer program (SPSS for windows, statistical analysis software package / version 9 / 1989 SPSS Inc., Chicago, USA).

2.5.3. Cellular morphology

Microscopic examination of human tested cancer cell lines was checked by using Inverted microscope (Nikon, TMS-F, New York, USA).

2.6. Assessment of antimicrobial activity (Bioassay)

Silver-nanoparticles biosynthesized from aqueous extract of red gum (R1, R2, R3) and those prepared using aqueous extract of yellow gum (Y1, Y2, Y3) were tested against harmful pathogenic bacteria, yeast and fungi by the agar diffusion technique (Abd El Aty and Ammar, 2016).

2.6.1. Antibacterial assay

All prepared AgNPs were screened against pathogenic strains of Gram-positive (*Staphylococcus aureus* ATCC29213, *Bacillus subtilis* ATCC6633, *Lactobacillus cereus* ATCC14579) and Gram- negative (*Escherichia coli* ATCC25922, *Salmonella enterica* ATCC25566). Suspensions of all pathogenic strains were prepared and adjusted to be approximately (1×10^6 spores^{-ml}). 1 ml of each bacterial suspension was inoculated into a plate containing 50 ml of sterile nutrient agar medium (NA). Wells of about 15 mm in diameter were made in the solidified agar media and filled with 400 µl of AgNps colloidal solution, then they were left for 120 min at 4 ºC for compound diffusion. The plates were incubated for 24 h at 30 ºC for bacteria growth. The inhibition zones of all tested organisms were recorded in millimeters at three different points, and the average values are reported as Mean ± SD using MS Excel (Abd El Aty and Zohair, 2020).

2.6.2. Antifungal assay

The antifungal effects of biosynthesized AgNPs were tested against the unicellular yeast (*Candida albicans* ATCC10321) and filamentous fungus (*Aspergillus niger* NRC53). One ml of (1×10^8 spores^{-ml}) fungal suspensions was inoculated into 50 ml sterile potato dextrose agar (PDA) medium. 400µl of AgNps colloidal solution was added to each well separately and left for compound diffusion. The plates were incubated for 72 h at 28 ºC and inhibition zones were recorded in millimeters.

3. Results and Discussion

3.1. Gum extract preparation and protein content evaluation

Three different concentrations of *sarcocolla* gum (5,10 and 20 mg/ml) were prepared from the stock aqueous extract of (50 mg/ml, w/v) Fig. 1. Results of protein analysis according to Lowry *et al.* (1951) indicated the presence of higher protein content in stock aqueous extract of yellow-gum (5.458mg/ml), greater than the red-gum (3.161mg/ml) as shown in Table 1.

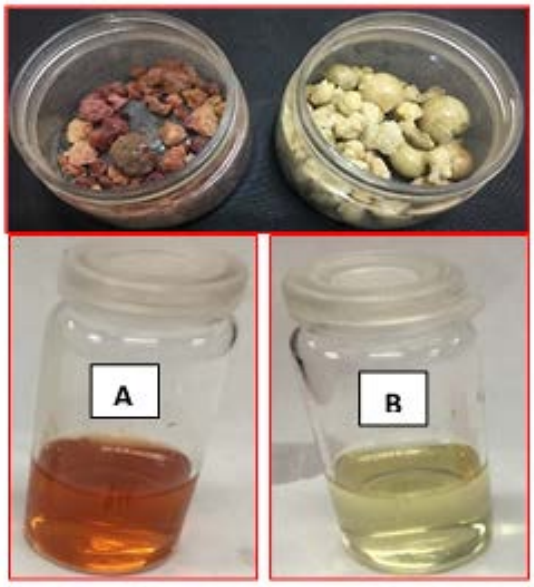

Figure 1. Photograph of *sarcocolla* gum. Stock aqueous extract of red (A) and yellow (B) gum at concentration of 50 mg/ml (w/v).

Table 1. Estimation of protein content of *sarcocolla* red and yellow gum.

Concentration of *sarcocolla* gum (mg/ml) (w/v)		**Protein content (mg/ml)**	
		Red-gum (RG)	**Yellow-gum(YG)**
Stock aqueous extract	50	3.161	5.458
Tested dilutions	5	RG1 (0.316)	YG1 (0.546)
	10	RG2 (0.632)	YG2 (1.092)
	20	RG3 (1.264)	YG3 (2.183)

3.2. Sarcocolla gum-mediated the synthesis of silver nanoparticles

The effect of gum-concentration on the formation of AgNPs was studied. Red and yellow aqueous extracts of 5, 10 and 20 mg/ml (w/v), containing different protein concentrations, were evaluated as reducing and capping agents for biosynthesis of nano-silver. The formation of the AgNPs during the reduction process is indicated first by the formation of reddish to dark brown color after mixing the gum extracts with $AgNO_3$, which can be visually observed. Roy *et al.,* (2015b) emphasized that the colour change resulted from the reduction of silver ions with free electrons excitation, which in turn forms surface plasmon resonance absorption (SPR) bands. In addition, the obtained reddish-brown color of the reaction mixture showed stability without any change at all experiments indicating the stability of the formed AgNPs, in accordance with (Nanda and Majeed, 2014; Ammar *et al.,* 2021).

Results obtained, indicated the ability of *sarcocolla* Gum-proteins to work as reducing and capping agent able to convert $AgNO_3$ into the nano form. All biosynthesized AgNPs were further characterized by UV-spectroscopy, TEM and DLS analyses.

3.3. Characterization of sarcocolla gum AgNPs

3.3.1. UV–Vis spectral analysis

The UV–visible absorption spectra of the AgNPs prepared with different concentrations of red-gum (RG) with 0.316, 0.632 and 1.264 mg/ml protein content respectively are recorded and shown in **Fig. 2.** The UV-vis spectra strong peaks with maxima around 425–440 nm were observed, which correspond to the typical surface plasmon resonance of silver nanoparticles (Kora and Arunachalam, 2012; Mudhafar *et al.*, 2021). In addition, the SPR band broadened with the high gum concentration (RG3) and shifted from 425 to 440 nm, indicating an increase in particle size of AgNPs-RG3, So, the low gum-concentration sample is preferred for synthesis of small sized uniform particles.

Silver-nanoparticles biosynthesized using yellow gum were scanned by UV–Visible spectrophotometer in the ranges of 200 to 800 nm. The result in **Fig. 3** showed that surface plasmon resonance of AgNPs -YG1, YG2 and YG3 appeared at 425, 420 and 420, respectively. The appearance of these peaks is due to the plasmon resonance and inters band transition of AgNPs which proved the biosynthesis of nanoparticles (Ammar *et al.*, 2021). These characteristics are similar to AgNPs synthesized by Kora and Arunachalam, (2012) who detected the formation of AgNPs from Gum tragacanth (*Astragalus gummifer*).

Results obtained in Fig. 3 emphasized that the absorbance intensity increased directly from 2.23 to 2.47 and 3.12 respectively, with increasing the concentration of the yellow-gum extracts. It is also observed that the surface plasmon peak that occurs at 425 nm with the lowest concentration is slowly shifted toward lower wavelength 420nm at high extract concentrations. This shift mainly depends on the particle size and shape (Lee and El-sayed 2006).

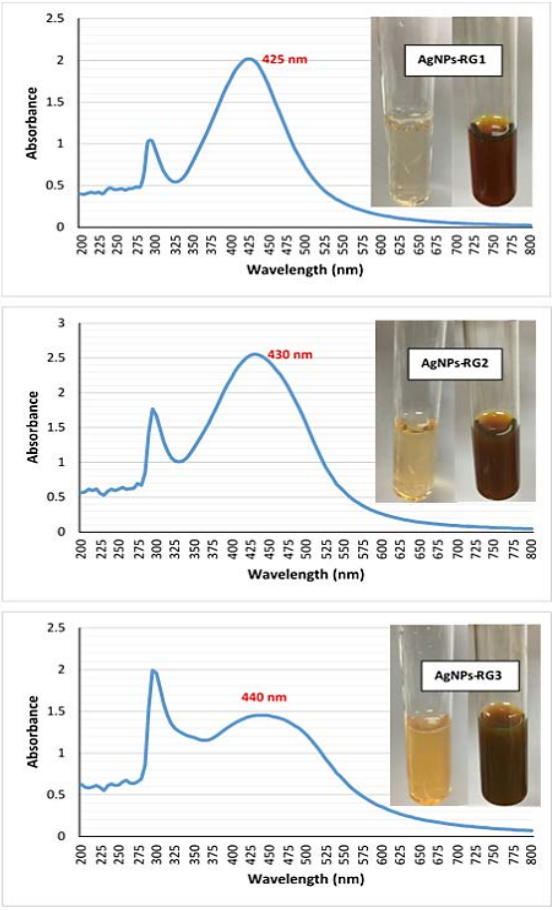

Figure 2. UV–vis spectroscopy of biosynthesized silver-nanoparticle from *Sarcocolla* red gum at 5 (RG1), 10 (RG2) and 20 (RG3) mg/ml concentration.

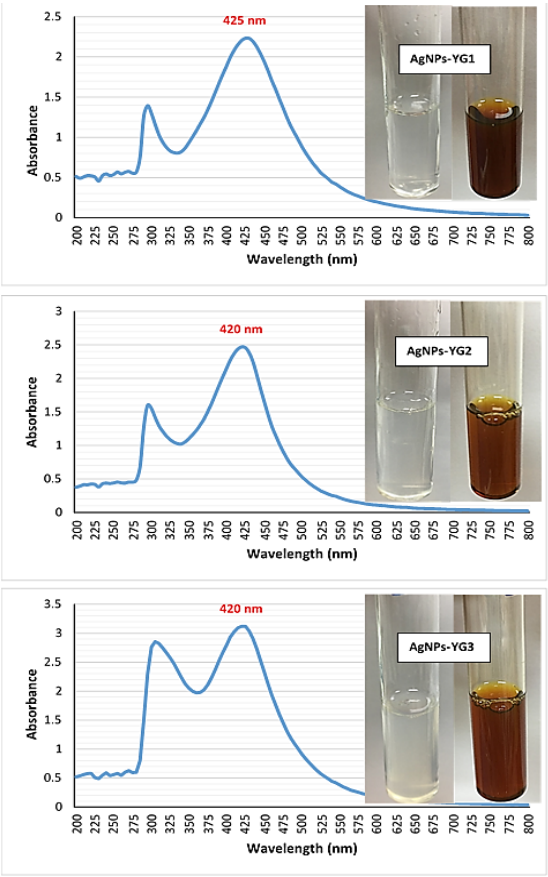

Figure 3. UV–vis spectroscopy of biosynthesized silver-nanoparticle from *Sarcocolla* yellow gum at 5 (YG1), 10 (YG2) and 20 (YG3) mg/ml concentration.

3.3.2. TEM analysis

TEM images of the silver nanoparticles synthesized with 5, 10 and 20 mg/ml red gum showed different shapes varying from spherical, cubic to semi rounded particles with a size range of 9.23±3.66 nm for AgNPs-RG1, 11.36±9.57 nm for AgNPs-RG2 and 15.72±10.79 nm for AgNPs-RG3. TEM analysis (**Fig. 4)** also showed well-dispersed AgNPs biosynthesized using low concentrations of red gum (RG1& RG2). On the other hand, some aggregations were observed with samples prepared with high gum concentration (RG3).

Silver-nanoparticles biosynthesized from yellow gum were spherical to cubic, polydispersed particles with different sizes depending on the gum concentration. AgNPs-YG1 showed sizes from 2.00–17.82 nm, and the average particle size was about 10.92 ± 5.48 nm. When the concentration of yellow gum was increased from 5 to 10 and 20 mg/ml, the particle size of the formed nanoparticles increased to about 12.36 ± 8.37 nm and 15.16 ±6.30 nm respectively as showed in Fig. 5.

The increase in average particle sizes with increase in concentration of the *Astragalus gummifer* gum was also demonstrated by Kora and Arunachalam, (2012). Based on the obtained results, we concluded that the particle size of the nanoparticles can be controlled by varying the gum type and concentration.

The crystallinity of the synthesized nanoparticles was confirmed from the observed clear lattice fringes in high-resolution image, and the concentric rings with intermittent bright dots appeared in the selected-area electron diffraction (SAED) pattern as shown in Figs. 4 and 5.

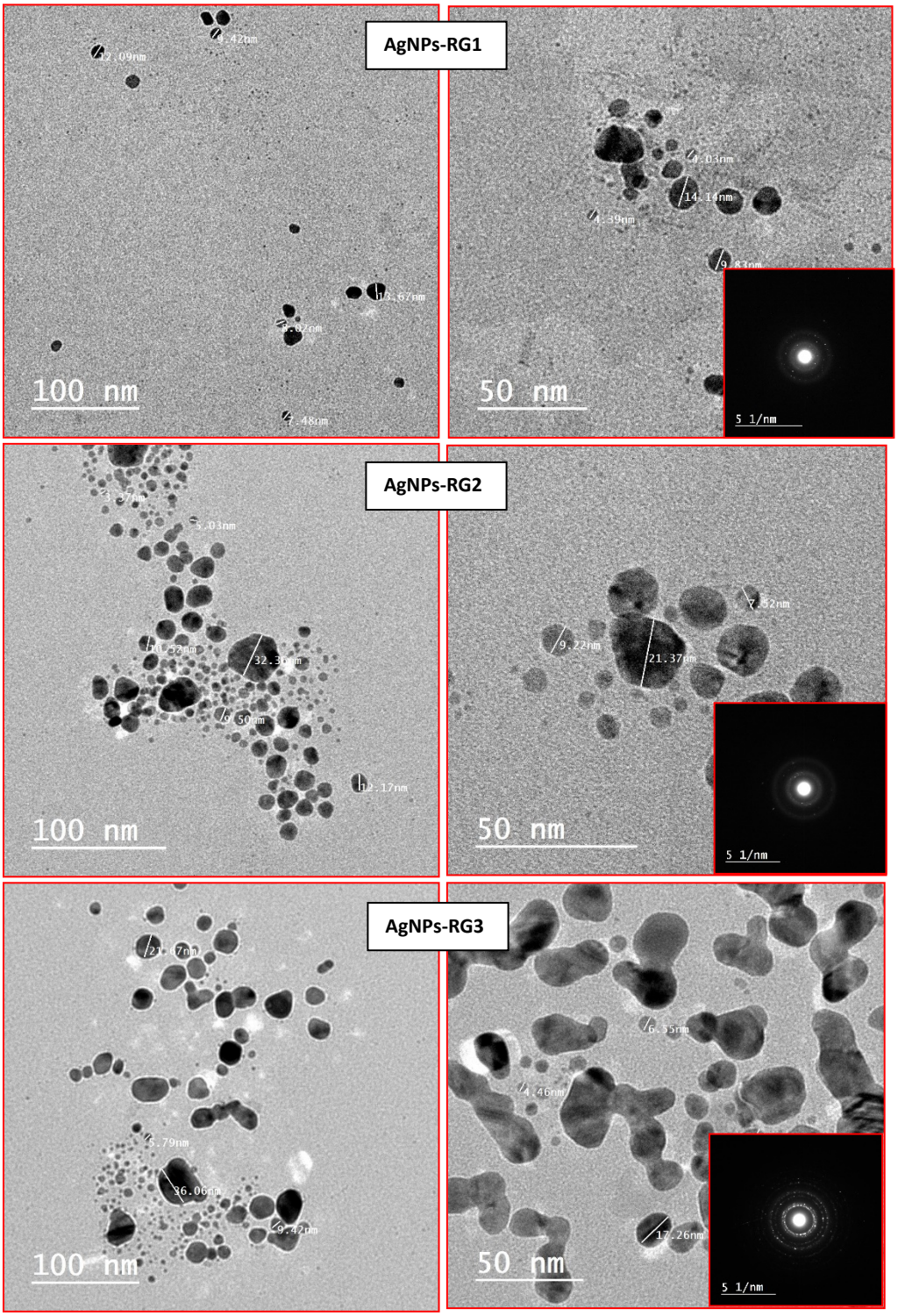

Figure 4. TEM for three synthesized AgNPs using *Sarcocolla* red gum at 5 (RG1), 10 (RG2) and 20 (RG3) mg/ml concentration. Inset shows selected area electron diffraction (SAED) patterns of AgNPs.

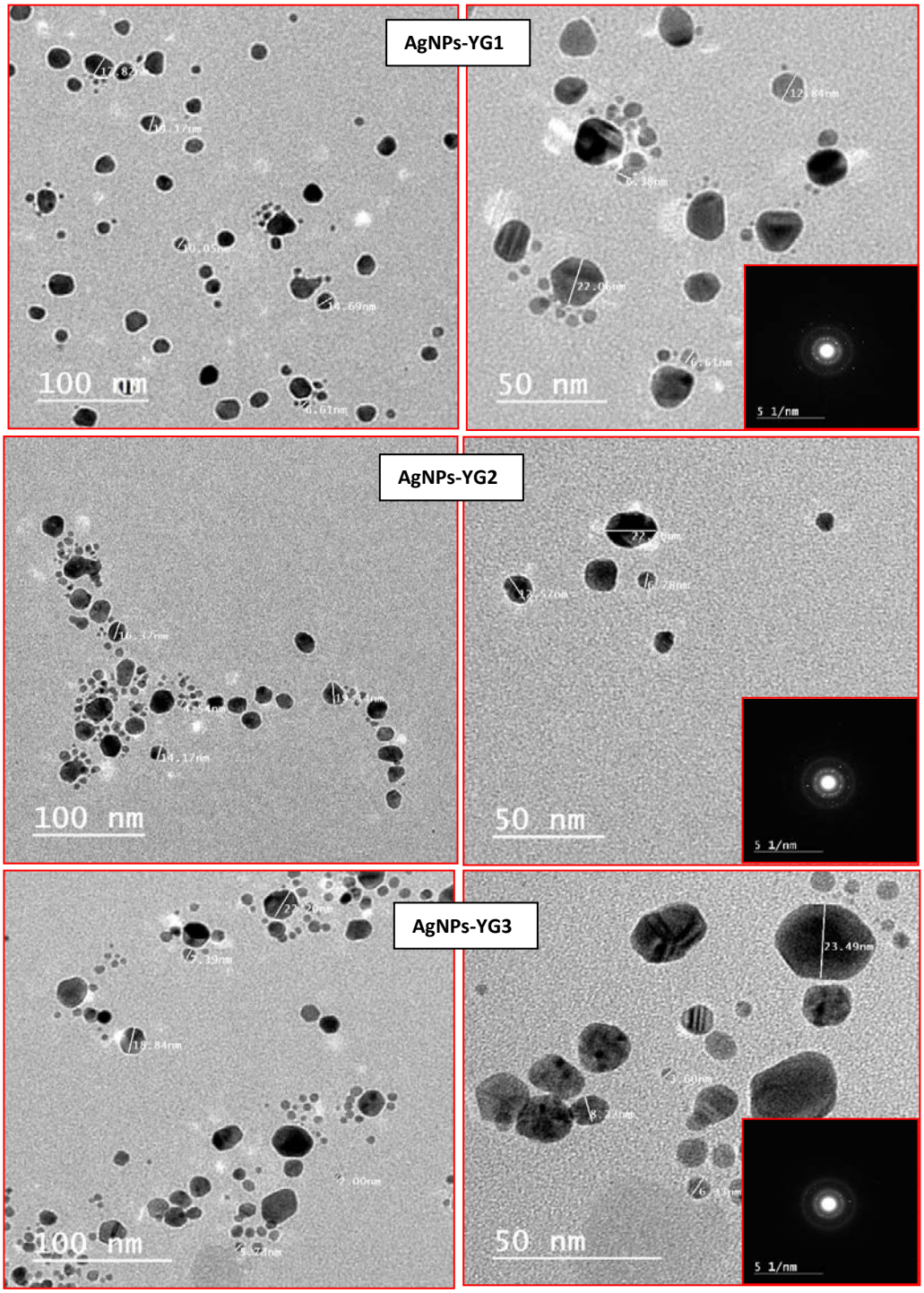

Figure 5. TEM for three synthesized AgNPs using *Sarcocolla* yellow gum at 5 (YG1), 10 (YG2) and 20 (YG3) mg/ml concentration. Inset shows selected area electron diffraction (SAED) patterns of AgNPs.

3.3.3. Dynamic light scatter analysis (DLS)

Dynamic light scatter analysis (DLS) was applied for the most active biosynthesized silver–nanoparticles, AgNPs-RG1 and AgNPs-YG1 to confirm the formation of particles in nano-size. To detect the average size distribution of AgNPs synthesized using low concentrations of red and yellow gums, two different techniques, INTENSITY-Weighted Gaussian Distribution and Zeta potential were applied. Intensity-weight Gaussian Distribution was found to be 48.2 and 74.2 nm, respectively. And their Zeta potential were -41.32 and −30.54 mv, respectively, which indicated their good stability Fig. 6.

High negative values of AgNPs-RG1 and YG1 appeared clearly to be advantageous for long-term colloidal stability, as mentioned by Eltarahony *et al.* (2018), who indicated that the values less than (−25 mV) or greater than (+25 mV) display higher electrical charge on nano-particles surface, which prevents agglomeration, but Alshammari and Abd El Aty (2022), showed slightly low surface charges of -6.70, -8.73 and 0.16 mv

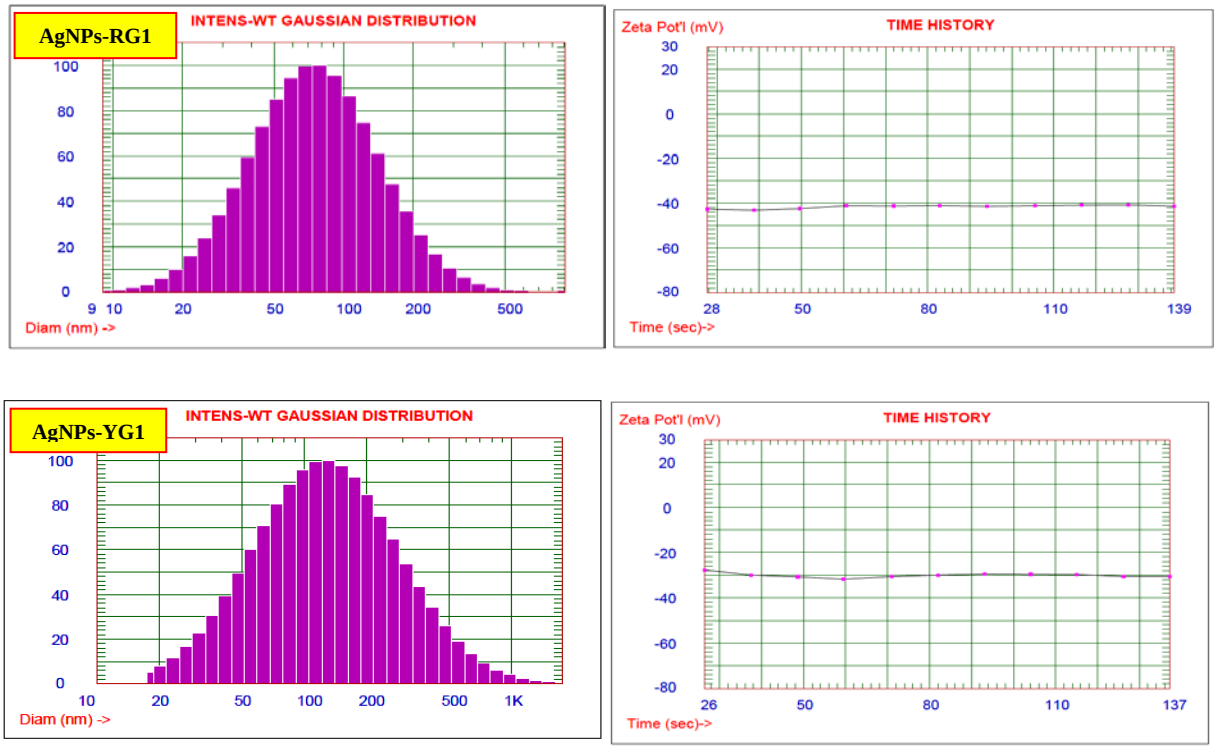

Figure 6. Gaussian distribution and Zeta potential of AgNPs biosynthesized by RG1 and YG1.

3.4. Biomedical applications of sarcocolla gum-AgNPs

3.4.1. Cytotoxicity assay

Silver-nanoparticles biosynthesized from aqueous extract of red gum (RG1, RG2, RG3) and that prepared using aqueous extract of yellow gum (YG1, YG2, YG3) were tested for their cytotoxic effect against five human cancer cells and one normal cells Table 2. The results, expressed as IC_{50} values are reported in Table 3.

The results showed that, out of three biosynthesized silver–nanoparticles of red gum aqueous extract, the AgNPs-RG1 was the most active and possessed high cytotoxic effect against four cancer cells, namely A549, pc3, Mcf7 and paca2 with IC_{50} values (88.4,75.6, 72.2& 55.0 ug/ml, respectively) and showed low cytotoxic effect (20 % at 100ug/ml) against human normal cells (BJ-1). On the other hand, AgNPs-RG2 showed cytotoxic effect against only paca2 cell line with IC 50 (47.0ug/ml) and AgNPs-RG3 showed only cytotoxic effect against mcf-7 with IC_{50} (74.4ug/ml), but two nanoparticles of (AgNPs-RG2 and AgNPs-RG3) showed highly cytotoxic effect against normal cells IC_{50} (46.8 and 76.4ug/ml). Devanesan *et al.*, (2020) showed good cytotoxicity of As-AgNPs biosynthesized from the plant *Ferula foetida* (asafoetida gum) against MCF-7 cell lines. Good cytotoxicity of silver-nanoparticles against human cancerous cells mainly occurs due to the high proliferation rate and abnormal metabolism of cancerous cells, which in turn causes the high uptake of nanoparticles by these cells more than normal cells (Park *et al.*, 2010; Madunić *et al.*, 2018).

Results also emphasized that silver-nanoparticles biosynthesized from different concentrations of yellow gum aqueous extract possessed various cytotoxic activity. AgNPs-YG1 showed high cytotoxic effect against three cancer cells (PC3, MCF-7 and paca2) with IC_{50} values (75.0, 82.8 and 81,6ug/ml respectively), and normal cells (BJ-1) with IC_{50} value (81.8ug/ml). Another study of Sánchez-Navarro *et al.*, (2018) also confirmed that the lower concentration of *Annona muricata* aqueous extract exhibited cytotoxicity oral fibroblasts. On the other hand, AgNPs-YG3 has high cytotoxic effect against tow cancer cells (MCF-7 and paca2) with IC_{50} values (52.6 and 90.3ug/ml respectively), with low cytotoxic effect against normal cells (Bj-1) 13.6% at 100 ug/ml. AgNPs-YG2 possessed high cytotoxic effect against only breast cancer cell (IC50=72.2).

The cytotoxic effect of the AgNPs-RG1 and AgNPs-YG1 indicates the possible application of these AgNPs as chemotherapeutic agents (Ahamed and AlSalhi, 2010).

Table 2. Cytotoxic effect of *Sarcocolla* Gum-AgNPs against five different human cancer cell lines and normal cell line (BJ-1).

Treatment	Cytotoxicity %*					
	A549	PC3	HCT-116	MCF-7	Paca2	Normal cells (BJ-1)
AgNPs-RG1	55.3	60.8	18.6	64.6	91.5	20.8
AgNPs-RG2	14.5	46.4	4.4	27	97	100
AgNPs-RG3	19.9	10	9.1	65	55.7	69.5
AgNPs-YG1	22.5	58.3	27.7	57.9	94.3	64.6
AgNPs-YG2	22.2	2.8	21.7	64	40.3	38.2
AgNPs-YG3	36.2	26.6	28.4	76	52.1	13.6
Doxorubicin	98.2	96.6	99.4	97.6	98.3	99.8

* Cytotoxicity % of AgNPs measured at 100ug/ml against different cancer cell lines.

Table 3. IC $_{50}$ µg/ml of *Sarcocolla* Gum-AgNPs samples.

Treatment	IC50 ug/ml					
	A549	PC3	HCT-116	MCF-7	Paca2	BJ-1
AgNPs-RG1	88.4	75.6	-	72.2	55.0	-
AgNPs-RG2	-	-	-	-	47.0	46.8
AgNPs-RG3	-	-	-	74.4	81.6	76.4
AgNPs-YG1	-	75.0	-	82.8	50.7	81,8
AgNPs-YG2	-	-	-	72.2	-	-
AgNPs-YG3	-	-	-	52.6	90.3	-
Doxorubicin	21.6	21.6	26.1	37.6	28.3	13.5

3.4.2. Cellular morphology

The effects of the *Sarcocolla*-AgNPs-RG1 and AgNPs-YG1 on cellular morphology were observed directly using Inverted microscope as shown in Fig. 7. Untreated cancer cells were homogeneously distributed on a cultured field, exhibiting a uniform polygonal shape. Following incubation with the silver-nanoparticles, various morphological changes were observed. Photos also showed that exposure of the cells to the AgNPs transformed the shapes of the cells from polygonal to circular and resulted in cell shrinkage. The non-active nanopartcles did not show any significant morphological change. Notably, these morphological alterations were observed at 100 µg/ml concentration.

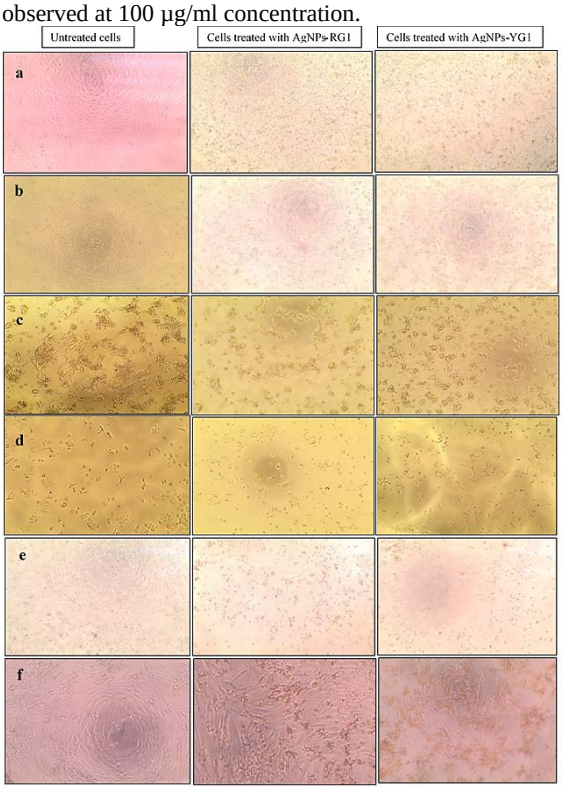

Figure 7. Microscopic examination of *Sarcocolla*-AgNPs-RG1 and AgNPs-YG1 treated and untreated cells of (a) A549, (b) PC3, (c) HCT-116, (d) MCF-7, (e) Paca2, (f) Normal cells (BJ-1).

3.4.3. Antimicrobial assay

Antibacterial and antifungal activities of the synthesized red and yellow gum-mediated AgNPs with different sizes and shapes were investigated against Gram-positive (*S. aureus*, *B. subtilis*, *L. cereus*) and Gram-negative (*E. coli*, *S. enterica*) bacteria using the agar diffusion method. Results in Table 4 indicated that AgNPs-RG1, RG2 and YG1 exhibited broad spectrum antimicrobial effects against all tested pathogenic bacteria, yeast and fungi, but no antimicrobial activity was displayed by AgNPs-RG3, YG2 and YG3, this negative effect may be due to large sized particles and aggregations.

Figs. 8 and 9 showed good antibacterial activity of AgNPs-RG1, RG2 and AgNPs-YG1 against gram-positive strains with inhibition zone diameter in range from 19-25 mm and from 19-26 mm respectively. Also, the gram-negative strains were highly inhibited after treatment with AgNPs-YG1 (IZD in range from 22-24 mm), followed by AgNPs-RG1 (IZD in range from 19-23 mm) and AgNPs-RG2 (IZD in range from 19-22 mm).

Ramdath *et al.* (2021) emphasized that the bactericidal effects observed in all bacterial strains caused as a result of releasing silver-cations. Researchers showed the ability of AgNPs to bind on to the surface of bacterial cells and directly affect the sulphur and phosphorous moieties of the cell-membrane; therefore, the cell metabolism has been failed leading to the bacterial death (Rawani *et al.*, 2013; Bindhu and Umadevi, 2015).

Results also observed that both the AgNPs-RG1 and YG1 solutions exhibit similar antifungal activity in the unicellular yeast *C. albicans* (21 and 20 mm respectively) and the filamentous fungus *A. niger* (17 and 18 mm respectively), but AgNPs -RG2 showed only an inhibitory effect against *C. albicans* 22mm.

In most cases, the antifungal mechanism of silver ions on microorganisms, due to their effects on the function of membrane-bound enzymes, inactivation of cellular proteins and enzymes essential to DNA replication (Min et al., 2009; Ammar et al., 2021).

In general, the findings suggested the AgNPs-RG1 and YG1 as good potential antibacterial and antifungal agents.

Table 4. Antibacterial and antifungal activity of the biosynthesized AgNps against pathogenic bacteria and fungi.

Samples (400µl/ well)	Inhibition zone diameter (IZD)						
	Gram-negative bacteria		**Gram-positive bacteria**			**Yeast**	**Fungi**
	Escherichia coli ATCC25922	*Salmonella enterica* ATCC25566	*Staphylococcus aureus* ATCC29213	*Bacillus subtilis* ATCC6633	*Lactobacillus cereus* ATCC14579	*Candida albicans* ATCC10321	*Aspergillus niger* NRC53
Red -Gum extract (C)	N.A	N.A	N.A	N.A	N.A	N.A	N.A
AgNPs RG1	23±0.17	19±0.28	25±0.42	22±0.16	21±0.35	21±0.18	17±0.17
AgNPs RG2	22±0.38	19±0.44	19±0.17	22±0.51	25±0.24	22±0.34	N.A
AgNPs RG3	N.A	N.A	N.A	N.A	N.A	N.A	N.A
Yellow- Gum extract (C)	N.A	N.A	N.A	N.A	N.A	N.A	N.A
AgNPs YG1	24±0.18	22±0.17	26±0.44	19±0.31	21±0.17	20±0.25	18±0.28
AgNPs YG2	N.A	N.A	N.A	N.A	N.A	N.A	N.A
AgNPs YG3	N.A	N.A	N.A	N.A	N.A	N.A	N.A

N.A. no activity

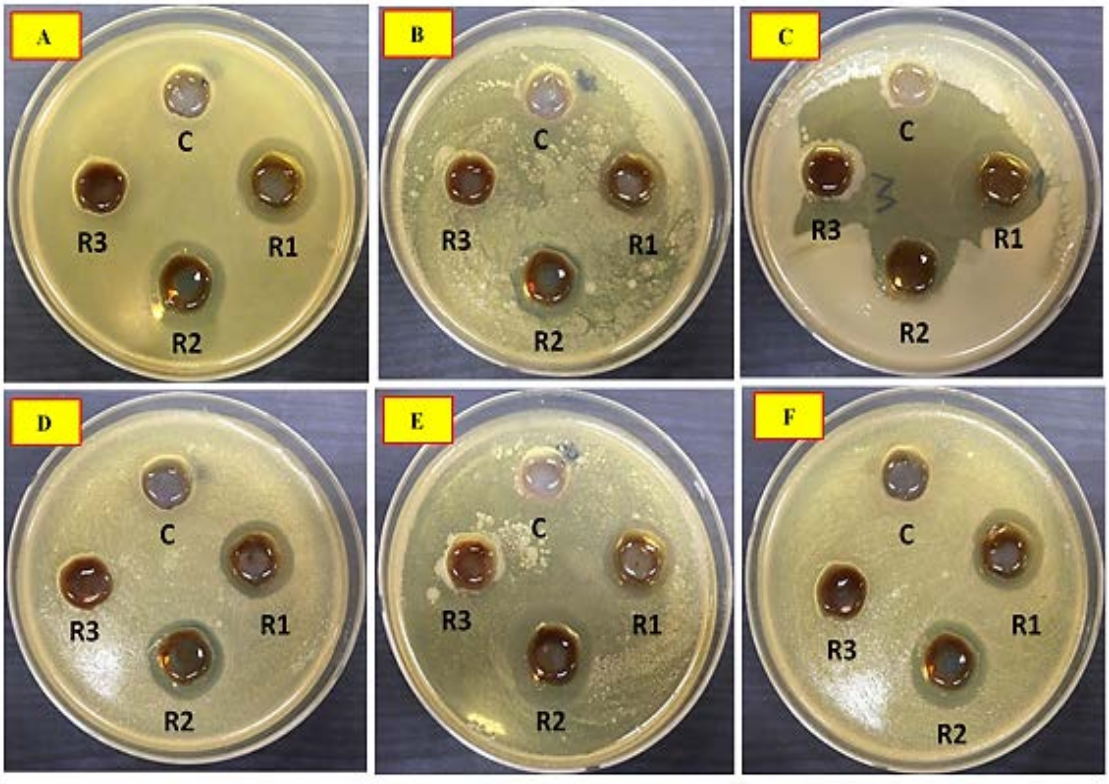

Figure 8. Photos of the antimicrobial effect of biosynthesized AgNPs using *sarcocolla* red gum at 5 (RG1), 10 (RG2) and 20 (RG3) mg/ml concentration against *E. coli* (A), *S. enterica* (B), *S. aureus* (C), *B. subtilis*(D). *L. cereus* (E) and *C. albicans* (F).

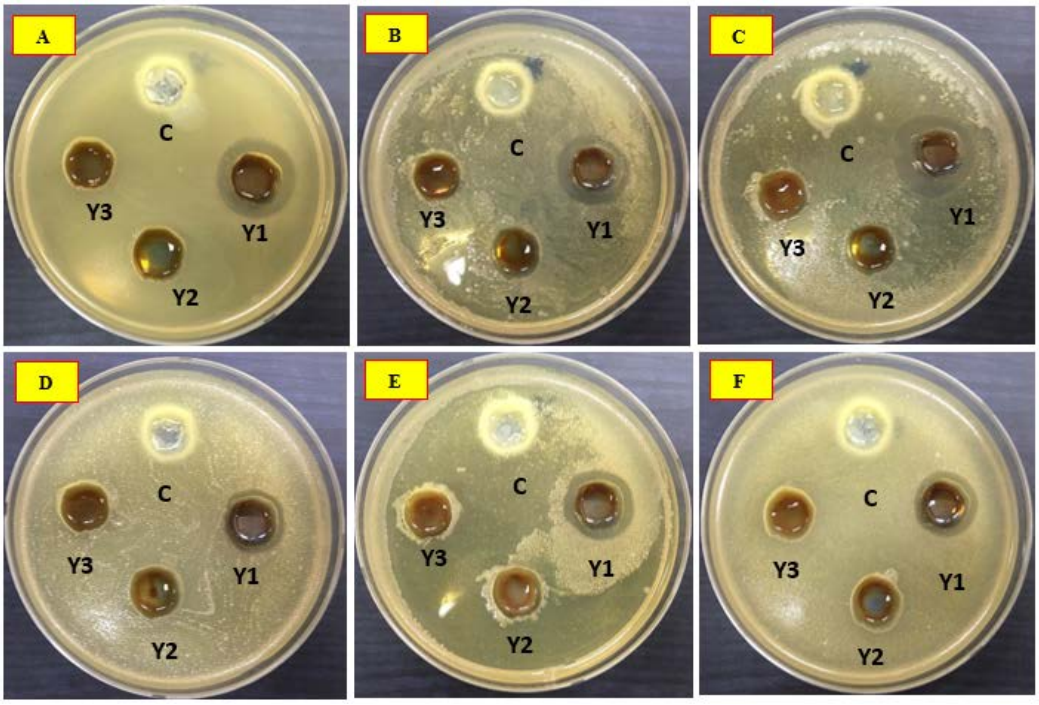

Figure 9. Photos of the antimicrobial effect of biosynthesized AgNPs using *sarcocolla* yellow gum at 5 (YG1), 10 (YG2) and 20 (YG3) mg/ml concentration against *E. coli* (A), *S. enterica* (B), *S. aureus* (C), *B. subtilis*(D). *L. cereus* (E) and *C. albicans* (F).

4. Conclusion

This paper, showed a novel simple, cost effective, eco-friendly green method using aqueous extract of red and yellow *Astragalus sarcocolla* gum. All characterization studies emphasized the biosynthesis of stable nanoparticles with different shapes and sizes specially at low gum concentrations, which in turn indicated the good application of *sarcocolla* gum as a reducing and stabilizing agent instead of using toxic chemical entities. Anticancer and antimicrobial potential of six gum-mediated silver nanoparticles was investigated. AgNPs-RG1 and AgNPs-YG1 showed the best cytotoxic effects against four cancer cells namely A549, pc3, Mcf7 and paca2, and the inverted microscope examination showed various morphological changes in the cells treated with AgNPs compared with untreated cancer cells, which confirmed the toxic effect of AgNPs. In addition, AgNPs-RG1, RG2 and AgNPs-YG1 exhibited good inhibition zones against all tested pathogenic bacteria, yeast and fungi.

Acknowledgement

The authors extend their appreciation to the Deanship of Scientific Research, University of Hafr Al Batin, for funding this work through the research group project No (0006-1443-S).

Conflict of interest

The authors declare that they have no conflict of interests.

References

Ababutain I M. 2017. Antimicrobial Activity and Phytochemical Screening of Sarcocolla Gum Resin. *Pak. J. Biol. Sci.* **20 (11)**: 571-576. DOI: 10.3923/pjbs.2017.571.576

Abd El Aty A A and Ammar H A. 2016. Potential characterization and antimicrobial applications of newly bio-synthesized silver and copper nanoparticles using the novel marine-derived fungus Alternaria tenuissima KM651985. *Res. J. Biotechnol.* **11(8):** 71-82.

Abd El Aty A A and Zohair M M. 2020. Green-synthesis and optimization of an eco-friendly nanobiofungicide from Bacillus amyloliquefaciens MH046937 with antimicrobial potential against phytopathogens. *Environ. Nanotechnol. Monit. Manag.*,**14**,100309.https://doi.org/10.1016/j.enmm.2020.100309

Abd El Aty A A, Mohamed A A, Zohair M M and Soliman A A F. 2020. Statistically controlled biogenesis of silver nano-size by Penicillium chrysogenum MF318506 for biomedical application. *Biocatal. Agric. Biotechnol*, **25**: 101592. https://doi.org/10.1016/j.bcab.2020.101592

Ahamed M and AlSalhi M S. 2010. Siddiqui MKJ. Silver nanoparticle applications and human health. *Clin Chim Acta*. **411**: 1841–1848. doi:10.1016/j.cca.2010.08.016

Akram M, Iqbal M, Daniyal M and Khan A U. 2017. "Awareness and current knowledge of breast cancer," *Biol. Res.*, **50 (1):**1–23.

Alharbi RM, Soliman A A F and Abd El Aty A A. 2020. COMPARATIVE STUDY ON BIOSYNTHESIS OF VALUABLE ANTIMICROBIAL AND ANTITUMOR NANO-SILVER USING FRESH WATER GREEN AND BLUE-GREEN MICROALGAE. *J. Microbiol. Biotechnol. Food Sci.*, **10(2)** https://www.jmbfs.org/wp-content/uploads/2020/10/1852-Main-document-manuscript-preprint.pdf

Alharbi R M, Alshammari S O and Abd El-Aty A A. Statically-improved Fungal Laccase-mediated the Biogenesis of Silver Nanoparticles with Antimicrobial Applications. *J. Appl. Pharm. Sci..,* **13(01),** 241-253, 2023. DOI: 10.7324/JAPS.2023.130105

Alshammari S O and Abd El Aty A A. 2022. Statically controlled mycogenic-synthesis of novel biologically active silver-nanoparticles using Hafr Al-Batin desert truffles and its antimicrobial efficacy against pathogens. *Saudi J Biol Sci.,* **29:** 103334. https://doi.org/10.1016/j.sjbs.2022.103334.

Ammar H A, Abd El Aty A A and El Awdan S A. 2021. Extracellular myco-synthesis of nano-silver using the fermentable yeasts Pichia kudriavzeviiHA-NY2 and Saccharomyces uvarumHA-NY3, and their effective biomedical applications. *Bioprocess Biosyst Eng*., **44 (4):** 841-854. https://doi.org/10.1007/s00449-020-02494-3

Bindhu M R and Umadevi M. 2015. "Antibacterial and catalytic activities of green synthesized silver nanoparticles," Spectrochimica Acta Part A: *Mol. Biomol. Spectrosc.,* **135**:373–378.

Bisht S, Mizuma M, Feldmann G. et al., 2010. "Systemic administration of polymeric nanoparticle-encapsulated curcumin (NanoCurc) blocks tumor growth and metastases in preclinical models of pancreatic cancer," *Mol. Cancer Ther.,* **9 (8):** 2255–2264.

Daniel M and Astruc D. 2004. Gold nanoparticles: assembly, supramolecular chemistry, quantum-size-related properties, and applications toward biology, catalysis, and nanotechnology. *Chem Rev*. **104**: 293–346.

Demchenko V, Riabov S, Sinelnikov S, Radchenko O, Kobylinskyi S and Rybalchenko N. 2020. "Novel approach to synthesis of silver nanoparticles in interpolyelectrolyte complexes based on pectin, chitosan, starch and their derivatives," *Carbohydr. Polym..*, **242**, Article ID 116431.

Devanesan S, Ponmurugan K, AlSalhi MS and Al-Dhab NA. 2020. Cytotoxic and Antimicrobial Efficacy of Silver Nanoparticles Synthesized Using a Traditional Phytoproduct, Asafoetida Gum. *Int. J. Nanomedicine*. **15**: 4351–4362.

Eltarahony M, Zaki S and Abd-El-Haleem D. 2018. Concurrent Synthesis of Zero- and One-Dimensional, Spherical, Rod-, Needle-, and Wire-Shaped CuO Nanoparticles by Proteus mirabilis 10B, *J. Nanomater.,* 1849616: https://doi.org/10.1155/2018/1849616

Kokila T, Ramesh P S and Geetha D. 2015. Biosynthesis of silver nanoparticles from Cavendish banana peel extract and its antibacterial and free radical scavenging assay: a novel biological approach. *Appl Nanosci.* **5**: 911–20. doi:10.1007/s13204-015-0401-2

Kora A J and Arunachalam J. 2012. Green fabrication of silver nanoparticles by gum tragacanth (Astragalus gummifer): a dual functional reductant and stabilizer. *J Nanomater*. **1–8**. doi:10.1155/2012/869765.

Kora A J, Beedu S R and Jayaraman A. 2012. Size-controlled green synthesis of silver nanoparticles mediated by gum ghatti (*Anogeissus latifolia*) and its biological activity. *Organic Med Chem Lett.* **2**: 17. doi:10.1186/2191-2858-2-17.

Lee , Kyeong-Seok and El-Sayed M A. 2006. Gold and silver nanoparticles in sensing and imaging: sensitivity of plasmon response to size, shape, and metal composition. *J Phys Chem B.* **110 (39):** 19220-5. doi: 10.1021/jp062536y.

Lee S and Jun B-H. 2019. "Silver nanoparticles: synthesis and application for nanomedicine," *Int J Mol Sci* , **20 (4):** 865.

Li T, Park H G and Choi S-H. 2007. γ-Irradiation-induced preparation of Ag and Au nanoparticles and their characterizations. *Mater Chem Phys.* **105**: 325–30. doi:10.1016/j.matchemphys.2007.04.069.

Lowry O H, Rosebrough NJ, farr AL and Randall RJ. 1951. Protein measurement with the folin Phenol reagent, *J. Biol. Chem*., **193**: 265-275.

Mackey T K, Liang B A, Cuomo R, Hafen R, Brouwer K C and Lee D E. 2014. "Emerging and reemerging neglected tropical diseases: a review of key characteristics, risk factors, and the policy and innovation environment," *Clin. Microbiol. Rev.* **27 (4):** 949–979.

Madunić J, Madunić IV, Gajski G, Popić J and Garaj-Vrhovac V, 2018. Apigenin: a dietary flavonoid with diverse anticancer properties. *Cancer Lett.* **413**: 11–22. doi:10.1016/j.canlet.2017.10.041

Mehndiratta P and Jain A. 2013. Srivastava S, Gupta N. Environmental pollution and nanotechnology. *Environ Pollut.* **2**: 49–58. doi:10.5539/ep.v2n2p49.

Min JS, Kim KS, Kim SW, Jung JH, Lamsal K, Kim SB, Jung M and Lee YS. 2009. Effects of colloidal silver nanoparticles on sclerotium-forming phytopathogenic fungi. *Plant Pathol J.* **25:** 376–380.

Mosmann T. 1983. Rapid colorimetric assay for cellular growth and survival: application to proliferation and cytotoxicity assays. *J. Immunol. Methods* **65**: 55–63.

Mudhafar M, Zainol I, Alsailawi H A and Aiza Jaafar C N. 2021. Green Synthesis of Silver Nanoparticles using Neem and Collagen of Fish Scales as a Reducing and Stabilizer Agents. *Jordan J. Biol. Sci.* **14**: 899 – 903. https://doi.org/10.54319/jjbs/140503

Murali Krishna I, Bhagavanth Reddy G, Veerabhadram G and Madhusudhan A. 2015. Ecofriendly green synthesis of silver nanoparticles using salmalia malabarica: synthesis, characterization, antimicrobial, and catalytic activity studies. *Appl Nanosci*. doi:10.1007/s13204-015-0479-6.

Nanda A and Majeed S. 2014. Improved bactericidal property of silver nanoparticles from *Penicillium pinophilum* (MTCC 2192) in a combined form with carbicillin and moxifoxacin. *Int J Pharm Pharm Sci.* **6**:609–612.

Pandey S and Mishra SB. 2014. Catalytic reduction of p-nitrophenol by using platinum nanoparticles stabilized by guar gum. *Corbopol.* **113**: 525–31. doi:10.1016/j.carbpol.2014.07.047.

Pandey S, Mishra SB. 2016. Au nanocomposite based chemiresistive ammonia sensor for health monitoring. *Am Chem Soc*. **1(1):** 55–62. doi:10.1021/ acssensors.5b00013.

Park EJ, Yi J, Kim Y, Choi K and Park K. 2010. Silver nanoparticles induce cytotoxicity by a Trojan-horse type mechanism. Toxicol in Vitro. **24**: 872–878. doi:10.1016/j.tiv.2009.12.001

Parveen M, Ahmad F, Malla AM and Azaz S. 2016. Microwave-assisted green synthesis of silver nanoparticles from Fraxinus excelsior leaf extract and its antioxidant assay. *Appl Nanosci*. **6**: 267–76. doi:10.1007/s13204-015-0433-7

Qi F, Zhao L, Zhou A et al. 2015. "+e advantages of using traditional Chinese medicine as an adjunctive therapy in the whole course of cancer treatment instead of only terminal stage of cancer," *Biosci. Trends.* **9 (1):** 16–34.

Raghavendra G M, Jung J, kim D and Seo J. 2016. "Step-reduced synthesis of starch-silver nanoparticles," *Int. J. Biol. Macromol.* **I 86**:126–128.

Raju D, Paneliya N and Mehta U J. 2014. Extracellular synthesis of silver nanoparticles using living peanut seedling. *Appl. Nanosci.* **4**: 875–9. doi:10.1007/s13204-013-0269-y

Ramdath S, Mellem J and Mbatha LS. 2021. Anticancer and Antimicrobial Activity Evaluation of Cowpea-Porous-Starch-Formulated Silver Nanoparticles. *J. Nanotechnol.*. Article ID 5525690, 13 pages. https://doi.org/10.1155/2021/5525690

Rastogi L, Sashidhar RB, Karunasagar D and Arunachalam J. 2014. Gum kondagogu reduced/stabilized silver nanoparticles as direct colorimetric sensor for the sensitive detection of Hg2+ in aqueous system. Talanta. **118**: 111–7. doi:10.1016/j.talanta.2013.10.012.

Rawani A, Ghosh A and Chandra G. 2013. "Mosquito larvicidal and antimicrobial activity of synthesized nano-crystalline silver particles using leaves and green berry extract of Solanum nigrum L. (Solanaceae: Solanales)," *Acta Trop.* **128 (3):** 613–622.

Roy K, Sarkar C K and Ghosh C K. 2015a. Photocatalytic activity of biogenic silver nanoparticles synthesized using yeast (*Saccharomyces cerevisiae*) extract. *Appl Nanosci*. **5(8):** 953–959 35.

Roy K, Sarkar CK and Ghosh CK. 2015b. Plant-mediated synthesis of silver nanoparticles using parsley (*Petroselinum crispum*) leaf extract: spectral analysis of the particles and antibacterial study. *Appl Nanosci*. **5**: 945–51. doi:10.1007/s13204-014-0393-3

Sánchez-Navarro M C, Ruiz-Torres CA, Niño-Martínez N, et al. 2018. Cytotoxic and bactericidal effect of silver nanoparticles obtained by green synthesis method using annona muricata aqueous extract and functionalized with 5-fluorouracil. *Bioinorg Chem Appl*. 1–8. doi:10.1155/2018/6506381.

Song JY and Kim BS. 2009. Rapid biological synthesis of silver nanoparticles using plant leaf extracts. *Bioprocess Biosyst Eng.* **32**: 79–84. doi:10.1007/s00449-008-0224-6

Vasan N, Baselga J and Hyman D M. 2019. "A view on drug resistance in cancer," *Nature*. **575 (7782):** 299–309.

Wang X, Yuan L, Deng H and Zhang Z. 2021. "Structural characterization and stability study of green synthesized starch stabilized silver nanoparticles loaded with Isoorientin," *Food Chem*, **338**, Article ID 127807.

JJBS

Volume 16, Number 1,March 2023
ISSN 1995-6673
Pages 55 – 61
https://doi.org/10.54319/jjbs/160108

Jordan Journal of Biological Sciences

Localized Depletion of Drosophila *Upf1* and *Upf2* in the Central Nervous System Leading to Anatomical Defects of the CNS of the Embryo and Larva

Sanusi Ahmed Jega[1,5,*], Ahmed Adebowole Adedeji[1,3], Marta Vicente-Crespo[2,4]

[1]*Department of Biochemistry, Faculty of Biomedical Sciences, Kampala International University, Ishaka-Bushenyi, Uganda;* [2]*Institute of Biomedical Research, Kampala International University, Ishaka-Bushenyi, Uganda;* [3]*Foresight Institute of Research and Translation, Ibadan Nigeria;* [4]*African Population and Health Research Center, Nairobi Kenya;* [5]*Department of Biochemistry, Faculty of Science, Kebbi State University of Science and Technology Aliero, Nigeria*

Received: June 8, 2022; Revised: July 14, 2022; Accepted: July 28, 2022

Abstract

Nonsense-mediated mRNA decay (NMD) is a quality control pathway that degrades mRNAs with premature termination codons, (PTC), which otherwise will result into a truncated protein with a potential dominant-negative effect. NMD is also an RNA turnover regulatory mechanism for controlling a significant percentage of wild type mRNAs. The pathway functions via coordination of some proteins known as NMD factors. The core NMD factors are Upf1, Upf2, and Upf3, which, in coordination with other important factors tag and mobilize an mRNA for degradation. The role of NMD in the architectural development of central nervous system (CNS) in different organisms has been studied. However, these *in vivo* studies of the involvement of NMD presented some challenges due to the lethality of Upf1 and Upf2. In this work, we studied the CNS localized loss of function and considered the effect of depletion of Upf1, Upf2, and Upf3 at an early and late *Drosophila* embryogenesis on the overall anatomical structures of the CNS in the embryo and the larvae. We found that depletion of Upf1 and Upf2 at early embryogenesis caused a significant reduction in the hatching and viability of the embryos. Also, the area of the ventral nerve cord in relation to the total area of the embryo was significantly reduced. However, the Upf3 depleted embryos exhibited normal hatching rates, viability, and ventral nerve cord area when compared with the control. Additionally, CNS localized depletion of Upf1 and Upf2 but not Upf3 at the late stage of embryogenesis resulted in the reduction of the optic lobe of the third instar larval brain. Our findings suggest that NMD factors Upf1 and Upf2 are necessary during the early and late *Drosophila* CNS development. Their absence in the CNS interferes with its developmental processes.

KeyWords: Nonsense-mediated mRNA decay, NMD factors, Central nervous system, Drosophila melanogaster, Embryogenesis

1. Introduction

RNA is the central conduit via which gene information is expressed. Consequently, controlling the half-life of RNA (RNA turnover) as an essential way of regulating the expression of gene information and the level of protein (Serin *et al.*, 2001; Bicknell and Ricci, 2017; Cheng *et al.*, 2017). A major RNA turnover mechanism is nonsense-mediated mRNA decay (NMD). NMD is a highly conserved surveillance pathway that cleans the system from aberrant mRNA harboring premature termination codon (PTC), which, if translated, will lead to possibly undesirable proteins with dominant-negative effect (Ghosh and Jacobson, 2010; Hug *et al.*, 2016; Nickless *et al.*, 2017). Beyond the cleaning task, NMD regulates a considerable percentage of wild-type mRNAs, having thus a gene regulatory function in addition to the quality assurance function (Wittkopp *et al.*, 2009; Nasif *et al.*, 2017). The essential player proteins of the NMD (NMD factors) in *Saccharomyces cerevisae*, *Caenorhabditis elegans*, *Drosophila melanogaster*, and vertebrates are Up-frameshift suppressor (Upf) proteins (Upf1, Upf2, and Upf3) (Peccarelli and Kebaara, 2014; Fatscher *et al.*, 2015; Son *et al.*, 2017). These core NMD factors in coordination with other factors in rather controversial modes activate and execute NMD functions.

NMD has demonstrated significance in the general development and architectural arrangement of CNS in different organisms (Laumonnier *et al.*, 2010; Barone and Bohmann, 2013). For example, NMD is essential in the development and maintenance of synapse structure and function in *Drosophila* (Metzstein and Krasnow, 2006; Long *et al.*, 2009; Giannandrea *et al.*, 2013). Similarly, NMD is indispensable for the proper development of the brain in zebrafish (Wittkopp *et al.*, 2009). In humans, Upf3B-NMD was associated with proper nervous system function (Tarpey *et al.*, 2007; Chan *et al.*, 2009). Furthermore, Upf3 and Upf2 NMDs were associated with neurophysiological abnormalities in humans, mice, and flies (Huang *et al.*, 2018; Johnson *et al.*, 2019; Jega *et al.*, 2020). *In vitro* studies with mouse cell lines have shown that the Upf1-NMD function is critical for neural differentiation (Lou *et al.*, 2014), and Upf3 was associated

* Corresponding author. e-mail: nibrasjega@gmail.com.

with an increase in the self-renewal of primary neural progenitor cells at the expense of their differentiation (Jolly *et al.*, 2013). In another *in vitro* study, Upf3B has shown an influence on the hippocampal neurite growth. The knockdown mutants were found to have altered expression of SIX3 and ROBO1 genes, a master regulator of cortical development and axon guide genes respectively (Nguyen *et al.*, 2012; Alrahbeni *et al.*, 2015).

Nevertheless, developmental processes are diverse and intricate with different requirements of gene products across the developmental stages and organism classes. Typically, the requirement of NMD factors was also variable across organisms and physiological processes (Avery *et al.*, 2011; Fatscher *et al.*, 2015). For instance, in *Drosophila*, Upf1 and Upf2 mutations have shown lethality independent of Upf3 by arresting cell division and survival. On the contrary, Upf3 and SMG1 (another NMD factor) lack any essential role in growth and development (Avery *et al.*, 2011). Depletion of Upf3 orthologue SMG4 in *C. elegans* has proven to only mildly affect the NMD target degradation during development. However, no noticeable effect was seen in the development and differentiation in upf1-3 mutants *S. cerevisae* (Metzstein and Krasnow, 2006; Vicente-Crespo and Palacios, 2010; Alex *et al.*, 2014). In contrast, the loss of Upf proteins in mice was accompanied by severe implications on growth and development (Takahashi and Yamanaka, 2006; Schweingruber *et al.*, 2013). The three Upf proteins and SMG1 are known to be required for NMD in mammalian cells (Serin *et al.*, 2001). Although NMD factors play a role in mammalian neuronal differentiation and survival of neural progenitors *in vitro* (Lou *et al.*, 2014) and synaptic architecture and synaptic vesicle cycle efficacy (Long *et al.*, 2009), testing its *in vivo* role and the stepwise involvement of the NMD factors in nervous system development and function has presented challenges due to the requirement for organism viability of most essential NMD factors. In this research, we used functional genetics and other Drosophila manipulation tools and techniques to study the effect of the loss of function of the core NMD factors in the development of CNS in the early and late embryogenesis.

2. Materials and Methods

2.1. Flies Used

Bloomington Stock number is designated as BM followed by a number. Initials stand for the donors of the flies: MM, AG, and FC for Mark Metzstein, University of Utah Salt City; Acaimo Gonzalez Reyes; and Fernando Casares, Centro Andaluz de Biologia del Desarrollo, Sevilla, Spain (CABD) respectively. The fly stocks used in this work are as follows:

yw GFP hsFLP neoPFRT19A/ yw neoFRT19A (AG), ovo D FRT19A/ c (1) Dx; FLP12 (BM 23880), yw FRT19A Upf1^{13D}/FM7c (MM), yw FRT19A Upf2^{29AA}/FM7c (MM), w; Upf3^{1}/SM6a (MM), Upf3[Df]/SM6 (BM 9424), SP/cyo; UASGFP/TM6B (FC), w;;SimGal4 (FC), neoPFRT19A/ovoDhsFLPFRT19A,Upf1^{13D}FRT19A/ovoD hsFLPFRT19AUpf2^{29AA}FRT19A/ovoDhsFLPFRT19A, SimGal4;UASGFP, Sim Gal4;UAS-Upf1i, Sim Gal4;UAS-Upf2i, SimGal4;UAS-Upf3i.

2.2. Generation and analysis of mutant embryos of Upf1 and Upf2

To analyze the effect of complete loss of *Upf1* or *Upf2* from early embryogenesis, mutant embryos of *Upf1* or *Upf2* were generated from the germline of the sterile mothers of *ovoD* (Avery *et al.*, 2011). Mutant flies were obtained following classical mating scheme (Roote & Prokop, 2013). The mutant virgin female flies Upf1 or Upf2 genes which are on chromosome X - were crossed with mutant males of ovoD also on chromosome X. The chromosomes were inherited following Mendelian rules, and the appropriate mutations were selected against the balancer chromosomes, FM7 for chromosome X. The embryos were collected hourly for 12hours, stained with mouse anti-Repo (1:100) and anti-mouse Cy3 (1:100) as primary and secondary antibodies respectively, and then the CNS was viewed and imaged under fluorescent microscope LEICA DM6000 (Cao *et al.*, 2006).

2.3. Generation of embryos with CNS localized loss of function of NMD factors

To generate wild type embryos with a localized absence of NMD factors in the nervous system, Male and female flies (1-3 days old) in a ratio of 1:1 were collected from each of the following: *Sim-Gal4>UAS-Upf1RNAi, Sim-Gal4>UAS-Upf2RNAi, Sim-Gal4>UAS-Upf3RNAi* (experiments) *and Sim-Gal4>UAS* (control) and placed in a food vial with dry yeast for two days at 18^{o}C. The flies were then placed in an apple juice agar for egg collection. For the early expression of RNAi, the embryos were placed in a 25^{o}C incubator (activation temperature of the Gal4>UAS recombination) 1hr after laying. Meanwhile, for the late expression of the RNAi, the Gal4>UAS recombination was supposedly activated at 25^{o}C; thus, the embryos were first kept at 18^{o}C (inactive temperature for Gal4>UAS) until after 14 hours of laying; they were then transferred to 25^{o}C (active temperature for Gal4>UAS). This was a way of circumventing the activation of the Gal4>UAS recombination until at the late stage of embryogenesis. The embryos were then analyzed for hatching and CNS development.

2.4. Viability and Antibody staining of the embryos

For viability, the hatching and survival index of the embryos were analyzed. To study the CNS structure, embryos were stained with a glial marker [Rabbit anti-repo (1:100)], as a primary antibody to examine the distribution of glial cells as a representation for the overall shape of the CNS and [Rabbit Cy3 (1:100)] was used as a secondary antibody (Cao *et al.*, 2006).

2.5. Immunostaining of the third Instar Larval Brain

To study the larval brain, third instar larvae were selected from the RNAi embryos in which the SimGal4 was expressed at the late stage of embryogenesis among the control (SimGal4>UAS), SimGal4>UAS-*Upf1i*, SimGal4>UAS-*Upf2i* and SimGal4>UAS-*Upf3i*. The larvae were dissected and the brains were collected and stained with a primary antibody [rabbit anti-Dachshund (dac) (1:500)] and a secondary antibody [Cy2 rabbit 1:100] (Cao *et al.*, 2006).

2.6. Measurement of VNC versus the embryo area

The image was converted to gray scale 8bit then measurement and scale were set to area and mm^2

respectively. The VNC was bordered with a free selection tool and the area of the VNC was displayed. Subsequently, the whole embryo was selected in the same way and the area of the embryo was displayed. The area proportion of the VNC was obtained by dividing the area of the VNC by the total area of the embryo multiplied by a hundred

2.7. Microscopy and image analysis

Stack images of Brains were obtained under the Leica SPE DM2500 confocal microscope using Obj. imm x20 with a Zoom Factor of 1 and a pinhole size of 1 Airy unit. Brain images were scanned and stored in a series of 76 images with a vertical spacing of 3µm (Z step). To analyze the stacked images obtained from the confocal microscope, Image J software was used. Z-projects were constructed for each brain. The central brain, optic lobe, and ventral nerve code areas were measured and compared against the control.

3. Results

To assess the role of core NMD factors in the development of the nervous system, we studied the effect of the loss of function of those factors in CNS development. For complete embryonic loss of function, mutant embryos of Upf1 or Upf2 were generated from the germline of a sterile female fly carrying the ovoD mutation. By doing this, it was ensured that any egg laid by these flies was maternally mutant for the selected Upf gene. These upf1 and upf2 maternal mutant eggs showed incompatibility with life as very few hatched (5.35% and 8.35% for Upf1 and Upf2 respectively), and only 0.82% and 1.78% for Upf1 and Upf2 respectively developed to second instar larval stage and none developed to the third instar larval stage. Many of these embryos are characterized by having irregular dorsal appendages, (94.02% and 90.82% for Upf1 and Upf2 respectively) and abnormally high yolk (Table 1).

Similarly, the ventral nerve cord failed to be established in most of the embryos, 96.02% and 89.3% for Upf1 and Upf2 respectively (Figure 1).

Table 1. Development analysis of the maternally mutant embryos

Average hatching, presence of regular dorsal appendages and shape, the yolk condition, and survival to the second instar larval stage of the maternally mutant embryos. FRT19A /ovoD FRT19A (control), Upf1 [13D] FRT19A /ovoD FRT19A (Upf1 mutants) and Upf2 [29AA] FRT19A /ovoD FRT19A (Upf2 mutants).* indicate significant difference compared to control ($p<0.001$, ANOVA, and Tukey's pairwise). Data are presented as means ± SEM

Genotype (no of female flies, N= 20)	Average No. of eggs laid	% Embryos hatched	% Embryos with regular dorsal appendages and shape	% Embryos with abnormally high yolk	% Embryos survived to 2nd instar
FRT19A /ovoD FRT19A	115 ± 4.16	90.5 ± 1.09	98.61 ± 1.91	1.31 ± 0.29	74.02 ± 2.11
Upf1 [13D] FRT19A /ovoD FRT19A	179 ± 21.7	5.35 ± 0.73*	3.98 ± 0.46*	94.02 ± 1.69*	0.82 ± 0.71*
Upf2 [29AA] FRT19A /ovoD FRT19A	118 ± 6.69	8.35 ± 0.89*	10.7 ± 0.70*	90.82 ± 1.61*	1.78 ± 0.32*

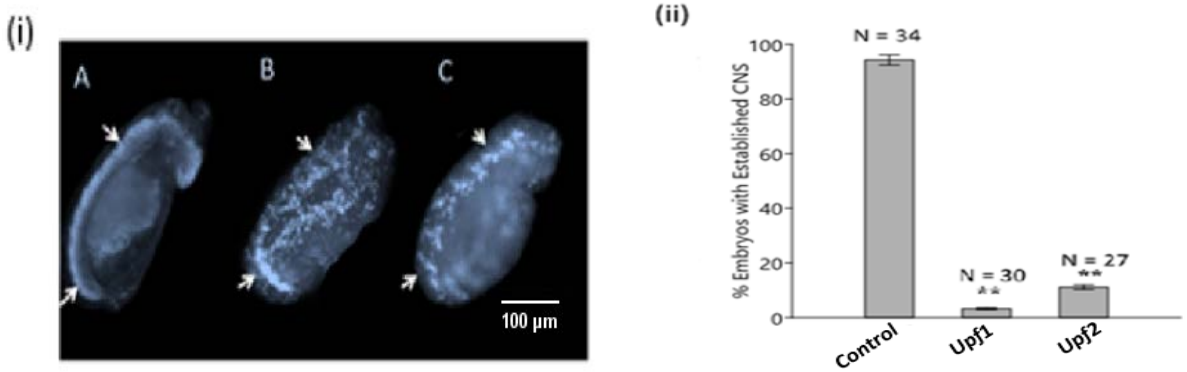

Figure 1. Central nervous system establishment in *Upf*1 and *Upf*2 mutant embryos**. (i)** Lateral confocal images of the central nervous system in embryos. Anti-repo staining (a glial marker) showing the ventral nerve cord of stage 12 to 14 in **(A)** Control, (**B)** and **(C)** maternal mutant embryos of *Upf*1 and *Upf*2 respectively displaying unestablished CNS. Arrows point to the position of the nerve cord. Anterior end on the right. **(ii)** Percentage of embryos with established CNS in FRT19A (control embryos), $Upf1^{13D}$ (maternal homozygous *Upf*1 mutant embryos), and $Upf2^{29AA}$ (maternal *Upf*2 mutant embryos). * Indicates significant difference compared to control ($p<0.0001$, ANOVA, and Tukey's pairwise). Data are presented as means ± SEM

Subsequently, temperature-sensitive SimGal4>UAS-*RNAi* was used to drive the localized depletion of Upf1, Upf2, and Upf3 in the CNS at an early and late stages of embryogenesis (stages 5 and 13 respectively). The result showed a significant reduction of hatching in both the early and late stage depleted embryos of Upf1 and Upf2 but not Upf3. However, there was slight improvement of hatching in the embryos of late expression of RNAi. The embryos that hatched displayed high chances of reaching adulthood as indicated by the percentage of larva adult escapers (Table 2).

Table 2. Hatching analysis of the embryos with Upf loss of functions localized in the CNS

Average hatching and survival of the genotypes: *Sim-Gal4>UAS* (control), *Sim-Gal4>UASUpf1i (Upf1-RNAi), Sim-Gal4>UASUpf2i (Upf2-RNAi)* and *Sim-Gal4>UASUpf3i (Upf3-RNAi).* *Indicate significant difference compared to the control ($p<0.001$), † Indicate significant difference when compares with the Upf3-RNAi ($p<0.05$). The proportion of survival is calculated as P = f/n; n is the total number of larvae collected for rearing; f = number of larvae reaching the adult stage

Time of expression of Gal4	Genotype (no of female flies, N= 25)	Average No. of eggs laid	Percentage hatching	Percentage of larva adult escapers
Early Embryogenesis	*Sim-Gal4>UAS*	131.2±5.5	95.12±5.1	96.31±5.4
	Sim-Gal4>UAS-Upf1i	122.8±3.9†	12.05±2.1*†	78.38±2.5*
	Sim-Gal4>UAS-Upf2i	105.6±5.0	21.97.0±4.5*†	84.48±3.2
	Sim-Gal4>UAS-Upf3i	159.6±8.4	65.04±3.9	94.22±4.8
Late Embryogenesis	*Sim-Gal4>UAS*	252.2±6.9	83.98±0.8	93.31±3.0
	Sim-Gal4>UAS-Upf1i	116.1±4.4†	37.51±4.3*†	81.18±1.9
	Sim-Gal4>UAS-Upf2i	124.6±5.0	32.74±1.7*†	87.25±6.8
	Sim-Gal4>UAS-Upf3i	207.7±3.2	65.05±4.2	91.70±2.0

Furthermore, the lateral view of the Upf1 and Upf2 embryos showed a significant reduction in the area of VNC with respect to the total area of the embryo in the early depleted embryos of Upf1 and Upf2 (Figure 2). However, no significant difference is noticed when the depletion was delayed till the late stage of embryogenesis (Figure 3)

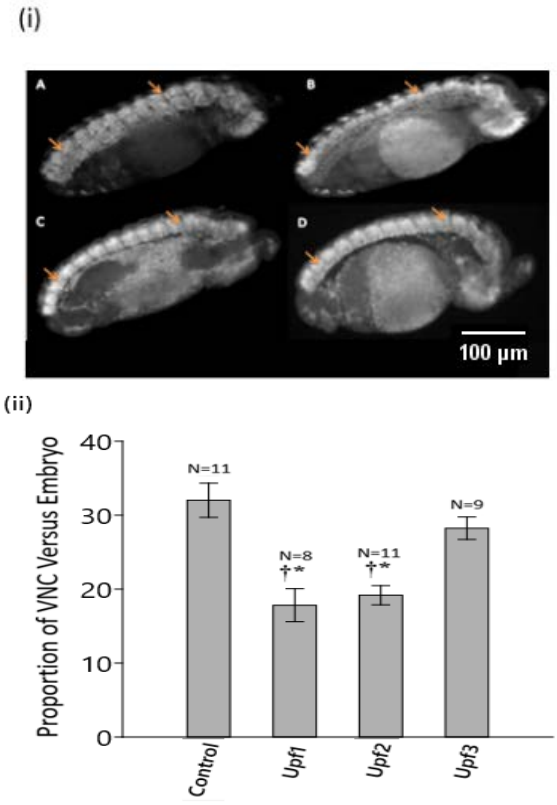

Figure 2. Central nervous system establishment in embryos with early *Upf* loss of functions localized in the CNS. (i) Lateral view of CNS of embryos. (A) Control, (B) *Upf1*i, (C) *Upf2*i, *and* (D) *Upf3*i. Arrows point to the ventral nerve cord. (ii) The area of ventral nerve cord compared to the total area of the embryos in the genotypes: Control (*Sim-Gal4>UAS*), *Upf1i* (*SimGal4UASUpf1i*), *Upf2i* (*Sim-Gal4>UASUpf2i*) and *Upf3i* (*Sim-Gal4>UASUpf3i*); *indicate significant difference when compared with the control, $p<0.001$. †Indicate significant difference compared to the *Upf3*i, $p<0.05$. (ANOVA and then Turkey's pairwise were used for the statistical analysis).

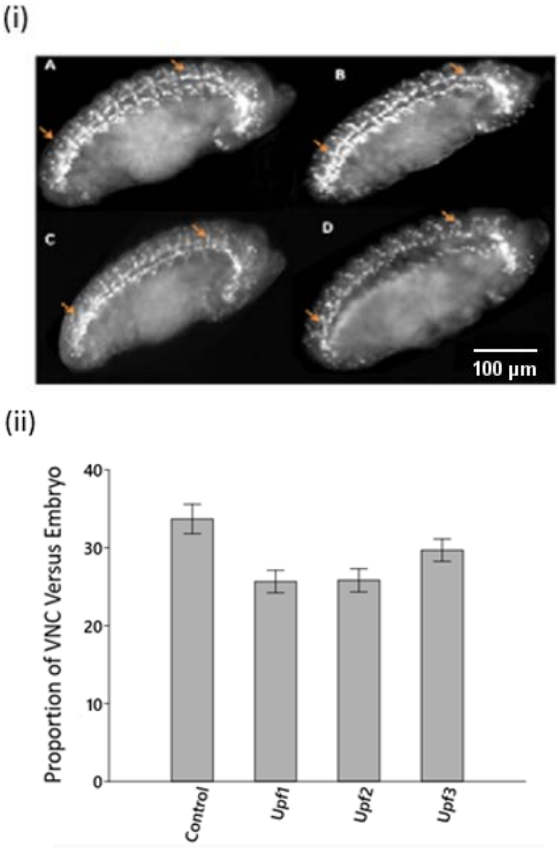

Figure 3. Central nervous system establishment in embryos with late Upf loss of functions localized in the CNS. (i) Lateral view of CNS of embryos. (A) Control (Sim-Gal4>UAS), (B) Upf1i (SimGal4UASUpf1i), (C) Upf2i (Sim-Gal4>UASUpf2i), and (D) Upf3i (Sim-Gal4>UASUpf3i). Arrows point to the ventral nerve cord (ii) The area of ventral nerve cord compared to the total area of the embryos in the genotypes: Control (Sim-Gal4>UAS), Upf1i (SimGal4UASUpf1i), Upf2i (Sim-Gal4>UASUpf2i) and Upf3i (Sim-Gal4>UASUpf3i);

Due to the observed improvement in hatching and survival of the embryos with delayed depletion of Upf1 and Upf2, the resultant third instar larva brains of these embryos were analyzed. The result showed normal VNC development but a significant reduction in the area of optic lobes of Upf1 and Upf2 mutant larval brains, but there was no significant reduction of any parameter noticed in the Upf3 mutants' larval brain (Figures 4 and 5).

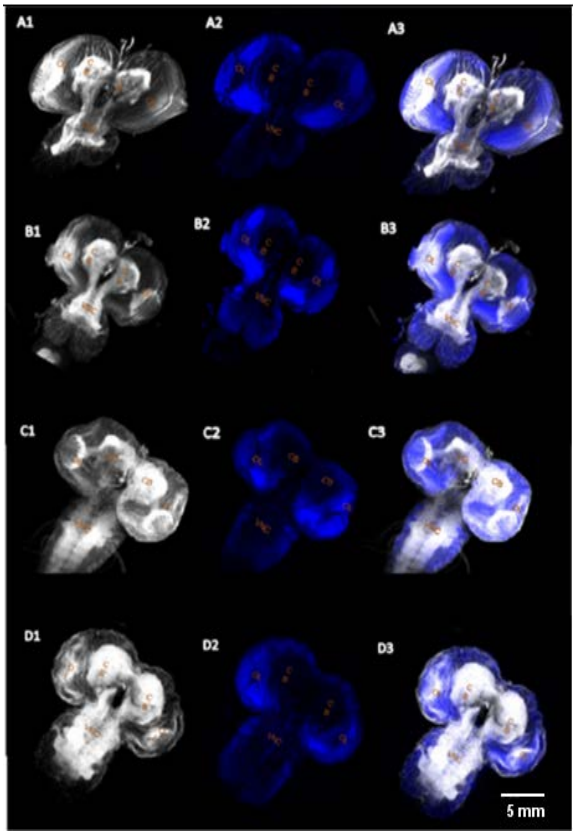

Figure 4. The central nervous system of mutant larvae. Confocal images of third instar larvae brains stained with a dachshund (gray) labeling the CNS tissues and Hoechst (blue) for nuclei. (A1 – A3) brain from the control (Sim-Gal4>UAS-GFP). (B1 – B3) Brain from the *Upf1*i (SimGal4>UAS-*Upf1*i). (C1 – C3) Brain from the *Upf2*i (SimGal4>UAS-*Upf2*i). (D1 – D3) Brain from the *Upf3*i (SimGal4>UAS-*Upf3*i). A1, B1, and C1: Dachshund; A2, B2, C2: Hoechst; A3, B3, C3: composite images; OL: optic lobe; CB: central brain; VNC: ventral nerve cord.

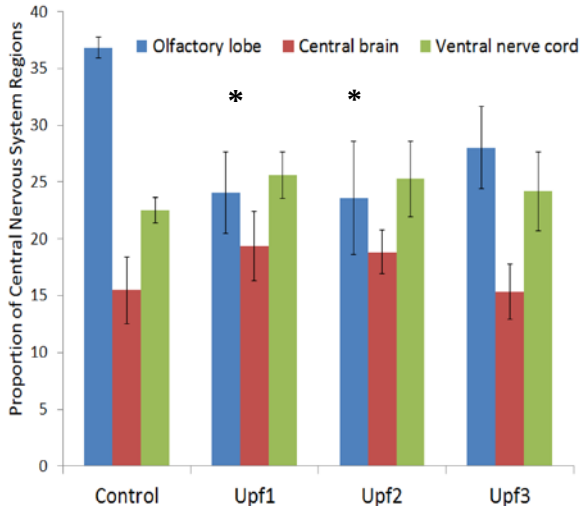

Figure 5. The proportion of central nervous system regions in larvae with loss of function of NMD factors in late NS development. The proportion of the area of OL (optic lobes), CB (central brains) and VNC (ventral nerve cords) to the total area of the larval brain, for the genotypes: Control (*Sim-Gal4>UAS*), *Upf1i* (*Sim-Gal4>UAS-Upf1i*), *Upf2i* (*Sim-Gal4>UAS-Upf2i*) and *Upf3i* (*SimGal4UASUpf3i*). *Indicate significant difference when compared with the control ($p<0.001$; ANOVA and Tukey's pairwise).

4. Discussion

NMD machinery ensures the production of functional proteins by eliminating mRNAs with PTC. Studying the developmental involvement of this pathway has proven important in pursuit of potential therapies in cancer and developmental biology. Similarly, NMD factors show promising roles in mammalian neuronal differentiation and survival of neural progenitors *in vitro* (Lou *et al.*, 2014) and in synaptic architecture and synaptic vesicle cycle efficacy (Long *et al.*, 2009), but their *in vivo* role in nervous system development and function has been hard to test due to the requirement for viability of most core NMD factors. In this work, we focused on the development of CNS during early embryonic and larval stages of *Drosophila*, in the absence of core NMD factors *Upf1*, *Upf2*, and *Upf3*, Owing to the remarkable similarities of insects with vertebrate in brain and nerve cord development, especially regarding the expression and function of homologous genes (Holley *et al.*, 1995; Arendt and Nübler-Jung, 1999; Denes *et al.*, 2007). Thus, we checked the ventral nerve cord (VNC) development in *Upf1* and *Upf2* maternally mutant embryos and found that VNC failed to be established in most of the embryos (Figure 1). The embryos were incompatible with life, very few survived to the second instar larvae stage, and none survived to adulthood (Table 1)

To investigate the localization effect of NMD absence in the CNS development, we used a temperature-sensitive GAL4/UAS system to derive the expression of *RNAi* and depleted the *Upf1*, *Upf2* and *Upf3* at early stage of embryogenesis specifically during the midline cells development. We found that there was a slight improvement in the survival and establishment of VNC compared to the maternally mutant embryos, but lethality was still near 80 percent. Also, significant reduction in the area size of the VNC of *Upf1* and *Upf2* depleted embryos was also observed in those embryos (Table 2). Although the restriction of the repression of the mutant core NMD factors to the midline reduced the burden of early cellular damage as noticed in the maternally mutant embryos, high mortality and reduced VNC were still noticed (Figure 3). This indicates that the expression of NMD factors in the nervous system at this stage of development is necessary for organismal viability. Nevertheless, delaying the depletion of Upf1 and Upf2 till the late stage of embryogenesis slightly improved the hatching approximately from 12% to 38% and 22% to 33% for Upf1 and Upf2 respectively (Figure 2). Still there was significant difference when compared with the control or Upf3 depleted embryos. These findings suggest that NMD plays a role in both early and late embryogenesis.

Dpp protein is implicated in the determination of the initial dorsal-ventral pattern of *Drosophila* embryo, by providing the signal for the border establishment along the domains of the dorsal-ventral axis, which happen before gastrulation at the cellular blastoderm stage (stage 5-6) 2-3hours after egg laying (Raz and Shilo, 1993). Previous work showed that the elimination of the *Drosophila* zygotic Dpp pathway resulted in embryos with no ventral structures including CNS (Raz and Shilo, 1993). The work of Shum *et al.*, (2016) in hESCs that established the role of NMD in regulating TGF-β and BMP signaling

(mammalian orthologue pathways of *Drosophila* Dpp*) in* ectoderm and mesoderm differentiation suggests that activation of Dpp (TGF-β homolog) may have been disturbed due to the absence of NMD and, consequently, the establishment of CNS (VNC in this case) was interfered with. In support of this hypothesis, our analysis of GSCs showed that Dpp signaling was disrupted in *Drosophila* germline stem cells (Unpublished). Avery *et al* (2011) showed that the localization of Gurken-Torpedo signaling pathway (TGF-alpha – EGF in vertebrates) that targets Broad-Complex (BR-C) was adequate in NMD mutant eggs. Since the restriction of BR-C expression depends on the interaction between EGF (Gurken) and BPM (Deng and Bownes, 1997), then the integrity of DPP signaling in this system might have been disrupted in the CNS phenotype described in this work.

The loss of NMD at midline cells developmental stage in Sim>Gal4 embryos might have affected the characteristic cell division of the neuroectoderm. Consequently, the patterning of the *Upf1* and *Upf2* depleted embryos during embryogenesis is compromised (Chang *et al.*, 2000), resulting in the reduced area of the VNC (Figure 4 and 5). Another possibility could be the compromised establishment and maintenance of the ventral epidermal and neuronal cell lineage (Chang *et al.*, 2000) due to the loss of NMD. This may have caused molecular deficit and defects in the establishment of the VNC, which results in the observed low survival rate.

Full establishment of cellular identities within ventral ectoderm and the differentiation of the ventral epidermis are achieved at the end of stages 9 and 12 of embryonic development respectively (Raz and Shilo, 1993). At stage 13, the ganglion mother cells will start differentiating into neurons. When expression of the RNAi was delayed to the beginning of stage 13, a dramatic improvement of viability and hatching of the embryos was noticed, indicating that the requirement of NMD for viability is due to its role in early embryogenesis. Moreover, analysis of the third instar larval brain from those embryos showed no reduction in the size of the central brain and the ventral nerve cords of the mutant larvae. However, we found a significant reduction in the optic lobes of the *Upf1* and *Upf2* larva but not in *Upf3* mutants (Figure 4). Interestingly, Lou *et al* shows that the deficit of *Upf1* and *Upf3B* in mouse neuronal stem cells led to reduced proliferation and increased differentiation into neural progenitors which expressed some markers of mature neurons (Lou *et al*., 2014). A similar mechanism could be at play in *Drosophila* optic lobes since the formation of vesicles of the optic lobes from the OL precursors begins at stage 13 (Hartenstein, 1993; Spindler and Hartenstein, 2010). However, NMD is a strictly regulated process in guiding the neuronal development. The *Upf1* and *Upf2* also have other non NMD functions that makes it difficult to tell whether the phenotypic expression is a result of NMD malfunction or other non NMD functions of the factors. Furthermore, the staining method employed was a proxy to determining the overall structure of the CNS using glial cells. The distribution, organization and complexity in relationship between the glial cells and neural formation are yet to be fully encompassed (Bahrampour *et al*., 2017). As such, the interference of glial cells factors in the observed defects may not be ruled out. Thus, an unbiased analysis of the house keeping genes in relation to these phenotypes may provide better explanation for NMD regulation and also the level of NMD participation in the phenotypes.

5. Conclusion

Our work has demonstrated neurodevelopmental and neurophysiology defects in flies mutants for core NMD factors. We showed the failure to establish CNS in *Upf1* and *Upf2* maternally mutant embryos. When the loss of *Upf1* and *Upf2* was localized in the nervous system, the result is nearly lethal with death occurring at the embryonic stage. We also revealed that those flies with loss of function of *Upf1* and *Upf2* localized to the NS exhibited a reduction of the areas of the ventral nerve cord in embryos and the optic lobes in the larvae.

Acknowledgements

The authors would like to thank the following for their contributions in making this work a possibility: Nigerian Tertiary Education Trust Fund (Tetfund) for providing the study grant and the Spanish Ministry of Economics for providing the travel grant to Centro Andaluz de Biologia del Desarrollo, Universidad de Pablo Olavide, Sevilla, Spain under the program i-COOP+2015. We also like to appreciate Acaimo González Reyes for providing the lab, facilities and moral support and Fernando Casares for his technical support. Lastly, we appreciate Isabel Palacios and Mark Metzstein for donating the flies used in this work.

References

Alex C, Hao H, Shawn GR, Julie H, Mark Y, Metzstein, MM. 2014. In vivo determination of direct targets of the nonsense mediated decay pathway in Drosophila. G3: Genes|Genomes|Genetics. 4(3): 485–496.

Alrahbeni T, Sartor F, Anderson J, Miedzybrodzka Z, McCaig C, Müller B. 2015. Full UPF3B function is critical for neuronal differentiation of neural stem cells. Mol Brain. 27;8:33.

Arendt D and Nübler-Jung K. 1999. Comparison of early nerve cord development in insects and vertebrates. Development. 126(11): 2309–2325.

Avery P, Vicente-Crespo M, Francis D, Nashchekina O, Alonso CR, Palacios IM. 2011. Drosophila Upf1 and Upf2 loss of function inhibits cell growth and causes animal death in a Upf3-independent manner. RNA. 17(4):624-38

Bahrampour S, Gunnar E, Jonsson C, Ekman H, and Thor S. 2017. Neural Lineage Progression Controlled by a Temporal Proliferation Program. Developmental Cell 43, 332–348

Barone MC, Bohmann D. 2013. Assessing neurodegenerative phenotypes in Drosophila dopaminergic neurons by climbing assays and whole brain immunostaining. J Vis Exp. 24;(74):e50339.

Bicknell AA, Ricci EP. 2017. When mRNA translation meets decay. Biochem Soc Trans. 15;45(2):339-351

Cao J, Brett J, Pellock KW, and Laurel, AR. 2006. A commercial phospho-Smad antibody detects endogenous BMP signaling in Drosophila tissues. Dros. Inf. Serv, 89: 131–135.

Chan WK, Bhalla AD, Le Hir H, Nguyen LS, Huang L, Gécz J, 2009. Wilkinson MF. A UPF3-mediated regulatory switch that maintains RNA surveillance. Nat Struct Mol Biol. 200916(7):747-53.

Chang J, Kim IO, Ahn JS, Kwon JS, Jeon SH, Kim SH. 2000. The CNS midline cells coordinate proper cell cycle progression and identity determination of the Drosophila ventral neuroectoderm. Dev Biol. 227(2):307-23

Cheng J, Maier KC, Avsec Ž, Rus P, Gagneur J. 2017. Cis-regulatory elements explain most of the mRNA stability variation across genes in yeast. RNA. 23(11):1648-1659

Denes AS, Jékely G, Steinmetz PR, Raible F, Snyman H, Prud'homme B, Ferrier DE, Balavoine G, Arendt D. 2007. Molecular architecture of annelid nerve cord supports common origin of nervous system centralization in bilateria. Cell. 129(2):277-88.

Deng WM, Bownes M. 1997. Two signalling pathways specify localised expression of the Broad-Complex in Drosophila eggshell patterning and morphogenesis. Development. 124(22):4639-47

Fatscher T, Boehm V, Gehring NH. 2015a. Mechanism, factors, and physiological role of nonsense-mediated mRNA decay. Cell Mol Life Sci. 72(23):4523-44

Ghosh S, Jacobson A. 2010. RNA decay modulates gene expression and controls its fidelity. Wiley Interdiscip Rev RNA. 1(3):351-61.

Giannandrea M, Guarnieri FC, Gehring NH, Monzani E, Benfenati F, Kulozik AE, Valtorta F. 2013. Nonsense-mediated mRNA decay and loss-of-function of the protein underlie the X-linked epilepsy associated with the W356× mutation in synapsin I. PLoS One. 8(6):e67724

Hartenstein, V. 1993. Atlas of Drosophila Development. Atlas of Drosophila Development, Cold Spring Harbor Laboratory Press. 94th Edition pp. 1–57.

Holley SA, Jackson PD, Sasai Y, Lu B, De Robertis EM, Hoffmann FM, Ferguson EL. 1995 A conserved system for dorsal-ventral patterning in insects and vertebrates involving sog and chordin. Nature. 376(6537):249-53.

Huang L, Low A, Damle SS, Keenan MM, Kuntz S, Murray SF, Monia BP, Guo S. 2018. Antisense suppression of the nonsense mediated decay factor Upf3b as a potential treatment for diseases caused by nonsense mutations. Genome Biol. 15;19(1):4.

Hug, N., Longman, D. and Cáceres, JF. 2016. Mechanism and regulation of the nonsense-mediated decay pathway. Nucleic Acids Research. 44(4):1483-1495.

Jega, SA, Adedeji, AA and Vicente-crespo, M 2020. Manifestation of Functional Defects of Nervous System in Upf3 Mutants Drosophila melanogaster at Larval and Adult Stages. Advances in Biochemistry. 8(2):38-44.

Johnson JL, Stoica L, Liu Y, et al. 2019. Inhibition of Upf2-Dependent Nonsense-Mediated Decay Leads to Behavioral and Neurophysiological Abnormalities by Activating the Immune Response. Neuron. 104(4):665-679.e8.

Jolly LA, Homan CC, Jacob R, Barry S, Gecz J, 2013. The UPF3B gene, implicated in intellectual disability, autism, ADHD and childhood onset schizophrenia regulates neural progenitor cell behaviour and neuronal outgrowth. Hum Mol Genet. 22(23):4673-87.

Laumonnier F, Shoubridge C, Antar C, Nguyen LS, Van Esch H, Kleefstra T, Briault S, Fryns JP, Hamel B, Chelly J, Ropers HH, Ronce N, Blesson S, Moraine C, Gécz J, Raynaud M. 2010. Mutations of the UPF3B gene, which encodes a protein widely expressed in neurons, are associated with nonspecific mental retardation with or without autism. Mol Psychiatry. 15(7):767-76.

Long AA, Mahapatra CT, Woodruff EA 3rd, Rohrbough J, Leung HT, Shino S, An L, Doerge RW, Metzstein MM, Pak WL, Broadie K. 2010. The nonsense-mediated decay pathway maintains synapse architecture and synaptic vesicle cycle efficacy. J Cell Sci. 1;123(Pt 19):3303-15.

Lou HC, Ada S., Eleen YS., Josh LE, Lulu HR, Karam MF. 2014. Posttranscriptional Control of the Stem Cell and Neurogenic Programs by the Nonsense-Mediated RNA Decay Pathway. Cell Rep. 6(4):748–764.

Metzstein, MM. and Krasnow, MA. 2006. Functions of the Nonsense-Mediated mRNA Decay Pathway in Drosophila Development. PLoS Genetics. 2(12):20180.

Nasif, S., Contu, L. and Mühlemann, O. 2017. Beyond quality control: The role of nonsense-mediated mRNA decay (NMD) in regulating gene expression. Semin Cell Dev Biol. 75:78-87

Nguyen LS, Jolly L, Shoubridge C, *et al.* 2012. Transcriptome profiling of UPF3B / NMD-deficient lymphoblastoid cells from patients with various forms of intellectual disability. Molecular Psychiatry. 17(11):1103–1115.

Nickless, A., Bailis, JM. and You, Z. 2017. Control of gene expression through the nonsense-mediated RNA decay pathway. Cell Biosci, 7:26.

Peccarelli, M. and Kebaara, BW. 2014. Regulation of natural mRNAs by the nonsense-mediated mRNA decay pathway. Eukaryotic Cell, 13(9):1126–1135.

Raz, E. and Shilo, B. 1993. Establishment of ventral cell fates in the Drosophila embryonic ectoderm requires DER , the EGF receptor homolog, Genes & Dev. 7:1937–1948.

Rehwinkel J, Letunic I, Raes J, Bork P, Izaurralde E. 2005.Nonsense-mediated mRNA decay factors act in concert to regulate common mRNA targets. RNA, Oct;11(10):1530-44.

Roote J, and Prokop A. (2013). How to Design a Genetic Mating Scheme: A Basic Training Package for Drosophila Genetics. Investigation, 3(February), 353–358.

Schweingruber C, Rufener SC, Zünd D, Yamashita A, Mühlemann O. 2013. Nonsense-mediated mRNA decay - mechanisms of substrate mRNA recognition and degradation in mammalian cells. Biochim Biophys Acta, 1829(6-7):612-23.

Serin G, Gersappe A, Black JD, Aronoff R, Maquat LE. 2001. Identification and characterization of human orthologues to Saccharomyces cerevisiae Upf2 protein and Upf3 protein (Caenorhabditis elegans SMG-4). Mol Cell Biol. 21(1):209-23.

Son H, Seo M, Ham S, et *al*. 2017. RNA surveillance via nonsense-mediated mRNA decay is crucial for longevity in daf-2/insulin/IGF-1 mutant C. Elegans. Nature Communications. 8, 14749.

Spindler SR. and Hartenstein V. 2010. The Drosophila neural lineages : a model system to study brain development and circuitry. Dev Genes Evol, 220:1–10.

Takahashi K. and Yamanaka S. 2006. Induction of Pluripotent Stem Cells from Mouse Embryonic and Adult Fibroblast Cultures by Defined Factors. Cell, 126(4), pp. 663–676.

Tarpey PS, Raymond FL, Nguyen LS, et al. 2007. Mutations in UPF3B , a member of the nonsense- mediated mRNA decay complex , cause syndromic and nonsyndromic mental retardation. Nature Genetics, 39(9):1127–1133.

Vicente-Crespo, M. and Palacios, IM. 2010. Nonsense-mediated mRNA decay and development : shoot the messenger to survive. Biochem. Soc. Trans, 38, pp. 1500–1505.

Wittkopp N, Huntzinger E, Weiler C, Saulière J, Schmidt S, Sonawane M, Izaurralde E. 2009. Nonsense-mediated mRNA decay effectors are essential for zebrafish embryonic development and survival. Mol Cell Biol. 29(13):3517-28.

JJBS

Volume 16, Number 1,March 2023
ISSN 1995-6673
Pages 63 – 71
https://doi.org/10.54319/jjbs/160109

Jordan Journal of Biological Sciences

The ability of *Lactobacillus helveticus -13* (*Lh-13*) Isolate Isolated from Lactic Acid Products to form A biofilm by Applying Modern Microscopy Methods

Zhanerke Amirkhanova[1,2], Saule Akhmetova[2,*], Samat Kozhakhmetov[3], Almagul Kushugulova[3], Rahat Bodeeva[1], Leila Ahvlediani[4], Anara Turmukhambetova[2]

[1]Buketov Karaganda University, University Street, 28, Karaganda, Kazakhstan; [2]Karaganda medical university, Gogol Street, 40, Karaganda, Kazakhstan; [3]Laboratory of Human Microbiome and Longevity "National Laboratory Astana" Nazarbayev University, Kabanbay Batyr Ave., 53, Astana, Kazakhstan; [4]Batumi International University, Fridon khalvashi street, 237, Batumi, Georgia.

Received: May 30, 2022; Revised: October 8, 2022; Accepted: October 21, 2022

Abstract

This article presents the study of the morpho-cultural properties and biofilm formation of lactobacilli isolated from lactic acid products (irimchik, suzbe, cheese, ashygan kozhe) produced in different districts of the Karaganda region. The species of the isolated lactic acid bacillus isolates were identified by using a MALDI-TOF mass spectrometer.

The evaluation of the resistance of the isolates to various stress factors, such as the ability to survive at low acidic pH values and in the presence of bile, made it possible to identify some promising isolates – *Lactobacillus helveticus -13* (*Lh-13*) and *Lactiplantibacillus plantarum* – 5 (*Lpl-5*), for studying antimicrobial and biofilm-forming activity.

The antimicrobial activity of *Lh-13*, *Lpl-5* was closely studied. They have a certain level of antibacterial and fungicidal activities, which indicates their pronounced inhibition against indicator microorganisms.

Using a laboratory robot, *TecanEVolizer100 (Tecan)*, the optical density of *Lh-13*, *Lpl-5* was studied in the wells of polystyrene plates, reflecting the intensity of biofilm formation along their surface. Using laser capture microdissection, the images of cell morphology in biofilm of *Lh-13* isolates included in the matrix were obtained. The atomic force microscopy made it possible to study the two and three-dimensional morphological images of biofilm-forming isolates of *Lh-13*.

Keywords*: lactobacilli, mass spectrometry (MALDI-TOF MS), biofilm, laser capture microdissection, atomic force microscopy, antimicrobial activity.*

1. Introduction

The advances in the sciences of human and animal microbiota confirm the beneficial health effects of lactic acid foods and probiotics containing probiotic bacteria, which can adhere and colonize on the inner wall of the intestinal tract, form microbial communities, and regulate the balance of intestinal microflora, etc. (Hill *et al.,* 2014; George *et al.,* 2018; Yue *et al.,* 2020; Bechelaghem *et al.,* 2022).

There are many lactic acid products and probiotics on the market right now. They are used to provide alleged health benefits based on the probiotic properties of specific strains of lactic acid bacteria (Casey *et al.,* 2004; Mitropoulou *et al.,* 2013; Singh *et al.,* 2012). The effectiveness of probiotic agents and functional food products primarily depends on the properties of the species of various strains of lactic acid bacteria included in their composition. Lactobacilli are a key component of starter cultures for such products (Corona-Hernandez *et al.,* 2013; Taverniti *et al.,* 2014). Lactobacilli, along with other members of the normal microbiota of human and animal mucous membranes, plays an important role in the body's anti-infectious defense and the formation of microorganism colonization resistance (Ghosh *et al.,* 2019; Zeng *et al.,* 2020).

In the modern biomedical practice, they can be used as methods of personalized medicine: the probiotic culture of lactobacilli exhibits antimicrobial activity against the pathogenic flora of the patient as well as stimulates antagonism and is not inhibited by pathogens (Ejtahed *et al.,* 2017; Torres and Tovar, 2021; Schupack *et al.,* 2022).

The viability and survival of lactobacilli under stressful conditions are the most important parameters for ensuring therapeutic functions. This parameter is also considered an important criterion for the selection of an active probiotic strain. In addition, the beneficial properties of lactobacilli are in their ability to form biofilms, which allows them to withstand environmental conditions, resulting in successful colonization and maintenance of their population (Guarner *et al.,* 2005; Son *et al.,* 2017).

A biofilm, according to current concepts, is a community of microorganisms connected by the surface and enclosed in a matrix composed of extracellular polymeric substances synthesized by them, as well as polysaccharides and proteins. Biofilm formation by probiotic bacteria such as lactic acid bacteria is considered

* Corresponding author. e-mail: S.Ahmetova@qmu.kz.

a beneficial property as it can promote colonization and longer persistence in the host mucosa avoiding colonization by pathogenic bacteria (Salas-Jara *et al.,* 2016; Tatsaporn and Kornkanok , 2020).

The scientifically established phenomenon of the protective function of the lactobacilli's biofilm is promising for further use in the medical, pharmaceutical, food and agricultural industries, which is a priority for Kazakhstan (Aitzhanova *et al.,* 2020).

In this regard, the above mentioned conditions prompted the search for new unique candidates for probiotic cultures of lactobacilli with highly active probiotic properties having *the GRAS status* (*generally recognized as safe)* (Wu *et al.,* 2017).

The search and study of the probiotic properties of domestic competitive starter cultures isolated from traditionally natural ethnical products, such as those traditionally produced, is an effective way to obtain genetically stable strains of probiotic cultures as a constant source of the strains for the needs of the country to improve the quality of microbiological resources in the national stocks.

The present study is aimed at screening the probiotic properties (tolerance to acidic pH and bile) of lactic acid bacillus isolates isolated from national lactic acid products in order to assess the ability to form biofilms and to study the morphology of cells in biofilm using laser capture microdissection and atomic force microscopy.

2. Materials and methods

Materials. For the given study, the isolates of lactobacilli isolated from traditional home-made national lactic acid products produced in different districts of the Karaganda region, Kazakhstan were used (Table 1).

Table 1. National lactic acid products and number of samples from different regions.

National lactic acid products (Number of samples)	Regions				
	Karkaraly	Zhanaarka	Aktogay	Bukhar-Zhyrau	Osakarov district
Irimchik	2	1	3	2	-
Suzbe	2	2	3	2	-
Cheese	-	-	-	3	1
Ashygan kozhe	1	-	2	-	-
Total	24				

Note: The results of the primary screening are published earlier in the given work: «Screening of Antimicrobial and Adhesive Activity of Lactobacilli Isolated from the National Food Products from Different Districts of the Karaganda Region (Kazakhstan)» Open Access Macedonian Journal of Medical Sciences. 2021 Sep 24; 9(A):827-832.

2.1. Isolation and identification of lactobacilli from dairy products

One of each sample (irimchik, suzbe, cheese, ashygan kozhe) was taken aseptically and transferred to a 10 ml phosphate buffered saline and then vortexed. The 1 ml of the produced homogenate was then inoculated in a 10 ml MRS broth contained in screw caped tube, and incubated under anaerobic conditions for 24 hours at 37°C. Further on, the serial dilutions prepared from each obtained culture were spread over the MRS (deMan, Rogosa, Sharpe) agar-1 plates and incubated anaerobically for 48 hours at 37° C (Lin *et al.,* 2006; Mulaw *et al.,* 2019). After incubation, the isolated colonies underwent both the Gram stain and catalase test. Only rod-shaped, gram-positive, catalase-negative isolates were selected for the tests. The individual colonies were subcultured in the MRS broth for 48 hours at 37°C, and the control smears were taken. The selected strains were stored in the MRS broth containing 20% glycerol at -22°C for further analysis. The isolates were activated in the MRS broth prior to each analysis (Wang *et al.,* 2016).

The pure cultures of lactobacilli were identified using MALDI-TOF MS (*Matrix Supported Laser Desorption / Ionization Flight Time Mass Spectrometry, Bruker, Germany*). The bacterial spectra were matched against the MALDI-TOF MS biotype reference library (Alatoom *et al.,* 2011; Schulthess *et al.,* 2014).

2.2. Tolerance to acidic pH and bile

The acid resistance of the bacterial isolate was observed by incubating lactobacilli at pH3 in the MRS broth. 9 ml of the acidified MRS broth (adjusted to pH3 by 5N HCl) and 1 ml of the MRS broth containing 10^9 CFU/ml of the test isolate of lactobacilli were added to each tube. The tubes with the suspension were further incubated at 37°C for 24 hours under anaerobic conditions. The growth of the isolates was monitored for 0h, 3h and 6h by measuring the absorbance of the culture broth at 492 nm using a spectrophotometer. The growth of lactobacilli in the MRS broth without HCl was used as a control (Kim *et al.,* 2019). The experiment was repeated three times.

The isolated isolates were tested for bile tolerance. To study the tolerance of lactic acid bacillus isolates to bile, a medicinal bile preparation containing natural gallbladder bile of cattle was used. Bile medicine tolerance of the isolated bacteria was examined by inoculating the freshly cultured isolates at 10^7 CFU / ml into the MRS broth containing bile medicine at different concentrations (0.3%; 0.5%; 1%). The medium was then incubated at 37°C in anaerobic conditions. The growth of the isolates was monitored at 0h and 3h by measuring the absorbance of the culture broth at 492 nm using a spectrophotometer. The growth of lactobacilli in the MRS broth without bile was used as a control (Tambekar and Bhutada, 2010). The experiment was repeated three times.

2.3. Antimicrobial properties isolates against indicator microorganisms

The study of the bactericidal and antifungal activity of antagonist strains in relation to test strains to opportunistic microorganisms of different groups was determined by *the deferred-antagonism method* (Bohora *et al.,* 2019).

The antimicrobial activity of the isolated lactic acid bacillus isolates was assessed using indicator microorganisms: *Staphylococcus aureus NCTC 12973, Escherichia coli NCTC 12923, Salmonella typhimurium NCTC 12023* and *Candida albicans NCPF 3179* (test strains from the *Laboratory of Human Microbiome and Longevity "National Laboratory Astana", Nazarbayev University (Nur-Sultan, Kazakhstan).* The antimicrobial

activity was assessed by the zone of no growth of test strains around the colony of the tested isolate of lactobacilli; the studies were repeated three times with the results expressed as an arithmetic mean.

2.4. Study of biofilm formation of strains

The ability of each individual strain to form a biofilm was assessed using the O'Toole method (O'Toole, 2010). The biofilm - synthesizing ability of *Lh-13*, *Lpl-5* was determined by a 96-well polystyrene plate (flat-bottomed, transparent, sterile, U-shaped bottom) for enzyme immunoassay. The sterile plastic plates were used. The 150 µl of the MRS broth and the prepared bacterial culture of lactobacilli were added to each well. The initial optical density of bacterial cultures in the medium was 0.1 unit (OD (490nm) = 0.1). At the same time, each strain was introduced into 4 wells, 50 µl each. The 50 µl of the MRS broth was used for further control. It was incubated for 48 hours at 37°C under anaerobic conditions. To assess the state of biofilms, the contents of the wells were removed by phosphate buffer pH = 7.2 three times, and dried in a thermostat at 60°C for 60 minutes. Further on, it was stained with a solution of gentian violet (2% crystal violet) in the volume = 150 µl for 15 minutes at room temperature. Afterwards, the dye solution was sucked out, washed off under a stream of distilled water, shake out and dried in the air at room temperature. The dye was eluted with 95% ethyl alcohol (150 µl per well). The plate was covered with a lid, left for 30 minutes and measured by a *TecanEVolizer100 laboratory robot (Tecan)* at a wavelength of 490 nm.

The results were interpreted in accordance with the optical density of the colored solvent. The efficiency of biofilm formation was assessed by the method (Stepanović *et al.*, 2007). The biofilm biomass formation: ODc≤ ~ ≤ 2*Odc – no/weak; 2*ODc <~ ≤ 4*Odc – moderate; > 4*Odc – dense. The experiment was repeated three times.

2.5. Study of biofilm formation by a laser capture microdissection

To visually assess the ability of *Lh-13* to form biofilms on the surface of the slide, the sterile Petri dishes with a diameter of 100 mm were used. A sterile glass slide was placed in the dish (Lenz *et al.*, 2008), a bacterial suspension with a density of 1.0 McF and a volume of 1 ml was applied to a sterile glass slide and placed in a thermostat at 37°C and kept for 4 hours for the cells to bind, then 5 ml MRS broth was added after 4 hours and incubated at 37°C for 24h and 48h respectively.

In 24 hours and 48 hours after incubation, the culture medium was carefully removed with a dispenser, the glass surface was washed three times with 1.15 M phosphate buffer, fixed with 96°alcohol, dried, stained with gentian violet solution (2% crystal violet) (Azeredo *et al.*, 2017) for 2 minutes at room temperature, after which washed with a phosphate buffer. After staining, the samples were covered with coverslips and embedded in the vitrogel mounting medium (12–005, Biovitrum). Further on, the samples were microscoped by laser capture microdissection *ArcturusXT ™ LaserCapture Microdissection (LCM)* in the Differential Interference Contrast mode.

The laser capture microdissection studies were carried out in the shared laboratory of the NCJSC Medical University of Karaganda. After obtaining the images of the cell surface, the data was processed using *Arcturus XT* software.

2.6. Study of biofilm formation by an atomic force microscope (AFM)

A microscope slide was used as a support. The *Lh-13* isolate was cultivated on a glass slide according to the above-mentioned method, the material was fixed using a 2.5% glutaraldehyde solution (Chao *et al.*, 2011) with an exposure for 2 hours at a temperature of 4°C, after which the prepared agent was thoroughly washed with bi-distilled water and dried in the air at room temperature. The biofilm formation ability of *Lh-13* isolate isolated from lactic acid products of the Karaganda region was assessed using the method of atomic force microscopy in a semi-contact mode. The advantage of the semi-contact scanning method is that a cantilever does not touch its surface for the most of the oscillation period and, therefore, does not damage the object under study.

The atomic force microscope was used to carry out the research in the laboratory of solid-state Physics of the Astana branch of the Institute of Nuclear Physics. The AFM samples were measured using an *AIST-NT SmartSPM* microscope in a semi-contact mode with an amplitude of 50 nm. The high-resolution silicon AFM cantilevers of the NSG10 series with a resonance frequency of about 210 kHz were used as a probe. After obtaining images of the cell surface, the data was processed using the *IAPro 3.2.2* software.

2.7. Statistical analysis

The obtained results are presented as mean ± standard error, obtained as a result of three-fold repetition of the experiment (Statistica 8.0 software was used) (Kabanikhin *et al.*, 2021).

3. Results

3.1. Isolation of lactobacilli and identification

Thirteen isolates of lactobacilli were isolated from 24 samples of irimchik, suzbe, cheese, ashygan kozhe produced by the traditional home-made method from different districts of the Karaganda region (Kazakhstan). All 13 isolated isolates are gram-positive with the cells located: singly, in pairs, chain-shaped. The isolates are immobile and catalase-negative. They do not form spores (lactobacilli do not have catalase thus, no gas formation in the sample with hydrogen peroxide was observed). On the MRS agar-1, the colonies are small, white, round, not pigmented, with the smooth edges, 1-3 mm in diameter, grow well at 37°C for 48 hours under anaerobic conditions. The figure illustrates the morphological (Figure 1 a, b, c, d) and cultural (Figure 1. e, f, g, h) characteristics of some isolated lactobaccili isolates.

As a result of the identification of isolates on the mass spectrometer, the following isolates were detected: *Lactobacillus helveticus (6 strains), Lacticaseibacillus rhamnosus (2 strains), Lactiplantibacillus plantarum (1 strains), Lacticaseibacillus paracasei (3 strains), Limosilactobacillus fermentum (1 strains).*

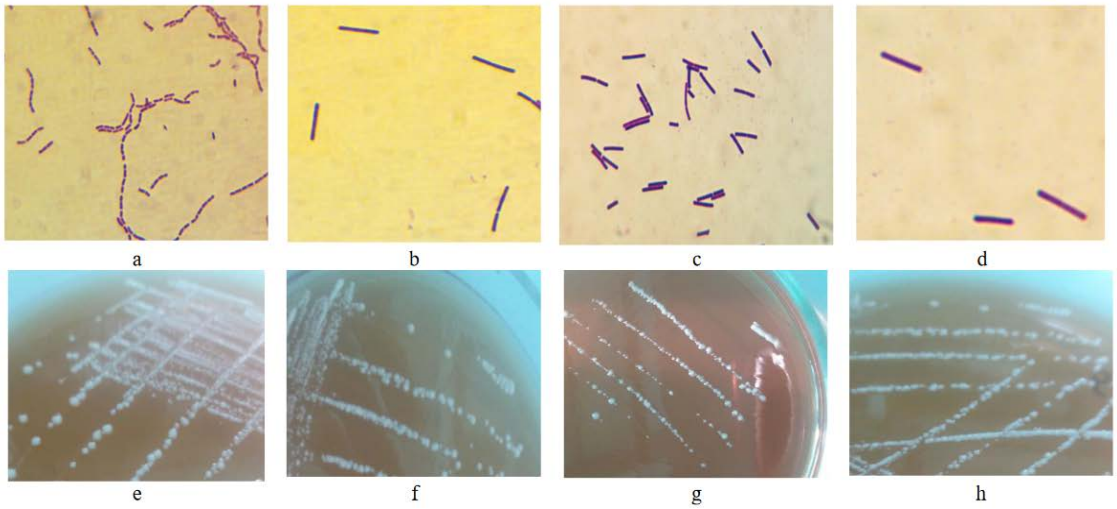

Figure 1. Morphological (100x objective) and cultural properties of the isolated lactobacilli: a-e) *Lpc-5/1*; b-f) *Lpl-5*; c-g) *Lh-13*; d-h) *Lrh-24.*

3.2. Tolerance to low acidic pH and bile salts

All thirteen lactobacilli isolates were tested for acidic pH resistance. As a result of the experiment, not all strains were resistant to acidic pH. The results demonstrated that 9 of 13 lactic acid bacillus isolates showed resistance to pH 3 for 0h, 3h and 6h despite differences in viability (growth with marked turbidity of the broth).

The isolates of *Lactobacillus helveticus-13 (Lh-13), Limosilactobacillus fermentum-18 (Lf-18), Lacticaseibacillus rhamnosus-24 (Lrh-24), Lacticaseibacillus paracasei -5/1 (Lpc-5/1), Lactiplantibacillus plantarum -5 (Lpl-5)* were found to be more resistant to acid stress. However, the isolates *Lactobacillus helveticus-14 (Lh-14), Lactobacillus helveticus -22 (Lh-22), Lacticaseibacillus paracasei -12 (Lpc-12), Lacticaseibacillus paracasei – 44 (Lpc-44)* did not tolerate low pH, yet some growth of isolates was observed (Figure 2).

The results of experimental studies have shown that the degree of resistance to acidic pH does not depend on the species; they differ among strains of the same species. These results are consistent with those obtained in the previous similar in vitro studies. The previous studies showed the ability of strains of lactobacilli to maintain their viability when exposed to the pH values of 3 (Mishra and Prasad , 2005; Guo *et al.*, 2010; Grosu-Tudor *et al.*, 2012; Menconi *et al.*, 2014).

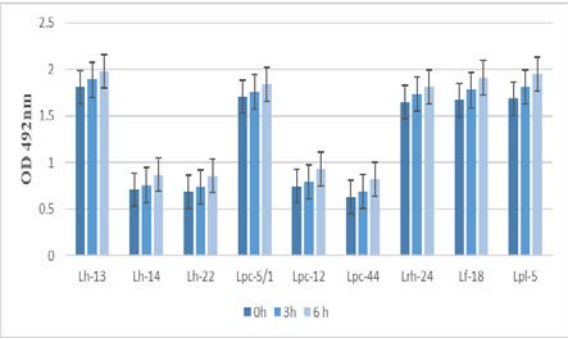

Figure 2. Acid resistance of lactobacilli isolates (mean±SD, three replicates).

The survival of 5 isolates of lactobacilli in the MRS broth containing 0.3, 0.5, 1% bovine bile was studied after incubation for 3 hours, and the results of optical density (OD) varied. According to the results (refer to Figure 3), lactic acid bacillus isolates retained their viability after exposure to 0.3-0.5% bovine bile for 3 hours (which reflects the time spent in the small intestine). The isolates of *Lh-13, Lpl-5* showed maximum growth at 0.3-0.5% bovine bile concentration compared to *Lf-18, Lrh-24, Lpc-5/1* (despite their acid resistance).

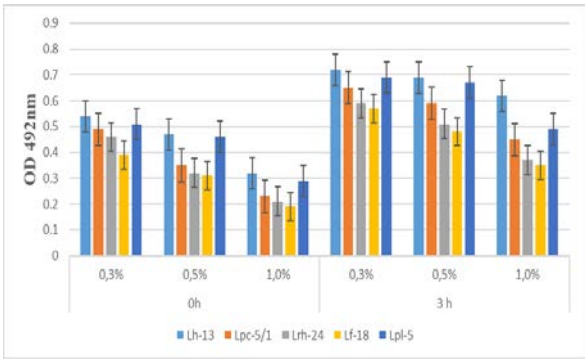

Figure 3. Survival of selected *Lh-13, Lf-18, Lrh-24, Lpc-5/1, Lpl-5* isolates in the MRS broth supplemented with 0.3%, 0.5%, 1.0% bovine bile (mean±SD, three replicates).

One could observe stable growth in *Lh-13, Lpl-5* at 1% bovine bile concentration, and optical density (OD) varied slightly. Despite the observed properties, such as acid resistance, the growth rate of the isolates of *Lf-18, Lrh-24, Lpc-5/1* decreased with an increase in the concentration of 1% bovine bile.

As a result of screening, *Lh-13, Lpl-5* have shown resistance to bovine bile and have been further tested for probiotic properties *in vitro.*

3.3. Detection of antibacterial activity of the isolates

The isolates of *Lh-13, Lpl-5* were tested for antimicrobial activity against gram-positive, gram-negative and yeast indicator microorganisms. The carried-out studies made it possible to establish that the *Lh-13, Lpl-5* showed antibacterial activity against indicator microorganisms, but the zone of inhibition of the test

strains varied. The antifungal activity was found in only one *Lh-13* isolate (Table 2).

Table 2. Antibacterial and antifungal activity of *Lh-13*, *Lpl-5* isolates

Isolated Lactobacilli isolates (symbols)	S. aureus NCTC 12973	E. coli NCTC 12923	S. typhimurium NCTC 12023	C. albicans NCPF 3179
	Zone of inhibition (diameter in mm)			
Lh-13	13.0±1.0	17.0±2.0	15.0±2.0	8.0±2.6
Lpl-5	14.0±3.0	15.0±2.0	16.0±1.0	0±0

Note: the diameters of inhibition zones (in mm) are presented as mean + SD, the research is repeated three times.

Thus, *Lh-13* possesses a certain level of antibacterial and fungicidal activity, which indicates their pronounced antimicrobial properties in relation to some opportunistic test strains.

3.4. Study of biofilm formation of isolated isolates

According to the study, the tested *Lh-13*, *Lpl-5* after 48 hours of incubation at 37°C in the standard MRS broth medium used to form biofilms on lactic acid bacteria on plastic plates varied in optical density (Figure 4).

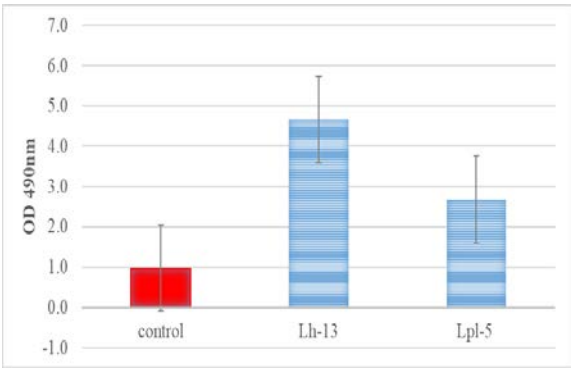

Figure 4. Assessment of the optical density of biofilm on plastic plates: Average optical density of the dye in the wells of polystyrene plates, reflecting the intensity of biofilm formation on their surface, by *Lh-13*, *Lpl-5* strains isolated from the national lactic acid products of the Karaganda region (mean±SD, three replicates).

According to the studied parameters, the intensity of biofilm formation shown by the *Lpl-5* (OD_{490nm}-2.686) expressed moderate intensity, and the one shown by the *Lh-13* strain expressed high intensity.

Microscopy is the simplest and fastest method to observe morphology of microorganisms attached to a surface. This observation allows researchers to compare the morphology of bacteria in a biofilm. In this regard, indicators reflecting the high intensity of *Lh-13* (OD_{490nm}-4.672) biofilm formation strains were studied by using a laser capture microdissection and an atomic force microscope.

3.5. Microscopy of the morphology of lactobacilli cells in biofilm using a laser capture microdissection

As a result of the study, in the morphology of the cells in the biofilm of the *Lh-13* by a laser capture microdissection in the DIC mode after 24 hours of incubation, one can observe some adhesion of single rod-shaped bacteria (Figure 5a). The bacteria adhere to a glass slide the most intensively with further compact microcolonies formed as they are united by an extracellular polymer matrix-mucus. Microcolonies gradually increase in size.

After 48 hours, homogeneous (rod-shaped) microbial communities were observed in the preparation; the structure on the outside is presented in the form of a protective film that unites all cells into a single system (Figure 5b). The increased thickness of the biofilm formed its specific structures, namely depressions and voids between them.

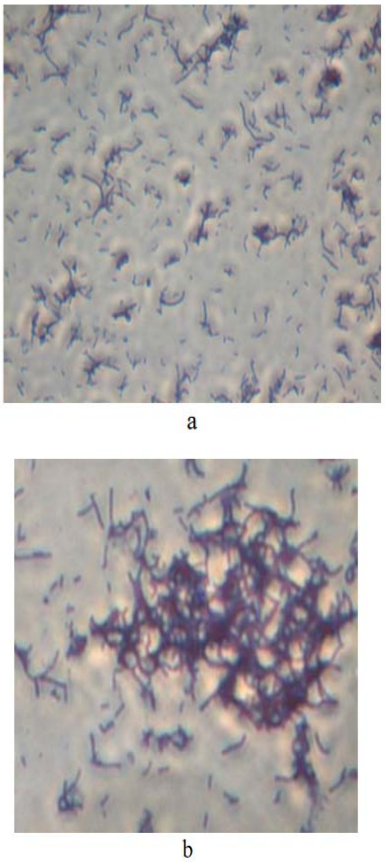

Figure 5. Cell morphology of *Lh-13* isolate in the biofilm (a) *Lh-13* after 24-hour incubation, (b) *Lh-13* after 48-hour incubation, a laser capture microdissection microscopy, homogeneous (rod-shaped) microbial communities, 60x objective.

Thus, using the resources of the laser capture microdissection allowed viewing the images of microcolony morphology and macro-colony of *Lh-13* isolate.

3.6. Study of the morphology of lactobacillus cells in the biofilm using an atomic force microscopy (AFM)

The AFM images obtained by scanning in the semi-contact mode made it possible to establish the morphology of cells in the biofilm. The advantage of the semi-contact scanning method of the sample is that a cantilever does not touch its surface for most of the oscillation period and, therefore, does not damage the object under study.

As a result of the study, one could observe adhesion to the surface of the glass slide and the distribution of the cell mass of the *L. hel-13* isolate after 24 hours. The bacterial cells are rod-shaped, homogeneously accumulated with sharp dips, which refer to depressions and voids between

them (Figure 6a). After 48 hours of incubation, one could observe some dense accumulations of rod-shaped biomass of *Lh-13* cells linked to each other. The architectonics of the adhered cells of the *Lh-13* isolate is supported by an exopolysaccharide matrix of microcolonies accompanied by the formation of clusters with the round channels around them. The microcolonies got increased largely (Figure 6c).

AFM provides 3D imaging of surface ultrastructures with molecular resolution in real time and under physiological conditions. Using the AFM resources, it was possible to get a clearer visualization to present the sample in a 3D image (Figure 6 b, d). The biofilm surface is not smooth, having numerous irregularities; *Lh-13* isolate is located in space randomly, but uniformly.

With the help of AFM, a biofilm surface roughness profile is constructed (Figure 6 e-j). The biofilm surface roughness is a set of surface irregularities. The roughness parameters were determined from the obtained images of surfaces with a microscopic field size of 20 × 20 μm. The differences in the roughness of the biofilm surface in their linear dimensions are associated with the relative position of the cells of the *Lh-13* isolate and matrix.

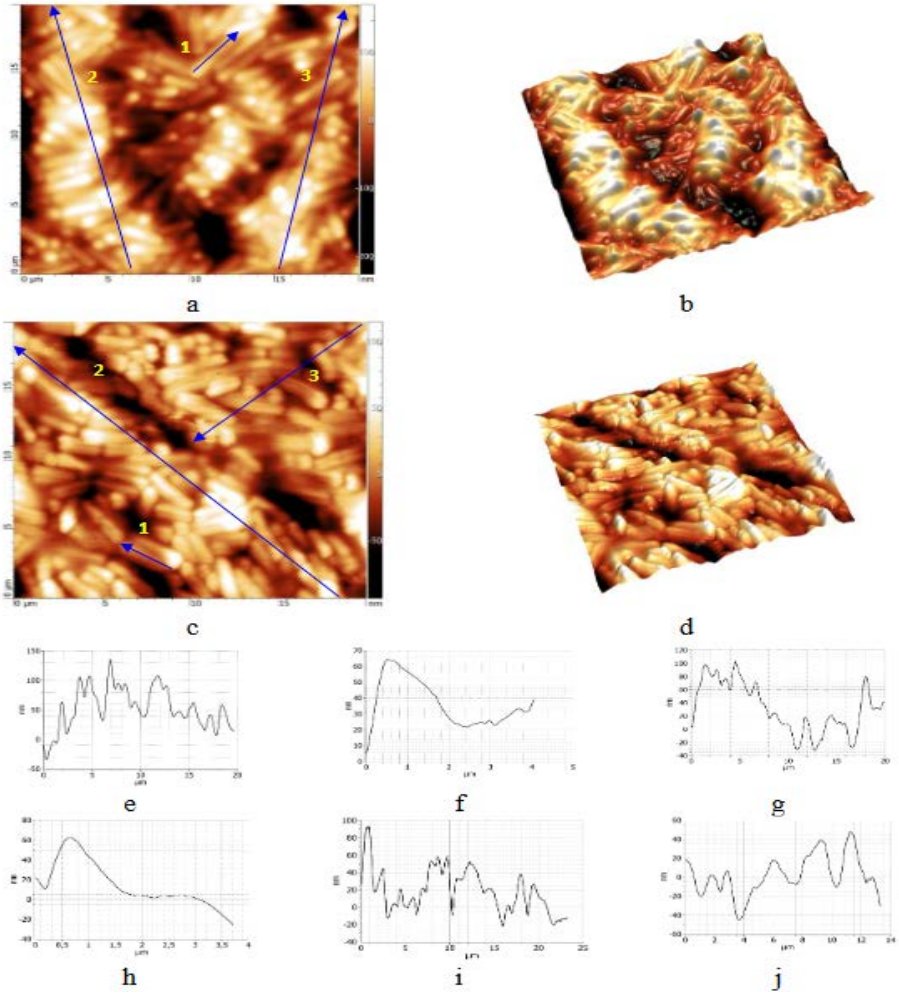

Figure 6. Cell morphology of *Lh-13* isolate in the biofilm, atomic force microscopy: a-b) 2D and 3D images of *Lh-13* after 24 hours of incubation; c-d) 2D and 3D images of *Lh-13* -13 after 48 hours of incubation; e-j) biofilm surface roughness profile. The biofilm surface roughness profile was measured by plotting the surface profile along the line: (e, h) directed along the maximum cell length; (f, i) where the long biomass of the cell accumulation of *Lh-13* is formed; (g, j) where a large number of the *Lh-13* aggregates (dense layers) is attached.

Thus, the study of the biofilm by an atomic force microscopy made it possible to study the morphology of the biofilm-forming strain in 2D and 3D projections, displaying the relief and topographic image of the biofilm of the *Lh-13* isolate.

4. Discussion

The isolates isolated by morpho-cultural characters and identification (Zheng *et al.*, 2020) by MALDI-TOF MS indicate that they refer to: *Lactobacillus helveticus (6 strains), Lacticaseibacillus rhamnosus (2 strains), Lactiplantibacillus plantarum (1 strain), Lacticaseibacillus paracasei (3 strains), Limosilactobacillus fermentum (1 strain).*

The mimicking conditions of the gastrointestinal tract made it possible to identify promising isolates of *Lh-13*, *Lpl-5* to study antimicrobial and biofilm-forming activity. The study of antimicrobial activity under conditions of intermicrobial relations enabled to witness the antimicrobial activity of *Lh-13* as the result the production of antimicrobial substances.

A detailed screening of *Lh-13* and *Lpl-5* isolates was carried out by the *TecanEVolizer100 (Tecan)* operating system. During such screening, *Lh-13* showed a high level of density (OD_{490nm}-4.672) during biofilm formation in the wells of polystyrene plates.

There is a large number of methods for visualizing the image of the obtained biofilms and studying their properties: from measuring the optical density to various options for light and electron microscopy (Relucenti *et al.,* 2021). Thanks to the use of lasers, highly sensitive light detectors, digital photography and computer technology, the methods of studying the cell's morphology and biofilm formation of bacteria have been transformed to provide objective studies in microscopy. A special role in forming this methodology was played by computer methods for processing and analyzing digital images. They made it possible not only to simplify, accelerate and automate many of the existing microscopy methods, but also ensured the acquisition of previously inaccessible images (Chang *et al.,* 2012; Babu and Singh, 2014).

The specialized microscopy bank made it possible to visualize the image and compare two methods: a laser capture microdissection and an atomic force microscopy, using the example of *Lh-13*. Both methods recorded the homogeneity of morphological properties with equal efficiency. The laser capture microdissection showed that *Lh-13* cells were rod-shaped, and the bacterial cells were in the extracellular matrix in the form of a homogeneous massive accumulation. Working in the mode of the investigated method, a distinctive feature is the use of gentian violet staining performed according to the above-mentioned technique, which gives a volumetric image, focusing on the clear lines and boundaries of the accumulation of microorganisms as the enveloping effect of biofilm.

The atomic force microscopy allows studying biological objects and processes without using complex fixation methods as well as obtaining images of bacterial cells with high resolution (Alsteens, 2012). By using an atomic force microscope, the two and three-dimensional morphological relief images were accurately studied, with an indication of the profile of surface roughness, a homogeneous massive accumulation is visually observed, reflecting the active biofilm formation of lactobacilli, 100% preserving the true topography.

The microscopic methods used, namely a laser capture microdissection and an atomic force microscopy, complement each other in the visualization of the experiment.

The expediency of using microscopic research methods is based on the fact that only visual control is able to assess the morphological state of both the strains of lactobacilli themselves and the matrix of biofilms.

The results of our own research and literature reviews (Flemming and Wingender, 2010; Gavrilova *et al.,* 2019) allow stating that the biofilm of lactobacilli is a community of cells attached to the surface and united by the extracellular matrix. In addition to adhesins, mucoid capsules and surface polysaccharides of bacterial cell walls can stimulate the formation of biofilms on the surface of solid substrates. After colonization, bacteria begin to actively secrete exopolysaccharides, which ensure the formation of a biofilm while filling the intercellular space (Spangler *et al.,* 2019; Barzegari *et al.,* 2020). In this case, communicative connections are regulated by means of special substances released into the environment, namely autoregulators with an established chemical structure. It is known that microbial cells in biofilms produce exopolysaccharides, mainly composed of polysaccharides, proteins and nucleic acids, which form a protective gel-like matrix around the cells (Aoudia *et al.,* 2016). According to the literature, the *L. helveticus* strain has a probiotic ability, in particular antimicrobial activity, and is able to produce mucus-binding proteins and proteins of the surface layer, having the properties of EPS formation and cell aggregation, proteolytic activity and bacteriocin production (Li *et al.,* 2015; Gómez *et al.,* 2016; Fontana *et al.,* 2019).

It is experimentally confirmed that *Lh-13* isolate can form biofilms in vitro on the surface of the glass slide, indicating their ability to colonize, having tolerance to acidic pH and bovine bile, and antimicrobial activity.

The given study has several limitations. When studying the cell morphology of *Lh-13* isolate in biofilm using the atomic force microscopy (AFM), an integrated approach was not taken into consideration. This approach includes three methods: semi-contact, mismatch, phase imaging, morphometric parameters of the cell (height, width, length, diameter), adhesive properties of the substrate, bacteria, biofilm (determination of adhesion forces between biofilm and substrate, as well as adhesion strength). These studies are in perspective.

We were able to visualize biofilms on a substrate (a microscope slide) using atomic force microscopy; due to the uniqueness of the biofilm creation approach; the image was augmented by a laser microdissection method. Because there was no scanning microscope in the lab, a stained image of the morphology and topography of the *Lh-13* cells in both singular and biofilm form was obtained.

This investigation enabled the selection of a biologically active (biofilm-forming) *Lh-13* isolate with antibacterial capabilities as a probiotic candidate; nevertheless, further studies of this isolate's probiotic properties are required.

5. Conclusions

The work's results established the groundwork for further study on the probiotic characteristics of isolate *Lh-13*. More research is needed to establish how biofilms and their active chemicals suppress foodborne pathogens, adhesive activity, antibiotic resistance, and so on.

These physiologically active strains of *Lh-13* will hopefully be used in vivo as probiotics for the nutritional needs of both people and animals in the near future.

Acknowledgements

The authors express their sincere gratitude to the employee of the laboratory of solid-state Physics of the Astana branch of the Nuclear Physics Institute, Shlimas I. Dmitriy, for assisting during the research with an atomic force microscope and to the Head of the laboratory of the NPJSC Medical University of Karaganda, Akhmaltdinova L. Lyudmila, for her active assistance during the research with the laser capture microdissection.

References

Aitzhanova AA, Oleinikova EA, Saubenova MG, Daugalieva ST, and Berzhanova, RZ. (2020). Selection of antagonistically active strains of lactic acid bacteria from milk of various animal species. *Bull. KazNU. Biol. series*, **83(2)**:72-81.

Alatoom AA, Cunningham SA, Ihde SM, Mandrekar J, Patel R. (2011). Comparison of direct colony method versus extraction method for identification of gram-positive cocci by use of Bruker biotyper matrix-assisted laser desorption ionization-time of flight mass spectrometry. *J Clin Microbiol.*, **49(8)**:2868-2873.

Alsteens D. (2012). Microbial cells analysis by atomic force microscopy. *Methods Enzymol.*, **506**:3-17.

Aoudia N, Rieu A, Briandet R, Deschamps J., Chluba J, Jego G, Garrido C, Guzzo J. (2016). Biofilms of Lactobacillus plantarum and Lactobacillus fermentum: Effect on stress responses, antagonistic effects on pathogen growth and immunomodulatory properties. *Food Microbiol.*, **53** (Pt A):51-59.

Azeredo J, Azevedo NF, Briandet R, Cerca N, Coenye T, Costa AR, Desvaux M, Di Bonaventura G, Hébraud M, Jaglic Z, Kačániová M, Knøchel S, Lourenço A, Mergulhão F, Meyer RL, Nychas G, Simões M, Tresse O and Sternberg C. (2017). Critical review on biofilm methods. *Crit Rev Microbiol.*, **43(3)**:313-351.

Babu R and Singh E. (2014). Atomic Force Microscopy: A source of investigation in biomedicine. *Int. J. Energy Environ. Eng.*, **7(1):** 59-66.

Barzegari A, Kheyrolahzadeh K, Mahdi S, Khatibi H, Sharifi S, Memar MY and Vahed SZ. (2020). The battle of probiotics and their derivatives against biofilms. *Infect Drug Resist.*, **13**:659-672.

Bechelaghem N, Djibaoui R, Ergün Y, Ettalhi M. (2022). *Lactobacillus reuteri* and *Lactobacillus salivarius*, two prevalent vaginal species isolated from healthy women in Western Algeria. *Jordan J. Biol. Sci.*,**15(1)**:133-137.

Bohora AA, Kokate SR, Khedkar S and Vankudre A. (2019). Antimicrobial activity of probiotics against endodontic pathogens: - A preliminary study. *Indian J Med Microbiol.*, **37(1):**5-11.

Casey PG, Casey GD, Gardiner GE, Tangney M, Stanton C, Ross RP, Hill C and Fitzgerald GF. (2004). Isolation and characterization of anti-Salmonella lactic acid bacteria from the porcine gastrointestinal tract. *Lett Appl Microbiol.*, **39(5)**:431-438.

Chang KC, Chiang YW, Yang CH and Liou JW. (2012). Atomic force microscopy in biology and biomedicine. *Tzu Chi Med. J.*, **24(4)**: 162-169.

Chao Y and Zhang T. (2011). Optimization of fixation methods for observation of bacterial cell morphology and surface ultrastructures by atomic force microscopy. *Appl Microbiol Biotechnol.*, **92(2)**:381-392.

Corona-Hernandez RI, Alvarez-Parrilla E, Lizardi-Mendoza J, Islas-Rubio AR, de la Rosa LA, Wall-Medrano A. (2013). Structural stability and viability of microencapsulated probiotic bacteria: A review. *Compr Rev Food Sci Food Saf.,* **12(6):** 614-628.

Ejtahed HS, Hasani-Ranjbar S, Larijani B. (2017). Human microbiome as an approach to personalized medicine. *Altern Ther Health Med.*, **23(6)**:8-9.

Flemming HC and Wingender J. (2010). The biofilm matrix. *Nat Rev Microbiol.*, **8(9)**:623-633.

Fontana A, Falasconi I, Molinari P, Treu L, Basile A, Vezzi A, Campanaro S, Morelli L. (2019). Genomic comparison of Lactobacillus helveticus strains highlights probiotic potential. *Front. Microbiol.*, **10:**1380.

Gavrilova E, Anisimova E, Gabdelkhadieva A, Nikitina E, Vafina A, Yarullina D, Bogachev M, Kayumov A. (2019). Newly isolated lactic acid bacteria from silage targeting biofilms of foodborne pathogens during milk fermentation. *BMC Microbiol.*, **19(1)**:248.

George Kerry R, Patra JK, Gouda S, Park Y, Shin HS, Das G. (2018). Benefaction of probiotics for human health: A review. *J Food Drug Anal.*, **26(3)**:927-939.

Ghosh C, Sarkar P, Issa R, Haldar J. (2019). Alternatives to conventional antibiotics in the era of antimicrobial resistance. *Trends Microbiol.*, **27(4)**:323-338.

Gomez NC, Ramiro JM, Quecan BX, de Melo Franco BD. (2016). Use of potential probiotic lactic acid bacteria (LAB) biofilms for the control of Listeria monocytogenes, Salmonella typhimurium, and Escherichia coli O157: H7 biofilms formation. *Front. Microbiol.*,**7:863:**

Grosu-Tudor SS and Zamfir M. (2012). Probiotic potential of some lactic acid bacteria isolated from Romanian fermented vegetables. *Ann Rom Soc Cell Biol.,* **17(1)**:234-239.

Guarner F, Perdigon G, Corthier G, Salminen S, Koletzko B, Morelli L. (2005). Should yoghurt cultures be considered probiotic? *Br J Nutr.*, **93(6)**:783-786.

Guo XH, Kim JM, Nam HM, Park SY, Kim JM. (2010). Screening lactic acid bacteria from swine origins for multistrain probiotics based on in vitro functional properties. *Anaerobe*, **6(4)**:321-326.

Hill C, Guarner F, Reid G, Gibson GR, Merenstein DJ, Pot B, Morelli L, Canani RB, Flint HJ, Salminen S, Calder PC, Sanders ME. (2014). Expert consensus document: The international scientific association for probiotics and prebiotics consensus statement on the scope and appropriate use of the term probiotic. *Nat Rev Gastroenterol Hepatol*., **11(8)**:506-514.

Kabanikhin S, Krivorotko O, Takuadina A, Andornaya D, Zhang S. (2021). Geo-information system of tuberculosis spread based on inversion and prediction. *J. Inverse Ill-Posed Probl.,* **29(1)**:1-20.

Kim JH and Baik SH. (2019). Probiotic properties of Lactobacillus strains with high cinnamoyl esterase activity isolated from jeot-gal, a high-salt fermented seafood. *Ann. Microbiol.,* **69:**407–417.

Lenz AP, Williamson KS, Pitts B, Stewart PS, Franklin MJ. (2008). Localized gene expression in Pseudomonas aeruginosa biofilms. *Appl Environ Microbiol.*, **74(14)**:4463-4471.

Li W, Xia X, Chen X, Rui X, Jiang M, Zhang Q, Zhou J, Dong M. (2015). Complete genome sequence of Lactobacillus helveticus MB2-1, a probiotic bacterium producing exopolysaccharides. *J Biotechnol.,* **209**:14-15.

Menconi A, Kallapura G, Latorre JD, Morgan MJ, Pumford NR, Hargis BM, Tellez G. (2014). Identification and characterization of lactic acid bacteria in a commercial probiotic culture. *Biosci Microbiota Food Health*, **33(1)**:25-30.

Mishra V and Prasad DN. (2005). Application of in vitro methods for selection of Lactobacillus casei strains as potential probiotics. *Int J Food Microbiol.*, **103(1)**:109-115.

Mitropoulou G, Nedovic V, Goyal A, Kourkoutas Y. (2013). Immobilization technologies in probiotic food production. *J Nutr Metab*, **2013:**1-15.

O'Toole GA. (2010). Microtiter dish Biofilm formation assay. *J. Vis. Exp.,* **(47)**:2437.

Relucenti M, Familiari G, Donfrancesco O, Taurino M, Li X, Chen R, Artini M, Papa R, Selan L. (2021). Microscopy methods for biofilm imaging: Focus on sem and VP-SEM pros and cons. *Biology*, **10(1)**:51.

Salas-Jara MJ, Ilabaca A, Vega M, García A. (2016). Biofilm forming lactobacillus: new challenges for the development of probiotics. *Microorganisms*, **4(3)**:35.

Schulthess B, Bloemberg GV, Zbinden R, Böttger EC, Hombach M. (2014). Evaluation of the bruker MALDI biotyper for identification of gram-positive rods: Development of a diagnostic algorithm for the clinical laboratory. *J Clin Microbiol*., **52(4)**:1089-1097.

Schupack DA, Mars RAT, Voelker DH, Abeykoon JP, Kashyap PC. (2022). The promise of the gut microbiome as part of individualized treatment strategies. *Nat Rev Gastroenterol Hepatol***., 19(1)**:7-25.

Singh TP, Kaur G, Malik RK, Schillinger U, Guigas C, Kapila S. (2012). Characterization of Intestinal Lactobacillus reuteri Strains as Potential Probiotics. *Probiotics Antimicrob. Proteins*, **4(1)**:47-58.

Son SH, Jeon HL, Jeon EB, Lee NK, Park YS, Kang DK, Paik HD. (2017). Potential probiotic Lactobacillus plantarum Ln4 from kimchi: Evaluation of β-galactosidase and antioxidant activities. *Food Sci. Technol.,* **85** (A):181-186.

Spangler JR, Dean SN, Leary DH, Walper SA. (2019). Response of lactobacillus plantarum WCFS1 to the gram-negative pathogen-associated quorum sensing molecule N-3-oxododecanoyl homoserine lactone. *Front. Microbiol*., **10**:715.

Stepanović S, Vuković D, Hola V, Di Bonaventura G, Djukić S, Cirković I, Ruzicka F. (2007). Quantification of biofilm in microtiter plates: Overview of testing conditions and practical recommendations for assessment of biofilm production by staphylococci. *APMIS*, **115(8)**:891-899.

Tambekar DH and Bhutada SA. (2010). Studies on antimicrobial activity and characteristics of bacteriocins produced by lactobacillus strains isolated from milk of domestic animals. *Internet J. Microbiol*.,**8(2)**:1-5.

Tatsaporn T and Kornkanok K. (2020). Using Potential Lactic Acid Bacteria Biofilms and their Compounds to control biofilms of foodborne pathogens. *Appl. Biotechnol. Rep.,* **26** (e00477):1-8.

Taverniti V, Scabiosi C, Arioli S, Mora D, Guglielmetti S. (2014). Short-term daily intake of 6 billion live probiotic cells can be insufficient in healthy adults to modulate the intestinal Bifidobacteria and Lactobacilli. *J Funct. Food.,* **6(1):** 482-491

Torres N and Tovar AR. (2021). The present and future of personalized nutrition. *Rev Invest Clin*, **73(5)**:321-325.

Wang D, Liu W, Ren Y, De L, Zhang D, Yang Y, Bao Q, Zhang H, Menghe B. (2016). Isolation and identification of Lactic acid bacteria from traditional dairy products in Baotou and Bayannur of Midwestern Inner Mongolia and q-PCR analysis of predominant Species. *Korean J Food Sci Anim Resour*, **36(4)**:499-507.

Wu C, Huang J, Zhou R. (2017). Genomics of lactic acid bacteria: Current status and potential applications. *Crit Rev Microbiol*., **43(4)**:393-404.

Yue Y, Xu X, Yang B, Lu J, Zhang S, Liu L, Nassar K, Zhang C, Zhang M, Pang X, Lv J. (2020). Stable colonization of orally administered Lactobacillus casei SY13 Alters the Gut Microbiota. *Biomed Res Int.,* **2020**:1-8.

Zeng Y, Li Y, Wu QP, Zhang JM, Xie XQ, Ding Y, Cai SZ, Ye QH, Chen MT, Xue L, Wu S, Zeng HY, Yang XJ, Wang J. (2020). Evaluation of the Antibacterial Activity and Probiotic Potential of Lactobacillus plantarum Isolated from Chinese Homemade Pickles. *Can. J. Infect. Dis. Med. Microbiol.,* **2020**:1-11.

Zheng J, Wittouck S, Salvetti E, Franz CMAP, Harris HMB, Mattarelli P. et al. (2020.) A taxonomic note on the genus Lactobacillus: Description of 23 novel genera, emended description of the genus Lactobacillus Beijerinck 1901, and union of Lactobacillaceae and Leuconostocaceae. *Int. J. Syst. Evol. Microbiol.* **70(2)**:2782–2858.

JJBS

Volume 16, Number 1,March 2023
ISSN 1995-6673
Pages 73 – 84
https://doi.org/10.54319/jjbs/160110

Jordan Journal of Biological Sciences

Optimization, Characterization of Newly Immobilized Mannanase on Activated Chitosan Beads and Its Applications

Siham, A. Ismail[1]; Shaimaa, A. Nour[1] ; Mohamed, E. Hassan[2] ; Nivien, A. Abosereh[3]; Om Kalthoum, H. Khattab[4]; Amany, A. Abo-Elnasr[4]; Mohamed M. I. Helal[1] and Amal, M. Hashem[1,*]

[1]*Department of Chemistry of Natural and Microbial Products, Pharmaceutical and Drug Institute Research Division, National Research Centre, El Buhouth St., Dokki, Giza;* [2]*Center of Scientific Excellence-Group of Advanced Materials and Nanotechnology, Chemistry of Natural and Microbial Products Department, National Research Center, El Behouth Street, Cairo 12622, Egypt;* [3]*Department of Microbial Genetics, Division of Genetic Engineering and Biotechnology, National Research Centre, Giza;* [4]*Department of Plant and Microbiology, Science Collage, Helwan University, Egypt.*

Received: May 30, 2022; Revised: October 2, 2022; Accepted: October 21, 2022

Abstract

Mannanase produced by mutant *Penicillium citrinium* Egy5 LC368457 isolated from Pharaoh Mummies of Ancient Egyptian Museum, Cairo, Egypt**,** was covalently immobilized onto activated chitosan beads by Polyethyleneimine, glutaraldehyde and dopamine. Loading time, enzyme's units, pH and temperature were optimized. The immobilized enzyme can keep its maximum activity at a broader range of pH and make it more stable at higher temperatures, including 60 °C, which is preferred to reduce microbial contamination of the enzyme. The reusability test indicated the high stability of immobilized enzymes that were still active at 75.82% of their activity at cycle number 9 and in the production of mannooligosaccharides, which showed antioxidant and prebiotic activity.

Keywords: *Penicillium citrinium;* reusability; β-Mannanases; immobilization technique; mannooligosaccharides

1. Introduction

According to the most recent Enzyme market analysis, the sum spent for enzymes in the global market reached up to $7,652.0 million, and the expanded catalyzed interest for enzyme are for the most part for nourishment and beverage industries.

The purpose of the immobilization technique is to improve an enzyme's operational presentation for industrial applications. The immobilized enzymes are more increasingly impervious to natural conditions. They can be effectively removed at the end of the reaction; the product is not contaminating with the enzyme and even more the immobilized enzymes can be reused as often as possible. In order to optimize the performance of immobilized enzymes, many matrices have been described in the literature. (Nadaroglu and Sonmez, 2016; and Mohapatra 2021).

In the constantly increasing biotechnology industry, hemicellulases have emerged as essential enzymes (Ismail *et al.*, 2022 and Nour *et al.*, 2022). Because of their diverse qualities, they gain a wide array of industrial applications. β-mannanases are an important group within hemicellulases that attack the mannan backbone's glycosidic linkages to release -1,4-manno-oligosaccharides (Chauhan *et al.*, 2012). Mannanase with biological origins has a broad range of applications in a variety of industries, such as production of manno-oligosaccharides which have prebiotic activity, pharmaceutical preparation, and pulp biobleaching, and as pre-treatment of plant biomass for second biofuel generation. The determination method of immobilization β-mannanase is necessary to prevent enzyme activity loss by avoiding changes in the chemical structure and reactive groups in the enzyme's binding site.

Adsorption, covalent coupling, entrapment, and cross-linking are the most well-known ways of enzyme immobilization (Hashem *et al*., 2016). Immobilized enzymes are more tight and resistant to environmental changes than unbound enzymes, which increases their thermal operational stability and recoverability. (Zhao *et al*., 2011).

The biocatalyst is more resistant to harsh industrial processes when organic (alginate, chitosan, collagen, and carrageenan) and manufactured (polyacrylamide, amberlite, and polyvinyl alcohol) components are adsorbed on the surface of different polymers (Sirisha *et al.*, 2016).

Because of its abundance, biocompatibility, biodegradability, and nontoxicity, chitosan nanoparticles have become a popular immobilized matrix in recent years (Mohapatra 2021). The high surface-to-area ratio of immobilization on nano-sized particles aids in increased enzyme loading, faster reaction rates, and resistance to fouling and diffusion. (Ansari *et al.,* 2016 and Verma *et al.,* 2016). The surface covalent attachment of an enzyme onto chitosan nanoparticles is achieved by using a crosslinker on the nanoparticles (e.g. glutaraldehyde). As a

* Corresponding author. e-mail: amal_mhashem@yahoo.com.

result, the biocatalytic –CHO groups in glutaraldehyde interact with the –Amino group molecules in glucosamine Nadaroglu and Sonmez (2016). The enzymatic activity showed that mannanase enzyme obtained from fungal Clitocybegeotropa was immobilized on magnetite (Fe_3O_4) nanoparticles using adsorption method for the clarification of some fruit juices (Verma *et al.*, 2016).

The properties of free and activated chitosan-immobilized *β*-mannanase from the gamma mutant *Penicillium citrinium* Egy5 LC368457 are described in this paper, in addition to the the biological activities of manno-oligosaccharides produced from the immobilized *β*-mannanase.

2. Materials and methods

2.1. Materials

Locust bean gum was obtained from sigma (St. Louis, Mo., USA). Chitosan, dopamine was purchased from Fluka. Polyethyleneimine (PEI) (50%, w/v) (MW: 423), Cat # 468533, was purchased from Aldrich. Glutaraldehyde, Dowex-IXD particle size 0.0730-0.15 mesh, acrylamide, bisacrylamide, TEMED, Potato dextrose agar and TLC cards coated with silica gel, layer thickness 0.2mm were obtained from Merck KGaA 64271 Darmstadt Germany. Coffee beans were bought from local market, Giza, Egypt. The rest of the reagents were of analytical quality.

2.2. Microorganism and its maintenance medium

Penicillium citrinium Egy5 LC368457 was isolated from Pharaoh Mummies of Ancient Egyptian Museum, Cairo, Egypt**.** The fungus was grown on potato dextrose agar (PDA) and grown for 7 days at 30°C until being maintained at 4°C and subculturing on a monthly basis. The probiotic beneficial bacteria *Pediococus lactis 1,2* , *Lactobacillus lactis, Lactobacillus acidophilus* and *Lactobacillus planterum* compared to that of pathogenic *Escherichia coli* cultured on MRS-medium (containing the sample as sole carbon source). The five probiotics were cultivated on MRS mixture for 24 hours, whereas *E. coli* was grown on nutritive broth medium for 24hrs with in laboratory.

2.3. Cultivation conditions and enzyme preparation

2.3.1. Mutagenesis with gamma rays treatment

Mutagenesis was carried out using gamma rays produced from Cobalt-60 (Co60) as a source of gamma radiation (by Egyptian Atomic Energy Authority) (Abosereh *et al.*, 2019).

2.3.2. Production of β- mannanase

The mutant *Penicillium citrinium* Egy5 LC368457 was used for the production of β- mannanase as previously described by (Khattab *et al.*, 2020 and Foda *et al.*, 2022). The medium used contain (g/L): KH_2PO_4, 8.5; Nitrogen complex (peptone + ammonium sulfate+ Urea), 1.8 and Coffee waste (10g/flask). The pH of the medium was adjusted at 5 before autoclaving. Each Erlenmyer flask contain 50ml inoculated with 8 percent spore suspension (on potato dextrose agar) cultured for 12 days from a 7-day-old age fungus shaking at 120rpm at 30°C. The crude extract was partially purified by fractional precipitation using ammonium sulfate. All the fractions were dialyzed.

2.3.3. Enzyme activity and Protein content

The Nelson–Somogyi method was used to determine the enzyme's activity (Smogi *et al*., 1952). The partial pure enzyme was added to 1ml of locust bean gum (1% (w/v) for 10 minutes at 50°C in sodium citrate buffer (50mM) at pH 5.5 (Hashem *et al.*, 2001). Under the assay conditions, the quantity of enzyme that releases 1 mol of mannose per minute is defined as one unit of mannanase (U). Lowery-Folin technique was used to determine the protein content (lowery *et al.*, 1951).

2.4. Screening for the best carrier

48 carriers were screened individually for immobilization of β-mannanase according to Hashem *et al*. (2016). These carriers were made by dissolving their components in distilled water, then using an encapsulator, dropping the polymer solutions into 3 percent CaCl2, 3 percent KCl, or 0.05 M FeCl3 to form homogenous gel beads. To complete the hardening process, the gel beads were placed in the same solution for three hours. The gel pellets were submerged in a 4 percent (v/v) polyethylenimine (PEI) liquid at pH 9.5 for three hours to set up them for immobilization via covalent bonds of the enzyme, and then steeped in glutaraldehyde (GA) 2.5 percent for three hours before rinsing with dist. After soaking in H_2O, the pellets were available for enzyme immobilization.

2.5. Immobilization of enzyme

1g of the previously manufactured gel beads carrier was combined with 1 milliliter of partly purified mannanase. The mixture was allowed at room temperature overnight to immobilize the beads, which were then rinsed with buffer solution and stored at 4°C for following studies, the Yield of Immobilization was computed using the equation as follows:

$$\text{The Yield of Immobilization (\%)} = \frac{\text{Immobilized enzyme activity (U/g carrier)}}{\text{Enzyme added (U/g carrier)} - \text{Unbound enzyme (U/g carrier)}} \text{ (\%).}$$

2.6. Optimum conditions for enzyme immobilization process

2.6.1. Effect of different chitosan with different concentrations enzyme

Different activated gel beads with different aldehyde groups were used to determine the enzyme concentration required to react with all of the aldehyde groups identified on the gel beads:

A. Chitosan+dopamine

chitosan + glutraldhyde (2.5%)+ polyethelene+ dopamine were soaked in different concentrations of enzyme (9.16, 20.02 and 29.65 IU). Enzyme activity was determined as mentioned before. Unbounded enzyme was determined.

2.6.2. Effect of different concentration of glutraldhyde

The effect of different glutraldhyde concentrations (1, 2.5, 3.5, 5 and 7%) on the catalytic activity of the immobilized enzyme was determined by soaking aminated chitosan beads in different concentrations of glutraldhyde for 3hrs at room temperature on a shaker (150 rpm).

2.6.3. Loading time for immobilization of β-mannanase

The effect of time loading of partially purified β-mannanase on chitosan beads treated with 3.5% glutraldhyde at various time periods (2, 4, 6, 8, 20, 24 and 26 h) at room temperature on a rotary shaker (150 rpm) was studied.

2.6.4. Different pHs of enzyme solution

The effect of pH of loading partially purified β-mannanase on chitosan beads treated with glutraldhyde at different pHs of enzyme (4, 4.5, 5, 5.5, 6 and 6.5) at room temperature on a shaker (150 rpm) after 6hrs was determined.

2.6.5. Effect of different temperature of enzyme solution

The effect of different temperatures of loading partially purified β-mannanase on chitosan beads ranged from 20 to 37°C with 3.5% glutraldhyde at pH 5.5 on a shaker (150 rpm) after 6hrs was studied.

2.6.6. Operational stability

This was done by incubating 0.5 g of immobilized β-mannanase with locust bean gum at 60°C for 10 minutes, comprising roughly 20.02 IU of the enzyme. The pellet was removed by filtration at the conclusion of the reaction period, washed with buffer, to start a new run; the pellets were re-suspended in freshly prepared substrate. The activity of β-mannanase was measured in the supernatant.

2.7. Characterization of the gel beads

2.7.1. Infrared Fourier Transform (FT-IR)

Fourier transform infrared spectroscopy was used to record the infrared spectra of all formulations (chitosan), (chitosan + PEI), (chitosan +PEI + dopamine), (chitosan + PEI + dopamine + GA), and (chitosan + PEI + dopamine + GA + Enzyme) (FTIR-8300, Shimadzu, Japan). At room temperature, FT-IR spectra were collected in the wavelength range of 4000 to 400 cm^{-1}.

2.7.2. Scanning Electron Microscope (SEM)

The various gel compositions' surfaces (chitosan), (chitosan + PEI), (chitosan +PEI + dopamine), (chitosan + PEI + dopamine + GA) and (chitosan + PEI + dopamine + GA + enzyme) Scanning electron microscopy was used to investigate the samples. (SEM, S-590, HITACHI)

2.8. Stability and optimization of free and immobilized β-mannanase

The following studies were carried out to verify the effectiveness of the novel carriers for mannanase immobilization in industry.

2.8.1. The pH Effect

Identical reaction mixes of free and immobilized enzymes were incubated in sodium citrate buffer (0.05M) in this experiment at different pHs ranging from 4 – 6.5 at 50^{o}C for 10 min. The enzyme assay was done in normal circumstances.

2.8.2. Effect of temperature

The kinetics on the activity of free and immobilized mannanase was evaluated with executing the reaction for 20 minutes at various temperatures varying between 40 and 70°C., in agreement to Nagar *et al.* (2012). The activation energy (Ea) including both free and immobilized mannanase was estimated utilizing the Arrhenius plot, as shown in equation (1):

$$\text{Slope} = -\text{Ea}/R \quad (1)$$

Where R denotes the gas constant

Both free and the immobilized enzyme was investigated in the absence of the substrate at temperature range from 40-70°C up to 60min to determine the thermal stability. The residual activity of the free and the immobilized enzyme was determined at the optimum condition previously calculated. Without pre-incubation, the enzyme's activity was assumed to be 100 percent.

2.8.3. Thermodynamic research

A regression plot of log relative activity (percent) versus time was used to get the kd (min). For both free and immobilized mannanase, the t1/2 (the time it takes for activity to fall to half of its original level) and D-value (the time required to reduce 90 percent of enzyme activity) were calculated from the Eq. (2, 3).

$$t_{1/2} = \ln 2/kd \quad (2)$$

$$D-\text{value} = \ln 10/kd \quad (3)$$

A plot of log denaturation rate constants (lnkd) vs reciprocal of absolute temperature was used to determine the activation energy (Ed) for both free and immobilized mannanase denaturation (K) using the Eq. (4)

$$\text{Slope} = -E_d/R \quad (4)$$

2.8.4. pH stability

The free and immobilized enzymes were treated to varied pH values ranging from 4 to 7 for different time intervals in the absence of the substrate (15, 30, 45, 60, 90 and 120 min.). The residual activities were then tested under the same conditions as before.

2.8.5. Effect of substrate concentrations and kinetic constant determination

For the determination of Michaelis-Menten kinetic parameters, different initial locust bean gum concentrations were used ranging from (2.5- 17mg/ml). The partial pure enzyme's dynamical parameters were calculated using the Lineweaver-Burk plot (Lineweaver and Burk, 1934), which was plotted using the formula giving:

$$1/V = (1/V_{max}) + (K_m/V_{max})\,(1/S) \quad (8)$$

$$K_{cat} = V_{max}/e \quad (9)$$

where V is the partial pure enzyme's activity (U/mL), Vmax is the maximal activity, Km is the Michaelis-Menten constant, S is the locust bean gum concentration (mg/mL), Kcat is the turnover number, and e is the enzyme concentration.

2.8.6. Effect of different salts on β-mannanase activity

The effect of Cu^{2+}, Zn^{2+}, Ca^{2+}, Hg^{2+}, Mn^{2+}, SDS, EDTA and Mercapto ethanol in concentration (1mM) for 30 minutes at 30°C on β-mannanase activity was determined. Each was added separately to free and immobilized β-mannanase at 1mM final concentration.

2.8.7. The immobilized β -mannanase's operating stability

0.5 g of immobilized β-mannanase was carried out in the experiment (wet), which contained approximately

20.02 IU of the enzyme. The immobilized form was incubated for 10 minutes at 60°C with Locust bean gum (10mg). It was filtered out at the conclusion of the reaction period, rinsed to start a new run, and re-suspended in solution with prepared substrate and pure water. The activity of β-mannanase was measured in the supernatant.

2.8.8. Thin – layer chromatography

Carbohydrates were separated and primary detected by (TLC) techniques using silica gel plates. The samples were spotted on plates with different authentic for mono, di, tri, tetra sugars. Plates were developed at room temperature in a saturated chamber containing the mobile phase which is propanol: water (8.5:1.5 v/v). Sugars were recognized using a spraying procedure. The dried plates were then added to the phenol-sulphuric acid reagent (3 g of phenol and 5 ml of concentrated sulphuric acid in 95 ml of ethyl alcohol), followed by incubation at 100 C in an oven for 10-15 min. (Adachi, 1965).

2.9. The biological actions of the manno-oligosaccharides synthesized (MOS)

Antimicrobial and antioxidant activity were measured for MOS's according to the following methods:

2.9.1. Antioxidant activity

The antioxidant activity of the samples was examined according to the approach provided; the scavenging activity of 1, 1-diphenyl-2-picrylhydrazyl (DPPH) radicals was determined by Brand-Williams *et al.,* (1995). The reaction was carried out by adding 0.1mL of the sample solution to 3.9mL of methanol solution of DPPH radical (1.1×10^{-4}mol/L). The reaction allowed for 30 minutes of standing in the dark. Using Trolox as a standard, the decrease in absorbance was determined spectrophotometrically at 515 nm. The outcomes are given in μMTrolox Equivalents (TE)/μg sample.

2.9.2. Determination of prebiotic activities

The oligosaccharide DP_4 was used as carbon sources for growing the three probiotics and (in parallel) a pathogenic strain *E. coli.* A medium-containing blank made out of uninoculated mannooligosaccharides (Hussein *et al.,* 2010). *E. coli* was cultured on nutritional broth medium, while probiotics were produced on conventional MRS broth medium. The optical densities of the growths were obtained at 625nm after 24 hours of incubation at 37°C, and The following formula was used to computed the prebiotic factor:

$$\text{Prebiotic factor} = \frac{\text{O.D of Bifido genic growth of culture}}{\text{O.D of pathogenic growth of culture}}$$

The prebiotic activity is determined by comparing the densities of growths of the probiotic beneficial bacteria *Pediococus lactis* 1,2, *Lactobacillus lactis*, *Lactobacillus acidophilus*, and *Lactobacillus planterum* cultured on MRS-medium with those of the pathogenic *Escherichia coli* (containing the sample as sole carbon source). The five probiotics were cultivated on MRS medium for 24 hours, whereas E. coli was grown on nutritional broth medium for 24 hours. As an inoculation, stock solutions of 0.1 ml of each resulting bacterial suspension were used. For a 10-ml study medium, including the researched material as a supply of carbohydrates. A carbohydrate source of 150 mg per 10 ml MRS-base medium was used to make this medium.

The resultant bacterial growth was detected at 625 nm after incubation during 24hrs at 37°C, against a blank made up of uninoculated MOS's including medium table (3).

The "Prebiotic factor" was used to determine the prebiotic activity: Prebiotic factor = Bifidogenic bacterial growth O.D. versus *E. coli* growth O.D. All studies were carried out in three different ways, and the findings are given as means SD (n= 3).

3. Result and discussion

3.1. Enzyme production

β-mannanase can be produced by microbes and filamentous organisms (Adigazel *et al.,* 2015 and Ismail *et al.,* 2019). The mutant *P. citrinium* β-mannanase was reported in our previous work as a good producer of β-mannanase that produce351 IU/ml with specific activity 21.57 U/mg protein (Ismail *et al.,* 2019).

3.2. Partial purification

The fraction brought precipitation at 60-70% ammonium sulphate saturation represented 34.03% of the total recovered activity with 7.99 fold increase in the specific activity. Our previous work (Ismail *et al.,* 2019) reported that the fraction determined at 60-70% (w/v) ammonium sulphate provided the most specific activities (27.83 U/mg proteins). Nadaroglu and Snomez (2016) and Olaniyi & Adebowale (2017) reported partial purification of mannanase using ammonium sulphate.

3.3. Enzyme immobilization

An important parameter in determination the economic viability of the industrial use is the reusability which shows the significance of the generated enzyme's immobilization (Fernandes *et al.,* 2013).

Among 48 different tested carriers, the immobilization by covalent binding with Chitosan-NaOH+ dopamine+ Polyethylenimine was the best giving the highest immobilization yield (34.41 %), which agrees with Mohy Eldin *et al.* (2012) who mentioned that covalent binding is progressively ideal as it leads to stable enzyme derivatives.

The immobilization process was optimized with different factors. The optimum conditions were the loading of 20.02 IU/ml on activated chitosan with glutraldhyde, polyethylenimine and dopamine, sufficient for achieving maximal immobilization yield (58.86%), while it was only 19.41%, in case of activated chitosan directly. Fig. 1 (A, B) showed the change in the surface of the beads for different gel formulation.

The increase in the loading enzyme decreases the immobilization yield, and this may be attributed to the increase on the surface of beads hamper diffusion of the substrate to the enzyme's active site (De Medeiros *et al.,* 2020 and Fernandez *et al.,* 2017).

The yield of immobilization increased to 61.7% with 3.5% glutraldhyde (fig, 1C). Covalent binding through glutraldhyde most likely increased the carrier local surface area and, accordingly decreased the streric impediment that surrounds the active site (Siso *et al.,* 1990). Blibech *et al*., (2011) reported that 2.5% glutraldhyde was optimum for the immobilization yield.

In addition, the effect of different pH and time of loading enzyme was studied. The optimum yield was achieved (69.07%) at pH 6 after 6h (Fig, 1D) and (Fig, 1E). Also, the temperature affected the yield of immobilization. A yield of 77.2% was achieved at 20°C but decreased to 8.12% at 37°C (Fig, 1F). Similarly, Nadaroglu and Sonmez (2016) found that the immobilization of β-mannanse was significantly enhanced at the mild acidic pH 5 and at 20°C.

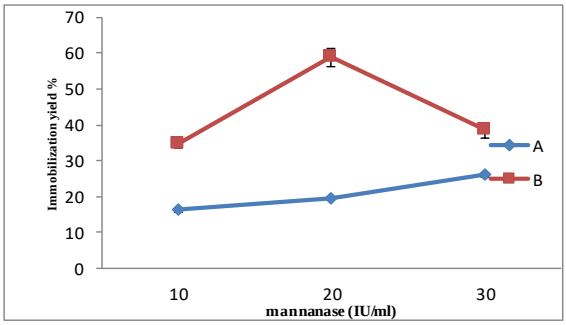

Figure (1A, B): Effect of different treatment of chitosan with different concentrations of enzyme
A-Chitosan+dopamine

chitosan + glutraldhyde(2.5%)+polyethelene+dopamine

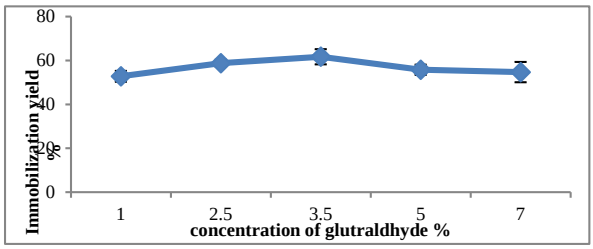

Figure (1C): Effect of different concentrations of glutraldhyde %

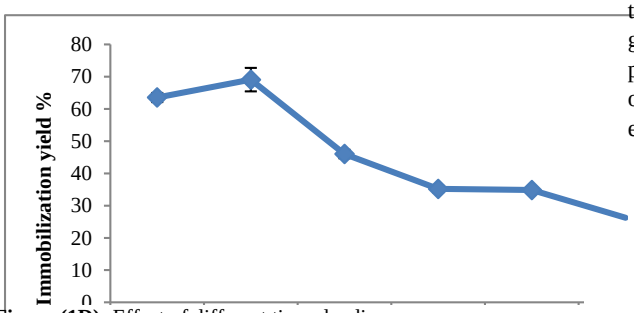

Figure (1D): Effect of different times loading

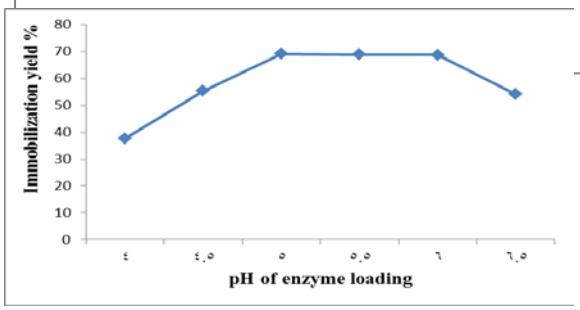

Figure (1E): Effect of different pHs of enzyme loading

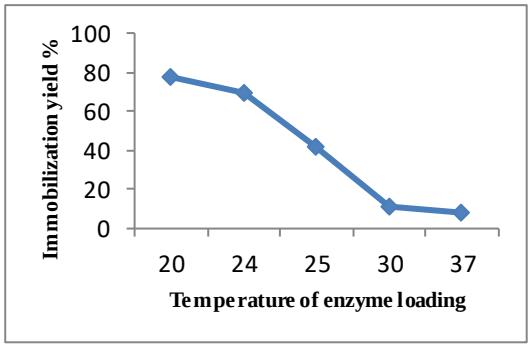

Figure (1F): Effect of different temperatures of enzyme loading

3.4. Characterization of the untreated and treated immobilized enzyme

3.4.1. Fourier Transform Infrared (FT-IR)

From 400 to 4000 cm-1, FT-IR spectroscopic investigation of chitosan with gel particles, triggered particles, and immobilized beads was done. (Fig,2). Chitosan gel beads had distinct peaks in their infrared spectra (curve A); in this figure the peak of amine group is clear at 3429cm^{-1} which is corresponding to NH_2 group. The spectra for aminated beads show that the peak at 3429 cm^{-1}became broader that more amine groups were found on the surface of the beads, indicating their existence (curve B). After treatment with dopamine, a distinguishable band appeared at 1109 cm^{-1}, corresponding to the C–O of the phenol group (curve C). Beads that have been activated with glutaraldehyde display two additional peaks. The first was at 1631 cm-1, referring to the (C=N-) group formed by the reaction of NH2 end groups with glutaraldehyde, and the second was at 1429 cm-1, referring to the (C=O) group formed by a free aldehyde end of glutaraldehyde (curve D). Finally, the immobilized beads produced a larger signal at 3433 cm^{-1}, reflecting a naturally occurring increase in the quantity of amino groups in the enzyme

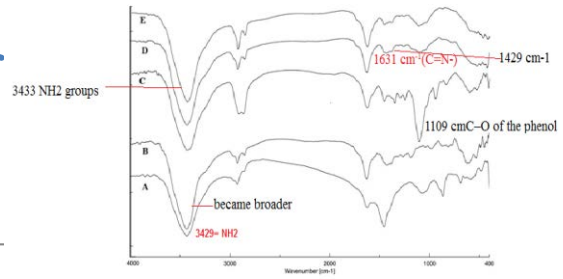

Figure 2. The examination of chitosan gel beads, activated beads, and immobilised beads using FT-IR spectroscopy

The FTIR spectra of the immobilized enzyme agree with novel *Streptomyces* β-mannanase Mohapatra (2021) and immobilized lipase from *Rhizomucor meihei* (Collins *et al.*, 2011) and β-galactosidase from *kluyveromyces lactis* (Klein *et al.*, 2012), and alginate lyase from Arthrobacter species AD-10 Mohapatra (2021).

3.4.2. Scanning Electron Microscope (SEM)

The results shown in Fig (3) showed the changes in the different gel formulation after each step of the immobilization.

The surface of chitosan beads was smooth, and after activation with glutraldhyde molecule accumulated on the surface (figure, 3B) and finally Figure 3C shows the shape of beads homogenous, symmetrical and spherical beads, agree with (Zhao *et al*., 2016).

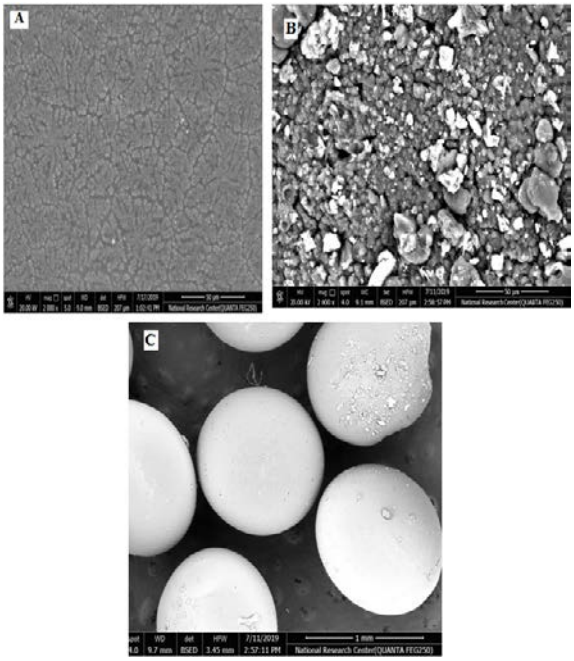

Figure 3. Scanning Electron Microscope (SEM) shows the shape of the beads

3.5. Effect of pH value of the reaction

The influence of pH on the activity of partly purified β-mannanase in a reaction combination and immobilized enzyme was studied in sodium citrate buffer (0.05M) at pH ranged from 4 – 6.5 at 50^{0}C. The results in Fig. 8 indicated that β-mannanase was optimally active at pH 5.5 (control) for both free and immobilized enzymes. The optimum pH of the free and immobilized enzyme was at pH 5.5 (Fig, 4A), and the immobilized enzyme still active (98.97%) at pH 5 and 98.67% at pH 6.0. These results indicated that the immobilized enzyme can keep its maximum activity at a broader range of pH.

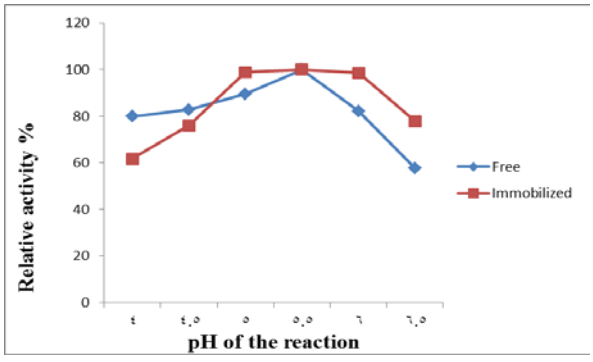

Figure 4A. Effects of varying pH levels on free and immobilized enzyme activity

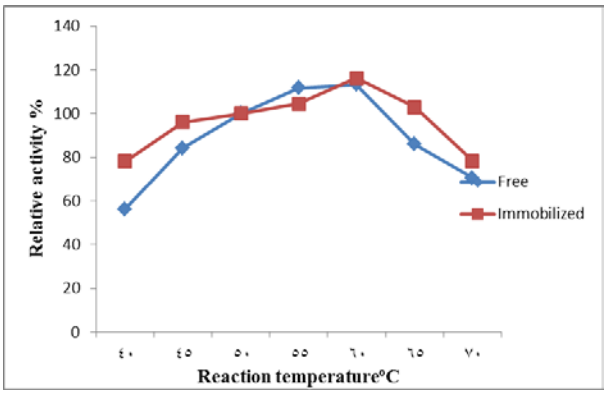

Figure 4B. Optimum temperature profile of free and immobilized mannanase.

Shalaby *et al.*, (2017) For *P. chrysogenum* mannanase, the optimal pH for the free and immobilized forms was found to be 6.0 and 6.5, respectively, respectively. Nadaroglu and Sonmez (2016) found that the immobilization of β-mannanase was determined at pH 5.0.

Most fungal β-mannanases have been found to be most active in the 4.0-5.0 acidic pH range (Lim *et al.*, 2012; Katrolia *et al.*, 2013), whereas β-mannanase is derived from *A. terreus* FBCC1369 was most active at pH 7.0. The optimal pH, according to Mohapatra (2021), is 7.5.

Additionally, the immobilized enzyme shows good pH stability that retained 100% of its activity at pH 5.5 and 6 for 2hr and retained more than 92% and 95% after 2hr at pH 6.5 and 5.0. Panwar *et al.* (2017) reported that between pH 6 and 10, the immobilized β-mannanase of *Bacillus sp.* CFR1601 was stable.

3.6. Effect of temperature

One of the most critical elements determining enzyme activity is temperature. With rising temperature, the activity of both free and immobilized β-mannanase enhanced up to 60°C. The free and immobilized enzyme showed activity of 113.28% and 116.26% of the control (50°C), respectively. Further increase of the reaction temperature up to 65°C leads to decrease of free β-mannanase activity (85.94%), while the immobilized one reaches 102.86%) (Fig. 4B). These findings revealed that the immobilized enzyme was more active than the free enzyme at higher temperatures. Covalent connections were formed between functional groups in enzyme molecules and the carrier surface, strengthening the flexibility of the enzyme's molecular structure and minimizing the effect of temperature on enzymes dissociation, may be referred to as shifting in the optimal temperature (Martin *et al.*, 2001 and Ferrarotti *et al.*, 2006). Covalent immobilization is one among the most extensively distributed utilized strategies for improving enzyme activity at high temperatures in enzyme engineering (Nwagu *et al.*, 2012 and Gill *et al.*, 2006). In general, high temperature is preferred and required for the majority of enzyme activity since it promotes conversion rates. Furthermore, high temperatures enhance the solubility of the substrate while also reducing microbial contamination (Ismail *et al.*, 2019).

The optimal temperature at previous studies were 40°C for Streptomyces galbus (Kansoh *et al.*, 2004), 50°C *Bacillus sp*. CFR1601 (Srivastava *et al.*, 2015), and 58°C *Streptomyces lividans* (Arcand *et al.*, 1993), and for the immobilized enzyme at 60°C for *Clitocybe geotropa*

(Nadaroglu *et al.*, 2016), and at 70°C for *Bacillus sp. CFR1601* (Panwar *et al.*, 2017) and *Penicillium occitanis* (Blibech *et al.*, 2011).

Arrhenius plots were used to compute the activation energy (Ea) of immobilized and free mannanase (Fig. 5). The energy needed to form enzyme- substrate complex was 2.5 higher than the immobilized enzyme. The lower activation energy needed in the immobilized enzyme makes it more suitable for the industrial application, and this would reduce the total cost of the industrial process (Naggar *et al.*, 2012).

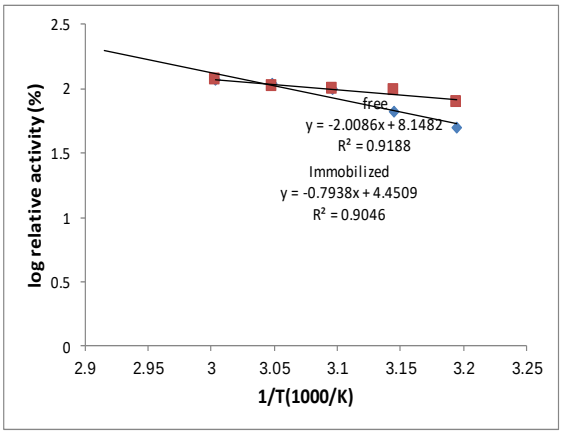

Figure 5. Calculation of activation energy (Ea) for free and immobilized enzymes using Arrhenius plots.

Many studies have suggested that the rise in the optimal temperature for immobilized mannanase is linked to a rise in the reaction's energy barrier as a result of the activation energy (Ea) (Guo *et al.*, 2017 and Arrhenius *et al.*, 1889).

Thermal stability profile (Fig, 6A, B) showed that the immobilized enzyme improved the stability of the enzyme at temperature from 50-60°C. After 2 hours at 50°C, the immobilized enzyme maintained 86.4 percent of its activity, compared to 56.27 percent for the free enzyme. After 2 hours at 60°C, the immobilized enzyme preserved 54.9 percent of its activity while the free enzyme was completely destroyed. This could be because of the covalent interaction between free enzyme and nanoparticles reduces protein unfolding and denaturation by enhancing structural rigidity and lowering thermal vibrations (Hanefeld *et al.*, 2009).

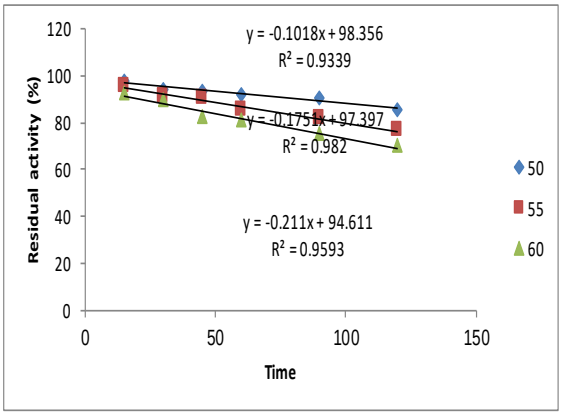

Figure 6A.Thermale-stability profile of immobilized mannanase.

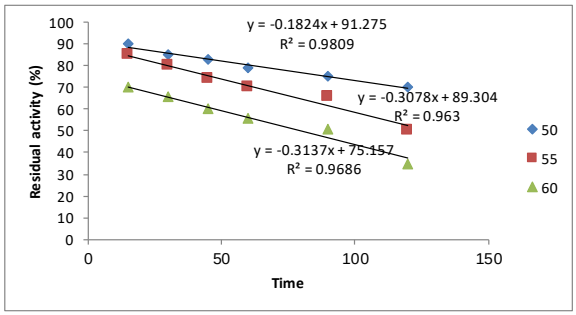

Figure 6B.Thermal-stability profile of free mannanase.

At temperatures of 50-60°C, the heat inactivation rate of free and immobilized mannanase were examined. Plotting the log of residual activity against time yielded a linear relationship, confirming a first-order kinetic response of the free and immobilized enzyme (Fig. 7A, B). The stability of enzymes was investigated as a function of temperature in this thermodynamic study. The thermal stability parameters of free and immobilized mannanase were shown in Table, 1. It was evident that as the temperature was raised, the $t_{1/2}$ fell, as did the (kd), the first order thermal deactivation rate constant (Fig, 8 A, B).

When the half-lives of free and covalently immobilized mannanase on chitosan beads were compared, the difference was striking, especially at higher temperatures. The results showed that the lower the kd the greater is the thermal stability of the enzyme which agrees with what was mentioned by Tayefi-Nasrabadi *et al.*, 2008. Furthermore, after covalent immobilization, D-values of mannanase increased, confirming the enhanced thermal stability of the immobilized mannanase. Previous studies also concluded that after immobilization, the enzyme's half-life increases (Mateo *et al.*, 2007).

Table 1. Thermodynamic parameters for thermal inactivation of free and immobilized mannanase.

	Free enzyme				Immobilized enzyme		
Temp ºC	50 ºC	55 ºC	60 ºC	Temp ºC	50 ºC	55 ºC	60 ºC
kd (min-1)	0.001	0.002	0.0027	*kd* (min-1)	0.0005	0.0009	0.0011
t1/2 (min)	693	346.5	256.67	*t1/2* (min)	1389.29	770.164	630.134
D-value (min)	2303	1151	852.96	*D*-value (min)	4605.17	2558.428	2302.585

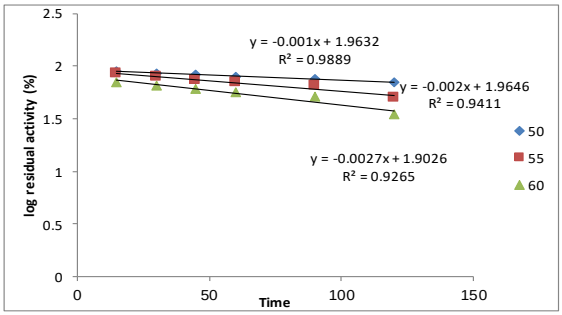

Figure 7A. Arrhenius plot for Kd calculation of free mannanase (free)

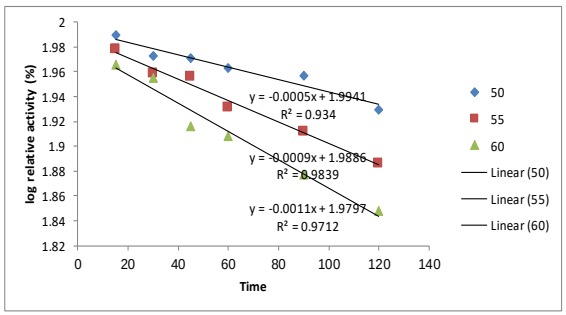

Figure 7B. Arrhenius plot for Kd calculation of immobilized mannanase (immobilized)

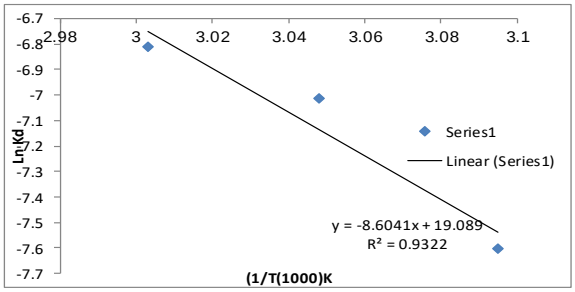

Figure 8A. Arrhenius plot to calculate activation energy (Ed) for denaturation (immobilized mannanase)

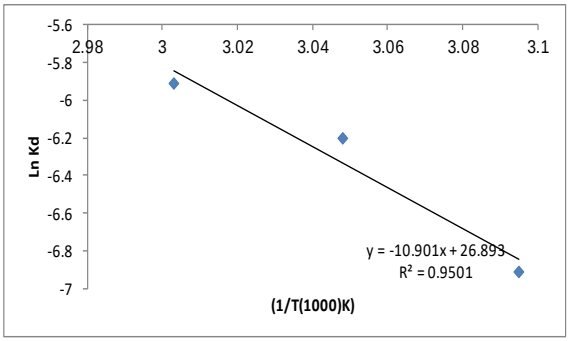

Figure 8B. Arrhenius plot to calculate activation energy (Ed) for denaturation (free mannanase)

coli with the highest activity of 24.9 and 15.65 times recorded for *Pediococus lactis 2 and Lactobacillus planterum*, respectively.

3.6.1. Antioxidant activity

By measuring the scavenging activity of the generated mannooligosaccharides mixture against the 1,1-diphenyl-2-picrylhydrazyl (DPPH) radical, the antioxidant activity of the mixture was determined. The results indicated that the produced oligosaccharides possessed antioxidant activity of about 166 µM Trolox Equivalents (TE)/mg. This result agrees with Amna *et al.* (2018) who indicated that the hydrolysate (rich in mannooligosaccharides) of konjac gum (linear mannan polymer) possessed significant antioxidant activity.

4. Conclusion

In our production, the Mannanase enzymeproduced by the mutant *Penicillium citrinium* Egy5 LC368457 was covalently immobilized onto activated chitosan beads by Polyethyleneimine, glutaraldehyde and dopamine. The immobilized enzyme possessed high stability and reusability as it retained 75.82% of its activity at cycle number 9. Furthermore, they produced mannooligosaccharides, which showed antioxidant and prebiotic activity. The influence of different substrate concentrations

In Lineweaver–Burk graph Fig. (9), the activities of free and immobilized enzymes for locust bean gum concentrations were plotted, and maximal activities (V_{max}) and Michaelis–Menten constants (K_m) values were computed. The results showed an increase in the K_m value of the immobilized enzyme. For free and immobilized enzyme, the K_m was 5 and 5.5 mg ml-1, respectively. In addition, the free and immobilized enzymes had V_{max} of 20 and 25 mg/min/ml, respectively. K_m value commonly increases after immobilization (Park *et al.*, 2005). Mohapatra (2021) reported 4.94mg/ml and 93.5U/mg protein as K_m and V_{max} value for the immobilized Streptomyces species ALg-S25 mannanase. Nadaroglu and Sonmez (2016) reported a K_m value of 0.122mg/ml for *Clitocybe geotropa*. Panwar *et al.*, (2017) reported a K_m value of 6.7mg/ml for *Bacillus sp. CFR1601*.K_m and V_{max} values are mostly determined by the enzyme's source, and hence represent the enzyme's sensitivity to the substrate.

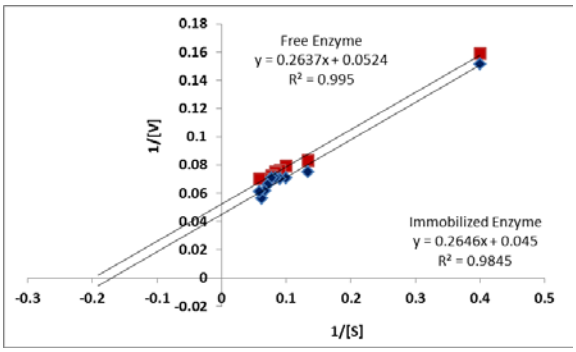

Figure 9. Effect of substrate (locust bean gum) concentrations on the activity of the free and immobilized *Penicillium citrinium* 150GY β-mannanase

4.1. The effect of metal ions on free and immobilized β-mannanase activity

The effects of different metal ions on the free and immobilized enzymes were investigated. The results indicated that EDTA stimulated both free and immobilized enzymes, resulting in increased activity by 14.3% and 15.6% respectively. Also, Ca^{+2} increased the activity by 12.9 and 8.2%, respectively. On the other hand, Hg^{2+} and Mn^{2+}decreased the activity of both free and immobilized enzyme (Fig. 10). Different concentration of EDTA ranged from 0.5 to 5M were examined, and the results showed that the activity reached its maximum at 3mM after 30 min

incubation reached 170.8% and 180.5% for free and immobilized enzyme, respectively (Table, 2). Mohapatra (2021) recorded that EDTA had strong inhibition on the free and immobilized enzyme, and different effect cation action of the enzyme may be due to adopt different geometrics in the same site in the absence of substrate.

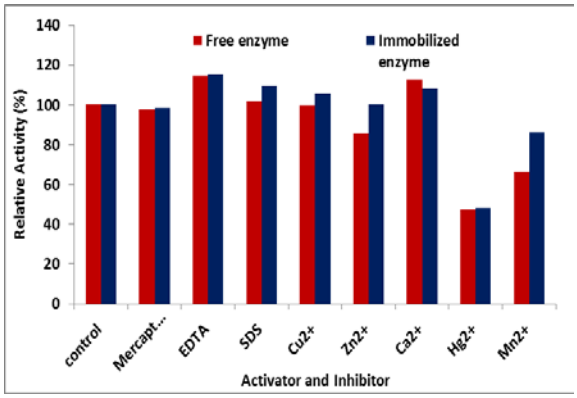

Figure 10. Effect of different activators and inhibitors on the activity of the free and immobilized enzyme

Table 2. Effect of different concentration of EDTA with different incubation time on the activity of the free and immobilized enzyme

conc	Time	Relative activity (%)	
		Free enzyme	Immobilized enzyme
0.5	30 min	129.34	128.92
	60 min	132.58	140.50
1	30 min	168.25	180.48
	60 min	148.35	163.94
3	30 min	170.78	180.48
	60 min	150.78	164.67
5	30 min	152.35	149.04
	60 min	143.28	135.82

4.2. Production of manno-oligosaccharides

L.B.G was more suitable substrate for hydrolysis; therefore, different incubation periods (1hr, 2hr, 3hr, 4hr, 5hr, 6hr, 21hr and 24hr) for hydrolysis of gum locust bean (1%) were applied at 45°C and with 2.5 IU/ml for free and immobilized enzyme. The results showed that in each case for free and immobilized enzyme the hydrolysis increased by increasing the time of the reaction. The 1h hydrolysis reaction yielded 4.39 and 3.1mg/ml for free and immobilized enzyme, respectively, while the 24 h reaction yield was enhanced and reached 8.16 and 7.5 mg/ml of reducing sugars for free and immobilized enzyme, respectively. The TLC indicated that as the time increased the production of MOS (visualized by the spot intensity on TLC plate) increased and the production of monomer increased (Fig. ١١A).

The degree of polymerization of the produced mannooligosaccharide was detected by HPLC and indicated that the enzyme hydrolyzed the locust bean gum to DP4 which has several biological activities (Fig. 11B). The significant item freed from L.B.G was manotetraose (M4) with minor of di, tri oligosaccharides and mannose. Our outcomes concur with Hakamada *et al*. (2014).

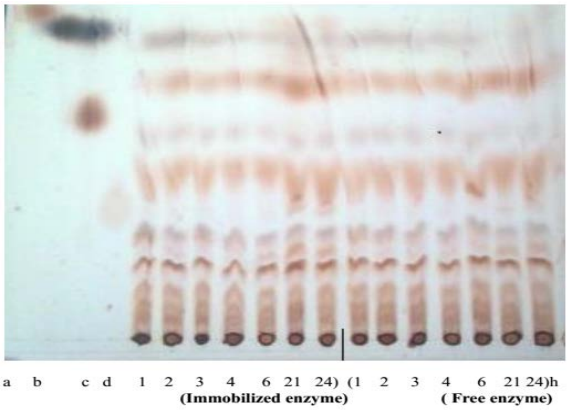

Figure 11A. TLC plate of hydrolysis product of LBG by (Immobilized enzyme and Free enzyme) of mutant of *P.citrinium*150GY β-mannanases at various periods 1, 2, 3, 4, 5, 6 and 7h.
Lan a: mannose, lanb: melibiose, lanc: raffinose, lan d :stachyose, lan 1: 1h, lan 2: 2h, lan 3: 3h, lan 4:4h, lan 5: 6h, lan 6:21h, lan 7: 24h

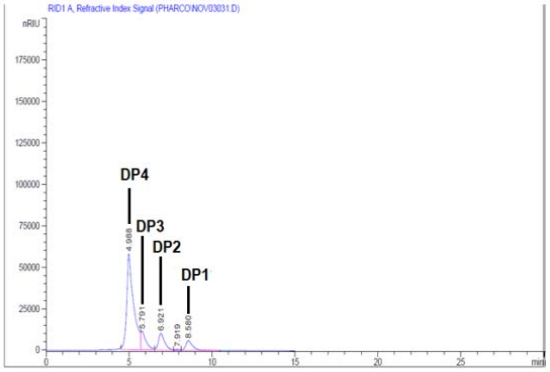

Figure 11B. HPLC for hydrolysis of locust bean gum

4.3. Operational stability

The immobilized enzyme was stable until 5th cycle as it retains 100% of its activity. The enzyme retained 75% of its activity at cycle number 9. The activity then dropped, which might be attributed to the released sugar during hydrolysis or the leaking of the enzyme from the carrier (Gouda *et al.*, 2002). The successive reuse of the immobilized enzyme is a major advantage of this technique due to enhancing the economic value (Fig. 12 A, B).

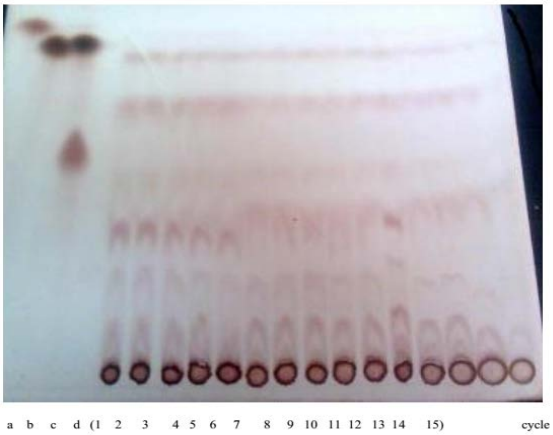

Figure 12A. TLC plate of hydrolysis product of LBG by immobilized enzyme and its reusability.

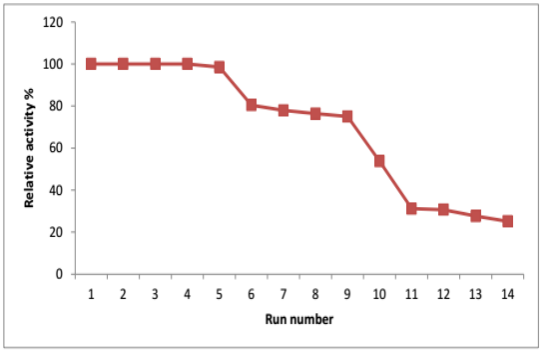

Figure 12B. Operational stability of immobilized from *Penicillium citrinium*150GY

Biological activities of galactomanno-oligosaccharide

4.3.1. Prebiotic activity

Mannooligosaccharides had been previously estimated as prebiotic compounds. They can increase the growth of good bacteria, such as *Lactobacillus* and *Bifidobacterium*, specifically. They can also prevent *Salmonella* and *E. coli* bacteria from attaching to each other in the digestive system (Chauhan *et al.*, 2014 and Dhawan *et al.*, 2015). In the current study, the prebiotic activity of the produced mannooligosaccharides mixture was evaluated by comparing its effect on the growth of various probiotic bacteria including *Pediococus lactis 1,2*, *Lactobacillus lactis*, *Lactobacillus acidophilus* and *Lactobacillus planterum* with that of the pathogenic *E. coli*. The results in table 3 indicated that the produced oligosaccharide mixture possessed a positive effect on the growth of all the tested probiotic strains as compared to the growth of *E.*

Table 3. Prebiotic activity of MOS

Probiotic microorganism	Ratio againt *E. coli*
Pediococus lactis 1	13.06
Pediococus lactis 2	24.9
Lactobacillus lactis	3.2
Lactobacillus acidophilus	4.7
Lactobacillus planterum	15.65

Reference

Abosereh NA, Ismail SA, Khattab OK, Nour SA, Abo-Elnasr AA and Hashem AM. 2019. Genetic improvement of fungal β-mannanase and its molecular differentiation. *Egypt. Pharm. J.*, **18(4):** 403.

Adachi S. 1965. A rapid method for the assay of lactulose. *Anal. Biochem.*, **12:** 137-142.

Adiguzel A, Nadaroglu H and Adiguzel G. 2015. Purification and characterization of β-mannanase from *Bacillus pumilus* (M27) and its applications in some fruit juices. *J. Food Sci. Technol.*, **52:** 5292–5298.

Amna KS, Park SY, Choi M, Kim SY, Yoo AY and Park J. K. 2018. Antioxidant activity of Manno-oligosaccharides derived from the hydrolysis of polymannan by extracellular carbohydrase of *Bacillus N3*. *J. Mar. Biosci. Biotechnol.*, **10(1):** 9-17.

Ansari SA and Husain Q. 2012. Potential applications of enzymes immobilized on/in nano materials: a review. *Biotechnol Adv.*, **30(3):** 512–523.

Arcand N, Kluepfel D and Paradis FW. 1993. β-mannanase of *Streptomyces lividans 66*: cloning and DNA sequence of the man A gene and characterization of the enzyme. *Biochem J.*, **290(3):** 857–863.

Arrhenius S. 1889. Uber die reaktionsgeschwindigkeitbei der inversion von rohrzucker durch sauren. *Z. fur Phys. Chem.*, **4(1):** 226–248.

Bayramoglu G, Altintas B, Yilmaz M and Arica MY. 2011. Immobilization of chloroperoxidase onto highly hydrophilic polyethylene chains via bioconjugation: catalytic properties and stabilities. *Bioresour. Technol.*, **102:** 475–482.

Blibech M, Ghorbel RE, Chaari F, Dammak I, Bhiri F, Neifar M and Chaabouni SE. 2011. Improved mannanase production from *Penicillium occitanis* by fed-batch fermentation using acacia seeds. *ISRN Microbiol.*, 1-5.

Brand-Williams W, Cuvelier ME and Berset CLWT. 1995. Use of a free radical method to evaluate antioxidant activity. *LWT - Food Sci. Technol.*, **28(1):** 25-30.

Chauhan PS, Puri N, Sharma P and Gupta N. 2012. Mannanases: microbial sources, production, properties and potential biotechnological applications. *Appl. Microbiol. Biotechnol.*, **93:** 1817–1830.

Chauhan PS, George N, Sondhi S, Puri N and Gupta N. 2014. An overview of purification strategies for microbial mannanases. *Int J Pharma Bio Sci.*, **5 (1):** 176- 192.

Collins SE, Lassalle V and Ferreira ML. 2011. FTIR-ATR characterization of free *Rhizomucor meihei* lipase (RML), Lipozyme RM IM and chitosan-immobilized RML. *J Mol Catal B Enzym.*, **72 (3–4):** 220–228.

de Medeiros Dantas JM, da Silva NS, de Araújo Padilha CE, de Araújo NK and dos Santos ES. 2020. Enhancing chitosan hydrolysis aiming chitooligosaccharides production by using immobilized chitosanolytic enzymes. *Biocatal Agric Biotechnol.*, **28:** 101759.

Dhawan S, Singh R and Kaur J. 2015. A β-mannanase from *Paeenibacillus sp*. Optimization of production and its possible prebiotic potential. *Biotechnol. Appl. Biochem.*, **63(5):** 669-678.

Fernandes KF, Cortijo-Triviño D, Batista KA, Ulhoa CJ and García-Ruiz PA. 2013. Chitin hydrolysis assisted by cell wall degrading enzymes immobilized of *Thichoderma asperellum* on totally cinnamoylated D-sorbitol beads. *Mater Sci Eng C.*, **33(5):** 3077-3081.

Fernandez - Lopez L, Pedrero SG, Lopez - Carrobles N, Gorines B C, Virgen - Ortíz JJ and Fernandez - Lafuente R. 2017. Effect of protein load on stability of immobilized enzymes. *Enzym Microb Technol.*, **98:** 18-25.

Ferrarotti SA, Bolivar JM, Mateo C, Wilson L, Guisan JM and Fernandez-Lafuente R. 2006. Immobilization and stabilization of a cyclodextrin glycosyltransferase by covalent attachment on highly activated glyoxyl-agarose supports. *Biotechnol. Prog.*, **22(4):** 1140-1145.

Foda DS, Nour SA, Ismail SA and Hashem AM. 2022. Safety Evaluation of β-mannanase Enzyme Extracted from the Mutant Pathogenic Fungal Strain *Penicillium citrinum* in Female Wistar Rats. *Int. J. Vet. Sci.*, **11(1)**: 74–81

Gill PK, Manhas RK and Singh. P. (2006). Hydrolysis of inulin by immobilized thermostable extracellular exoinulinase from *Aspergillus fumigatus*. *J. Food Eng.*, **76(3):** 369-375.

Gouda MK and Abdel-Naby MA. (2002). Catalytic properties of the immobilized *Aspergillus tamarii* xylanase. *Microbiol. Res.*, **157(4):** 275-281.

Guo Y, Liu J, Zhang K, Zhang H, Li Y and Lei Z. 2017. Synthesis of stimuli-responsive support material for pectinase

immobilization and investigation of its controllable tailoring of enzymatic activity. *Biochem. Eng. J.,* **121:** 188-195.

Hakamada Y, Ohkubo Y and Ohashi S. 2014. Purification and characterization of *β*-mannanase from *Reinekea* sp. KIT-YO10 with transglycosylation activity. *Biosci. Biotechnol. Biochem.,***78(4):** 722–728.

Hanefeld U, Gardossi L and Magner E. 2009. Understanding enzyme immobilisation. *Chem Soc Rev.,* **38(2):** 453–468.

Hashem AM, Ismail AMS, El-Refai MA and Abdel-Fattah AF. 2001. Production and properties of β-Mannanase by free and immobilized cells of *Aspergillus oryzae* NRRL 3488. *Cytobios.,* **105:** 115-130.

Hashem AM, Gamal AA, Hassan ME, Hassanein NM and Esawy MA. 2016. Covalent immobilization of *Enterococcus faecalis* Esawy dextransucrase and dextran synthesis. *Int. J. Biol. Macromol.,* **82:** 905-912.

Hussein MM, Kheiralla ZMH, Helal MMI and Saker EAE. 2010. The prebiotic activities of oligosaccharides derived from partial hydrolysis of commercial Algal polysaccharides. *Egypt. Pharm. J.*,**19:** 1-23.

Ismail SA, Khattab OK H, Nour SA, Awad GE, Abo-Elnasr AA and Hashem AM. 2019. A Thermodynamic Study of Partially-Purified Penicillium humicola β-mannanase Produced by Statistical Optimization. *Jordan J. Biol. Sci.,* 12(2).

Ismail SA, Nour SA and Hassan AA. 2022. Valorization of corn cobs for xylanase production by *Aspergillus flavus* AW1 and its application in the production of antioxidant oligosaccharides and removal of food stain. *Biocatal. Agric. Biotechnol.,* **41**: 1878-8181.

.Kansoh AL and Gammal A. 2001. Xylanolytic activities of *Streptomyces sp*. taxonomy production, partial purification and utilization of agricultural wastes. *Acta Microbiol. Immunol. Hung.,* **48:** 39-52.

Katrolia P, Yan Q, Zhang P, Zhou P, Yang S and Jiang Z. 2013. Gene cloning and enzymatic characterization of an alkali-tolerant endo-1, 4-β-mannanase from *Rhizomucor miehei*. *J. Agric. Food Chem.,*. **61(2):** 394-401.

Khattab OK, Ismail SA, Abosereh NA, Abo-Elnasr AA, Nour S A and Hashem AM. 2020. Optimization and comparative studies on activities of β-mannanase from newly isolated fungal and its mutant. *J. Agric. Food Chem.,* **19(1):** 29.

Klein MP, Nunes MR, Rodrigues RC., *et al*., 2012. Effect of the support size on the properties of β-galactosidase immobilized on chitosan: advantages and disadvantages of macro and nanoparticles. *Biomacromolecules.,* **13(8):** 2456–2464.

Lim JL, Bakar FDA, Yusof HM and Murad AMA. 2012. Cloning and expression of a *Trichoderma longibrachiatum* β-mannanase gene in *Pichia pastoris*. *Afr. J. Biotechnol.,* **11(7):** 1705-1718.

Lowry OH, Rosebrough NH, Farr AL and Randall R. 1951. Protein measurement with the Folin phenol reagent. *J. Biol. Chem.,* **193:** 265–275.

Martin MT, Alcalde M, Plou FJ, Dijkhuizen L and Ballesteros A. 2001. Synthesis of malto-oligosaccharides via the acceptor reaction catalyzed by cyclodextrin glycosyltransferases. *Biocatal. Biotransformation.,* **19(1):** 21-35.

Mateo C, Palomo JM, Fernandez-Lorente G, Guisan JM and Fernandez-Lafuente R. 2007. Improvement of enzyme activity, stability and selectivity via immobilization techniques. *Enzyme Microb. Technol.,* **40(6):** 1451-1463.

Mohapatra BR. 2021. Characterization of β-mannanase extracted from a novel *Streptomyces species* Alg-S25 immobilized on chitosan nanoparticles. *Biotechnol Biotechnol Equip.,* **35(1):** 150-161.

Mohy Eldin MS, El Enshasy HA, Hassan ME, Haroun B and Hassan EA. 2012. Covalent immobilization of penicillin G acylase onto amine functionalized PVC membranes for 6APA production from penicillin hydrolysis process. II. Enzyme immobilization and characterization. *J. Appl. Polym. Sci.,* **125(5):** 3820-3828.

Nadaroglu H and Sonmez Z. 2016. Purification of an endo-beta 1, 4-mannanase from *clitocye geotropa* and immobilization on chitosan-coated magnetite nanoparticles: *application for fruit juices.* ***Enzyme.,*** **1:** 2.

Nagar S, Mittal A, Kumar D, Kumar L and Gupta VK. 2012. Immobilization of xylanase on glutaraldehyde activated aluminum oxide pellets for increasing digestibility of poultry feed. *Process Biochem.,* **47(9):** 1402-1410.

Nagar S, Mittal A, Kumar D, Kumar L and Gupta VK. 2012. Immobilization of xylanase on glutaraldehyde activated aluminum oxide pellets for increasing digestibility of poultry feed. *Process Biochem.,* **47(9):** 1402-1410.

Nour SA, El-Sayed GM, Taie HAA, Emam MTH, El-Sayed AF, Salim RG. 2022. Safe production of *Aspergillus terreus* xylanase from *Ricinus communis*: gene identification, molecular docking, characterization, production of xylooligosaccharides, and its biological activities. *J Genet Eng Biotechnol*., **20**:121.

Nwagu TN, Aoyagi H, Okolo BN and Yoshida S. 2012. Immobilization of a saccharifying raw starch hydrolyzing enzyme on functionalized and non-functionalized sepa beads. *J. Mol. Catal.,* **78:** 1-8.

Olaniyi OO and Adebowale O. 2017. Production and Partial Purification of Beta-Mannanase from *Aspergillus niger* Associated with Ilaje Lake, Ondo State, Nigeria. *J Bacteriol Mycol.,* **5(3):** 00132.

Panwar D, Kaira GS and Kapoor M. 2017. Cross-linked enzyme aggregates (CLEAs) and magnetic nanocomposite grafted CLEAs of GH26 endo-b-1,4-mannanase**:** improved activity, stability and reusability. *Int J Biol Macromol.,* **105(1):**1289–1299.

Park H, Brothers EN and Merz KM. 2005. Hybrid QM/MM and DFT investigations of the catalytic mechanism and inhibition of the dinuclear zinc metallo-β-lactamase CcrA from *Bacteroides fragilis. J. Am. Chem. Soc.,* **127(12):** 4232-4241.

Shalaby AG, Esawy MA and Hussein MM. 2017. Comparative study between free and immobilized *Penicillium chrysogenum* mannanase: a local fungal isolate. *Biocatal Agric Biotechnol.,* **7(06):** 97-104.

Sirisha V, Jain A and Jain A. 2016. Enzyme immobilization: an overview on methods, support material, and applications of immobilized enzymes. *Adv Food Nutr Res.,* **79:**179–211.

Siso MIG, Graber M, Condoret JS and Combes D. 1990. Effect of diffusional resistances on the action pattern of immobilized alpha-amylase. *J. Chem. Technol. Biotechnol.,* **48(2):** 185-200.

Smogyi M. 1952. Notes on sugar determination. *Journal Biol. chem.,* **195:** 19-23.

Srivastava PK, Panwar D, Harish Prashanth KV and Kapoor M. 2015. Hydrolysis of Locust Bean Gum by GH-26 Endo-Mannanase: Generation of Un-Substituted and terminally-Substituted Mannooligosaccharides and their In-Vitro Fermentability (under Communication).

Tayefi-Nasrabadi H and Asadpour R. 2008. Effect of heat treatment on buffalo (Bubalus bubalis) lactoperoxidase activity in raw milk. *J Biol Sci.*, **8(8):** 1310-1315.

Verma ML, Puri M and Barrow CJ. 2016. Recent trends in nanomaterials immobilised enzymes for biofuel production. *Crit Rev Biotechnol.*, **36(1):** 108–119.

Zhao JQ, Wang YJ, Luo GS and Zhu SL. 2011. Immobilization of penicillin G acylase on macro-mesoporous silica spheres. *Bioresour. Technol.*, **102:** 529–535.

Zhao Y, Byshkin M, Cong Y, Kawakatsu T, Guadagno L, De Nicola A, ... and Dong B. 2016. Self-assembly of carbon nanotubes in polymer melts: simulation of structural and electrical behaviour by hybrid particle-field molecular dynamics. *Nanoscale.*, **8(34):** 15538-15552.

JJBS

Volume 16, Number 1,March 2023
ISSN 1995-6673
Pages 85 – 92
https://doi.org/10.54319/jjbs/160111

Jordan Journal of Biological Sciences

Optimization of the Process of Reducing the Bitterness of Bitter Melon with Response Surface Methodology

Ummi Rohajatien[1,*], Teti Estiasih[2], Mazarina Devi[1], Soenar Soekopitojo[1], Aly Imron[3] Norfezah Binti Md Nor[4], Luqman Ali Shah[5], Roy Hendroko Setyobudi[6], and Damat Damat[7]

[1]Department of Industrial Technology, State University of Malang, Jl. Semarang No.5, Malang 65145, East Java, Indonesia; [2]Department of Food Science and Technology, Faculty of Agricultural Technology, Brawijaya University, Jl. Veteran, Malang 65145, East Java, Indonesia; [3]Departement of English Language, State Polytechnic of Malang, Jl. Soekarno Hatta, Malang 65141, East Java, Indonesia; [4]Department of Food Service Management, Faculty of Hotel and Tourism Management,Universiti Teknologi Mara Cawangan Pulau Pinang, Jl. Permatang Pauh, 13500 Bukit Mertajam, Pulau Pinang, Malaysia ;[5]National Center of Excellence in Physical Chemistry (NCEPC), University of Peshawar 25120, Pakistan; [6]Department of Agriculture Science, Postgraduate Program, University of Muhammadiyah Malang, Jl. Tlogomas No. 246, Malang, 65144, East Java, Indonesia; [7]Department of Food Technology, Faculty of Agriculture and Animal Science, University of Muhammadiyah Malang, Malang, 65144, Indonesia.

Received: Jan 23, 2023; Revised: Feb 11, 2023; Accepted Feb 21, 2023

Abstract

Bitter melon fruit (*Momordica charantia*, Linn.) is rich in vitamins and minerals, antioxidants, and steroid saponins, which taste bitter and are not liked. Steroid saponin compounds have a good role in biological activities such as antidiabetic, anti-hypercholesterolemia, anti-obesity, anti-tumor, anti-inflammatory, analgesic, antiviral, and antidepressant. Currently, many efforts have been made to reduce the bitter taste, such as salting. To optimize the salting process, the response surface method with the developed model was employed. The design in this study was a 2k or partial factorial design with two levels for each variable coded -1 and +1 and expanded with a value of α, where α = 2k/4, and k = number of variables. To check the accuracy of the second-order polynomial model, the observations were repeated five times at the center point (X1 = 0 and X2 = 0). Bitter taste response parameters were measured using descriptive sensory tests and LC-MS chromatographic analysis of diosgenin compounds. The optimization results show that the quadratic polynomial regression equation is Y = 2.468 – 0.1053X1- 0.0176X2 + 0.0153X12 + 0.0178X22 + 0.085X1X2 where X1 = salt concentration and X2 = salting time. A minimal bitter taste response was obtained at a salt concentration of 5 % and 15 min of salting time with a desirability value of 94.1%. In the condition of a minimum bitter taste response of 2.145, the optimum point for each variable is a stationary point, considered the optimum response.

Keywords: Bitter gourd, Bitter cucumber, Reduce bitter taste, Herbal medicine, Medicinal vegetable, *Momordica charantia* L., Optimization decrease, Salting treatment

1. Introduction

The bitter melon plant belongs to the Cucurbitaceae family; and the distribution includes China, India, and Southeast Asia. Bitter melon or bitter gourd fruit (*Momordica charantia*, Linn.) is rich in nutrients, especially vitamins, minerals, and fiber, and contains many complexes of beneficial bioactive compounds, and antioxidants, among other alkaloids, terpenoids, steroids, tannins, and saponins (Nursal and Yeanny 2019), which contribute to extraordinary versatility in treating diseases. Several researchers (Asmawati *et al*., 2022; Damat *et al*., 2019, 2020, 2021; Gangakhedkar *et al*., 2021, Setyobudi *et al*., 2019; Sur and Ray, 2020; Ummi *et al*., 2019) stated that fiber and antioxidants have good roles in supporting biological activities and act as anti-diabetic, anti-hypercholesterolemic, anti-obesity, antitumor, anti-inflammatory, analgesic, antiviral, and antidepressant. The people of southern Japan use bitter melon as a laxative and anthelmintic (Shubha *et al*., 2018). Bitter melon extract in India is used as a diabetic drug, rheumatic drug, liver disease drug, and lymphatic disease drug (Ee Shian *et al*., 2015).

Bitter melon in Indonesia, apart from being known as a vegetable, is also traditionally used as a phlegm laxative, fever reducer, and appetite enhancer. Bitter melon leaves are used as a menstrual laxative, burn medicine, skin disease medicine, and worm medicine (Bahagia *et al*., 2018). Since it is known that the bitter melon plant is productive for health, several researchers have tried to identify and isolate the material that depends on the bitter melon plant. Various kinds of treatment can be done to reduce the bitter taste of bitter melon before the culinary/cooking process is carried out. One way is often done is by salting treatment (Ummi *et al*., 2019). Various methods of salting are carried out by the community, squeezing bitter melon fruit that has been sliced

* Corresponding author. e-mail: ummi.rohajatien.ft@um.ac.id.

longitudinally and transversely to become bitter melon slices using fingers for a specific time and adding a certain amount of salt. Indonesia, an archipelagic country consisting of thousands of islands, has various tribes, languages , and cultures. Each region also has a distinctive food, processed using local ingredients and favored by the local community and then referred to as the area's traditional food. This food can change regarding ingredients and processing methods (Weaver, 2018). Even more interesting is consuming food with essential elements derived from plants and animals locally with natural processing (Wijaya, 2019). The problem is more in the way Indonesian people process their food. Almost all traditional Indonesian food is processed using heating until it is cooked. In addition, especially for vegetable processing, the vegetable ingredients are often washed, boiled, and the water removed, then the vegetables are kneaded before being mixed with spices and served. This way, some nutrients, such as vitamins and minerals that are soluble in water, will be wasted through washing, and some that are not heat resistant will be damaged during the cooking process (Reis *et al*., 2015; Xu *et al*., 2014). Setyobudi *et al*. (2021, 2022) reported a decrease in vitamin C and vitamin A levels when heating above 50 °C. This high temperature has a negative impact because these two vitamins are enchangers in the absorption of Fe non-heme nutrients in the human body. Another adverse effect is the damage to antioxidants. Therefore, this research was carried out to avoid damage to the valuable ingredients in bitter melon by developing a model for optimizing the salting process.

2. Material and Methods

Optimization of the bitter melon pre-treatment process by adding salt and pressing was carried out using the Response Surface Methodology (RSM). The research design using the RSM method, which many statisticians have developed to construct a second-order response surface design with two variables, is the Central Composite Design (CCD). The design of this study is a 2k factorial or partial factorial (fractional factorial) with two levels on each variable coded -1 and +1 and expanded with a value of α, where $\alpha = 2\ k/4$ and k = number of variables. The second-order polynomial model is tested for accuracy by making observations repeated five times at the midpoint (X1 = 0 and X2 = 0) (Kumari and Gupta, 2019). In addition, before compiling the primary research with a composite design, a preliminary study was carried out to determine the optimum point of each optimized variable. These points are considered process conditions that produce the optimal response.

3. Results and Discussion

3.1. Preliminary research

This preliminary study optimized the concentration of added salt (KK) and kneading time (KW). In addition, preliminary research was conducted to determine the optimum point of each optimized variable in the initial treatment of squeezing bitter melon slices that had been added with salt. This point is suspected to be a condition that produces an optimum response, namely a minimal bitter taste response (Y). The results of Y response data obtained from preliminary research from each optimization variable are presented in Figure 1 and Figure 2.

Based on Figure 1, it can be seen that the minimum score, which is the optimal value in the preliminary study of the salting optimization process, is found in the 7.5 % concentration treatment with a duration of 15 min with an average score of 2.4. This score shows the minimum bitter taste response score. Figure 2 shows that the minimum mean score of 2.4 is found in the 10 % salt concentration treatment and the salting time of 10 min. This minimum score is the optimum value at the preliminary research stage of the salting optimization process. This optimum value indicates a minimal bitter taste response. The optimum value at the initial research stage of the optimization of the salt kneading process is then used as the optimum level and the experimental area in the primary research stage of the optimization of the salt kneading process.

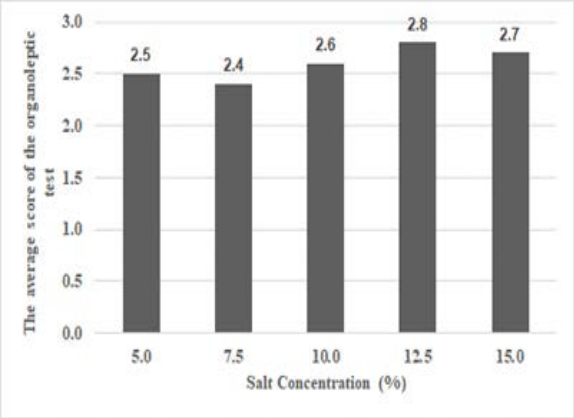

Figure 1. Histogram of preliminary research on the optimization of the squeezing process at 15 min

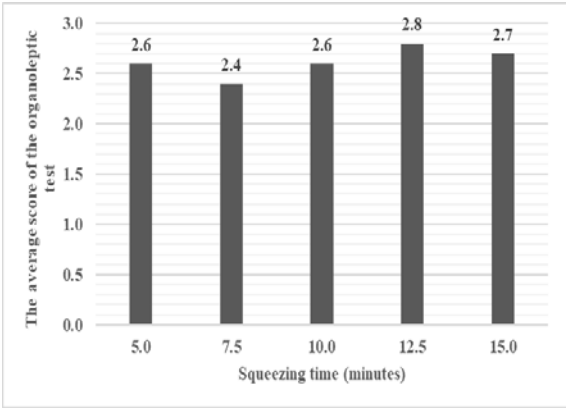

Figure 2. Histogram of preliminary research on process optimization salting at 10 % salt concentration

As a comparison material in the preliminary research on the optimization of the salting kneading process with this descriptive sensory test, a test was carried out by measuring the levels of bitter taste compounds in bitter melon fruit by LC-MS chromatographic method. Diosgenin compounds are known to have a bitter taste in bitter melon. Diosgenin is a steroidal saponin compound with a bitter taste (Joseph and Jini, 2013). The chromatogram of the results of the analysis of the diosgenin content of bitter melon in a preliminary study of optimization of the salting squeezing process of bitter melon before culinary processing is contained in the

appendix. In comparison, the table of diosgenin levels on the optimization of salt concentration and salting time variables is presented in Figures 3 and Figure 4. The chromatography results of the diosgenin content in Figure 3 show that the combination treatment of 7.5 % salt concentration and 15 min of squeezing time resulted in the lowest diosgenin level of 0.461 mg g^{-1}. Meanwhile, the chromatography results of diosgenin levels on optimization of squeezing time with a salt concentration are presented in Figure 4.

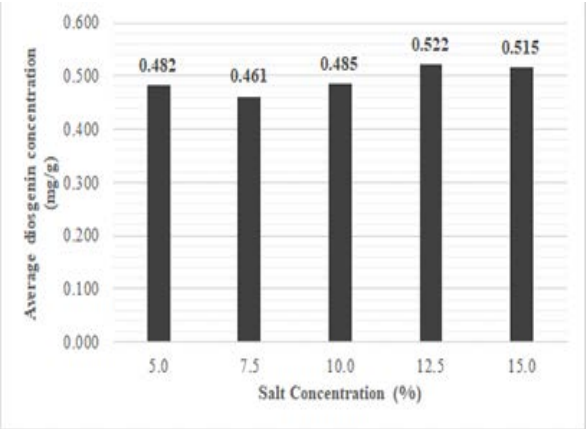

Figure 3. The levels of diosgenin compounds are corrected for the bitter taste in optimization of salt concentration with 15 min

The lowest diosgenin level shown in Figure 4 is 0.470, namely the 10 % salt concentration treatment with a kneading time of 10 min. Low diosgenin levels indicate a lot of diosgenin is wasted after squeezing bitter melon slices with added salt. In addition, low diosgenin levels indicate a minimal bitter taste response. The points of the lowest diosgenin levels in Figure 3 and Figure 4 are the points that are thought to produce an optimum response, namely a minimal bitter taste response (Y), while the level of treatment that will be the center point of the experiment in the main study is the level of treatment that produces a minimal bitter taste response in each optimized variable.

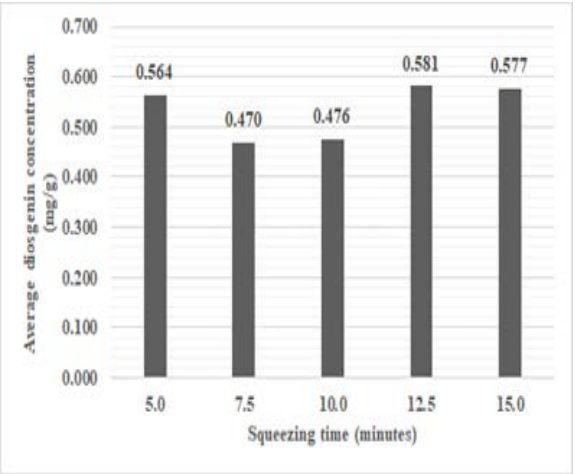

Figure 4. Levels of bitter-tasting compounds (diosgenin) on optimization of squeezing time with 10 % salt concentration

Based on Figure 1 and Figure 3, the minimal bitter taste response with a mean score of 2.4 and the lowest diosgenin level with a concentration of 0.461 mg g^{-1} was obtained at a salt concentration of 7.5 %, while Figure 2 and Figure 4 show a minimal bitter taste response with the same average score (2.4) and the lowest diosgenin level of 0.470 mg g^{-1} obtained at 10 min of squeezing. The variables with minimal bitter taste response and the lowest diosgenin levels were then used as the center point for the primary research with the coded variable (0,0). The treatment for coded variables with a central point (0.0) was expanded by taking two inflection points from each variable, namely at the point before the level (coded -1) and at the point after the level (coded +1) from the optimum level. Therefore, the two inflection points for the salt concentration variable are 5 % (code -1) and 10 % (code +1), while the two inflection points for the variable length of extraction time are 5 min (code -1) and 15 min (code + 1). These points are then used to develop experimental designs in the primary research.

3.2. Main research process optimization

The primary research was carried out using three levels on each variable which was assumed to be the optimum level and the experimental area obtained from the preliminary research. Determining the desired optimum point in the response surface analysis with a central composite design requires an experimental area around the center point. The experimental area consists of two levels of each variable coded with -1 and +1 and expanded with the value of α. The formula set for the value of α is where k is the number of variables being tested (Kumari and Gupta, 2019) so that the value of α is set at 1.414. Code variables -1 and +1 indicate the level of variables that are before and after the optimum point. The distance between the coded variable -1 and the optimum variable 0 is the same as the distance between the coded variable +1 and the optimum variable 0.

The experimental design used in this main study is the Central composite design with a combination treatment of the processes obtained from the introduction, namely the salt concentration of 7.5 % and the duration of 10 min repeated five times. Further expansion of the treatment was carried out by combining the points before and after the optimum conditions for the concentration variables of 5 % (code -1) and 15 % (code +1) and for the variable length of time 5 min (code -1) and 15 min (code +1). In determining the second-order equation, the treatment is further expanded by combining each optimum condition with points – α and – α. The point α for the concentration variable was determined at 3.965 % (code -1) and 11.035 (code +1), while for the time variable, it was determined for 2.93 min (code -1) and 17.07 (code +1). The composite design of this research center is presented in Table 1.

Table 1. Central composite design for pre-salting process conditions for Bitter melon

Condition Process	Original variable		Code Variable		Response of Bitter taste	
	Concentration (%)	Time (min)	X_1	X_2		
1	5	5	-1	-1	2.87± 0.06	bit bitter
2	5	15	-1	+1	2.1± 0.05	bit bitter
3	10	5	+1	-1	2.5± 0.03	bit bitter
4	10	15	+1	+1	2.47± 0.06	bit bitter
5	7.5	10	0	0	2.53± 0.08	bit bitter
6	7.5	10	0	0	2.5± 0.05	bit bitter
7	7.5	10	0	0	2.57± 0.05	bit bitter
8	7.5	10	0	0	2.47± 0.03	bit bitter
9	7.5	10	0	0	2.5± 0.07	bit bitter
10	3.965	10	-1.414	0	2.33± 0.05	bit bitter
11	11.035	10	+1.414	0	2.37± 0.03	bit bitter
12	7.5	2.93	0	-1.414	2.67± 0.03	bit bitter
13	7.5	17.07	0	+1.414	2.47± 0.03	bit bitter

Score description: 1 to 1.99: less bitter ; 2 to 2.99: slightly bitter ; 3 to 3.99: bitter ; 4: very bitter

3.2.1. Response surface methodology analysis (RSM)

3.2.1.1. Model selection analysis

Statistical model selection analysis was conducted to determine the appropriate model for describing the significance of the research results obtained. The model selection analysis was based on: i) the description of the sum of squares (Sequential Model Sum of Squares), ii) the inaccuracy test of the model (Lack of Fit Test), and iii) the summary of the statistical model (Summary of Statistics). Several models may be selected, including linear models, 2-factor interaction models, and quadratic and cubic models.

3.2.1.2. Model selection based on the number of squares

The selection of the model based on the number of squares is based on the highest value of the polynomial degree with the condition that the model is accepted if the p-value < 0.05 (the probability of error from the model is less than 5 %), which means the model has a significant effect on the response. The table of the model selection results based on the description of the number of squares is presented in Table 2. Based on the analysis of the Sequential Model Sum of Squares (Table 2), it is found that a model can be chosen to describe the phenomenon of the effect of salt concentration and to knead time on the resulting bitter taste. Therefore, the analysis results obtained that matches the selected model (Suggested) is of quadratic model design.

The model selection based on the number of squares starts from the linear model. The linear model has a p-value of 0.0856 (8.56 %), indicating that the probability of model error is more than 5 % (the p-value in the program has been set < 5 %), which means that the model is not significant (not significant) on the response. The next model observed is 2FI (interaction between two variables). Based on Table 2, it can also be seen that the p-value for the 2FI model is 0.0057 (0.57 %), which indicates the model error is less than 5 % which means that the 2FI model is significant to the response. The following model observation is the Quadratic form with a p-value of 0.0529 (5.29 %) – indicating that the probability of error from the model is close to 5 % – which means that the Quadratic model has a significant (significant) effect on the response, making it the best design and selected as "Suggested" referring to the sum of the squares description. The Cubic model has a p-value of 0.0121 (1.21 %), which indicates that the probability of error from the model is less than 5%, which means that the Cubic model has a significant effect on the response. The program declares the Cubic model "Aliased" (not recommended) because it is suspected that the model is too complex and impossible to use.

Table 2. The results of model selection based on the description of the sum of squares

Source Diversity	Number of Squares	db	Square Mean	F Count	P value Prob>F	Information Model
Mean vs Total	80.50	1	80.50			
Linear vs Mean	0.15	2	0.073	3.18	0.085 6	
2FI vs Linear	0.14	1	0.14	13.04	0.005 7	
Quadratic vs 2FI	0.054	2	0.027	4.61	0.052 9	Suggested
Cubic vs Quadratic	0.034	2	0.017	12.13	0.012 1	Aliased
Residual	0.006 97	5	0.001 39			
Total	80.88	13	6.22			

3.2.1.3. Model selection based on model inaccuracy test

The selection of the second model is based on the model inaccuracy test (Lack of Fit Test). Kumari and Gupta (2019) state that the main criterion for the accuracy of the model is based on the lack of fit test because a model is considered appropriate if the model inaccuracy test is not statistically significant and is considered inappropriate to explain a problem from an analyzed if the model's inaccuracy is statistically significant. In contrast to the previous model selection criteria, the model selection criteria based on the model's inaccuracy is determined by a p-value > 5 %, where the model is accepted if it has a p-value > 5 %, which means the model inaccuracy is not significant to the response. The calculation of the model selection results based on the model inaccuracy test is presented in Table 3.

Table 3. Results of model selection based on inaccuracy of the test model

Source Diversity	Number of Squares	db	Square Mean	F Count	P value Prob>F	Information
Linear	0.23	6	0.038	26.30	0.0035	
2FI	0.089	5	0.018	12.42	0.0151	
Quadratic	0.035	3	0.012	8.18	0.0351	Suggested
Cubic	0.001 25	1	0.001 25	0.87	0.4027	Aliased
Pure Error	0.005 72	4	0.001 43			

The p-value in the analysis of the model's inaccuracy in Table 3 for the Quadratic model shows a result of 0.0351 (3.51 %), which means that the inaccuracy of the Quadratic model has a significant effect on the response, and so the Quadratic model is not accepted. Still, compared with other values, the Quadratic model has a p-value close to 0.05, and so the test suggests using the Quadratic model (suggested). For the Cubic model, a p-value of 0.4027 (40.27 %) was obtained, which indicates that this model is not significantly different, but the Cubic model is not recommended (aliased). In the Linear and 2FI models, each has a p-value of 0.0035 (0.52 %) and 0.0151 (0.30 %), indicating a p-value of less than 5 %, and so the two models are significantly different and the model is conclusively incorrect.

3.2.1.4. Model selection based on statistical model summary

The selection of the third model is based on the summary statistical model analysis (model summary statistics), namely the calculation analysis of the conclusions from the previous calculations. According to Montgomery (2013), determining the best model is focused on the maximum adjusted R2 and Predicted R2 values. Furthermore, the model selection also focuses on the minimum PRESS (Prediction Error Sum of Squares) value (Arham *et al*., 2013). The analysis of the model based on the complete summary of the statistical model is presented in Table 4.

Table 4. The results of the model selection based on the summary description of the statistical model

Source Diversity	Standard Deviation	R^2	Adjusted R^2	Prediction R^2	PRESS	Information
Linear	0.15	-0.325 4	0.388 4	0.266 1	0.50	
2FI	0.10	0.312 7	0.750 2	0.667 0	0.26	
Quadratic	0.076	0.317 1	0.892 2	0.815 1	0.26	Suggested
Cubic	0.037	0.764 9	0.981 6	0.955 8	0.089	Aliased

The statistical parameter used to select the suitable model is the model with the lowest standard deviation and PRESS. The low standard deviation and PRESS indicate that the level of variance and prediction of the number of squares error is low. Based on Table 4, the lowest standard deviation is owned by the Cubic model, but the model has a high PRESS value, so the Cubic model cannot be selected. In addition, the complexity of the Cubic model makes this model Aliased status. The model that has the lowest standard deviation value is the Quadratic model. The quadratic model has a standard deviation of 0.076, and the lowest PRESS is 0.26, which makes this model a Suggested status (recommended to be selected).

The quadratic model has an R2 value of 0.3171, which indicates that the salt concentration factor, soaking time in salt solution in the study, has an effect of 31.71 % on the diversity of bitter taste responses while the remaining 68.29 % is influenced by other factors not included in the model. The adjusted R2 value is 0.892 2, which means the close relationship between salt concentration and soaking time in a salt solution to the bitter taste response is 89.22 %. The difference between the R2 and Adjusted R2

is thought to be caused by the emergence of insignificant additional variables in the development of the model. Montgomery (2013) states that a decrease in Adjusted R2 will occur if the variables added to the modeling have no effect.

3.2.2. Analysis of variance (ANOVA) of RSM on bitter taste response

From the results of the three model selection processes, the Quadratic model was chosen as the model used to explain the relationship between the variables X1 (salt concentration) and X2 (squeezing time) to the Y response (bitter taste). After selecting the model, an analysis of variance was carried out on the Quadratic model. The results of the study of variance for the Y response (ethanol content) with the complete Quadratic model are presented in Table 3. The analysis of variance (ANOVA) presented in Table 5 shows that the model significantly affects the response, where the p-value is less than 0.05 (5 %). A lack of fit or significant test inaccuracy of 0.0351 indicates that the model only matches some design values. This is because the p-value is smaller than 0.05. The analysis of variance showed that the soaking time, the interaction between the salt concentration and the soaking time, and the salt concentration (squared) had a significant (significant) effect on the response. Other factors, namely salt concentration (linear) and soaking time (squared), had no significant (not significant) impact on the response.

Table 5. Results of analysis of variance (ANOVA) of the quadratic model

Source Diversity	Sum of Squares	df	Mean Square	F Value	p-value Prob > F	Information
Model	0.34	5	0.068	11.58	0.002 8	significant
A-Concentration	4.000E-004	1	4.000E-004	0.069	0.800 9	not significant
B-Time	0.15	1	0.15	25.15	0.001 5	significant
AB	0.14	1	0.14	23.49	0.001 9	significant
A^2	0.040	1	0.040	6.85	0.034 6	significant
B^2	8.160E-003	1	8.160E-003	1.40	0.275 3	not significant
Residual	0.041	7	5.829E-003			
Lack of Fit	0.035	3	0.012	8.18	0.035 1	significant
Pure Error	5.720E-003	4	1.430E-003			
Cor Total	0.38	12				

Description: A = Variable X_1/Salt Concentration (% v v^{-1}); B = Variable X_2 (soaking time h^{-1}) , AB, A_2, B_2 = interaction between treatments

3.2.3. Response graph of the effect of salt concentration and salting time on the decrease in the bitter taste of bitter melon.

The response graph is used to facilitate the description in knowing the effect of the variable on the bitter taste response. The bitter taste response is depicted in 3-dimensional curves and plot contours. A contour plot is a 2-dimensional plot, a cross-section of a 3-dimensional curve. Contour plots help analyze the effect of interaction between factors on responses Oliveira (2019). Figure 5 depicts dimensional curves and plot contours for optimizing the process of squeezing bitter melon with the addition of salt. Each figure shows the effect of the two parameters on the fruit-squeezing process. The values listed in the boxes on the contour plots indicate bitter taste in the studied squeezing process conditions. Figure 5 shows that the shape of the saddle shape curve depicts the possibilities of the variables at the maximum and minimum points. Such a contour system is called a saddle or minimax system. The interaction between salt concentration and soaking time is shown in Figure 5. The x-axis and y-axis in Figure 5(a) show the optimized variables. The x-axis shows the salt concentration variable, while the y-axis shows the soaking time variable. Circular lines indicate the response. The optimal response is characterized by the presence of a flag in the middle of the contour, which shows the optimal point information located at the point (node) displayed on the flag. The contour plot indicates the optimum salt concentration at the point (node) at 5 % (v v^{-1}) and and 15 min.

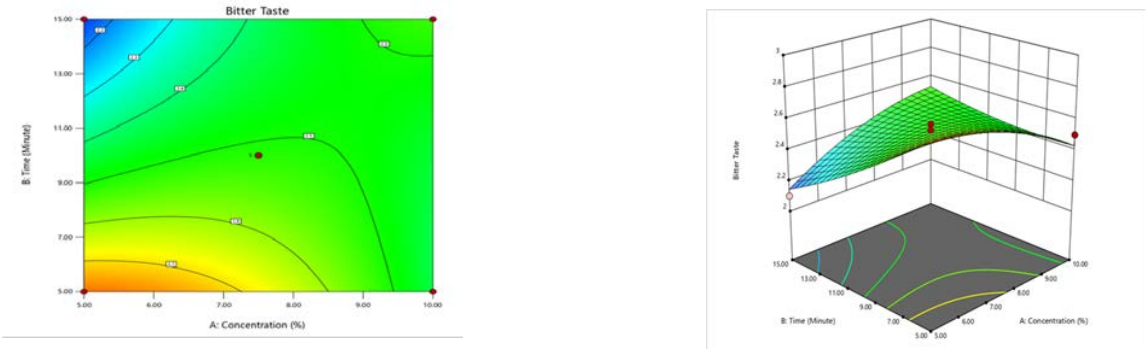

(a) (b)

Figure 5. (a) Contour plot and (b) response surface curve (three dimensions) salt concentration and duration of concentration on bitter taste respons

3.2.4. Determination of optimum conditions

Software Design Expert 7.1.5 was used to identify the best combination of bitter taste reduction process parameters to optimize bitter taste response. A desirability is a tool used to explain how well the optimal solution offered follows the objectives of the response A desirability value of 1 indicates the perfect case, but a desirability value of 0 indicates the response must be discarded. In this study, the optimal solution offered by the model is a salt concentration of 5 % (v v^{-1}), and a soaking time of 15 min for predicting the bitter taste response is the same as the optimization, which is 2.145 with a desirability value of 0.941. The optimum point of each variable is a stationary point which is assumed to be the optimum response.

4. Conclusion

The optimum treatment for removing the bitter taste of bitter melon can be done by squeezing the bitter melon, which has been sliced lengthwise and crosswise for 15 min with the addition of 5% salt concentration. This treatment is optimal for salting bitter melon with a minimum bitterness response score of 2.145. The optimization results show that the quadratic polynomial regression equation is Y= 2.468–0.1053X1- 0.0176X2 + 0.0153X12 + 0.0178X22 + 0.085X1X2, where X1=salt concentration and X2=stirring time. This salting process changes several parameters of nutritional content and bioactive compounds, such as total carbohydrate, crude protein, fat, total sugar, pectin, soluble and insoluble food fiber, vitamin C, β-carotene, diosgenin, β-sitosterol, stigmasterol, and campesterol.

Acknowledgments

Thanks go to the Dean of Engineering Faculty for funding this research and the Head of the Department of Industrial Technology at the State University of Malang that has permitted researchers to use the Food Industry Laboratory facilities.

References

Arham NA, Mohamad NAN, Jai J. Krishnan J and Yusof NM.2013.Application of response surface methodology in extraction of bioactive component from palm leaves (*Elaeisguineensis*). *Int. J. Sci. Eng*., **5(2)**:95–100. https://doi.org/10.12777/ijse.5.2.95-100

Asmawati A, Marianah M, Atoum MFM, Sari DA, Iqrar I, Hussain Z, Setyobudi RH and Nurhayati N. 2022. The potential of cashew apple waste as a slimming agent. *Jordan J Biol. Sci.*,**15(5)**: 887–892. https://doi.org/10.54319/jjbs/150518

Babu VS and Radhamany PM. 2021. Phytochemical profiling and in vitro α-amylase inhibitory activityof *Glycosmis pentaphylla* (Retz.) DC. *Jordan J. Biol. Sci*., **14(2)**:199–203. https://doi.org/10.54319/jjbs/140201.

Bahagia W, Kurniawaty E, and Mustafa S.2018. Potential of bitter melon extract (*Momordhica charantia*) as a blood glucose lowering level: Benefits behind the bittertaste.*Majority*,**7(2)**:177–181.

Damat D, Anggriani R, Setyobudi RH and Soni P. 2019. Dietary fiber and antioxidant activity of gluten-free cookies with coffee cherry flour addition. *Coffee Sci*., **14(4):**493–500. http://dx.doi.org/10.25186/cs.v14i4

Damat D, Setyobudi RH, Soni P, Tain A, Handjani H and Chasanah U. 2020. Modified arrowroot starch and glucomannan for preserving physicochemical properties of sweet bread. *Ciênciae Agrotecnologia*, **44(014820):**1–9. https://doi.org/10.1590/1413705420204401482O.

Damat D, Setyobudi RH, Burlakovs J, Vincevica-Gaile Z, Siskawardani DD, Anggriani R and Tain A. 2021. Characterization properties of extruded analog rice developed from arrowroot starch with addition of seaweed and spices. *Sarhad J. Agric*. **37 (Special Issue 1)**:159–170. https://dx.doi.org/10.17582/journal.sja/2021.37.s1.159.170

Gangakhedkar PS, Machewad GM, Deshpande HW, Katke S and Hemanth M. 2021. Studies on physico-chemical characteristics of Bitter Gourd powder. *J. Pharm. Innov*. **10(8)**: 718–721

Hifnawya MS, Issaa MY, El-Seedi H, Mahrousa AMK and Ashour RMS. 2021. Phytochemical study, nutritional evaluation and *in vitro* antiobesity potential of fruits pericarp and seeds of *Livistona carinensis* and *Thrinax parviflora*. *Jordan J. Biol. Sci***. 14(1):**163–173. https://doi.org/10.54319/jjbs/140121

Joseph B and Jini D. (2013). Antidiabetic effects of *Momordica charantia* (Bitter melon) and its medicinal potency. *Asian Pac J Trop Dis*., **3(2)**:93–102. https://doi.org/10.1016/S2222-1808(13)60052-3.

Kamari FE, Ousaaid D, Taroq A, Atki YE, Aouam I, Lyoussi B and Abdellaoui A. 2021. Bioactive ingredients of different extracts of *Vitexagnus-castus* L. fruits from Morocco and their antioxidant potential. *Jordan J. Biol. Sci.*,**14(2)**:267–270. https://doi.org/10.54319/jjbs/140210

Kumar RS, Ashih J and Satish N. 2011. *Momordica charantia* Linn.: A mini review. *Int. J. Biomed. Res*.**2(11)**:579–587.

Kumari M and Gupta SK. 2019. Response surface methodological (RSM) approach for optimizing the removal of trihalomethanes (THMs) and its precursor's by surfactant modified magnetic nanoadsorbents (sMNP) - An endeavor to diminish probable cancer risk. *Sci Rep* **9**(18339):1–11. https://doi.org/10.1038/s41598-019-54902-8

Montgomery D.C. 2013. **Design and Analysis of Experiments** 8ed. John Willey & Sons. Arizona StateUniversity, USA.

Nursal and Yeanny MS. 2019. The egg hatchability and the development of *Aedes aegypti* mosquitoes in ethanol extracts of the leaves of Bitter Melon (*Momordica charantia* L.) and Basil (*Ocimum basilicum* L.). *IOP Conf. Ser.: Earth Environ. Sci*. **305 (012048)**: 1–8. https://doi.org/10.1088/1755-1315/305/1/012048

Oliveira L, Oliveira L, Paiva AP, Balestrassi PP and Ferreira JR. 2019. Response surface methodology for advanced manufacturing technology optimization: theoretical fundamentals, practical guidelines, and survey literature review. *Int. J. Adv. Manuf. Technol.* **104**:1785–1837 https://doi.org/10.1007/s00170-019-03809-9.

Reis LCD, de Oliveira VR, Hagen ME, Jablonski A, Flores SH and de Oliveira Rios A. 2015. Effect of cooking on the concentration of bioactive compounds in broccoli (*Brassica oleracea* var. avenger) and cauliflower (*Brassica oleracea* var. alphina F1) grown in an organic system. *Food Chem.* **172**:770–777. https://doi.org/10.1016/j.foodchem.2014.09.124..

Setyobudi RH, Zalizar L, Wahono SK, Widodo W, Wahyudi A, Mel M, Prabowo B, Jani Y, Nugroho YA, Liwang T and Zaebudin A. 2019. Prospect of Fe non-heme on coffee flour made from solid coffee waste: Mini review. *IOP Conf. Ser. Earth Environ. Sci*.,**293 (012035)**:1–24. https://doi.org/10.1088/1755-1315/293/1/012035

Setyobudi RH, Yandri E, Nugroho YA, Susanti MS, Wahono SK, Widodo W, Zalizar L, Saati EA, Maftuchah M, Atoum MFM, Massadeh MI, Yono D, Mahaswa RK, Susanto H, Damat, D, Roeswitawati D, Adinurani PG, and Mindarti S. 2021. Assessment on coffee cherry flour of Mengani Arabica coffee, Bali, Indonesia as iron non-heme source. *Sarhad J. Agri.*, **37(Special Issue1):**171–183. https://doi.org/10.17582/journal.sja/2022.37.s1.171.183

Setyobudi RH, Atoum MFM, Damat D, Yandri E, Nugroho YA, Susanti MS, Wahono SK, Widodo W, Zalizar L, Wahyudi A, Saati EA, Maftuchah M, Hussain Z, Yono D, Harsono SS, Mahaswa RK, Susanto H, Adinurani PG, Ekawati I, Fauzi A and Mindarti S. 2022. Evaluation of coffee pulp waste from some coffee cultivation areas in Indonesia as iron booster.*Jordan J Biol. Sci*.,**15(3)**: 475–488. https://doi.org/10.54319/jjbs/150318

Shian ET, Aminah A, Kartinee NK and Hisham SZA. 2015.Antioxidant and hypoglycaemic effects of local bitter gourd fruit (*Momordica charantia*). *Int. J. Pharmtech Res*., **8(1):**46–52.

Shubha AS, Devaraju, Sharavati MB, Srinivasa V, Kantharaj Y, Ravi CS, Akshay A, Yalleshkumar HS and Shanwaz A.. 2018. Medicinal and nutritional importance of Bitter melon: A review article. *J Pharmacogn Phytochem*, **7(3S)**:297–300.

Snee LS, Nerurkar VR, Dooley DA. Efird JT, Shovic AC and Nerurka PV. 2011. Strategies to improve palatability and increase consumption intentions for *Momordica charantia* (Bitter melon): A vegetable commonly used for diabetes management. *Nutr J***10**, 78. https://doi.org/10.1186/1475-2891-10-78

Sur S and Ray RB. 2020. Bitter melon (*Momordica charantia*), a nutraceutical approach for cancer prevention and therapy. *Cancers*, **12 (8,2064):**1–22. https://doi.org/10.3390/cancers12082064

Thakur A, Singh S and Puri S. 2021. Nutritional evaluation, phytochemicals, antioxidant and antibacterial activity of *Stellaria monosperma* Buch.-Ham. Ex D. Don and *Silene vulgaris* (Moench) Garcke: wild edible plants of Western Himalayas. *Jordan J. Biol. Sci.*, **14(1):**83–90. https://doi.org/10.54319/jjbs/140111

Ummi R, Harijono, Teti E and Endang S. 2019. The effect of innovation in the culinary processing of Bitter melon (*Momordica charantia*) on Wistar rats' change in glucose level (*Rattus norvegicus*) *Int. J. Innov. Creativity Chang*., **8(1)**:398–414.

Weaver CM, Dwyer J, Fulgoni VL, King JC, Leveille GA, MacDonald RS, Ordovas J and Schnakenberg D. 2014. Processed foods: contributions to nutrition**.** *Am. J. Clin. Nutr*.**, 99(6)**:1525–1542. https://doi.org/10.3945/ajcn.114.089284.

Wijaya S. 2019. Indonesian food culture mapping: A starter contribution to promote Indonesian culinary tourism. *J. Ethn. Foods*, **6(9):**1–10. https://doi.org/10.1186/s42779-019-0009-3

Xu F, Zheng Y, Yang Z, Cao S, Shao X and Wang H. 2014. Domestic cooking methods affect the nutritional quality of red cabbage. *Food Chem*., **161**:162–167. https://doi.org/10.1016/j.foodchem.2014.04.025

Yusof NM, Yee Y and Zakaria Z. 2020. Application of response surface methodology on sensory properties in the development of mushroom-based patties from grey oyster mushroom (*Pleurotus pulmonarius*). *IOP Conf. Ser.: Earth Environ. Sci*.**765(012042):** 1–11.https://doi.org/10.1088/1755-1315/765/1/012042

JJBS

Volume 16, Number 1,March 2023
ISSN 1995-6673
Pages 93 – 103
https://doi.org/10.54319/jjbs/160112

Jordan Journal of Biological Sciences

Therapeutic Potential of Ginger Extract on the Embryotoxicity and Nephrotoxicity Induced by Labetalol in Rat Fetuses

Hend T. El-Borm*, Marwa S. Gobara, Gamal M. Badawy

Zoology Department, Faculty of Science, Menoufia University, Egypt.

Received: May 27, 2022; Revised: September 21, 2022; Accepted: October 6, 2022

Abstract

Labetalol is a widely used antihypertensive drug, especially during pregnancy. However, its adverse effects on fetuses are unclear. This study aimed to evaluate the therapeutic role of ginger extract on embryonic and renal toxicity induced by labetalol in 20-day-old rat fetuses. Sixty pregnant rats were divided into four groups. Group I served as the control, group II received 200 mg/kg aqueous extract of ginger orally from the 6th to the 15th day of pregnancy, group III received 300 mg/kg labetalol orally over the same period, and group IV received labetalol and aqueous extract of ginger orally. At the end of the experiment, i.e. on the 20th day, renal specimens from the rat fetuses were processed for light and electron microscopic examination and flow cytometric analysis of the cell cycle and apoptosis. Additionally, embryotoxicity and morphological parameters were assessed. The labetalol group showed a significant increase in embryo resorption and high growth retardation in the 20-day-old fetuses. Fetal kidneys displayed renal corpuscles with shrunken, narrowed urinary spaces, podocyte affection, tubular cell degeneration, hemorrhage, and hyalinization of tubules. Flow cytometric analysis demonstrated G0/G1 phase cell cycle arrest and a significant increase in apoptosis and necrosis. Administration of ginger with labetalol prevented most of these morphological, histological, and molecular changes. Prenatal exposure to labetalol caused embryonic and nephrotoxicity when administrated during the organogenesis phase. Ginger ameliorated these toxicities.

Keywords: Ginger; Labetalol; Embryotoxicity; Nephrotoxicity; Apoptosis; Cell cycle.

1. Introduction

Labetalol is a combined α- and β-adrenoceptor blocker widely used to treat high blood pressure and long-term angina. This includes essential hypertension, hypertensive emergencies, and hypertension during pregnancy (Podymow and August, 2011). It is used alone or in combination to treat high blood pressure, which increases the workload of the heart and the arteries. This can damage blood vessels in the brain, heart, and kidneys, resulting in stroke or heart or kidney failure (Campese and Krol, 2002). Common side effects of labetalol include orthostatic hypotension, dizziness, headache, and nausea (Lee, 2003; Whelan et al., 2020). Serious side effects may include severe bradycardia, hypotension, cardiac impairment, bronchospasm, respiratory distress, hypoglycemia, cardiotoxicity, and hepatotoxicity (Rosenthal and Oparil, 2002; Grassin *et al.*, 2008; Whelan *et al*., 2020; El-Borm *et al*., 2021). Moreover, various β-adrenoceptor blocking agents are associated with perinatal mortality and fetal growth retardation (Petersen *et al*., 2012; Ersbøll *et al.*, 2014).

Ginger is a common natural spice widely used as a powder or a fresh root. It is a subtropical rhizome of the plant *Zingiber officinale* (*Z. officinale)* Roscoe (Zingiberaceae family) (Johari *et al.*, 2013). It contains several compounds, such as gingerol, shogaol, zingiberence, paradol, resin, starch, volatile oil, and vitamins C and A (Dhanik *et al.*, 2017; Kim *et al*., 2022). Ginger has antioxidant, antimicrobial, antiviral, gastroprotective, antidiabetic, antihypertensive, cardioprotective (El-Borm *et al.*, 2021), anticancer, and immunomodulatory effects (Dissanayake *et al.*, 2020).

Many studies advise using ginger as an effective treatment for nausea during the first and second trimesters of pregnancy (Bryer, 2005; Abu Baker, 2013). Moreover, ginger treatment during pregnancy does not increase the risk of congenital malformations, stillbirth, perinatal death, preterm birth, or low birth weight (Weidner and Sigwart, 2000; Heitmann *et al.*, 2013). Furthermore, the therapeutic role of ginger against renal damage has been demonstrated (Tzeng *et al.*, 2013; Gholampour *et al.*, 2017; Pratap *et al.*, 2017; El-Bahr *et al.*, 2022).

In this study, we investigated whether co-administration of an aqueous extract of ginger with labetalol to pregnant rats prevented labetalol-induced embryotoxicity and nephrotoxicity in 20-day-old fetuses. We measured the mother's body weight and percentage of embryonic absorption, fetal morphology, histopathological examination of the fetal kidney using light and transmission electron microscopy, and apoptosis rates and cell cycle analysis using flow cytometry.

* Corresponding author. e-mail: Hend.elbarm@science.menofia.edu.eg;Hendtarek98@yahoo.com.

2. Materials and Methods

2.1. Preparation of ginger water extract

Fresh ginger rhizomes (*Z. officinale*) were purchased from a local market at Shebeen El-Koom, Menoufia, Egypt, and were shade-dried and crushed into a powder. 125 g ginger powder was soaked in 1000 ml distilled water for 12 h at room temperature and filtered to obtain an aqueous extract (Kamtchouing *et al.*, 2002). The extract concentration was 24 mg/ml.

2.2. Animals

The principles of animal care and use of laboratory animals guide approved by the Faculty of Science, Menoufia University, Egypt (Approval No. MUFS/F/EM/1/20) and the National Institutes of Health guide for the care and use of laboratory animals (NIH publications No. 8023, received 1978) were carefully followed while conducting this study. Sixty healthy mature virgin females and 30 fertile males of Wistar albino rats (*Rattus norvegicus*) weighing 160 ± 10 g and aged 17 ± 1 weeks were purchased from Helwan Farm, Ministry of Health, Cairo, Egypt. Before the study, the animals were housed in plastic cages under hygienic conditions with good ventilation in the animal house of the Faculty of Science, Menoufia University. They were kept under controlled ambient temperature (25°C ± 2°C) and lighting (12 h light/dark cycle) and were allowed free access to water and food. Two weeks before the experiment, females were checked daily to determine the estrous cycle stage. Only animals in the persistent anestrus (diestrus) stage were included in the experiment. Mating was induced by housing females and males overnight at a ratio of 2:1. The initiation of pregnancy was determined when the vaginal copulatory plug was present, and the vaginal smear was positive.

2.3. Experimental design

The pregnant females were divided equally into four groups (15 in each group) as follows:

- Group I (control group) received 1 ml of distilled water.
- Group II (ginger group) was administrated an aqueous extract of ginger (200 mg/kg) (Abd El-Aty and Morgan, 2011).
- Group III (labetalol group) was administrated labetalol (300 mg/kg). Labipress tablets (each containing labetalol hydrochloride 100 mg) were manufactured by DBK for pharmaceutical industries (Cairo, Egypt). The tablets were ground and dissolved in distilled water (Mahmoud *et al.*, 1993).
- Group IV (labetalol + ginger group) received labetalol (300 mg/kg) followed by ginger (200 mg/kg) 1 h later.

All groups were orally administrated distilled water, labetalol, and/or ginger via an intragastric tube from the 6th to 15th day of gestation (Badawy *et al*., 2019a). By the end of the experiment, i.e. on the 20th day of gestation, the pregnant rats were euthanized and dissected. The whole uterus was removed, weighed, and photographed with a digital camera. Embryos were excised from the uterus, and those that were alive were euthanized and subjected to gross examination to investigate morphological abnormalities under a dissection microscope. The morphological assessment was carried out by counting the number of implants, live, resorbed, and dead fetuses.

2.4. Investigated parameters

2.4.1. Morphological parameters

The crown-rump length (cm) of fetuses and body weight (g) of both the mothers and their fetuses were recorded.

2.4.2. Histopathological investigation

For examination with a light microscope, fetal kidney specimens were fixed in 10% formalin to prepare paraffin blocks. 5-µm sections were cut using a rotary microtome (IHC World, China), stained with hematoxylin and eosin (Suvarna et al., 2018), and photographed with an Olympus microscope (BX41, Japan).

2.4.3. Ultrastructural investigation

For transmission electron microscope (TEM) analysis, fetal kidney specimens were separated, immediately fixed in 2.5% glutaraldehyde, and manipulated according to the method by Kuo (2007) as described in El-Borm *et al.* (2021). Examination and photography were done using the JEOL electron microscope (TEM-1400Plus, Japan), Electron Microscope Unit, Alexandria University.

2.4.4. DNA fragmentation assay

DNA extraction was performed according to the method by El-Garawani and Hassab El-Nabi (2016) and described in detail in Sakr *et al.* (2014).

2.4.5. Cell cycle analysis

Fresh fetal kidney samples were transported in isotonic saline and prepared according to the method of Reichard and Asosingh (2018). The material was washed with isotone Tris EDTA buffer, 3.029 g of 0.1 M Tris (hydroxymethyl aminomethane, 1.022 g of 0.07 M sodium chloride, and 0.47 g of 0.005 M EDTA. These were dissolved in 250 ml distilled water. Then, the pH was adjusted to 7.5 with 1 N HCl. The samples were centrifuged at 1800 rpm for 10 min, and the cells were fixed in approximately 1 ml of ice-cold 96%–100% ethanol (BDH) for each sample.

After at least 12 h of fixation, the samples were centrifuged again, and excessive ethanol was removed. 200 µl of cell suspension in citrate buffer was placed into a 15-ml Falcon tube. Then, propidium iodide (PI) was added. The samples were filtered through a 30-Mm pore diameter nylon mesh filter to eliminate nuclear clumps into another 5-ml tube (12 × 75 mm, cat. no.2058, Falcon). The samples were run in a flow cytometer within 1 h after adding PI. The flow cytometer used in the current study was Accuri C6 (Becton Dickinson, Sunnyvale, CA, USA), equipped with a compact air-cooked low-power 15 mwat argon ion laser beam (488 nm). Data analysis was conducted using the DNA analysis program MODFIT (v.2.0).

2.4.6. Annexin-V/PI dual staining assay

The cell suspensions (1 mL) in phosphate buffer were resuspended in 2ml 1x binding buffer (1ml of 10x buffer+99ml dist. H2O) then 100 µl of cells suspensions were added to 5µl of annexin-V (Cat. No.556547 BD pharmingen FITC apoptosis Kit) then directly 5 µl PI (PE label) was added. The cells were resuspended in 200 µl 1X

binding buffer and immediately analyzed by the flow cytometer Accuri C6 (Becton Dickinson, Sunnyvale, CA, USA).

2.5. Data evaluation and statistical analysis

All data were expressed as mean ± standard error of the mean (SEM). The differences between groups were tested by analysis of variance (one-way ANOVA) using SPSS for Windows v.22 (IBM Corp., Armonk, NY USA), followed by an LSD test for multiple comparisons. $P < 0.05$ was considered statistically significant. The significance of the obtained data was classified into two categories, $P < 0.001$ and $P < 0.05$.

3. Results

3.1. Body weight of mothers

Fig. 1a displays the changes in body weight gain of the mothers. The mothers that received ginger exhibited a gradually progressive increase in body weight, similar to the control group. On the contrary, the body weight of the labetalol group gradually decreased until the 15th day of gestation. The weight slowly decreased until the 18th day, after which the body weight gradually increased slightly until the 20th day. The mothers in the labetalol + ginger group exhibited a gradual increase in body weight but lower than that of the control group.

3.2. Morphology of the uteri

The uteri of the control and ginger groups had a healthy, bright appearance and normal fetal implantation between the two horns. Four pregnant rats from the labetalol group showed some resorbed sites, while two from the same group showed resorption of all fetuses, giving the uterus a dark color. The labetalol + ginger group had an improved number of fetuses and the appearance of the uteri (Fig. 1b).

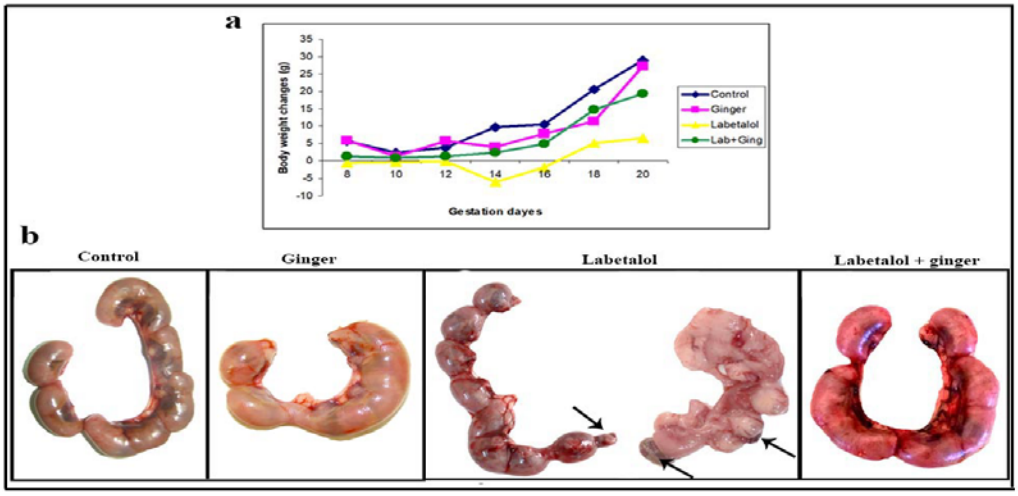

Figure 1: (a) Graph showing changes in the body weight gain of mothers in different groups. **(b)** Photographs showing different uteri of pregnant rats at the 20th day of gestation. Control and ginger groups showed normal appearance and implantation. The Labetalol group showed partial or complete resorption of fetuses (arrow). The Labetalol+ginger group showed normal implantation.

3.3. The average weight of the uteri and the percentage of resorption

As shown in Table 1, there was no significant difference in the uterine weight of pregnant rats from the ginger group (53.5 g) compared with that of the control group (51.95 g). In contrast, the average weight of the uteri from pregnant rats administrated labetalol showed a highly significant decrease (16.83 g) compared to the control group (51.95 g). Meanwhile, the average weight of the uteri of the combined group exhibited a highly significant increase (43.25 g) when compared with that of the labetalol-only group (16.83 g) and a slight decrease compared with that of the control group (51.95 g).

The control and ginger groups showed no embryonic resorption in their uteri, while the uteri with partial or complete resorption in the labetalol group recorded 40%. However, the percentage of uteri with resorption in the combined group decreased to 13.3% compared with that of the labetalol group (Table 1).

Table 1: Average weight of uteri and the percentage of resorption at the 20th day of gestation.

Groups	Total no. of sacrificed rats	Uteri		With resorption C%	Without resorption C%
		Average weight of uteri (g)	C%		
Control	15	51.95±0.025	0 (0%)	0 (0%)	15 (100%)
Ginger	15	53.5±0.013	1.55 (2.9%)	0 (0%)	15 (100%)
Labetalol	15	16.83±0.12***	-35.1 (67.6%)	6 (40%)	9 (60%)
Labetalol+ Ginger	15	43.25±0.065*a	-8.7 (-16.7%)	2 (13.3%)	13 (86.6%)

C%= percentage of change compared with control.
Asterisks (*** P< 0.001, * P< 0.05) refer to the P value compared with the control group.
a= highly significant (P<0.001) compared with labetalol group.

3.4. Body weight and crown-rump length of the fetuses

The body weight and crown-rump length of fetuses from the ginger-treated group showed insignificant changes compared with controls. Compared with controls, there was a highly significant decrease in the weight and length of fetuses from the labetalol group. However, the fetal weight and length of the combined treatment group showed a highly significant increase compared with the labetalol-only group and a slightly significant difference compared with controls (Figs. 2a–c).

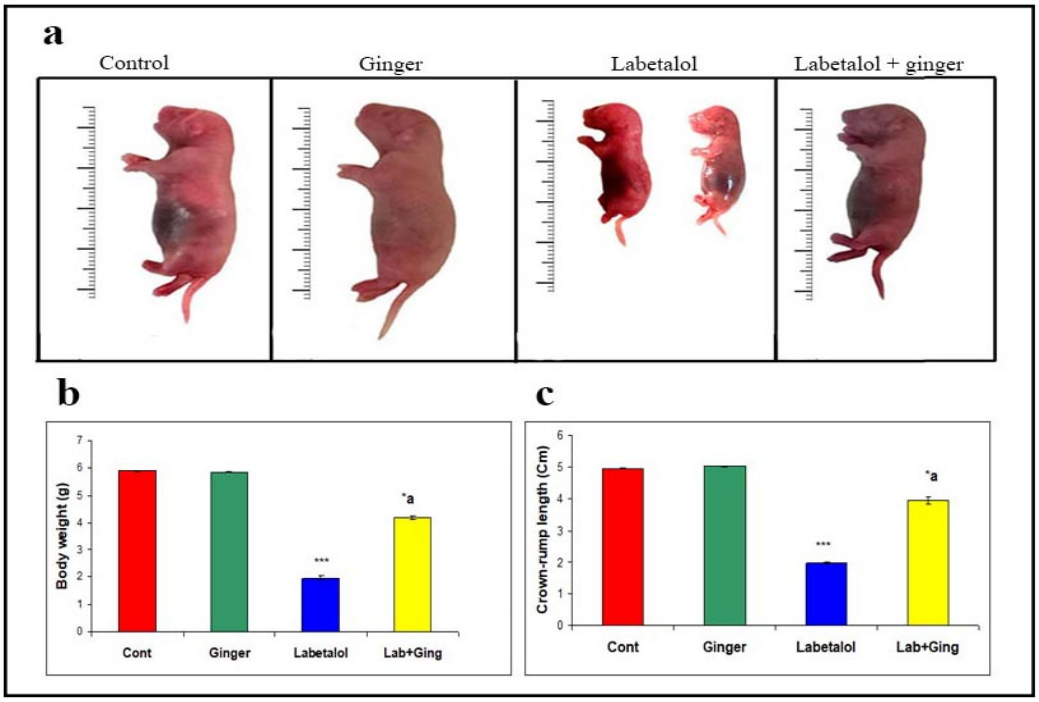

Figure 2: (a) Photographs of fetuses aged 20-day (n=40/group). **(b)** graph of the body weight of the fetuses. **(c)** graph of the crown-rump length of the fetuses in different groups. Asterisks (*** P< 0.001, * P< 0.05) refer to P values compared with the control group. a= highly significant (P<0.001) compared with the labetalol group.

3.5. Histopathological observation

The renal cortex of the control fetuses displayed two zones: the subcapsular and the juxtamedullary zones. The subcapsular zone contained immature renal corpuscles, while the juxtamedullary zone contained mature renal corpuscles and proximal and distal convoluted tubules. Medullary rays were observed as extending between the two zones (Fig. 3a). The ginger group showed a normal structure, like that of the control group (Fig. 3b).

The fetal kidney of the labetalol group exhibited degenerated renal corpuscles, which appeared shrunken with increased preglomerular space. Moreover, the proximal and distal convoluted tubules showed lumen dilation and epithelium vacuolation (Figs. 3c and 3d). Hemorrhage, hyalinization of tubules, hypertrophy of renal glomeruli, and tubular cell degeneration were also seen (Fig. 3e–g). The kidneys of the combined-treatment group showed improvement; the glomeruli and tubules regained their normal appearance, and there were no areas of obvious degeneration (Fig. 3h).

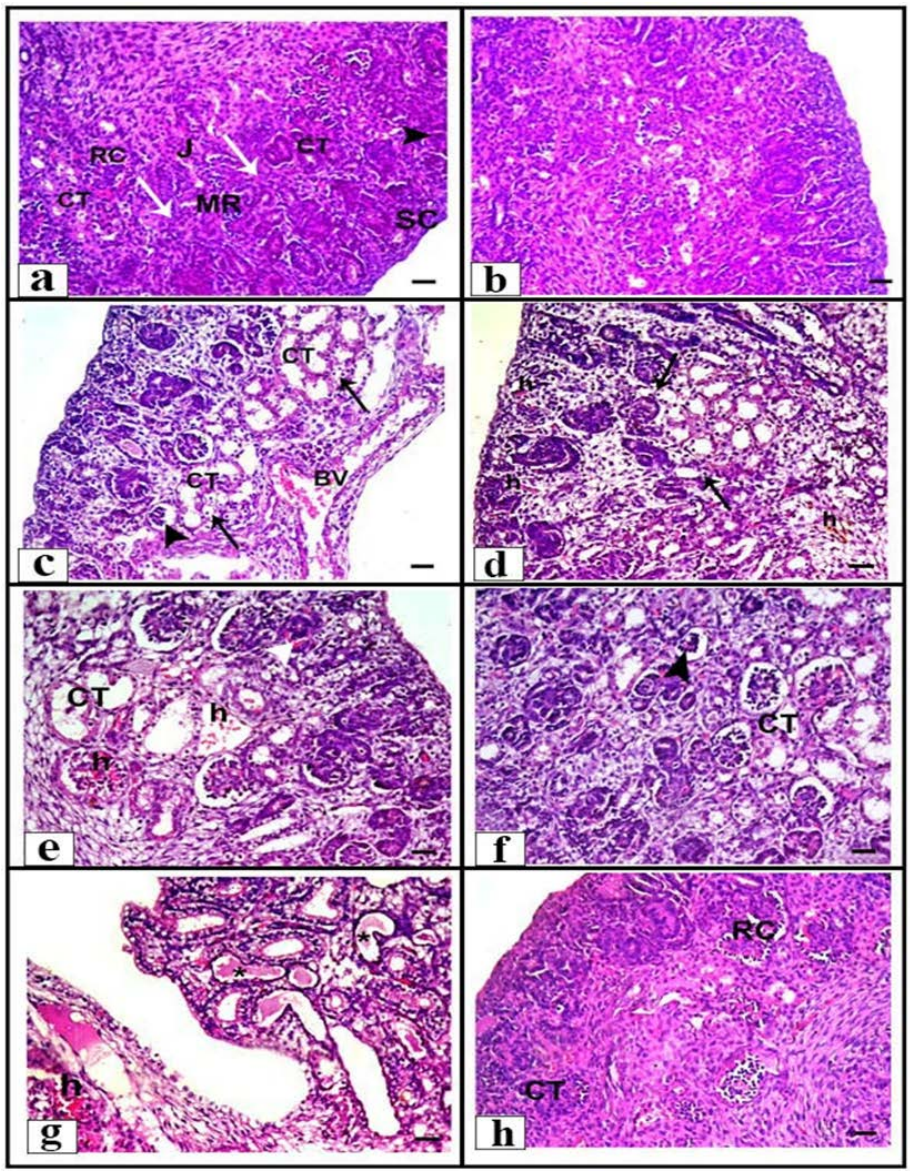

Figure 3: Photomicrographs of transverse histological sections in the 20-day-old fetal kidney. **(a)** control showing subcapsular zone (SC), immature forms of renal corpuscles (Arrowhead), the juxtamedullary (J), mature renal corpuscles (RC), convoluted tubules (CT), medullary rays (MR), nephrogenic mesenchyme (White Arrow), **(b)** ginger showing the normal structure, **(c-g)** Labetalol showing disrupted glomeruli (arrowhead), dilated and congested blood vessel (BV), degenerated convoluted tubules (CT), vacuolation in the epithelium of the convoluted tubules (Arrow), hemorrhage (h), congested renal corpuscles (White Arrowhead), shrinkages in the glomeruli (arrowhead) and tubular hyalinization (Star) **(h)** Labetalol + ginger group showing renal corpuscles (RC) and the convoluted tubules (CT). (H&E) Scale bare = 15µm.

3.6. TEM observation

The renal cortex of control fetuses showed normal glomeruli containing podocytes with many foot processes, a glomerular basement membrane, and a wide urinary space (Fig. 4a). The proximal convoluted tubule cells rested on a thin basal lamina and contained a basal euchromatic nucleus with a prominent nucleolus, an intact nuclear envelope, and a well-formed apical brush border. The cytoplasm was electron-dense with numerous rod-like mitochondria of various sizes between the basal folds (Fig. 4b). The distal convoluted tubules contained large basal euchromatic nuclei, numerous mitochondria, thin basal lamina, and few microvilli at the apical surface (Fig. 4c). The renal cortex of fetuses from the ginger group had the same structure as those of the control group (Fig. 4d–e).

The fetal renal cortex of the labetalol group showed many degenerative changes, including glomerular basement membrane thickening and urinary space narrowing. The podocyte nuclei were electron-dense with an irregular nuclear envelope (Fig. 4f). The proximal tubule cells showed electron-dense and shrunken nuclei, a degenerated brush border in some areas, and swollen mitochondria. The basal membrane enfolding was destroyed (Fig. 4g–h). Other cells appeared vacuolated with a ruptured cell membrane and basal lamina (Fig. 4i). Most nuclei were fragmented with electron-dense shapes (Fig. 4j). The cells lining the distal convoluted tubules exhibited various degrees of nuclear damage. The nuclei were irregular and ruptured in some places with chromatin clumps, while others were fragmented (Fig. 4k).

The convoluted tubule cells from the combined-treatment group showed normal cytoplasm and organelles, an intact brush border, euchromatic nuclei, mitochondria with preserved crista, and a thin basal lamina (Fig. 4l).

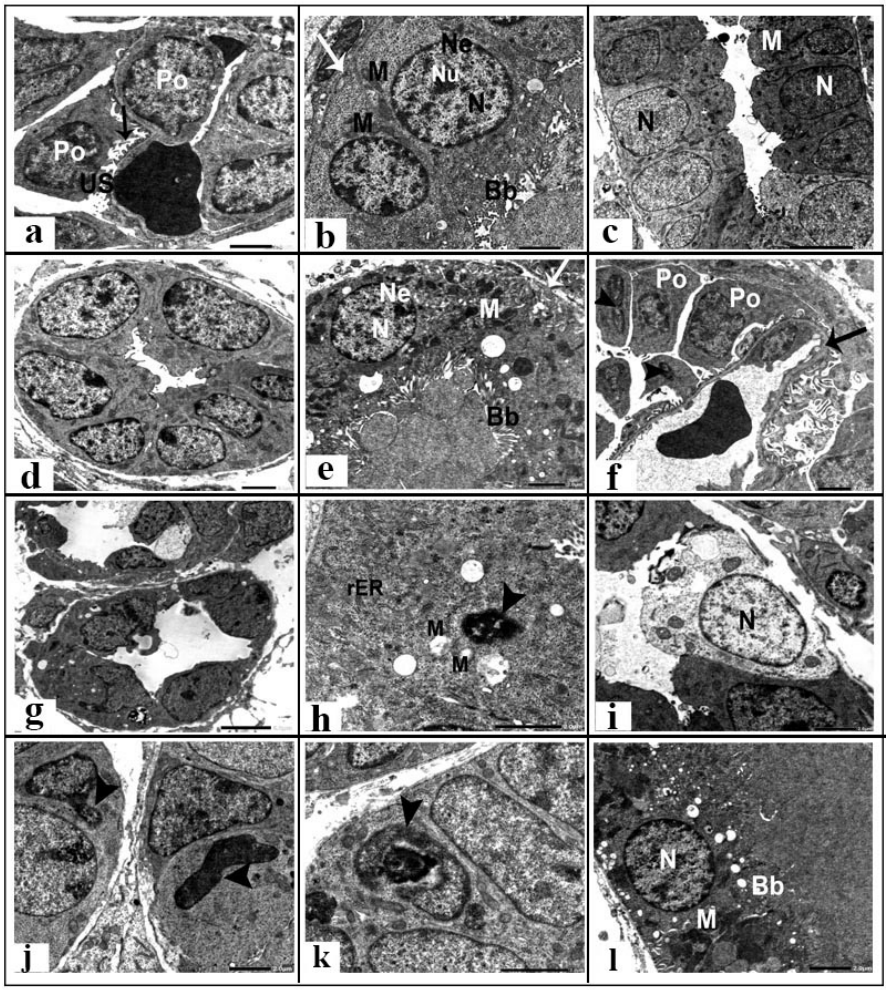

Figure 4: Transmission electron micrographs of fetal renal cells. **(a-c)** control group showing podocytes and their foot processes, thin basement membrane, proximal convoluted tubule cells and distal convoluted tubule cells. **(d-e)** ginger group. **(f-k)** labetalol group showing degenerated podocytes, degenerated proximal convoluted tubules, and degenerated distal convoluted cells. **(l)** labetalol + ginger group. podocytes (Po), basement membrane (Arrow), visible urinary space (US), apical brush border (Bb), euchromatic nucleus (N), nucleolus (Nu), nuclear envelope (Ne), mitochondria (M), rough endoplasmic reticulum (rER), degenerated and pyknotic nuclei (Arrowhead). Scale bare = 2µm for all except (**c** and **g**) =5µm.

3.7. DNA fragmentation

Administration of labetalol caused marked DNA damage in the renal cells of fetuses. In Fig. 5, lane 3 shows the migration of DNA fragments compared with the control and ginger groups (lanes 1 and 2, respectively). Meanwhile, the administration of ginger after labetalol resulted in less DNA fragmentation than in the control and ginger groups (Fig. 5).

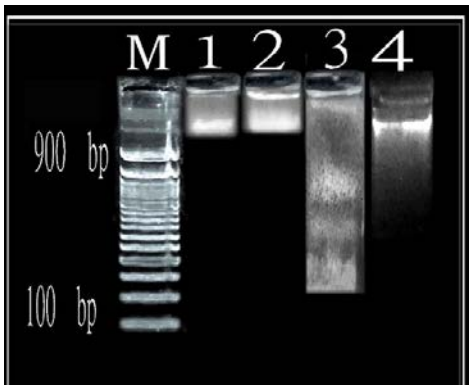

Figure 5: Photomicrograph of an agarose gel showing an evident variation of the DNA fragmentation in the renal tissue extract of 20-days-old rat fetuses treated with labetalol with/without ginger. bp: base pair, M: marker DNA (100 bp DNA Ladder, New England Bio-labs, Ipswich, MA, USA), 1: control, 2: ginger, 3: labetalol, and 4: labetalol + ginger.

3.8. Cell cycle distribution

Flow cytometric analysis of PI-stained renal cells of the labetalol group showed the accumulation of most cells in the G0/G1 phase (80.8%). In comparison, the fraction of cells in the S phase was non-significantly increased (17.6 %) compared with that of the control (14.8%) and ginger groups (17.6) (Table 2 and Fig. 6). The percentage of cells in G2/M revealed a highly significant decrease compared with that of controls (2.7% and 20.8% for the labetalol and control groups, respectively). However, co-administration of ginger with labetalol caused a highly significant reduction in G0/G1 phase cells (69.1%) and a highly significant increase in cells in the G2/M phase (15%) compared with the labetalol group (Fig. 6 and Table 2).

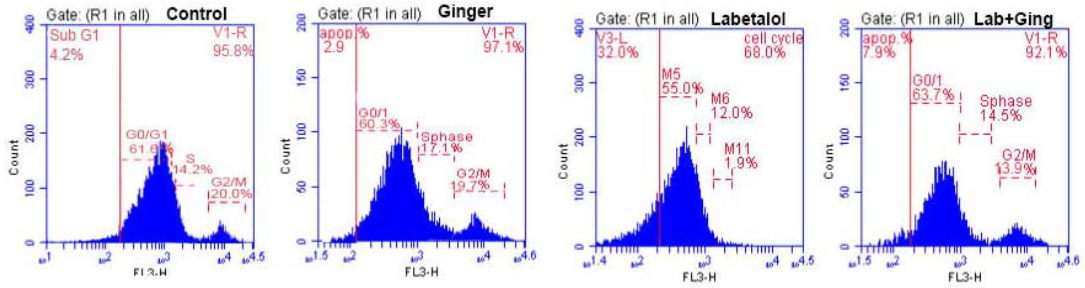

Figure 6: Representative flow cytometry graphs of cell cycle distribution of renal cells.

Table 2: Percentage of total apoptosis and cell cycle distribution in renal cells of 20-day-old fetuses.

Cells% / Groups	% Sub G1 (Apoptosis)	% No. Cells/Cell cycle	% cells analyzed G0/G1	S	G2/M
Control	4.2±0.01	95.8±0.15	64.3±0.08	14.8±0.11	20.8±0.06
Ginger	2.9±0.08	97.1±0.13	62.1±0.21	17.6±0.09	20.2±0.03
Labetalol	32.0±0.01	68.0±0.02	80.8±0.012***	17.6±0.03	2.7±0.138***
Lab+Ginger	7.9±0.05	92.1±0.17	69.1±0.12a	15.7±0.14	15.0±0.043*a

Data are represented as mean ± SEM.

Asterisks (***P< 0.001, *P<0.05) refer to the P value compared with the control group.

a= highly significant (P< 0.001) compared with labetalol group.

3.9. Dual detection of apoptosis by Annexin-V/PI

Annexin V/PI analysis of fetal renal cells from the ginger group showed that most cells were viable (95.4%). On the other hand, the labetalol group showed a 59.1% reduction in the number of viable cells and a highly significant increase in the apoptosis and necrosis rates (24.4% and 16.5%, respectively) compared with the control group, as shown in Figs. 7a and b. Administration of ginger after labetalol caused a noticeable amelioration (86%, 8.2%, and 5.8% for viable, apoptotic, and necrotic rates, respectively) compared with those of the labetalol group.

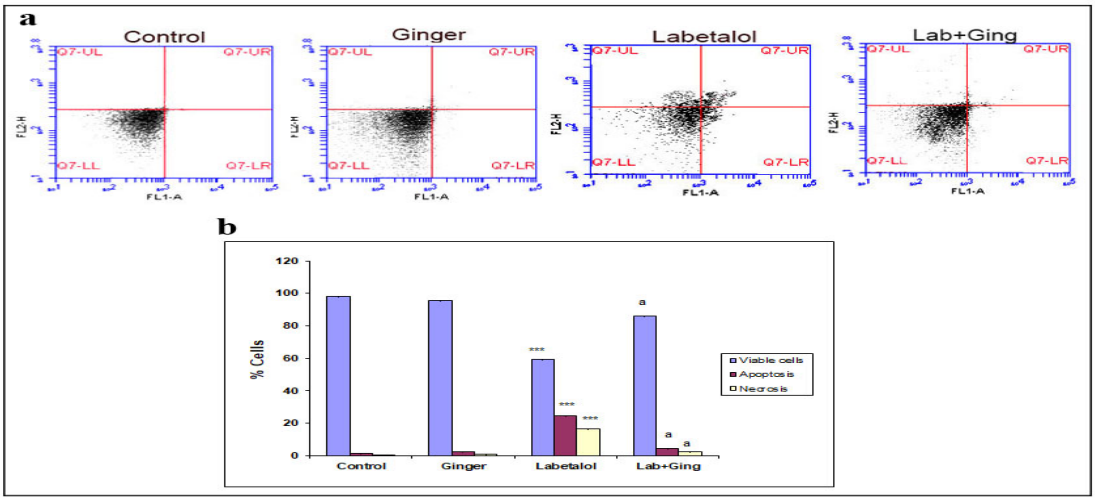

Figure 7: (a) Fluorocytograms of fetal renal cells; (FL1-A) = Annexin V +ve cells and Y-axis (Fl2-H)= PI-labeled cells. The lower left portion (Q7-LL) of the fluorocytogram (-ve for both stains) shows viable cells, whereas the lower right portion (Q7-LR) (+ve for Annexin) shows early apoptotic cells, the upper right portion (Q7-UR) (+ve for both stains) shows late apoptotic cells and the upper left portion (Q7 UL) (+ve for PI) shows necrosis. **(b)** Graph showing the percentage of viable, apoptotic, and necrotic renal populations in experimental groups. Asterisks (*** P< 0.001) refer to P values compared with the control group. a= highly significant (P<0.001) compared with the labetalol group.

4. Discussion

As observed in this study, all females treated with labetalol survived but showed significant weight loss compared with the control group. The reduction in maternal body weight may be due to reduced food intake or the developmental toxicity of the drug as displayed by reduced weight of the gravid uterus due to reduced mean fetal weight and the increased incidence of early and later resorption. Alternatively, this may be due to metabolic disorder in the mothers (Bateman *et al.,* 2012). Our study shows that treated rats displayed an asymmetrical distribution of fetuses in the two uteri horns and a reduced uterine weight. Also, the uterine horns displayed clearly visible embryonic resorption sites. An increase in resorption sites resulted in a significant reduction in uterine weight compared with the control group.

Oral administration of labetalol to female rats from the 6^{th} day until the 15^{th} day of gestation induced growth retardation, represented by a decrease in fetal body weight and length. β-blockers, especially atenolol, have been linked to fetal growth retardation when given early in pregnancy (Lydakis *et al.,* 1999). Other studies showed that β-blocker use during pregnancy increases the risk of fetuses that are small for gestational age, premature birth, perinatal mortality, and neonatal hypoglycemia (Petersen *et al.,* 2012; Ersbøll *et al.,* 2014), but some studies have reached the opposite conclusion (Heida *et al.,* 2012).

In contrast, a study by Rashidi *et al.* (2012) displayed that a carvedilol (5 mg/kg) injection at the 9^{th} to 11^{th} day of gestation in pregnant rats had protective effects on cleft palate induced by caffeine in rat fetuses. Injection of nifedipine and amlodipine at three dose levels each (5, 10, and 20 mg/kg, and 0.5, 1, and 2 mg/kg, respectively) showed no developmental toxicity in rat fetuses (Ramadan and Ashry, 2010; Jaiswal *et al.,* 2019). Also, Broulõk *et al.* (2001), reported that losartan (2 mg/kg b.wt) and enalapril (0.4 mg/kg b.wt) exerted no significant effects on body weight.

Although β-blocker exposure may increase the risk of small for gestational age, stillbirth, and growth retardation, the reasons remain unclear. Most β-blockers are thought to cross the placenta (Lennestål *et al.,* 2009), which is associated with various adverse effects, including intra-uterine growth retardation, neonatal respiratory depression, bradycardia, and hypoglycemia (Bateman *et al.,* 2012; Ishibashi *et al.,* 2017). A mechanism of β-blockers on placental hemodynamics has been proposed, suggesting that the decrease in placental blood flow is due to the selective vasoconstriction of placental vessels caused by the effect of β-blockers, which also leads to the absence of intrinsic sympathomimetic activity (Liu *et al.,* 2019). Other mechanisms might contribute to fetal bradycardia caused by β-blocker exposure, negatively affecting fetal cardiac output and development. The negative inotropic and chronotropic effects of β-blockers can reduce maternal cardiac output, affecting fetal growth (Gelson *et al.,* 2011). This effect could, at least in part, explain fetal growth retardation.

Labetalol induced many histological and ultrastructure changes in the kidney tissue of rat fetuses. Seleem (2016) observed similar effects, finding that verapamil caused atrophy and shrinkage of the renal corpuscles and degeneration of the kidney tubules. Also, Sánchez *et al.* (2008) showed that administration of losartan during pregnancy resulted in severe renal abnormalities in both newborn and one-week-old animals. Moreover, Swelim and Sakr (2004) demonstrated that injection of captopril to pregnant mice resulted in degenerative changes in the renal tissue.

In contrast, a study by Abdelhamid et al. (2019) reported that carvedilol (20 mg/kg), nebivolol (10 mg/kg), and nadolol (50 mg/kg) have a mild protective effect on the histopathological changes in the kidneys of hypertensive rats. Additionally, carvedilol and nebivolol have protective effects against nephropathy and acute renal failure in rats (Akgullu *et al.,* 2015; Atwa *et al.,* 2016). Similarly, captopril (60 mg/kg/day) had ameliorative effects on the renal cortex of chronic hypertensive rats (Rezk and Ibraheim, 2017). Furthermore, captopril had a protective effect against cisplatin nephrotoxicity (Gad *et al.,* 2016), and amlodipine acted against gentamicin-induced nephrotoxicity (Abdel-Rahman and Kandeel, 2012).

Many studies have shown that antihypertensive drugs induce apoptosis and cell cycle arrest (Koyama *et al.,* 2014; Oura *et al.,* 2017). Similarly, we showed that according to flow cytometric analyses, labetalol administration during organogenesis induced cell cycle arrest at the G0/G1 phase and a noticeable increase in apoptosis and necrosis rates in renal cells.

These findings were further corroborated by Attiq *et al.* (2018), who reported that carvedilol and celecoxib had genotoxic and cytotoxic effects on peripheral blood mononuclear cells. Losartan-treated rats at a dose of 15 mg/kg per day showed an increased percentage of cells in the G1 cell cycle phase in vascular smooth muscle cells (Bravo *et al.,* 2001). Also, Salman *et al.* (2011) reported that antihypertensive drugs such as clonidine, methyldopa, amlodipine, ramipril, and rilmenidine have a toxic effect on DNA in rat uterus tissue. This genotoxicity and cytotoxicity may be attributed to the overproduction of free radicles caused by labetalol administration, which impairs the innate antioxidant defense system of cells. This, in turn, induces a different type of DNA damage, cell cycle arrest, and apoptosis (Finkel and Holbroork, 2000).

This study confirms the ameliorative activity of ginger against the toxic developmental effects of labetalol, represented by the increase in maternal weight and fetal weight and length. This agrees with Abd-Allah and Sharaf El-Din (2013), who reported that ginger at a dose of 200 mg/kg had an ameliorative role against a methotrexate-induced reduction in body weight. Similarly, El-Aziz *et al.* (2018) concluded that injection of *Z. officinale* (250 mg/kg) before cadmium chloride resulted in a noticeable improvement in the body weight and gravid uterine weight of pregnant rats. Moreover, Faried *et al.* (2013) indicated the effectiveness of ginger extraction in regaining body weight loss in diabetic rats.

Injection of ginger tea during the organogenesis of rats resulted in no maternal toxicity or morphologic malformations (Wilkinson, 2000). Additionally, Weidner and Sigwart (2000) investigated the effect of *Z. officinale* in different doses (100, 333, and 1000 mg/kg/day) on organogenesis in rats, and no developmental or maternal toxicity was observed. Moreover, Yon *et al.* (2012) reported that [6]-gingerol has a protective effect against ethanol-induced teratogenicity during mouse

embryogenesis *in vitro*. Furthermore, Badawy *et al.* (2019b) demonstrated that the administration of ginger from the 6th to 15th day of gestation in rats reduced the incidence of malformation and growth retardation induced by gabapentin. Also, it increased the mother's body weight and uterine weight.

This study revealed that ginger significantly ameliorated the histological and ultrastructural effects induced by labetalol in fetal renal tissue. Many recent studies confirmed the therapeutic effect of ginger against nephrotoxicity (Dawood *et al.*, 2022; El-Bahr *et al.*, 2022). Ali *et al.* (2020) reported that the ethanolic extract of *Z. officinale* (200 mg orally for 8 weeks) had a protective effect on the renal damage induced by mercuric chloride in rats. Moreover, Badawy *et al.* (2019a) reported that ginger extract at a dose of 200 mg/kg had a protective effect against gabapentin-induced nephrotoxicity in rat fetuses. Similarly, a study by Mohammad *et al. (*2013) indicated that ginger extract at a dose of 2 g/kg/day daily in drinking water for 40 d acted against cadmium bromide-induced nephrotoxicity in adult female albino rats. Abdulhameed *et al*. (2017) found that the ginger plant protects against CCL4-induced kidney damage in mice. Sheriff *et al*. (2018) reported that ginger extract at a dose of 400 mg/kg protects against contrast media-induced nephrotoxicity in rats. Additionally, ginger extract ameliorates renal damage in high-fat diet-induced obesity in rats (Bin-Meferij *et al*., 2019). Moreover, Ali *et al.* (2015) reported that injection of ginger at a dose of 120 mg/kg every other day for 4 weeks in rats resulted in clear improvements in the acute renal damage induced by cisplatin.

Ginger extract can also prevent DNA damage in rats (Makpo *et al*., 2020) and genotoxicity induced by toxicants (Lee *et al.*, 2011; Yang *et al.*, 2011). Moreover, Hosseinzadeh *et al.* (2017) revealed that ginger extract reduces oxidative stress and mitochondrial apoptosis induced by IL-1β chondrocytes. Recently, ginger extract decreased DNA damage, chromosomal abnormalities, and micronucleus formation in both bone marrow cells and sperm caused by radiation in rats (Abd El-Monem and Elwakeel, 2020). The rhizome of *Z. officinale* have high flavonoid level and a high antioxidant activity (Ghasemzadeh *et al.*, 2010). This study revealed that ginger extract ameliorated labetalol-induced genotoxicity. This effect may be mediated either by its direct free radical scavenging activity or the antioxidant defense system.

5. Conclusion

Taken together, maternal administration of labetalol during 6th to 15th of gestation induced embryotoxicity and nephrotoxicity in rat fetuses as indicated by increases in embryo resorption, fetal growth retardation, renal tissue degeneration, G0/G1 phase cell cycle arrest, and a significant increase in both apoptosis and necrosis rates. However, treatment with ginger extract reduced these toxicities. Ginger can be used during pregnancy as a therapeutic agent to alleviate the nephrotoxicity and embryotoxicity induced by labetalol.

Funding

This research did not receive any funding.

Declaration of competing interest

The authors declare that they have no known competing financial interests or personal relationships that could influence the work reported in this paper.

References

Abd-Allah O and Sharaf El-Din A. 2013. The possible protective effect of ginger against intestinal damage induced by methotrexate in rats. Med J Cairo Univ, 81:1073-1084.

Abd El-Aty O and Morgan E. 2011. Ginger administration has a protective effect on the liver of albino rats treated with 6-mercaptopurine drug. J Am Sci, 7:737-745.

Abd El-Aziz AS, Mustafa HN, Saleh HA and El-Fark MO. 2018. *Zingiber officinale* alleviates maternal and fetal hepatorenal toxicity induced by prenatal cadmium. Biomed Pharmacol J, 1(3):1369-1380.

Abdelhamid A, Moustafa A, Sekinah A, Abbas N, Rashed H and Hussein S. 2019. Carvedilol and nebivolol protect the kidney against renal ischemia in Wistar rats. ZUMJ, 25(3):335-343.

Abd El-Monem D and Elwakeel S. 2020. The harmful biological effects of IR can be induced directly via the ionization of biological molecules or the formation of free radicals, such as superoxide. Int J Radiat Res, 18(1):43-55.

Abdel-Rahman M and Kandeel M. 2012. Effect of amlodipine and trimetazidine on gentamicin-induced nephrotoxicity in rats. J Am Sci, 8(6):328-335.

Abdulhameed I, Al-Mohamadamin D, Abed A and Abid W. 2017. The Effect of Ginger Plant (*Zingiber officinale*) Aqueous Extract on Function and Histological Structure of Kidney in Mice Treated with Carbon Tetrachloride. Int. J Chemtech Res, 10(12):208-219.

Abu Baker S. 2013. Effect of ginger on the histological structure of some organs of female rats and their embryos during pregnancy. Life Sci J, 10:1225-1232.

Akgullu C, Hekim T, Eryılmaz U, Boyacıog M, Gungor H, Meteoglu I, Karul A and Onbasili O. 2015. The usefulness of carvedilol and nebivolol in preventing contrast nephropathy in rats. Ren Fail Early Online, 37(3):511-517.

Ali D, Abdeen A, Ismail M and Mostafa M. 2015. Histological, ultrastructural and immunohistochemical studies on the protective effect of ginger extract against cisplatin-induced nephrotoxicity in male rats. Toxico Indust Health, 31(10): 869-880.

Ali S, Kadhem M and Ali H. 2020. Protective effect of ethanolic extract of *Zingiber Officinale* against mercuric chloride induced renal toxicity in rats. Indian J Public Health Res Dev, 11:1119-1123.

Attiq A, Ashraf M, Jalil J, Javeed A, Anjum A, Ullah A, Umair M and Ali S. 2018. Augmented cytotoxic, mutagenic and genotoxic response triggered by carvedilol and celecoxib combinations. Braz J Pharm Sci, 54.

Atwa A, Hegazy R, Shaffie N, Yassin N and Kenawy S. 2016. Protective effects of vasodilatory βeta-blockers carvedilol and nebivolol against glycerol model of rhabdomyolysis-induced acute renal failure in rats. Open Access Maced J Med Sci, 4(3):329-336.

Badawy G, Atallah M and Sakr S. 2019a. Ginger ameliorates the nephrotoxicity induced by gabapentin in rat fetuses. GSJ, 7:2320-9186.

Badawy G, Atallah M and Sakr S. 2019b. Morphological and skeletal malformations induced by gabapentin in rat fetuses and their amelioration by ginger. Asian J Adv Basic Sci, 7(1):1-12.

Bateman B, Hernandez-Diaz S, Huybrechts K, Palmsten K, Mogun H, Ecker J and Fischer M. 2012. Patterns of outpatient

antihypertensive medication use during pregnancy in a medicaid population. Hypertension, 60:913-920.

Bin-Meferij M, El-Kott A, Shati A and Eid R. 2019. Ginger extract ameliorates renal damage in high fat diet induced obesity in rats: biochemical and ultrastructural study. Int J Morphol, 37(2):438-447.

Bravo R, Somoza B, Ruiz-Gayo M, González C, Ruilope L and Fernández-Alfonso M. 2001. Differential effect of chronic antihypertensive treatment on vascular smooth muscle cell phenotype in spontaneously hypertensive rats. Hypertension, 37(5):E4-E10.

Broulõk P, Tesař V, Zima T and Jirsa M. 2001. Impact of antihypertensive therapy on the skeleton: Effects of enalapril and at1 receptor antagonist losartan in female rats. Physiol Res, 50:353-358.

Bryer E. 2005. A literature review of the effectiveness of ginger in alleviating mild-to-moderate nausea and vomiting of pregnancy. J Midwifery Women Health, 50:1-3.

Campese V and Krol E. 2002. Neurogenic factors in renal hypertension. Curr Hypertens Rep, 4:256-260.

Dawood SM, Farah M and Padiya R. 2022. Zingerone alleviates cadmium-induced nephrotoxicity in rats via its antioxidant and anti-apoptotic properties. Rev Ciênc Farm Básica Apl, 43:e759.

Dhanik J, Arya N and Nand V. 2017. A Review on *Zingiber officinale*. J Pharmacol Phytochem, 6:174-184.

Dissanayake K, Waliwita W and Liyanage R. 2020. A review on medicinal uses of *Zingiber officinale* (Ginger). Inter. J of Health Sci Res, 6(7):142-148.

El-Bahr S, Elzoghby R, Alfattah M, Kandeel M and Hamouda A. 2022. Aqueous ginger (*Zingiber officinale*) extract ameliorates the harmful effects of high-dose lornoxicam in albino male rats. BioMed Research International, 2022:1-15.

El-Borm H, Gobara M and Badawy G. 2021. Ginger extract attenuates labetalol induced apoptosis, DNA damage, histological and ultrastructural changes in the heart of rat fetuses. Saudi J Biol Sci, 28:440-447.

El-Garawani I and Hassab El-Nabi S. 2016. Increased sensitivity of apoptosis detection using staining method and integration of Acridine Orange as an alternative safer fluorescent dye in agarose gel electrophoresis and micronucleus test. CJPAS, 10:3865-3871.

Ersbøll A, Hedegaard M, Søndergaard L, Ersbøll M and Johansen M. 2014. Treatment with oral beta-blockers during pregnancy complicated by maternal heart disease increases the risk of fetal growth restriction. BJOG, 121:618-626.

Faried M, Mansour F, Zolfakar A and El-Kholy W. 2013. Experimentally induced diabetic keratopathy in albino rats and the possible protective role of ginger. J Am Sci, 9(12):206-220.

Finkel T and Holbroork N. 2000. Oxidants, oxidative stress and the biology of ageing. Nature, 408:239.

Gad A, Abd El-Raouf O, El-Sayeh B, Fawzy H and Abdallah D. 2016. Antiapototic effect of captopril in cisplatin-induced kidney injury in rats. Egypt J Hosp Med, 65:573-582.

Gelson E, Curry R, Gatzoulis M, Swan L, Lupton M, Steer P and Johnson M. 2011. Effect of maternal heart disease on fetal growth. Obstet Gynecol, 117(4):886-891.

Ghasemzadeh A, Jaafar H and Rahmat A. 2010. Antioxidant activities, total phenolics and flavonoids content in two varieties of Malaysia young ginger (*Zingiber officinale* Roscoe). Molecules, 15(6):4324-4333.

Gholampour F, Ghiasabadi F, Owji S and Vatanparast J. 2017. The protective effect of hydroalcoholic extract of Ginger (*Zingiber officinale* Rosc.) against iron-induced functional and histological damages in rat liver and kidney. Avicenna J Phytomed, 7 (6):542-553.

Grassin Delyle S, Duverneuil-Mayer C, Abe E, Mathieu B, Grandmaison G, Charlier P and Alvarez J. 2008. Fatal intoxication with labetalol (Trandate). Forensic Sci Int, 178(2-3): e19–e21.

Heida K, Zeeman G, Van Veen T and Hulzebos C. 2012. Neonatal side effects of maternal labetalol treatment in severe preeclampsia. Early Hum Dev, 88:503-507.

Heitmann K, Nordeng H and Holst L. 2013. Safety of ginger use in pregnancy: results from a large population-based cohort study. Eur J Clin Pharmacol, 69:269-277.

Hosseinzadeh A, Juybari KB, Fatemi M, Kamarul T., Bagheri A, Tekiyehmaroof N and Sharifi A. 2017. Protective effect of ginger (*Zingiber officinale* Roscoe) extract against oxidative stress and mitochondrial apoptosis induced by interleukin-1β in cultured chondrocytes. CTO, 204:241-250.

Ishibashi K, Aiba T, Kamiya C, Miyazaki A, Sakaguchi H, Wada M, *et al*. 2017. Arrhythmia risk and β-blocker therapy in pregnant women with long QT syndrome. Heart, 103:1374-1379.

Jaiswal S, Bhardwaj D and Brashier D. 2019. Teratogenicity study in rats of commonly used calcium channel blockers. Int J Basic Clin Pharmacol, 8(12): 2701-2705.

Johari H, Delirnasab F, Sharifi E, Hemayat-Khah V, Pourdanesh M, Kargar H, Nikpour M and Yazdani M. 2013. The effects of hydro-alcoholic extract of *zingiber officinale* on prevention from plumbism in kidney tissue of neonatal rats. ZJRMS, 15:13-17.

Kamtchouing P, Mboungue–Fandis G, Dimo T and Jasta H. 2002. Evaluation of androgenic activity of *zingiber officinale* and pentadiplandrabrazzanae in male rats. Asian j Androl, 4:299-301.

Kim S, Cheon C, Kim B and Kim W. 2022. The Effect of ginger and its sub-components on Pain. Plants, 11: 2296.

Koyama N, Nishida Y, Ishii T, Yoshida T, Furukawa Y and Narahara H. 2014. Telmisartan induces growth inhibition, DNA double-strand breaks and apoptosis in human endometrial cancer cells. PLoS One, 9:e93050.

Kuo J. 2007. Electron Microscopy. Methods and Protocols, 2 ed. Humana Press Inc. Totowa, New Jersey, pp. 369.

Lee WM. 2003. Drug-induced hepatotoxicity. N Engl J Med, 349 (05):474-485.

Lee C, Park G, Kim C and Jang J. 2011. [6]-Gingerol attenuates b-amyloid induced oxidative cell death via fortifying cellular antioxidant defense system. Food Chem Toxicol, 6:1261-1269.

Lennestål R, Olausson P and Källén B. 2009. Maternal use of antihypertensive drugs in early pregnancy and delivery outcome, notably the presence of congenital heart defects in the infants. Eur J Clin Pharmacol, 65:615-625.

Liu Q, Ling G, Zhang S, Zhai W and Chen Y. 2019. The effects on fetal outcome of the use of beta-blockers during pregnancy: a systematic review and meta-analysis. Int J Clin Exp Med, 12(12):13943-13950.

Lydakis C, Lip G, Beevers M and Beevers D. 1999. Atenolol and fetal growth in pregnancies complicated by hypertension. Am J Hypertens, 12:541-547.

Mahmoud T, Bjornsson S and Calder A. 1993. Labetalol therapy in pregnancy induced hypertension effects on fetoplacental circulation and fetal outcome. Eur J Obstet Gynecol Reprod Biol, 50:109-113.

Makpo S, Sani N, Hakimi N, Rani N, Zakaria S, Rasid A, Gunasekaran G, Sahardi N, Tan J, Ghafar N and Nordin M. 2020. *Zingiber officinale* Roscoe prevents DNA damage and improves muscle performance and bone integrity in old Sprague Dawley rats. Evid Based Complementary Altern Med, 2020:1-18.

Mohammad S, Mustafa I and Abdulqader S. 2013. Ameliorative effect of the aqueous extract of *Zingiber officinale* on the cadmium-induced liver and kidney injury in female rats. JJBS**, 6:**231-234**.**

Oura K, Tadokoro T, Fujihara S, Morishita A, Chiyo T, Samukawa, E, Yamana Y, Fujita K, Sakamoto T, Nomura T, Yoneyama H, Kobara H, Mori H, Iwama H, Okano K, Suzuki Y and Masaki T. 2017. Telmisartan inhibits hepatocellular carcinoma cell proliferation in vitro by inducing cell cycle arrest. Oncology Reports, 38:2825-2835.

Petersen M, Jimenez-Solem E, Andersen J, Petersen M, Brødbæk K, Køber L, Torp-Pedersen C and Poulsen H. 2012. Beta-Blocker treatment during pregnancy and adverse pregnancy outcomes: a nationwide population-based cohort study. BMJ Open, 2:1-7.

Podymow T and August P. 2011. Antihypertensive drugs in pregnancy. Sem in Nephrol, 31:70-85.

Pratap M, Jyothi M and Baburao G. 2017. Nephroprotective effect of ginger (*zingiber officinale*) extract against lead induced renal toxicity in male albino rats. Int J Recent Sci Res, 8(12):22523-22528.

Ramadan F and Ashry K. 2010. Outcome of angiotensin ii inhibition in pregnant irradiated rats and their embryos. J Rad Res Appl Sci, 3:1193 -1209.

Rashidi F, Mahabady M, Ranjbar R and Varzi N. 2012. The effects of caffeine and carvedilol on skeletal system of rat embryos in prenatal period. AJPP, 6(29): 2229-2234.

Reichard A and Asosingh K. 2018. Best Practices for Preparing a Single Cell Suspension from Solid Tissues for Flow Cytometry. Cytometry A, 95 (2): 219-226.

Rezk H and Ibraheim A. 2017. Histopathological effects of therapeutic doses of combined XO-Inhibitors and ace-inhibitors on the expression of VEGF-A in the myocardium and renal cortex in chronic hypertensive albino. Wulfenia J, 24:35-79.

Rosenthal R and Oparil S. 2002. The effect of antihypertensive drugs on the fetus. Journal of Human Hypertension, 16, 293-298.

Sakr S, Badawy G and El-Borm H. 2014. Ultrastructural and molecular changes in the developing small intestine of the toad *Bufo regularis.* Sci World J, 2014:1-13.

Salman S, Kumbasar S, Gursan N, Kumtepe Y, Borekci B, Polat B, Hakan H, Sener M and Suleyman H. 2011. Investigation of the Relationship of Some Antihypertensive Drugs with Oxidant/Antioxidant Parameters and DNA Damage on Rat Uterus Tissue. Inter J Fertil Steril, 5(2):96-103.

Sánchez S, Seltzer A, Fuentes L, Forneris M and Ciuffo G. 2008. Inhibition of Angiotensin II receptors during pregnancy induces malformations in developing rat kidney. Eur J Pharmacol, 588(1):114-123.

Seleem A. 2016. The protective effect of bee venom against verapamil embryotoxicity during prenatal liver and kidney development of mice Mus musculus. J Basic Appl Zoo, 75:13-27.

Sheriff M, Abas A and Zaitoun L. 2018. Protective effect of ginger extract against contrast media-induced nephrotoxicity in rats. Biochemistry letters, 13(17):202-222.

Suvarna K, Layton C and Bancroft J. 2018. Bancroft's Theory and Practice of Histological Techniques.8th ed., Elsevier.

Swelim H and Sakr A. 2004. Ultrastructural study of renal tubular damage induced by captopril in adult and fetal mice. Egypt J Hosp Med, 17:20-43.

Tzeng T, Liou S, Chang C and Liu I. 2013. The Ethanol Extract of *Zingiber zerumbet* Attenuates Streptozotocin-Induced Diabetic Nephropathy in Rats. Evid Based Complement Alternat Med, 2013:1-8.

Weidner M and Sigwart K. 2000. Investigation of the teratogenic potential of a *Zingiber officinale* extract in the rat. Reprod Toxic, 15:75-80.

Whelan A, Izewski J, Berkelhammer C, Walloch J and Kay H. 2020. Labetalol-Induced Hepatotoxicity during Pregnancy: A Case Report. Am J Perinatol Rep, 10:e210-e212.

Wilkinson J. 2000. Effect of ginger tea on the fetal development of Sprague-Dawley rats. Reproductive toxicology (Elmsford, N.Y.), 14:507-512.

Yang G. Zhong L, Jiang L, Geng C, Cao J, Sun X, Liu X, Chen M and Ma Y. 2011. 6-gingerol prevents patulin-induced genotoxicity in HepG2 cells. Phytother Res, 10:1480-1485.

Yon J, Baek I, Lee S, Kim M, Hong J, Yong H and Lee B. 2012. Protective effect of [6]-gingerol on the ethanol-induced teratogenesis of cultured mouse embryos. Arch Pharm Res, 35:171-178.

JJBS

Volume 16, Number 1,March 2023
ISSN 1995-6673
Pages 105 – 115
https://doi.org/10.54319/jjbs/160113

Jordan Journal of Biological Sciences

Anti-nephrolithiatic Evaluation of Partitioned Ethanol Extract of *Calotropis procera* Leaf in Wistar Rats

Nafiu, Mikhail Olugbemiro*,Ogunsola, Ibukun James

Department of Biochemistry, University of Ilorin, P.M.B. 1515, Ilorin, Nigeria.

Received: August 3, 2022; Revised: October 8, 2022; Accepted: October 16, 2022

Abstract

Nephrolithiasis is a common urinary disease that elicits excruciating pains and could be managed through alternative therapy. This investigation was planned to evaluate the action of partitioned fractions of ethanol *Calotropis procera* leaf extract in nephrolithiasis treatment. *In vitro* anti-nephrolithiatic and antioxidant tests were assayed using varying concentrations of the ethanol extract and its n-hexane and ethyl acetate fractions to determine which had the optimum activity. Thirty albino rats (101 ± 3 g) were randomly divided among six groups. (n=5). Group A (control) received drinking water and pellets daily. Groups B-F were made lithiatic by daily administration of 2% Ammonium Chloride and 0.75% ethylene glycol in drinking water and fed pellets. Groups C, D, E and F received 750 mg//kg body weight (b.w.) Cystone (reference drug), 25, 50 and 100 mg/kg b.w. n-hexane fraction of *Calotropis procera* ethanol leaf extract (HFCPL) respectively for 10 days. Urine samples were pooled on day eleven for electrolytes and uric acid estimation. Serum and tissue homogenates were assayed for antioxidant, liver and kidney function assessments. Organ tissues from the liver and kidney were fixed for histological analysis. The extract indicated saponin, flavonoid, alkaloid, tannins, terpenoids and phenolics as secondary metabolites. The HFCPL gave the highest 2,2-diphenyl-1-picrylhydrazyl (DPPH) scavenging activity, a higher nucleation and aggregation activity and reduced uroliths *in vitro* better than the ethanol extract and the ethyl acetate fraction. HFCPL treated animals displayed decreased stone formation in the urine, a significantly ($p < 0.05$) increased urinary calcium and elevated magnesium levels. Significant decrease was recorded in lipid peroxidation activity with corresponding increase ($p < 0.05$) in superoxide dismutase, catalase and reduced glutathione levels. These findings indicated an effectiveness of HFCPL in the management of nephrolithiasis, and hence it may be a good alternative treatment regimen.

Keywords: Nephrolithiasis, *Calotropis procera*, calcium oxalate, nucleation, aggregation

1. Introduction

Nephrolithiasis is the third most common urinary disorder (Divakar *et al.*, 2010) and a complex process that occurs because of an imbalance between promoters and inhibitors in the kidneys (Jehti *et al.*, 1983). It is a succession of several physicochemical events including supersaturation, nucleation, growth, aggregation and retention within the kidneys (Yadav and Jain, 2011) occurring in both men and women but with higher risk in men (Selvem, 2002). The prevalence of nephrolithiasis has been increasing over time. In a survey demonstrated in adults aged 20-74 years, the outcome reflected 3.2% in 1976-1980 to 5.2% in 1988-1994 while overall prevalence increased to 8.8% by 2007-2010. A study estimates the prevalence of renal stones in the US as 7.1% in women and 10.6% in men (Ziemba and Matlaga, 2017). According to estimates, the patient's chance of developing secondary stones again is between 10 and 23 percent per year, 50 percent after five to ten years, and 75 percent within twenty years (Moe, 2006). One in eleven Americans in the country experience kidney stones, and it is believed that 600,000 Americans experience KSD each year (Scales *et al*., 2012). Urinary stones are predicted to affect about 13% of Indians, and half of them could eventually lose their ability to function (Joseph *et al.*, 2005). Calcium stones comprise about 80% of all urinary calculi (Coe and Worchester, 2005) and the principal component of calcium stone is brushite or hydroxyapatite. Factors that contribute to calcium stone formation include hypercystinuria, hyperoxaluria, hyperuricoxuria, hypomagnesuria and urinary pH of 5.0 - 6.5. Struvite or magnesium phosphate stones occur in around 10-15% of cases of chronic urinary tract infections (El Zoghby *et al*., 2012). These infections cause the production of urease (Barbasa *et al.*, 2002), which is required to break down urea into ammonia and CO_2 and raise the pH of the urine. A high-purine diet, particularly one heavy in animal protein like meat and fish, can result in hyperuricosuria, reduced urine volume, and low pH (Kumar *et al.*, 2012).

Similar to other disorders, the treatment of renal calculi has steadily advanced clinically, with techniques including classic open surgery, percutaneous nephrolithotomy, retrograde intra-renal surgery, and extracorporeal shockwave

* Corresponding author. e-mail: olumikail@unilorin.edu.ng.

lithotripsy (Chung *et al.*, 2019). Nephrolithotomy is performed if large stones (up to 8 mm in width) lodge inside or adjacent to the kidneys using a telescopic tool (Aggarwal *et al.*, 2017). A sufficient amount of fluid intake lowers urine saturation and dilutes calcium oxalate crystallization promoters (Xu et al., 2013). A high sodium diet raises the risk of forming stones by lowering the reabsorption of calcium by the renal tubules and increasing the calcium excreted in the urine (Park and Pearle, 2007).

Current medical management methods have been shown to possess disadvantages that include being highly expensive and with side effects such as hemorrhage, hypertension, tubular necrosis, subsequent fibrosis of the kidney and an increase in stone reoccurrence. Standard pharmaceuticals used to treat and prevent urolithiasis are not always effective and have a number of negative side effects (Sathyaa *et al.*, 2011). Phytotherapy, however, is currently the subject of scientific research because it has been shown to be essential for preventing the recurrence of stones (Gilhorta and Christina, 2011) and act by either allowing spontaneous passage of small calculi in urine or by producing antioxidant, anti-microbial, analgesic and anti-inflammatory activities (Soundarajan *et al*., 2006).

Calotropis procera is an anthelmintic, abortifacient, and whooping cough, colic, headaches, lice removal, diarrhea, painful gums, toothaches, sterility, swellings, and ulcers are among the conditions for which it is used in folk medicine. Its stem is used in treating skin diseases, intestinal worms and leprosy (Esmail and Al Snafi, 2015). The plant is known for its antifungal (Lahsini *et al.*, 1997) and analgesic activity (Hassan *et al.* 2006). Its latex is scientifically reported for the management of diabetes (Mohsin *et al.*, 1989), anti-diarrheal activity (Kumar *et al.*, 2005), while the antioxidant and polyphenolic contents were shown to be effective in cancer studies (Kumar *et al.*, 2001; Prabha and Vasntha, 2011).The milky sap (latex) is well known for its traditional medical uses (Iqbal *et al*., 2005), as food, especially in West Africa as a coagulation ingredient for cheese manufacturing (O'Connor 1993) and a source of energy (Parsons and Cuthbertson, 2001). Given its antioxidant property and secondary metabolites-enriched nature, this investigation was intended to determine the anti-nephrolithiatic activity of *Calotropis procera* ethanol leaf extract and to investigate its toxicity on the kidney, liver and serum indices in Wistar rats.

2. Materials and Methods

2.1. Experimental Animals

Thirty Wistar rats (*Rattus novergicus*) were obtained from the Faculty of Veterinary Medicine, University of Ilorin, Ilorin, Nigeria. The animals were housed in standard cages and acclimatized for twelve days at the Department of Biochemistry, University of Ilorin, Ilorin, Nigeria. They were maintained under standard conditions and fed rat pellets (Grand Cereals, A subsidiary of UAC, Nigeria) and water *ad libitum*.

2.2. Drugs and Chemicals

Alkaline phosphatase, aspartate transaminase, alanine transaminase, creatinine, urea, uric acid and bilirubin reagent kits were products of Randox Laboratory Ltd., U.K. Cystone (Himalaya Drug Company, India), ammonium chloride (Loba Chemie Pvt. Ltd.) and ethylene glycol (CDH Ltd, New Delhi) were also procured. Other reagents used were of analytical grade prepared using distilled water.

2.3. Plant Material

Calotropis procera leaves were obtained at Gaa Akanbi, Ilorin, Kwara State, Nigeria in November 2017. It was identified at the Department of Plant Biology, University of Ilorin, Ilorin, Nigeria, where a voucher specimen was deposited and a number (UILH/001/2019/1001) was assigned. The leaves were oven-dried at 50 °C for four days.

2.3.1. Preparation of Extract

The oven-dried leaves were pulverized using an electric blender. Exactly 200 g of the pulverized sample was infused in 800 ml ethanol for 24 hours in a conical flask. This was thereafter filtered with Whatman filter paper and the filtrate collected into a clean beaker. The process was repeated using ethanol for two more days to exhaustively obtain the extract. The total filtrate obtained was evaporated at 55 °C using a water bath (HH 420KW-1000DB) to obtain the crude extract. The crude ethanol extract was reconstituted in 50 ml distilled water, loaded in a separating funnel where 100 ml n-hexane was added. The n-hexane fraction was collected into a clean beaker and the solvent was allowed to evaporate. Ethyl acetate fraction was also collected after addition of 100 ml ethyl acetate to. The n-hexane and ethyl acetate fractions were stored in plain bottles and refrigerated. The percentage yield was then calculated. Secondary metabolites screening of the ethanol extract was carried out using standard procedures.

2.4. In vitro Anti-nephrolithiatic Activity

Nucleation and aggregation assays were performed according to the method described by Hess *et al.* (2000). A freshly prepared solution of 10 mM calcium chloride di-hydrate and 1.0 mM sodium oxalate, containing 200 mM NaCl and 10 mM sodium acetate trihydrate was adjusted to pH 5.7. All experiments were performed at 37 °C using a water bath (HH-420 KW-1000DB).

25 ml of sodium oxalate solution was transferred into beakers placed in the water bath and stirred continuously using a stirrer. 1 ml of distilled water, cystone and varying concentrations (62.5, 125, 250, 500 and 1000 µg/ml) of the ethanol extract and its fractions respectively were added and finally, 25 ml calcium chloride was added. The optical density was measured using spectrophotometer (UV 721, Axiom Medicals U.K.) at 620 nm at every 15 sec over 5 min and then every 1 min over 10 min. The percentage inhibition was calculated as:

$$(1- (Tsi/Tsc)) \times 100$$

Where Tsc is the optical density of control and Tsi, the optical density in presence of inhibitor.

The final solutions were viewed under a light microscope (B-Bran Olympus) to analyze the density of formed crystals in the solution.

2.5. DPPH Scavenging Activity

This assay was carried out using the method described by Molyneux (2004). Briefly, 1 ml varying concentrations (2, 4, 6, 8 and 10 mg/ml in methanol) of the extract and its n-hexane and ethyl acetate fractions and ascorbic acid were added to 4 ml 0.1 mM methanol solution of DPPH. A blank probe was obtained by mixing 4 ml 0.1 mM methanol DPPH solution and 200 µl of distilled water. After 30 min of incubation in the dark, the absorbance of samples and blank were taken at 517 nm (Visible Spectrophotometer 721, Axiom Medical, U. K.). Inhibition of free radicals by DPPH in percentage was calculated using the expression:

$$\% \text{ Inhibitioin} = 100 - ((ABS_{sample} - ABS_{blank})/ABS_{control}) \times 100$$

2.6. Acute Toxicity Testing (LD_{50})

The OECD (2002) guidelines for the Testing of Chemicals No. 420 were followed for conducting an acute toxicity investigation. After three rats were made to fast for 24 hours, the HFCPL was administered to them in steps at fixed doses of 5, 50, 300, and 2000 mg/kg body weight respectively, via gavage with a cannula in a single dosage. The rats were observed for physical changes on their bodies, hair loss, ease of movement, breathing pattern, etc.

2.7. In vivo Studies

Thirty Wistar rats were randomly divided into six groups (A-F) of five and subjected to different treatments. Animals in groups B-F were administered 2.0% ammonium chloride and 0.75% ethylene glycol in drinking water *ad libitum* for 10 days. Animals in group A (control) took only drinking water, those in group B were untreated (negative control group). Group C was administered 750 mg/kg cystone (reference drug), while groups D-F were administered 25, 50 and 100 mg/kg body weight HFCPL respectively. 0.5 ml of 750 mg/kg cystone and HFCPL doses and were administered to the respective groups using a cannula for 10 days.

Diethyl ether was used to anesthetize the rats, blood was collected using jugular puncture into plain bottles and centrifuged to get the serum. Serum was drawn out with a Pasteur pipette, which was then placed in plain sample vials and refrigerated. Portions of the kidney and liver were homogenized in 0.25M sucrose solution and refrigerated, while the rest were preserved in 10% formalin for histological studies.

2.7.1. Urinary Microscopy

As a way to validate the onset and resolution of kidney stone disorder following the injection of ethylene glycol, ammonium chloride, and the HFCPL treatment, respectively, urinary microscopy was performed. Animal urine was collected on slides and analyzed under a microscope (B-Bran Olympus) at a magnification of 400.

2.7.2. Biochemical Indices

The serum was used to estimate the ALP, AST and ALT activities. The concentrations of the serum functional parameters (albumin, creatinine, urea, bilirubin and globulin) were then determined using methods described in the respective kits. Histological studies (H & E staining's) were done on the liver, kidney and pancreas of the rats and viewed under the light microscope.

2.8. Gas Chromatography-Mass Spectrometer (GC-MS) Analysis

GC-MS (model QP2010SE, Shimadzu, Japan) was employed to conduct a GC-MS analysis of the HFCPL in accordance with the instructions from the manufacturer. For the analysis, 10 ml of n-hexane were used to dissolve 1g of the extract. The injector and column oven temperatures were set at 60 ℃ and 250 ℃, respectively. The split ratio was set at 10:1 and the pressure was kept at 144.4 kPa while the flow control mode was maintained at a linear velocity of 46.3 cm/sec. The interface temperature was 250 ℃, while 230 ℃ was the temperature of the ion source. The mass to charge ratio (m/z) was 35 at the beginning and 700 at the conclusion (35-700 m/z). The retention time, % height and peaks were obtained and integrated after the analysis.

2.9. Statistical Analysis

The information was presented as the mean of five determinations ± SEM. One-way ANOVA and the Tukey Post-Hoc Test were used in the statistical study. At $p < 0.05$, all data were taken as statistically significant.

3. Results

3.1. Percentage yield

A yield of 8.42 g of ethanol extract was obtained from the leaf. On partitioning, the n-hexane fraction gave a percentage yield of 1.025 % while the ethyl acetate fraction yielded 0.885 %.

3.2. 3.2 Quantitative Secondary Metabolite Constituents

The analysis of secondary metabolite constituents of the ethanol extract of *C. procera* leaf revealed the presence of saponins, flavonoids, alkaloids, tannins, glycoside and phenolics (Table 1).

Table 1: Concentration of detected Secondary Metabolite Constituents of ethanol extract C. *procera* leaf

Secondary Metabolite	Concentration (mg/100 g)
Saponins	38.62 ± 0.02
Flavonoids	361.07 ± 17.69
Alkaloids	48.24 ± 0.11
Tannins	19.75 ± 0.37
Terpenoids	57.26 ± 0.09
Phenolics	34.46 ± 0.86

3.3. DPPH Scavenging Activity

There was a progressive increase as concentrations increase in the inhibition of DPPH with the highest values recorded in the n-hexane fraction (IC_{50} 10.2 ± 0.8) which compared favorably with the ascorbic acid standard (IC_{50} 8.01 ± 0.2) (Table 2).

Table2: *In vitro* DPPH Scavenging Activity of C. *procera* leaf ethanol extract and its n-hexane and ethyl acetate fractions.

Concentration (mg/ml)	% Inhibition Ethanol	% Inhibition Ethyl acetate	% Inhibition n-Hexane	% Inhibition Ascorbic acid
2	47.47 ± 0.07	65.88 ± 0.22	66.88 ± 0.28	66.91 ± 0.02
4	62.92 ± 0.26	72.50 ± 0.13	79.25 ± 0.20	79.39 ± 0.00
6	69.81 ± 0.19	76.37 ± 0.09	80.54 ± 0.25	80.42 ± 0.05
8	76.46 ± 0.11	80.36 ± 0.18	84.19 ± 0.17	85.12 ± 0.00
10	82.68 ± 0.10	82.00 ± 0.30	86.18 ± 0.32	91.75 ± 0.01

3.4. In vitro Anti-nephrolithiatic Activity

The results of nucleation (Fig. 1) gave an indication that the n-hexane fraction displayed better inhibitory potentials compared to the ethanol extract of *C. procera* and the ethyl acetate fraction at varying concentrations. Upon aggregation (Fig. 2), the findings demonstrated that, at various doses, the n-hexane fraction of the *C. procera* extract had the strongest inhibitory potentials in comparison to the ethanol and ethyl acetate extracts. The microscopy of the solution gave a progressive decrease in the number of stones *in vitro* (Fig. 3).

With results from the *in vitro* studies, the n-hexane fraction had the best activity across the parameters investigated and hence; it was further used to carry out *in vivo* studies.

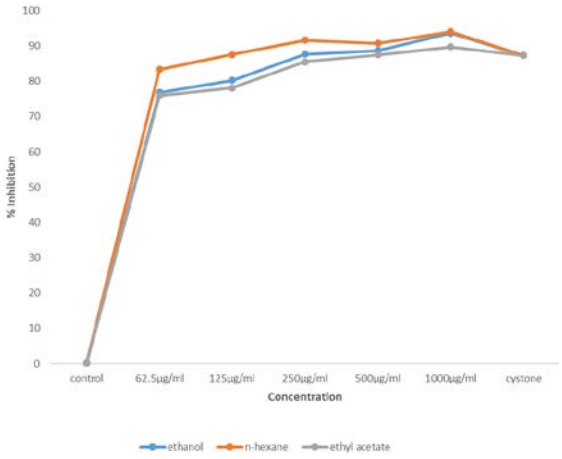

Figure 1: *In vitro* nucleation assay of *C. procera* leaf ethanol extract and its n-hexane and ethyl acetate partitioned fractions.

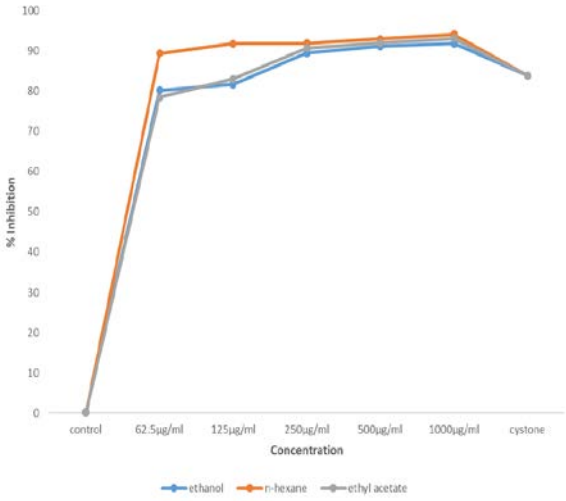

Figure 2: *In vitro* aggregation assay of *C. procera* leaf ethanol extract and its n-hexane and ethyl acetate partitioned fractions.

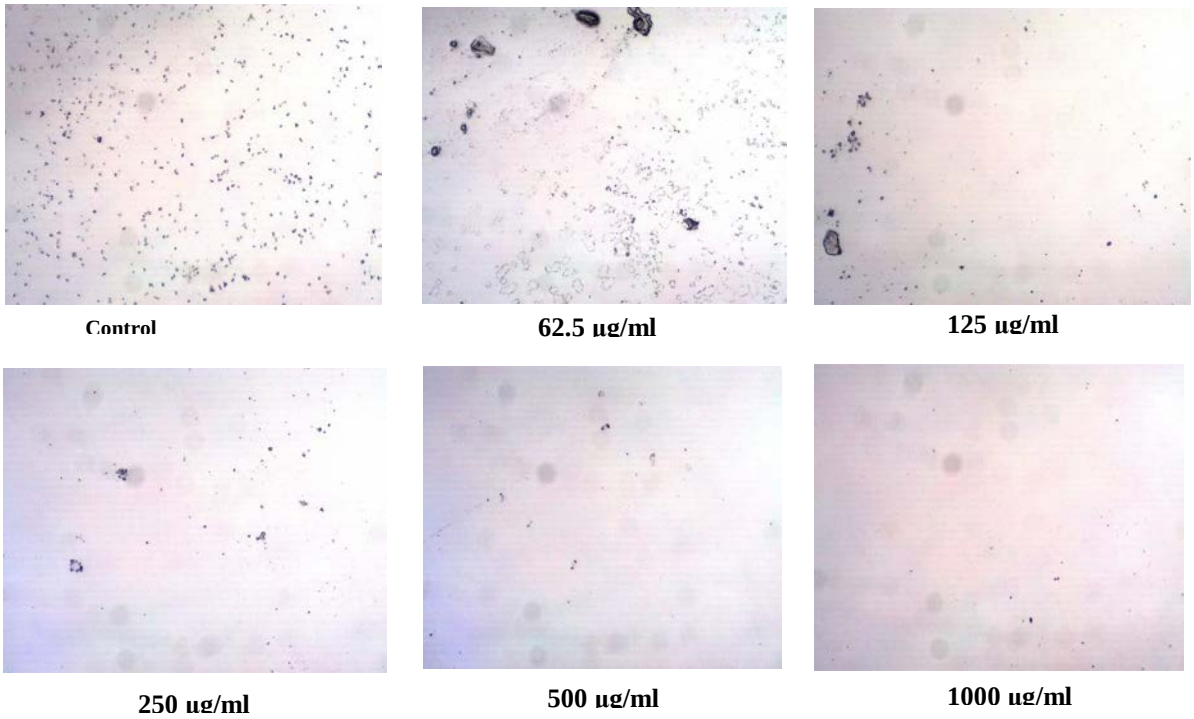

Figure 3: Photomicrograph of inhibition of urolith by various doses of HFCPL ethanol extract *in vitro*.

3.5. Electrolyte Parameters

The magnesium level was higher in the urine samples in comparison to the serum (Table 3). However, at a dose of 25 mg/kg there was a substantial drop ($p < 0.05$) in the blood magnesium level compared to the control, as well as a significant lower level ($p < 0.05$) in the urine magnesium. At doses of 25 and 50 mg/kg, there was a notable decline ($p < 0.05$) in urinary calcium levels compared to the control; however, there was no discernible alteration in serum calcium levels.

Table 3: Effect of hexane fraction of *Calotropis procera* leaf (HFCPL) ethanol extract on some electrolyte parameters of nephrolithiatic rats.

Group	Serum Calcium (mmol/l)	Serum Magnesium (mg/dl)	Urine Calcium (mmol/l)	Urine Magnesium (mg/dl)
Control + dw	2.03 ± 0.10 [a]	1.79 ± 0.29 [a]	2.26 ± 0.25 [a]	2.70 ± 0.04 [a]
Lithiatic + dw	2.50 ± 0.48 [a]	1.26 ± 0.01 [b]	1.01 ± 0.13 [b]	2.52 ± 0.02 [b]
Lithiatic + 750 mg/kg bw cystone	1.80 ± 0.09[b]	1.51 ± 0.24 [a]	2.65 ± 0.30 [a]	2.83 ± 0.01[c]
Lithiatic + 25 mg/kg bw HFCPL	2.24 ± 0.34 [a]	1.32 ± 0.20[b]	1.69 ± 0.17[c]	2.58 ± 0.07 [b]
Lithiatic + 50 mg/kg bw HFCPL	1.97 ± 0.06[a]	1.61 ± 0.18[a]	1.81 ± 0.08 [c]	2.60 ± 0.11 [a]
Lithiatic + 100 mg/kg bw HFCPL	2.59 ± 0.59 [a]	1.65 ± 0.16 [a]	2.41 ± 0.15 [a]	2.71 ± 0.15 [a]

Values are expressed as Means ± SEM of 5 replicates. Values with superscripts different from the control are significantly different ($p < 0.05$).

3.6. Kidney FunctionTests

All HFCPL-treated groups experienced a substantial rise in creatinine concentration ($p < 0.05$) in contrast to the control (Table 4). Among all treated and untreated groups, there was no discernible difference in the amounts of either urea or uric acid ($p < 0.05$). The globulin concentration was discovered to be considerably less ($p < 0.05$) in the cystone and 25 mg/kg body weight groups compared to the control. At 25 mg/kg, the bilirubin level significantly increased ($p < 0.05$) compared to the control, whereas at 50 mg/kg, it significantly reduced ($p<0.05$). Only at a dose of 25 mg/kg compared to the other groups did albumin level show a significant value ($p < 0.05$).

Table 4: Effect of hexane fraction of *Calotropis procera* leaf (HFCPL) ethanol extract on kidney function parameters of nephrolithiatic rats

Group	Albumin (g/dl)	Globulin (mg/dl)	Bilirubin(mg/dl)	Creatinine(mg/dl)	Urea (mg/dl)	Uric Acid(mg/dl)
Control + dw	4.47 ± 0.90[a]	10.41 ± 1.69[a]	1.08 ± 0.00[a]	0.71 ± 0.00[a]	16.42 ± 0.28[a]	5.07 ± 0.46[a]
Lithiatic + dw	3.99 ± 0.18[b]	10.34 ± 1.66[b]	0.75 ± 0.05[b]	0.77 ± 0.01[b]	14.51 ± 0.85[b]	5.14 ± 0.66[a]
Lithiatic + 750 mg/kg bw cystone	4.04 ± 0.53[a]	8.37 ± 1.02[c]	0.93 ± 0.16[a]	0.73 ± 0.06[ab]	16.54 ± 0.31[a]	5.13 ± 0.39[a]
Lithiatic + 25 mg/kg bw HFCPL	2.21 ± 1.46[c]	8.13 ± 1.88[c]	1.93 ± 0.39[c]	0.95 ± 0.01[c]	17.58 ± 1.84[a]	5.99 ± 0.79[a]
Lithiatic + 50 mg/kg bw HFCPL	3.44 ± 0.91[ab]	10.12 ± 1.12[ab]	0.56 ± 0.11[d]	0.74 ± 0.01[d]	16.23 ± 1.38[a]	6.23 ± 0.83[a]
Lithiatic + 100 mg/kg bw HFCPL	4.24 ± 0.58[a]	9.52 ± 1.03[ab]	1.20 ± 0.25[a]	0.85 ± 0.04[e]	16.20 ± 1.43[a]	5.79 ± 0.85[a]

Values are expressed as Means ± SEM of 5 replicates. Values with superscripts different from the control are significantly different ($p < 0.05$).

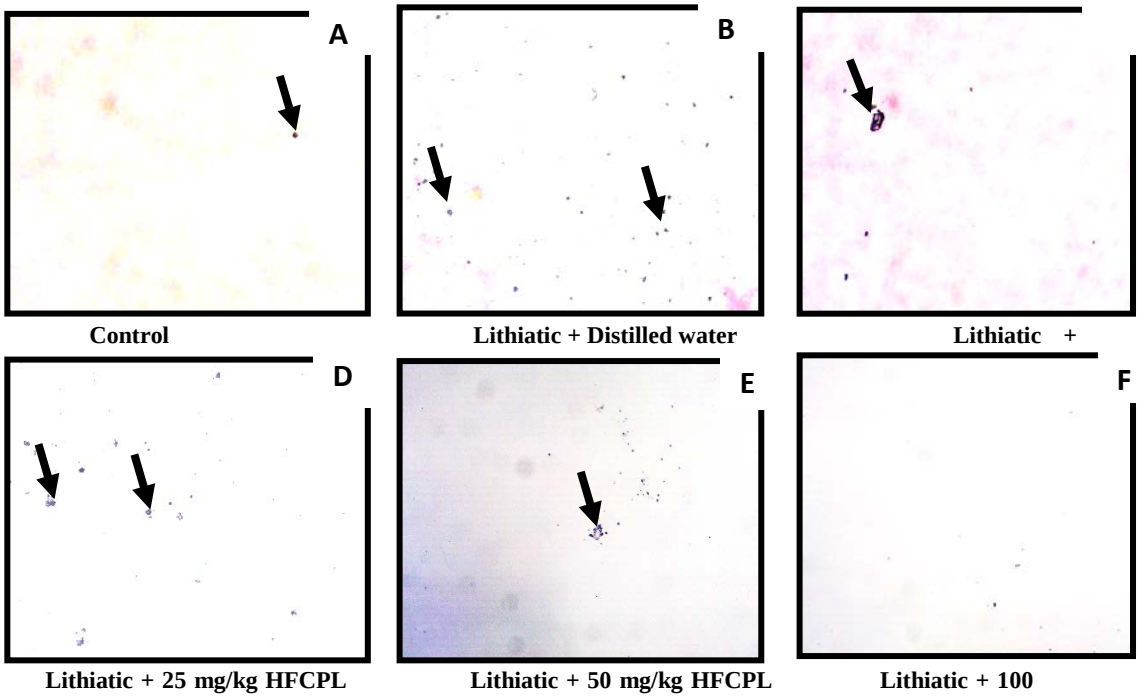

Figure 4: Photomicrograph of urine samples of lithiatic rat treated with HFCPL ethanol extract showing kidney stones (arrows)

3.7. Enzyme Activity

All doses and the cystone group saw a substantial rise ($p< 0.05$) in the actions of the enzymes alanine transaminase and aspartate transaminase; however, only the 25 and 100 mg/kg body weight groups saw a similar increase ($p <0.05$) in alkaline phosphatase activity (Table 5).

Table 5: Serum enzyme activity in nephrolithiatic rats treated with hexane fraction of *Calotropis procera* leaf (HFCPL) ethanol extract

Group	ALT (U/I)	AST (U/I)	ALP (U/I)
Control + dw	6.49 ± 0.18[a]	24.31 ± 0.26[a]	0.62 ± 0.41[a]
Lithiatic + dw	7.34 ± 0.21[b]	26.59 ± 0.24[b]	2.09 ± 0.29[b]
Lithiatic + 750 mg/kg bw cystone	9.12 ± 0.47[c]	35.72 ± 0.44[c]	0.32 ± 0.16[a]
Lithiatic + 25 mg/kg bwHFCPL	11.12 ± 0.46[d]	41.05 ± 3.22[d]	1.69 ± 0.35[b]
Lithiatic + 50 mg/kg bw HFCPL	8.32 ± 0.37[c]	26.51 ± 0.32[b]	0.37 ± 0.11[a]
Lithiatic + 100 mg/kg bw HFCPL	10.80 ± 0.11[d]	36.06 ± 1.61[d]	1.52 ± 0.18[b]

Values are expressed as Means ± SEM of 5 replicates. Values with superscripts different from the control are significantly different ($p < 0.05$).

3.8. Antioxidant Enzyme Activity

All of the dosages significantly differed from the control in terms of liver glutathione activity ($p <0.05$). But both the cystone and 100 mg/kg groups showed a statistically significant increase ($p< 0.05$) in the kidney glutathione activity (Table 6). When compared to the control and standard medication, kidney MDA activity was significantly lower in all doses of HFCPL ($p< 0.05$). The only group in which the liver's MDA activity rose considerably ($p< 0.05$) in comparison to the control was the one that received cystone at a dose of 25 mg/kg. When equated to the control group, the kidney's catalase activity considerably decreased ($p <0.05$) in both groups. In contrast to the untreated groups, SOD activity considerably increased ($p <0.05$), reaching its peak at a dose of 50 mg/kg.

Table 6: Effect of hexane fraction of *Calotropis procera* leaf(HFCPL) ethanol extract on antioxidant parameters in nephrolithiatic rats (×10^4 mg/protein).

Group	Liver GSH	Kidney GSH	Liver MDA	Kidney MDA	Kidney SOD	Kidney Catalase
Control + dw	0.89 ± 0.01[a]	0.86 ± 0.02[a]	1.63 ± 0.15[a]	2.22 ± 0.15[a]	3.50 ± 0.81[a]	0.74 ± 0.25[a]
Lithiatic + dw	0.80 ± 0.02[b]	0.87 ± 0.01[a]	2.41 ± 0.13[b]	2.53 ± 0.06[b]	0.81 ± 0.33[b]	0.15 ± 0.02[b]
Lithiatic + cystone	0.90 ± 0.05[a]	0.91 ± 0.01[b]	2.03 ± 0.19[c]	2.25 ± 0.10[a]	1.87 ± 0.42[c]	0.49 ± 0.03[c]
Lithiatic + 25 mg/kg bwHFCPL	1.03 ± 0.07[c]	0.88 ± 0.00[a]	2.17 ± 0.14[b]	1.53 ± 0.15[c]	1.76 ± 0.21[c]	0.64 ± 0.09[a]
Lithiatic + 50 mg/kg bwHFCPL	1.00 ± 0.03[c]	0.88 ± 0.01[a]	1.43 ± 0.08[a]	1.87 ± 0.18[c]	4.46 ± 0.88[a]	0.23 ± 0.17[c]
Lithiatic + 100 mg/kg bw HFCPL	0.99 ± 0.02[c]	0.94 ± 0.02[b]	1.55 ± 0.16[a]	0.96 ± 0.01[d]	2.20 ± 0.40[a]	0.32 ± 0.13[c]

Values are expressed as Means ± SEM of 5 replicates. Values with superscripts different from the control are significantly different ($p < 0.05$)

3.9. GCMS Analysis

The GCMS analysis revealed the presence of five active principles in the n-hexane fraction of ethanol extract of *C. procera* leaf. The compound 9, 12, 15-Octadecatrien-1-ol (61.22 %) had the highest percentage abundance while 5-Methyldocosane (2.81 %) had the lowest (Table 7).

Table 7: Bioactive constituents of hexane fraction of *Calotropis procera* Leaf(HFCPL) ethanol extract

S/N	Name of Compounds	Retention Time	Peak area %
1.	n-Hexadecanoic acid	37.758	27.21
2.	Phytol	38.584	5.83
3.	9,12,15-Octadecatrien-1-ol	38.859	61.22
4.	Tetrabenzo[e,i,o,s][1,4,7,11,14,18] dithiatetraazacycloeicosine	39.410	2.94
5.	5-Methyldocosane	40.504	2.81

4. Discussion

Results from the analysis of the secondary metabolites revealed that ethanol extract of *C. procera* leaf contains saponins, alkaloids, flavonoids, tannins and terpenoids (Table 1). It has been reported that saponins (Touhami *et al.*, 2007; Rad *et al.*, 2011), flavonoids and alkaloids (Rad *et al.*, 2011) possess anti-nephrolithiatic activity, the concentrations of which might have contributed significantly to the clearance of uroliths in the lithiatic rats. Saponins (Kenner and Requena, 1996) boosts the immune system, tannins (El Marie and Jonah, 2001); alkaloids and flavonoids (Aliero *et al.*, 2008) possess antibacterial property and are phytotherapeutic agents capable of clearing uroliths. From the study, both the ethanol extract and its partitioned fractions could prevent the calculi formation at all the nucleation and aggregation stages of stone formation. As the concentration increases, the inhibitory effect also increased. The number of stones in the solution microscopy reduced progressively with the dose, confirming the anti-nephrolithiatic effect of *C. procera* leaf. Nafiu *et al.* (2008) similarly asserted that saponin extract of *Dianthus bausticus* exhibited the highest nucleation inhibitory activity based on its antioxidant-rich potentials. The antioxidant test demonstrated the plant's capacity to function as a free radical scavenger. *Calotropis procera* leaf extract and its fractions can prevent the development of stones because DPPH has a proton free radical and pairs with it in the presence of a free radical scavenger (Chang *et al.*, 2002).

Divakar *et al.* (2010) reported that experimental mice given ethylene glycol and ammonium chloride experienced elevated renal oxalate retention and excretion as well as the development of calculi primarily made of calcium oxalate. Urinal microscopy validates the potency of the n-hexane fraction at reducing the sizes and quantity of calculi in the urine. The stones clearance at 25 mg/kg body weight with a further increase at higher dose concentrations confirms the anti-nephrolithiatic activity of HFCPL. Previous studies indicate that plants lower kidney stone formation by causing a reduction in stone number and size (Rushton and Spector, 1982). Kidney stones block the urinary tract, and hence the obstruction in the passage of urine.

The production of stones in the urine is frequently accompanied by a low amount of magnesium. By joining with calcium oxalate to produce a soluble complex and lowering the concentration at which calcium oxalate can form, magnesium has been found to effectively inhibit the crystallization of calcium oxalate in vitro (Lemann *et al.*, 1991). The increase in urinary magnesium concentration in all doses indicates the efficacy of C. *procera* in the management of kidney stones by clearing the oxalate concentration available for stone formation. This supports studies that magnesium levels recover to normal following medication therapy, with decreases in CaOx growth and nucleation rate in nephrolithiasis-affected rats (Grases *et al*., 1989; Patel *et al.*, 2016).

The danger of precipitation, stone formation, and stone growth are reduced because calcium and uric acid are eliminated through the urine. Hypercalciuria at all the doses validates the potency of *C. procera* in the inhibition and regulation of stone development characteristic of nephrolithiasis. This is further substantiated by the urinary microscopy (Fig. 5) result, which showed the quantity and sizes of stones across all groups. In this study, uric acid level showed no significant difference, contrary to reports by Patel *et al.* (2016) that uric acid level in lithiatic rats decrease after drug treatment. This suggests that kidney stone disease poses no threat to the production and elimination of uric acid.

According to Wright and Plummer (1974), alkaline phosphatase is a plasma membrane marker enzyme that is necessary for healthy organ function in particular levels and is essential to evaluating the integrity of the plasma membrane. The metabolism of xenobiotics and the preservation of biological homeostasis in an organism both depend heavily on the liver. Due to these important roles,

liver enzymes are used as makers in the assessment of drugs (Satyapal *et al.*, 2008). The reported increase in AST and ALT activity across all dose groups indicate impairment of the liver function (Huang *et al.*, 2002). At 50 mg/kg body weight dose, the observation of no significant difference in the serum suggests absence of hepatic injury which could cause elevation of ALP levels in the blood.

It was reported that antioxidant enzyme activity decreases in kidney stone patients, hence an increase in lipid peroxidation. An increase in MDA characterizes calculi formation with a progressive reduction in levels of SOD, catalase and GSH in CaOx induced rats. The observed decrease in MDA (Huang *et al.*, 2002) and the corresponding increase in antioxidant enzymes level (Patel *et al.*, 2016) are in line with previous nephrolithiatic studies that used phytotherapy as a drug alternative in the disease management. The HFCPL potency is also supported by its DPPH scavenging potentials, hence protecting against oxidative stress.

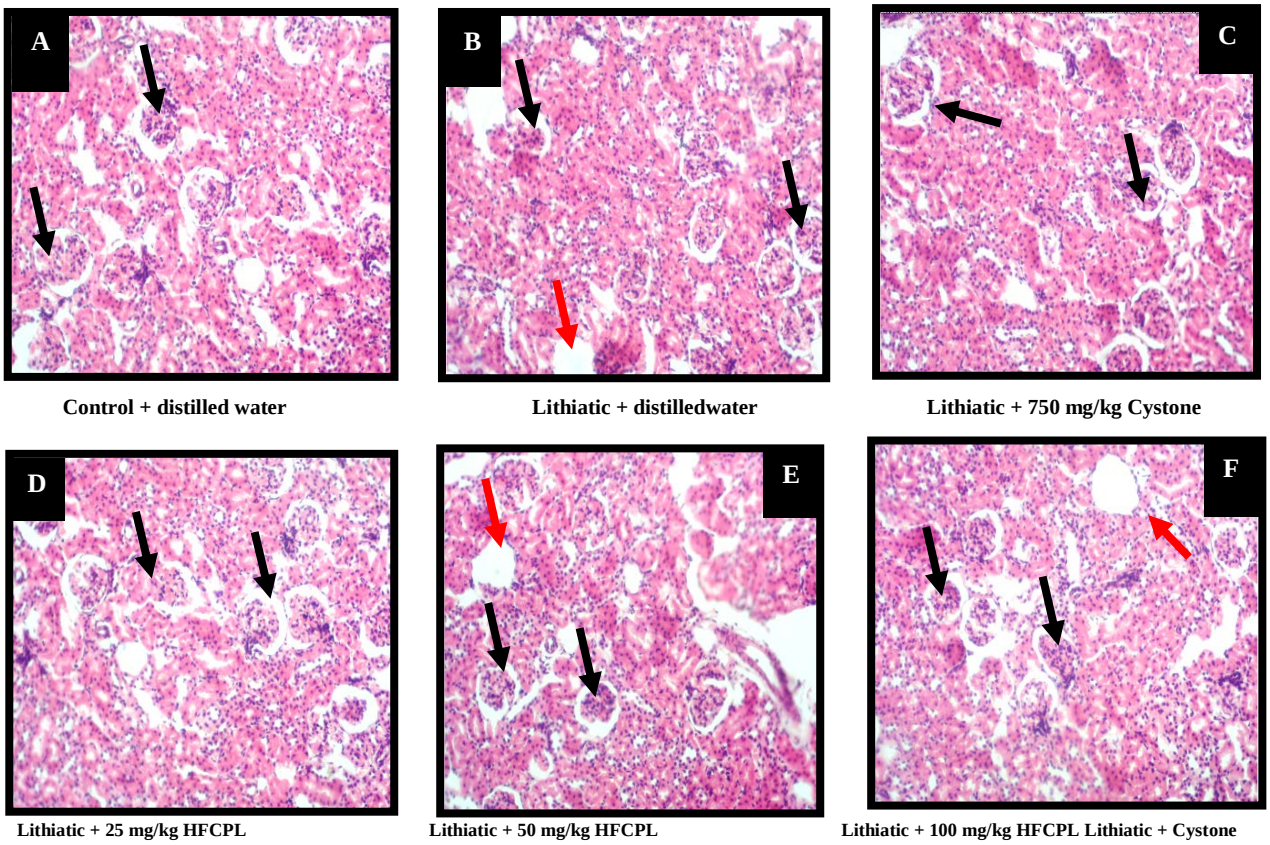

Figure 5: Photomicrographs of the kidney of experimental rats showing the renal cortex and distribution of renal corpuscles (black arrow) and possible corpuscular degeneration (red arrow). Figures A, C and D represent normal renal cortical morphology and histo-architecture with intact renal corpuscles and staining characteristics. B, E and F present corpuscular degeneration suggesting pathological alteration. H and E stain (Mg x 400).

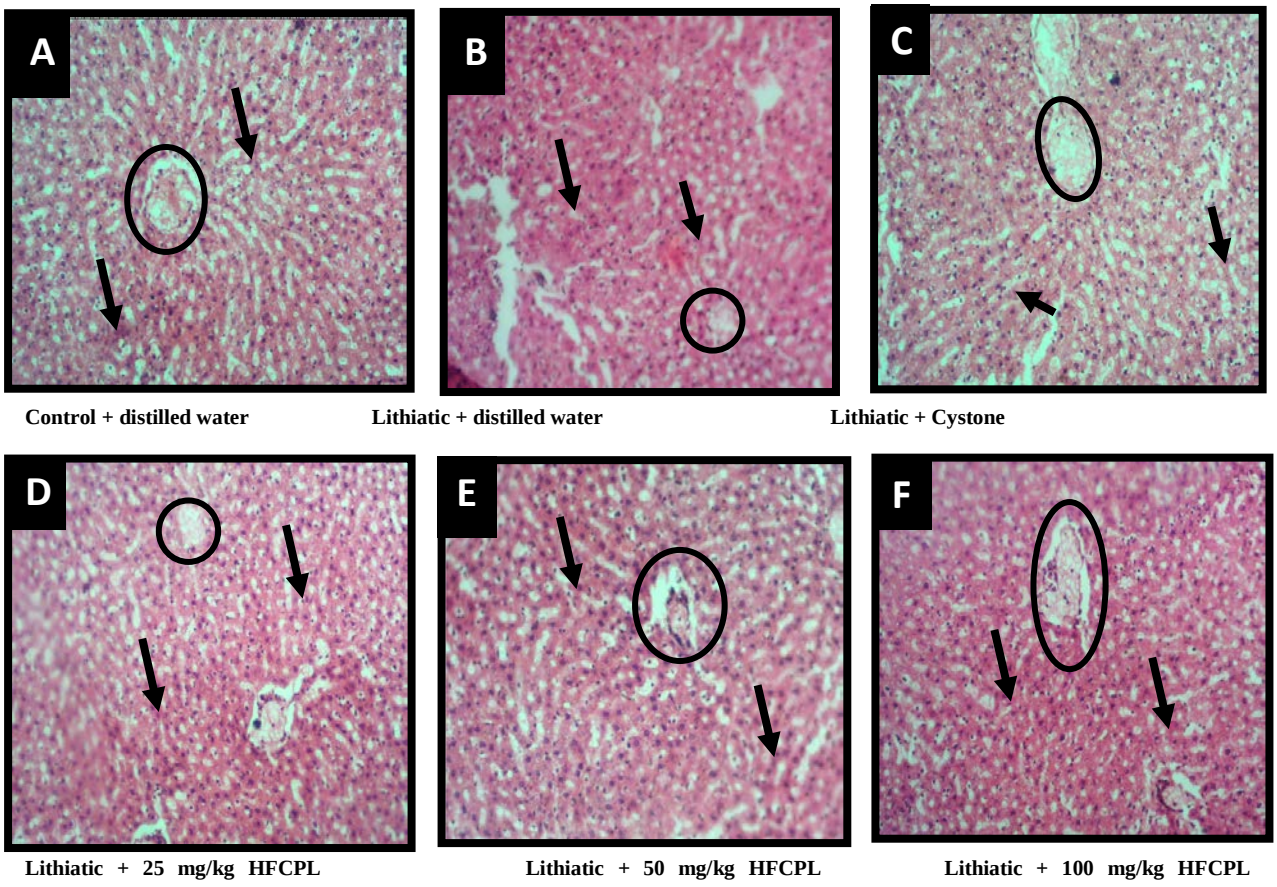

Figure 6: Photomicrograph of the liver of lithiatic rat treated with HFCPL ethanol extract showing the central veins (black circles) and densely packed hepatocytes (black arrow). The photomicrographs appear characteristically normal with no pathological alteration though with sings of cellular delineation, fatty liver and cholestasis.

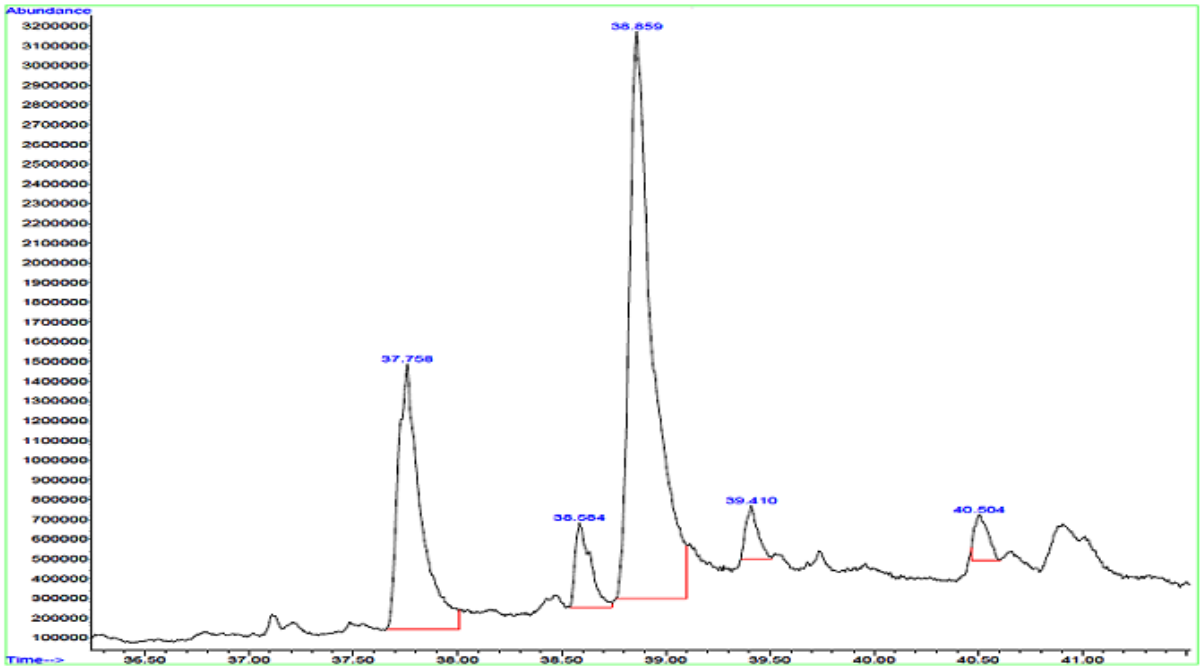

Figure 7: Gas Chromatography-Mass Spectrophotometry (GC-MS) chromatogram of hexane fraction of *Calotropis procera* leaf (HFCPL) ethanol extract.

Normal urea concentration at all dose groups in relation to the control could be indicative of adequate kidney functioning in excretory, regulatory and endocrine processes (Judykay, 2007). According to Adebayo *et al*. (2003), elevated urea levels predict a decline in the nephrons' capacity to filter waste, leading to waste accumulation, whereas a drop could be ascribed to insufficient protein catabolism that results in lesser urea production. Whelton *et al.* (2002) stated that an increase in creatinine concentration suggests impaired renal function. The increase observed in creatinine level is, therefore, suggestive of a distorted function of the kidney in the HFCPL treated rats.

To assess an animal's proper liver function, a combination of molecules called albumin, total bilirubin, and globulin can be employed (Rasekh *et al.*, 2008). With both biological and diagnostic relevance, bilirubin is a significant byproduct of blood catabolism. The increase in bilirubin generation at 25 mg/kg dose may be due to oxidative stress, hepatic injury, or impaired liver function (Moudgil *et al.*, 1989). The main serum protein components are albumin and globulin, and their concentrations can provide some insight into the health of the immune system and diet. Low albumin to globulin ratios can indicate either excessive globulin production, as in autoimmune illnesses, or albumin deficiency, as in cirrhosis, or even selective albumin removal from circulation. The lack of any discernible variation in serum albumin and globulin indicates adequate protein synthesis.

The kidney corpuscular degeneration at higher doses after the histological examination is suggestive of pathological alteration. The aggregation of stones in the kidney of the rats after induction causes severe damages in the kidney pending treatment because of impaired urine excretion. However, the normal liver morphology without pathological alteration shows that interactions between promoters and inhibitors had no effect on the tissue; hence, HFCPL displayed a good hepatoprotective agent.

The analysis of the active ingredients in the n-hexane fraction indicated the presence of chemical compounds that might enhance the plant's therapeutic qualities. Phytol acts as an antioxidant by the removal of hydroxyl radicals which may be capable of inhibiting cell damage caused by this radical (Camila *et al.*, 2013). The presence of this compound corroborates the antioxidant potential of the plant which was able to lower lipid peroxidation *in vivo*. It occurs naturally in green tea and is used in the synthesis of vitamins E and K. Hexadecanoic acid is a surfactant used in soap making, which might account for the high foaming capacity of the plant. Vasudevan *et al.* (2012) reported that hexadecanoic acid possesses anti-inflammatory property upon its kinetic assessment.

5. Conclusion

From this study, *Calotropis procera* leaf may be used in the management of kidney stone disease, a novel outcome in the phytotherapy potentials of the plant. This is probable because of its antioxidant, nucleation and aggregation properties that promote inhibition of stone formation. The n-hexane fraction is effective in stone clearance with no alteration in biochemical indices. When administered at higher dose concentrations, the fraction poses a threat to tissue morphology; hence, pathological alterations occur.

Conflicting Interests

The authors certify that they have no business or personal connections that would have improperly impacted their authorship of this work.

Data Availability Statement: The corresponding author, Nafiu MO., will provide the data supporting the study's conclusions upon reasonable request.

Funding Information: The research, writing and/or publication of this paper were not funded in any way.

References

Adebayo JO, Yakubu MT, Egwin CE, Owoyele BV and Enaibe BU. 2003.Effect of ethanolic extract of *Khaya senegalensis* on some biochemical parameters on rat kidney. *J. Ethnoparm.* **88**: 69-72.

Aggarwal R, Srivaster A, Jain SK, Sud R and Singh R. 2017. Renal stones: A clinical review. *EMJ Urol* **5(1):** 98-103.

Aliero AA, Aliero BL and Buhari U. 2008. Preliminary phytochemical and antibacterial screening of *Scadous maltiforus. Int J of Pure and Appl Sci.* **2(4):** 13-17.

Barbasa C, Garciaa A, Saavedraa L and Muros M. 2002. "Urinary analysis of nephrolithiasis markers." *J of Chroma B.* **781(1-2):** 433–455.

Camila PS, Salvadori MS, Mota VG, Costa LM, de Almeida AA, de Oliveira GA, Costa JP, de Sousa DP and de Freitas R. 2013. Antinociceptive and antioxidant activities of phytol *in vivo* and *in vitro* models. *Neuro SciJ*, **949452**: 1-9.

Chang LW, Yen WJ, Huang SC and Duh PD. 2002. Antioxidant activities of sesame coat. *Food Chem.* **78**: 347-54

Chung KJ, Kim JH, Min JE, Park HK, Li S, del Giudice F, Han DK and Chung BI. 2019. Changing trends in the treatment of Nephrolithiasis in the real world. *J of Endourol.* Doi: 10.1089/end.2018.0667.

Coe F, Evan A and Worcester E. 2005. Kidney stone disease.*J of Clin Inves* **115(10):** 2598–2608.

Divakar K, Pawar AT, Chandrasekhar SB, Dighe SB and Divakar G. 2010. Protective effect of the hydro-alcoholic extract of *Rubia cordifolia* roots against ethylene glycol induced urolithiasis in rats. *Food and Chem Toxicol.* **48(4):**1013-1018.

El Marie VW and Jonah CP. 2001. Purification and identification of active antibacterial component in *Carpobrotus edulis. J of Ethnopharm.* **76**: 87-91.

El-Zoghby M, Lieske JC and Foley RN. 2012. "Urolithiasis and the risk of ESRD." *Clin J of the Ame Soc of Nephro* **7(9):** 1409–1415.

Esmail A and Al Snafi. 2015. The constiuents and pharmacological properties of *Calotropis procera*- an overview. *Int J of Pharm Rev and Res.* **5(3)**: 259-275.

Gilhorta KR and Christina JM. 2011. Effect of *Rotula aquatic* Lour. on ethylene-glycol induced urolithiasis in rats. *Int J Drug Dev and Res.* **3**: 273.

Grases FA, Genestar C, Conte A, March P and Costa-Bauza A. 1989. Inhibitory effect of pyrophosphate, citrate, magnesium and chondroitin sulphate in calcium oxalate urolithiasis. *Biochem J Inter.* **64(3)**: 235-237.

Hassan SW, Bilbis FL, Ladan MJ, Umar RA and Danagogo SM. 2006. Evaluation of antifungal activity and phytochemical analysis of leaves, roots and stem bark extracts of *Calotropis procera* (asclepiadaceae). *Pak J Bio Sci.* **9(14):** 2624-2629.

Hess B, Hasler-StrubU, Ackermann D and Jaeger P. 2000. Metabolic evaluation of patients with recurrent idiopathic calcium nephrolithiasis. *Neprol Dial Transplant* **12**:1362.

Huang HS, Ma MC, Chen J and Chen CF. 2002. Changes in the oxidant-antioxidant balance in the kidney of rats with nephrolithiasis induced by ethylene glycol. *J Urol.* **167**: 2584-93.

Iqbal Z, Lateef M, JabbarA, Muhammad G and Khan MN. 2005. Anthelmintic activity of *Calotropis procera* (Ait.) Ait.F. flowers in sheep. *J Ethnopharm.* **102(2):** 256-261.

Jehti RK, Duggal B, Sahota RS, Gupta M and Sofat JB. 1983. Important plants used in stone. *India J Med Res.* 78: 422-25.

Joseph KC, Bharat B, Parek H and Joshi MJ. 2005. Inhibition of growth of urinary type calcium hydrogen phosphate dehydrate crystals by tartaric acid and tamarind. Current Science **88**: 1232-1238.

Judykay T. 2007. Nutrition for reducing urea and creatinine in the blood. *Diab Care.* **27**: 2191-2192.

Kumar SB, Kumar KG, Srinivasa V and Bilal S. 2012. A review on urolithiasis.*Int J of Uni Pharm and Life Sci.* **2(2):** 269–280.

Kumar VL, Padhy BM, Shelgal R and Roy S. 2005. Antioxidant and protective effect of latex of *Calotropis procera* against alloxan-induced diabetes in rats. *J of Ethnopharm.* **102(3):** 470-473.

Lahsini M, Bousaid M, Lazrec HB and Jana M. 1997.Evaluation of antifungal and molluscidcal properties of extracts of *Calotropis procera*. *Filorapia.* **68**: 371-373.

Lemann J, Worcester E and Gray R. 1991. Hypercalciuria and stress. *Am. J Kidney Dis.* **27**: 386-391.

Moe OW. 2006. Kidney stones: pathophysiology and medical management.*Lancet* **367(9507):** 333–344.

Mohsin A, Shah AH, Alaha MA, Tanqi MO and Ageel AM. 1989. Analytic antipyretic activity and phytochemical screening of some plants used in traditional Arab system of medicine. *Filorapia.* **60(3):** 174-177.

Molyneux P. 2004. The use of the stable free radical diphenylpicryl-hydrazyl (DPPH) for estimating antioxidant activity. *Songklana J Sci Technol*. **26(2):** 211-219.

Moudgil KD, Narang BS and Moudgil KD.1989. Textbook of Biochemistry and Human Biology. 2nd Edn. *New Delhi, India: Prentice-Hall of India Limited* pp. 271-273.

Nafiu MO, Ashafa AO and Sabiu S. 2018. Antinephrolithiatic potentialand the protective role of saponin-rich extract of *Dianthus bausticus*against acetaminophen induced damage in HEK 293 cells. *Indian J Nat Prod Resour*. **9(2):** 117-125.

O'Connor C. 1993. Traditional cheese making in West Africa. *Dairy Tech Paper.* **3(2):** 14-18.

OECD. 2002. OECD Guidelines for the Testing of chemicals Test No. 420: Acute oral toxicity- fixed dose procedure. *OECD Publishing, Paris.* Section 4. http://doi.org/10.1787/9789264070943-en.

Orwa C, Mutua A, Kindt R, Jamnadass R and Anthony S. 2009. Agroforestry Database: as tree reference and selection guide version 4.0. *World Agroforestry Centre, Kenya*.

Park S and Pearle MS. 2007. "Pathophysiology and management of calcium stones." *Urol Clin of N America*, **34(3):** 323–334.

Parsons WT and Cuthbertson EG. 2001. Noxious weeds of Australia. *CSIRO Pub*. Pg. 712.

Patel PK, Vyas BA, Joshi SV and Gandhi TR. 2016. Evaluation of Antiurolithiatic Effect of *Pedalium murex* Fruit Extract in Ethylene Glycol-induced Nephrolithiasis in Rat. *Indian J of Pharm Sci*.

Prabha MR, and Vasntha K. 2011. Antioxidant, cytotoxicity and polyphenolic content of *Calotropis procera* R. Br. Flower. *J of App Pharm Sci.* **1(7):** 136-140.

Rad AK, Hadjadeh M, Rajael Z, Mohammadian N and Valiolahi S. 2011. The beneficial effect of *Cynodon dactylon* fractions on ethylene glycol induced kidney calculi in rats. *Uro J.* **8(3):** 179-84.

Rasekh HR, Nazari P, Kamil-Nejad N and Hosseinzaden L. 2008. Acute and subchronic toxicity of *Galega officinalis* in rats. *J Ethnopharmacol* **116**:21-26.

Sathyaa M, Kokilavani R, Ananta KS and Balakrishnan A. 2011. Supplementation of ethanolic extract of *Acalpha indica* Linn prevents hyperoxaluria in experimental urolithic rats. *J for Bloomers of Res.* **4**: 293.

Satyapal SU, Kadam VJ and Ghosh R. 2008. Hepatoprotective activity of Livobond, a polyherbal formation against CCl_4 induced hepatotoxicity in rats. *Int. J. Pharmacol* **4**:472-6

Scales CD, Smith AC, Hanley JM and Saigal CS. 2012."Prevalence of kidney stones in the United States" *EuroUrol*. **62(1):** 160–165.

Selvem R. 2002. Calcium oxalate stone disease: role of lipid peroxidation and antioxidants. *Uro Res.* 30(1): 35-47.

Soundararajan P, Mahesh R, Ramesh T and Begum VH. 2006. Effect of *Aerva lanata* on calcium oxalate urolithiasis in rats. *Ind J of Exp Bio* **44(12):** 981.

Touhami M, Laroubi A, Elhabazi K, Loubna F and Zara I. 2007. Lemon juice has protective activity in a rat urolithiasis model. *BMC Uro.* 7-18.

Vasudevan A, Kalarickal VD, Pradeep KM, Ponnuraj K, Chittalakkottu S and Haridas M. 2012. Antiinflammtory property of n-hexadecanoic acid: Structural Evidemce and Kinetic Assessment. *Chem Bio & Drug Des*, **80(3):** 14-18.

Wright PJ and Plummer DT. 1974. The use of urinary enzymes measurement to detect renal damage caused by nephrotoxic compounds. *Biochem Pharmacol* **23**: 65-73.

Xu H, Zisman A, Coe F and Worcester E. 2013. "Kidney stones: an update on current pharmacological management and future directions." *Expert Opin on Pharmacoth*, **14(4):** 435–447.

Yadav RD and Jain SK. 2011. Herbal plants used in the treatment of urolithiasis, a review. *Intl J of Pharm Sci and Res* **2(6):** 1412-142.

Ziemba JB and Matlaga BR. 2017. Epidemiology and economics of nephrolithiasis. *Invest Clin Urol* **58(5):** 299-306.

JJBS

Volume 16, Number 1,March 2023
ISSN 1995-6673
Pages 117 – 123
https://doi.org/10.54319/jjbs/160114

Jordan Journal of Biological Sciences

The Antioxidative, Anticancer and Hepatoprotective of Quercetin Nanoparticles *In-vitro* and *In-vivo*

Uzma A Faridi[1,*],Nahla S Zidan[2,3], Fahad M. Almutairi [1], Adel I. Alalawy[1], Hebatallah H. Atteia[4,5], Yahya S.Al-Awthan [6,7] , Md. Qussen Akhtar[8], Mohamed I. Sakran[1,9]

[1]*Biochemistry Department, Faculty of Science, University of Tabuk, Saudi Arabia ufaridi@ut.edu.sa;* [2] *Department of Home Economics, Faculty of Specific Education, Kafr ElShaikh University, Egypt;* [3]*Department of Nutrition and Food Science, Faculty of Home Economics, University of Tabuk, Tabuk 71491, Saudi Arabia;* [4]*Department of Pharmaceutical Chemistry, Faculty of Pharmacy, University of Tabuk, Tabuk, Saudi Arabia;* [5]*Department of Biochemistry, Faculty of Pharmacy, Zagazig University, Zagazig, Egypt;* [6]*Department of Biology, Faculty of Science, University of Tabuk, Tabuk, Saudi Arabia;* [7]*Department of Biology, Faculty of Science, Ibb University, Ibb, Yemenm;* [8]*Biotechnology Division, CSIR-Central Institute of Medicinal and Aromatic Plants, Lucknow, Uttar Pradesh, Indi;* [9]*Department of Chemistry, Faculty of Sciences, Tanta University, Tanta 31527, Egypt*

Received: September 8, 2022; Revised: October 8, 2022; Accepted: October 18, 2022

Abstract

Quercetin is a flavonoid found in many plants, such as berries and green tea. It has several therapeutic properties, including anticancer, antioxidative, and hepatoprotective. Although quercetin has numerous health benefits and is a valuable phytomedicine, it does have some drawbacks, including low solubility and bioavailability. In the present study, to overcome these drawbacks, quercetin nanoparticles were synthesized and studied for *in-vitro* and *in-vivo* antioxidative, anticancer, and hepatoprotective properties. The results indicated that the quercetin nanoparticles show significantly improved activity in both *in-vitro* and *in-vivo* studies.

Keywords: Quercetin; quercetin nanoparticles; antioxidant activity; cytotoxic activity

1. Introduction

In addition to providing us with food, the plants have several ethnomedicinal benefits without causing harm. When it comes to nutrition and disease prevention, these fruits and vegetables are indispensable (Manna K *et al*., 2016, Prakash D *et al*., 2012). These polyphenols, flavonoids, and isoflavonoids present in fruits, seeds, herbs, and vegetables also contain phytochemicals that have a variety of health benefits at different stages of their life cycles (Shikov AN *et al*., 2017). One of the phytomolecules, quercetin, a flavonoid found in fruits and vegetables, has antioxidative, anticancer, anti-inflammatory, and other therapeutic properties (Figure 1). Quercetin's hepatoprotective and anti-inflammatory properties have been extensively studied (Inal ME & Kahraman A, 2000)(Kanadaswami C *et al*., 2005). Although, quercetin contains a variety of health benefits, it still has disadvantages over other flavonoids as it has very low water solubility and it is a very easily degradable molecule, which limits its uses as a drug (Frenzel M & Steffen-Heins A. 2015). One of the solutions to the solubility and bioavailability problems of quercetin could be nanoparticles. Less than 1000 nm in size, nanoparticles can enhance the bioavailability and absorption of medicines (Dai J *et al*., 2004) (Salatin S *et al*., 2017) (Hsu CH *et al*., 2003). In the current study, the antioxidative, anticancer, and hepatoprotective properties of QNPs in contrast to pure quercetin were examined after the QNPs were produced and *in-vitro* and *in-vivo* testing were conducted.

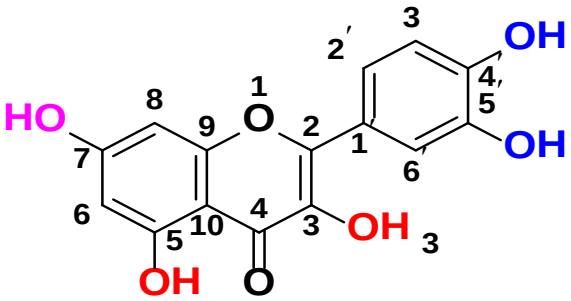

Figure1. Chemical structure of Quercetin

2. Materials and Methods

2.1. Chemicals

The chemicals utilized in this study were purchased from the American company Sigma Aldrich Chemical Co.

2.2. Synthesis and Characterization of QNPs:

QNPs were synthesized by an improved anti-solvation precipitation method by Bilati *et al*., (Bilati U *et al*., 2005) Briefly, PVA solution was infused with 300 mg of quercetin that was dissolved in 200 ml of ethyl alcohol. The solution was homogenized for 1 hour at 20,000 rpm, and the sample was then freeze dried after removal to

* Corresponding author. e-mail: ufaridi@ut.edu.sa.

remove ethyl alcohol. Furthermore, the lyophilized powder was stored in a moisture-proof container until needed. The morphology of quercetin nanoparticles was observed using a 20 kV SEM (Quanta 3D FEG/FEI).

The QNPs were initially analyzed by using FTIR to identify functional groups, phytochemical constituents, and other factors involved in the reduction and stabilization of the synthesized nanoparticles by using the Jasco FTIR 4100's attenuated total reflectance mode (Japan). The data was recorded between 4000 cm^1 and 400 cm^1. CuK1-X Ray diffractometer radiation (= 1.5406 A°) was used to confirm the presence of ZnO in the powdered sample as well as to analyze the crystallite structure and size. An NMR spectrometer (BRUKER) was used to measure the 1H NMR 400MHz spectra using DMSO.

2.3. Cell Lines:

The cell lines used in the study were obtained from the ATCC, U.S.A. and maintained in cell culture as per ATCC guidelines. For long-term usage, the cell lines were cryopreserved in liquid N2 containers. A total of two cell lines, Human Tumor Cell Line (Huh-7) (ATCC, U.S.A.) and Human Epithelial Amnion Cell Line (WISH) were used in the present study.

2.4. Antioxidant activity

The method outlined by Braca *et al.* was used to measure the free radical scavenging activity of quercetin and quercetin nanoparticles based on the scavenging activity of the stable 1,1-diphenyl-2-picrylhydrazyl (DPPH) free radical (Braca A *et al*., 2002). Three milliliters of a 0.004% methanol solution of DPPH were mixed with various amounts of quercetin and QNPs. After 30 minutes, the absorbance at 517 nm was measured. To determine the percentage inhibitory activity, the formula [(A0-A1)/A0] x 100 was used, where A0 represents the absorbance of the control and A1 represents the absorbance of the quercetin/QSRs or ascorbic acid (Standard). Inhibition curves were created in order to get IC50 values.

2.5. Sub culturing of cell lines:

The monolayer culture was transferred to a second vessel by diluting the cells with trypsin. After the cell reached 80% confluency, the culture flask was removed from the CO2 incubator. The old medium was completely removed from the flask and washed with 3ml of 1X PBS. Trypsin (3 ml, 0.25%) was added to that flask for 60 seconds and removed, leaving a few drops in the flask. The culture flasks were kept at 37^0 C for 20 minutes until all the cells were released from the surface in the residual trypsin solution. Furthermore, the required amount of growth medium (10 ml) was added to suspend the cells with the help of a Pasteur pipette, and the cells were distributed equally in two flasks. Finally, the culture flasks were incubated at 37^0C with 5% CO2.

2.6. In-vitro cytotoxic activity using human cancer and normal cell lines using SRB assay:

SRB assays were used to test the in-vitro cytotoxic activity of quercetin and QNPs (Houghton PJ *et al*., 1994]. In order for the 3x103 cells per well to adhere to the 96-well microtiter plates, 150 l of fresh media were incubated with the cells for 24 hours. After 24 hours, quercetin and quercetin nanoparticles were added in triplicate along with 0, 12, 5, 25, 50, and 100 g/ml. The plates were subsequently incubated once more for 24 hours with quercetin and quercetin nanoparticles present. Cell growth was examined in the last stage (Vichai V & Kirtikara K. 2006). Immediately after the operation, the cells were fixed by adding 50 l of cool, 40% (w/v) trichloroacetic acid, and they were once more kept at 4 °C for an hour. The plates with wells were thoroughly cleaned with distilled water after the supernatant was removed from them. Following the procedure, the cells were fixed by adding 50 l of cool, 40% (w/v) trichloroacetic acid, and they were once more maintained for an hour at 4 °C. After removing the supernatant from the plates containing wells, they were thoroughly cleaned with distilled water. 50 l of SRB solution was added to each well after the plate had dried, and it was left to incubate for 30 min at room temperature. The unconnected SRB was eliminated by repeatedly washing the plate in 1% acetic acid. To solubilize the dye, 100 l of 10 mM Tris base was then added to each well. The plates were placed on a plate and gently shaken for 20 minutes. After that, the absorbance (OD) was measured at 570 nm using an ELISA reader. The formula below was used to compute the cell's survival percentage.

Percentage cell survival = O.D. (treated cells)/ O.D. (control cells).

2.7. In-vivo toxicity assay:

Thirty adult male albino rats were used in this study. The animals were divided into four groups: the control group (A), animals treated with diethylnitrosamine and acrylamide to induce oxidative stress and hepatocarcinoma (B, C, and D), and animals not treated. The group B mice were considered as positive controls. The rest of the C and D group mice were treated with the different concentrations of quercetin and QNPs via intraperitoneal injection, after the four weeks of diethylnitrosamine and acrylamide administration. The liver function test was performed after the treatment of quercetin and QNR.

Decapitation was used to sacrifice animals by cervical dislocation, and the cardiac puncture technique was used to collect five milliliters of blood in gel tubes. The blood samples were then centrifuged for 15 minutes at 3000rpm. Human Germany provided standard reagents for the Humalyser 3000, a semi-automatic chemistry analyzer. Before and after the experiment, blood (5 mL) was taken from the vein. Lver function tests were carried out by analysing the AST, ALP, and ALP enzymes (Exarchou V *et al*., 2002).

2.8. Histopathological examination:

The liver tissues of the respective animals were fixed using 10% formaldehyde for 24 hours and embedded into paraffin after 16 h. Five to five m thick sections of each sample were obtained from the paraffin blocks. Each sample was stained using hematoxylin and eosin. The results were analyzed using a light microscope (Babu BH *et al*., 2002).

2.9. Statistical analysis

SPSS v16 was used to analyze the results of our study, with all values expressed as a mean standard error of mean. For ANOVA, P values of 0.05 and 0.01 were measured as statistically significant.

3. Results and Discussion

3.1. Characterization of synthesized QNPs:

3.1.1. FTIR spectroscopic analysis:

Figure 2 displays the quercetin IR spectrum. The bands of absorption at 3325 cm 1 correspond to the hydroxyl group. The C-H bond peak can be found at 3060 cm 1. Stretching of the aromatic C=C bond at 1604 cm-1, where hydroxyl group intensity reduced following QNPS synthesis, indicates the presence of an aromatic nucleus. The findings made it abundantly evident that intermolecular hydrogen bonding took place in the QNPs. **(Figure 3)**.

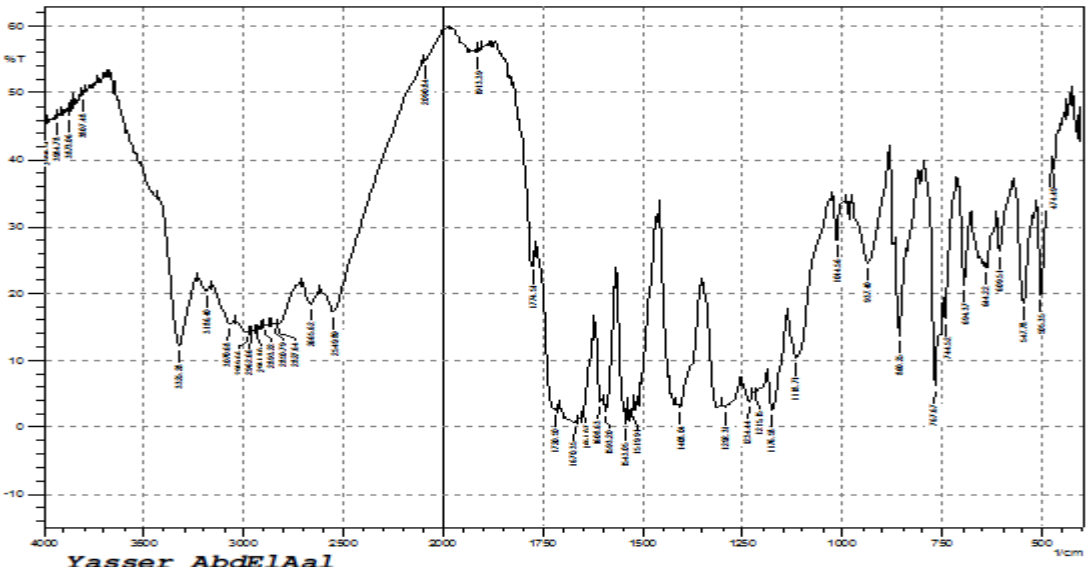

Figure2. IR spectrum of Quercetin

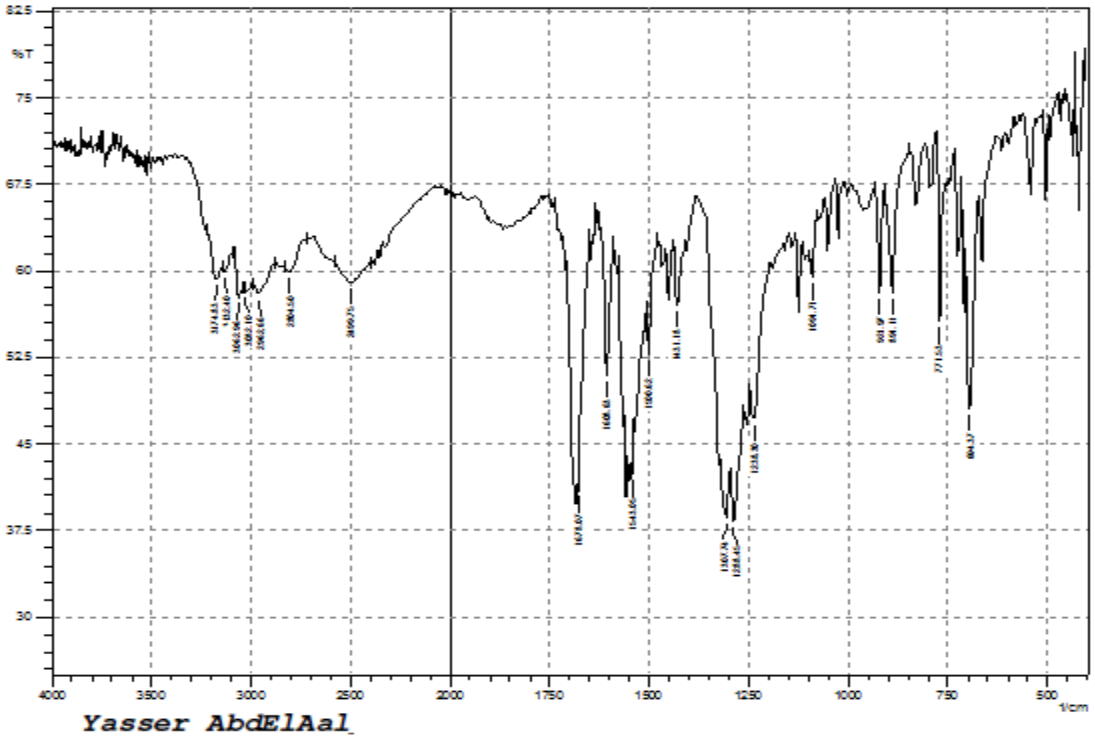

Figure3. IR spectrum of Quercetin nanoparticles

3.1.2. [1] H NMR spectrum of Quercetin and Quercetin nanoparticles:

The following values are displayed in the 1H-NMR spectra of quercetin in DMSO-d6 at 400 MHz: 11.24 (1H, s, C7-OH), 11.56 (1H, s, C4' -OH); 7.92 (1H, d, H-6), 7.94 (1H, d, H-8), 7.98 (1H, d, H-5'), 9.57 (1H, d, H-6'), and 9.87 (1H, s, H-2'). Furthermore, the aromatic proton had peaks in the 1H-NMR spectrum at C-6, C-8, C-5, C-6, and C-2, respectively (Figure 4). The spectra showed protons on aromatic groups ranging from 6 to 8 ppm, strong intramolecular hydrogen bonding at 12.62 ppm, a characteristic shift for intramolecular six-membered ring hydrogen bonding of the C5-OH and C4 O moiety. The QNP's results showed that the H6 and H8 aromatic protons had shifted upfield (Figure 5).

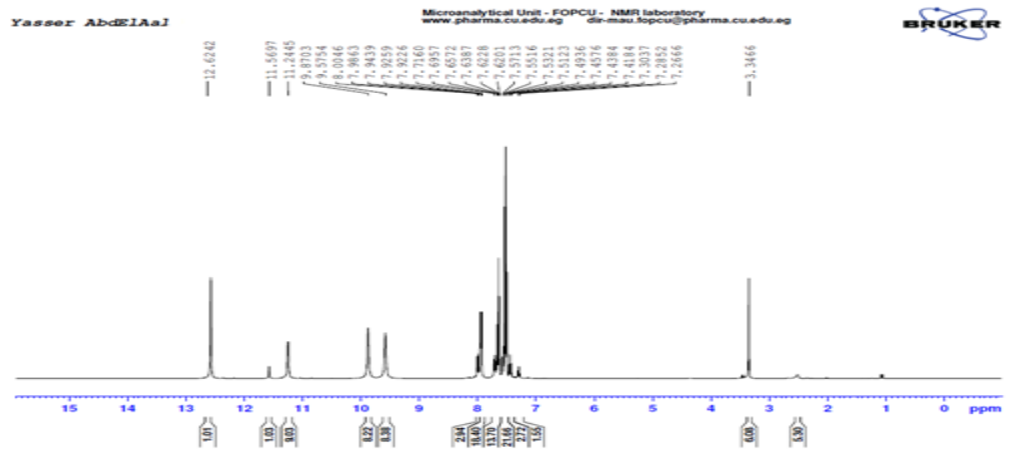

Figure4. [1] H NMR spectrum of Quercetin

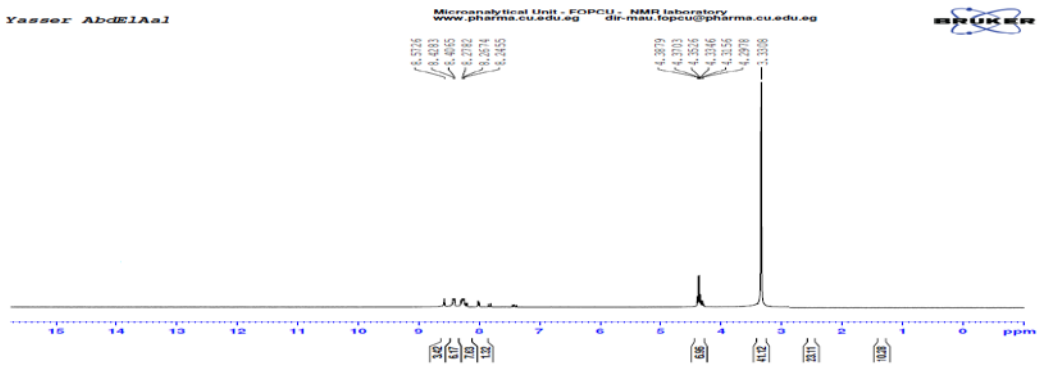

Figure5. [1] H NMR spectrum of Quercetin nanoparticles

3.1.3. XRD analysis:

By using X-ray diffraction, the dried crystalline quercetin nanoparticles were evaluated. The Quercetin nanocrystals' X-ray diffraction patterns are displayed in Figure 6. Numerous distinct peaks of 12.61°, 14.5168°, 16.09°, 17.1714°, 18.62°, 20.19°, 21.17°, 23.78°, 26.10°, 27.91°, and 29.1808° were visible in the X-ray patterns of the QNPs (Figure 6).

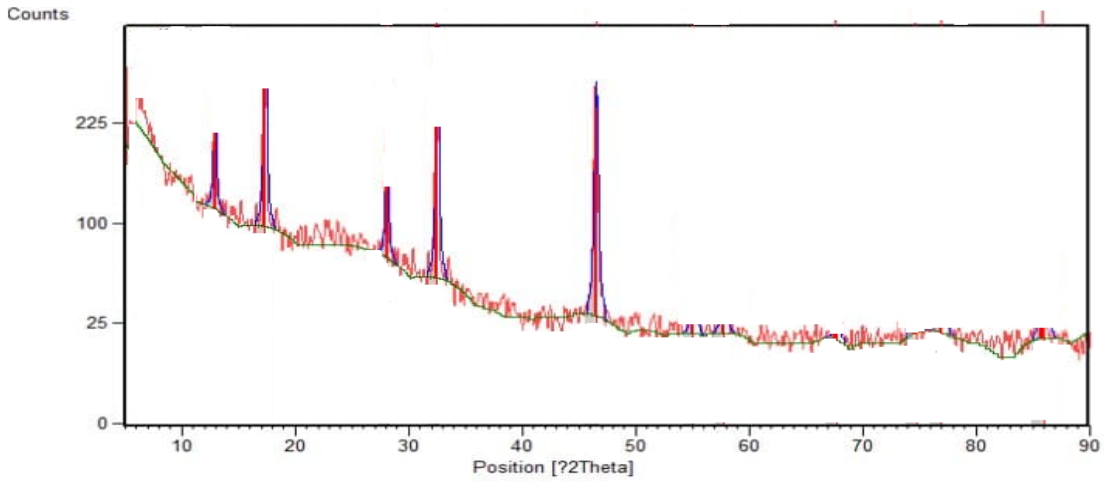

Figure6. X-ray diffraction of Quercetin nanoparticl

3.1.4. SEM analysis:

The size and crystalline properties of the produced NPs were studied by SEM examination. The QNPs' particle diameter was 17.25 nm at a flow rate of 8 ml/min. (Figure7).

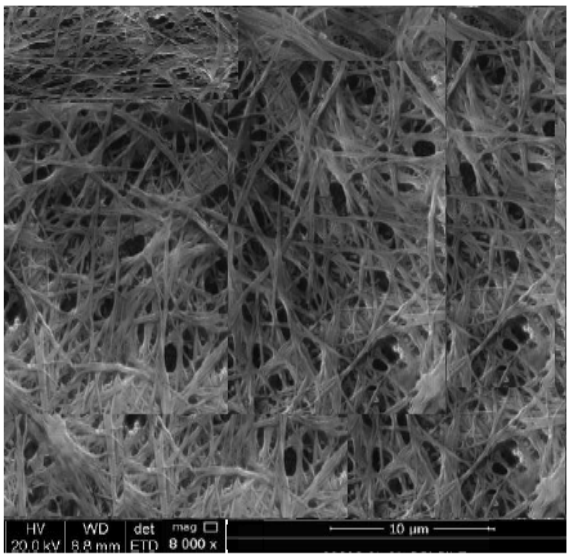

Figure7. SEM photographs of Quercetin nanoparticles at flow rate (8ml/ min)

3.2. Biological activities:

3.2.1. Antioxidant activity:

A Quantitative analysis of quercetin and quercetin nanoparticles using the DPPH radical-scavenging method was then performed. Antioxidant activity using DPPH increased in a focus-dependent manner. In comparison to Ascorbic acid, Quercetin nanoparticles had a lower IC50 value of 19.21 micrograms/ml (Table 1).

Table 1. Antioxidant activity of Quercetin and Quercetin nanoparticles, using DPPH free radical scavenging method

Conc.(µg/ml)	Quercetin	Quercetin nanoparticles	Ascorbic Acid
20	25.3 ±0.23	45.12 ± 1.21	42.12 ± 0.22
40	27.11 ± 1.12	56.11 ± 0.21	47.13 ± 1.10
60	33.54 ± 2.12	62.3 ± 0.13	50.4 ± 1.11
80	35.7 ± 1.11	64.1 ± 1.53	55.1 ± 0.03
100	40.31 ± 0.19	69.32 ± 2.44	56.312 ± 0.11
IC_{50}	55.05	19.21	31.16

3.3. Cytotoxic activity:

3.3.1. In-Vitro cytotoxicity assay:

Human hepatocellular liver carcinoma (Huh-7) and a normal liver cell (WISH) were used to test the cytotoxicity of quercetin and quercetin nanoparticles. For each cell line, IC50 value was used to determine the toxicity. On the whole, quercetin nanoparticles were cytotoxic to human hepatocellular liver carcinoma (Huh-7, IC50 8.35 g/mL) but showed significantly less toxicity towards normal cells (Table 2).

Table 2. Percentage cell survival of Quercetin and Quercetin nanoparticles different cell lines

Conc.(µg/ml)	Quercetin	Quercetin nanoparticles	WISH
	Huh-7		
0.0	2.000	1.068	1.160
12.5	1.868	0.600	1.891
25	1.659	0.415	1.531
50	1.222	0.325	1.375
100	1.232	0.222	1.291
IC_{50}	29.23	8.35	37.52

3.4. In-Vivo assay:

3.4.1. Biochemical analysis:

Earlier studies found that quercetin nanoparticles were highly effective against a liver cancer cell line (Huh-7). It was, therefore, decided to test the same cell line with quercetin nanoparticles *in-vivo*. The levels of AST (87.00 percent at 200 mg/kg.b.wt), ALT (50.00 percent at 200 mg/kg.b.wt), and albumin (317.11 at 200 mg/kg.b.wt) all showed dose-dependent anticancer activity (Table 3). The anticancer activity of quercetin nanoparticles (Figure 8) was confirmed by histopathology.

Table 3. In-vivo result of Quercetin and Quercetin nanoparticles

Parameter / Groups	AST	ALT	ALP
Control group (A)	83.50±1.500	50.67±0.27	312.23±1.182
Untreated group (B)	302.50±0.51	88.51±1.59	424.01±1.11
Treated group (C) Quercetin	91.00 ±1.01	67.01±1.01	397.21±1.02
Treated group (D) with Quercetin nanoparticles	87.00±1.21	50.00±1.05	317.11±1.11

(Mean±SD)

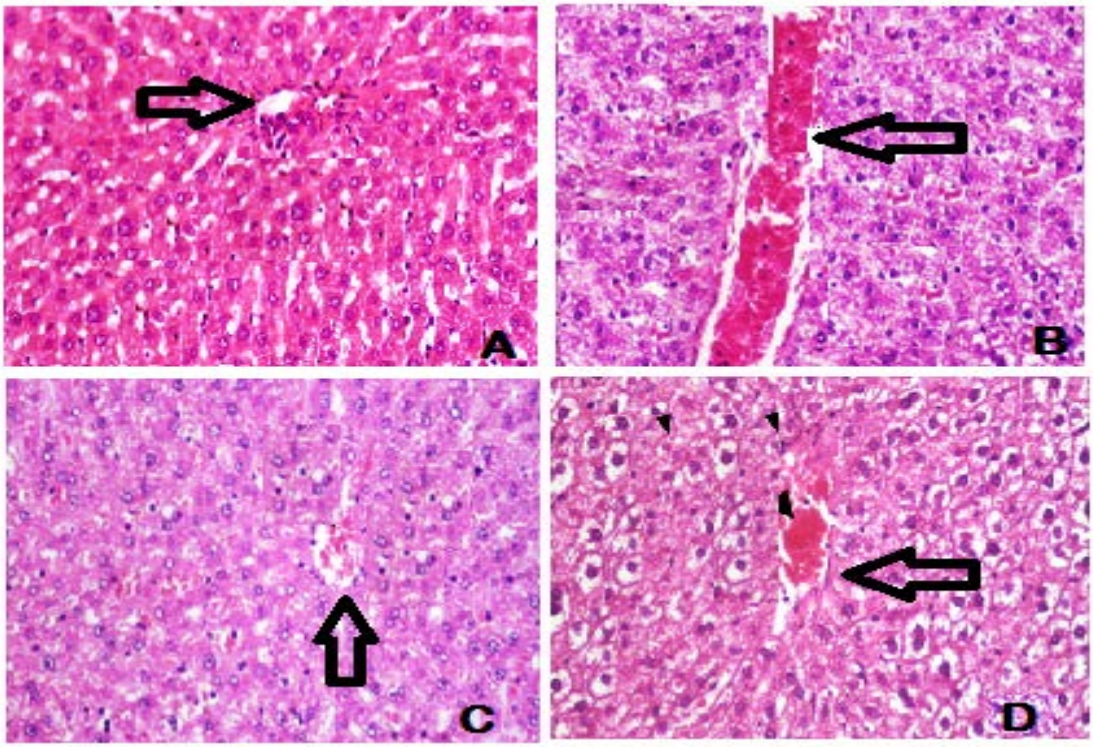

Figure 8: effect of Quercetin and Quercetin nanoparticles on livers section of different groups: **A)** of control rats revealed normal histological**; B)** induced control group (acrylamide) untreated with new compound; **C);** Experimental group treated with Quercetin and **D);** Experimental group treated with Quercetin nanoparticles.

3.5. Histopathological examination:

The hepatic lobules in the livers of rats in group 1 were found to be normal histologically (Figure 8A). Hepatocyte necrosis and fibroplasia were found in the portal triad in rats from group 2 (Figure 8B). Features include anaplastic carcinoma cells that are characterized by large hyperchromatic nuclei (Figure 8B). The quercetin treatment caused the acrylamide-induced rats to exhibit some nuclear pyknosis, granular and vacuolar degeneration, necrosis, and activation of Kupffer cells in the liver (Figure 8C).

Quercetin nanoparticle treated mice showed good restoration of the hepatic parenchymal cells with mild hepatocellular vacuolar degeneration and a few scattered necrotic cells (Figure 8D).

4. Conclusions

Quercetin is considered as one of the best naturally occurring flavonoids, consisting of several therapeutic properties, including anti-oxidative and anticancer (Butler MS. 2004) (Cho EJ *et al*., 2003). Despite having several therapeutic properties, quercetin shows low bioavailability. According to Ren K *et al*., (2017) QNPs displayed significant anticancer activity against, Hep3B, HCCLM3 and Bel7402MHCC97H (Ren K *et al*., 2017). To overcome the problem of bioavailability and solubility, we also synthesized QNPs and then compared the *in-vitro* and *in-vivo* anticancer and antioxidative properties of quercetin and its nanoparticle QNP. The results indicated that the QNPs have an advantage over quercetin molecules as the QNPs showed better antioxidative and anticancer activity in *in-vitro* and *in-vivo* studies in comparison with quercetin molecules.

References

Babu BH, Shylesh BS, Padikkala J. 2002. Tumour reducing and anticarcinogenic activity of Acanthus ilicifolius in mice. J. Ethnopharmacol., **79(1):**27-33

Bilati U, Allémann E, Doelker E. 2005. Development of a nanoprecipitation method intended for the entrapment of hydrophilic drugs into nanoparticles. Eur J Pharm Sc., **24(1):**67-75

Braca A, Sortino C, Politi M, Morelli I, Mendez J. **2002**. Antioxidant activity of flavonoids from Licania licaniaeflora. J. Ethnopharmacol., **79(3):**379-81.

Butler MS. 2004. The role of natural product chemistry in drug discovery. J. Nat. Prod.,**67(12):**2141-53

Cho EJ, Yokozawa T, Rhyu DY, Kim SC, Shibahara N, Park JC. 2003. Study on the inhibitory effects of Korean medicinal plants and their main compounds on the 1, 1-diphenyl-2-picrylhydrazyl radical. Phytomedicine. **10(6-7):**544-51.

Dai J, Nagai T, Wang X, Zhang T, Meng M, Zhang Q. 2004. PH-sensitive nanoparticles for improving the oral bioavailability of cyclosporine A. Int. J. Pharm., 280(1-2):229-40.

Exarchou V, Nenadis N, Tsimidou M, Gerothanassis IP, Troganis A, Boskou D. 2002. Antioxidant activities and phenolic composition of extracts from Greek oregano, Greek sage, and summer savory. J. Agric. Food Chem., **50(19):**5294-9.

Frenzel M, Steffen-Heins A. 2015. Impact of quercetin and fish oil encapsulation on bilayer membrane and oxidation stability of liposomes. Food Chem., **185**:48-57.

Houghton PJ, Photiou A, Uddin S, Shah P, Browning M, Jackson SJ, Retsas S. **1994.** Activity of extracts of Kigelia pinnata against melanoma and renal carcinoma cell lines. Planta med., **60(05)**:430-3.

Hsu CH, Cui Z, Mumper RJ, Jay M. 2003. Preparation and characterization of novel coenzyme Q10 nanoparticles engineered from microemulsion precursors. AAPS Pharm SciTech., **4(3):**24-35.

Inal ME, Kahraman A. 2000. The protective effect of flavonol quercetin against ultraviolet a induced oxidative stress in rats. Toxicology., **154(1-3)**:21-9

Kanadaswami C, Lee LT, Lee PP, Hwang JJ, Ke FC, Huang YT, Lee MT. 2005. The antitumor activities of flavonoids. In-vivo., **19(5)**:895-909.

Lee ES, Lee HE, Shin JY, Yoon S, Moon JO. 2003. The flavonoid quercetin inhibits dimethylnitrosamine-induced liver damage in rats. *J Pharm Pharmacol*., **55(8):**1169-74.

Manna K, Debnath B, Das M, Marwein S. 2016. A comprehensive review on pharmacognostical investigation and pharmacology of Typhonium trilobatum. J. Nat. Prod., **6(3):**172-8.

Omoregie ES, Oikeh EI. 2015. Comparative studies on the phytochemical composition, phenolic content and antioxidant activities of methanol leaf extracts of Spondias mombin and Polyathia longifolia. *Jordan J. Biol. Sci*., **147(3427):**1-5.

Prakash D, Gupta C, Sharma G. 2012. Importance of phytochemicals in nutraceuticals. *J. Chin. Med. Res*., **1(3)**:70-8.

Ren K, Li Y, Wu G, Ren J, Lu H, Li Z and Han X: 2017.Quercetin nanoparticles display antitumor activity via proliferation inhibition and apoptosis induction in liver cancer cells. Int J Oncol., **50**: 1299-1311,

Salatin S, Barar J, Barzegar-Jalali M, Adibkia K, Kiafar F, Jelvehgari M. 2017. Development of a nanoprecipitation method for the entrapment of a very water soluble drug into Eudragit RL nanoparticles. Res Pharm Sci., **12(1**):1

Shikov AN, Tsitsilin AN, Pozharitskaya ON, Makarov VG, Heinrich M. 2017. Traditional and current food use of wild plants listed in the Russian Pharmacopoeia. Frontiers in pharmacology., **8**:841

Vichai V, Kirtikara K. 2006. Sulforhodamine B colorimetric assay for cytotoxicity screening. Nature prot., **1(3)**:1112-6

JJBS

Volume 16, Number 1,March 2023
ISSN 1995-6673
Pages 125 – 130
https://doi.org/10.54319/jjbs/160115

Jordan Journal of Biological Sciences

Cultivation of Edible Ectomycorrhizal Mushrooms (*Phelobopus portentosus*) Associated with *Sesbania javanica* Miq

Thalisa Yuwa-amornpitak*, Luchai Butkhup, Pa-Nag Yeunyaw,Kannika Chookietwattana

[1]*Department of Biotechnology, Faculty of Technology, Mahasarakham University, Kantharawichai,Maha Sarakham, 44150 Thailand*

Received: July 16, 2022; Revised: September 28, 2022; Accepted: October 27, 2022

Abstract

Phlebopus portentosus is a popular wild edible mushroom that is found growing on both forest trees and fruit trees. Because it can grow either with various trees or without a host tree, it is reported that it is not a mycorrhizal fungus and may not be an obligate ectomycorrhizae. Furthermore, it was recognized that *P. portentosus* can be found in association with leguminous plants, such as *Sesbania javanica* Miq. The aims of this study were to cultivate *P. portentosus* with bioinoculants in solid and liquid forms and track the ectomycorrhizal association with *Sesbania javanica* Miq. A pure mycelium culture of this fungus was isolated, and the growth parameters, temperature, medium pH, and types of medium were examined. The mycelium grew very well on synthetic media such as MPDA and YM. The optimum pH and temperature were pH 4 and 30^{o}C, respectively. Bioinoculants of *P. portentosus* were inoculated on seedbeds of *Sesbania javanica* Miq. After inoculation, ectomycorrhizal-like roots were found at 6 months, and sporocarps were found at 8.5 months. To prove this, the ITS rDNA sequences were aligned, and the results revealed that all sequences of the ectomycorrhizal-like root tips and sporocarps that developed on seedbeds of S. *javanica* Miq. and black bolete used as a bioinoculant were 100% identical to those of *P. portentosus* MN962534 (GenBank database). This finding indicates that *P. portentosus* can form ectomycorrhizae with *S. javanica* Miq.

Keywords: ectomycorrhiza, edible mushroom, symbiosis, cultivation, ITS region, *Phelebopus portentosus*, *Sesbania javannica* Miq.

1. Introduction

Worldwide, approximately 2.2-3.8 million species are included in the fungus kingdom (Howksworth and Lücking, 2017), while only 35,000 species produce macroscopic fruiting bodies (He et al., 2019). Mycelium fungi that can form fruiting bodies are called “mushrooms.” Mushrooms consist of various types with different shapes, colors, and sizes. In addition to their varied morphology, mushrooms also have various habitats: belowground, aboveground, and saprophytes. Most below-ground and above-ground mushrooms are ectomycorrhiza (ECM). Ectomycorrhizal mushrooms are mostly symbiotic with woody plants. In temperate regions, ECM are associated with many species including birch, spruce, beech, willow, pine, fir, poplar, and oak. The Dipterocarpaceae species in Southeast Asia are mostly mutualistic with ECM. Both the plant and fungus benefit from each other. In addition to protecting against plant root diseases and providing drought resistance, fungi help plants to absorb more nutrients and water. In turn, the plants provide carbohydrates and growth factors to the fungi (Smith and Read, 2008).

Edible mushrooms have been used as food for a long time because they are rich in protein, vitamins, and minerals. Essential amino acids that humans cannot synthesize are found in mushrooms such as *Pleurotus ostreatus* (Chirinang and Intarapichet, 2009), *Agaricus bisporus*, *Boletus edulis* (Jaworska and Bernaś, 2013), and in wild edible mushrooms (Yuwa-amornpitak et al., 2020). Aside from their nutritional value, mushrooms are a source of bioactive compounds with antimicrobial (Titilawo et al., 2022; Muhsin et al., 2011) and anticancer (Oyetayo et al., 2013) properties.

P. portentosus is placed in the Boletinellaceae family and is distributed in tropical regions in Asia (Watling R.,2001). It is found in the central, northern, and northeastern parts of Thailand and is also found in China (Zhang et al., 2017), Laos (Mortimer et al., 2012), Myanmar (Zhang et al., 2015), and Sri Lanka (Berkeley and Broome, 1873). The fruiting bodies of *P. portentosus* mostly form on the ground under trees during the rainy season. The fungus can form associations with various tree species, such as *Mangifera indica*, *Dimocarpus longan*, *Elaeocarpus hygrophilus*, *Syzygium cumini*, Quercus spp., and *Minosa pigra*. With a good texture and rich nutritional value (Zhang, 2010), *P. portentosus* is a tasty wild edible mushroom that appeals to local people and mushroom hunters. Furthermore, *P. portentosus* contains high concentrations of bioactive compounds, such as phenolic compounds (Kaewnarin et al., 2016); pyrrole alkaloids (phlebopines); 2-[2-forml-5-(methoxy methyl)-1H-pyrrole-1-yl] propanoate; inotopyrrole B; and 1-isopentyl-2-formyl-5-hydroy-methylpyrrole (Hou et al., 2014). Sun et al. (2018) also found that inotopyrrole B exhibits

* Corresponding author. e-mail: ythalisa@yahoo.com.

neuroprotective effects against hydrogen peroxide-induced neuronal-cell damage in human neuroblastoma SH-Sy5Y cells.

In contrast to other wild edible ectomycorrhizal mushrooms, *P. portentosus* is associated with various tree species, not only with forest trees but also with fruit trees. Kumla et al. (2016) also reported that *P. portentosus* has the ability to form ECM-like structures in *Pinus kesiya* after 1 year of inoculation with fungal mycelium. Furthermore, it can be produced as basidiomes without a host plant, and this method shows an ability to produce basidiomes 2 years after original isolation from tissues (Kumla et al., 2012). Zhang et al. (2017) reported that *P. portentosus* creates a tripartite association with mealy bugs and roots. The fungus has a symbiotic association with soil mealy bugs and creates special fungus-insect galls. The galls grow on plant roots with parasitic habits. Fang et al. (2020) reported that mealy bugs excreted honeydew inside or outside the galls. Honeydew is rich in amino acids and sugars that promote mycelial growth. An annual plant such as *Sesbania javannica* Miq., is also found on the seedbedalong with *P. portentosus*. However, there are no reports on the association between them.

The objectives of this study were to cultivate and examine the association of black bolete with *Sesbania javannica* Miq. by using two types of bioinoculants (solid and liquid bioinoculants). The mycelium growth parameters were studied and used as growth conditions to propagate solid bioinoculants in sorghum grains. To prove the association of the fungus with the root tree, the sequences of the ITS region from black bolete, ECM from *Sesbania javannica* Miq. root, and sporocarps on the seedbed were aligned.

2. Materials and methods

2.1. Pure mycelium isolation

Basidiocarps of *P. portentosus*(black bolete) were purchased from a local market in Maha Sarakham Province in the rainy season (May-October 2019-2020). A pure mycelium culture was isolated from fresh sporocarps using aseptic techniques by cutting a small piece and transferring it onto a modified potato dextrose agar plate, MPDA (potato juice extract from 200 g boiling in water 1 liter for 30 min, glucose 20 gl^{-1}, yeast extract 2 gl^{-1}, peptone 2 gl^{-1}, malt extract 3 gl^{-1}, agar 20 gl^{-1}). The plates were incubated at 30^{o}C until the mycelia growth fully covered the plate. The pure culture was transferred onto a new medium plate after 3-4 weeks of age for further study.

2.2. Growth study

The temperature, initial pH of the medium, and types of media were the important parameters for fungal growth. In this study, temperatures ranging from 25^{o}C to 35^{o}C, pH levels ranging from 4 to 9, and three medium types were investigated: MPDA, YM (yeast malt agar; glucose 10 gl^{-1}, yeast extract 3 gl^{-1}, peptone 5 gl^{-1}, malt extract 3 gl^{-1}, and agar 20 gl^{-1}), and starch medium (starch 10 $gl^{-1}$and agar 20 gl^{-1}). One piece of fungus mycelium (diameter 0.5 cm) was transferred from the inoculum plate (mycelium on YM agar plate) to the center of a new plate and incubated at 30^{o}C. Each studied parameter had three replicates. The growth diameters of the fungi were measured and analyzed.

2.3. Solid bioinoculant preparation

A solid bioinoculant was prepared from the mycelium growth on sorghum grains. Sterilized sorghum grains were prepared by soaking in water for 3-5 h or overnight, decanting and cleaning. Sorghum grains were boiled until the grains were softened, and the water was decanted. The grains were used to fill containers (plastic bags or bottles) after they had cooled down. After that, they were sterilized at 121^{o}C for 15 min in an autoclave sterilizer. Then, 1-2 pieces of fungus mycelium were aseptically transferred (Figure 1-A) to a container with sorghum grains and incubated at 30^{o}C until the mycelium covered the sorghum grains (3-4 weeks, Figure 1-B).

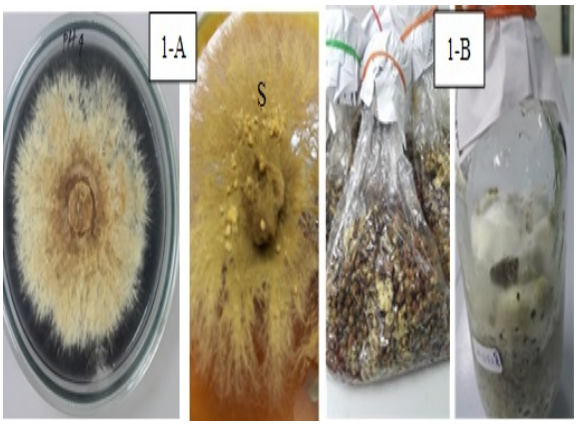

Figure 1. Bioinoculant of *P. portentosus* (black bolete) on sorghum grains**:**1-A shows mycelium growth on an agar plate with and without activated charcoal;1-B shows mycelium growth on sorghum grains used as a bioinoculant.S in Fig. 1-A represents sclerotia

2.4. Liquid bioinoculant preparation

Fresh and mature *Phebopus portentosus* sporocarps were used as spore suspension inocula (liquid bioinoculants). The sporocarps were pulverized with clean water. Mushroom debris was separated by sieving through a strainer for a long period. The spore suspension was placed in a bottle and kept at room temperature. If the liquid bioinoculant was immediately used, there was no need to remove the debris. The sporocarps could be separated by pulverizing only the tubes (spores are present inside these parts) to provide a high spore density.

2.5. Plantation and inoculation with bioinoculants

The planting area was prepared by tilling, removing weeds, constructing three seedbeds (1 m x 6 m), and adding organic matter such as compost. *S. javannica* Miq. seeds were immersed in water overnight, decanted and cleaned before sowing. The seeds were sown on the seedbeds, covered with rice stalks and watered twice a day. When the plants were at least 50 cm tall, the soil around the roots was carefully removed (plant roots were not disturbed) to reveal the plant roots, and *P. portentosus* bioinoculants on sorghum grains and liquid bioinoculants were inoculated on the roots of *S. javannica* Miq., then covered with soil, compost, rice stalks, and watered. For the spores to germinate and mycelia to grow, the seedbeds were not watered after 2 or 4 days of inoculation. The seedbeds were still watered twice each day, and compost and rice stalks were regularly added.

2.6. ECM on plant roots and fruiting bodies on seedbeds

Plant roots of *S. javannica* Miq. were sampled from the seedbeds by using four randomly selected samples per seedbed after inoculation for 4, 5 and 6 months. Samples were kept in plastic bags and stored in a refrigerator until examination under a stereomicroscope (Olympus SZ61, Japan). Soil and debris were removed from the samples by cleaning with water. The ECM-root-like structures at the fine root tips were kept in absolute ethanol and stored in a refrigerator.

Fruiting bodies on the seedbeds, including plant roots near or connecting to the fruiting bodies, were collected. Small pieces of mushroom were cut and kept in absolute ethanol and stored in a refrigerator. Plant roots were kept in plastic bags and stored in a refrigerator. Plant root tips were examined for ectomycorrhizal-root-like interactions under a stereomicroscope. The ECM-root-like morphological descriptions followed Agerer (1987-1998).

2.7. DNA extraction and sequencing

DNA was extracted from mushroom (*P. portentosus*) samples obtained from the local market, fruiting bodies from seedbeds, and ECM-root-like structures that were kept in absolute ethanol. Ethanol was removed from the samples until they dried. DNA was ground with a micropestle and extracted with a DNA preparation kit (Vivantis, GF1). The internal transcribed spacer of the nuclear ribosomal repeats (ITS1 and ITS2) was amplified from the genomic DNA using the forward primer, ITS5 (‘5-GGAAGTAAAAGTCGTAACAAGG-3’) and reverse primer ITS4 (‘5’-TCCTCCGCTTATTGATATGC-3’) (White et al., 1990). The PCR mixture contained 1 µl of DNA template, 1 µl of each primer at a concentration of 20 pmol/µl, 12 µl of master mix with Taq DNA polymerase (Vivantis), and deionized water in a total volume of 25 µl. The PCR conditions were performed by using a DNA thermal cycler (FINEMOULD PRECISION IND.CO, South Korea) as follows: initial denaturation at 94^{o}C for 3 min, followed by 30 cycles of denaturation at 94^{o}C for 40 s, annealing at 55^{o}C for 40 s, and extension at 72^{o}C for 1 min. A final extension to complete the unfinished strands was performed at 72^{o}C for 7 min. The PCR products of the ITS region were sequenced by the Sanger Coulson’s method (Sanger et al., 1980) using an ABI BigDye Terminator v3.1 Cycle Sequencing Kit (Applied Biosystems).

2.8. Molecular identification

To identify the ECM-root-like structures (at the fine root tips of *S. javannica* Miq.) that developed from the *P. portentosus* bioinoculant, the sequences of the ECM-root-like, mushrooms collected from seedbeds and sporocarps of *P. portentosus* samples obtained from the local market were searched for the most similar sequences by using the BLASTn tool in the GenBank database (https://blast.ncbi.nlm.nih.gov/Blast). After that, their sequences were aligned again with the most similar sequences retrieved from the GenBank database by Clustal Omega (https://www.ebi.ac.uk/Tools/msa/clustalo/).

2.9. Statistical analysis

One-way analysis of variance (ANOVA) in SPSS version 23 for Windows (SPSS Inc., Chicago, Illinois) was used to analyze the data. Duncan’s multiple range test was used to determine the significant differences ($p \leq 0.05$) between treatments from three replicates of each experiment.

3. Results

3.1. Effects of medium type, temperature, and initial pH on mycelial growth

The growth of pure mushroom mycelia on three media types (MPDA, YM, and starch medium) at 30^{o}C was studied. It was found that mycelia could use these media well. However, MPDA and YM produced the best growth, and the mycelia grew throughout the plate at 20 days (Figure 2-A). Furthermore, *P. portentosus* can be grown on starch medium at approximately 60% of the growth on MPDA and YM. The results indicate that all three media can be used as C-sources. However, MPDA and YM contained glucose that the fungus could use directly. Because fungi in the starch medium must synthesize and secrete enzymes to hydrolyze starch into glucose, the growth in the starch medium was slower than that in MPDA and YM. Furthermore, the growth of the fungus in MPDA and YM was nearly the same. Then, YM was chosen for pH and temperature growth studies because it is a synthetic culture medium that is commonly used for microbial growth and is easy to prepare.

Temperatures of 25, 30, and 35^{o}C were used for the mycelium growth study. Growth was assessed as the mycelium diameter on YM agar plates (Figure 2-B). The results indicated that the highest growth occurred at 30^{o}C with a nearly full plate at Day 20. The fungal growth amounts at temperatures of 25°C and 35°C were lower than that at 30^{o}C. Furthermore, mycelial growth at 25^{o}C was faster than that at 35^{o}C. At Day 20, the mycelial growth amounts at 25^{o}C, and 35°C were approximately 48% and 24% of the growth at 30°C, respectively. These results indicated that 30^{o}C was the optimum temperature for mycelium growth of *P. portentosus*.

The effects of the initial medium pH on black bolete growth were examined on YM medium at 30^{o}C. The mycelium growth diameters at various pH values are shown in Figure 2-C. The results indicated that the mycelia of the fungus grew well for a wide range of pH values from 4-9. However, mycelia slowly grew at pH 5-9, and growth clearly declined at pH 9. This study concluded that a medium at pH 4 was optimum for mycelium growth of the fungus.

Figure 2. Effects of *P. portentosus* growth on various media (2-A), various temperatures (2-B), and various pH values (2-C). Data are presented as the means, and the error bar for each graph indicates the ± standard deviation based on three replicates. Each graph's different letters for the same factors indicate significant differences ($p \leq 0.05$).

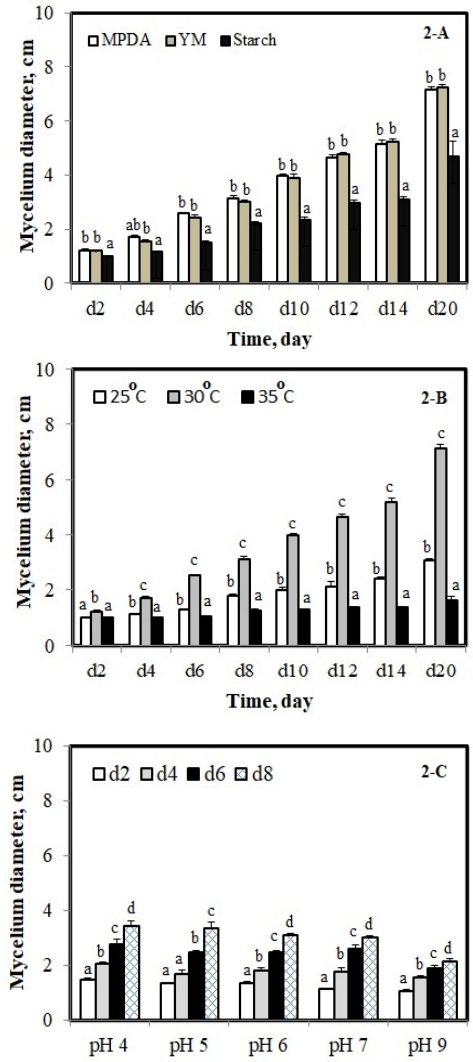

3.2 Plant–fungus colonization

Root tips of *S. javannica* Miq. were examined for ectomycorrhizal root-like structures under a stereomicroscope by obtaining samples from the seedbeds after inoculation for 4, 5, and 6 months. It was discovered that at month 6, the morphologies of some plant root tips developed ectomycorrhizal root-like structures. After that, the plant's root system was not disturbed when adding compost and covering it with rice stalks. The soil should contain some moisture all day and should not be flooded for a long period. Finally, sporocarps appeared at month 8.5 (Figure 3-B). In the morphology study, the sporocarps were bolete, and the caps and stalks were colored plain brown. Tube trama (hymenophoral) or pores where spores were produced were present under the caps. The mushroom color may be dark brown depending on the color of the soil and the environmental stage of the mushrooms (the mature stage has a darker-brown color than the early stage). Clamp connections were commonly found in basidiomycetes and were also found in this mushroom mycelium. Its spores were oval in shape. The caps of the sporocarps were soft. Ectomycorrhizae that colonized at the root tips and were connected to the mushrooms are shown in Figure 3-A. The ECM root tips were not branched, and their surface aggregates formed loose mycelial strands, as shown in Figures 3-C and 3-D. The root tip colors of the ECM were brown and dark brown.

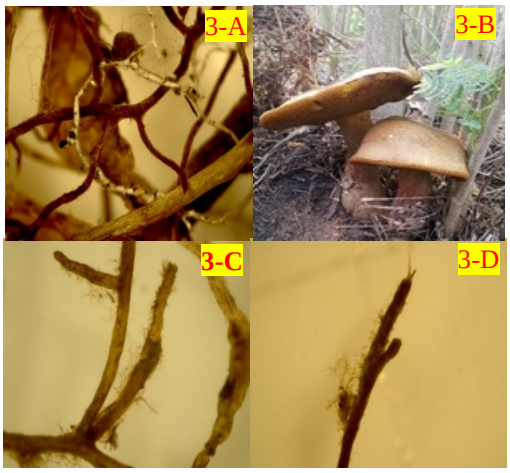

Figure 3. Ectomycorrhizae colonization associated with the plant root tips of *S. javannica* Miq. (3-A), fruiting bodies on the seedbed (3-B) at 8.5 months after inoculation, and ectomycorrhizal-like root tips (3-C and 3-D) from plant roots

3.2 Molecular Identification

To confirm that the ectomycorrhizal root tips and sporocarps on the seedbeds of *S. javannica* Miq. were the same species as the fruiting bodies of *P. portentosus* (black bolete), their ITS rDNA sequences were aligned together with sequences retrieved from GenBank using Clustal Omega. The results showed that the ITS sequences of the fruiting bodies that developed on the seedbeds and the ectomycorrhizal root tips connected to the sporocarps were 100% identical to those of *P. portentosus* MN962534 (GenBank database), as shown in Figure 4, including the black bolete sequence with 730 base pairs that was used as a bioinoculant. This finding indicated that the *P. portentosus* bioinoculant can associate with the root tips of *S. javannica* Miq. and develop sporocarps. Even though this method takes a long time (8.5 months) for fruiting body development, it is the most sustainable method to cultivate edible ectomycorrhizal mushrooms. This technique can be used in mass production and can control mushroom production by adding biofertilizer and watering.

```
P._portentosus(MN962534)    cattatcgaaagcacaaagtccgaaggggggaaaaaaaagagggtgatgctaggtgggac  60
Fruiting_body               cattatcgaaagcacaaagtccgaaggggggaaaaaaaagagggtgatgctaggtgggac  60
ECMlike                     cattatcgaaagcacaaagtccgaaggggggaaaaaaaagagggtgatgctaggtgggac  60
Black_bolete                cattatcgAaagcacaaagtccgaaggggggaaaaaaaagagggtgatgctaggtgggac  60
                            ************************************************************

P._portentosus(MN962534)    gactgtcgctggcatatatcgtatgcatgtgcacgtcgaaaccttggctcgccccttctc  120
Fruiting_body               gactgtcgctggcatatatcgtatgcatgtgcacgtcgaaaccttggctcgccccttctc  120
ECMlike                     gactgtcgctggcatatatcgtatgcatgtgcacgtcgaaaccttggctcgccccttctc  120
Black_bolete                gactgtcgctggcatatatcgtatgcatgtgcacgtcgaaaccttggctcgccccttctc  120
                            ************************************************************

P._portentosus(MN962534)    ctttcggcgtaatgcttaatacacctgtgaacctgttgtaggttgttcccctacgagcag  180
Fruiting_body               ctttcggcgtaatgcttaatacacctgtgaacctgttgtaggttgttcccctacgagcag  180
ECMlike                     ctttcggcgtaatgcttaatacacctgtgaacctgttgtaggttgttcccctacgagcag  180
Black_bolete                ctttcggcgtaatgcttaatacacctgtgaacctgttgtaggttgttcccctacgagcag  180
                            ************************************************************

P._portentosus(MN962534)    taggaggacgatctatgtctttccatcacactacatgtatgtctacagaacgttgaaagt  240
Fruiting_body               taggaggacgatctatgtctttccatcacactacatgtatgtctacagaacgttgaaagt  240
ECMlike                     taggaggacgatctatgtctttccatcacactacatgtatgtctacagaacgttgaaagt  240
Black_bolete                taggaggacgatctatgtctttccatcacactacatgtatgtctacagaacgttgaaagt  240
                            ************************************************************

P._portentosus(MN962534)    cgtctcgacccttgacggggttggacgcaaaactataatacaacttttcagcaacggatct  300
Fruiting_body               cgtctcgacccttgacggggttggacgcaaaactataatacaacttttcagcaacggatct  300
ECMlike                     cgtctcgacccttgacggggttggacgcaaaactataatacaacttttcagcaacggatct  300
Black_bolete                cgtctcgacccttgacggggttggacgcaaaactataatacaacttttcagcaacggatct  300
                            ************************************************************

P._portentosus(MN962534)    cttggctctcgcatcgatgaagaacgcagcgaattgcgataagtaatgtgaattgcagat  360
Fruiting_body               cttggctctcgcatcgatgaagaacgcagcgaattgcgataagtaatgtgaattgcagat  360
ECMlike                     cttggctctcgcatcgatgaagaacgcagcgaattgcgataagtaatgtgaattgcagat  360
Black_bolete                cttggctctcgcatcgatgaagaacgcagcgaattgcgataagtaatgtgaattgcagat  360
                            ************************************************************

P._portentosus(MN962534)    tttcagtgaatcatcgaatctttgaacgcaccttgcgctccttggtattccgaggagcat  420
Fruiting_body               tttcagtgaatcatcgaatctttgaacgcaccttgcgctccttggtattccgaggagcat  420
ECMlike                     tttcagtgaatcatcgaatctttgaacgcaccttgcgctccttggtattccgaggagcat  420
Black_bolete                tttcagtgaatcatcgaatctttgaacgcaccttgcgctccttggtattccgaggagcat  420
                            ************************************************************

P._portentosus(MN962534)    gcctgtttgagtgtcatcgaattctcaaccatgtcttgatgttaactttcgaggcatggc  480
Fruiting_body               gcctgtttgagtgtcatcgaattctcaaccatgtcttgatgttaactttcgaggcatggc  480
ECMlike                     gcctgtttgagtgtcatcgaattctcaaccatgtcttgatgttaactttcgaggcatggc  480
Black_bolete                gcctgtttgagtgtcatcgaattctcaaccatgtcttgatgttaactttcgaggcatggc  480
                            ************************************************************

P._portentosus(MN962534)    ttggacttgggagctttgctggttggaccccccctctcttcgaggggggaatgtcagctct  540
Fruiting_body               ttggacttgggagctttgctggttggaccccccctctcttcgaggggggaatgtcagctct  540
ECMlike                     ttggacttgggagctttgctggttggaccccccctctcttcgaggggggaatgtcagctct  540
Black_bolete                ttggacttgggagctttgctggttggaccccccctctcttcgaggggggaatgtcagctct  540
                            ************************************************************

P._portentosus(MN962534)    cctcaaaagcattagcaaaagggacgtgttcgtcgcatgaactgacggccttcgacgtga  600
Fruiting_body               cctcaaaagcattagcaaaagggacgtgttcgtcgcatgaactgacggccttcgacgtga  600
ECMlike                     cctcaaaagcattagcaaaagggacgtgttcgtcgcatgaactgacggccttcgacgtga  600
Black_bolete                cctcaaaagcattagcaaaagggacgtgttcgtcgcatgaactgacggccttcgacgtga  600
                            ************************************************************

P._portentosus(MN962534)    taatgatcgtcgtggctggaggggaaaagtgtgatggcgaaggtctgtcctagcttctaat  660
Fruiting_body               taatgatcgtcgtggctggaggggaaaagtgtgatggcgaaggtctgtcctagcttctaat  660
ECMlike                     taatgatcgtcgtggctggaggggaaaagtgtgatggcgaaggtctgtcctagcttctaat  660
Black_bolete                taatgatcgtcgtggctggaggggaaaagtgtgatggcgaaggtctgtcctagcttctaat  660
                            ************************************************************

P._portentosus(MN962534)    caaaggcgaggggcttgtgtcacgcatgccctctgtcttatcgaaccttgacctcaaatc  720
Fruiting_body               caaaggcgaggggcttgtgtcacgcatgccctctgtcttatcgaaccttgacctcaaatc  720
ECMlike                     caaaggcgaggggcttgtgtcacgcatgccctctgtcttatcgaaccttgacctcaaatc  720
Black_bolete                caaaggcgaggggcttgtgtcacgcatgccctctgtcttatcgaaccttgacctcaaatc  720
                            ************************************************************

P. portentosus (MN962534)   aggtaggact                                                  730
Fruiting_body               aggtaggact                                                  730
ECMlike                     aggtaggact                                                  730
Black_bolete                aggtaggact                                                  730
                            **********
```

Figure 4. Sequence alignments of ITS rDNA of ectomycorrhizal-like root tips, sporocarps from the seedbeds of *S. javannica* Miq. (fruiting body), and black bolete (bioinoculum) with 100% identity to *P. portentosus* (MN962534), as determined by Clustal Omega

4. Discussion

Kumla et al. (2011) reported that *P. portentosus* mycelia were able to grow between pH 3-9 and grew well at pH 4. The optimal temperature was 30^{o}C, and there was no growth at 40^{o}C. They also found that modified Murashige & Skoog (MMS) and fungal host media were best for mycelium growth. Sanmee et al. (2010) found that *P. portentosus* mycelia grew well on modified Gamborg, modified Melin Norkans and MS media at 30^{o}C and pH 4. Kumla et al. (2020) found that *P. spongiosus* mycelia grew well on L-modified Melin-Norkans and Murashige and Skoog agar at 30^{o}C at an initial pH of 5. Siri-in et al. (2014) studied the growth conditions of pure *Scleroderma sinnamariense* mycelia. The optimal temperature and pH were 30^{o}C and 5, respectively. The results of our study on temperature and pH agree with the studies of Kumla et al. (2011) and Sanmee et al. (2010). According to Kumla et al. (2011), Sanmee et al. (2010) and this study, *P. portentosus* could grow well in various types of media. However, this study found that *P. portentosus* mycelia could grow well on common media, such as MPDA and YM. Thus, YM was chosen for the growth study and used as the inoculum media to prepare bioinoculants from sorghum grains. This was done because this approach is not complicated, and the medium is easy to prepare.

The features of the ECM root tips examined in this study are similar to those of the ECM root tips of *P. portentosus* on *Pinus kesiya* (Sanmee, et al., 2010). Further study by the same group reported by Kumla et al. (2016) confirmed the mutualistic relationship between *P. portentosus* and Pinus trees by using carbon ($^{13}C/^{12}C$) and nitrogen ($^{15}N/^{14}N$) isotopes measurements. Based on carbon assimilation studies, ECM fungi derive simple sugars from plant photosynthesis, while saprotrophic fungi obtain sugars from wood decay. Nitrogen from soil was absorbed by ECM fungi and transferred to their host plants. In contrast, saprotrophic fungi obtained nitrogen from decaying substrates (Hobbie et al., 1999). Although the lifestyle of *P. portentosus* is also found in saprophytic habits, it was proven that it was cultivated without a host plant (Sanmee et al. 2010, Ji et al. 2011). However, the ITS region of the rDNA sequence is a popular tool used for fungal identification. In this study, sporocarps that developed in seedbeds were of the same species as both the bioinoculants and ECM-root-like structures. These results confirmed that *P. portentosus* can be associated with an annual plant and that it is an ectomycorrhizal fungus. Because it can develop ECM-root structures, *P. portentosus* is a special species because it can adapt its lifestyle to be a saprophyte or ectomycorrhiza depending on the environment.

5. Conclusions

Attempts to overcome the difficulties associated with ECM mushroom cultivation are very challenging endeavors. This study demonstrated that bioinoculants of sorghum (pure mycelia) and liquid-formed (spores from mature sporocarps) have the potential to colonize the fine root tips of *S. javannica* Miq. Furthermore, the findings also prove that *P. portentosus* is an ectomycorrhizal mushroom and has a symbiotic association with the fine roots of *S. javannica* Miq. *P. portentosus* is a boletus

mushroom that may not be an obligate ECM. The host plants of the fungus are not only woody plants and fruit trees but also annual plants such as *S. javannica* Miq. However, to succeed in cultivating ectomycorrhizal mushrooms, biofertilizer and watering are needed.

Acknowledgments

This study was supported by grants from the Biodiversity-based Economy Development Office (Public Organization, BEDO) based on the plant genetic conservation project under the Royal Initiative of Her Royal Highness Princess Maha Chakri Sirindhorn**.** Mahasarakham University and the Faculty of Technology are thanked for providing facility support.

References

Agerer R. 1987-1998. Color atlas of ectomycorrhizae: 1st – 11th edn. Einhorn, Schwäbisch Gmünd.

Berkeley MJ and Broome CE. 1873. Enumeration of the Fungi of Celon. Part II., containing the remainder of the Hymenomycetes, with the Remaining Established Tribes of Fungi. J. Linnean Soc. London, Bot., 14 (73): 29-64.

Chiriang P and Intarapichet K. 2009. Amino acids and antioxidant properties of the oyster mushrooms, *Pleurotus ostreatus* and *Pleurotus sajor-caju*. Sci. Asia. 35(4): 326-331.

Fang YW, Wang WB, He MX, et al. 2020. Relationship between the honeydew of mealy bugs and growth of *Phlebopus portentosus*. PLOS ONE. 15(6): e0233710. https://doi.org/ 10.1371/journal.pone.

He MQ, Zhao RL, Hyde KD, Begerow D, Kemler M, Yorkov A, McKenzie HHC, et al. 2019. Notes, outline and divergence times of Basidiomycota. Fungal Divers., 99: 105-367.

Hobbie EA, Macko Sa and Shugart HH. 1999. Insights into nitrogen and carbon dynamics of ectomycorrhizal and saprotrophic fungi from isotopic evidence. Oecologia. 118: 353-360.

Hou Y, Ding X, Hou W, Song B, Wang T, Wang F, Li J, Zeng Y, Zhong J, Xu T, et al. 2014. Pharmacological evaluation for anticancer and immune activities of a novel polysaccharide isolated from *Boletus speciosus* Frost. Mol. Med. Rep. 9:1337-1344. Online DOI: 10.3892/mmr.2014.1976.

Howksworth DL and Lücking R. 2017. Fungal diversity revisited: 2.2 to 3.8 million species. Microbiol. Spectr., 5(4). doi: 10.1128/microbiolspec.FUNK-0052-2016.

Jaworska G and Bernas E. 2013. Amino acid content of frozen *Agaricus bisporus* and *Boletus edulis* mushrooms: effects of pretreatments. Inter. J. Food Prop. 16:139-153.

1532-2386 online DOI: 10.1080/10942912.2010.526278

Ji KP, Cao Y, Zhang C, He M, Lui J, Wang W and Wang Y. 2011. Cultivation of *Phlebopus portentosus* in southern China. Mycol. Pro. 10:293-300.

Kaewnarin K, Suwannarach N, Kumla L and Lumyong S. 2016. Phenolic profile of various wild edible mushroom extract from Thailand and their antioxidant properties, anti-tyrosinase and hyperglycaemic inhibitory activities. J. Funct. Foods., 27: 352-364.

Kumla J, Danell E, Bussaban B and Lumyong S. 2011. Suitable growth conditions and nutrition factors on *in vitro* culture of *Phlebopus portentosus* (Boletales). Chiang Mai J. Sci., 38(1): 156-159.

Kumla J, Bussaban B, Suwannarch N and Lumyong S. 2012. Basidiome formation of an edible wild, putatively ectomycorrhizal fungus, *Phlebopus portentosus*without host plant. Mycologia., 104(3): 597-603.

Kumla J, Hobbie EA, Suwannarach N and Lumyong S. 2016. The ectomycorrhizal status of a tropical black bolete, *Phlebopus portentosus*, assessed using mycorrhizal synthesis and isotopic analysis. Mycorrhiza., 26: 333-343. https;//link.springer.com/article/10.1007/s00572-015-0672-1

Kumla J, Suwannarach N and Lumyong S. 2020. A new report on edible tropical bolete, *Phlebopus spongiosus* in Thaialand and its fruiting formation without the need for a host plant. Mycobiology. 48(4):263-275.

Mortimer PE, Karunarathna SC, Li QH, Gui H, Yang XO, Yang XF et al. 2012. Prized edible Asia mushrooms: ecology, conservation and sustainability. Fung. Divers., 56(1): 31-47.

Muhsin TM, Al-Duboon AHA and Khalaf KT. 2011. Bioactive compounds from a polypore fungus *Ganoderma applanatum* (Per s. ex Wallr.) Pat. Jordan J. Biol. Sci. 4(4): 205-212.

Oyetayo VO, and Ariyo OO. 2013. Micro and Macronutrient properties of *Pleurotus ostreatus* (Jacq:Fries) cultivated on different wood substrates. Jordan J. Biol. Sci. 6(3): 223-226.

Sanger F, Coulson AR, Barrell BG, Smith AJ and Roe BA. 1980. Cloning in single-stranded bacteriophage as an aid to rapid DNA sequencing. J. Mol. Bio., 143(2): 161-178.

Sanmee R, Lumyong P, Dell B and Lumyong S. 2010. In vitro cultivation and fruit body formation of the black bolete, *Phlebopus portentosus*, a popular edible ectomycorrhizal fungus in Thailand. Mycoscience., 51: 15-22.

Siri-in J, Kumla J, Suwannarach N and Lumyong S. 2014. Culture conditions and some properties of pure culture of ectomycorrhizal fungi, *Scleroderma sinnamariense*. Chiang Mai. J. Sci. 41(2); 275-285.

Smith SE and Read D. 2008. Mycorrhizal Symbiosis. third ed. Academic Press London.

Sun Z, Hu M, Sun Z, Zhu N, Yang J, Ma G and Xu X. 2018. Pyrrole alkaloids from the edible mushroom *Phlebopus protentosus* with their bioactive activities. Molecules., 23: 1198.

Titilawo MA, Faseum AO, Akinde SB, Olaitan JO and Odeyemi O. 2022. Bioactivity of four Nigerian wild mushrooms against some typed clinical isolates. Jordan J. Biol. Sci. 15(1): 67-73.

Watling R. 2001. The relationships and possible distribution patterns of boletes in south-east Asis. Mycol. Res., 105:1440-1448.

White TJ, Bruns T, Lee S and Taylor J. 1990. Amplification and direct sequencing of fungal ribosomal RNA genes for phylogenetics *In* Innis M., Gelfand D., Sninsky J., White T. [eds], PCR protocals: a guide to methods and applications, 315-322. Academic Press, San Diego, California, USA.

Yuwa-amornpitak T, Butkhup L and Yeunyaw P. 2020. Amino acids and antioxidant activities of extracts from wild edible mushrooms from a community forest in the Nasrinual District, Maha Sarakuam, Thailand. Food Sci. Technol. 40(3): 712-720.

Zhang CX, Ji KP, He MX, Cao Y, Liu J and Wang WB. 2010. Analysis on nutrient components of *Phlebopus portentosus* fruit bodied. J. Yunnan Uni., 32:527-532.

Zhang CX, He MX,Cao Y, Lui J, Gao F, Wang WB, Ji KP, Shao SC and Wamg Y. 2015. Preliminary studies on trophic relationships of *Phlebopus portentosus*, soil mealy bug and plant. Edible Medic. Mush.,23(6):359-363.

Zhang C, He M, Liu J, Xu X, Cao Y, Gao F, Fang Y, Wang W and Wang Y. 2017. Brief introduction to a Unique edible bolete*Phlebopus portentosus* in southern China., J. of Agri. Sci. Technol. B., 7:386-394.

JJBS

Volume 16, Number 1,March 2023
ISSN 1995-6673
Pages 131 – 136
https://doi.org/10.54319/jjbs/160116

Jordan Journal of Biological Sciences

Detection and Epidemiological Features of Human Coronaviruses in Patients with Acute Gastroenteritis in Northern Jordan

Mamdoh M. Meqdam[1,*], Malak I. Abusamha[2], Asem M. Alkhateeb[2] , Ziad M. Bataineh [3], Khadija F. Maho[1], and Ayat M. Gogazeh[1]

[1]*Applied Medical Sciences Faculty, Jordan University of Science and Technology;* [2]*Arts and Sciences Faculty, Jordan University of Science and Technology;* [3]*Medicine Faculty, Jordan University of Science and Technology*

Received: June 27, 2022; Revised: October 16, 2022; Accepted: November 19, 2022

Abstract

Fecal specimens collected from patients with acute gastroenteritis among the Northern Jordan population were screened for human coronaviruses-229E, human coronaviruses-NL63, human coronaviruses-HKU1, and human coronaviruses-OC43 by Reverse Transcriptase- Polymerase Chain Reaction (RT-PCR) and PCR. Out of the 401 analyzed specimens, 42(10.5%) specimens were found positive for at least one human coronavirus. Of the 42 specimens, 57.1% were positive for human coronaviruses-229E, 33.3% for human coronaviruses-NL63, and 9.5% for human coronaviruses-HKU1. The human coronaviruses-OC43 virus was not detected in the tested specimens. None of the fecal specimens collected from healthy individuals were found positive for human coronavirus strains. No significant association was found between human coronavirus infection and gender (P>0.05). Most infected cases were in the age group >60 years old (23.8%), followed by the age group 0–1-year-old (19.0%). Most cases of human coronaviruses were detected in the winter season (42.9%) with a significant association recorded with human coronaviruses-NL63 (P = 0.006), and the lowest in the spring season (4.8%).The relationship between the human coronavirus-229E and fever (P = 0.04) and between human coronavirus-HKU1 and weakness (P = 0.04) were significant. No association (P> 0.05) between respiratory disease and positive human coronaviruses fecal specimens. The average symptom duration was 2-3 days. Among the viral-positive specimens, 38.1% were under antibiotic treatment. The provided data will help in patient care control of viral acute gastroenteritis.

Keywords: Gastroenteritis; Human Coronaviruses; RT-PCR; PCR; Jordan

1. Introduction

Acute gastroenteritis (AGE) is a diarrheal illness that could be associated with many clinical manifestations and death worldwide and the most AGEcases in developing countries were in young children (Kotloff , 2017, Bányai *et al.,* 2018, Lo Vecchio, 2020). Viruses are the leading cause of acute gastroenteritis globally, accounting for the majority of diagnosed acute episodes of community-acquired diarrhea. About 50-70% of AGE was caused by viral infections(Luo*et al.,* 2019). Today, it is regarded as a major cause of mortality and morbidity in children under 5 years old (De Francesco*et al*., 2021, Thwiny*et al*., 2022). Moreover, in 2013 diarrheal disease accounted for 9% of total deaths around the world (Liu*et al*., 2015). The World Health Organization defines diarrhea as three or more occurrences of loose or watery stools per day, for three days or more, and less than 14 days (WHO 2005).Enteric viruses causing AGE varied from watery diarrheal along with symptoms such asanorexia,vomiting, nausea, fever, or malaise, to severe dehydration that needs hospitalization or leads to death (Lee*et al.,* 2020, Xiong *et al.,* 2020). Enteric viruses causing gastroenteritis were rotaviruses (Gupta*et al*., 2019,Omatola and Olaniran*et al*., 2022), enteric adenoviruses (Biscaro *et al*., 2018), astroviruses (Vu*et al*., 2017), caliciviruses (norovirus and sapovirus)(Desselberger *et al*., 2017). New viruses, human bocavirus (Guido *et al.,* 2016), human coronavirus (Owusu*et al*., 2021), aichivirus (Chuchaona *et al*., 2017), klassevirus (Pei*et al.*,2016), salivirus (Lasure *et al*., 2016) were increasingly detected in AGE cases from different countries. As most enteric viruses cannot be grown in cell culture, electron microscopy is considered the mainstay of diagnosis(Zhao*et al*., 2019,Donelli *et al*., 2021). Applying more accurate methods for viral antigen detection in fecal specimens using immunoassay and molecular biology techniques has enhanced the diagnosis of new viruses causing gastroenteritis(Malik *et al*., 2019).

Human coronaviruses (HCoVs) have been identified in the late 1960s, involvingHCoV-229E, HCoV-HKU1, HCoV-NL63, and HCoV-OC43, severe acute respiratory syndrome coronavirus, Middle East respiratory syndrome coronavirus, and SARS-CoV-2 (the newly detected HCoV in late 2019) (Owusu*et al*., 2021).Coronavirus (CoV) is a member of the

* Corresponding author. e-mail: meqdam@just.edu.jo.

Coronaviridae family including alpha (α), beta (β), gamma (γ), and delta (δ), with a single-stranded positive-sense RNA genome, and infects humans and a diversity of animals. HCoVs are widely known as respiratory pathogens. In 1975, some researchers noticed coronavirus-like particles (CVLPs) in fecal specimens collected from patients with diarrhea (Payne *et al* 1986). Following that, human coronavirus was detected in children with AGE and in necrotizing enterocolitis in babies (Osborne *et al*., 2015, Xiong*et al*., 2020).

The current study aimed to explore the presence of HCoVsin patients with AGE and to examine the relationship between AGE and the clinical data obtained from all age groups of patients.

2. Materials and Methods

2.1. Patients and Specimens

The Institutional Review Board Committee of Jordan University of Science and Technology, Jordan approved this study (No. 13/124/2019). The fecal specimens were collected from four hospitals in Northern Jordan; King Abdullah University Hospital, Prince Rashid Ben Al-Hasan Military Hospital, Princess Basma Teaching Hospital, and Princess Rahma Teaching Hospital in Northern Jordan. A convenience sampling technique was used to collect 401fecal specimens, during the period from Sep. 2019 until Aug. 2020. This study includes patients with AGE symptoms. Clinical profiles containing significant information such as gender, age, stool properties, symptoms, etc., were gathered in a particular form. The fecal suspension was prepared for each sample by adding 0.5 ml of stool to 450 µl of phosphate buffer saline in a 1.5 ml sterile Eppendorf tube. After that, the suspension was vortexed and centrifuged for 5 min at 3000 rpm for clarification purposes. The supernatant for each sample was transferred to a new sterile Eppendorf tube and preserved at -20°C until processed.

2.2. RNA Extraction

The human coronavirus RNAwas extracted from the stool supernatant through the DNA/RNA Path Miniprep (Zymo USA), as instructed by the manufacturer. All extraction steps were carried out at room temperature (unless specified) and centrifuged for 30 seconds at 10,000 rpm.

2.3. Reverse Transcription (RT)

To synthesize the cDNA, the protocol described by Kang *et al*. (2009) was used to reverse transcribe the extracted RNA using randomprimers by Maxime RT PreMix-iNtRON kit (South Korea).Using the Thermal Cycler TC9610-230 (Mayfield Avenue Edison, USA), the cDNA synthesis reaction was performed as follows: 45°C for 60 min, followed by inactivating the RTase at 95°C for 5 min. As an internal expression control, the β-actin gene was used.

2.4. Polymerase Chain Reaction (PCR)

The primers used to detect the presence of specific genes in HCoVs were in Table 1. As described by Gouvea *et al*. (1990), the PCR reaction was carried out using the PCR master mix solution of i-TaqTM -iNtRON kit (South Korea).GeneBank ® tool was used to design the positive control and generated by GeneScript® biotech company (New Jersey, USA).Positive control and a mixture without a cDNA template as negative control were added in each run.

Table 1. Oligonucleotide primers used for detection of HCoVs.

Virus	Primer	Target region	Sequence (5′ to 3′)	Size	Ref.
HCoV- OC43	N gene	O1 Forward	CCCAAGCAAACTGCTACCTCTCAG	309bp	(Vabret *et al*., 2005)
		O3 Reverse	GTAGACTCCGTCAATATCGGTGCC		
HCoV- 229E	N gene	E1 Forward	AGGCGCAAGAATTCAGAACCAGAG	309bp	(Vabret *et al*., 2001)
		E3 Reverse	AGCAGGACTCTGATTACGAGAAAG		
HCoV- KU1	1B gene	Forward	GGTTGGGATTATCCTAAATGTGA	440bp	(Esper*et al* ., 2006)
		Reverse	CCATCATCACTCAAAATCATCATA		
HCoV-NL63	S gene	Forward	ACCGCTGTTAATGAGTCTAGATATG	523bp	(Vabret *et al*., 2005)

2.5. Gel Electrophoresis

Gel electrophoresis was performed as described by Gouvea *et al*. (1990).A volume of 5 µl of the amplified PCR products for each specimenwas analyzed using a1.5 % agarose in 100 ml of 1 x tris-borate ethylenediaminetetraacetic acid buffer and stained with 0.5 µg/ml ethidium bromide (Fisher Scientific, UK) to visualize the amplified product. The electrophoresis was performed at 120 volts at room temperature for 1 hour and the bands were imaged under a Gel Documentation System.

2.6. Statistical Analysis

The package of Social Science (SPSS) software (IBM, USA) version 1.0.0.1447 and Chi-square (X^2) test was used for statistical analysis and comparison of groups.

3. Results

The fecal specimens were analyzed by PCR to detect 4 different strains of HCoVs(HCoV 229E, HCoV HKU1, HCoV NL63, and HCoV OC43). Out of the 401 fecal

specimens,10.5% were found positive for at least one HCoV strain. HCoV 229E was the most detected virus (6.0%),

while 1.0% of cases were detected with HCoV HKU1 and HCoV. OC43 was not detected in any sample (Table 2). Figures 1-3, represent gel electrophoresis for PCR amplified products of the HCoVs detected strains. HCoVs detection among gender was demonstrated in Table 3, without significant associations (*P*> 0.05)between males and females.

Table 2: HCoVsdistribution in 401 fecal specimens

Pathogen	No. (%)
HCoV 229E	24 (6.0%)
HCoV NL63	14 (3.5%)
HCoV HKU1	4 (1.0%)
Total	42 (10.5%)

Fig. 4 demonstrated the number of positive results of 3 different viruses (HCoV 229E, HCoV NL63, and HCoV HKU1) stratified by age. Of the 401 fecal specimens, 104 (26.0%) and 60 (15.0%) specimens were obtained from children younger than 1 and equal to or more than 60 years of age, respectively. The positive rate of HCoV 229E was distributed among the age groups, 16.7 % for those aged 0-4 age group, and 14.3% for those aged 60 years or older, whereas the rate of HCoV NL63 was 14.3 % for those 0-4 age groups. The HCoV HKU1 was found only in two age groups with a percentage of 4.8% in each of the 10-19 age group and for those aged 60 years or older.

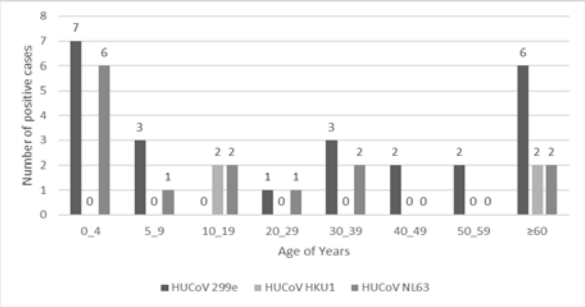

Figure 1: Distribution of human coronaviruses by patients age groups.

Table 3: The association between human coronaviruses infections and gender

Gender	HCoV 229E +ve No. (%)	HCoV 229E –ve No. (%)	HCoV HKU1 +ve No. (%)	HCoV HKU1 –ve No. (%)	HCoV NL63 +ve No. (%)	HCoV NL63 –ve No. (%)
Male	15(62.5)	211(56.1)	2 (50.0)	224 (56.6)	9 (64.3)	218 (56.3)
Female	9 (37.5)	165 (43.9)	2(50.0)	172 (43.4)	5 (35.7)	169 (43.7)
Total	24 (6)	376 (94)	4(1)	396(99)	14(3.5)	387(96.5)
P value	0.54		0.79		0.55	

The HCoVs detection varied in the four seasons (Table 4). The HCoV 229E was detected in the four seasons; winter (37.5%), autumn (29.2%, summer (25.0%), and spring were detected in two patients (8.3%), without significant associations between the HCoV 229E and seasons (*P* =0.51). A significant association was seen between the seasons and HCoV NL63 (*P* = 0.006), without any detection in spring.

Table 4: The association between human coronaviruses infection and seasons.

Season (Months)	HCoV 229E +ve No. (%)	HCoV 229E –ve No. (%)	HCoV HKU1 +ve No. (%)	HCoV HKU1 –ve No. (%)	HCoV NL63 +ve No. (%)	HCoV NL63 –ve No. (%)
Autumn	7(16.7)	119(31.6)	2 (4.7)	125 (31.6)	3 (7.2)	124 (32.0)
Winter	9(21.5)	92(24.5)	0 (0.0)	101 (25.5)	9 (21.5)#	92(23.8)
Spring	2(4.7)	35(9.3)	0 (0.0)	37(9.3)	0 (0.0)	37(9.2)
Summer	6(14.3)	130(34.6)	2 (4.7)	133(33.6)	2 (4.7)	134(34.6)
P value	0.51		0.55		0.006#	

Statistically significant at *P* =0.006

The HCoVs strains detection relationship with respiratory tract disease was demonstrated in Table 5. The HCoV 229E was detected in 2 patients with respiratory tract infection (8.3%), without significant associations (*P*=0.92).

Table 5. The association between human coronaviruses infection and respiratory tract disease.

Respiratory tract disease	HCoV 229E No. (%)	HCoV HKU1 No. (%)	HCoV NL63 No. (%)
Yes	2(8.3)	0(0.0)	0(0.0)
No	22(52.3)	4(9.6)	14(33.4)
Total No. (%)	24(57.0)	4(9.6)	14(33.4)
P value	0.92	0.72	0.27

Table 6 demonstrated the HCoVs relationship with clinical observations. A significant association was seen between the presence of HCoV 229E and fever (P = 0.04) and between HCoV HKU1 and weakness (P = 0.04). The range of symptoms duration was 2-3 days. In relation to the antibiotics treatment, 38.1% (16 out of 42) of infected patients were under antibiotics treatment.

Thirty fecal specimens were collected as control from healthy individuals to detect the presence of HCoV 229E, HCoV HKU1, HCoV NL63, and HCoV OC43 strains). Results showed that the HCoVs strains were not detected in healthy individuals.

Table 6: The association between HCoVsinfection and clinical observations

Observation	HCoV 229E+ve No. (%)	HCoV 229E –ve No. (%)	*P* value	HCoV HKU1 +ve No. (%)	HCoV HKU1 –ve No. (%)	*P* value	HCoV NL63 +ve No. (%)	HCoV NL63 –ve No. (%)	*P*value
Clinical diagnosis									
Dehydration	0(0.0)	6(1.6)	0.53	0(0.0)	6(1.5)	0.80	0(0.0)	6(1.5)	0.63
No dehydration	24(100)	371(98.4)		4(0.0)	390(98.5)		14(100)	381(98.5)	
Weakness	13(54.1)	167(44.3)	0.35	4(100)	177(44.5)	0.04#	8(57.1)	173(44.7)	0.35
No weakness	11(45.9)	210(55.7)		0(0.0)	220(55.5)		6(42.9)	214(55.3)	
Vomiting	3(12.5)	85(22.5)	0.24	0(0.0)	88(22.1)	0.28	2(14.2)	86(22.2)	0.48
No vomiting	21(87.5)	292(77.5)		4(100)	308(77.9)		12(85.8)	301(77.8)	
Fever	2(8.3)	102(27)	0.04#	0(0.0)	105(26.4)	0.23	5(35.7)	99(17.4)	0.39
No fever	22(91.7)	274(73)		4(100)	292(73.6)		9(64.3)	288(82.6)	
Abdominal pain	7(29.1)	135(35.8)	0.50	0(0.0)	143(36)	0.13	2(14.2)	140(37)	0.09
No Abdominal Pain	17(70.9)	242(64.2)		4(100)	254(64)		12(85.8)	247(63)	
Duration of Symptoms (days)									
1	5(20.8)	124(33)	0.28	3(75)	126(31.7)	0.17	6(42.8)	124(95.4)	0.64
2-3	17(70.9)	204(54)		1(25)	220(55.8)		7(50)	214(96.8)	
> 4	2(8.3)	48(13)		0(0)	50(12.5)		1(7.2)	49(98.0)	
Antibiotics received									
Yes	7(29.1)	142(37.6)	0.39	1(25)	148(37.2)	0.61	8(57)	141(37.2)	0.11
No	17(70.8)	234(62.3)		3(75)	248(62.8)		6(43)	246(62.8)	

Significant associations were seen between the presence of HCoV 229E and fever (P = 0.04) and between HCoV HKU1 and weakness (P = 0.04)

4. Discussion

Acute gastroenteritis was the main cause of mortality in children globally in the last two decades, with 10%of deaths in hospitalized children (Wang *et al*., 2016). In 2015, more than 1.3 million deaths due to diarrhea illness were reported including 146000 deaths among children <5 years old (Wang *et al*., 2016). The literature review showed that this study was the first study in Jordan that detected and associated HCoVs strains with AGE among all age groups of patients.

In this study, we collected fecal specimens from AGE patients to screen for the presence of HCoV 229E, HCoV HKU1, HCoV NL63, and HCoV OC43 strain as possible causes of AGE.

Human coronaviruses have already been considered pathogens infecting the respiratory tract since their discovery. However, the detection of HCoVs strains in fecal specimens was recorded in the United Kingdom since 1975 using electron microscope. After that, it had been detected in fecal specimens of AGE in many studies but with a very low prevalence rate. In a Slovenia study (Jevsnik *et al*., 2016), HCoV particles were detected in 8.7% of the tested specimens. Another study in Saudi Arabia (Kheyami *et al*., 2010) showed a 6% prevalence of HCoVs in AGE patients. A Finnish study (Risku *et al*., 2010) using molecular methods showed a 2.5% prevalence rate of HCoVs and distributed as follows: 45.5% HCoV-OC43, 27.3% HCoV-HKU1 and 18.2% HCoV-NL63. In the current study, HCoVs were detected in 10.5% of the tested specimens, and distributed as follows: 57.2 % HCoV-229E, 33.3 % HCoV-NL63, and 9.5 % HCoV-HKU1. A study from Ghana (Owusu *et al*., 2021) also reported that HCoV-229E was the most isolated strain. The HCoV-OC43 virus was not detected in the tested specimens. However, the detection rate of each strain of HCoVs varied in different regions, and the detection

of the predominant types of HCoVs associated with AGE is still unclear and needs further study.

The age distribution of HCoVs strains in this study was mostly in patients in the age groups below 5 years and equal to or above 60 years old, 31 % and 23.8%, respectively. Our results were in part similar to the result in a previous study that showed that the range of children age infected with HCoVs was 42 months (Kheyami *et al*., 2010). Another study showed that the age group affected was children less than 2 years old (Risku *et al*., 2010). No significant association was found between HCoVs infection and gender (P >0.05). The percentage of males to females was similar to previous studies (Risku *et al*., 2010).

Most cases of HCoVs were detected in the winter season (42.9%), with a significant association recorded with HCoV NL63 (P =0.006) and the lowest in the spring season (4.8%). Compared with a previous study, Risku *et al*. (2010) recorded the highest percentage of cases in both winter and spring each with 45.4%, which may be attributed to the low sample collection due to COVID-19pandemic. Paloniemi *et al*. (2015) detected HCoVs in both fecal specimens and nasopharyngeal swaps with a higher viral load in patients associated with AGE compared with respiratory tract disease, which may indicate that the source of the virus in fecal specimens is the respiratory tract.

In this study, the detected HCoVs appeared as the significant pathogens and were supported by the fact that thirty specimens collected from healthy individuals were found negative for HCoVs.

Due to a lack of published data concerning the clinical observations of AGE patients infected with HCoVs to compare with, in this study we presented the clinical observations from patients as follows: all the detected cases have a weakness; HCoV HKU1 recorded 100% weakness with significant association (P = 0.04). HCoV NL63 and HCoV 229E recorded similar percentages, 57.1%, and 54.1%, respectively. Vomiting was shown at 14.2% and 12.2% in HCoV NL63 and HCoV 339E, respectively. Also, fever recorded a significant association with HCoV 229E (P = 0.04) which represented 8.3% and HCoV NL63 recorded a higher rate in 53.7% of patients with fever. A significant association between fever and infection with human coronaviruses was also reported by Wen *et al*., 2022. The percentages of patients suffering from abdominal pain were 29.1% and 14.2% of the HCoV 339E and HCoV NL63. There were no positive cases recorded for HCoVs infection with dehydration. The duration of symptoms varies between the HCoVs strains and patients with AGE; HCoV 229E and HCoV NL63 recorded the highest percentages of duration as 2-3 days with 70% and 50%, respectively, while HCoV HKU1 recorded 75% for the one-day duration. Patients infected with HCoVs and under antibiotic treatment were 38.1%, which indicates the need for a laboratory test to diagnose viral AGE and minimize the use of unnecessary antibiotics.

5. Conclusions

The study provided data about the epidemiological features of human coronaviruses in patients with acute gastroenteritis with the association between AGE and the clinical data collected from patients in Northern Jordan. The provided data has demonstrated a 10.5% of specimens were found positive for at least one HCoVs with the highest percentage for HCoV-229E (57.1%) in Northern Jordan. Most infected cases (23.8%) were in the age group >60 years old. Among the positive specimens, 38.1% were under antibiotic treatment, necessitating viral diagnoses setting to enhance patient safety by reducing antibiotic overuse.

Acknowledgment

Jordan University of Science and Technology supported this study with Grant No. 20190332

References

Bányai K, Estes RIMK, Martella V, and Parashar UD. 2018. Viral Gastroenteritis. *Seminar*,175–86.

Biscaro V, Piccinelli G, Gargiulo F, Ianiro G, Caruso A, Caccuri F, et al. 2018. Detection and

Molecular Characterization of Enteric Viruses in Children with Acute Gastroenteritis in Northern Italy. *Infect, Genet and Evol*, **60**:35-41.

Chuchaona W, Khamrin P, Yodmeeklin A, Kumthip K, Saikruang W, Thongprachum A, et al. 2017. Detection and Characterization of Aichi virus 1 in Pediatric Patients with Diarrhea in Thailand. *J Med Virol*.,**89(2)**:234–8.

Desselberger U. 2017. Viral gastroenteritis. Vol. 45, Medicine (United Kingdom). Elsevier. p. 690–4.

De Francesco MA, Lorenzin G, Meini A, Schumacher RF, and Caruso A. 2021. Nonenteric Adenoviruses Associated with Gastroenteritis in Hospitalized Children.*Microbiol Spectr*. **9(1)**:e0030021. doi: 10.1128/Spectrum.00300-21. Epub 2021 Jul 28.

Donelli YG, Ruggeri FM, Tinari A, Marziano ML, Menichella D, Caione D, et al. 2021. A Three-Year Diagnostic and Epidemiological Study on Viral Infantile Diarrhoea in Rome. *Epidem Inf.,* **100:**311–20.

Esper F, Weibel C, Ferguson D, Landry ML, and Kahn JS. 2006. Coronavirus HKU1 Infection in the United States. *Emerg Infect Dis.*,**12(5)**:775–9.

Guido M, Tumolo MR, Verri T, Romano A, Serio F, De Giorgi M, et al. 2016. Human Bocavirus: Current Knowledge and Future Challenges. *World j gastroenterol*.,**22(39)**:8684.

Gouvea V, Glass RI, Woods P, Taniguchi K, Clark HF, Forrester B, and Fang ZY. 1990. Polymerase Chain Reaction Amplification and Typing of Rotavirus Nucleic Acid from Stool Specimens. J Clin Microbiol., **28(2):** 276-282

Gupta S, Chaudhary S, Bubber P, and Ray P. 2019. Epidemiology and Genetic Diversity of Group

A rotavirus in Acute Diarrhea Patients in Pre-Vaccination Era in Himachal Pradesh, India. *Vaccine*. **37(36):**5350-5356. doi: 10.1016/j.vaccine.2019.07.037. Epub 2019 Jul 19.

Jevsnik M, Steyer A, Pokorn M, Mrvič T, Grosek S. 2016. The Role of Human Coronaviruses in Children Hospitalized for Acute Bronchiolitis, Acute Gastroenteritis, and Febrile Seizures: A 2-Year Prospective Study. *PLOS ONE* DOI:10.1371/journal.pone.0155555

Kheyami AM, Nakagomi T, Nakagomi O, Getty B, Hart CA, and Cunliffe NA. 2010. Detection of Coronaviruses in Children with Acute Gastroenteritis in Maddina, Saudi Arabia. *Ann Trop Paediatr.*,**30(1)**:45–50.

Kang Sc, Jung JY, Yang HS, Park BK, Kim DY, , and Kim, JH. 2009. Detection of Potentially Xenozoonotic Viruses in the Porcine Ovary in Korea. *Korean J Vet Res.*,**49(3):** 215-220.

Kotloff KL. 2017. The Burden and Etiology of Diarrheal Illness in Developing Countries.*Pediatr*

*Clin North Am.***64(4):** 799-814. doi: 10.1016/j.pcl.2017.03.006.

Lasure N and Gopalkrishna V. 2016. Infection, Genetics and Evolution Clinico-epidemiology and genetic diversity of Salivirus in acute gastroenteritis cases from Pune , Western India : 2007 – 2011. *MEEGID.*,**44**:425–30.

Lee B, Damon CF, Platts-Mills JA. 2020. Pediatric Acute Gastroenteritis Associated with Adenovirus 40/41 in low-Income and Middle-Income Countries.*Curr Opin Infect Dis*.

33(5):398-403. doi: 10.1097/QCO.0000000000000663.

Liu L, Oza S, Hogan D, Perin J, Rudan I, Lawn JE, et al. 2015. Global, Regional, and National Causes of Child Mortality in 2000-13, with Projections to Inform Post-2015 Priorities: An Updated Systematic Analysis. *The Lancet*. 31(385) (9966):430–40.

Lo Vecchio A, Basile FW, Bruzzese D, Di Dato F, Aol P, Omona V. 2020. Diarrhea in Children with Plasmodium falciparum Malaria: A Case-Control Study on the Prevalence and Response to Antimalarial Treatment.*Am J Trop Med Hyg.***14;104(2)**:659-665. doi:

10.4269/ajtmh.20-0287.

Luo L, Gu Y, Wang X, Zhang Y, Zhan L. 2019. Epidemiological and Clinical Differences Between Sexes and Pathogens in a Three-Year Surveillance of Acute Infectious gastroenteritis in Shanghai. *Scientific Reports* 9(9993) https://doi.org/10.1038/s41598-019-

46480-6

Malik YS, Verma AK, Kumar N, Touil N, Karthik K. 2019. Advances in Diagnostic Approaches for Viral Etiologies of Diarrhea: From the Lab to the Field. *Front. Microbiol*, **10(1957)**: 1-

18.https://doi.org/10.3389/fmicb.2019.01957

Payne CM, Ray CG, Borduin V, Minnich LL, and Lebowitz MD. 1986. An Eight-Year Study of the Viral Agents of Acute Gastroenteritis in Humans: Ultrastructural Observations and Seasonal Distribution with a Major Emphasis on Coronavirus-Like Particles. *Diagn Microbiol Infect Dis.*,**5(1)**:39–54.

Paloniemi M, Lappalainen S, and Vesikari T. 2015. Commonly Circulating Human Coronaviruses do not have a Significantrole in the Etiology of GastrointestinalInfections in Hospitalized children. *J Clin Virol.*,**1**(62):114–117

Pei N, Zhang J, Ma J, Li L, Li M. 2016. First Report of Human Salivirus/Klassevirus in Respiratory Specimens of a Child with Fatal Adenovirus Infection.*Virus Genes*,**52**:620–624.

Omatola CA and Olaniran AO. 2022. Rotaviruses: from Pathogenesis to Disease Control— aCritical Review. *Viruses*, **14(875):** 1-34.

Osborne CM, Montano AC, Robinson CC, Schultz-Cherry S,and Dominguez1, SR. 2015. Viral Gastroenteritis in Children in Colorado 2006-2009. *J Med Virol*. **87**:931–939.

Owusu M, Sylverken AA, El-Duah P, Acheampong G, Mutocheluh M, and Adu-Sarkodi Y. 2021. Sero-epidemiology of Human Coronaviruses in Three Rural Communities in Ghana. *PAMJ.*, **38(244):** 1-12.

Thwiny HT, Alsalih NJ, Saeed ZF, Al-Yasari AMR, et. al. 2022. Prevalence and Seasonal Pattern of Enteric Viruses among Hospitalized Children with Acute Gastroenteritis in Samawah, Iraq.*J Med Life*. **15(1):**52-57. doi: 10.25122/jml-2021-0158.

Risku M, Lappalainen S, Räsänen S, Vesikari T. 2010. Detection of Human Coronaviruses in Children with Acute Gastroenteritis. *J Clin Virol.*,**48(1)**:27–30.

Vabret A, Mouthon F, Mourez T, Gouarin S, Petitjean J, and Freymuth F. 2001. Direct Diagnosis of Human Respiratory Coronaviruses 229E and OC43 by the Polymerase Chain Reaction. *J Virol Methods.*, **97(1–2):**59–66.

Vabret A, Mourez T, Dina J, Van Der Hoek L, Gouarin S, Petitjean J, et al. 2005. Human coronavirus NL63, France. *Emerg Infect Dis.*, **11(8):**1225–9.

Vu DL, Bosch A, M. Pintó RM, Guix S. 2017. Epidemiology of Classic and Novel Human Astrovirus: Gastroenteritis and Beyond. *Viruses*, **9(330):** 1-23

Wen C, Sun L, Zhao MC, Duan SX, Wang L, and Cui XW. 2022. Clinical Study of Human Coronavirus NL63, OC43, 229E, HKU1 Indentions in Hospitalized Children from 2015 to 2020. *Infect Drug Resist.*, **15:** 1093–1101

World Health Organization, editor. 2005. The Treatment of Diarrhoea: a Manual for Physicians and other Senior Health Workers. In: World Health Organization. Geneva; 2005.

Xiong LJ, Zhou MY, He XQ, Wu Y, Xie XL. 2020. The Role of Human Coronavirus Infection in Pediatric Acute Gastroenteritis. *The Pediatr Infec Dis J*,**39(7):**645-649.

Zhao Y, Qu H, Hu J, Fu J, Chen R, 2019. Characterization and Pathogenicity of the Porcine Deltacoronavirus Isolated in Southwest China.*Viruses*. **11(1074):** 1-22. doi: 10.3390/v11111074.

JJBS

Volume 16, Number 1,March 2023
ISSN 1995-6673
Pages 137 – 147
https://doi.org/10.54319/jjbs/160117

Jordan Journal of Biological Sciences

Assessment on Drought Stress Resistance, Salinity Endurance, and Indole Acetic Acid Production Potential of Dryland-Isolated Bacteria

Henik Sukorini[1*], Ellynda Retno Tiana Putri[1], Erny Ishartati[1], Sufianto Sufianto[1], Roy Hendroko Setyobudi[2], Nguyen Ngoc Huu[3], and Sawita Suwannarat[4]

[1]Department of Agrotechnology, Faculty of Agriculture and Animal Science, University of Muhammadiyah Malang, Jl. Raya Tlogomas No.246, Malang, 65145, East Java, Indonesia ; [2]Department of Agriculture Science, Postgraduate Program, University of Muhammadiyah Malang, Malang, 65145, East Java, Indonesia ;[3]Department of Plant Biology, Faculty of Agriculture and Forestry, University of Tay Nguyen, 567 Le Duan St., 63100 Buon Ma Thuot City, Dak Lak Province, Vietnam ;[4]Department of Plant Pathology, Faculty of Agriculture, Kasetsart University, 50 Ngamwongwan Rd, Lat Yao, Chatuchak, Bangkok 10900, Tanah Thai, Thailand

Received: Sep 29, 2022; Revised: Feb 11, 2023; Accepted Feb 21, 2023

Abstract

Dryland lacks water, unfulfilled nutrient supply, lack of abiotic and biotic elements, and very little rainfall. The area of dry land in Indonesia reaches 144.47×10^6 ha. About 99.65×10^6 ha are dry land with potential for agriculture, and around 44.82×10^6 ha are dry land with no possibility for agriculture. Many arid lands in Indonesia cause significant problems, especially in the agricultural sector. The problem often occurs due to the constraints of plant growth factors, including planting media, water, light, wind, and nutrients. This study aims to determine the resistance of bacteria to drought stress and high salinity as well as their ability to produce IAA (Indole Acetic Acid). The method used is *in vitro*. The results obtained are various kinds of bacteria, the nature of bacteria in binding gram, and osmoprotectant bacteria. Bacteria tested from the dry land of annual plants could effectively survive on PEG 6000 media NaCl even at high concentrations. The best bacteria that can survive in the saline conditions were B7, B8, B9, B10, while the potential as plant growth hormone bacteria are B6, B7, B8, B9, B10.

Keywords: Arid land, Biofertilizer, Dry land microbe, Environmentally friendly, Improve soil quality, *In vitro* screening, Plant growth promoting rhizobacteria, Soil biological fertility

1. Introduction

Indonesia has a vast dry land potential reaching 148×10^6 ha. The dry land area with potential for agriculture is estimated at 76.22×10^6 ha (52 %), and most are in the lowlands (70.71×10^6 or 93 %) (Budiono, *et al*. 2019). There are several obstacles faced in developing dryland agriculture (Adinurani *et al*., 2018; Bafdal *et al*., 2015; Noerwijati, *et al*. 2021). Water availability is highly dependent on rainfall. In general, dry land in Indonesia is degraded due to erosion. Land degradation causes dryland organic matter to be at the lowest level (Goenadi *et al*., 2021; Prasetyo *et al*, 2022a; Purbajanti *et al*., 2016; Vincevica-Gaile *et al*., 2021). Rhizosphere bacteria are soil microorganisms that can establish a relationship with the physical and chemical conditions of the soil (Ekawati, 2019; Sukmawati *et al*. 2021; Xiong *et al*. 2021). These bacteria help plants absorb nutrients and minerals and increase tolerance to environmental stresses (Ahmed and El-Sayed, 2021; Dimkpa *et al*., 2009; Ekawati, 2019; Muhammad *et al*. 2021). Bacteria in the root rhizosphere are bacteria cultured in soil with 10^{-6} to 10^{-9} cm^{-3} living cells (Hafeburg and Kothe, 2007).

However, further research on dryland bacteria is needed to determine how bacteria survive and adapt to dry land. Under drought conditions, the development of microbial communities will be hampered. Thus, the application of plant growth-promoting microorganisms has been suggested (Anjori *et al*., 2021; Marulanda *et al*., 2006). In addition, the ability of certain bacteria to reduce the detrimental effects of stress on plants has been previously reported (Kasim *et al*., 2013; Marulanda *et al*., 2009). Therefore, it is necessary to apply inoculation technology to strengthen the potential of microbes in dry land to improve the soil's physical, chemical, and biological conditions (Barea *et al*., 2002; Ekawati, 2019; Goenadi *et al*., 2021; Prasetyo *et al*., 2022b; Sukmawati *et al*., 2021).

The role of bacteria in growth, nutrition, and drought tolerance under nutrient-limited conditions is based on various physiological and cellular mechanisms (Medina and Azcon, 2012; Shinwari *et al*., 2019). In this case, microorganisms can also reduce water stress by reducing cellular oxidative damage produced by plants under drought conditions (Ahmed and El-Sayed, 2021; Potters *et al*., 2010). Inocula formation in dry soil activates antioxidant metabolic pathways (Benabdellah *et al*., 2011; Nguyen *et al*., 2020). The dry environment determines the ability of microorganisms to reproduce in that habitat. Remarkable similarities exist between plants and bacteria in their cellular responses to osmotic pressure (Csonka, 1989; Purbajanti *et al*., 2019).

This study reports information about the relevance of cellular metabolic processes carried out on the production of microbes that survive unfavorable conditions (stress and

salinity) and the potential of Indole Acetic Acid (IAA) in growing media added with PEG (Polyethylene Glycol) to create osmotic pressure (Gordon and Paleg, 1957; Purbajanti *et al*, 2019). Bacterial IAA production will be used as a plant repair effect and under stress conditions to protect cells against the adverse effects of ROS and stabilize proteins. This compound increases resistance against water shortages, which is considered a good stress indicator. In addition, previous studies reported the mechanisms generally involved in plant growth-promoting bacteria, such as the production of phytohormones, especially IAA, which plays the most crucial role in promoting plant growth (Adinurani *et al.* 2021; Glick, 1995). Thus, it was selected as a representative index of bacterial efficiency. Plants and microorganisms that live in dry soil adapt to stressful conditions.

The microorganisms are applied to form vegetation cover to restore soil conditions (Tanveer *et al*., 2022) . However, adaptable/tolerant bacteria can increase plant growth and nutrition in drought conditions. Besides, physiological mechanisms can increase plant resistance to water stress. Increasing cellular osmolyte accumulation can increase drought tolerance by reducing stomatal conductance and evapotranspiration (Bates *et al.* 1973; Purbajanti *et al*., 2019).

Microbe-producing Plant Growth Promoting Rhizobacteria (PGPR) use different mechanisms to promote plant growth (Ekawati, 2019; Goenadi *et al*. 2021; Parmar and Dadarwal, 2003). Tryptophan – gained from root exudates or decaying cells – replaces IAA microbial biosynthesis in the soil. Endophytic and rhizosphere bacteria have other properties that allow them to reach and establish themselves more effectively in plants' rhizosphere and inner tissues (Martinez-Viveros *et al*, 2010). Therefore, *in vitro* screening of rhizosphere and endophytic bacteria for IAA potency can provide a reliable basis for selecting effective PGPR bacteria.

Based on this research method, the tested bacteria will be selected to stimulate plant growth. After choosing the best isolate, the ultimate goal is to introduce the isolate as a biological fertilizer (Ekawati 2019; Li *et al.*, 2008, Muhammad *et al*. 2021). In addition, several studies have reported that the endophytic microbial community originating from the soil and rhizosphere were the best isolates promoted as biofertilizer or biodegradation (Afzal *et al.* 2017; Elvira-Rescuenco and van Vuurde, 2000; Hallman *et al.*, 1997; Sturz *et al.*, 2000).

2. Materials and Methods

2.1. Soil sampling

Soil samples were taken from the annual plant rhizosphere of Shrub (*Chamaedaphane* Moench), rhizosphere of Sonokeling/Java palisander (*Dalbergia latifolia* Roxb.), and rhizosphere of Coconut (*Cocos nucifera* L.) located in the dryland forest area of of South Malang, East Java, Indonesia *i.e.* Pagak districts (112°29’66″ to 112°33’12″ BT and 8°11’46″ to 8°18’27″ LS) and Bantur districts (8°18′59.14″S to 112°34′40.91″E). The average annual rainfall (2013 to 2021) in Pagak is 152 mm, while in Bantur, it is 194 mm. According to Oldeman's criteria, climate types are categorized as D and C (Harahap *et al*., 2021). The average annual rainfall in South Malang is slightly lower than in North Malang (climatological station at Abdulrahman Saleh Airport), which is 225 mm (climate type C). The soil samples (Pagak — mediteran type and Bantur — alfisol type) were collected from the surface 10 cm below the surface and processed immediately.

2.2. Preparation of bacterial isolation media

Alternative growth media was needed for growing microorganisms containing nutrient-rich carbohydrates and proteins (Medina and Azcon, 2012). The media used was PDA (Potato Dextrose Agar — Merck P2182). Isolation of antagonistic bacteria was according to the method used by Chilcott and Wigley (1993) and Limbu *et al*. (2020). The 1 g of the soil sample was suspended in 9 mL sterile distilled water and shaken vigorously for 2 min. Then, the liquid was serially diluted in sterile distilled water, and a 0.1 mL sample of the dilutions 10^{-4} to 10^{-7} was added to 20 mL of melted 92008 Tryptone Bile Agar (TBA — Merck 92008). After solidification of the medium, the plates were incubated at 30 ℃ for 24 h to 48 h. Finally, the bacterial colonies that showed antagonism to the adjacent colonies were picked up and subcultured to make pure cultures, as explained by Dubey and Maheshwari (2002) and Kumar *et al*. (2021).

The dilution method was used to isolate bacteria. This isolation was carried out by taking 10 L of homogenized soil samples with different dilution levels. The samples were then flattened before poured into the Petri dish using a multilevel triangle. Finally, planting was made in three cups per dilution to maximize bacterial growth *in vitro*.

2.3. Purification

Purification was carried out by taking a suspension of bacteria that had grown to the same size and volume and streaking them on new solid PDA media. Purification was carried out by taking a growing bacterial suspension of the same size and volume. After streaking on new solid PDA media then storing in a sterile room for 3 d to 4 d, the suspension was ready for further testing.

2.4. Gram stain and bacterial morphological identification

To observe microscopic characterization, gram staining method was used (Thairu *et al.* 2014). It was carried out to determine bacteria morphology and their gram properties. It used four different colors: crystal violet, Lugol's iodine, 96 % ethanol, and safranin. Bacteria with gram-positive properties will be blue-purple, while bacteria with gram-negative properties will be red or pink.

2.5. PEG 6000 — drought test

Drought stress test using PEG 6000 + NB media (PEG —Merck, Sigma-Aldrich) (Nutrient Both — Chemical Athaya/Tokopedia), according to Susilowati *et al.* (2018). The concentrations tested in the drought stress test were different: 1 %, 2 %, 3 %, 4 %, 5 %, 6 %, 7 %, 8 %, 9 %, and 10 %. An amount of 10 mL of the media was put into the test tube according to the concentration, and two inoculating loops of bacteria inoculums were added. This drought stress test was carried out to determine the ability of bacteria to survive in drought conditions with relatively little water conditions and organic matter that did not match the needs of bacteria and very minimal nutrients. Observations were made by reading the Optical Density

(OD) value on a spectrophotometer (Genesys 10 S UV, USA) and recording each phase of bacterial growth marked on the number of OD values produced. Observation variables start from the lag phase, the exponential/logarithmic phase, the stationary phase, and the death phase (Myers *et al*., 2013).

2.6. NaCl salinity test

The salinity test was carried out to produce bacteria that can survive in osmotic stress or low water content due to the salt's high nature. The salinity test used NaCl + NB media (NaCl — Merck, CAS Number:7647-14-5) (Nutrient Both — Chemical Athaya/Toko Pedia) with 4 %, 5 %, 6 %, 7 %, 8 %, 9 %, 10 %. Observation variables include the value of OD (Optical Density), with an observation time interval of 3 h for 24 h (Khanghahi *et al.*, 2021). The OD value obtained will be recorded and presented on a bacterial growth. Suppose the resulting OD value increases at certain time intervals for 24 h. In that case, the bacteria can survive unfavorable conditions and if the suspension becomes cloudy, the bacteria can adapt to the media.

2.7. IAA potency test

Testing the potency of IAA using NB + L-Tryptophan media (Merck, CAS Number: 73-22-3) and added with Salkowski reagent (CV Nitra Kimia/Tokopedia) as a precursor to induce IAA in bacterial samples, according to Gang *et al*. 2019. Take the media at the concentration of 10 mL, add two inoculating loops of bacteria inoculum, homogenize it, and add 2 mL to 3 mL of Salkowski's reagent. Observations were conducted qualitatively after being in OD for 24 h with a 24 h observation interval. The bacteria can produce IAA hormone if the sample is pink after adding Salkowski's reagent.

2.8. Data analysis technique

Data analysis is based on in vitro experiments with qualitative descriptive study. The data obtained will be analyzed by bacterial growth during the initial 0 h observation and the final 24 h. The data will be presented by displaying macroscopic and microscopic observations of the morphology of bacterial growth, the shape of the bacteria, and the nature of the bacteria in binding color (Adinurani, 2022).

3. Results and Discussion

3.1. Purification, bacterial morphology, and bacterial physiology test

The results of bacterial purification that were successfully isolated and purified with different dilution levels from the Rhizosphere of Shrub, Rhizosphere of Sonokeling/*Java palisander*, and Rhizosphere of Coconut were shown in Table 1.

Table 1. Bacterial Isolation Results Based on The Bacterial Purification Index

No.	Inoculum sources	inoculums	Inoculum code
1.	Shrubs Location 1	B1 (five colonies)	B1
2.	Shrubs Location 2	B2 (three colonies)	B2
3.	Shrubs Location 3	B3 (two colonies)	B3
4.	Coconut Location 1	B1 (four colonies)	B4
5.	Coconut Location 2	B2 (three colonies)	B5
6.	Coconut Location 3	B3 (three colonies)	B6
7.	Coconut Location 4	B1 (two colonies)	B7
8.	Sonokeling Location 1	B2 (four colonies)	B8
9.	Sonokeling Location 2	B3 (two colonies)	B9
10.	Sonokeling Location 3	B4 (four colonies)	B10

Table 1 shows the purification results of bacteria from different plants with different dilution levels. In regards of the isolated sample selected based on the isolate purification index above, 32 inoculants were produced but only ten colonies were the difference. The morphological characteristics of bacterial colonies were presented in Table 2 to Table 4.

Table 2. Morphological characteristics of bacterial colonies of shrubs rhizosphere

Observation	Bacteria 1	Bacteria 2	Bacteria 3
Form	Circular	Circular	Circular
Elevation	Raised	Raised	Raised
Surface	Shiny	Shiny	Shiny
Edge	Entire	Entire	Entire
Color	Milky white	Milky white	Milky white
Cell shape	Coccus	Basil	Basil
Gram stain	Positive(+)	Negative (-)	Negative (-)

Table 3. Morphological characteristics of bacterial colonies of coconut rhizosphere

Observation	Bacteria 1	Bacteria 2	Bacteria 3	Bacteria 4
Form	Circular	Circular	Circular	Circular
Elevation	Raised	Raised	Raised	Raised
Surface	Shiny	Shiny	Shiny	Shiny
Edge	Undulate	Undulate	Undulate	Undulate
Color	Milky white	Milky white	Milky white	Milky white
Cell shape	Coccus	Basil	Coccus	Coccus
Gram stain	Positive (+)	Positive (+)	Positive (-)	Positive (+)

Table 4. Morphological characteristics of bacterial colonies of sonokeling rhizosphere

Observation	Bacteria 1	Bacteria 2	Bacteria 3
Form	Irregular	Irregular	Irregular
Elevation	Raised	Raised	Raised
Surface	shiny	Shiny	shiny
Edge	Undulate	Undulate	Undulate
Color	Milky white	Milky white	Milky white
Cell shape	Basilus	Basilus	Coccus
Gram stain	Positive (+)	Positive (+)	Positive (+)

Growth of 10 bacteria on media treated with NaCl to test whether the ten bacteria could grow in unfavorable environmental conditions, especially salinity. At 8 % salinity, all bacteria except bacteria B1, B2, and B3 showed an increasing trend, but at 9 % NaCl, only bacteria B7, B8, B9, and B10 still showed a growing trend, while other bacteria experienced a decrease in growth. At 10 % NaCl, only B7 and B10 bacteria survived (Figure 1). Salinity is a severe environmental problem. Salinity causes osmotic stress around the roots and causes a decrease in plant growth and productivity in dry areas that rely on irrigation or in dry areas without irrigation (Cicek and Cakirlar, 2002). Stress caused by salinity will affect plant metabolism. Excess salt in the soil solution can affect plant growth either through osmotic inhibition of water uptake by roots or the effect of specific ions. Salinity will increase Na^+ uptake, which in turn causes a decrease in Ca^{2+} and K^+ uptake (Kusmiyati *et al*., 2009; Yildirim *et al*., 2006). Bacterial B7 and B10 are able to survive at high concentrations of NaCl, and the two bacteria may be halotolerant bacteria. This type of bacteria can grow in the presence of high NaCl concentrations (Tortura, *et al.*, 1998), such as on the surface of the skin, which often has a high NaCl concentration (10 % NaCl) (Tsai *et al.*, 2016). This may suggest that the two bacteria may exhibit a better ability to overcome the osmotic shock due to NaCl. The ability of bacteria to survive in high salinity stress is due to the ability of bacteria to accumulate dissolved organic matter in their cytoplasm. The goal is to prevent the loss of fluid from inside the cell as a result of the high osmotic pressure outside the cell due to the increased concentration of dissolved organic matter NaCl. Halophilic bacteria can produce hydraulic enzymes, one of which is a protease. It can catalyze protein hydrolysis reactions into oligopeptides and their amino acids. That these microorganisms can thrive in hypersaline environments has been correlated with the high content of acidic amino acids in their proteins, which increases the negative surface potential of proteins, since these microorganisms were effectively used.

Bacteria able to survive at high salinity can be used further. It uses in the process of agronomic tests in terms of improving saline soil aggregates.

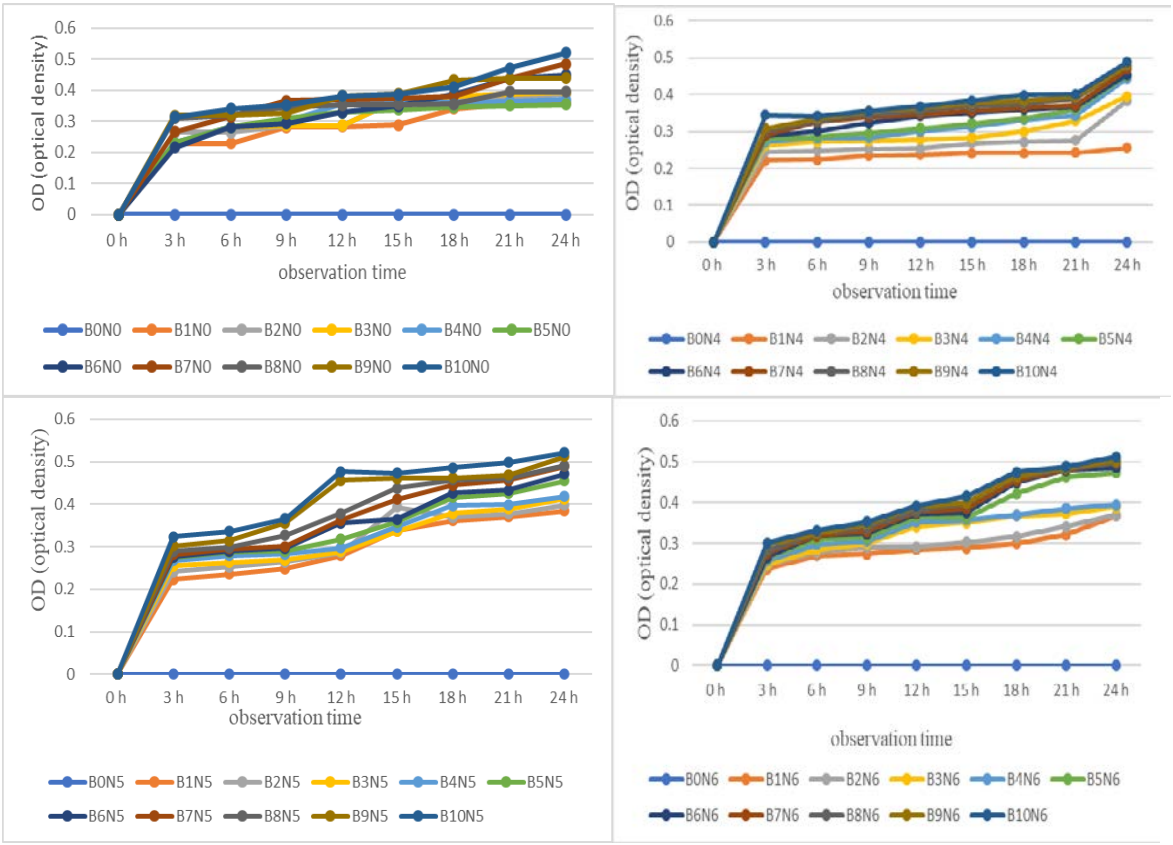

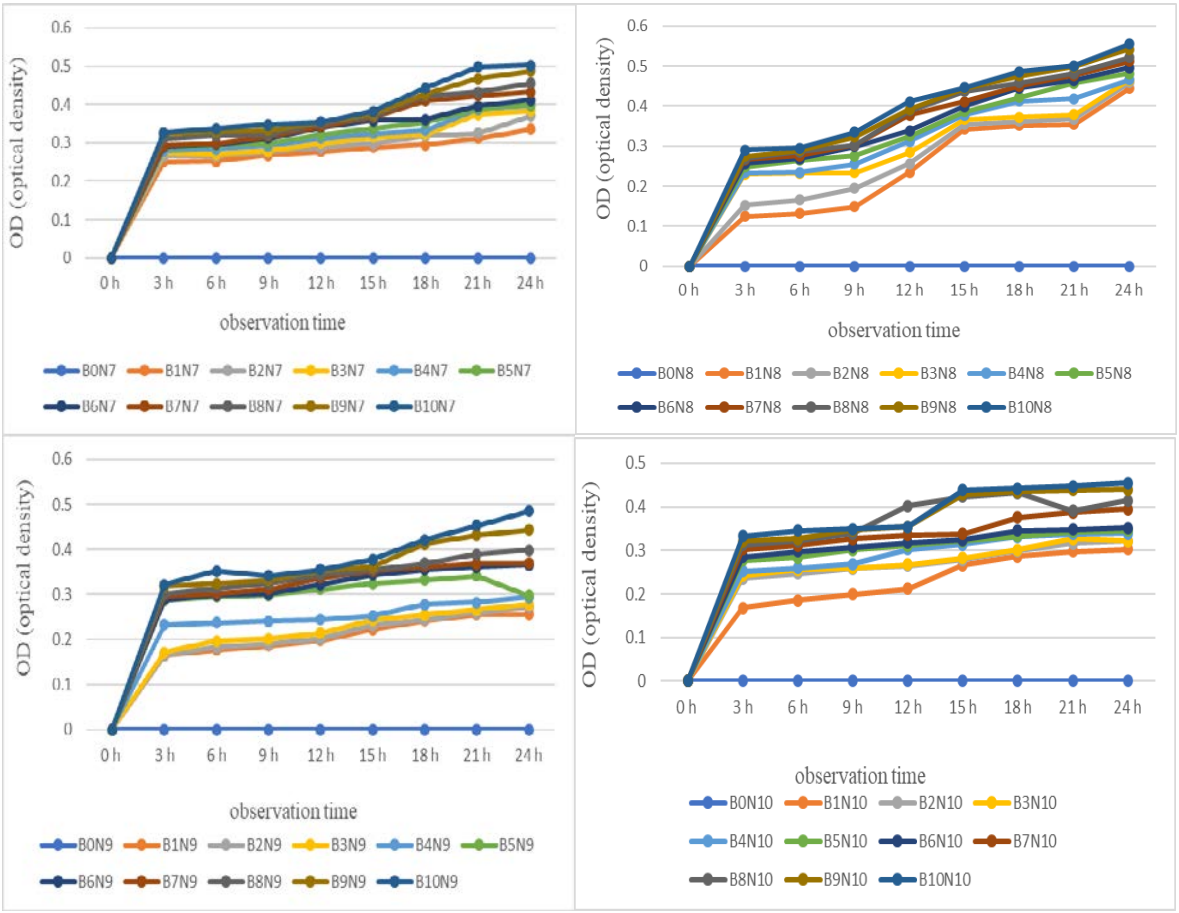

Figure 1. Bacterial growth at different NaCl concentrations. B0, B1, B2, B3, B4, B5, B6, B7, B8, B9, B10 were the types of bacteria tested. N0: NaCl 0 %; N4: NaCl 4 %; N5: NaCl 5 %; N6: NaCl 6 %; N7: NaCl 7 %; N8: NaCl 8 %; N9: NaCl 9 %; N10: NaCl 10 %

Growth of ten bacteria on media treated with PEG to test whether the ten bacteria could grow in unfavorable environmental conditions, especially water stress. All bacteria were able to grow on PEG-treated media from a concentration of 1 % to a concentration of 10 %, although there is a group of bacteria that consistently shows an upward growth trend and is always on top. These bacteria are B5, B6, B7, B8, B9, B10 (Figure 2). Drought or dry land is a major environmental problem that is currently emerging. This is the most formidable challenge for most countries in the world, apart from pest and disease attacks, because it causes a decrease in plant growth and yield. Therefore, it is necessary to find ways to increase plant growth and production under drought stress conditions. Microorganisms have the opportunity to overcome this. Arzanesh *et al.* (2011) analyzed the presence of siderophores and their relationship to drought resistance of the bacteria, and found that strains producing higher levels of siderophores were associated with excellent host plant resistance to drought. Siderophores are used by bacteria as one of the most important microbial survival strategies because they form complexes with Fe and increase its solubility and uptake under conditions of insufficient availability of iron (Rajkumar *et al*., 2017). Under stress conditions, *Pseudomo*nas sp., produces higher Exopolysaccharides (EPS) levels than conditions without stress. EPS formation in bacteria occurs as a reaction to stress (Ali *et al*., 2014). The ability to produce EPS by bacterial cells is used as a criterion for drought tolerance in bacteria (Sandhya *et al.*, 2009).

Incorporation of microorganisms as active and vital components in agricultural systems is imperial to stimulate drought tolerance. Cohen *et al.*, 2015 and Kang *et al.*, 2014, stated that among microorganisms, bacteria might promote plant growth by producing essential phytohormones and mineral solubilization. In addition, the bacteria may enhance the antagonistic effect against the pathogen. In plants grown under extreme stress conditions, inoculation of Plant Growth Promoting Bacteria (PGPB) improved stress tolerance, at least partly, by increasing root length and allowing better access to water (Enebe and Babalola, 2018).

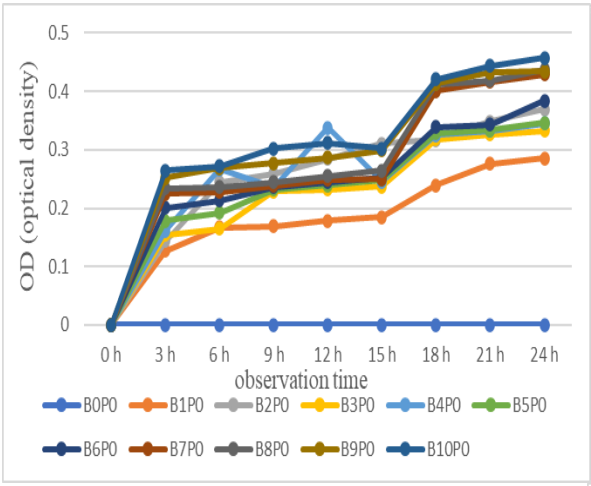

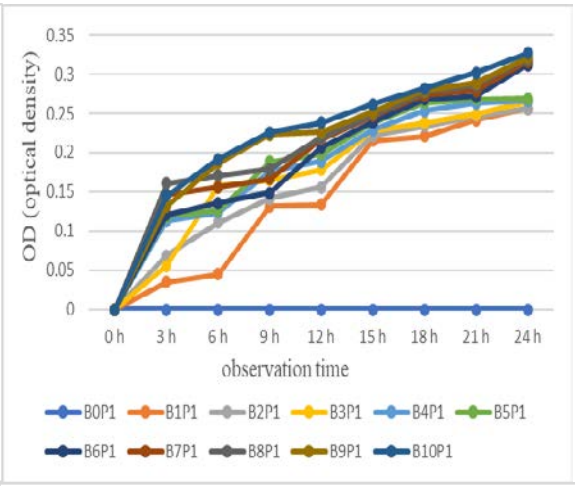

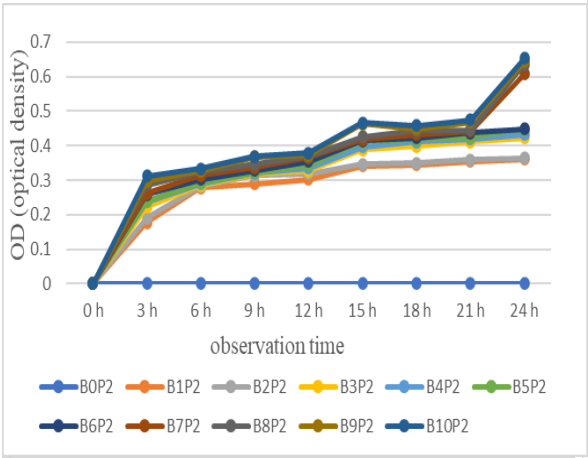

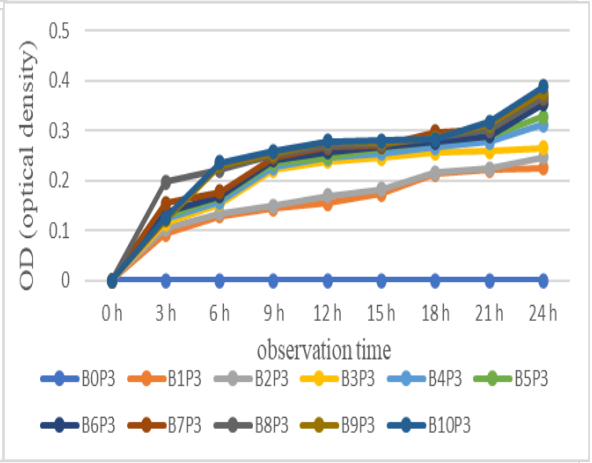

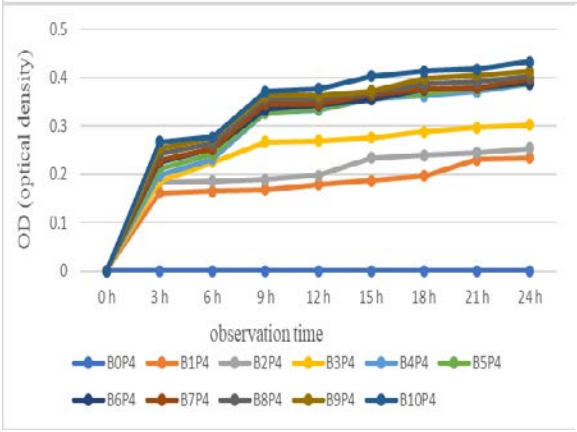

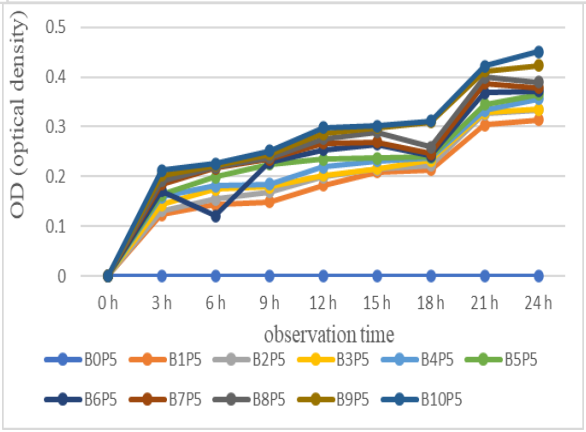

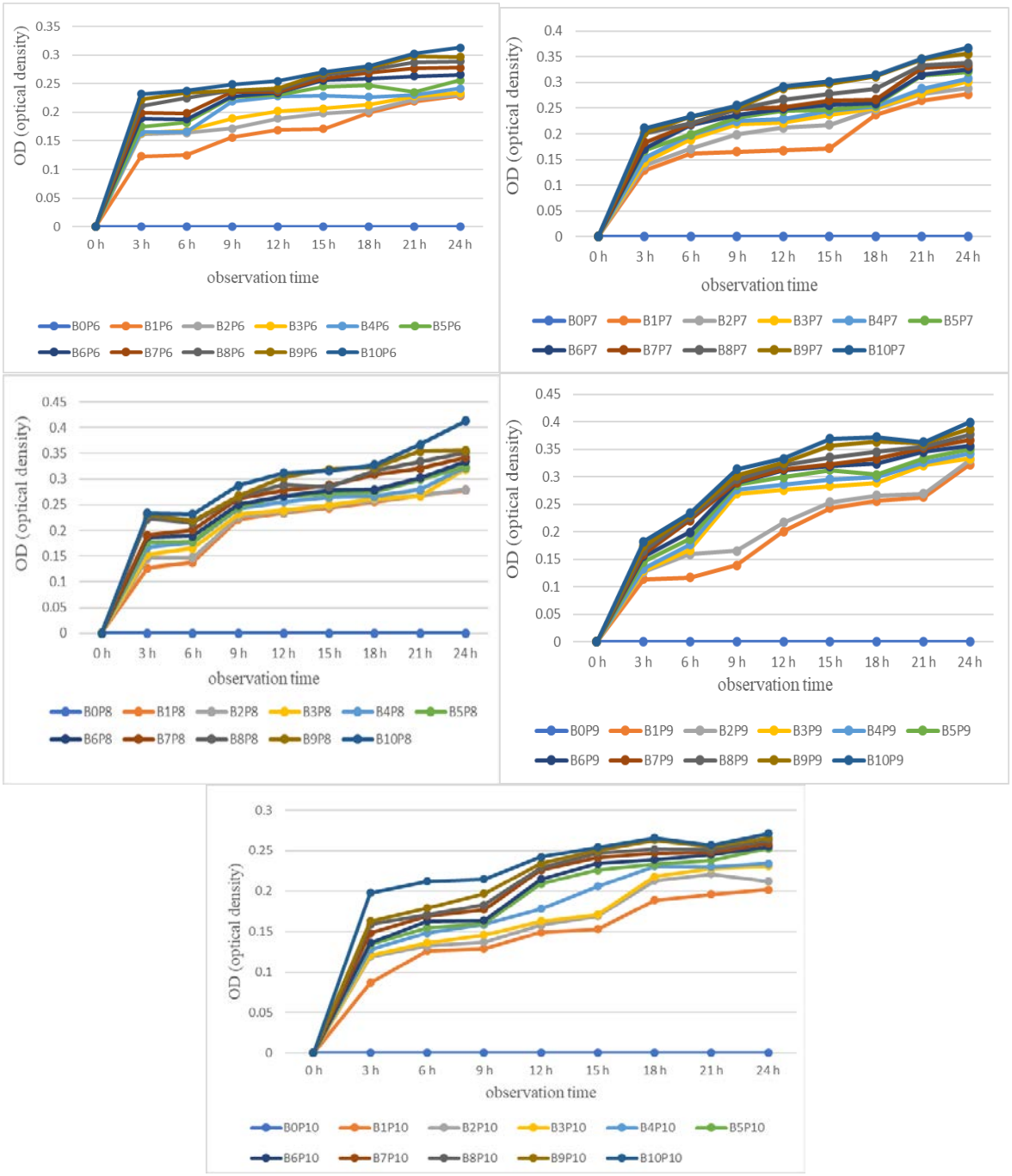

Figure 2. Bacteria growth trend on media with PEG in different concentrations. Name of bacteria: B0, B1, B2, B3, B4, B5, B6, B7, B8, B9, B10. P0: PEG 0 %; P1: PEG 1 %; P2: PEG 2 %; P3: PEG 3 %; P4: PEG 4 %; P5: PEG 5 %; P6: PEG 6 %; P7: PEG 7 %; P8: PEG 8%; P9: PEG 9 %; P10: PEG 10 %.

Ten isolates were identified as IAA-producing strains because the OD of all bacteria at 1 h to 24 h of observation showed an upward trend from (20 to 100) tryptophan concentrations. The top five bacteria are B6, B7, B8, B9, and B10. The five bacteria had the highest OD among the ten bacteria tested (Figure 3). IAA production by bacteria can vary between different species and strains besides being influenced by culture conditions, growth stages and substrate availability (Mohite, 2013). The technique for detecting IAA using the Van Urk Salkowski reagent is an essential option for qualitative and semi-qualitative determinations that guarantee the presence of hormones in bacterial culture supernatants or liquid formulations of biological inoculants. The amount of IAA produced by bacteria was within the detection limit of the Salkowski reagent (Ehmann, 1997). The results showed that the higher is the tryptophan concentration, the higher is the OD value. Indole production increased with increasing tryptophan concentration in testing Fluorescent Pseudomonas isolates for their ability to produce indole acetic acid in pure culture without the presence of and L-tryptophan (Karnwal, 2009).

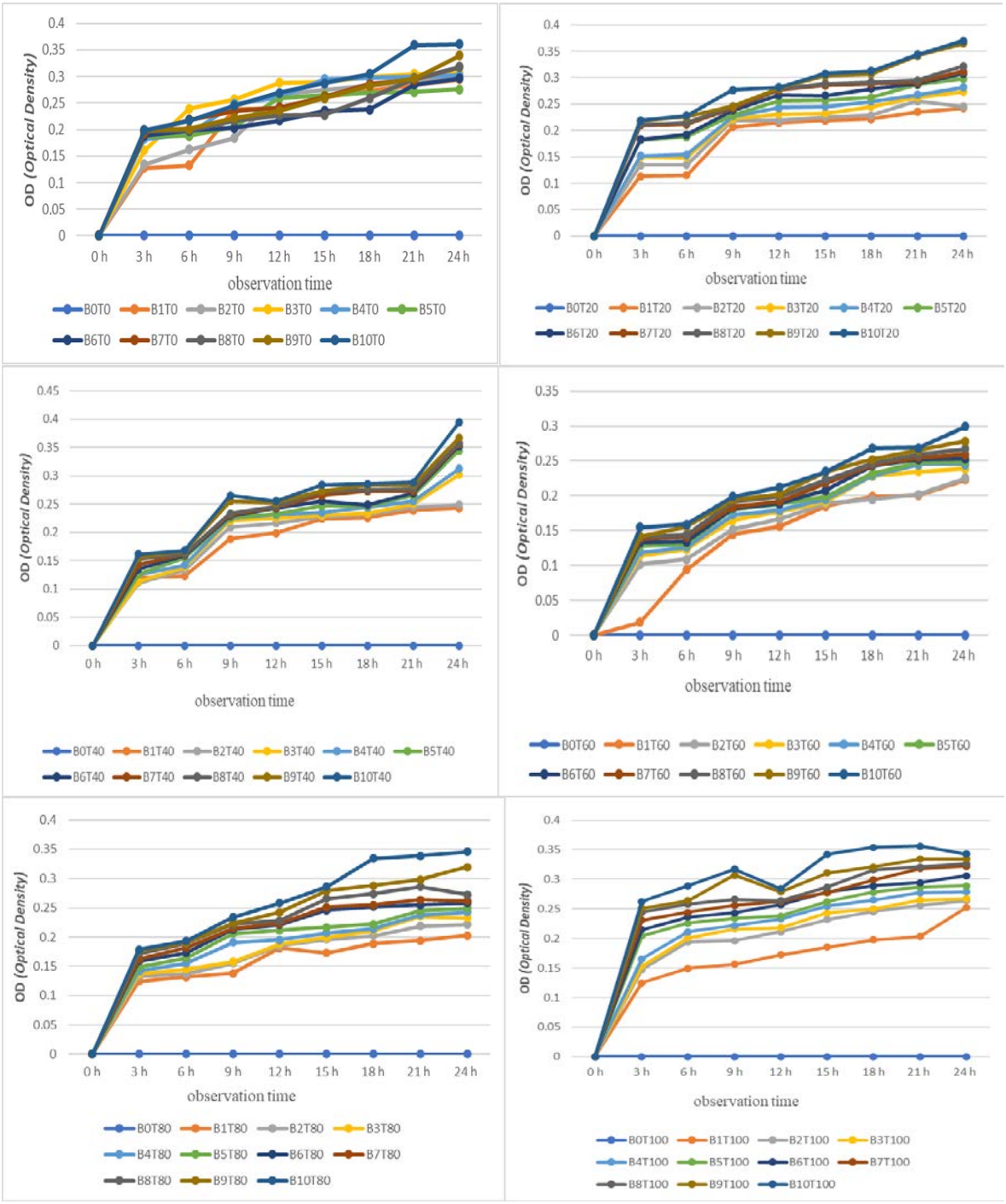

Figure 3. Bacteria growth trend on media with Tryptophan in different concentrations. Name of bacteria: B0, B1, B2, B3, B4, B5, B6, B7, B8, B9, B10. T0: Tryptophan 0 %; T20: Tryptophan 20 %; T40: Tryptophan 40 %; T60: Tryptophan 60 %; T80: Tryptophan 80 %; T100: Tryptophan 100 %

This study needs to relate soil organic matter content for future research directions to validate the conclusions. PGPR requires standard soil organic content to be efficient and effective (Adinurani *et al*., 2021; Ekawati, 2019; Goenadi *et al*. 2021; Medina and Azcón, 2012; Muhammad *et al*. 2021). It takes real action and collaboration between various stakeholders so that all organic waste —agricultural waste, livestock waste, kitchen waste, leftover food, and human excrement from pit latrines and septic tanks (Abdullah *et al*. 2020, Anukam and Nyamukamba, 2022; Manzoor *et al*., 2020; Prasetyo *et al*., 2022a and b, Setyobudi *et al*. 2021, Somorin, 2020; Susanto *et al*., 2020) can return to agricultural lands to maintain and increase soil fertility.

4. Conclusions

Based on the research on the ability to test drought stress, salinity, and potential IAA (Indole Acetic Acid) on bacterial isolates of dry land annual crops, the results are as follows:

(i) Various types of bacteria are produced from the purification process; the success of this bacterial

suspension is produced from the annual Sonokeeling, Shrubs, and Coconut plants.

(ii) Bacteria tested for drought and salinity can survive in unfavorable conditions. The high absorbance value at each observation time interval proves that the bacteria can live and have the potential to be used as biological fertilizers or PGPR.

(iii) The best bacteria that can survive in the saline conditions were B7, B8, B9, B10, while the potential as plant growth hormone bacteria are B6, B7, B8, B9, B10.

References

Abdullah K, Uyun AS, Soegeng R, Suherman E, Susanto H, Setyobudi RH., Burlakovs J, and Vincēviča-Gaile Z. 2020. Renewable energy technologies for economic development. *E3S Web of Conf*., **188(00016)**: 1–8. https://doi.org/10.1051/e3sconf/202018800016

Adinurani PG, Rahayu S, Budi LS, Nindita A, Soni P and Mel M. 2018. Biomass and sugar content of some varieties of sorghum (*Sorghum bicolor* L. Moench) on dry land forest as feedstock bioethanol. *Matec Web Conf*. **164(01035)**: 1–5. https://doi.org/10.1051/matecconf/201816401035

Adinurani PG, Rahayu S, Purbajanti ED, Siskawardani DD, Stankeviča K and Setyobudi RH. 2021. Enhanced of root nodules, uptake NPK, and yield of peanut plant (*Arachis hypogaea* L.) using rhizobium and mycorrhizae applications. *Sarhad J. Agric*., **37(Special issue 1):** 16–24. https://dx.doi.org/10.17582/journal.sja/2021/37.s1.16.24

Adinurani PG. 2022. **Non-Parametric Statistics (Agricultural Applications, Manuals and SPSS).** DeepPublish, Yogyakarta, Indonesia.

Afzal I, Iqrar I, Shinwari ZK and Yasmin A. 2017. Plant growth-promoting potential of endophytic bacteria isolated from roots of wild *Dodonaea viscosa* L. *Plant Growth Regul*., **81**, 399–408. https://doi.org/10.1007/s10725-016-0216-5

Ahmed ZG and El-Sayed MA.2021. Influence of drought stress on physiological traits of crossed okra varieties. *Jordan J. Biol. Sci*. **14(2):**253 –260. https://doi.org/10.54319/jjbs/140208

Ali, SZ, SandhyaV and Rao LV. 2014. Isolation and characterization of drought-tolerant ACC deaminase and exopolysaccharide-producing fluorescent Pseudomonas sp. *Ann. Microbiol*. **64 (2)**, 493–502. https://doi.org/10.1007/ s13213-013-0680-3.

Anjorin TS , Usman A, Fapohunda SO , Kwanashie A, Sulyok M and Krska R. 2021. Mycobiota and fungal metabolites in improved groundnut varieties in Nigeria. *Jordan J. Biol. Sci*. **14(4)**: 719–726. https://doi.org/10.54319/jjbs/140412

Anukam A and Nyamukamba P. 2022. The chemistry of human excreta relevant to biogas production: A review. In: Meghvansi M., Goel AK (Eds) **Anaerobic Biodigesters for Human Waste Treatmen**t pp 29–38. *Environmental and Microbial Biotechnology*. Springer, Singapore. https://doi.org/10.1007/978-981-19-4921-0_2

Arzanesh MH, Alikhani HA, Khavazi K, Rahimian HA, Miransari M. 2011. Wheat (*Triticum aestivum* L.) growth enhancement by Azospirillum sp. under drought stress. *World J. Microbiol. Biotechnol*. **27 (2),** 197–205. https://doi.org/ 10.1007/s11274-010-0444-1.

Bafdal N, Dwiratna S and Kendarto DR. 2015. Runoff management technology for integrated dry land agriculture in Jatinangor Research Center West Java, Indonesia. *Egypt. J. Desert Res*. **65(1):** 1–10. https://dx.doi.org/10.21608/ejdr.2015.5774

Barea JM, Azcon R and Aguilar CA. 2002. Mycorrhizosphere interactions to improve plant fitness and soil quality. *Antonie Van Leeuwenhoek*. **81:**343–351. https://doi.org/10.1023/A:1020588701325

Benabdellah K, Abbas Y, Abourouh M, Aroca R and Azcon R. 2011. Influence of two bacterial isolates from degraded and non-degraded soils and arbuscular mycorrhizae fungi isolated from semi-arid zone on the growth of Trifolium repens under drought conditions: Mechanisms related to bacterial effectiveness. *Eur. J. Soil Biol,*. **47(5):**303–309. https://doi.org/10.1016/j.ejsobi.2011.07.004

Budiono R, Adinurani PG and Soni P. 2019. Effect of new NPK fertilizer on lowland rice (*Oryza sativa* L.) growth. *IOP Conf. Ser: Earth Environ. Sci*., **293 (012034)**:1–10. https://doi.org/10.1088/1755-1315/293/1/012034

Bates LS, Waldren RP and Teare ID. 1973. Rapid determination of free proline for water-stress studies. *Plant Soil*. **39**:205–207. https://doi.org/10.1007/BF00018060

Chilcott CN and Wigley PJ. 1993. Isolation and toxicity of *Bacillus thuringiensis* from soil and insect habitats in New Zealand. *J. Invertebr. Pathol*., 61(3**)**:244–247. https://doi.org/10.1006/jipa.1993.1047

Cicek N and Cakirlar H. 2002. The effect of salinity on some physiological parameters in two maize cultivars. *Bulg J Plant Physiol*., **28(1–2**):66–74.

Cohen AC, Bottini R, Pontin M, Berli FJ, Moreno D, Boccanlandro H, Travaglia CN and Piccoli PN. 2015. *Azospirillum brasilense* ameliorates the response of *Arabidopsis thaliana* to drought mainly via enhancement of ABA levels. *Physiol. Plant*., **153 (1),** 79–90. https://doi.org/10.1111/ppl.2015.153.issue-110.1111/ ppl.12221.

Csonka LN. 1989. Physiological and genetic responses of bacteria to osmotic stress. *Microbiol. Mol. Biol. Rev*., **53(1**):121–147. https://doi.org/10.1128/mr.53.1.121-147.1989

Dimkpa C, Weinand T and Asch F. 2009. Plant–rhizobacteria interactions alleviate abiotic stress conditions. *Plant Cell Environ,*. **32(12):**1682–1694. https://doi.org/10.1111/j.1365-3040.2009.02028.x

Dubey RC and Maheshwari DK. 2012. **Practical Microbiology**. S. Chand Publishing. Uttar Pradesh, India.

Edbeib MF, Wahab RA and Huyop F. 2016. Halophiles: Biology, adaptation, and their role in decontamination of hypersaline environments. *World J Microbiol Biotechnol* **32(8):** 135. https://doi.org/10.1007/s11274-016-2081-9

Ehmanm A. 1977. The van URK-Salkowski reagent — a sensitive and specific chromogenic reagent for silica gel thin-layer chromatographic detection and identification of indole derivatives. *J. Chromatogr. A*. **132(2):**267–276. https://doi.org/10.1016/S0021-9673(00)89300-0

Ekawati. I. 2019. Smart farming: PGPR technology for sustainable dry land agriculture. Prosiding Seminar Nasional Ekonomi dan Teknologi, pp 615–622. Universitas Wiraraja, Sumenep, Madura, Indonesia.

Elvira-Recuenco M and van Vuurde JWL. 2000. Natural incidence of endophytic bacteria in pea cultivars under field conditions. *Can. J. Microbiol*. **46(11)**:1036–1041. https://doi.org/10.1139/w00-098

Enebe MC and Babalola OO. 2018. The influence of plant growth-promoting rhizobacteria in plant tolerance to abiotic stress: A survival strategy. *Appl. Microbiol. Biotechnol*. **102 (18)**: 7821–7835. https://doi.org/10.1007/s00253- 018-9214-z.

Glick BR. 1995. The enhancement of plant growth by free-living bacteria. *Can. J. Microbiol.* **41(2):**109–117. https://doi.org/10.1139/m95-015

Gordon SA and Paleg LG. 1957. Observations on the quantitative determination of indoleacetic acid. *Physiol. Plant.* **10(1):**39–47. https://doi.org/10.1111/j.1399-3054.1957.tb07608.x

Gang S, Sharma S, Saraf M, Buck M and Schumacher J. 2019. Analysis of Indole-3-acetic Acid (IAA) production in Klebsiellaby LC-MS/MS and the Salkowski method. *Bio Protoc.* **9(9):**e3230. https://doi.org/10.21769/BioProtoc.3230.

Goenadi DH, Setyobudi RH, Yandri E, Siregar K, Winaya A, Damat D, Widodo W, Wahyudi A, Adinurani PG, Mel M, Zekker I, Mazwan MZ, Siskawardani DD, Purbajanti ED and Ekawati I. 2021. Land suitability assessment and soil organic carbon stocks as two keys for achieving sustainability of oil palm (*Elaeis guineensis* Jacq.). *Sarhad J. Agri*., **37(Special issue 1)**: 184–196. https://dx.doi.org/10.17582/journal.sja/2022.37.s1.184.196

Haferburg G and Kothe E. 2007. Microbes and metals: Interactions in the environment. *J. Gen. Microbiol.* **47(6):**435–467. https://doi.org/10.1002/jobm.200700275

Hallman J, Quadt-Hallman A, Mahafee WF and Kloepper JW. 1997. Bacterial endophytes in agricultural crops. *Can. J. Microbiol.* **43(10):**895–914. https://doi.org/10.1139/m97-131

Harahap IS , Matondang IZ, Suryanto, Indah EK and Fitri I. 2021. Mapping climate classification of Oldeman in agricultural resources management in South Tapanuli district. *IOP Conf. Ser.: Mater. Sci. Eng.* **1156 (012002):**1–5 https://doi.org/10.1088/1757-899X/1156/1/012002

Kasim WA, Osman ME, Omar MN, El-Daim IAA, Bejai S and Meijer J. 2013. Control of drought stress in wheat using plant-growth-promoting bacteria. *J. Plant Growth Regul.* **32**:122–130. https://doi.org/10.1007/s00344-012-9283-7.

Kang SM, Khan AL, Waqas M, You YH, Kim JH, Kim JG, Hamayun M, Lee IJ. 2014. Plant growth-promoting rhizobacteria reduce adverse effects of salinity and osmotic stress by regulating phytohormones and antioxidants in *Cucumis sativus*. *J. Plant Interact.* **9 (1):** 673–682. https://doi.org/10.1080/ 17429145.2014.894587.

Karnwal A. 2009. Production of Indol acetic acid by fluorescent Pseudomonas in the presence of L-Tryptophan and rice root exudates. *J. Plant Pathol*., **91**: 61–63.

Khanghahi MY, Strafella S, Allegretta I and Crecchio C. 2021. Isolation of bacteria with potential plant-promoting traits and optimization of their growth conditions. *Curr Microbiol* **78**, 464–478. https://doi.org/10.1007/s00284-020-02303-w

Kumar S, Dubey RC, Maheshwari DK, Baliyan N and Dheeman S. 2021. Cyclic siloxane biosurfactant producing Bacillus Sp. BS14 biocontrol charcoal rot pathogen *Macrophomina phaseolina* and induce growth promotion in *Vigna mungo* L. *Arch Microbiol* **203**:5043–5054. https://doi.org/10.1007/s00203-021-02492-3

Kusmiyati F, Purbajanti ED and Kristanto BA. 2009. Macro nutrients uptake of forage grasses at different salinity stresses. *J. Indonesian Trop. Anim. Agric*., **34(3)**: 205–210. https://doi.org/10.14710/jitaa.34.3.205-210

Li JH, Wang ET, Chen WF and Chen WX. 2008. Genetic diversity and potential for promotion of plant growth detected in nodule endophytic bacteria of soybean grown in Heilongjiang province of China. *Soil Biol. Biochem.* **40(1)**:238–246. https://doi.org/10.1016/j.soilbio.2007.08.014

Limbu J, Shrestha, BK, Shakya J, Khatri SB and Khanal H. 2020. Isolation of *Bacillus thuringiensis* and its insecticidal effect against *Galleria mellonella*. *Himalayan Journal of Science and Technology*, **4**: 96–102. https://doi.org/10.3126/hijost.v4i0.33918

Manzoor M, Gul I, Iqrar I and Arshad M. 2020. Solid waste management practices in Pakistan. In: Agamuthu Pariatamby A, Hamid FS and Bhatti MS (Eds). **Chapter 10. Sustainable Waste Management Challenges in Developing Countries.** IGI Global. Pennsylvania, USA. https://doi.org/10.4018/978-1-7998-0198-6.ch010. pp. 248–269.

Marulanda A, Barea JM and Azcon R. 2006. An indigenous drought-tolerant strain of *Glomus* intraradices associated with a native bacterium improves water transport and root development in *Retama sphaerocarpa*. *Microb. Ecol.* **52:**670–678. https://doi.org/10.1007/s00248-006-9078-0

Marulanda A, Barea JM and Azcon R. 2009. Stimulation of plant growth and drought tolerance by native microorganisms (am fungi and bacteria) from dry environments: Mechanisms related to bacterial effectiveness. *J. Plant Growth Regul.* **28:**115–124. https://doi.org/10.1007/s00344-009-9079-6

Medina A and Azcón R. 2012. Reclamation strategies of semiarid mediterranean soil: Improvement of the efficiency of arbuscular mycorrhizal fungi by inoculation of plant growth promoting microorganisms and organic amendments. pp: 87–106. In: Hahdi M and Duponnois R (Eds.). **The Mycorrhizal Symbiosis in Mediterranean Environment: Importance in Ecosystem Stability and in Soil Rehabilitation Strategies**. Nova Science Publishers, Inc., Hauppauge, New York, USA.

Mohite B. 2013. Isolation and characterization of indole acetic acid (IAA) producing bacteria from rhizospheric soil and its effect on plant growth. *J. Soil Sci. Plant Nutr.*, **13(3):**638–649. http://dx.doi.org/10.4067/S0718-95162013005000051

Muhammad M, Isnatin U, Soni P, Adinurani PG. 2021. Effectiveness of mycorrhiza, plant growth promoting rhizobacteria and inorganic fertilizer on chlorophyll content in *Glycine max* (L.) cv. Detam-4 Prida. *E3S Web Conf.* **226 (00031)**: 1–5. https://doi.org/10.1051/e3sconf/202122600031

Myers JA, Curtis BS and Curtis WR. 2013. Improving accuracy of cell and chromophore concentration measurements using optical density. *BMC Biophys* **6(1)**:4 https://doi.org/10.1186/2046-1682-6-4

Nguyen NH, Trotel-Aziz P, Villaume S, Rabenoelina F, Schwarzenberg A, Nguema-Ona E, Clément C, Baillieul F and Aziz A. 2020. *Bacillus subtilis* and *Pseudomonas fluorescens* trigger common and distinct systemic immune responses in *Arabidopsis thaliana* depending on the pathogen lifestyle. *Vaccines* (Basel). 4;8(3)503:1–18. https://doi.org/0.3390/vaccines8030503.

Noerwijati K, Sholihin S, Wahyuni TS, Budiono R, Minh NV, Setyobudi RH, Vincēviča-Gaile Z and Husna L. 2021. Cluster analysis based selection in seedling population of cassava clones. *Sarhad J. Agric*, **37(2)**: 398-405. https://dx.doi.org/10.17582/journal.sja/2021/37.2.398.405

Parmar N and Dadarwal KR. 2003. Stimulations of plant growth of chickpea by inoculations of the flourencent Pseudomonas, *J. Appl. Microbiol*. **86(1)**:36–44. https://doi.org/10.1046/j.1365-2672.1999.00634.x

Potters G, Horemans N and Jansen MAK. 2010. The cellular redox state in plant stress biology – A charging concept. *Plant Physiol. Biochem.* **48(5):**292–300. https://doi.org/10.1016/j.plaphy.2009.12.007

Prasetyo H, Setyobudi RH, Adinurani PA, Vincēviča-Gaile Z, Fauzi A, Pakarti TA, Tonda R, Minh NV and Mel M. 2022a. Assessment on soil chemical properties for monitoring and maintenance of soil fertility in Probolinggo, Indonesia. *Proc. Pak. Acad. Sci.: B.*, **59(4):** 99–113. http://doi.org/10.53560/PPASB(59-4)811

Prasetyo H, Karmiyati D, Setyobudi RH, Fauzi A, Pakarti TA, Susanti MS, Khan WA, Neimane L and Mel M. 2022b. Local rice farmers' attitude and behavior towards agricultural programs and policies. *Pakistan Journal of Agricultural Research*, 35(4): 663–677. https://dx.doi.org/10.17582/journal.pjar/2022/35.4.663.677

Purbajanti ED, Kusmiyati F, Fuskhah E, Rosyida R, Adinurani PG, Vincēviča-Gaile Z. 2019. Selection for drought-resistant rice (*Oryza sativa* L.) using polyethylene glycol. *IOP Conf. Ser.: Earth Environ. Sci* . **293(012014):**1–8. https://doi.org/10.1088/1755-1315/293/1/012014

Purbajanti ED, Kusmiyati F, Slamet W, Praptiningsih Gamawati Adinurani PG. 2016. Chlorophyll, crop growth rate and forage yield of Brachiaria (*Brachiaria brizantha* Stapf.) as the result of goat manure in various nitrogen dosage. *AIP Conf Proc*., **1755 (130013):** 1–5. https://doi.org/10.1063/1.4958557

Rajkumar M, Bruno LB and Banu JR. 2017. Alleviation of environmental stress in plants: The role of beneficial Pseudomonas spp. *Crit. Rev. Environ. Sci. Technol*. **47 (6):** 372–407. https://doi.org/10.1080/10643389.2017.1318619.

Sandhya VD, Shaik ZA, Grover M, Reddy G and Venkateswarlu B. 2009. Alleviation of drought stress effects in sunflower seedlings by the exopolysaccharides producing Pseudomonas putida strain GAP-p45. *Biol. Fertil. Soils* **46(1)**: 17–26. https://doi.org/10.1007/s00374-009-0401-z.

Setyobudi RH, Yandri E, Atoum MFM, Nur SM, Zekker I, Idroes R, Tallei TE, Adinurani PG, Vincēviča-Gaile Z, Widodo W, Zalizar L, Van Minh N, Susanto H, Mahaswa RK, Nugroho YA. Wahono SK, and Zahriah Z. 2021. Healthy-smart concept as standard design of kitchen waste biogas digester for urban households. *Jordan J. Biol. Sci*., **14(3)**: 613 – 620. https://doi.org/10.54319/jjbs/140331

Shinwari ZK, Tanveer F and Iqrar I. 2019. Role of microbes in plant health, disease management, and abiotic stress management. In: Kumar V, Prasad R, Kumar M and Choudhary D (Eds). **Microbiome in Plant Health and Disease: Challenges and Opportunities.** Springer, Singapore. https://doi.org/10.1007/978-981-13-8495-0_11. pp. 231–250

Somorin TO. 2020. Valorisation of human excreta for recovery of energy and high-value products: A Mini-review. In: Daramola M, Ayeni A. (Eds) **Valorization of Biomass to Value-Added Commodities** pp 341–370. *Green Energy and Technology*. Springer, Cham. https://doi.org/10.1007/978-3-030-38032-8_17

Sukmawati S, Adnyana A, Suprapta DN, Proborini M, Soni P, Adinurani PG. 2021. Multiplication arbuscular mycorrhizal fungi in corn (*Zea mays* L.) with pots culture at greenhouse. *E3S Web Conf*. **226(00044)**:1–10. https://doi.org/10.1051/e3sconf/202122600044

Susanto H., Setyobudi RH.,Sugiyanto D, Nur SM, Yandri E., Herianto H., Jani Y, Wahono S.K., Adinurani PA, Nurdiansyah Y and Yaro A. 2020a. Development of the biogas-energized livestock feed making machine for breeders. *E3S Web Conf*., **188 (00010**): 1–13. https://doi.org/10.1051/e3sconf/202018800010

Susilowati, Puspita AA and Yunus A. 2018. Drought resistant of bacteria producing exopolysaccharide and IAA in rhizosphere of soybean plant (*Glycine max*) in Wonogiri Regency Central Java Indonesia. *IOP Conf. Ser.: Earth Environ. Sci.* **142 012058)**: 1–7. https://doi.org/10.1088/1755-1315/142/1/012058

Sturz AV, Christie BR and Nowak J. 2010. Bacterial endophytes: Potential role in developing sustainable systems of crop production. *CRC Crit Rev Plant Sci.* **19(1):**1–30. https://doi.org/10.1080/07352680091139169

Tanveer F, Iqrar I, Shinwari ZK and Gul I. 2022. Microbial biostimulants and their role in environmental bioremediation. In: Inamuddin, Adetunji CO, Ahamed MI and Altalhi T (Eds). **Chapter 8. Microbial Biostimulants and their Role in Environmental Bioremediation**, 1st edition. CRC Press, Boca Raton, Florida. USA. 12 p. https://doi.org/110.1201/9781003188032-8

Thairu Y, Nasir IA, Usman Y. 2014. Laboratory perspective of gram staining and its significance in investigations of infectious diseases. *Sub-Saharan Afr J Med* **1**:168–174

Tortura GJ, Funke BR and Case CL. 1998. **Microbiology: An Introduction**. 6th ed. Addison Wesly Longman Inc., USA.

Tsai M, Ohniwa RL, Kato Y, Takeshita SL, Ohta T, Saito S, Hayashi H and Morikawa K. 2011. *Staphylococcus aureus* requires cardiolipin for survival under conditions of high salinity. *BioMed Central Microbiol*., **11**: 13. https://doi.org/10.1186/1471-2180-11-13

Vincevica-Gaile Z, Stankevica K, Klavins M, Setyobudi RH, Damat D, Adinurani PG, Zalizar L, Mazwan MZ, Burlakovs J, Goenadi DH, Anggriani R and Sohail A. 2021. On the way to sustainable peat-free soil amendments. *Sarhad J. Agric*, **37(Special issue 1)**: 122–135. https://dx.doi.org/10.17582/journal.sja/2021.37.s1.122.135

Yildirim E, Taylor AG and Spittler TD. 2006. Ameliorative effects of biological treatments on growth of squash plants under salt stress. *Sci. Hortic*. **111(1):**1–6. https://doi.org/10.1016/j.scienta.2006.08.003

Xiong Q, Hu J, Wei H, Zhang H and Zhu J. 2021. Relationship between plant roots, rhizosphere microorganisms, and nitrogen and its special focus on rice. *Agriculture*, **11(234)**: 1–18. https://doi.org/ 10.3390/agriculture11030234

JJBS

Volume 16, Number 1,March 2023
ISSN 1995-6673
Pages 149 – 155
https://doi.org/10.54319/jjbs/160118

Jordan Journal of Biological Sciences

Epstein-Barr Virus Genotypes and Phylogeny among Cancer Patients in Sana'a City, Yemen

Anas Ahmed Al-Mahbashi[1], Abdul-Raoof Alshawkany[2], Khalid Mohammed Naji[3,4], Saeed Munassar Alghalibi[1], Qais Yusuf Abdullah[1], Eshraq Ahmed Al-Khalqi[1]

[1]Department of Biological Sciences, Faculty of Science, Sana'a University, Yemen; [2]Faculty of Veterinary Medicine, Sana`a University, Yemen; [3]Department of Chemical, Faculty of Science,Sana'a University, Yemen; [4] Department of Chemical Ecology/Biological Chemistry, Konstanz University, Konstanz, Germany.

Received: February 8, 2022; Revised: June 12, 2022; Accepted: August 4, 2022 [*]

Abstract

Epstein-Barr virus (EBV) is a ubiquitous virus that infects more than 90% of the world's population. It is a tumorigenic herpes virus that causes infectious mononucleosis (IM) and has been linked to the development of several malignant tumours such as Burkitt`s lymphoma, Hodgkin`s lymphoma, Nasopharyngeal carcinoma and Gastric carcinoma. This study was designed to detect EBV DNA and to identify the EBV genotypes and phylogeny among cancer patients' group (Case) and healthy individuals' group (Control) in Sana'a city, Yemen. One hundred subjects were enrolled in the study. Fifty individuals were clinically diagnosed to have cancer. The remaining 50 individuals were healthy controls. Serum IgM antibody against EBV viral capsid antigen (VCA) were tested by an enzyme-linked immunosorbent assay (ELISA).EBV-DNA detection was done using conventional polymerase chain reaction while genotyping and sub-genotyping were performed by Nested polymerase chain reaction of EBNA-2 gene and LMP-1 gene, respectively. Results showed that the prevalence rate of EBV-VCA IgM antibodies among cancer patients was 12% while in healthy individuals was 8%. EBV-DNA positivity were 66.7% (4/6) and 50% (2/4) for cancer patients (cases) and controls, respectively. Also, all EBV-DNA positive cases in both cancer patients and controls were genotype 1 and sub-genotype Med- with a rate of 100% both of them. The results presented genotypes and sub-genotype of EBV circulating in Sana'a city. It is worth mentioning that genotype 1 and Med- strain was first time recorded in Yemen. This study concluded that genotype 1 and Med- strain being predominant in Sana'a city, Yemen. Clinical significance of these finding have not been investigated and shall be evaluated in future studies.

Keywords: anti-EBV-VCA IgM antibodies, Cancer, DNA, Epstein-Barr Virus, PCR, Sana'a city, Yemeni.

1. Introduction

Cancer is a major public health problem in developing countries and worldwide with increasing frequency, especial with increased modernization and predisposition to a large number of carcinogenic agents (Alwan, 1997; AL-Nabhi *et al*., 2017), whereas cancer is a major public health problem in Yemen. AL-Nabhi *et al*. (2017) mentioned that cancer registry in Yemen is still a big challenge in absence of national cancer surveillance. In 2021, the World Health Organization (WHO) suggested that out of Yemen's population (33,28 million inhabitants), approximately 35,000 Yemeni people currently have cancer, and more than 11,000 are newly diagnosed with the disease every year (O'Neill, 2021; WHO, 2021). The link between virus and cancer was one of the pivotal discoveries in cancer research. Therefore, it is generally agreed that viruses are involved in 10-20-% of all cancers (zur Hausen, 2001; Parkin, 2006).

The Epstein-Barr virus (EBV) is a ubiquitous oncogenic virus (Ayee *et al.*, 2020) initially discovered by electron microscopy within a cultured African Burkitt's lymphoma (BL) cell line in 1964 (Epstein *et al.*, 1964). EBV, a double-stranded, 170-kbp DNA virus packaged within an icosahedral capsid surrounded by an envelope, belongs to the subfamily gammaherpesvirinae in Herpesviridae family (Peh *et al*., 2003; Habibian *at al*., 2018). The viral genome exists in linear form in mature virions and in circular episomal form in latently infected cells, and encodes for more than 85 genes. This virus is ubiquitous, and infects more than 90% of the human population worldwide with a life-long, asymptomatic, latent infection (Peh *et al*., 2003). EBV is the causative agent of infectious mononucleosis, playing a significant role as a cofactor in the process of tumorigenesis and has consistently been associated with a variety of malignant tumours, including endemic Burkitt's lymphoma, nasopharyngeal carcinoma, certain B and T-cell lymphomas, Hodgkin's disease, gastric carcinomas, and other lymphoproliferative diseases (Mendes *et al*., 2008). Primary EBV infection usually occurs subclinically during childhood, and thereafter the virus establishes a latent infection of B lymphocytes that persists for life (Habibian *at al*., 2018). In latency, only small subset of viral genes is expressed, which include the six EBV nuclear proteins:

[*] Corresponding author. e-mail: i.alkhalqi@su.edu.ye.

EBNA-1, EBNA-2, EBNA-3A, EBNA-3B, EBNA-3C, EBNA-LP, and three latent membrane proteins: LMP-1, LMP-2A, LMP-2B (Santpere *et al*., 2014).

There are two different EBV genotypes: Type 1 and Type 2, also known as Type A and B, distinguished by

the differences in the EBNA-2 gene, where the rest of the EBV genes differ only by less than 5% in their sequence. The divergence in EBNA-2 reveals only 54% of homology between the two types, facilitating the distinction between each EBV type (Smatti *et al*., 2018). Two genotypes of the virus, namely genotypes 1 and 2, exist and exhibit variation in geographical distribution. Although EBV genotype 1 is globally distributed, it is predominantly found in American, Chinese, European and South-East Asian (SEA) populations, whereas genotype 2 is predominantly found in Africa (Ayee *et al.*, 2020). The two genotypes also vary in biological properties; EBV genotype 1 is more efficient in immortalizing B cells while genotype 2 has a higher lytic ability (Walling *et al*., 2003; Saechan *et al*., 2006). EBV genotypes 1 and 2 can further be subdivided into different virus strains based on the genetic diversity of LMP-1gene, which shows greater degree of polymorphism than most EBV genes (Walling *et al*., 2003). LMP-1 is a 356-amino acid protein, which consists of a short cytoplasmic N-terminus, six membrane spanning domains, and a long cytoplasmic C- terminal domain (Li and Chang, 2003). LMP1 plays an important role in signal transduction and cell survival (Bouvard *et al*., 2009). Variants in LMP-1 were classified into 7 main groups: B95-8, Alaskan, China 1, China 2, Mediterranean (Med+) and (Med−), and North Carolina (NC) (Bouvard *et al*., 2009; Tzellosand Farrell, 2012; Yakovleva *et al*., 2015). However, new strains were subsequently reported from different origins, including two new strains from Thailand, Southeastern Asia 1 (SEA1), and Southeastern Asia 2 (SEA2), which have unique amino acid substitutions (Saechan *et al*., 2006; Saechan *et al*., 2010). Multiple EBV variants could be detected within one individual, which could affect disease induction and prognosis (Walling *et al*., 2003). For example, a variant LMP-1 gene with 30 bp deletion gene was detected in virus isolated from NPC tumor and was associated with a higher transforming activity compared to the typical prototype LMP-1 (B95-8) (Hu *et al*., 1991; Blake *et al*., 2001).

Attempts to develop preventative vaccines against EBV have been largely unsuccessful. Thus, it increases the risk of EBV spread. The vast majority of published studies on EBV prevalence are focused on serological analysis rather than viremia detection (Adjei, *et al*., 2008; Van-Lant and Knipe, 2009; Suntornlohanakul, *et al*., 2015; de Paor *et al*., 2016; Cohen, 2018). Clearly, detection of circulating EBV DNA is a better indication of infection status, which can contribute to improving the level of medical care prevention measures (Kondo, *et al*., 2004; Lin, *et al*., 2004). Previous studies from Middle Eastern countries such as Kuwait (Makar *et al.,* 2003), Saudi Arabia (Al-Diab *et al.,* 2003), Jordan (Vasef *et al.,* 2004), the UAE (Al-Salam *et al.,* 2008), Egypt (Audouin *et al.,* 2010), and Syria (Al Moustafa *et al.,* 2016) have investigated EBV and its association with certain diseases such as Hodgkin's lymphoma (ranging from 28% to 87%), but not among other cancer patients and healthy individuals. To the best of our knowledge, no studies have been conducted in Sana'a, Yemen or Middle East countries concerning EBV detection and genotypes and sub-genotypes identification in neither cancer patients or healthy individuals except in Qatar, where the circulating genotypes and sub-genotypes of EBV in healthy blood donors were determined by Smatti *et al.* (2017). Nasher (2012) determined the prevalence of the high-risk HPV type 16 and 18 and EVB in some Yemeni patients with oral squamous cell carcinoma. From this point, this study aimed at detection of EBV using ELISA and PCR method and identifying the EBV genotypes and sub-genotypes (strains) circulating within various study groups in Sana'a city, Yemen. Furthermore, this information will enable the health officials in Sana'a city to consider the development of new policies that aim at reducing the burden of communicable diseases related to malignancies.

2. Materials and Methods

2.1. Study Population and Design

This study is a case-control study. Sample size was calculated by Epi info version 7 (CDC, Atlanta, USA). A total number of 100 participants were included in this study. The study was conducted in two groups. The first group consisted of 50 cancer patients, who were clinically diagnosed with Burkitt's lymphoma, Hodgkin's lymphoma, Nasopharyngeal and Gastric carcinoma by a physician and also considered clinically suspected cases of EBV infection, in addition to those who attended the national oncology center in Sana'a city. The second group consisted of 50 healthy individuals from the general population who were considered controls.

2.2. Sample Collection

Venous blood (5 mL) was collected from each participate using venous puncture techniques and divided into equal shares. One part (2.5 ml of blood specimen) was added into vacutainer serum tube free from anticoagulant agent and left to dot at room temperature, then the blood was centrifuged for five minutes at 3000 rpm. The gel in the tubes formed a physical barrier between the serum and the red blood cells during centrifugation. Then each serum sample was separated into Eppendorf tube, until performing serological assay. The other 2.5 ml of the blood specimen was added into an EDTA tube and stored as a whole blood sample until performing molecular assay. The sera and whole blood samples were stored at -20^{o}C until performing tests.

2.3. Serological Assay

Sera from all specimens were analyzed for Epstein-Barr virus IgM viral capsid antigen (VCA) using opened system (manual) Enzyme-Linked Immunoassay (ELISA) diagnostic kits provided by (DIA. PRO, Italy). Quality control was performed according to manufactured instructions (DIA. Pro, Italy). According to the information included in the kits insert, the immunoassay used has sensitivity >98% and specificity >98%.

2.4. Molecular assay

Molecular identification of Epstein-Barr virus was performed using Conventional Polymerase Chain Reaction (PCR). The EBV IgM positive specimens were used in the molecular assay.

2.4.1. DNA Extraction

Total viral DNA were extracted from 200 µl of human whole blood specimens using the *AccuPrep®* Genomic DNA Extraction kit (K-3032) (Bioneer, Inc., Korea) according to the manufacturer's instruction. Extracted DNA samples were then stored at -20 °C for further testing.

2.4.2. Primers used in molecular assay

Specific genomic sequences (primers) synthesized by Bioneer, Inc., Korea were used in this investigation to detect EBV DNA, and to identify EBV genotypes and sub-genotypes table (1).

Table (1): The sequences of EBV virus primers used for EBV detection, genotyping and sub-genotypes during this study (Smatti *et al.*, 2017).

Primer type	Primer sequences	Amplicon Size
E2p1	5'-AGGGATGCCTGGACACAAGA-3'	596pb
E2p2	5'-TGGTGCTGCTGGTGGTGGCAA T-3'	
Ap1	5'- TCTTGATAGGGATCCGCTAGGATA-3'	497pb
Ap2	5'-ACCGTGGTTCTGGACTATCTGGATC-3'	
Bp1	5'-CATGGTAGCCTTAGGACATA-3'	150pb
Bp2	5'-AGACTTAGTTGATGCCCTAG-3'	
A1	5'-AGTCATAGTAGCTTAGCTGAA-3'	602pb
A2	5'-CCATGGACAACGACACAGT -3'	
B1	5'-AGTCATAGTAGCTTAGCTGAA-3'	587pb
B2	5'- CAGTGATGAACACCACCACG-3'	

2.4.3. EBV DNA detection by PCR

Detection of EBV DNA in all extracted samples were performed by a Conventional PCR using the *AccuPower®HotStart* PCR PreMix kit (K-5050) (Bioneer, Inc., Korea), and primers (E2p1 and E2p2) that have previously been reported (Table, 1). PCR amplification was preformed according to the manufacturer's instructions (Bioneer, Inc., Korea). Briefly, primer solutions were thawed, and genomic DNA was prepared. 4 µl(5Mm/µl) of diluted primers mix was distributed into the each *AccuPower®HotStart* PCR PreMix tube. 4 µl (100ng/µl) of genomic DNA was added to the individual PCR tube. Distilled water was added to *AccuPower®HotStart* PCR PreMix tube until the total volume of mixture became 20 µl. The lyophilized blue pellet was dissolved by vortexing and spin-down. The PCR tube was placed in TProfessional *TRIO* Thermocycler (Biometra Ltd, Germany) and the cycling program was started, whereas PCR reaction cycling conditions involved initial denaturation at 95°C for 5 min, followed by 35 cycles of amplification with denaturation at 95°C for 0.45 s, annealing at 56°C for 0.45 s, extension at 72°C for 0.45 s, and a find extension at 72°C for 5 min. A negative control (without genomic DNA) was used. Afterward, PCR amplified products were separated on 1.5% ethidium bromide-stained agarose gel and visualized using UV light trans illuminator, then a photo was taken by a Sony digital camera.

2.4.4. EBV genotyping by nested PCR of the EBNA-2 gene

Extracted samples that showed EBV DNA positive results were used in the genotypes assay. EBV genotyping was performed by nested PCR targeting the EBNA-2 gene as described by Smatti *et al.* (2017) and Ayee *et al.* (2020), using specific primers as previously reported (Table, 1), with slight modification to cycling conditions. The first round of the PCR was done by amplifying a common region of EBNA-2 using Apl and Ap2 as sense and antisense primers, respectively. Each PCR reaction mixture of 20 µl contains the following components with the final concentrations: *AccuPower®HotStart* PCR PreMix (produced by Bioneer, Inc. Korea), 2 µl (5Mm/µl) each of the forward and reverse primers, and 3 µl (100ng/µl) of genomic DNA. The volume was made up with nuclease-free water. The cycling conditions for the PCR reaction were as follow: initial denaturation at 95°C for 5 min, followed by 35 cycles of amplification with denaturation at 95°C for 0.45 s, annealing at 56°C for 0.45 s, extension at 72°C for 0.45 s, and a find extension at 72°C for 5 min. A second round PCR (nested) was performed using 0.5 µl of the amplicons from the first round as template; all other reaction components were the same as the first-round reaction mixture, except for the primers. A forward primer (Bp1) and reverse primers (Bp2) were used for the second-round amplification. The reaction was carried out at initial denaturation at 95°C for 5 min, followed by 35 cycles of amplification with denaturation at 95°C for 0.45 s, annealing at 56°C for 0.45 s, extension at 72°C for 0.45 s, and a find extension at 72°C for 5 min. Afterward, PCR amplified products were separated on 1.5% ethidium bromide-stained agarose gel and visualized using UV light trans illuminator then a photo was taken by a Sony digital camera. In all experiments, a negative control (without genomic DNA) was used.

2.4.5. EBV sub-genotyping by sequencing of LMP-1 gene

EBV sub-genotyping was done using nested PCR targeting the LMP-1 gene as described by Smatti *et al.* (2017), using specific primers as previously reported (Table, 1), with slight modification to cycling conditions. The first round of the PCR was done by amplifying a common region of LMP-1 using Al and A2 as sense and antisense primers, respectively. Each PCR reaction mixture of 20 µl contains the following components with the final concentrations: *AccuPower®HotStart* PCR PreMix (produced by Bioneer, Inc. Korea), 2 µl (5Mm/µl) each of the forward and reverse primers, and 4 µl(100ng/ µl)of genomic DNA. The volume was made up with nuclease-free water. The cycling conditions for the PCR reaction were as follow: initial denaturation at 95°C for 5 min, followed by 35 cycles of amplification with denaturation at 95°C for 0.45 s, annealing at 56°C for 0.45 s, extension at 72°C for 0.45 s, and a find extension at 72°C for 5 min. A second round PCR (nested) was performed using 0.5 µl of the amplicons from the first round as template; all other reaction components were the same as the first-round reaction mixture, except for the primers. A forward primer (B1) and reverse primers (B2) were used for the second-round amplification. The reaction was carried out at initial denaturation at 95°C for 5 min, followed by 35 cycles of amplification with denaturation at 95°C for 0.45 s, annealing at 56°C for 0.45 s, extension at 72°C for 0.45 s, and a find extension at 72°C for 5 min. Afterward, PCR amplified products were separated on 1.5% ethidium bromide-stained agarose gel as previously described and visualized using UV light trans illuminator,

then a photo was taken by a Sony digital camera. In all experiments, a negative control (without genomic DNA) was used.

2.5. Phylogenetic analysis

LMP-1 PCR products (587 pb) were sent out to Germany at Eurofins Genomics for purification and determination of DNA sequence. Then, CLC Main Workbench 5 was used to run sequence alignments and construct the phylogenetic tree. For sequence homology comparison, sequences were compared to reference sequences representing the seven main EBV strains available in the GenBank database: B95.8 prototype strain (V01555), Med + with 30-bp deletion (AY337721), Med - without 30-bp deletion (AY493810), China 1 (AY337723), ina 2 (AY337724), Alaskan (AY337725), and NC strain (AY337726). As described by Lorenzetti *et al.* (2012) and Smatti *et al*. (2017). The phylogenetic tree was generated using the neighbor joining method. Bootstrapping and reconstruction were carried out with 100 replicates to obtain the confidence level of the phylogenetic tree.

3. Results and Discussion

3.1. Seroprevalence of EBV among study groups

Epstein-Barr virus VCA-IgM antibody were detected by Enzyme Linked Immunosorbant Assay (ELISA) test in 6 (12%) of the 50 cancer cases and in 4(8%) of the 50 controls (Table 2). In contrast, Salehi *et al.* (2016) reported that only 12/673 (8%) of blood samples were anti-VCA IgM antibodies positive, while 35% of the case group and 6% of the control group were positive for this antibody.

Table (2): Seroprevalence of EBV IgM antibody among cancer patients and control groups.

Groups	Seropositive of EBV IgM	
	Number	%
Cancerpatients (n=50)	6	12
Control groups (n=50)	4	8
Total	10	10

3.2. Molecular detection of EBV among study groups

All seropositive specimens of acute EBV infection (EBV IgM antibody) (n=10) were screened for the present of EBV-DNA using Conventional Polymerase Chain Reaction (PCR) assay. The number of EBV-DNA positive were 66.7% (4/6) and 50% (2/4) for cancer patients (cases) and controls, respectively (Figure1). In our study, not all samples classified serologically with reactive EBV infection (EBV-IgM positive) were positive by PCR. This could be explained by the cross-reaction with other antigenically related viruses, especially CMV (de Ory *et al.*, 2011and Guerrero-Ramos *et al.*, 2014). Also, serological testing only cannot confirm reactivation status or the exact reactivation time (Maurmann *et al.*, 2003). Therefore, EBV-DNA detection and viral load quantification is used to assist in the diagnosis of EBV reactivation, although discrepancies can be found between PCR and serology.

In the same respect, many studies have detected EBV-DNA in different types of cancer and healthy individuals. In Brazil, 43% (13/30) of the patients with HL had EBV-DNA and 8% (1/13) of healthy individuals were positive for EBV-DNA (Musacchio *et al.*, 2006). In India,EBV-DNA was detected in 49% (16/33) of HL patients and not in controls (Sinha *et al.*, 2016).In Iran, 35/56 (62.5%) of GC patients and 3/56 (5.4%) of controls, were EBV-DNA positive (Amoueian *et al.*, 2018). In Ghana, the number of EBV-DNA positives were 67% (37/55) and 92% (48/53) for NPC patients and controls, respectively (Ayee *et al.*, 2020). The differences in results might be due to:1. the small sample size of the reactivation group (n=10); 2.EBV detection by PCR is highly affected by the specimen used (whole blood versus PBMC versus serum) and the variation in sample types must always be considered when comparing different studies (Smatti *et al*., 2017); 3. several factors including; the methodology employed (e.g. relative sensitivities and the specificity of the tests used), undefined socioeconomic conditions, the geographic distribution and the immunity disturbance occasionally seen in cancer patients (Musacchio *et al*., 2006; Nasher, 2012; Sinhal *et al.*, 2016).

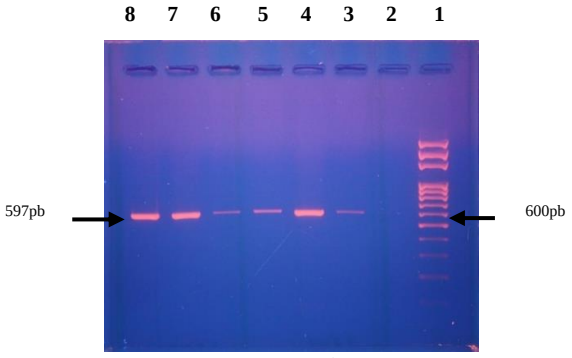

Figure (1): Electrophoretic pattern of EBV-DNA detection. Lane 1: molecular weight marker- 100 pb (Bioneer, Inc., Korea); lane 2: negative control (without genomic DNA); lane 3,4,5,6,7 and 8: positive samples

3.3. EBV Genotypes in cancer patients and controls of the study participants

All positive samples of EBV-DNA detected were tested for EBV genotyping using nested PCR targeting the EBNA2 gene showed 497pb and 150pb fragment which are characteristic of genotypes 1 and 2, respectively.

Results in figure (2), showed that the frequencies of EBV genotype 1 in blood samples of both cancer patients and controls were predominant 100%(6/6), while frequencies of EBV genotype 2 in blood samples were 0% (0/6) in both cancer patient and control samples, whereas genotype 1 is usually more prevalent in Europe, America, China, and South Asia (Hu *et al.*, 1991; Tzellos and Farrell, 2012), compared to genotype 2 that is more prevalent in African and Papua New Guinean populations (Bouvard *et al.*, 2009; Kwok *et al.*, 2015).Our findings are in agreement with the results of two studies in Iran and Malaysia. Only genotype 1 was detected in Iranian HL and NHL samples (Habibian *et al.*, 2018), and in Malaysian NPC, HL and BL patients (Peh *et al.*, 2003). In contrast, other studies reported the prevalence of genotypes 1&2 in several countries. In India, the prevalence of type A, B and both A and B was reported to be 32(45.7%), 2(2.9%) and 1(1.4%), respectively (Janani *et al.*, 2015). However, 37(72.5%) of type 1, 2(3.5%) of type 2 and 4% of both types were reported in Qatar (Smatti *et al.*, 2017). In Brazil,54(71.1%) EBV1, 13(17.1%) EBV 2 and 9(11.8%) EBV 1&2 were reported by Monteiro *et al.*

(2020). In China, type 1was detected in 59 (72%) of leukemia cases and in 31 (88.6%) of myelodysplastic syndrome (MDS), while type 2 was detected in 7 (8.5%) of

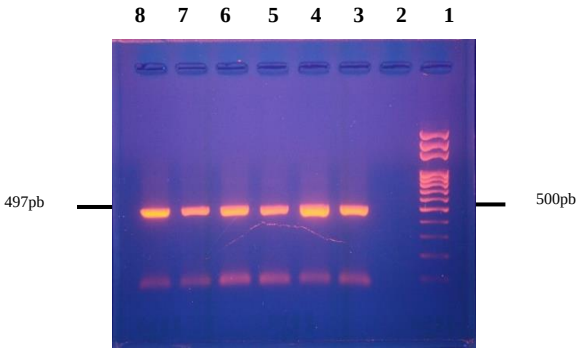

leukemia and in 3 (8.6%) of MDS, and both types 1&2 were detected in 16 (19.5%) of leukemia and 1 (2.8%) of MDS (Wanga *et al.*, 2021).

Figure (2): Electrophoretic pattern of EBV genotype 1. Lane 1: molecular weight marker- 100 pb; lane 2: negative control (without genomic DNA); lane 3,4,5,6,7 and 8: EBV positivity samples of genotypes 1.

3.4. EBV sub-genotypes in cancer patients and controls of the study participants

The 6 genotyped samples were further sub-genotyped by sequence analysis of the LMP1 gene C-terminus region. Nested PCR was used to amplify a 602pb and 587pb products as shown in figure (3&4). The second cycle of PCR products (587pb products) were sent out to Germany at Eurofins Genomics for purification and determination sequence DNA. After that, five DNA sequences were obtained from the sent samples, while the determination of the DNA sequence of one sample failed. Generated sequences were aligned in comparison to previously reported EBV strains (prototype B95-8(V01555), Med+(AY337721), Med-(AY493810), China 1(AY337723), China 2(AY337724), Alaskan(AY337725), NC (AY337726) using CLC Main Workbench 5. The phylogenetic tree was generated using the neighbor joining method.

Data in figure (5) showed that all EBV genotype positive cases in both cancer patients and controls were Med- (Mediterranean -) strain with a rate of 100%. In contrast to our results, there are several previous studies that have reported different strains of EBV in many countries including Hong Kong where LMP1-defined strains, China 1, China 2 and Mediterranean+ were reported to be the most common strains observed among infectious mononucleosis (IM) patients and asymptomatic individuals (AS) with primary EBV infection (Kwok *et al*., 2015). In Qatar, Smatti *et al*. (2017) revealed the presence of four variants among healthy blood donors including Mediterranean, B95.8, China 1 and North Carolina strains. In China, Wang *et al.* (2021) reported that four distinct sequence patterns were found in the specimens of patients with leukemia and myelodysplastic syndrome (MDS): B95-8, China 1, China 2, and Med (Mediterranean). These differences in results could be explained according to the suggestion of Gurtsevitch and Smirnova (2021) that direct sequencing of the C-terminal domain of LMP1(showing a high degree of heterogeneity compared to other EBV genes) in biological materials (blood, saliva, and tumor tissue) of cancer patients and healthy individuals from different geographic regions mismatched LMP1variants.

To the best of our knowledge, this study is the first which determined the genotype and the sub-genotype of EBV in Sana'a city, Yemen and provides a baseline information on the prevalence and co-infection patterns of the genotypes and sub-genotype among four types of cancer patients and healthy individuals in Sana'a city, Yemen and Middle East countries.

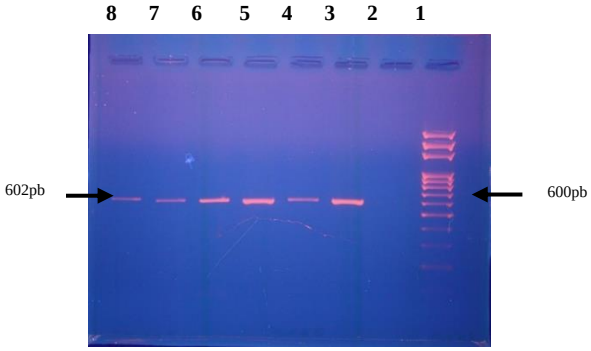

Figure (3): Electrophoretic pattern of EBV sub-genotype. Lane 1: molecular weight marker- 100 pb; lane 2: negative control (without genomic DNA); lane 3,4,5,6,7 and 8: EBV genotyped samples tested of sub-genotypes with amplicon of 602pb.

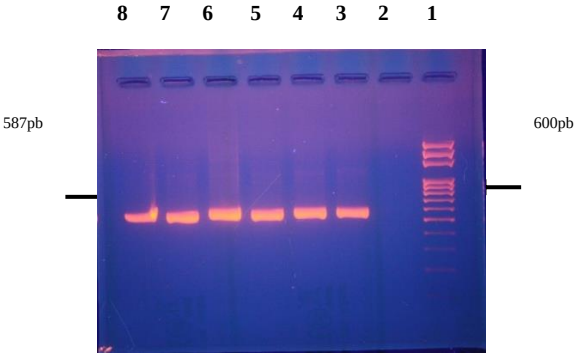

Figure (4): Electrophoretic pattern of EBV sub-genotype. Lane 1: molecular weight marker- 100 pb; lane 2: negative control (without genomic DNA); lane 3,4,5,6,7 and 8: EBV genotyped samples tested of sub-genotypes with amplicon of 587pb.

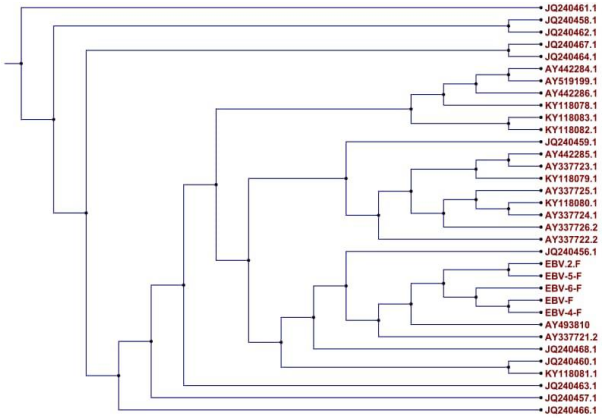

Figure (5): Phylogenetic tree of the C-terminus of LMP-1.

4. Conclusion

This is the first report for the predominance of EBV genotype 1, and sub-genotype Med- strain in the studied

Yemeni population. Identification of the virulent EBV genotype 1 in Yemen indicates a possible risk factor in the development of cancer in Yemeni patients.

5. Ethical approval

Ethics statement of the study a known ledged distinctive consent forms the Committee of Biological Sciences Department, Faculty of Science, Sana'a University and from the National Oncology Center of sample collection in Sana'a city, Yemen.

Acknowledgement

We acknowledge Department of Biological Sciences, Faculty of Science, Sana'a University, Yemen, and my sincere gratitude goes to Dr. ***Khalid Al-Shaibani***, the general manager of the Med Labs, for providing me with valuable guidance and appropriate place (Med. Labs) to conduct laboratory experiments in this work. Thank You!

Conflict of interest

The authors verify having no interest in competition and no conflict of interests.

References

Adjei AA, Armah HB, Gbagbo F, Boamah I, Adu-Gyamfi C and Asare I.2008. Seroprevalence of HHV-8, CMV, and EBV among the general population in Ghana, West Africa. *BMC Infect Dis*.,**8(1):**111.

Al-Diab AI, Siddiqui N, Sogiawalla FF and Fawzy EM.2003. The changing trends of adult Hodgkin's Disease in Saudi Arabia. *Saudi Med J*.,**24(6):**617-622.

Al Moustafa AE, Al-Antary N, Aboulkassim T, Akil N, Batist G and Yasmeen A. 2016. Co-Prevalence of Epstein- Barr Virus and high-risk Human Papillomaviruses in Syrian women with breast cancer. *Hum Vaccin Immunother*.,**12(7):**1936-1939.

AL-Nabhi A, Algharati AMT, Abdul Hamid G, Al-Nehmi A and Shamlan A. 2017. Pattern of cancer in Yemen: first result from the national oncology center, Sana'a, 2007. *EJPMR*.,**4(1):** 149-154.

Al-Salam S, John A, Daoud S, Chong SM and Castella A. 2008. Expression of Epstein-Barr Virus in Hodgkin Lymphoma in a population of United Arab Emirates Nationals. *Leuk Lymphoma*.,**49(9):**1769-1777.

Alwan A. 1997. Noncommunicable disease: a major challenge to public health in the region. *EMHJ*.,**3(1):** 6-16.

Amoueian S, Attaranzadeh A and Allahyari A. 2018. Epatein-Barr virus infection in adult patients with gastric cancer in Northeast of Iran. *Indian J Med Paediatr Oncol*.,**39(2):** 206-209.

Audouin J, Diebold J, Nathwani B, Ishak E, Maclennan K, Mueller-Hermelink HK, Armitage JO and Weisenburger DD.2010. Epstein-Barr Virus and Hodgkin's Lymphoma in Cairo, Egypt. *J Hematop*.,**3(1):**11-18.

Ayee R, Ofori MEO, Wright E and Quaye O. 2020. Epstein Barr Virus associated lymphomas and Epithelia cancer in humans. *J Cancer*.,**11(7):** 1737-1750.

Blake SM, Eliopoulos AG, Dawson CW and Young LS. 2001. The transmembrane domains of the EBV-encoded latent membrane protein 1 (LMP1) variant CAO regulate enhanced signalling activity. *Virol*.,**282 (2):**278–287.

Bouvard V, Baan R, Straif K, Grosse Y, Secretan B, El Ghissassi F, Benbrahim-Tallaa L, Guha N, Freeman C, GalichetL and Cogliano V. 2009. A review of human carcinogens-Part B: biological agents. *Lancet Oncol*.,**10(4):**321–322.

Chan KA, Zhang J, Chan AT, Lei KI, Leung S-F, Chan LY, Chow KC and Lo YD. 2003. Molecular characterization of circulating EBV DNA in the plasma of nasopharyngeal carcinoma and lymphoma patients. *Cancer Res*.,**63:** 2028–2032.

Cohen JT. 2018. Vaccine development for Epstein-Barr virus. *Adv Exp Med Biol*.,**1045:** 477-493.

Epstein M A, Achong BG and Barr YM. 1964. Virus particles in cultured lymphoblasts from Burkitt's lymphoma. *Lancet I*.,**1(7335):** 702-703.

Guerrero-Ramos A, Patel M, Kadakia K and Haque T. 2014. Performance of the architect EBV antibody panel for determination of Epstein-Barr virus infection stage in immunocompetent adolescents and young adults with clinical suspicion of infectious mononucleosis. *Clin Vaccine Immunol*.,**21(6):** 817–823.

Gurtsevitch V and Smirnova K. 2021. Epstein-Barr Virus (EBV) genome sequence variations, virus strain classifications and EBV-associated tumors. *Virol Immunol J*.,**5(1):** 1-3.

Habibian A, Makvandi M, Samarbaf-Zadeh A, Neisi N, Soleimani-Jelodar R, Makvandi K and Izadi S. 2018. Detection and Genotyping of Epstein-Bar Virus Among Paraffin Embedded Tissues of Hodgkin and Non-Hodgkin's Lymphoma Patients in Ahvaz, Iran. *Acta Medica Iranica*.,**56(7):** 434- 440.

zur Hausen H. 2001. Oncogenic DNA viruses. *Oncogene*., **20(54):** 7820–7823.

Hu LF, Zabarovsky ER, Chen F, Cao SL, Ernberg I, Klein G and Winberg G.1991. Isolation and sequencing of the Epstein-Barr virus BNLF-1 gene (LMP1) from a Chinese nasopharyngeal carcinoma. *J Gen Virol*.,**72(10):**2399–2409.

Janani MK, Malathi J, Rela M, Farouk M, Jand P and Madhavan HN. 2015. Genotypic detection of Epstein-Barr virus in pediatric transplant recipients from India. *Indian Pediatr*.,**52:** 946-950.

Kondo S, Horikawa T, Takeshita H, Kanegane C, Kasahara Y, Sheen TS, Sato H, Furukawa M and Yoshizaki T. 2004. Diagnostic value of serum EBV-DNA quantification and antibody to viral capsid antigen in nasopharyngeal carcinoma patients. *Cancer Sci*.,**95(6):**508–513.

Kwok H, Chan KW, Chan KH and Chiang AK. 2015. Distribution, persistence and interchange of Epstein-Barr virus strains among PBMC, plasma and saliva of primary infection subjects. *PLoS ONE*.,**10(3):**1-18.

Li HP and Chang YS. 2003. Epstein-Barr virus latent membrane protein 1: structure and functions. *J Biomed Sci*.,**10(5):**490–504.

Lin JC, Wang WY, Chen KY, Wei YH, Liang WM, Jan JS and Jiang RS. 2004. Quantification of plasma Epstein-Barr virus DNA in patients with advanced nasopharyngeal carcinoma. *N Engl J Med*.,**350(24):** 2461– 2470.

Makar RR, Saji T and Junaid TA. 2003. Epstein-Barr virus expression in Hodgkin's lymphoma in Kuwait. *Pathol Oncol Res*.,**9(3):**159-165.

Maurmann S, Fricke L, Wagner HJ, Schlenke P, Hennig H, Steinhoff J and Jabs WJ. 2003. Molecular parameters for precise diagnosis of asymptomatic Epstein-Barr virus reactivation in healthy carriers. *J Clin Microbiol*.,**41(12):**5419–28.

Mendes TM, Oliveira LC, Yamamoto L, Del Negro GM and Okay TS. 2008. Epstein- Barr virus nuclear antigen-2 detection and typing in immunocompromised children correlated with lymphoproliferative disorder biopsy findings. *Braz J Infect Dis*.,**12(3):**186–91.

Monteiro TAF, Costab IB, Costab IB, Corrêab TLS, Coelhob BMR, Silvab AES, Ramosb FLP, Filhob AJM, Monteirob JLF, Siqueirac JAM, Gabbayc YB and Sousad RCM. 2020. Genotypes of Epstein–Barr virus (EBV1/EBV2) in individuals with infectious mononucleosis in the metropolitan area of Belém, Brazil, between 2005 and 2016. *Braz J Infect Dis*.,**24(4):** 322-329.

Musacchio JG, Carvalho MGC, de Morais JCO, Silva NH, Scheliga A, Romano S and Spector N. 2006. Detection of free circulating Epstein-Barr virus DNA in plasma of patients with Hodgkin's disease. *Sao Paulo Med J*.,**124(3):** 154-7.

Nasher ATM. 2012. Prevalence of Human Papilloma (type 16 & 18) and Epstein-Barr viruses in oral squamous cell carcinoma and their association with other risk factors in some Yemeni patients (2009-2012). Ph.D. Thesis, Medical & Health Studies Board, The Graduate Collage, University of Khartoum, Sudan.

O'Neill 2021. Yemen: Estimated total population from 2016 to 2026. Available at https://www.statista.com/statistics/524126/total-population-of-yemen/

de Ory F, Guisasola ME, Sanz JC and Garcı´a-Bermejo I. 2011. Garcia-Bermejo I. Evaluation of four commercial systems for the diagnosis of Epstein-Barr virus primary infections. *Clin Vaccine Immunol*.,**18(3):** 444–8.

de Paor M, O'BrienK, Fahey T and Smith SM. 2016. Antiviral agents for infectious mononucleosis (glandular fever). *Cochrane Database Syst Rev*.,**12:** 1-45.

Parkin DM. 2006. The global health burden of infection-associated cancers in the year 2002. *Int. J. Cancer*.,**118(12):**3030–3044.

Peh SC, Kim LH, Mun KS, Tan EL, Sam CK and Poppema S. 2003. Epstein-Barr virus (EBV) subtypes and variants in malignant tissue from Malaysian patients. *J. Clin. Exp. Hematopathol*.,**43(2):** 61-69.

Saechan V, Mori A, Mitarnun W, Settheetham-Ishida W and Ishida T. 2006. Analysis of LMP1 variants of EBV in Southern Thailand: evidence for strain-associated T-cell tropism and pathogenicity. *J Clin Virol*.,**36(2):**119–125.

Saechan V, Settheetham-Ishida W, Kimura R, Tiwawech D, Mitarnun W and Ishida T. 2010. Epstein-Barr virus strains defined by the latent membrane protein 1 sequence characterize Thai ethnic groups. *J Gen Virol*.,**91(8):**2054–2061.

Salehi H, Salehi M, Roghanian R, Bozari M, Taleifard S, Salehi MM and Saleh M. 2016. Comparison of serological and molecular test for diagnosis of infectious mononucleosis. *Adv Biomed Res*.,**5(1):** 95.

Santpere G, Darre F, Blanco S, Alcami A, Villoslada P, Mar Albà M, et al. 2014. Genome-wide analysis of wild-type Epstein-Barr virus genomes derived from healthy individuals of the 1,000 Genomes Project. *Genome Biol Evol*.,**6(4):**846-860.

Sinha M, Rao CR, Shafiulla M, Shankaranand B, Viveka BK, Lakshmaiah KC, Jacob LA, Babu GK and Jayshree RS. 2016. Plasma Epstein Barr viral load in adult-onset Hodgkin Lymphoma in South India. *Hematol Oncol Stem Cell Ther*.,**9:** 8– 13.

Smatti MK, Yassine HM, AbuOdeh R, AlMarawani A, Taleb SA, Althani AA and Nasrallah GK. 2017. Prevalence and molecular profiling of Epstein Barr virus (EBV) among healthy blood donors from different nationalities in Qatar. *PLoS ONE*.,**12(12):**1-20.

Smatti MK, Al-Sadeq DW, Ali NH, Pintus G, Abou-Saleh H and Nasrallah GK. 2018. Epstein–Barr Virus Epidemiology, Serology, and Genetic Variability of LMP-1 Oncogene Among Healthy Population: An Update. *Front Oncol*.,**8:** 211.

Suntornlohanakul R, Wanlapakorn N, Vongpunsawad S, Thongmee T, Chansaenroj J and Poovorawan Y. 2015. Seroprevalence of Anti-EBV IgG among Various Age Groups from Khon Kaen Province, Thailand. *Asian Pac J Cancer Prev*.,**16(17):** 7583–7587.

Tzellos S and Farrell PJ. 2012. Epstein-Barr virus sequence variation-biology and disease. *Pathogens*.,**1(2):**156–175.

Van-Lant AL and Knipe DM. 2009. Herpesviruses. Harvard Medical School, Boston, MA, USA.

Vasef MA, Ubaidat MA, Khalidi HS, Almasri NM, Al-Abbadi M and Annab HZ. 2004. Association between Epstein-Barr virus and classic Hodgkin lymphoma in Jordan: A comparative study with Epstein-Barr virus-associated Hodgkin lymphoma in North America. *South Med J*.,**97(3):**273-277.

Walling DM, Brown AL, Etienne W, Keitel WA and Ling PD. 2003. Multiple Epstein-Barr virus infections in healthy individuals. *J Virol*.,**77(11):**6546–6550.

Wanga HY, Sun L, Li P, Liu W, Zhang ZG and Luo B. 2021. Sequence variations of Epstein-Barr virus-encoded small noncoding RNA and latent membrane protein 1 in hematologic tumors in northern China. *Intervirology*.,**64:** 69–80.

WHO (World Health Organization) 2021. Cancer patients in Yemen face the compounded pain of disease and conflict? Available at http://www.emro.who.int/yemen/news/cancer-patients-in-yemen-face-the-compounded-pain-of-disease-and-conflict.html

Yakovleva LS, Senyuta NB, Goncharova EV, Scherback LN, Smirnova RV, Pavlish OA and Gurtsevitch VE. 2015. Epstein Barr Virus LMP1 oncogene variants in cell lines of different origin. *Mol Biol (Mosk).*,**49(5):**800 – 810.

JJBS

Volume 16, Number 1,March 2023
ISSN 1995-6673
Pages 157 – 164
https://doi.org/10.54319/jjbs/160119

Jordan Journal of Biological Sciences

Leaf Blade Growth and Development in Red, Pink, and Yellow Petiole Cultivars of the Swiss Chards Grown in Floating Culture System

Benyamin Lakitan[1, 2*], Susilawati Susilawati[1], Andi Wijaya[1], Rofiqoh Purnama Ria[1], Strayker Ali Muda[1]

[1] *College of Agriculture, Universitas Sriwijaya, Inderalaya 30662, Indonesia;* [2] *Research Center for Sub-optimal Lands, Universitas Sriwijaya, Palembang 30139 Indonesia*

Received: March 28, 2022; Revised: June 25, 2022; Accepted: July 6, 2022

Abstract

Adaptability of the Swiss chard to the tropical climate opens opportunity to grow this leafy vegetable all year around. Colorful petiole and leaf blade of this vegetable have attracted urban community to grow them. Objectives of this research were to study the morphological and growth characteristics of the Swiss chard, especially leaf growth rate, time to reach full size, and non-destructive measurement of the leaf area. The Swiss chards used were red, pink, and yellow petiole cultivars. The plants were cultivated using the floating culture system. Relative leaf elongation and widening rates were higher at early leaf development, i.e. soon after the leaf blade was unfolded. Then, the rates were gradually declined and completely halted at about 12 days. In this study, combination of the zero-intercept linear model and the length × width (LW) as predictor were accurate for estimation leaf area (LA) of the red (R^2=0.981), pink (R^2=0.975), and yellow (R^2=0.980) petiole cultivars. The non-destructive measurement on selected morphological and/or weight traits should be useful for continuously monitoring of leaf growth, predicting yield at any time during plant growth, and determining the time to harvest.

Keywords: continuous monitoring, time to harvest, non-destructive measurement, yield prediction, zero-intercept regression.

1. Introduction

The western part of the Indonesian archipelago is classified as the tropical rain forest climate zone and characterized by high annual rainfall. Waterlogging occurs periodically in lowlands and coastal areas during rainy season. Floating culture is a reliable solution for avoiding the vegetables from submergence during the rainy season (Jaya et al., 2021; Siaga et al., 2018).

Swiss chard is a suitable leafy vegetable for cultivation during cool summer in the temperate climate zone, yet this vegetable can also tolerate the heat and humid tropical climate as long as water is available for maintaining soil moisture. Swiss chard is also grown well under full sunlight or partial shade. In the tropics, this vegetable is potentially grown all-year around. Leaf is obviously the most valuable organ in leafy vegetable.

Leaf has some specific roles, including capturing sunlight, absorbing CO_2, controlling inner temperature, and synthesizing carbohydrate. Leaf is also a good source of vitamins, minerals, fibers, pigments, antioxidants, and other beneficial substances for human health. Leaves also very significantly contribute to quality of environment. Furthermore, vibrant colors of leaf blade and petiole, such as in Swiss chard plant, also contribute to aesthetic value in urban living space.

Studies have focused on leaf from many different perspectives has aroused (Katifori, 2018; Smithers *et al*., 2019). Vanhaeren *et al*. (2015) explained that leaf emerged as a group of cells at the shoot apical meristem, then developed into planar, a complicated organ through different interrelated cellular events. Leaf development is driven by cell proliferation and cell expansion. However, active suppression on leaf meristem decelerated and, at the end, halted leaf growth (Alvarez *et al*., 2016)

Leaf shape and size were controlled by multiple genes. Modern technology helped to identify numerous genes that contributed to the final size of leaves and unraveled the complex cellular and molecular mechanisms that underlie leaf growth. Numerous genes have been identified to play significant role in inducing cell proliferation and/or size during leaf growth (Vercruysse *et al*., 2020).

The problem in the cultivation of leafy vegetables, such as Swiss chard, is the difficulty in determining the right time for harvesting in order to get an optimal quantity of yield and excellent quality of vegetables, namely the leaves are not too old at time of harvest. It was hypothesized that the Swiss chard leaf enlargement follows the Sigmoid curve and takes less than 10 days to reach the optimal leaf size.

Objectives of this research were to compare amongst Swiss chard with different petiole colors on their leaf morphological and growth characteristics, including probable changes in two-directional leaf growth, patterns

* Corresponding author e-mail: blakitan60@unsri.ac.id.

of midrib elongation and blade widening in growing leaf, number of days for individual leaf to reach its full size, development of accurate and reliable model for non-destructive leaf area estimation, and monitoring daily growth of Swiss chard leaves.

2. Materials and Methods

The research was conducted during dry season (31^{o} C and RH ± 51%) in tropical lowland climate at the Jakabaring Outdoor Research Facilities, Palembang, Indonesia. Planting material used was seeds of three Swiss chard cultivars with different petiole colors, i.e. red, pink, and yellow (Figure 1). The seeds were soaked in warm water (30^{o}C) for 15 minutes for enhancing imbibition process, then sown in seedling trays filled soil-chicken manure mixture (2:1 v/v).

The seedlings with two true leaves were transplanted to plastic pot at 14 days after sowing (DAS). The size of pot was 27.5 cm in inner-upper diameter and 19.8 cm in inner-lower diameter. The pots were loaded with the soil-manure mix similar to those used in nursery up to 20 cm in height. Prior to transplanting, the mix was pre-treated with bio-sterilant at dose of 2 gram/liter. Each pot was applied with 200 ml bio-sterilant solution. Nutrient was applied at non-flooded, well-aerated, upper layer of the substrate within each pot.

A floating cultivation system was conducted in an experimental pond. Three cultivation rafts were used. The raft dimensions were 2.0 m (length) × 1.0 m (width) × 0.078 m (height); constructed using 66 units of 1500 mL polyethylene terephthalate (PET) bottles as the floater. The water-substrate interface (WSI) was adjusted to 1.5 cm depth. The WSI is the thin (1-2 cm) water-saturated layer at bottom part of growing substrate which maintaining physical connection between the substrate and water surface. The pots were placed on the raft. The raft was submerged in water such that 1-2 cm growing substrate within the pots were always in contact with water surface. Each pot has 4 holes at the bottom. Substrate moisture is relatively stable between 15% to 20% due to the upward movement of water through the bottom 4 holes of the pot driven by the capillarity force.

Split plot experimental design was used. Three cultivation systems were assigned as the main plot, i.e., floating bottom-wet, and conventional. On each raft in floating culture consisted of 3 cultivars of Swiss chards were assigned as the subplots, 3 replications in each cultivar, and 2 pots in each replication. In total, 18 pots were placed on each raft in floating culture system.

2.1. Data collection

Length of leaf midrib (L) and width of leaf blade (W) were daily measured for 16 consecutive days and used as predictors for non-destructive estimation of LA. Measurement begins when the leaves begin to be unfolded on each individual leaf.

Leaf blade discontinued to enlarge in less than 2 weeks. Multiplication of the L×W was used as a secondary predictor for the LA. Accuracy of the LA estimation model was based on value of the coefficient of determination (R^2). The developed model was validated by comparing estimated value of LA and direct measurement of LA using a digital image analysis software LIA32, designed by Kazukiyo Yamamoto, Nagoya University, Japan.

Figure 1. Swiss chard with red, pink, and yellow petioles

2.2. Data analysis

Various types of regression models and predictors had been evaluated, and it was found that there were 3 most accurate models for leaf area estimation, namely: (a) the zero-intercept linear model uses the length × width of the leaf blade as a predictor; (b) the power and (c) the polynomial models if the length or width of the leaf blade is used as a predictor (Lakitan *et al*., 2017; 2018a; 2021). Therefore, in this study, the LA estimation was conducted using the zero-intercept linear, quadratic, and power regressions. The three regressions were intentionally chosen based on their performances in the previous studies.

Predictors used were L, W, and L×W. Curves of the relative leaf elongation, the relative leaf widening, and the leaf area enlargement were fitted using polynomial order-3 regression for mimicking the S-curve or reversed S-curve. Other secondary parameters were also calculated, including absolute leaf elongation rate (LER), absolute leaf widening rate (LWR), relative LER, relative LWR, length/width (L/W) ratio, average days to full leaf size (DFS), and non-destructive LA estimation. Calculations of the growth analysis formula were based on Hunt (2012).

3. Results

Leaf blade growth is three directional, i.e. length, width, and thickness; however, leaf thickened did not significantly contribute to light capturing activity, CO2 uptake, transpiration, and heat exchange. Thickness does not contribute significantly (<1%) to the total surface area of the leaves, except for succulent plants. The stomata are also never on the thickness edge of the leaf blade. Instead, the main leaf area is determined by length and width of the blade. Therefore, the two directional growth of midrib elongation and blade widening are the focus in this study (Figure 2). Midrib elongation rate of the yellow-petiole chard was significantly faster (7.69 mm/d) than those of red- and pink-petiole chard. The elongation rates of red- and pink-petiole chard were slightly more than 6 mm/d. The blade widening rates in all three cultivars of Swiss chard were almost similar at around 3.3 mm/d. Higher daily midrib elongation rate in yellow-petiole chard morphologically shaped its leaf to a slimer leaf blade compared to the other two cultivars of Swiss chard.

Ratio of length/width reflects shape of the leaf. The higher ratio value indicates a slimer leaf shape. Most of leaves have ratio of length/width higher than 1. Leaf can change its shape through a gradual process. In Swiss chard leaf, the ratios were 3.26 (red), 3.27 (pink), and 3.66 (yellow) at the early half of their development, then decreased to 2.08, 2.07, and 2.53, respectively, at the rest half, until the leaves stopped expanding. The leaves transformed into a more rounded shape as they got older. Midrib elongation and blade widening rates of individual leaf in all three cultivars of Swiss chards were relatively consistent (Figure 3).

Days required to reach full size leaf were significantly different between Swiss chard plants with red and yellow petiole colors. The fastest relative elongation and widening rates occurred at the first day after the leaf blade unfolded (Table 1). This phenomenon was mainly associated with rapid cell multiplication in the young leaves. Midrib length on the first measurement was less than 5 mm.

Relative leaf elongation and widening rates were very high at early growth in all Swiss chard cultivars studied but then gradually declined and completely halted at age less than 2 weeks (Figure 4). Knowledge on when the leaf blade stops to expand is beneficial for vegetable farmers, since this knowledge can be used as base of decision on the best time to harvest the specified leaf. Furthermore, farmers can develop their schedule for leaf harvesting of Swiss chard plants if the frequency of new leaf developed has also been known.

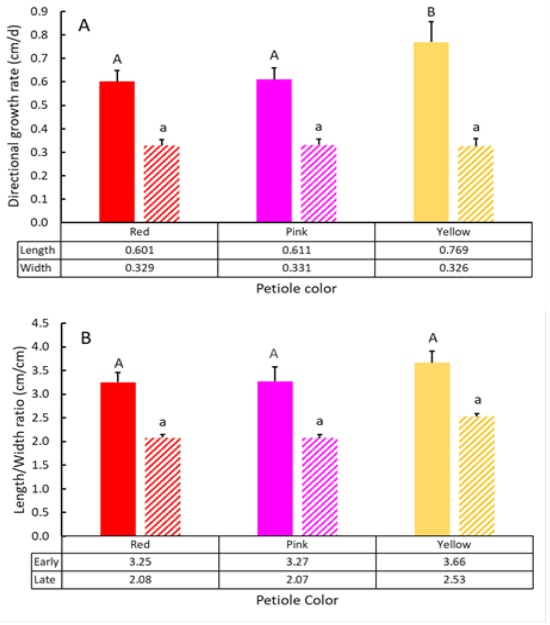

Figure 2. The two-directional growth of the leaf and leaf/width ratio in red-, pink-, and yellow-petiole Swiss chards. Solid bar is for leaf length and striped bar is for leaf width. Means followed by different letter was significantly different at $LSD_{0.05}$. The data in the table is used to show the magnitude of the difference.

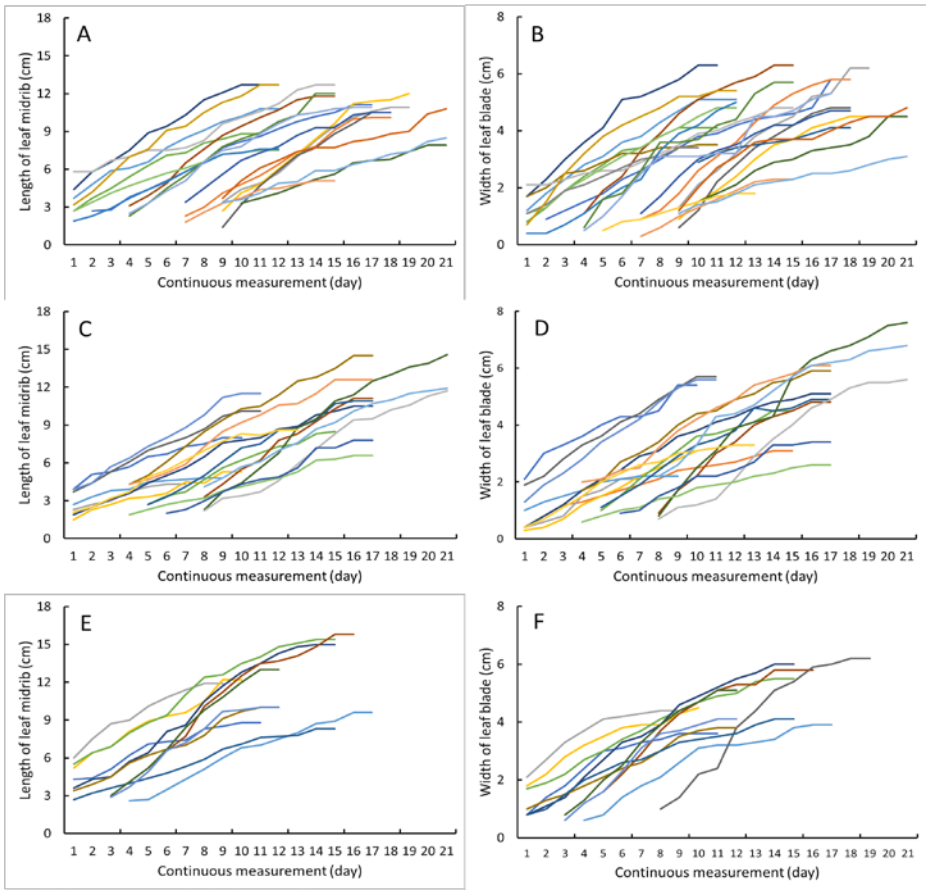

Figure 3. Elongation of midrib (A, C, and E) and widening of blade (B, D, and F) of individual leaf in Swiss chard with red (A-B), pink (C-D) and yellow (E-F) petiole colors. Each line represents the monitored individual leaf.

Table 1. Some leaf growth characteristics in red-, pink-, and yellow-petiole Swiss chard

	Growth characteristics	Petiole color		
		Red	Pink	Yellow
1.	Average number of days to reach full size leaf (d) [a]	11.60 ± 0.36 a	12.26 ± 0.56 b	12.00 ± 0.59 ab
2.	Fastest relative elongation rate (mm/mm/d) [b]	2.697	2.358	2.045
3.	Fastest relative widening rate (mm/mm/d) [b]	5.514	4.786	4.116

[a] Count was started at the first day since leaf blade unfolded. Means followed by different letter was significantly different at $LSD_{0.05}$.
[b] Predicted value using polynomial order-3 regression at the $R^2 > 0.95$ for both elongation and widening.

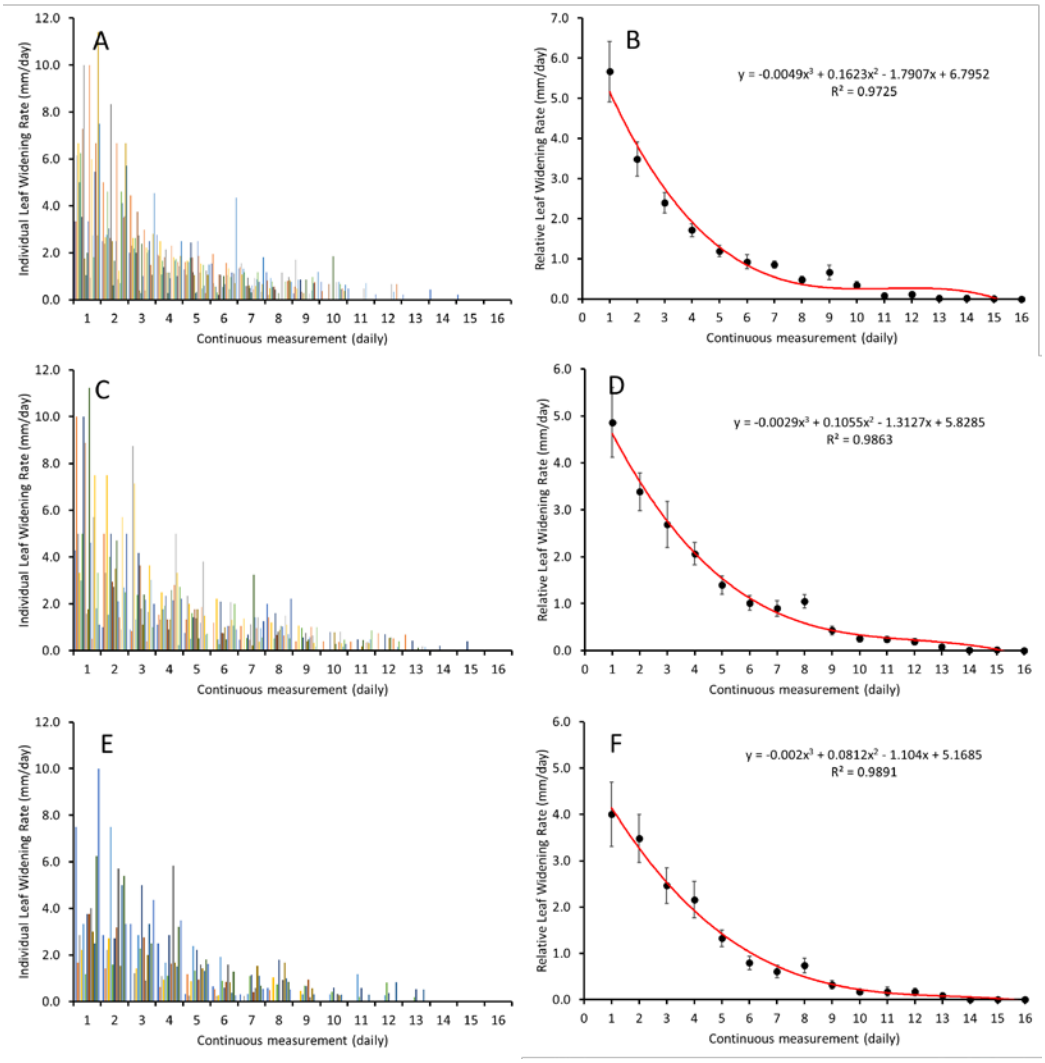

Figure 4. Elongation rate of individual leaf (A, C, and E) and declining trend of relative elongation rate (B, D, and F) in Swiss chard plants with red (A-B), pink (C-D), and yellow (E-F) petioles.

Leaf elongation and widening were halted at the same day. The slopy declining patterns of the midrib elongation were relatively similar to that of leaf blade widening, although the values of the two rates were different (Figure 5).

Leaf elongation and widening were halted at the same day. The slopy declining patterns of the midrib elongation were relatively similar to that of leaf blade widening, although the values of the two rates were different (Figure 5).

Leaf area estimation model is a prerequisite before the leaf expansion rate (LER) can be calculated based on LA measured non-destructively on each individual leaf. Most of the cases for the regular non-compound leaf, LA can be accurately estimated ($R^2 > 0.95$) using the zero intercept linear regression and L×W as predictor. Results in Figure 6 confirmed that combination of the chosen regression model and the selected predictor were accurate in estimating LA of all three Swiss chard cultivars, i.e. red-, pink-, and yellow-petiole cultivars.

Flattened S-curve was barely recognized in LA increased during 16-day period starting after the young leaf was naturally unfolded (Figure 7). LA of the yellow-petiole cultivar was much higher than those of red- and pink-petiole cultivars. Average calculated-LA of red-, pink, and yellow-petiole cultivars were 825.16 cm^2, 941.10 cm^2, and 1252.65 cm^2, respectively. Variability in leaf size increased as the plants grew older.

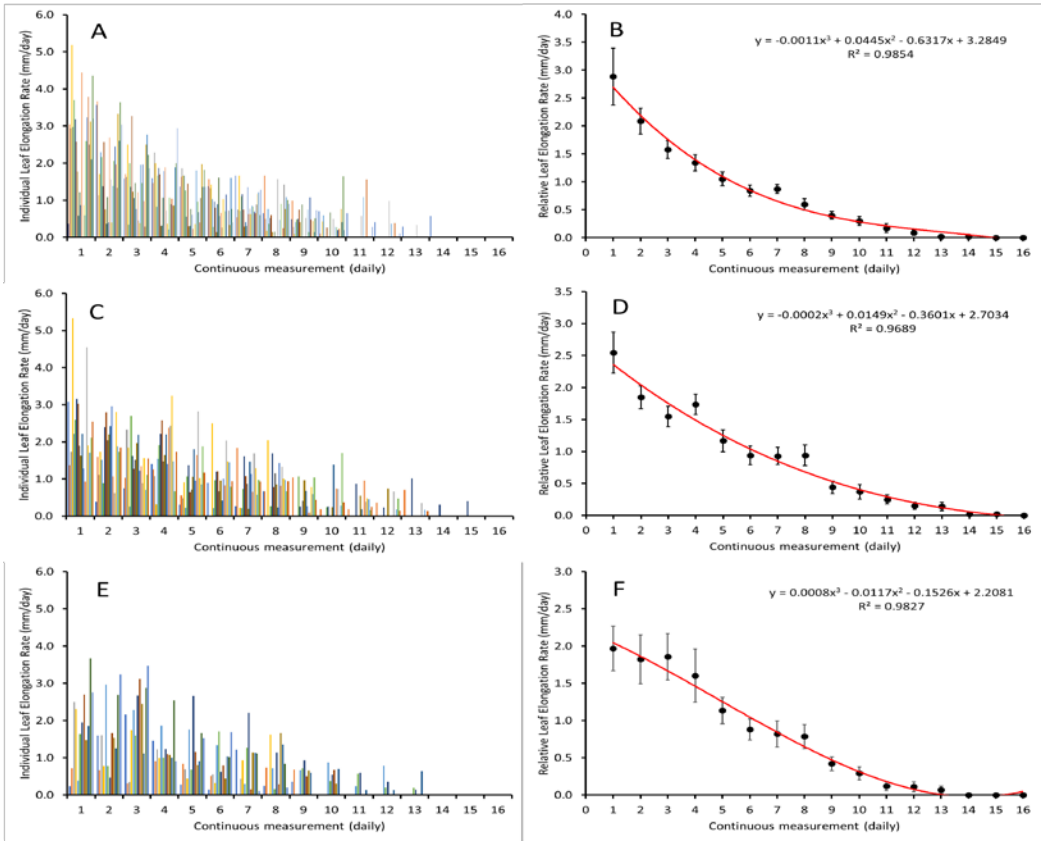

Figure 5. Widening rate of individual leaf (A, C, and E) and declining trend of relative widening rate (B, D, and F) in Swiss chard plants with red (A-B), pink (C-D), and yellow (E-F) petioles.

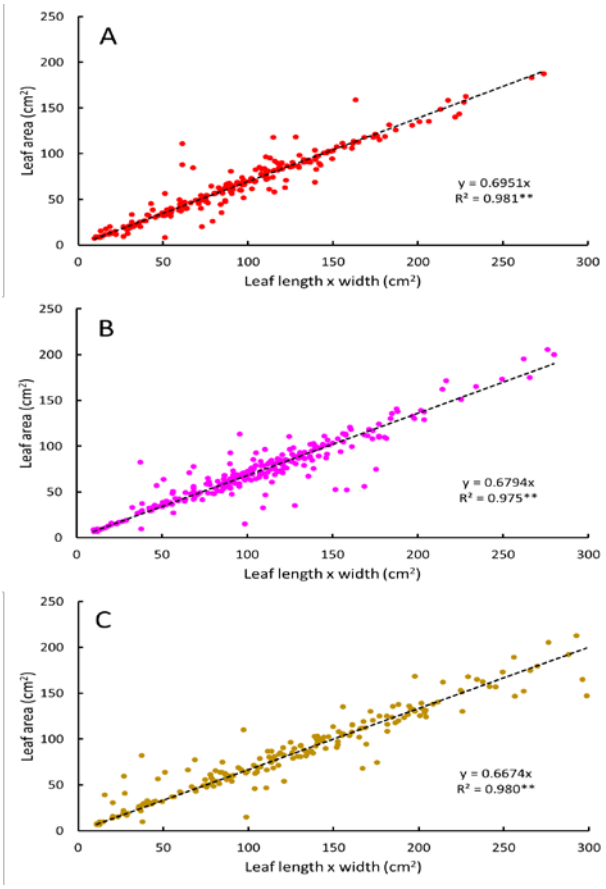

Figure 6. Leaf area estimation using L×W as predictor and the zero-intercept linear regression as selected model for Swiss chards with red (A), pink (B) and yellow (C) petioles.

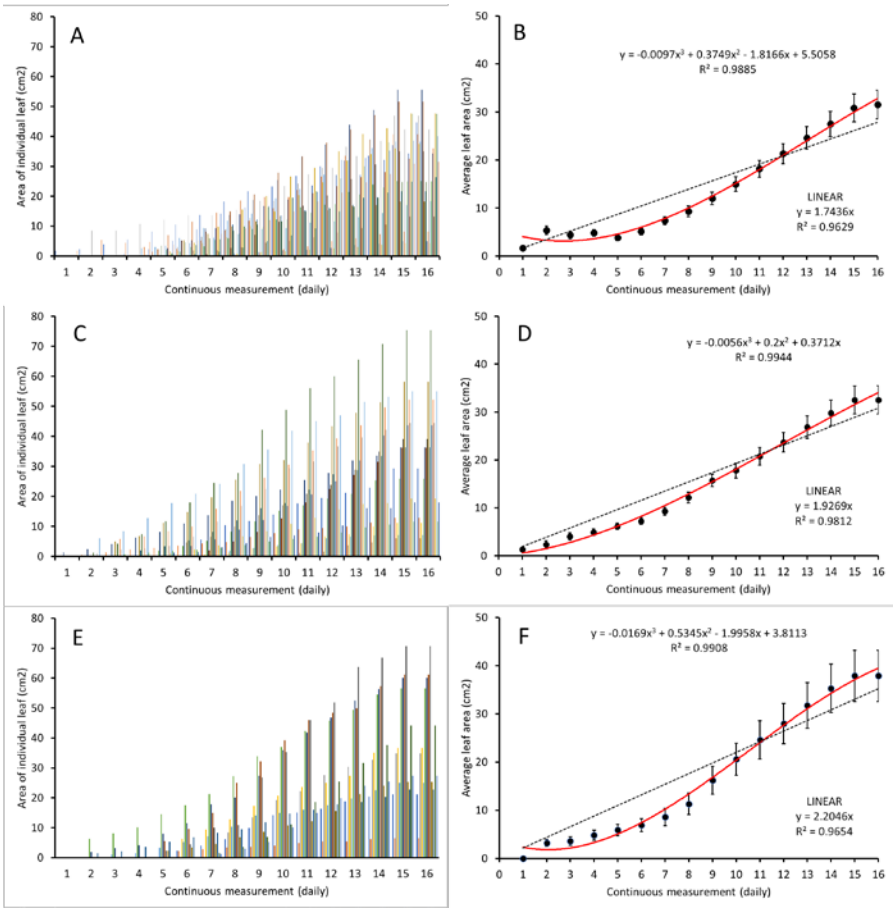

Figure 7. Leaf area of individual leaves (A, C, E) and average leaf area of Swiss chard (B, D, F) in red (A,B), pink (C, D) and yellow (E, F) petiole cultivars.

4. Discussion

4.1. Number of days to reach the maximum leaf size

Most studies related to leaf enlargement do not consider that the process takes place in two directions, which is formed from a combination of increasing the length and width of the leaves. In this study, differences due to lengthening were distinguished by the influence due to widening, because the ratio of length/width indicated whether the shape of the leaves was static or changed during the leaf enlargement process.

Nelissen *et al*. (2016) reported that leaf growth was temporally regulated with cell division ceasing earlier at the tip and continuing longer at the base of the leaf which may altered leaf shape. Leaf growth was enhanced by self-regulating pathways but affected by increase in cell number and growing conditions. The final size of leaf was closely controlled by environmental and genetic factors (Gonzalez *et al*., 2010). The growth rate started to decline soon after the division zone regressed. Despite leaf size differences at time of unfolding, the leaves of common bean (*Phaseolus vulgaris*) attained their full size in approximately 9 days (Lakitan *et al*., 2018a).

4.2. Leaf growth rate

Leaf growth was fluctuated during each 24-hour period. Relative leaf expansion rate (RLER) at night was significantly higher than daytime RLER in bean (Lakitan *et al*., 2018a) and tomatoes (Meihana *et al*., 2017). Higher nocturnal RLER was associated with higher leaf water content due to lower transpiration rate. Daytime leaf elongation rate (LER) was mainly temperature-dependent. LER at night was influenced by temperature and relative humidity (Stuerz and Asch, 2021). Leaf widening revealed a strong sensitivity to plant intercepted light and weak reaction to evaporative demand. Leaf elongation was receptive to evaporative demand and was not affected by the intercepted light (Lacube *et al*., 2017). Scoffoni *et al.* (2016) found the core for synchronization of hydraulic and photosynthetic physiology. Their reliance on climate confirms the function of water transport in photosynthetic activities.

Smithers *et al*. (2019) argued that plant growth was a highly mechanical process. Mathematics could provide an underlying framework for probing the fundamental unrevealed mechanisms and concluded that interdisciplinary collaborations were vital for tackling the challenge to understand plant growth mechanics. A similar argument was brought up by Katifori (2018) that the moves towards unraveling the problems of plant physiology and ecology could only be accomplished with collaboration amongst scientists in biology, computer science and physics.

Armon *et al*. (2021) identified that a growing leaf was a prototypical active solid and the cells were its active units. During the out-of-equilibrium process of cellular growth, the leaf increased its area, yet maintained a proper flat shape. Moreover, leaf growth strongly fluctuated in time and position. Growth isotropy did not homogenize in time. Mechanical analysis indicated that a leaf could stay flat

only if the fluctuations were regulated. How this was achieved in the lack of a central control was unknown.

4.3. Leaf shape

Leaf shape is only a common concern in plant species identification and generally leaf shape is assumed to be static, although in fact in some types of plants the shape of the leaves sometimes changes during the leaf development process. In this study, leaf shape in Swiss chard did not change during leaf development. In agronomic and physiological studies, leaf deformation rarely receives attention.

Li *et al*., (2020) observed that there was significant spatial and temporal intraspecific variation in leaf size and shape in response to climate. Leaf size changing over time was positively correlated with precipitation, whereas leaf shape changes were mostly correlated with temperature. Quantitative models apprehending genetic diversity and environmental plasticity required understanding on the evolution and development of the leaf shape and its response to environmental stresses (Chitwood and Sinha, 2016).

Odiyi and Eniola (2015) reported that acid rain caused leaf morphological alterations, including leaf folding. Kumar and Pandey (2017) reminded that the high levels of UV-B radiation augmented total leaf abnormality. However, these changes might be temporal. Mahdid et al. (2021) described that leaf growth was recovered after termination of an abiotic stresses. The recovery rate was linked to the propensity of osmotic adjustment in the elongation zone. Furthermore, Qi *et al*. (2017) argued that mechanical heterogeneity of the cell wall within tissue might underlie organ shape asymmetry which might include alteration of the leaf shape.

4.4. Leaf area estimation

Estimation of LA is commonly done for further use in non-destructive continuous data collection for calculating absolute and relative leaf expansion rate respectively and other LA-based secondary morphological traits, including continuous measurement of specific leaf area, specific leaf weight. LA estimation was using length of midrib (L), width of leaf blade (W), or L×W as predictor. Several regression models had been evaluated for their accuracy in estimating LA. For single regular-shape leaf, such as Swiss chard leaf, the zero-intercept linear regression has been proven to be a very accurate LA estimator if L×W is used as predictor (Lakitan *et al*., 2018b; Widuri *et al*., 2017). Result of this study confirmed that combination of the zero-intercept linear regression and L×W as predictor was an accurate LA estimation.

5. Conclusion

Leaf is the most important organ in leafy vegetable, including Swiss chard; therefore, leaf growth rate and reliable information on how long it takes for a leaf to reach its full size are beneficial for farmers on deciding the best time to harvest the leaf. Monitoring leaf growth rate should be non-destructively done. Length of midrib, width of leaf blade, and combination of these two morphological traits (L×W) can be used as reliable predictors for continuous leaf area (LA) estimation. For single-blade and regular-shape Swiss chard leaves, highly accurate estimation model was achieved by using the zero intercept linear regression and L×W as the predictor. The slopes were 0.695, 0.679, and 0.667 for red, pink, and yellow petiole cultivars, respectively. Based on the estimated LA, it was found that the yellow-petiole cultivar grew significantly faster than both red and pink cultivars. However, the leaves of all cultivars reached their full size at around 12 days after the tiny young leaf blade was unfolded. It is recommended that Swiss chard leaves should be regularly harvested within 12 days after the unfolded immature leaf blade has been recognizable, i.e. at midrib length of about 1 cm.

Acknowledgement

High gratitude goes to the editor-in-chief of the Jordan Journal of Biological Sciences and all supporting staff. We also would like to deeply appreciate the comments and suggestions given by the anonymous reviewers of our manuscript. This research was funded by Indonesian Ministry of Education, Culture, Research, and Technology, Grant No. 057/E5/PG.02.00.PT/2022.

References

Alvarez JP, Furumizu C, Efroni I, Eshed Y and Bowman JL. 2016. Active suppression of a leaf meristem orchestrates determinate leaf growth. *Elife*, **5**: e15023.

Armon S, Moshe M and Sharon E. 2021. The multiscale nature of leaf growth fields. *Comm Phys*, **4**: 1-7.

Chitwood DH and Sinha NR. 2016. Evolutionary and environmental forces sculpting leaf development. *Curr Biol.*, **26**: 297-306.

Gonzalez N, de Bodt S, Sulpice R, Jikumaru Y, Chae E, Dhondt S, and Inzé D. 2010. Increased leaf size: different means to an end. *Plant Physiol.*, **153**: 1261-1279.

Hunt, R. (2012). **Basic growth analysis.** Unwin Human Ltd., London.

Jaya KK, Lakitan B and Bernas SM. 2021. Responses of leaf celery to floating culture system with different depths of water-substrate interface and NPK-fertilizer application. *Walailak J Sci Technol*., **18:** e19823.

Katifori E. 2018. The transport network of a leaf. *C R Phys*, **19**: 244-252.

Kumar G and Pandey A. 2017. Effect of UV-B Radiation on chromosomal organization and biochemical constituents of *Coriandrum sativum* L. *Jordan J Biol Sci.*, **10**: 85-93.

Lacube S, Fournier C, Palaffre C, Millet EJ, Tardieu F and Parent B. 2017. Distinct controls of leaf widening and elongation by light and evaporative demand in maize. *Plant Cell Environ.*, **40**: 2017-2028.

Lakitan B, Widuri LI and Meihana M. 2017. Simplifying procedure for a non-destructive, inexpensive, yet accurate trifoliate leaf area estimation in snap bean (*Phaseolus vulgaris*). *J Appl Hort.*, **19**: 15-21.

Lakitan B, Kadir S and Wijaya A. 2018a. Tolerance of common bean (*Phaseolus vulgaris* L.) to different durations of simulated shallow water table condition. *Aust J Crop Sci.*, **12**: 661-668.

Lakitan B, Iwanaga H, Kartika K, Kriswantoro H and Sakagami JI. 2018b. Adaptability to varying water levels and responsiveness to NPK fertilizer in yellow velvetleaf plant (*Limnocharis flava*). *Aust J Crop Sci.*, **12**: 1757-1764.

Lakitan B, Kartika K, Susilawati S and Wijaya A. 2021. Acclimating leaf celery plant (*Apium graveolens*) via bottom wet

culture for increasing its adaptability to tropical riparian wetland ecosystem. *Biodiversitas J Biol Div*., **22**: 320-328.

Li Y, Zou D, Shrestha N, Xu X, Wang Q, Jia W and Wang Z. 2020. Spatiotemporal variation in leaf size and shape in response to climate. *J Plant Ecol.*, **13**: 87-96.

Mahdid M, Kameli A and Simonneau T. 2021. Rapid osmotic adjustment in leaf elongation zone during polyethylene glycol application: Evaluation of the imbalance between assimilation and utilization of carbohydrates. *Jordan J Biol Sci.*, **14**: 147-155.

Meihana M, Lakitan B, Harun MU, Widuri LI, Kartika K, Siaga E and Kriswantoro H. 2017. Steady shallow water table did not decrease leaf expansion rate, specific leaf weight, and specific leaf water content in tomato plants. *Aust J Crop Sci*., **11**: 1635-1641.

Nelissen H, Gonzalez N and Inze D. 2016. Leaf growth in dicots and monocots: so different yet so alike. *Curr Opin Plant Biol.*, **33**: 72-76.

Odiyi BO and Eniola AO. 2015. The Effect of simulated acid rain on plant growth component of Cowpea (*Vigna unguiculata*) L. Walps. *Jordan J Biol Sci.*, **8**: 51-54.

Qi J, Wu B, Feng S, Lu S, Guan C, Zhang X, Qiu D, Hu Y, Zhou Y, Li C, Long M and Jiao Y. 2017. Mechanical regulation of organ asymmetry in leaves. *Nature Plant*, **3**: 724-733.

Scoffoni C, Chatelet DS, Pasquet-Kok J, Rawls M, Donoghue MJ, Edwards EJ and Sack L. 2016. Hydraulic basis for the evolution of photosynthetic productivity. *Nature Plant*, **2**: 1-8.

Siaga E, Lakitan B, Bernas SM, Wijaya A, Lisda R, Ramadhani and Meihana M. 2018. Application of floating culture system in chili pepper (*Capsicum annum* L.) during prolonged flooding period at riparian wetland in Indonesia. *Aust J Crop Sci.*, **12**: 808-816.

Smithers ET, Luo J and Dyson RJ. 2019. Mathematical principles and models of plant growth mechanics: from cell wall dynamics to tissue morphogenesis. *J Exp Bot.*, **70**: 3587-3600.

Stuerz S and Asch F. 2021. Responses of rice growth today and night temperature and relative air humidity—Leaf elongation and assimilation. *Plants*, **10**: e134.

Vanhaeren H, Gonzalez N and Inzé D. 2015. A journey through a leaf: Phenomics analysis of leaf growth in *Arabidopsis thaliana*. **The Arabidopsis Book**, **13**: e0181.

Vercruysse J, Baekelandt A, Gonzalez N and Inzé D. 2020. Molecular networks regulating cell division during Arabidopsis leaf growth. *J Exp Bot.*, **71**: 2365-2378.

Widuri LI, Lakitan B, Hasmeda M, Sodikin E, Wijaya A, Meihana M, Kartika K and Siaga E. 2017. Relative leaf expansion rate and other leaf-related indicators for detection of drought stress in chili pepper (*Capsicum annuum* L.). *Aust J Crop Sci.*, **11**: 1617-1625.

JJBS

Volume 16, Number 1,March 2023
ISSN 1995-6673
Pages 165 – 170
https://doi.org/10.54319/jjbs/160120

Jordan Journal of Biological Sciences

Effects of Dietary Lysine for River Catfish Juveniles on Protein Digestibility and Body Composition

Diana Rachmawati[1,*], Istiyanto Samidjan[1], Dewi Nurhayati[1], Putut Har Riyadi[2], Roy Hendroko Setyobudi[3], and Olga Anne[4]

[1]*Department of Aquaculture, Faculty of Fisheries and Marine Sciences, Diponegoro University, Jl. Prof. Soedarto, SH, Tembalang, Semarang 50275, Central Java, Indonesia;* [2]*Department of Fishery Technology, Faculty of Fisheries and Marine Sciences, Diponegoro University, Jl. Prof. Soedarto, SH, Tembalang, Semarang 50275, Central Java, Indonesia;* [3]*Department of Agriculture Science, Postgraduate Program, University of Muhammadyah Malang, Jl. Raya Tlogomas No 246 Malang 65114, East Java, Indonesia;* [4]*Marine Technology and Natural Sciences Faculty of Klaipeda University, H. Manto g. 84, Klaipėda 92294, Lithuania*

Received: Sep 8, 2022; Revised: Feb 26, 2023; Accepted Feb 27, 2023

Abstract

The success of intensive aquaculture for river catfish juveniles (*Pangasius hypophthalmus* Sauvage, 1878) is determined by the availability of good quality feed. Good quality feed does not only contain protein required by the fish; it should also contain essential amino acids to support fish growth. Lysine is a constraint of amino acids in the formulation diet due to the characteristics of the plant-based protein with lysine deficiency. This study was conducted to determine the dietary effects of lysine river catfish juveniles on protein digestibility, body composition, and relative growth rate. The river catfish juveniles used in the study had a mean weight of 8.21 g ± 0.32 g fish^{-1}. The test feed contained 37.1 % and 19.76 MJ kg^{-1}. Doses of lysine in the feed were added in an increase of 0.25 g 100 g^{-1} [1.48 g; 1.73 g; 1.98 g; 2.23 g; 2.48 g, and 2.67 g] 100 g^{-1} dry diet)]. The results showed that a lysine-added diet with the dose of 2.23 % 100 g^{-1} dry diet generated the highest values of protein digestibility (ADCp), relative growth rate (RGR), and fish body composition compared to other treatments. The optimal dose of lysine in feed for protein digestibility and relative growth rate of river catfish juveniles were 2.22 % to 2.24 % dry diet.

Keywords: Amino acid essential, Diet formulation, Fish growth, Fish nutrition, Intensive aquaculture, Lysine deficiency, *Pangasius hypophthalmus* (Sauvage, 1878), Quality of feed

1. Introduction

The availability of high-quality feed determines the success of intensive aquaculture. The excellent quality of diet formulation of feed does not only contain protein required by the fish; it should also contain essential amino acids to support fish growth. Ten types of amino acids are necessary for the feed to help maximum growth (Setyobudi *et al*., 2021; Yun *et al*., 2016). Lysine is a constraint of amino acids in the diet formulation of feed due to the characteristics of the plant-based protein that has lysine deficiency (Xie *et al.*, 2012a). Lysine is one of the amino acids the fish highly require since it is discovered in high concentration in the carcasses of most species (NRC, 2011). For example, adding 1.93 % lysine from the total feed could increase the growth of orange-spotted rabbitfish (*Siganus guttatus* Bloch, 1787) (Nhu *et al*., 2022). Furuya *et al*. (2012) also indicated that adding 1 % lysine from the total feed can increase the efficiency of protein utilization by Nile tilapia (*Oreochromis niloticus* Linnaeus, 1758), which is followed by an increase in growth rate. Lysine is needed to support growth, normal physiological function, and protein synthesis. Lysine is a limiting amino acid for river catfish (*Pangasius hypophthalmus* Sauvage, 1878) species, and if feed diets are formulated to meet the minimum lysine requirement, all other amino acids should be in excess (Yun *et al*., 2016). Moreover, metionin lysine has a role in carnitine synthesis, transporting fat acid to create energy through oxidation reactions (Furuya *et al.* (2012).

Lysine deficiency in the fish causes slow growth, not maximal protein utilization, and losing appetite (Nguyen and Davis, 2016). Excess lysine in the feed also causes low growth (Yang *et al*., 2011). The lysine deficiency due to using a plant-based diet can be compensated for by adding lysine to the feed (NRC, 2011). The addition of lysine to the diet can increase fish weight (Khan and Abidi, 2011). The additional lysine in the diet also reduces lipid content in the fish (Nguyen and Davis, 2016), increases protein retention, and metabolizes mass growth (Cao *et. al*., 2012). Some studies have been done on the lysine needs of some fish species, such as *Oncorhynchus mykiss* Walbaum, 1792 (Yun *et al*., 2016), *Heteropneustes fossilis* Bloch, 1794 (Farhat and Khan, 2013), *Ictalurus punctatus* Rafinesque, 1818 and *Oreochromis niloticus* Linnaeus, 1758 (Nguyen and Davis, 2016), *Oreochromis niloticus* Linnaeus, 1758 (Ovie and Eze, 2013), *Siganus guttatus* Bloch, 1787 (Nhu *et al*., 2022), *Trachinotus blochii* Lacépède, 1801 (Ebeneezara *et*

* Corresponding author. e-mail: dianarachmawati1964@gmail.com

al., 2019), *Pseudosciaena crocea* Richardson, 1846 (Xie *et al*., 2012a).

The river catfish (*P. hypophthalmus*) is a freshwater cultivated fish that is highly preferred and consumed in Indonesia. The river catfish is one of the original fish in Indonesian waters that have been successfully domesticated, as superior fish and economical; besides, the cultivation development is quite prospective. Support for developing this fish is quite easy to access – farming areas, farmers, cultivation technology, even markets. For catfish cultivation, the environment needed is not complicated because catfish is included in the class of catfish that can survive in bad aquatic environments such as circumstances with lack of oxygen (Rachmawati and Prihantoro, 2019). The taste of river catfish meat is unique, tasty, and delicious. These characteristics make people like the Catfish (Rachmawati and Prihantoro, 2019). The need for protein for the growth of Catfish juveniles is 37.12 %, as reported by Jayant *et al*. (2018); however, there are still few studies on the optimal requirement of lysine for Catfish juveniles that justify studying the matter.

2. Materials and Methods

2.1. Research design and test fish

The study method used an experimental design conducted at the Laboratory of Freshwater Hatchery and Aquaculture of Muntilan Subdistrict, Magelang District, Central Java, Indonesia, from April to June 2021. Test fish was obtained from the laboratory. Adaptation for the fish on cultivation media and feed was made 1 wk before the study was conducted. Fish were acclimatized and reared in fiber containers with the dimension of 1.50 m × 1 m × 1 m filled with 600 L water. During adaptation, amino acid lysine-free feed was administered. One day prior to the experiment, the fish fasted to remove any metabolic waste. Test fish were healthy with homogenous size, normal organs, and pathogen-free (Rachmawati *et al*., 2017).

The containers used in this study were 18 aquariums. The study consisted of six treatments, and each treatment was replicated three times. The fish (weight of 8.21 g ± 0.32 g fish^{-1}) was reared in the aquariums with the dimension of 100 cm × 80 cm × 80 cm equipped 20 fish stocked recirculation systems each. The test diet was given at the fixed rate of 5 % of the mass weight three times a day (07.00, 12.00, and 17.00). The study was conducted for 49 d. Each fish was weighed on weekly basis to determine the growth.

2.2. Test feed

The lysine used was L-lysine HCI which is produced by PT. Cheiljedang, Indonesia. Test feed consisted of isonitrogenous feed (37.1 %) and isoenergetic feed (19.76 MJ kg^{-1}) based on the study of Jayant *et al*. (2018). Doses of lysine in the feed were added an increase of 0.25 g 100 g^{-1} (1.48 g; 1.73 g; 1.98 g; 2.23 g; 2.48 g and 2.67 g) 100 g^{-1} dry diet, equals 3.99 %, 4.66 %, 5.34 %, 6.01 %, 6.68 % and 7.19 % protein diet. The ratio of casein-gelatin (4:1) accounted for the minimum of amino acids, and other maximum amino acids were maintained to increase the isonitrogenous diet as lysine increased but by sacrificing non-essential amino acid, glycine, to decrease. Crystalized lysine amino acid was weighed according to the treatments and stirred in hot water (Hotplate Stirrer Ika Hs-7, Germany) at 80 °C. In a separate container, the gelatine was diluted in the water and constantly stirred, then mixed with the amino acid solution (Xie *et al*., 2012b). Diet ingredients were mixed with amino acid and gelatine solution and added with NaOH 6 N to reach pH 7.0 (Ebeneezar *et al*., 2019). After the diet mixture had been ready, the mixture was formed as pellets with a size of 4.2 mm (MKS-PLT10, Indonesia) and dried in the oven (Memmert, UF30Plus Universal, Italy) at 70 ºC for 3 h. After the pellets had been dried, the pellets were saved in cold storage (Gea AB2226R, China) at 4 ºC until the pellets were ready to be used. Formulation of test feed used for determining the dietary lysine content of juvenile Catfish was shown in Table 1.

Table 1. Formulation of tests feed used for Catfish juveniles

Ingredients (g 100 g^{-1}, dry diet)	**Diets**					
	P_1	**P_2**	**P_3**	**P_4**	**P_5**	**P_6**
Casein[a]	20	20	20	20	20	20
Gelatin[b]	5	5	5	5	5	5
Amino acid mix[c]	29.95	29.70	29.45	29.20	28.95	28.70
Dextrin	21.15	19.24	19.24	19.24	19.24	19.24
Corn oil	4	4	4	4	4	4
Cod liver oil	3	3	3	3	3	3
Mineral mix[d]	3	3	3	3	3	3
Vitamin mix[e]	4	4	4	4	4	4
Carboxymethyl cellulose	10	10	10	10	10	10
α- cellulose	0.06	0.06	0.06	0.06	0.06	0.06
Lysine	1.25	1.5	1.75	2.0	2.25	2.5
Cr_2O_3	0.5	0.5	0.5	0.5	0.5	0.5
Total	100	100	100	100	100	100
Analyzed lysine	1.48	1.73	1.98	2.23	2.48	2.67
Proximate composition [(*)]						
Crude protein (%)	36.85	37.13	36.76	37.12	37.05	37.08
Crude Lipid (%)	7.43	7.46	7.45	7.51	7.25	7.45
Ash (%)	8.33	8.30	8.32	8.28	8.36	8.27
Gross energy (kcal 100 g^{-1}, dry diet)	471.87	471.89	471.88	471.87	471.87	471.88

[a]Crude protein (76 %)

[b]Crude protein (96 %)

[c]Amino acid mixture (g 100 g^{-1}) tryptophan 0.45; alanine 1.23; methionine 1.03; valine 1.67; proline 0.952; tyrosine 0.94; aspartie acid 0.09; cystine 0.85; arginine 1.20; glulamic acid 0.08; histidine 0.37; serine 0.06; isoleucine 2.15; leucine 1.89; threoinne 1.02; phenyla-lanine 1.55; lysine variable; glycine variable.

[d]Mineral mixture (g 100 g^{-1}) magnesium sulphate 13.20; potassium iodide 0.015; zinc sulphated $7H_2O$ 0.40; sodium chloride 4.35; magnus sulphated H_2O 0.080; calcium biphosphate 13.57; calcium lactate 32.69; potassium phosphate 23.98; alumunium chloride $6H_2O$ 0.0154; cuprous chloride 0.010; cobalt chloride $6H_2O$ 0.10; sodium biphosphate 8.72; ferric citrate 2.97 (Xie *et al*., 2012b).

[e]Vitamin mixture diluted in choline chloride 0.5 g 100 g^{-1}; pyridoxine hydrochloride 0.005; vitamin B12 0.00001; alpha cellulose 3 g 100 g^{-1}; biotin 0.0005; vitamin E as α-tocopherol 0.04; thiamin hydrochloride 0.005; ascorbic

acid 0.10; niacin 0.075; calcium pantothenate 0.05; riboflavin 0.02; menadione 0.004; folic acid 0.0015; inositol 0.20 (Loba Chemic India)

*) Animal Nutrient Laboratory, Faculty of Husbandry and Agriculture, Diponegoro University (2021)

2.3. Proximate analysis

Based on the method of Latimer (2019 and Setyobudi *et al*. (2018), AOAC proximate analysis was used to analyze diet and carcasses of the fish. Ash content was attained by incinerating the sample fish in the furnace (HPE, Indonesia) at a temperature of 550 °C for 24 h. The cooled and stable ash results were then weighed so that the formula can calculate the total ash content:

$$\text{Ash (\%)} = \frac{W_1 - W_2}{W} \times 100\ \% \quad (1)$$

W = Sample weight before turn to ashes (g)

W_1 = Sample weight + porcelain dish after turn to ashes(g)

W_2 = Weight of an empty porcelain dish (g)

The fat level was measured with the eter extraction method based on the Soxhlet (FOSS Soxtec 2043, Denmark) method. Samples with known constant weight were put into Soxhlet extracted using hexane or petroleum ether. After extraction, the sample was removed from the Soxhlet and dried.

$$\text{Crude lipid (\%)} = \frac{\text{Initial weight (g)} - \text{Final weight (g)}}{\text{Final Sample weight (g)}} \times 100\ \% \quad (2)$$

Protein content was measured with a semi-automatic Kjeldahl system (FOSS Kjeltec 2300, Denmark). Samples (2 g) were digested in the digestion unit for 45 minutes. The digester was then distilled in a distillation unit (Kjeldahl system, Indonesia). It was titrated with 0.2 N Hydrochloric acid HCL, and crude protein was obtained by multiplying the total nitrogen by a conversion factor of 6.25 (Setyobudi *et al*. 2021, Tonda *et al*., 2022)

$$\text{Crude protein (\%)} = \frac{\text{mL titration} \times N \times 14{,}007 \times 6.25 \times 100\ \%}{\text{Weight the sample (g)} \times 1\ 000} \quad (3)$$

2.4. Protein digestibility analysis

The indirect method of adding Cr_2O_3 0.5 % in the diet to measure protein digestibility was employed (Pérez-Jiménez *et al*., 2014). Before the feces of the fish were collected, the fish was acclimated to the diet containing chromium for 1 wk. After the 8th day, the feces were collected for 49 d every morning, noon, and afternoon after the fish was fed. The collection process was performed 2 h after feeding – a small plastic hose of which tip was attached to a wooden stick for easy moving was used for the purpose, and the feces were put in a bucket. Then the feces were filtered with a plankton cloth net; the filtered feces were placed in small plastic bottles and stored in cold storage. Before the feces were analyzed, they were dried in the oven (Memmert, UF30Plus Universal, Italy) at 6 °C for 24 h. After that, protein and Cr_2O_3 content in the feces were analyzed using a spectrophotometer (SSA 320N, Denmark) with a wavelength of 350 nm (Pérez-Jiménez *et al*., 2014).

2.5. Water quality

Observation of water quality, including temperature, pH, and dissolved oxygen, was conducted every day during the study. Meanwhile, the observations of ammonia-nitrogen (NH_3-N), nitrite-nitrogen (NO_2-N), and nitrate-nitrogen (NO_3-N) were done on the first and final day of the study. The quality of water was still in accordance condition of Catfish aquaculture. Those values for the temperature ranged from 26.4 °C to 30.5 °C; pH ranged 7.3 to 8.5; dissolved oxygen (DO) ranged from (4.6 to 6.8) mg L^{-1}; ammonia-nitrogen (NH_3-N) ranged between (0.002 to 0.002) mg L^{-1}; nitrite-nitrogen (NO_2-N) ranged (0.001 to 0.002) mg L^{-1}; nitrate-nitrogen (NO_3-N) ranged from (0.02 to 0.04) mg L^{-1} (Ut *et al*., 2016).

2.6. Observed variables

Variables that were observed included average growth weight (AWG), total feed consumption (TFC), relative growth rate (RGR), feed conversion ratio (FCR), protein efficiency ratio (PER), and survival rate (SR). The measurement of those variables was based on the method of Rachmawati *et al*. (2021), while protein digestibility (ADCp) and Efficiency Feed Utilization (EFU) measurement followed the method of Rachmawati and Prihantoro (2019). The Equation used to calculate the variables were in (4) to (11)

$$\text{AWG (\%)} = \frac{\text{Final weight (g)} - \text{Initial weight (g)}}{\text{Initial weight (g)}} \times 100\ \% \quad (4)$$

$$\text{TFC (g)} = \text{Amount of feed the first day + Amount of feed the second day + Amount of feed day n} \quad (5)$$

$$\text{SGR (\%)} = \frac{\text{Log final weight} - \text{Log initial weight}}{\text{Number of days}} \times 100\ \% \quad (6)$$

$$\text{ADCp (\%)} = 100 - \left\{ \frac{100 \times Cr_2O_3\ \text{feed (\%)} \times \text{protein feces (\%)}}{Cr_2O_3\ \text{feed (\%)} \times \text{protein feed (\%)}} \right\} \quad (7)$$

$$\text{AWG (\%)} = \frac{\text{Final weight (g)} - \text{Initial weight (g)}}{\text{The weight of feed consumed (g)}} \times 100\ \% \quad (8)$$

$$\text{FCR} = \text{feed consumtion (g) / body weight gain (g)} \quad (9)$$

$$\text{PER} = \text{body weight gain (g) / protein intake (g)} \quad (10)$$

$$\text{SR (\%)} = 100\ (\text{final count/initial count}) \quad (11)$$

2.7. Amino acid analysis

Analyze lysine of 1.48 %, 1.73 %, 1.98 %, 2.23 %, 2.48 %, and 2.67 % dry diet (Table 2) was determined by the HPLC (Column Chiller EW-42650-80, Japan) method followed by Ebeneezar *et al*. (2019), Setyobudi *et al.* (2021).

2.8. Statistic analysis

Data on growth performance and feed utilization variables before ANOVA analysis were tested for homogeneity, additivity, and normality. Analysis of

Variance (ANOVA) was used to determine growth performance and feed utilization variables. Duncan's Multiple Range Test was used to identify specific differences between means (Adinurani 2016, 2022). Finally, the Polynomial Orthogonal test was used to determine the optimum dose of lysine in the test feed (Xie *et al*., 2012a). The ethical clearance of this research was issued by the research ethics committee of Brawijaya University, Malang, East Java, Indonesia (No.114-KEP-UB-2021).

3. Results and Discussion

3.1. Result

3.1.1. Amino acids of test feed

The results were as shown in Table 2. It can be incurred that the essential amino acids in the test feed contains the lysine dose of 2.23 % dry diet, which was close to Catfish juveniles' essential amino acid profile

3.2. Composition of fish carcasses

The results of the proximate test of the fish carcasses, which were fed with various doses of lysine, are depicted in Table 3. The protein content in fish carcasses given additional lysine was higher than in the initial fish carcasses. The treatment with 2.23 % lysine in a dry diet showed the highest range of protein in the carcasses. The level of water, lipid, and ash contents decreased as the lysine in the fish increased.

Table 2. Content of amino acid on test feed (% dry matter)

Amino acid essential	Analyzed dietary lysine levels (% dry diet)						*P.hypophthalmus**
	1.48	1.73	1.98	2.23	2.48	2.67	
Threonine	1.69	1.58	1.55	1.40	1.29	1.28	1.358
Lysine	1.48	1.73	1.98	2.23	2.48	2.67	2.268
Phenylalanine	1.13	1.22	1.59	1.47	1.50	1.58	1.398
Arginine	1.18	1.26	1.39	1.45	1.47	1.49	1.447
Methionine	0.86	0.84	0.83	0.76	0.80	0.84	0.755
Leucine	3.59	3.64	3.68	4.09	4.20	4.25	4.128
Isoleucine	1.38	1.59	1.80	2.10	2.18	2.21	2.019
Histidine	0.81	0.83	0.82	0.84	0.82	0.81	0.841
Valine	1.52	1.63	1.74	1.81	1.90	1.98	1.805

Note : * Jayant *et al*. (2018)

Table 3. Body composition of Catfish juveniles containing different doses of lysine

g 100 g^{-1} wet weight	Analyzed dietary lysine doses (% dry diet)						
	Initial	1.48	1.73	1.98	2.23	2.48	2.67
Moisture	70.4 ± 0.1	70.2 ± 0.2	70.1 ± 0.2	70.0 ± 0.1	69.6 ± 0.3	68.6 ± 0.3	67.9 ± 0.1
Protein	11.6 ± 0.3	14.4 ± 0.2	15.7 ± 0.3	17.8 ± 0.2	19.5 ± 0.3	18.3 ± 0.1	17.0 ± 0.5
Lipid	9.6 ± 0.1	8.3 ± 0.3	7.5 ± 0.4	6.5 ± 0.3	6.2 ± 0.1	5.2 ± 0.2	5.0 ± 0.2
Ash	5.4 ± 0.1	4.4 ± 0.2	4.0 ± 0.2	3.5 ± 0.3	3.4 ± 0.2	3.2 ± 0.3	3.0 ± 0.2

Responses of Catfish juveniles fed with various dosages of lysine were displayed in Table 4. During the research, diseases that caused fish mortality were not found. The research study showed that the responses of AWG, TFC, ADCp, EFU, RGR, FCR, and PER were significant ($P < 0.01$) due to the availability of lysine in the feed; however, the existence of lysine in the feed did not affect SR. The highest values of AWG, TFC, ADCp, EFU, RGR, FCR, and PER were obtained in the fish which was given the feed containing lysine of a 2.23 % dry diet. The polynomial orthogonal test resulted in the optimum lysine dosages on ADCp and RGR as much as 2.24 % and 2.22 % dry feed, respectively (Figure 1 and Figure 2).

Table 4. Feed utilization and growth performance of juvenile catfish feed diets containing varying dietary lysine doses

Variables	Dietary lysine doses					
	1.48	1.73	1.98	2.23	2.48	2.67
Initial weight	8.21 ± 0.32	8.20 ± 0.30	8.25 ± 0.28	8.28 ± 0.18	8.20 ± 0.15	8.21 ± 0.30
Final weight	19.38 ± 0.12^{f}	24.51 ± 0.16^{e}	31.52 ± 0.10^{b}	42.56 ± 0.11^{a}	30.75 ± 0.12^{c}	27.73 ± 0.14^{d}
AWG (%)	11.17 ± 0.22^{f}	16.31 ± 0.23^{e}	23.27 ± 0.19^{b}	34.28 ± 0.14^{a}	22.55 ± 0.14^{c}	19.52 ± 0.22^{d}
TFC (g)	95.10 ± 0.26^{f}	96.53 ± 0.78^{dc}	97.43 ± 0.75^{b}	99.76 ± 0.42^{a}	96.83 ± 0.36^{c}	96.02 ± 0.27^{e}
ADCp (%)	58.27 ± 0.19^{f}	63.53 ± 0.14^{e}	75.15 ± 0.16^{c}	85.27 ± 0.14^{a}	77.63 ± 0.12^{b}	70.31 ± 0.17^{d}
EFU (%)	60.27 ± 0.12^{f}	65.17 ± 0.15^{e}	76.51 ± 0.18^{c}	85.24 ± 0.17^{a}	78.25 ± 0.15^{b}	71.46 ± 0.12^{d}
SGR (% d^{-1})	0.76 ± 0.08^{f}	0.97 ± 0.09^{e}	1.19 ± 0.12^{c}	1.45 ± 0.15^{a}	1.17 ± 0.12^{b}	1.08 ± 0.11^{d}
FCR	2.48 ± 0.10^{f}	2.12 ± 0.14^{e}	2.00 ± 0.10^{d}	1.43 ± 0.12^{a}	1.75 ± 0.13^{b}	1.98 ± 0.03^{c}
PER	1.78 ± 0.13^{f}	2.56 ± 0.10^{e}	3.05 ± 0.10^{c}	4.18 ± 0.13^{a}	3.78 ± 0.12^{b}	2.89 ± 0.11^{d}
SR (%)	93.85 ± 2.47^{a}	100 ± 0.00^{a}	100 ± 0.00^{a}	100 ± 0.00^{a}	100 ± 0.00^{a}	100 ± 0.00^{a}

Notes : Mean values with same superscript showed insignificant difference ($P > 0.05$)

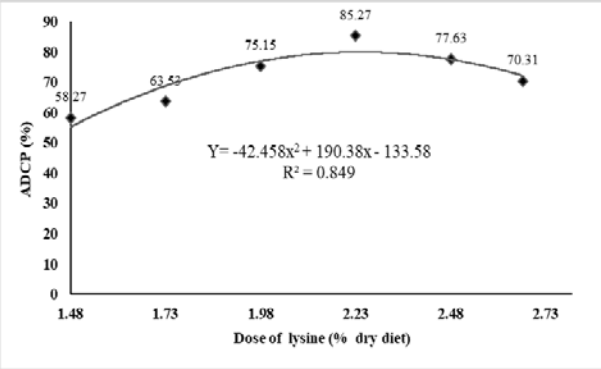

Figure 1. The correlation between the addition of lysine in the diet and ADCp

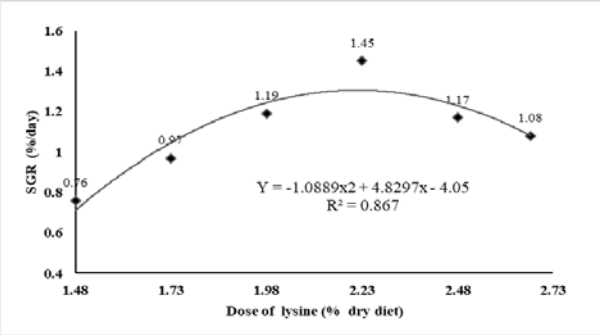

Figure 2. The correlation between the addition of lysine in the diet and SGR

4. Discussion

The river Catfish juveniles that were fed with a low dose of lysine caused low values of AWG, TFC, ADCp, EFU, SGR, FCR, and PER. Farhat and Khan (2013) disclosed that the lack of lysine caused low growth of the fish. The study results on *Litopenaeus vannamei* Boone, 1931 showed that lysine deficiency reduced appetite (Xie *et al*., 2012a). Otherwise, the results of this study proved that the river Catfish juveniles fed with various doses of lysine did not cause the fish appetite to decrease. The low values of ADCp, EFU, SGR, FCR, and PER were because of lysine deficiency. The lysine deficiency hindered protein synthesis and metabolism. The same results were discovered in several fish, such as in the *H. fossilis* (Farhat and Khan, 2013), *O. niloticus* (Ovie and Eze, 2013), *T. blochii* (Ebeneezara *et al*., 2019), *P. crocea* (Xie *et al*., 2012b), *O. mykiss* (Yun *et al*., 2016).

Besides the lack of lysine, the excess lysine also caused the values of TFC, ADCp, EFU, SGR, FCR, and PER to be low. However, the quantity of lysine did not indicate a toxic effect on the fish. So far, there is no information yet explaining the lysine toxicity in the fish. He *et al*. (2013) stated that the low growth of the fish fed with the excess lysine was due to the opposite function between lysine and arginine, although the mechanism has not been understood yet.

The protein content of fish carcasses fed with lysine supplementation was higher than that in the initial state. The increase in protein content in the fish carcass was due to the availability of lysine in the feed He *et al*. (2013). Hamid *et al*. (2016) expressed that lysine promotes protein formation in fish. Cao *et al*. (2012) noted that lysine could boost nitrogen retention. Lysine is essential to synthesize carnitine which transports fat acids and oxidizes fat to create energy. Wu (2013) also described that lysine is a critical factor for synthesizing keratin, which transports long-chain fatty acids from the cytoplasm to mitochondria for β-oxidation. Fat content in the fish carcass fed with a low dosage of lysine (1.48 % dry diet) was higher than those given with higher dosages of lysine (1.73 %, 1.98 %, 2.23 %, 2.48 %, and 2.67 % dry diet). The decrease in carnitine synthesis was thought to be due to lysine deficiency that hindered lipid metabolism and caused an excess of fat and energy. Similar studies were proclaimed by Xie *et al*. (2012b) in the white shrimp (*L vannamei*), Yang *et al*. (2011) in the silver perch (*Bidyanus bidyanus* Mitchell, 1838), Helland *et al*. (2011) in the Atlantic salmon (*S. salar*), Farhat and Khan (2013) in the black seabream (*Spondyliosoma cantharus* Linnaeus, 1758).

The highest values of AWG, TFC, ADCp, EFU, SGR, FCR, and PER were obtained from the fish fed with the lysine dosage of 2.23 % dry diet. It was thought that profile of amino acids in the feed containing lysine in a 2.23 % dry diet has a similar essential amino acids profile in the Catfish juveniles (Table 2). Therefore, He *et al*. (2013) declared that the appropriate feed for fish was the feed with a similar amino acid profile. Thus, the optimum lysine for protein digestibility and relative growth rate in the feed of Catfish juveniles ranged from 2.22 % to 2.24 % dry diet (5.96 % to 6.03 % protein feed).

NRC (2011) disclosed that the requirement of lysine among fish species and within the same species has various levels ranging from 3.32 % to 6.61 % protein feed. Therefore, the study's results were consistent with the need for lysine for fish, according to NRC (2011). The lack of lysine for Catfish juveniles (*P. hypophthalmus*) – 5.96 % to 6.03 % protein feed – was similar to the lysine requirement for stinging Catfish fingerlings (*H. fossilis*) at 5.3 % to 6.1 % (Farhat and Khan, 2013) and silver perch (*B. bidyanus*) at 6.0 % (Yang *et al.*, 2011), but lower than for *Trachinotus ovatus* Linnaeus, 1758 at 6.7 % (Du *et al*., 2011). However, it was higher than one for Indian major carp (*C. mrigala*) at 5.75 % (Ahmed and Khan, 2011), large yellow croaker (*P. crocea*) at 3.95 % (Xie *et al*., 2012), and juvenile Silver pompano (*T. blochii*) at 5.71 % to 5.83 % (Ebeneezara *et al*., 2019).

5. Conclusion

Supplementation of lysine in feed with the dose of 2.23 % dry diet generated the highest values of protein digestibility (ADCp), relative growth rate (SGR), and fish body composition compared to other treatments. The optimal dose of lysine in feed for protein digestibility and relative growth rate of juvenile Catfish were 2.22 % to 2.26 % dry diet.

Acknowledgements

The authors express special gratitude to the Head of Research and Community Service of Diponegoro University for granting the research funding through Grant for Research, Development and Applied Research as a support to the National Budget of Diponegoro University the year of 2020 with the letter assignment Number: 233-86/UN7.6.1/PP/2021.

References

Adinurani PG. 2016. **Design and Analysis of Agrotrial Data: Manual and SPSS**. Plantaxia, Yogyakarta, Indonesia

Adinurani, PG. 2022. **Agrotechnology Applied Statistics (Compiled According to the Semester Learning Plan)**. Deepublish, Yogyakarta, Indonesia.

Cao JM, Chen Y, Zhu X, Huang YH, Zhao HX, Li GL, Lan HB, Chen B and Pan Q. 2012. A study on dietary L-lysine requirement of juvenile yellow Catfish *Pelteobagrus fulvidraco*. *Aquac. Nutr.*, **18**: 35–45. https://doi.org/10.1111/j.1365-2095.2011.00874.x

Du Q, Lin HZ, Niu J, Ding X, Huang Z, Chen X and Chen YF. 2011. Dietary lysine requirements of juvenile pompano (*Trachinotus ovatus*). *Chin. J. Anim. Nutr*. **23**:1725–1732. https://doi.org/10.1016/j.aquaculture.2019.734234

Ebeneezara S, Vijayagopala P, Srivastavab PP, Gupta S, Sikendrakumarb, Vargheseb T, Prabua DL, Chandrasekara S, Varghesea E, Sayooja P, Tejpalc CS and Wilson L. 2019. Dietary lysine requirement of juvenile silver pompano, *Trachinotus blochii* (Lacepede, 1801). *Aquaculture.*, **511 (734234)**: 1–8. https://doi.org/10.1016/j.aquaculture.2019.734234

Farhat D and Khan MA. 2013. Dietary L-lysine requirement of fingerling stinging catfish, *Heteropneustes fossilis* (Bloch) for optimizing growth, feed conversion, protein and lysine deposition. *Aquac. Res.*, **44(4)**: 523–533. https://doi.org/10.1111/j.1365-2109.2011.03054.x

Furuya WM, Graciano TS, Vidal LVO, Xavier TO, Gon-gora LD, Righetti JS and Furuya VRB. 2012. Digestible lysine requirement of nile tilapia fingerlings fed arginine-to- lysine-balanced diets. *Rev. Bras. Zootec*. **41(3)**: 485–490. https://doi.org/10.1590/S1516-35982012000300003

Hamid SNIN, Abdullah MF, Zakaria Z, Yusof SJHM and Abdullah R. 2016. Formulation of fish feed with optimum protein-bound lysine for African Catfish (*Clarias gariepinus*) fingerlings. *Procedia Eng*., **148**:361–369.

https://doi.org/10.1016/j.proeng.2016.06.468

He JY, Titan LX, Lemme A, Gao W, Yang HJ, Niu J, Liang GY, Chen PF and Liu YJ. 2013. Methionine and lysine requirements for maintenance and efficiency of utilization for growth of two sizes of tilapia (*Oreochromis niloticus*). *Aquac.Nutr.*, **19**: 629–640. https://doi.org/10.1111/anu.12012

Helland GB, Gatlin DM, Corrent E and Helland SJ. 2011. The minimum dietary lysine requirement, maintenance requirement and efficiency of lysine utilization for growth of Atlantic salmon smolts. *Aquac.Res.*, **42**:1509–1529. https://doi.org/10.1111/j.1365-2109.2010.02743.x

Jayant M, Muralidhar AP, Sahu NP, Jain KK, Pall AK, Pal AK and Srivastava PP. 2018. Protein requirement of juvenile striped Catfish, *Pangasianodon hypophthalmus*. *Aquac. Int.* **26(1)**:375–389. https://doi.org/10.1007/s10499-017-0216-0

Khan MA and Abidi SF. 2011. Effect of dietary L-lysine levels on growth, feed conversion, lysine retention efficiency and haematological indices of *Heteropneustes fossilis* (Bloch) fry. *Aquac. Nutr.*, **17(2):**e657–e667. https://doi.org/10.1111/j.1365-2095.2010.00815.x

Latimer GW. Jr. (Ed.) 2019. **Official Methods of Analysis of AOAC International 21st Edition**, 2019. AOAC International. Maryland, USA.

Nhu BM, Truong DV, Thi TTN, Duy TQN, That CT, Dan LV, Serrano AE. 2022. Effect of dietary lysine level on the growth performance of orange-spotted rabbit fish (*Siganus guttatus*) fingerlings. *Isr. J. Aquac.*, **74(1713744)**:1–13.

https://doi.org/10.46989/001c.36170.

Nguyen L and Davis DA. 2016. Comparison of crystalline lysine and intact lysine used as a supplement in practical diets of channel catfish (*Ictalurus punctatus*) and nile tilapia (*Oreochromis niloticus*). *Aquaculture*. **464**:331–339. https://doi.org/10.1016/j.aquaculture.2016.07.005

NRC (National Research Council). 2011. **Proteins and Amino Acids. Nutrient Requirements of Fish and Shrimp**. National Academy Press, Washington, D.C. pp. 57–101.

Ovie SO and Eze SS. 2013. Lysine requirement and its effect on the body composition of *Oreochromis niloticus* fingerlings. *J. Fish. Aquat. Sci*. **8(1)**: 94–100. https://doi.org/10.3923/jfas.2013.94.100

Pérez-Jiménez A, Peres H and Oliva-Teles A. 2014. Effective replacement of protein-bound amino acids by crystalline amino acids in Senegalese sole (*Solea senegalensis*) juveniles. *Aquac. Nutr.*, **20(1)**: 60–68. https://doi.org/10.1111/anu.12052

Rachmawati D, Istiyanto S and Maizirwan M. 2017. Effect of phytase on growth performance, feed utilizationefficiency and nutrient digestibility in fingerlings of *Chanos chanos* (Forsskal 1775). *Philipp J. Sci*., **146 (3):**237–245.

Rachmawati D and Prihantoro AA. 2019 Effect of papain enzyme supplementation on growth performance and nutrient utilization of Catfish (*Pangasius hypophthalmus*). *Malays Appl Biol.*, **48(5)**: 1–10.

Rachmawati D, Setyobudi RH, Burlakovs J, Elfitasari T and Purnomo AH. 2021. Impacts of immunostimulant yeast (*Saccharomyces cerevisiae*) supplemented feed on growth and blood profile of Java Barb (*Barbonymus gonionotus*). *Jordan J. Biol. Sci*., **14(2)**: 297– 302. https://doi.org/10.54319/jjbs/140215

Setyobudi RH, Wahono SK, Adinurani PG, Wahyudi A, Widodo W, Mel M, Nugroho YA, Prabowo B and Liwang T. 2018. Characterisation of Arabica coffee pulp – hay from Kintamani - Bali as prospective biogas feedstocks. *Matec Web of Conf.* **164 (01039)**:1–13. https://doi.org/10.1051/matecconf/201816401039

Setyobudi RH, Yandri E, Nugroho YA, Susanti MS, Wahono SK, Widodo W, Zalizar L, Saati EA, Maftuchah M, Atoum MFM, Massadeh MI, Yono D, Mahaswa RK, Susanto H, Damat D, Roeswitawati D, Adinurani PG and Mindarti S. 2021. Assessment on coffee cherry flour of Mengani Arabica coffee, Bali, Indonesia as iron non-heme source. *Sarhad J. Agric*., **37(Special issue 1)**: 171–183. https://dx.doi.org/10.17582/journal.sja/2022.37.s1.171.183

Tonda R, Zalizar L, Widodo W, Setyobudi RH, Hermawan D, Damat D, Purbajanti ED, Prasetyo H, Ekawati I, Jani Y, Burlakovs J, Wahono SK, Anam C, Pakarti TA, Susanti MS, Mahnunin R, Sutanto A, Sari DK, Hilda H, Fauzi A, Wirawan W, Sebayang NS, Hadinoto H, Suhesti E, Amri U and Busa Y. 2022. Potential utilization of dried rice leftover of household organic waste for poultry functional feed. *Jordan J. Biol. Sci*., **15(5)**: 879–886. https://doi.org/10.54319/jjbs/150517

Ut VN, Phu TQ, Phuong NT, Giang HT and Morales J. 2016. Assessment of water quality in Catfish (*Pangasianodon hypophthalmus*) production systems in the Mekong Delta. *Can Tho University. Journal of Sciences*. **3**:71–78. https://doi.org/10.22144/ctu.jen.2016.107

Wu G. 2013. **Amino Acids: Biochemistry and Nutrition**. CRC Press, Boca Raton, Florida, USA.

Xie F, Ai Q, Mai K, Xu W and Wang X. 2012a. Dietary lysine requirement of large yellow croaker (*Pseudosciaena crocea*, Richardson 1846) larvae. *Aquac. Res.*, **43**:917–928. https://doi.org/10.1111/j.1365-2109.2011.02906.x

Xie F, Zeng W, Zhou Q, Wang H, Wang T, Zheng C and Wang Y. 2012b. Dietary lysine requirement of juvenile Pacific white shrimp, *Litopenaeus vannamei*. *Aquaculture*, **358-359**: 116–121. https://doi.org/10.1016/j.aquaculture.2012.06.027

Yang SD, Liu FG and Liou CH. 2011. Assessment of dietary lysine requirement for silver perch (*Bidyanus bidyanus*) juveniles. *Aquaculture*. **312**:102–108. https://doi.org/10.1016/j.aquaculture.2010.12.011

Yun H, Park G, Ok I, Katya K, Hung S and Bai SC. 2016. Determination of the dietary lysine requirement by measuring plasma free lysine concentrations in rainbow trout *Oncorhynchus mykiss* after dorsal aorta cannulation. *Fish Aquatic Sci.* **19(4)**:1–8. https://doi.org/10.1186/s41240-016-0004-1.

Subscription

Jordan Journal of Biological Sciences

An International Peer – Reviewed Research Journal

Published by the Deanship of Scientific Research, The Hashemite University, Zarqa, Jordan

Name: ..... الاسم:

Specialty: ..... التخصص:

Address: ..... العنوان:

P.O. Box: ..... صندوق البريد:

City &Postal Code:..... المدينة: الرمز البريدي:

Country: ..... الدولة:

Phone: ..... رقم الهاتف

Fax No.: ..... رقم الفاكس:

E-mail: ..... البريد الإلكتروني:

Method of payment: ..... طريقة الدفع:

Amount Enclosed: ..... المبلغ المرفق:

Signature: ..... التوقيع:

Cheque should be paid to Deanship of Research and Graduate Studies – The Hashemite University.

I would like to subscribe to the Journal

For

- ☐ One year
- ☐ Two years
- ☐ Three years

One Year Subscription Rates

	Inside Jordan	Outside Jordan
Individuals	JD10	$70
Students	JD5	$35
Institutions	JD 20	$90

Correspondence

Subscriptions and sales:

The Hashemite University
P.O. Box 330127-Zarqa 13115 – Jordan
Telephone: 00 962 5 3903333
Fax no. : 0096253903349
E. mail: jjbs@hu.edu.jo

المجلة الأردنية للعلوم الحياتية
Jordan Journal of Biological Sciences (JJBS)

http://jjbs.hu.edu.jo

المجلة الأردنية للعلوم الحياتية: مجلة علمية عالمية محكمة ومفهرسة ومصنفة، تصدرعن الجامعة الهاشمية وبدعم من صندوق دعم البحث العلمي والإبتكار – وزراة التعليم العالي والبحث العلمي.

ترسل البحوث الى العنوان التالي:

رئيس تحرير المجلة الأردنية للعلوم الحياتية
الجامعة الهاشمية
ص.ب , 330127 , الزرقاء, 13115 , الأردن
هاتف: 0096253903333
E-mail: jjbs@hu.edu.jo, Website: www.jjbs.hu.edu.jo

المملكة الأردنية الهاشمية

المجلة الأردنية

للعلوم الحياتية

مجلة علمية عالمية محكمة

تصدر بدعم من صندوق دعم البحث العلمي و الابتكار

http://jjbs.hu.edu.jo/